



**UNIVERSIDADE FEDERAL DE UBERLÂNDIA  
INSTITUTO DE CIÊNCIAS BIOMÉDICAS  
PROGRAMA DE PÓS-GRADUAÇÃO EM IMUNOLOGIA E  
PARASITOLOGIA APLICADAS  
LABORATÓRIO DE ENSAIOS ANTIMICROBIANOS - LEA**

**ESTUDOS *IN VITRO* E *IN VIVO* DA PRÓPOLIS VERMELHA BRASILEIRA:  
POTENCIAL ANTIBACTERIANO, ANTIPARASITÁRIO E ANTIVIRAL FRENTE  
A MICRORGANISMOS PATOGÊNICOS**

**NAGELA BERNADELLI SOUSA SILVA**

**UBERLÂNDIA-MG  
2024**



UNIVERSIDADE FEDERAL DE UBERLÂNDIA  
INSTITUTO DE CIÊNCIAS BIOMÉDICAS  
PROGRAMA DE PÓS-GRADUAÇÃO EM IMUNOLOGIA E  
PARASITOLOGIA APLICADAS  
LABORATÓRIO DE ENSAIOS ANTIMICROBIANOS - LEA



ESTUDOS *IN VITRO* E *IN VIVO* DA PRÓPOLIS VERMELHA BRASILEIRA:  
POTENCIAL ANTIBACTERIANO, ANTIPARASITÁRIO E ANTIVIRAL FRENTE  
A MICRORGANISMOS PATOGÊNICOS

Tese de doutorado apresentado ao  
Colegiado do Programa de Pós-graduação  
em Imunologia e Parasitologia Aplicadas  
como requisito para obtenção do título de  
Doutora.

**Aluna:** Ma. Nagela Bernadelli Sousa  
Silva

**Orientador:** Prof. Dr. Carlos Henrique  
Gomes Martins (ICBIM/UFU)

UBERLÂNDIA-MG  
2024



Nagela Bernadelli Sousa Silva



ESTUDOS *IN VITRO* E *IN VIVO* DA PRÓPOLIS VERMELHA BRASILEIRA:  
POTENCIAL ANTIBACTERIANO, ANTIPARASITÁRIO E ANTIVIRAL FRENTE  
A MICRORGANISMOS PATOGÊNICOS

Tese de doutorado apresentado ao Colegiado do Programa de Pós-graduação em Imunologia e Parasitologia Aplicadas como requisito para obtenção do título de Doutora.

Uberlândia, Junho de 2024

**Banca examinadora:**

Prof. Dr. Carlos Henrique Gomes Martins, Universidade Federal de Uberlândia (**Presidente**)  
Profa. Dra. Eloisa Amália Vieira Ferro, Universidade Federal de Uberlândia  
Profa. Dra. Ana Paula Turrioni Hidalgo, Universidade Federal de Uberlândia  
Profa. Dra. Tânia Cristina de São Pedro Pires, Centro de Investigação de Montanha  
Dra. Junya de Lacorte Singulani, Universidade Federal de Minas Gerais

**Suplentes:** Dra. Ralciane de Paula Menezes, Universidade Federal de Uberlândia  
Prof. Dr. Samuel Cota Teixeira, Universidade Federal de Uberlândia

Ficha Catalográfica Online do Sistema de Bibliotecas da UFU  
com dados informados pelo(a) próprio(a) autor(a).

S586  
2024

Silva, Nagela Bernadelli Sousa, 1995-  
ESTUDOS IN VITRO E IN VIVO DA PRÓPOLIS VERMELHA  
BRASILEIRA: POTENCIAL ANTIBACTERIANO, ANTIPARASITÁRIO E  
ANTIVIRAL FRENTE A MICROORGANISMOS PATOGÊNICOS [recurso  
eletrônico] / Nagela Bernadelli Sousa Silva. - 2024.

Orientador: Prof. Dr. Carlos Henrique Gomes Martins.  
Tese (Doutorado) - Universidade Federal de Uberlândia,  
Pós-graduação em Imunologia e Parasitologia Aplicadas.  
Modo de acesso: Internet.  
Disponível em: <http://doi.org/10.14393/ufu.te.2024.390>  
Inclui bibliografia.  
Inclui ilustrações.

1. Imunologia. I. Martins, Prof. Dr. Carlos Henrique  
Gomes, 1968-, (Orient.). II. Universidade Federal de  
Uberlândia. Pós-graduação em Imunologia e Parasitologia  
Aplicadas. III. Título.

CDU: 612.017

Bibliotecários responsáveis pela estrutura de acordo com o AACR2:

Gizele Cristine Nunes do Couto - CRB6/2091  
Nelson Marcos Ferreira - CRB6/3074



## **ATA DE DEFESA - PÓS-GRADUAÇÃO**

Programa de Pós-Graduação em	Imunologia e Parasitologia Aplicadas				
Defesa de:	Tese de Doutorado nº 166				
Data:	11/07/2024	Hora de início:	09:00	Hora de encerramento:	12 h 07 min
Matrícula do Discente:	12013IPA001				
Nome do Discente:	Nagela Bernadelli Sousa Silva				
Título do Trabalho:	Estudos in vitro e in vivo da Própolis Vermelha brasileira: Potencial antibacteriano, antiparasitário e antiviral frente a microrganismos patogênicos				
Área de concentração:	Imunologia e Parasitologia Aplicadas				
Linha de pesquisa:	Biotecnologia empregada no diagnóstico e controle de doenças				
Projeto de Pesquisa de vinculação:	Ensaio Biológicos Antimicrobianos in vitro e in vivo de Produtos Naturais e Sintéticos				

Em 11 de julho de 2024, às 09:00 horas, reuniu-se por vídeo conferência, a Banca Examinadora, designada pelo Colegiado do Programa de Pós-graduação em Imunologia e Parasitologia Aplicadas, assim composta pelos membros titulares: Presidente: Carlos Henrique Gomes Martins - ICBIM/UFU(orientador da discente); Eloisa Amália Vieira Ferro - ICBIM/UFU; Tânia Cristina de São Pedro Pires - CIMO/IPB - Portugal; Ana Paula Turrioni Hidalgo - FOUFU/UFU; Junya de Lacorte Singulani - FF/UFMG.

Iniciando os trabalhos o(a) presidente da mesa, Prof. Carlos Henrique Gomes Martins, apresentou a Comissão Examinadora e a candidata, agradeceu a presença do público, e concedeu ao Discente a palavra para a exposição do seu trabalho. A duração da apresentação, o tempo de arguição e resposta foram conforme as normas do Programa.

A seguir o senhor(a) presidente concedeu a palavra, pela ordem sucessivamente, aos(às) examinadores(as), que passaram a arguir o(a) candidato(a). Ultimada a arguição, que se desenvolveu dentro dos termos regimentais, a Banca, em sessão secreta, atribuiu o resultado final, considerando o(a) candidato(a):

### **APROVADA**

Esta defesa faz parte dos requisitos necessários à obtenção do título de Doutor.

O competente diploma será expedido após cumprimento dos demais requisitos, conforme as normas do Programa, a legislação pertinente e a regulamentação interna da UFU.

Nada mais havendo a tratar foram encerrados os trabalhos. Foi lavrada a presente ata que após lida e achada conforme foi assinada pela Banca Examinadora.



Documento assinado eletronicamente por **Carlos Henrique Gomes Martins, Professor(a) do Magistério Superior**, em 11/07/2024, às 12:08, conforme horário oficial de Brasília, com fundamento no art. 6º, § 1º, do [Decreto nº 8.539, de 8 de outubro de 2015](#).



Documento assinado eletronicamente por **Ana Paula Turrioni Hidalgo, Professor(a) do Magistério Superior**, em 11/07/2024, às 12:08, conforme horário oficial de Brasília, com fundamento no art. 6º, § 1º, do [Decreto nº 8.539, de 8 de outubro de 2015](#).



Documento assinado eletronicamente por **Junya de Lacorte Singulani, Usuário Externo**, em 11/07/2024, às 12:08, conforme horário oficial de Brasília, com fundamento no art. 6º, § 1º, do [Decreto nº 8.539, de 8 de outubro de 2015](#).



Documento assinado eletronicamente por **Tânia Cristina De São Pedro Pires, Usuário Externo**, em 11/07/2024, às 12:08, conforme horário oficial de Brasília, com fundamento no art. 6º, § 1º, do [Decreto nº 8.539, de 8 de outubro de 2015](#).



Documento assinado eletronicamente por **Eloisa Amália Vieira Ferro, Professor(a) do Magistério Superior**, em 11/07/2024, às 12:09, conforme horário oficial de Brasília, com fundamento no art. 6º, § 1º, do [Decreto nº 8.539, de 8 de outubro de 2015](#).



A autenticidade deste documento pode ser conferida no site [https://www.sei.ufu.br/sei/controlador\\_externo.php?acao=documento\\_conferir&id\\_orgao\\_acesso\\_externo=0](https://www.sei.ufu.br/sei/controlador_externo.php?acao=documento_conferir&id_orgao_acesso_externo=0), informando o código verificador **5518740** e o código CRC **220BEDA2**.

*Á minha vó Ovidia, que não  
esta mais entre nós, mas onde  
estiver, ficará feliz e orgulhosa.*

## **Agradecimentos**

A Deus, que sempre me mostrou qual caminho seguir e me deu forças para continuar apesar das dificuldades.

Ao meu orientador, Prof. Dr. Carlos Henrique Gomes Martins, que me estendeu a mão e me deu a oportunidade de aprender, crescer e evoluir tanto profissionalmente quanto pessoalmente.

A todos os professores que me auxiliaram e ajudaram ao longo de toda a minha trajetória acadêmica, que foram fundamentais para que eu chegasse até aqui.

A minha família, por ser meu porto seguro, por me apoiar e me incentivar dia após dia e apesar das dificuldades, nunca mediram esforços para me ajudar. Não teria conseguido sem vocês.

Ao meu marido Emerson, que esteve ao meu lado toda a minha trajetória acadêmica, me incentivando e me ajudando nos momentos que eu mais precisei.

Aos meus amigos e colegas que me apoiaram e não me deixaram desanimar em nenhum momento.

Aos amigos e companheiros do LEA, pelo companheirismo, amizade, ajuda e por deixarem o ambiente de trabalho descontraído e leve.

A Fundação de Amparo a Pesquisa do Estado de Minas Gerais (FAPEMIG) pela concessão da minha bolsa de estudos durante o curso (bolsa Número 12138).

À Fundação de Amparo à Pesquisa do Estado de São Paulo (FAPESP), pelo auxílio financeiro no projeto temático “Realização de estudos químicos, analíticos, biológicos, farmacológicos e tecnológicos para preenchimento das lacunas no desenvolvimento do setor brasileiro de própolis”, processo 2017/04138-8.



*“O sucesso é a soma de  
pequenos esforços repetidos dia  
após dia.”*

*Robert Collier*

## RESUMO

As doenças infecciosas continuam a ser uma causa importante de milhares de mortes anualmente em todo o mundo. Portanto, o objetivo desse estudo foi avaliar a atividade antimicrobiana, antiviral e antiparasitária da Própolis Vermelha brasileira (PVB) frente a microrganismos causadores de infecções endodônticas, vírus Chikungunya e *Toxoplasma gondii*, utilizando abordagens *in vitro*, *in vivo* e *in silico* além de realizar avaliações toxicológicas desses produtos. A atividade antimicrobiana foi determinada pelo método de diluição em caldo e a atividade sinérgica pelo ensaio checkerboard. A atividade antibiofilme foi avaliada pela coloração com cristal violeta a 2% e contagem de microrganismos. A infecção *in vivo* foi realizada em larvas de *Caenorhabditis elegans* AU37 e a análise *in silico* foi realizada pelo docking molecular. O efeito na modulação do crescimento de *T. gondii* foi avaliado através de ensaio colorimétrico de  $\beta$ -galactosidase. No primeiro estudo, a PVB demonstrou atividade antiperiodontopatogênica frente a todos os microrganismos avaliados, bem como atividade antibiofilme frente a biofilmes monoespécies e multiespécies. Além disso, foi capaz de inibir até 96% a infecção pelo vírus Chikungunya. Em *C. elegans*, a própolis não demonstrou toxicidade nas concentrações terapêuticas determinadas no estudo. No segundo estudo, a PVB demonstrou atividade antibacteriana e antifúngica frente a todos os microrganismos avaliados. Além disso, as amostras de PVB inibiram de forma significativa a produção de biomassa e reduziu o número de células viáveis do biofilme, além de diminuir a agregação celular. As maiores concentrações do extrato bruto e Gutiferona E aumentaram a sobrevivência das larvas infectadas e tratadas e reduziram o risco de morte. As substâncias isoladas Gutiferona E e Oblongifolina B inibiram a proliferação intracelular de *T. gondii* e demonstraram diversos alvos de ação frente as bactérias e *T. gondii* na análise *in silico*. Os resultados apresentados nos dois artigos são promissores e constituem-se como um estudo base, para que futuramente a PVB possa ser utilizada como medicamento frente a microrganismos de relevância clínica.

**Palavras chave:** Atividade antibacteriana, atividade antiviral, atividade antifúngica, atividade antiparasitária, Própolis Vermelha Brasileira, toxicidade.

## ABSTRACT

Infectious diseases continue to be an important cause of thousands of deaths annually around the world. Therefore, the objective of this study was to evaluate the antimicrobial, antiviral and antiparasitic activity of Brazilian Red Propolis (BRP) against microorganisms that cause endodontic infections, Chikungunya virus and *Toxoplasma gondii*, using *in vitro*, *in vivo* and *in silico* approaches, in addition to carrying out evaluations toxicology of these products. Antimicrobial activity was determined by the broth dilution method and synergistic activity by the checkerboard assay. Antibiofilm activity was evaluated by staining with 2% crystal violet and counting microorganisms. *In vivo* infection was performed on *Caenorhabditis elegans* AU37 larvae and *in silico* analysis was performed using molecular docking. The effect on modulating the growth of *T. gondii* was evaluated using a  $\beta$ -galactosidase colorimetric assay. In the first study, BRP demonstrated antiperiodontopathogenic activity against all microorganisms evaluated, as well as antibiofilm activity against monospecies and multispecies biofilms. Furthermore, it was able to inhibit Chikungunya virus infection by up to 97%. In *C. elegans*, propolis did not demonstrate toxicity at the therapeutic concentrations determined in the study. In the second study, BRP demonstrated antibacterial and antifungal activity against all microorganisms included. The crude extract demonstrated additive activity in combination with amphotericin B against *C. albicans* (ATCC 28366). Furthermore, the BRP samples significantly inhibited biomass production and reduced the number of viable cells in the biofilm, in addition to reducing cell aggregation and causing damage to the cell wall of the microorganisms present in the biofilm. The highest concentrations of the crude extract and Gutiferone E of BRP increased the survival of infected and treated larvae and reduced the risk of death. The isolated substances Gutiferone E and Oblongifolin B inhibited the intracellular proliferation of *T. gondii* and demonstrated several targets of action against bacteria and *T. gondii* *in silico* analysis. The results presented in the two articles are promising and constitute a basic study so that in the future BRP can be used as a medicine against clinically relevant microorganisms.

**Keywords:** Antibacterial activity, antifungal activity, antiviral activity, antiparasitic activity, Brazilian Red Propolis, toxicity.

## LISTA DE ABREVIATURAS, SIGLAS E SÍMBOLOS

%	Porcentagem
<	Menor
>	Maior
AmB	Anfotericina B
ATCC	American Type Culture Collection
BHI	Brain Heart Infusion
BHK-21	Fibroblastos derivados de rim de hamster dourado sírio
BOD	Biochemical Oxygen Demand
BRP	Brazilian Red Propolis
CC <sub>50</sub>	Concentração citotóxica
CFU	Colony Forming Units
CG	Cromatografia gasosa
CHIKV	<i>Chikungunya</i>
CHIKV-nanoluc	<i>Chikungunya</i> –nanoluciferase
CHX	Clorexidina
CLSI	Clinical and Laboratory Standards Institute
DAPI	4',6'-diamino-2-fenil-indol,
DMSO	Dimethylsulfoxide
DNA	Ácido desoxirribonucleico
EIMS	Esetrometria de Massa por Ionização Eletrônica
EPS	Extracellular Polymeric Matrix
FCAV	Faculdade de Ciências Agrárias e Veterinárias
h	Horas
HCFMRP	Hospital das Clínicas da Faculdade de Medicina de Ribeirão Preto
HPLC	Cromatografia Líquida de Alta Eficiência
IBILCE	Instituto de Biociências, Letras e Ciências Exatas
IC <sub>50</sub>	50% Cell Growth Inhibition
ICBIM	Instituto de Ciências Biomédicas
LC <sub>50</sub>	Lethal Concentration
LEA	Laboratório de Ensaios Antimicrobianos
MBC	Minimum Bactericidal Concentration

MFC	Minimum Fungicidal Concentration
MIC	Minimum Inhibitory Concentration
MICB <sub>50</sub>	Minimum Inhibitory Concentration of Biofilm
MTT	3-(4,5-Dimethylthiazol-2-yl)-2,5-Diphenyltetrazolium Bromide)
NGM	Nematode Growth Media
°C	Graus Celsius
OD	Optical Density
PDA	Detector de matriz de fotodiodos
PI	Propidium iodide
PVB	Própolis Vermelha Brasileira
RPMI	Roswell Park Memorial Institute
SDA	Sabouraud Dextrose Agar
SEM	Scanning Electron Microscopy
TI	Índice terapêutico
UFU	Universidade Federal de Uberlândia
UNESP	Universidade Estadual Paulista
UNIFRAN	Universidade de Franca
USA	United States of America
USP	Universidade de São Paulo
WHO	World Health Organization

## LISTA DE FIGURAS

### Capítulo II-

**Figure 1.** Chromatographic profile of Brazilian red propolis extract and chemical structures of their main compounds. Numbers correspond to: vestitol (1); neovestitol (2); medicarpin (3); 7-O-methylvestitol (4); guttiferone E/xanthochymol; and oblongifolin B (6).

**Figure 2.** Antibiofilm activity of Brazilian Red Propolis crude hydroalcoholic extract samples and number of viable cells in monospecies biofilms formed by ATCC strains and clinical isolates included in the study. (a) *P. gingivalis* (ATCC 49417). (b) *P. gingivalis* (clinical isolate). (c) *P. intermedia* (ATCC 15033) (d) *P. intermedia* (clinical isolate). (e) *A. naeslundii* (ATCC 19039). (f) *F. nucleatum* (clinical isolate).

**Figure 3.** Antibiofilm activity of oblongifolin B and number of viable cells in monospecies biofilms formed by ATCC strains and clinical isolates included in the study. (a) *P. intermedia* (clinical isolate) (b) *P. intermedia* (ATCC 15033) (c) *A. naeslundii* (ATCC 19039). (d) *F. nucleatum* (clinical isolate).

**Figure 4.** Antibiofilm activity of guttiferone E and number of viable cells in monospecies biofilms formed by ATCC strains and clinical isolates included in the study. (a) *P. gingivalis* (ATCC 49417). (b) *P. gingivalis* (clinical isolate). (c) *P. intermedia* (ATCC 15033). (d) *A. naeslundii* (ATCC 19039) (e) *F. nucleatum* (clinical isolate).

**Figure 5.** Antibiofilm activity of samples of Brazilian Red Propolis crude hydroalcoholic extract, oblongifolin B and guttiferone E and number of viable cells in multispecies biofilms formed by bacteria from groups 1 (standard strains) and 2 (clinical isolates). (A) Crude extract. (B) Oblongifolin B. (C) Guttiferone E.

**Figure 6.** Cell viability and CHIKV replication rates in the presence of Brazilian Red Propolis crude hydroalcoholic extract and fractions.

**Figure 7.** Effects of isolated compounds at on CHIKV infection and cell viability.

**Figure 8.** Evaluation of the toxicity of the Brazilian Red Propolis crude hydroalcoholic extract and isolated compounds guttiferone E and oblongifolin B in the *C. elegans in vivo* model. (A) Crude hydroalcoholic extract. (B) Oblongifolin B. (C) Guttiferone E.

### Capítulo III-

**Figure 1:** Antibiofilm activity of Gutiferone E and crude extract against bacteria and yeasts causes oral infections. **A:** Antibiofilm activity of Gutiferone E against *E. faecalis* (clinical isolate). **B:** Antibiofilm activity of Gutiferone E against *Enterococcus faecalis* (ATCC 4082). **C:** Antibiofilm activity of Gutiferone E against *S. salivarius* (clinical isolate). **D:** Antibiofilm activity of Gutiferone E against *S. salivarius* (ATCC 25975). **E:** Antibiofilm activity of Gutiferone E against *S. aureus* (clinical isolate). **F:** Antibiofilm activity of Gutiferone E against *Lactobacillus paracasei* (ATCC 11578). **G:** Antibiofilm activity of crude extract against *Candida albicans* (ATCC 28366). **H:** Antibiofilm activity of crude extract against *Candida glabrata* (ATCC MYA-276).

**Figure 2:** Antibiofilm activity of antibiotic and antifungal used as controls against bacteria and yeast included in the study. **A:** Antibiofilm activity of chlorhexidine against *E. faecalis* (clinical isolate). **B:** Antibiofilm activity of chlorhexidine against *Enterococcus faecalis* (ATCC 4082). **C:** Antibiofilm activity of chlorhexidine against *S. salivarius* (clinical isolate). **D:** Antibiofilm activity of chlorhexidine against *S. salivarius* (ATCC 25975). **E:** Antibiofilm activity of chlorhexidine against *S. aureus* (clinical isolate). **F:** Antibiofilm activity of chlorhexidine against *Lactobacillus paracasei* (ATCC 11578). **G:** Antibiofilm activity of amphotericin B against *Candida albicans* (ATCC 28366). **H:** Antibiofilm activity of amphotericin B against *Candida glabrata* (ATCC MYA-276).

**Figure 3:** Fluorescence electron microscopy images of biofilms of oral pathogens included in the study, untreated and treated with BRP samples at MIC<sub>50</sub> concentration, stained with PI and DAPI solution. **A&B:** Biofilm of *E. faecalis* (ATCC 4082) untreated and treated with Gutiferone E, respectively. **C&D:** Biofilm of *E. faecalis* (clinical isolate) untreated and treated with Gutiferone E, respectively. **E&F:** Biofilm of *S. salivarius* (ATCC 25975) untreated and treated with Gutiferone E, respectively. **G&H:** Biofilm of *S. salivarius* (clinical isolate) untreated and treated with Gutiferone E, respectively. **I&J:** Biofilm of *L. paracasei* (ATCC 11578) untreated and treated with Gutiferone E, respectively. **K&L:** *S. aureus* biofilm (clinical isolate) untreated and treated with Gutiferone E, respectively. **M&N:** Biofilm of *C. albicans* (ATCC 28366) untreated and treated with BRP crude extract, respectively. **O&P:** Biofilm of *C. glabrata* (ATCC MYA-276) untreated and treated with BRP crude extract, respectively. **Q&A:** Biofilm of *C. albicans* (ATCC 28366) showing nuclear fragmentation after treatment, indicated by the red arrow.

**Figure 4:** Scanning electron microscopy images of biofilms of oral pathogens untreated and treated with BRP samples. **A&B:** Biofilm of *E. faecalis* (ATCC 4082) untreated and treated with Gutiferone E, respectively. The red arrow shows the decrease in cell aggregation and biomass. **C&D:** *E. faecalis* biofilm (clinical isolate) untreated and treated with Gutiferone E, respectively. The red arrow highlights the change in the morphology of bacterial cells after treatment compared to the control. **E&F:** Biofilm of *S. salivarius* (ATCC 25975) untreated and treated with Gutiferone E, respectively. **G&H:** Biofilm of *S. salivarius* (clinical isolate) untreated and treated with Gutiferone E, respectively. **I&J:** Biofilm of *L. paracasei* (ATCC 11578) untreated and treated with Gutiferone E, respectively. **K&L:** *S. aureus* biofilm (clinical isolate) untreated and treated with Gutiferone E, respectively. **M&N:** Biofilm of *C. albicans* (ATCC 28366) untreated and treated with BRP crude extract, respectively. **O&P:** Biofilm of *C. glabrata* (ATCC MYA-

276) untreated and treated with BRP crude extract, respectively.

**Figure 5:** Survival curve and concentration response of oral pathogen infection in *C. elegans* larvae. **A)** Larvae infected with *E. faecalis* (clinical isolate) and treated with different concentrations of Gutiferone E. **B)** Larvae infected with *E. faecalis* (ATCC 4082) and treated with different concentrations of Gutiferone E. **C)** Larvae infected with *S. salivarius* (clinical isolate) and treated with different concentrations of Gutiferone E. **D)** Larvae infected with *S. salivarius* (25975) and treated with different concentrations of Gutiferone E. **E)** Larvae infected with *S. aureus* (clinical isolate) and treated with different concentrations of Gutiferone E. **F)** Larvae infected with *L. paracasei* (ATCC 11578) and treated with different concentrations of Gutiferone E. **G)** Larvae infected with *C. glabrata* (ATCC MYA-276) and treated with different concentrations of the crude BRP extract. **H)** Larvae infected with *C. albicans* (ATCC 28366) and treated with different concentrations of BRP crude extract. Survival curves were plotted using the Kaplan–Meier method and survival curves were compared by log-rank test. CHX: Chlorhexidine; AmB: Amphotericin B.

**Figure 6.** Molecular docking simulations of Gutiferone E against *S. aureus* and *L. paracasei*. **A)** Binding affinity of Gutiferone E against *S. aureus* (left panel) and *L. paracasei* (right panel) ranked by the total energy. **B)** Best pose prediction of Gutiferone E upon *S. aureus* teichoic acid glycosyltransferase (tarP) colored in green. **C)** Best pose prediction of Gutiferone E against *L. paracasei* ribonuclease (rnz) colored in orange. The target surfaces are represented by the interpolated charge. The hydrophobic interactions, conventional hydrogen bond and carbon-hydrogen bond are colored in pink, green and blue, respectively. The carbon, oxygen and hydrogen atoms are shown in grey, red and black, respectively.

**Figure 7.** Molecular docking simulations of Gutiferone E against *S. salivarius* and *E. faecalis*. **A).** Binding affinity of Gutiferone E against *S. salivarius* (left panel) and *E. faecalis* (right panel) ranked by the total energy. **B).** Best pose prediction of Gutiferone E upon *S. salivarius* teichoic acid urease accessory protein (ureG) colored in magenta. **C).** Best pose prediction of Gutiferone E against *E. faecalis* mevalonate diphosphate decarboxylase (mvaD) colored in blue. The target surfaces are represented by the interpolated charge. The hydrophobic interactions, conventional hydrogen bond and carbon-hydrogen bond are colored in pink, green and blue, respectively. The carbon, oxygen and hydrogen atoms are shown in grey, red and black, respectively.

**Figure 8:** Host cell viability and *T. gondii* intracellular proliferation. BeWo cells were treated for 24 h in twofold serial dilutions (ranging from 256 to 4 µg/mL) with (a) Gutiferone E and (b) Oblongifolin B. Also, BeWo cells were treated with culture medium alone (control group), 1.2% DMSO (vehicle of compounds in the concentration of 256 µg/mL). Cell viability was expressed in percentages (Cell viability %), with the absorbance of cells incubated only with culture medium considered to be 100% viability. *T. gondii*-infected BeWo cells were exposed for 24 h to concentrations in twofold serial dilutions of (c) Gutiferone E and (d) Oblongifolin B (ranging from 256 to 4 µg/mL), sulfadiazine plus pyrimethamine (SDZ+PYR; 200 + 8 µg/mL, respectively)



or culture medium only (control group - considered as 100% parasite proliferation). Parasite intracellular proliferation was analyzed using a colorimetric  $\beta$ -galactosidase assay and expressed in percentage change in comparison with control (*T. gondii* proliferation %). Data are shown as means  $\pm$  standard error of the means (SEM). \*Comparison between infected/untreated cells and infected/treated cells. & Comparison to SDZ+PYR-infected/treated cells. Significant differences were analyzed using one-way ANOVA test with Dunnett's multiple comparison post-test to evaluate significant differences ( $P < 0.05$ ).

**Figure 9.** Molecular docking simulations of Guttiferone E and Oblongifolin B against *T. gondii*. **A).** Binding affinity of Guttiferone E (left panel) and Oblongifolin B (right panel) ranked by the total energy. **B).** Best pose prediction of Guttiferone E upon *T. gondii* uracil phosphoribosyltransferase (uprT) colored in red. **C).** Best pose prediction of Oblongifolin B against *T. gondii* prolyl tRNA synthetase (prs) colored in yellow. The target surfaces are represented by the interpolated charge. The hydrophobic interactions, conventional hydrogen bond and carbon-hydrogen bond are colored in pink, green and blue, respectively. The carbon, oxygen and hydrogen atoms are shown in grey, red and black, respectively.

## LISTA DE TABELAS

### Capítulo II-

**Table 1:** Minimum inhibitory concentration of the Brazilian Red Propolis crude hydroalcoholic extract and fractions against periodontopathogenic bacteria.

**Table 2:** Minimum inhibitory concentration of the BRP isolated compounds against periodontopathogenic bacteria.

**Table 3:** BHK-21 cell viability in the presence of the BRP crude hydroalcoholic extract or fractions at 50, 10, and 2  $\mu\text{g}/\text{mL}$ . BHK-21 cells were treated with the extracts for 16 hours, and viability was measured via the MTT assay. The results are presented as percentage.

**Table 4:** BHK-21 cell viability in the presence of the BRP isolated substances at 50, 20, 10, 2, and 0.4  $\mu\text{M}$  /mL. BHK-21 cells were treated with the propolis samples for 16 hours, and viability was measured via the MTT assay. The results are presented as percentage.

### Capítulo III-

**Table 1:** Values of Minimum Inhibitory Concentration (MIC), Minimum Bactericidal Concentration (MBC) and Minimum Fungicide Concentration (MFC) of brazilian red propolis samples against oral pathogens.

**Table 2:** FICI values of the BRP samples in combination with standard antimicrobials against oral pathogens.

Table 3: Evaluation of the cytotoxicity of the isolated substances Gutiferone E and Oblongifolin B in BeWo cells infected with *T. gondii*.

## SUMÁRIO

APRESENTAÇÃO.....	18
CAPÍTULO I.....	21
Fundamentação teórica.....	21
1. Infecções endodônticas.....	22
2. Periodontite.....	23
3. Vírus Chikungunya .....	24
4. <i>Toxoplasma gondii</i> .....	25
5. Produtos naturais: uma opção terapêutica promissora.....	27
6. Própolis Vermelha Brasileira .....	29
Objetivo Geral .....	31
Objetivos específicos .....	31
Referências .....	32
CAPÍTULO II.....	37
Potential <i>in vitro</i> anti-periodontopathogenic, anti-Chikungunya activities and <i>in vivo</i> toxicity of Brazilian red propolis .....	37
CAPÍTULO III.....	53
Brazilian red propolis reduces the adhesion of oral biofilm cells and the <i>Toxoplasma gondii</i> intracellular proliferation.....	53
CAPÍTULO IV .....	95
Considerações finais.....	95
ANEXOS .....	98

## APRESENTAÇÃO

Ao longo da história, a humanidade utiliza a natureza para suprir suas necessidades fundamentais no manejo de uma ampla gama de enfermidades. As plantas são especificamente as principais fontes de compostos ativos que podem ser utilizadas na prática terapêutica, devido à notável diversidade de metabólitos que produzem. Esses metabólitos podem demonstrar potenciais farmacológicos que oferecem oportunidades para a descoberta e o desenvolvimento de medicamentos inovadores (Newman and Cragg 2020). O homem moderno vive em uma era onde a resistência microbiana é um grave problema de saúde pública, devido a constante alteração no potencial patogênico dos microrganismos, o que leva a escassez de medicamentos disponíveis para o tratamento de doenças infecciosas, tornando de extrema urgência a busca por novos compostos com atividade antimicrobiana (Morrison and Zembower 2020; Dutra et al. 2016).

O Brasil é o país com a maior biodiversidade do planeta, sendo fonte inesgotável de bioativos importantes (Noguera et al. 2024). Dos produtos naturais, a Própolis Vermelha Brasileira (PVB) vem demonstrando potenciais biológicos relevantes, que incentivam novos estudos nessa temática. A PVB é uma substância coletada pelas abelhas da espécie *Apis mellifera* de superfícies de buracos feitos pelos insetos no tronco de *Dalbergia ecastophyllum* (Dos Santos et al. 2022). Devido à multipotencialidade dos componentes bioativos que a PVB contém, a própolis pode ser utilizada como uma alternativa terapêutica promissora frente a diversos microrganismos causadores de infecções humanas. Várias doenças de grande relevância para a saúde pública, como as infecções endodônticas e a toxoplasmose, embora existam fármacos disponíveis no mercado para tratamento, os mesmos não são totalmente eficientes e/ou eficazes. Além disso, outra doença infecciosa de grande relevância nos dias atuais, é a infecção viral causada pelo vírus Chikungunya (CHIKV), sendo considerada uma doença aguda preocupante e ainda sem tratamento. Portanto, a presente tese de doutorado objetivou a avaliação da atividade antibacteriana, antiviral e antiparasitária da PVB frente á bactérias causadoras de infecções endodônticas, vírus CHIKV e *Toxoplasma gondii*.

Essa pesquisa visa contribuir para o conhecimento da multipotencialidade da PVB frente á microrganismos que causam infecções humanas graves. Considerando que o Brasil não tem atuação destacada no mercado mundial de fitomedicamentos, ficando inclusive atrás de países menos desenvolvidos tecnologicamente, espera-se que essa

pesquisa contribua para estabelecer as condições necessárias para o desenvolvimento no futuro de novos medicamentos á base de própolis, que atendam aos requisitos de segurança, eficácia e qualidade, com a complementação dos estudos para a validação química e farmacológica desses produtos naturais. Além disso, é importante ressaltar que a presente pesquisa incentivará o fortalecimento do capital humano e social, na formação e capacitação de pesquisadores nessa importante área do conhecimento e com potencial de obtenção de grande reconhecimento em diferentes áreas científicas.

A presente tese foi subdivida em quatro capítulos, como descrito a seguir:

**Capítulo I-** Fundamentação teórica. Apresenta uma revisão da literatura atualizada sobre os microrganismos causadores das infecções endodônticas, vírus Chikungunya e *Toxoplasma gondii*, patógenos que foram tema da presente tese e que são responsáveis por infecções de alta relevância clínica. Além disso, será abordada a importância da PVB como opção terapêutica frente a essas infecções, descrevendo sua composição química e aplicações farmacológicas.

**Capítulo II:** Nesse capítulo será apresentado o artigo publicado intitulado: ``Potential *in vitro* anti-periodontopathogenic, anti-*Chikungunya* activities and *in vivo* toxicity of Brazilian red própolis ´´, publicado no periódico Scientific Reports (fator de impacto 4,6, Qualis CAPES A1 na área Ciências Biológicas III). Esse artigo avaliou o potencial antibacteriano, antibiofilme e antiviral do extrato bruto hidroalcoólico, frações e substâncias isolados da PVB frente a bactérias periodontopatogênicas e vírus CHIKV, bem como sua toxicidade *in vivo*. A atividade antibacteriana foi avaliada por microdiluição em caldo, determinando-se a Concentração Inibitória Mínima e a atividade antibiofilme através de ensaios para a determinação da Concentração Inibitória Mínima do Biofilme (CIMB<sub>50</sub>). Os ensaios antivirais foram realizados infectando células BHK-21 com CHIKV. A toxicidade foi avaliada no modelo animal *C. elegans*. Os resultados foram muito promissores, com valores de CIM e CIMB<sub>50</sub> baixos em comparação com outros estudos. A medicarpina, neovestitol e vestitol foram capazes de inibir a infecção por CHIKV em até 97%. Os testes para avaliar a toxicidade em *C. elegans* demonstraram que a PVB não foi tóxica nas concentrações consideradas terapêuticas no estudo. Os resultados constituem uma abordagem alternativa no tratamento de diversas doenças infecciosas.

**Capítulo III:** Nesse capítulo será apresentado o manuscrito intitulado: “ Brazilian red propolis reduces biomass and viable cells of oral biofilm cells and the *Toxoplasma gondii* intracellular proliferation” que será submetido no periódico Biomedicine & Pharmacotherapy (fator de impacto 7.5 Qualis CAPES A1 na área Ciências Biológicas III). Esse estudo avaliou a atividade antimicrobiana e antiparasitária do extrato bruto hidroalcolólico e substâncias isoladas da Própolis Vermelha Brasileira (PVB) frente a patógenos orais e *T. gondii*, utilizando abordagens *in vitro*, *in vivo* e *in silico*. A atividade antimicrobiana foi determinada através da método de diluição em caldo e a atividade sinérgica pelo ensaio de cheakboard. A atividade antibiofilme foi avaliada pela coloração com cristal violeta a 2% e contagem de microrganismos. Os ensaios *in vivo* foram realizados em larvas de *Caenorhabditis elegans* AU37 e a análise *in silico* pelo docking molecular. Os valores de Concentração Inibitória Mínima variaram de 3.12 a 400 µg/mL. O extrato bruto demonstrou atividade aditiva em combinação com a anfotericina B frente a *C. albicans* (ATCC 28366). Os valores da Concentração Inibitória Mínima do Biofilme variaram de 6,25 a 375 µg/mL, com significativa redução no número de células viáveis. A maior concentração das amostras de PVB avaliadas aumentou a sobrevivência das larvas infectadas com taxas de sobrevivência acima de 50%. Além disso, as amostras inibiram a proliferação intracelular de *T. gondii*. A análise de docking molecular aponta vários alvos das substâncias isoladas da PVB frente às bactérias e *T. gondii*. Esses resultados apresentados nesse estudo demonstram que a PVB possui diversas atividades biológicas, podendo ser utilizada futuramente como medicamento frente a esses patógenos.

**Capítulo IV – Considerações finais.** Principais conquistas obtidas com o estudo, contribuições e perspectivas futuras dos resultados da pesquisa.

Adicionalmente, em ANEXO será apresentada toda produção científica realizada pela doutoranda em colaboração com a equipe do Laboratório de Ensaio Antimicrobianos (LEA/UFU) e outras instituições desde seu ingresso no Programa de Pós-graduação em Imunologia e Parasitologia Aplicadas (PPIPA/UFU).

**CAPÍTULO I**  
**Fundamentação teórica**

## 1. Infecções endodônticas

A cavidade bucal humana possui aproximadamente 700 espécies de microrganismos. A composição da microbiota bucal varia em cada indivíduo, mas de modo geral, os gêneros de bactérias de maior prevalência em uma boca saudável são *Streptococcus* spp., *Actinomyces* spp., *Veillonella* spp., *Fusobacterium* spp., *Porphyromonas* spp., *Prevotella* spp., *Treponema* spp., *Neisseria* spp., *Haemophilus* spp., *Lactobacillus* spp., *Capnocytophaga* spp., *Staphylococcus* spp., entre outros. Os fungos estão presentes em menor quantidade, sendo os gêneros *Candida* spp., *Cladosporium* spp., *Saccharomyces* spp., *Aspergillus* spp., *Fusarium* spp. e *Cryptococcus* os mais frequentes (Liu et al. 2024). A saúde bucal está diretamente relacionada com essa interação microbiana, onde bons hábitos alimentares e higiene favorecem uma relação microbiana harmoniosa. Porém, quando o ambiente bucal sofre alterações, esse ecossistema entra em desequilíbrio (Furtado Junior et al. 2020). As Infecções endodônticas são infecções causadas por uma variedade de microrganismos que invadem o espaço endodôntico (Dioguardi et al. 2020). Podem ser classificadas em infecções primárias, caracterizadas por uma infecção inicial de patógenos orais na polpa dentária e infecções endodônticas secundárias, quando a infecção se espalha para um sítio anatômico adjacente (Heasman 2014). A polpa dentária é um tecido localizado em uma câmara rígida do dente, protegido pela dentina, responsável por fornecer proteção mecânica frente ao ambiente oral. Quando a polpa dentária sofre lesões ou danos, essa região fica totalmente vulnerável a ação de microrganismos (Yu and Abbott 2007). A adesão desses microrganismos a polpa dentária pode acarretar uma resposta inflamatória conhecida como pulpíte. À medida que a doença avança, esses patógenos formam um fator de virulência essencial para sua permanência e forte adesão a dentina, denominado como biofilme (Gliga et al. 2023). Biofilme é definido a adesão de microrganismos uns aos outros e a uma superfície, circundados por uma matriz extracelular formada de polissacarídeos (Furtado Junior et al. 2020). A matriz extracelular fornece proteção a essa comunidade microbiana, protegendo-os frente a alterações de pH, células do sistema imune, substâncias de limpeza e agentes antimicrobianos (Del Rey et al. 2024). O tratamento das infecções endodônticas inclui a desinfecção da região pulpar, tentativa de reparo da raiz perfurada ou uso de antimicrobianos (Heasman 2014; Mendez-Millan et al. 2024). Porém, o uso excessivo desses medicamentos contribui para o aumento da resistência bacteriana, acarretando em falhas no tratamento endodôntico e piora do quadro clínico (Mendez-Millan et al. 2024).



Estudos destacam a relação das infecções bucais com o surgimento de doenças sistêmicas. Quando não tratadas, essas infecções tornam-se um reservatório importante de patógenos que podem causar danos sistêmicos ao indivíduo. Portanto, o tratamento correto e eficaz das infecções endodônticas torna-se extrema urgência (de Araujo et al. 2024).

## 2. Periodontite

Após a infecção e necrose pulpar, os patógenos orais podem invadir o espaço periapical, causando a periodontite (Mendez-Millan et al. 2024). Como resposta as toxinas liberadas pelo agregado microbiano, durante o processo inflamatório são liberadas substâncias como a histamina e outras, que aumentam a permeabilidade dos vasos sanguíneos, acarretando na destruição óssea, sendo denominada essa condição patológica de doença periodontal ou periodontite (Furtado Junior et al. 2020). A periodontite pode ser classificada como crônica ou agressiva, sendo a prevalência da periodontite agressiva dependente de vários fatores como etnia e localização. Estima-se que 2,6% dos afro-americanos, 1 a 5% dos africanos, 0,2% dos asiáticos, 0,5% a 1% dos norte-americanos e 0,3% dos sul-americanos possuem periodontite na sua forma mais grave (Mehrotra and Singh 2019). A doença inicia-se quando bactérias chamadas de colonizadoras primárias, que na sua grande maioria são bactérias do gênero *Streptococcus* e *Actinomyces* e outras bactérias Gram-positivas, aderem-se na superfície do dente. As bactérias Gram-negativas anaeróbias e organismos filamentosos são considerados os colonizadores secundários, enquanto *Fusobacterium* é considerado um organismo intermediário, capaz de se ligar tanto aos colonizadores primários quanto aos secundários. Algumas bactérias são mais específicas e se agregam somente em determinadas espécies como o caso da simbiose entre *Treponema denticola* e *Porphyromonas gingivalis*. Os últimos colonizadores são as espiroquetas, que irão contribuir no desenvolvimento do biofilme e no progresso da doença. As espiroquetas são móveis, sendo capazes de invadir o tecido hospedeiro e provocar os principais sinais clínicos da periodontite que são vermelhidão gengival, inchaço e sangramento na sondagem (Furtado Junior et al. 2020; Escobar-Arregoces et al. 2024).

A periodontite causada por fungos depende do estado imunológico do paciente, sendo mais susceptíveis a infecções fúngicas, os indivíduos em tratamento de câncer, doenças renais e fatores ambientais como tabagismo e alcoolismo. As espécies de *Candida*, especialmente *C. albicans*, estão relacionadas com a forma mais grave da

periodontite, sendo capazes de coagregarem com os colonizadores iniciais dos biofilmes orais, o que aumenta a sua persistência na cavidade oral, formando conseqüentemente um biofilme fúngico. *P. gingivalis* e *C. albicans* estão presentes na periodontite de forma sinérgica, onde *C. albicans* favorece o crescimento de *P. gingivalis*, deixando-a mais virulenta, e *P. gingivalis* induz a formação do tubo germinativo em *C. albicans*, deixando as leveduras mais virulentas e invasivas (Hu et al. 2024).

### 3. Vírus Chikungunya

Os primeiros casos da transmissão do vírus Chikungunya (CHIKV) nas Américas foram reportados em 2013 na ilha de Saint Martin no Caribe, com rápida propagação para outras ilhas como a América Central. A doença causada por CHIKV era raramente vista nos Estados Unidos no século passado, porém foram observados aumentos nos casos com uma média de 28 por ano entre 2006 e 2013. No Brasil, o vírus CHIKV foi identificado no ano de 2014 e juntamente com os vírus da dengue e zika, tornou-se hiperendêmico no país (Slavov et al. 2018; Reilly et al. 2020).

O vírus CHIKV é pequeno, envelopado e pertencente ao grupo dos alfavírus e da família *Togaviridae*. Possui aproximadamente 11.800 nucleotídeos, um RNA de cadeia simples de sentido 5´7´ com regiões não traduzidas 5`3` e quatro proteínas não essenciais (Silva and Dermody 2017). O ciclo de vida do vírus começa através da ligação de glicoproteínas virais a membrana celular das células hospedeiras. Após a adesão, o capsídeo do vírus é liberado no citoplasma das células hospedeiras, onde acontecerá a replicação. As proteínas NS formam então o complexo de replicase viral e o mRNA subgenômico é traduzido em uma poliproteína, clivada posteriormente em proteínas estruturais C, E3, E2, 6k e E1, seguidos pelos componentes virais. Após todo esse processo, o vírus é liberado das células (Martins et al. 2020).

A maioria das pessoas infectadas desenvolve a febre *Chikungunya*, uma doença aguda preocupante pelo rápido início da febre, poliartralgia, artrite incapacitante, erupção cutânea, mialgia e dor de cabeça. Devido a fase aguda da doença ser semelhante aos sintomas da dengue, alguns casos retrospectivos sugerem que os surtos de CHIKV ocorreram no ano de 1779, mas foram erroneamente atribuídos ao vírus da dengue. Uma diferença entre a dengue e CHIKV é que a última afeta a parte musculoesquelética do indivíduo, principalmente articulações periféricas, que podem

persistir por meses ou até anos após a infecção aguda. A taxa de mortalidade da doença por CHIKV é baixa, porém leva a limitações de saúde e um prejuízo na qualidade de vida do indivíduo, bem como consideráveis consequências econômicas e comunitárias (Silva and Dermody 2017).

O surgimento dos alfavírus na sociedade leva a constantes emergências de saúde e o desenvolvimento de compostos antivirais potentes e seguros contra esses vírus, torna-se de extrema urgência. Somente ano de 2023, foram registrados 154.800 casos prováveis de CHIKV no Brasil e mais de 100 óbitos de acordo com o Ministério de Saúde (Health 2024).

Os antivirais ajudam a reduzir a gravidade da doença, bem como os sintomas da fase aguda da infecção. Além disso, a redução da carga viral em pacientes infectados através da terapia antiviral pode ajudar a diminuir a eficiência da transmissão do vírus pelo mosquito vetor. Algumas estratégias contra o vírus CHIKV já foram estudadas como a alteração do pH endossomal, inibição dos receptores do vírus nas células e alguns produtos naturais, entre outros estudos *in vitro* (Silva and Dermody 2017), porém até o presente momento não há nenhum tratamento regulamentado para a doença de CHIKV.

#### **4. *Toxoplasma gondii***

*Toxoplasma gondii* é um protozoário intracelular obrigatório, da família *Apicomplexa*, causador da toxoplasmose em humanos e animais. É considerado o parasito de maior sucesso na terra, conhecido por infectar até um terço da população humana global. A prevalência de *T. gondii* no mundo difere e algumas regiões possuem uma taxa mais elevada como o Brasil com 77,5%, São Tomé e Príncipe 75,2%, Irã 63,9%, Colômbia 63,5% e Cuba com 61,8% de pessoas infectadas (Zaki et al. 2024). O ciclo de vida de *T. gondii* é complexo e envolve hospedeiros intermediários e definitivos e fases sexuada e assexuada. A fase sexuada acontece em gatos, que é considerado seu hospedeiro definitivo e a fase assexuada acontece no homem e outros mamíferos, juntamente com as aves (Attias et al. 2020).

A fase assexuada se inicia quando um hospedeiro susceptível ingere oocistos maduros contendo esporozoítos encontrados em alimentos ou água contaminada, cistos contendo bradizoítos encontrados na carne crua, ou mais raramente taquizoítos

eliminados no leite. Cada forma evolutiva sofre intensa multiplicação intracelular e invadem vários tipos de células do organismo, dando início a fase inicial da doença ou fase aguda. Alguns parasitos evoluem para a forma de cistos, os quais poderão permanecer por longo prazo, caracterizando a fase crônica da doença. A fase sexuada acontece em felinos, onde após a ingestão de cistos, oocistos ou taquizoítos, os parasitos liberados no estomago, penetram nas células do epitélio do gato, onde darão origem aos merozoítos. Posteriormente, essas células parasitadas se rompem e se transformam em formas sexuadas masculinas e femininas, que darão origem a microgametas e macrogametas. O macrogameta permanecerá na célula epitelial, enquanto que os microgametas móveis sairão de uma célula e irão fecundar o macrogameta, formando ovo ou zigoto, que dará origem ao oocisto, que é a forma infectante da doença para seu hospedeiro intermediário (Attias et al. 2020).

A transmissão da toxoplasmose ocorre principalmente pela ingestão de carne crua ou mal cozida contendo cistos viáveis ou água contaminada contendo oocistos de *T. gondii*. As infecções em adultos são geralmente assintomáticas, apenas 10% dos pacientes podem apresentar linfadenopatia ou toxoplasmose ocular. Em pacientes imunocomprometidos, a toxoplasmose pode se manifestar na sua forma mais grave, podendo causar encefalite toxoplasmática fatal, miocardite e pneumonite. A transmissão congênita de *T. gondii* é outro problema de saúde grave, acometendo mais de 190 mil casos em todo o mundo, causando danos graves ao feto, como sequelas incapacitantes a longo prazo, natimortos ou morte fetal (Warschkau and Seeber 2023). A forma neurológica da toxoplasmose em humanos, também tem sido associada à esquizofrenia, transtornos psiquiátricos entre outros. A toxoplasmose é a quarta causa mais comum de hospitalização e a terceira principal causa de morte dentre as doenças causadas por alimentos contaminados (Symeonidou et al. 2023).

Atualmente, a pirimetamina combinada com sulfadiazina e trimetoprim combinado com sulfametoxazol e esperamicina são as drogas de primeira escolha no tratamento da toxoplasmose. Os fármacos de segunda escolha incluem atovaquona e epiroprim (Shammaa, Powell, and Benmerzouga 2021). Apesar da eficácia desses fármacos na cura da toxoplasmose, em aproximadamente 80% dos casos acontecem recidivas e 40% dos pacientes precisam interromper o tratamento devido a efeitos colaterais tóxicos, como alergias severas. Além disso, esses medicamentos combinados são eficazes somente na fase aguda da doença, não tendo efeito na fase latente. Outro desafio dos regimes terapêuticos atuais é que os mesmos não passam na barreira

hematoencefálica, não sendo útil no tratamento das doenças do sistema nervoso causadas pelo *T. gondii*. A vacina, que é considerada uma estratégia promissora para a prevenção de *T. gondii*, ainda está longe da fase final dos estudos (Smith et al. 2021). Outra dificuldade sobre os antiparasitários atuais é sobre o tratamento das infecções crônicas, pois alguns medicamentos não são eficazes frente a cistos teciduais (Kalogeropoulos et al. 2022). Com isso, são necessários estudos que avaliem a ação de novos compostos frente a esse parasito, que poderá vir a ser uma alternativa terapêutica frente à toxoplasmose.

## **5. Produtos naturais: uma opção terapêutica promissora**

Os medicamentos fitoterápicos podem ser definidos como aqueles provindos de plantas com propriedades terapêuticas e curativas. A natureza sempre foi motivo de grande interesse por parte do homem, devido a tantos recursos oferecidos, muitos ainda não estudados. Os medicamentos fitoterápicos são utilizados por cerca de 3,5 a 4 bilhões de pessoas em todo o mundo para o tratamento de diversas doenças (A. Srivastava 2019). Desde a antiguidade, os produtos naturais desempenham um papel essencial na descoberta de medicamentos, principalmente para doenças causadas por microrganismos. Esses produtos se destacam frente as moléculas sintéticas, devido a sua enorme diversidade de metabólitos secundários e complexidade estrutural (Atanasov et al. 2021; Chopra and Dhingra 2021). Segundo Newman and Cragg (2020), de 1981 a 2019, 78 medicamentos antibacterianos, um antiviral e dois antiparasitários derivados de produtos naturais foram aprovados para uso pelo Food Drug Administration (FDA). Ainda segundo esses autores, nenhum antifúngico derivado de produtos naturais foi aprovado para uso até 2019, estando dois medicamentos na fase III de testes.

A descoberta das ações farmacológicas dos produtos naturais iniciou-se em 1806, com a descoberta da morfina isolada da papoula, que marcou o início de uma intensa e promissora busca por novos produtos com efeitos terapêuticos (Zhang et al. 2020). Compostos sintéticos elaborados a partir de produtos naturais podem fornecer soluções viáveis para enfrentar essa era da multirresistência que o mundo enfrenta atualmente, pois esses produtos podem ser capazes de atuar em diferentes alvos, bem como desenvolver novos mecanismos de ação frente a patógenos (Atanasov et al. 2021). O Brasil possui a maior biodiversidade do planeta, compreendendo mais de 45.000

espécies de plantas e é um país que possui a tradição do uso de plantas medicinais no tratamento de diversas doenças. O Ministério da Saúde do Brasil já estabeleceu diretrizes segundo a Organização Mundial da Saúde (OMS) que regulamenta os medicamentos a partir de produtos naturais (Ministério da Saúde Secretaria de Ciência and Estratégicos 2016), sendo considerados medicamentos desde que seja comprovada sua segurança na utilização, eficácia e qualidade (Dutra et al. 2016).

O mercado mundial de fitoterápicos movimenta cerca de 27 bilhões de dólares americanos, distribuídos principalmente na Europa, Ásia e Estados Unidos. Portanto percebe-se que o Brasil precisa urgentemente entrar nesse mercado econômico promissor, pois é um país com extensa biodiversidade, mas que possui poucos fitoterápicos disponíveis e aprovados, em comparação com o grande número de publicações científicas a respeito das vantagens desses produtos (Dutra et al. 2016).

A busca por novos compostos derivados de plantas medicinais com atividade antimicrobiana torna-se de extrema relevância pois a maioria dos produtos naturais não são tóxicos ou apresentam baixa toxicidade para os seres humanos, podendo ser utilizados desde que sejam realizados testes para a comprovação de segurança. Além de compostos antimicrobianos, os produtos naturais podem atuar como agentes anticâncer, antiinflamatórios, analgésicos entre outros, constituindo-se como um recurso renovável e único para a descoberta de novas biomoléculas terapeuticamente ativas, possuindo diversas características estruturais e biológicas (Sen and Samanta 2015).

Boccolini et al. (2022) avaliaram as características sociodemográficas e de saúde da população brasileira e demonstraram que a utilização de plantas medicinais é maior nas regiões Norte e Nordeste. Nessas regiões podem ser encontradas diversas origens botânicas das própolis, um tipo de produto natural que vem demonstrando-se como promissor no tratamento de diversas doenças, devido a sua extensa variedade de compostos químicos que apresentam atividade farmacológica. Existem 14 tipos de própolis no Brasil que vem demonstrando grande potencial antibacteriano, antifúngico, antioxidante, entre outras (Nani et al. 2020). Em 2007, o 13th tipo de própolis foi descrita na literatura, sendo denominada Própolis Vermelha Brasileira (PVB) devido a sua cor avermelha.

## 6. Própolis Vermelha Brasileira

A Própolis Vermelha Brasileira (PVB) é substância resinosa de cor avermelhada encontrada na superfície dos buracos feitos pelos insetos no tronco de *Dalbergia ecastophyllum*, popularmente conhecida como rabo-de-bugio, considerada a origem botânica da PVB, sendo coletada pelas abelhas da espécie *Apis mellifera* (Moise and Bobis 2020). Diversos compostos da PVB já foram identificados tais como a elemicina, isoelemicina, metil isoeugenol, formononetina, biochanina A, isoliquiritigenina, liquiritigenina, medicarpina, homopterocarpana, quercetina e vestitol. Do extrato lipofílico foram isoladas as benzofenonas, polipreniladas, guttiferona E, xantochimol, oblongifolina A e B, entre outros. As isoflavonas, formononetina, biochanina A, pinocembrina e medicarpina são considerados seus marcadores químicos devido as suas elevadas concentrações. Além destes compostos, foram identificados o ácido cafeico, ácido ferúlico, ácido umbelico, ácido picumárico, genisteína, canferol, catequina, dalbergioidina, epicatequina, daidzein, 2'hidroxiformononetina, ácido evernico, naringenina, calicosina, (7S), dalbergifenol, tevetiaflavona, cicloartenol, guttiferona C e outros compostos (Aldana-Mejia et al. 2021). Os flavonoides constituem-se como uma das mais importantes classes químicas presentes na PVB, sendo responsáveis pelas principais atividades biológicas que a PVB exerce, presentes nas PVB em concentrações que variam de 6,2 a 18,8% (Moise and Bobis 2020). A extração desses compostos pode ser realizada utilizando-se diversas técnicas e solventes, sendo o etanol o solvente mais utilizado. Com relação aos métodos aplicados, muitos autores utilizam a Cromatografia Gasosa (GC), Espectrometria de Massa por Ionização Eletrônica (EIMS), cromatografia em coluna repetida em sílica gel com gradiente de n-hexano-acetona, Cromatografia Líquida de Alta Eficiência (HPLC) e a cromatografia líquida de ultra-alta eficiência (UHPLC) acoplada a um espectrômetro de massas (Moise and Bobis 2020).

Alguns componentes de natureza polar, também já foram identificados na PVB, o que a torna de grande interesse econômico devido à facilidade de solubilização para fins comerciais, podendo ser produzida em larga escala (Moise and Bobis 2020). Atualmente é o segundo tipo de própolis brasileira mais produzida e comercializada, sendo encontrada principalmente na região costeira do Brasil, mais precisamente no Estado de Alagoas (Dos Santos et al. 2022). Muitos compostos encontrados na PVB não foram encontrados em outros tipos de própolis brasileiras, o que a torna um produto de abelha singular (de Freitas et al. 2017).

O valor comercial da própolis vermelha é internacionalmente alto, sendo que 1 kg pode custar cerca de R\$ 500.00. O Brasil é atualmente o terceiro maior produtor mundial de própolis, perdendo apenas para a Rússia e a China (Pereira, Seixas, and Aquino Neto 2002). Apesar de representar de 10 a 15% da produção mundial, o Brasil atende cerca de 80% da demanda japonesa. Em Minas Gerais, dados da Federação de apicultores mostram que a própolis produzida na região Centro-Oeste do Estado é considerada a melhor do mundo pelo mercado japonês, onde o quilograma de produto saltou de US\$ 5 a US\$ 200 nos últimos anos (Pereira, Seixas, and Aquino Neto 2002).

A PVB possui diversas atividades biológicas promissoras como atividade antibacteriana, antifúngica, anti-inflamatória, imunomoduladora, antioxidante e antiproliferativa. A estrutura molecular desses produtos é moldada devido à força evolutiva, fazendo com que os compostos químicos sejam capazes de se ligar a diferentes alvos biológicos, sendo essa a possível explicação para a multipotencialidade demonstrada pela PVB (Freires, de Alencar, and Rosalen 2016). A atividade antibacteriana da PVB já foi demonstrada frente a diversas bactérias como *Staphylococcus aureus* resistentes a metilina (MRSA)(Ripari et al. 2023), *Helicobacter pylori* (Santiago et al. 2022), *Clostridioides difficile*, entre outras. Possui atividade antibacteriana promissora frente a microrganismos causadores de infecções endodônticas, como *Porphyromonas gingivalis*, *Fusobacterium nucleatum*, *Prevotella intermedia*, *Actinomyces naeslundii*, *Streptococcus mutans*, *Streptococcus sobrinus*, *Staphylococcus aureus* (Silva et al. 2022; Bueno-Silva, Alencar, et al. 2013; Bueno-Silva, Koo, et al. 2013; de Figueiredo et al. 2020; Miranda et al. 2019). A sua atividade antiviral, embora menos investigada, já foi avaliada frente ao coronavírus 229E (Silva-Beltran et al. 2023) e *Enterovirus surrogates*. A PVB também já foi avaliada frente a parasitos como *Shistosoma mansoni* (Silva et al. 2021), *Toxocara cati* (Sinott et al. 2019) *Trypanosoma cruzi* e *Leishmania Braziliensis* (Regueira-Neto et al. 2018).

O uso da PVB como medicamento pode reduzir o uso de antimicrobianos e antiparasitários sintéticos e constituir-se como uma nova estratégia frente a microrganismos causadores de infecções. Devido aos múltiplos componentes bioativos encontrados nos extratos de própolis, pode-se esperar um sinergismo com as drogas convencionais e um maior espectro de ação comparado com o uso apenas dos medicamentos (Silva-Beltran et al. 2020).

Poucos estudos demonstraram a atividade antibacteriana e antifúngica da PVB frente aos microrganismos incluídos no presente estudo. Além disso, esse é o primeiro



estudo a avaliar a toxicidade da PVB em larvas de *Caenorhabditis elegans*. Nenhum estudo avaliou a atividade antiviral da PVB frente ao vírus CHIKV e atividade antiparasitária frente a *T. gondii*, tornando o presente estudo original e pioneiro.

### **Objetivo Geral**

Avaliar a atividade antimicrobiana, antiviral e antiparasitária da Própolis Vermelha Brasileira frente a microrganismos causadores de infecções endodônticas, vírus Chikungunya e *T. gondii*.

### **Objetivos específicos**

- Determinar a Concentração Inibitória Mínima (CIM) frente a um painel de bactérias e leveduras causadoras de infecções endodônticas e frente a bactérias periodontopatogênicas;
- Determinar a Concentração Bactericida Mínima (CBM) frente a um painel de bactérias e leveduras causadoras de infecções endodônticas e frente a bactérias periodontopatogênicas;
- Determinar a atividade antibiofilme mono e multiespécies frente a um painel de bactérias e leveduras causadoras de infecções endodônticas e frente a bactérias periodontopatogênicas;
- Avaliar o efeito sinérgico com antimicrobianos, frente a microrganismos causadores das infecções endodônticas;
- Determinar a atividade antiproliferativa das substâncias isoladas Gutiferona E e Oblongifolina B frente ao parasito *Toxoplasma gondii*;
- Determinar a concentração efetiva de 50% (EC<sub>50</sub>) frente ao parasito *Toxoplasma gondii*;
- Determinar o índice de seletividade frente ao parasito *Toxoplasma gondii*.
- Determinar a atividade antiviral no ciclo replicativo do vírus Chikungunya;
- Determinar a concentração efetiva de 50% (EC<sub>50</sub>) frente ao vírus Chikungunya;
- Determinar o índice de seletividade frente ao vírus Chikungunya.
- Determinar *in silico* quais são os principais alvos das substâncias isoladas Gutiferona E e Oblongifolina B frente aos microrganismos causadores de infecções endodônticas e *T. gondii*

## Referências

A. Srivastava, P. Srivastava, A. Pandey, V.K. Khanna, A.B. Pant. 2019. 'Chapter 24 - Phytomedicine: A Potential Alternative Medicine in Controlling Neurological Disorders.' in, *New Look to Phytomedicine: Advancements in Herbal Products as Novel Drug Leads* (Academic Press). <https://doi.org/10.1016/B978-0-12-814619-4.00025-2>

Aldana-Mejia, J. A., G. V. Ccana-Ccapatinta, I. S. Squarisi, S. Nascimento, M. H. Tanimoto, V. P. Ribeiro, C. Arruda, H. Nicolella, T. Esperandim, A. B. Ribeiro, K. S. de Freitas, L. H. D. da Silva, S. D. Ozelin, L. T. S. Oliveira, A. L. A. Melo, D. C. Tavares, and J. K. Bastos. 2021. 'Nonclinical Toxicological Studies of Brazilian Red Propolis and Its Primary Botanical Source *Dalbergia ecastaphyllum*', *Chem Res Toxicol*, 34: 1024-33. <https://doi.org/10.1021/acs.chemrestox.0c00356>

Atanasov, A. G., S. B. Zotchev, V. M. Dirsch, Taskforce International Natural Product Sciences, and C. T. Supuran. 2021. 'Natural products in drug discovery: advances and opportunities', *Nat Rev Drug Discov*, 20: 200-16. <https://doi.org/10.1038/s41573-020-00114-z>

Attias, M., D. E. Teixeira, M. Benchimol, R. C. Vommaro, P. H. Crepaldi, and W. De Souza. 2020. 'The life-cycle of *Toxoplasma gondii* reviewed using animations', *Parasit Vectors*, 13: 588. <https://doi.org/10.1186/s13071-020-04445-z>

Boccolini, P. M. M., K. de Lima Sirio Boclin, I. M. C. de Sousa, and C. S. Boccolini. 2022. 'Prevalence of complementary and alternative medicine use in Brazil: results of the National Health Survey, 2019', *BMC Complement Med Ther*, 22: 205. <https://doi.org/10.1186/s12906-022-03687-x>

Bueno-Silva, B., S. M. Alencar, H. Koo, M. Ikegaki, G. V. Silva, M. H. Napimoga, and P. L. Rosalen. 2013. 'Anti-inflammatory and antimicrobial evaluation of neovestitol and vestitol isolated from Brazilian red propolis', *J Agric Food Chem*, 61: 4546-50. <https://doi.org/10.1021/jf305468f>

Bueno-Silva, B., H. Koo, M. L. Falsetta, S. M. Alencar, M. Ikegaki, and P. L. Rosalen. 2013. 'Effect of neovestitol-vestitol containing Brazilian red propolis on accumulation of biofilm in vitro and development of dental caries in vivo', *Biofouling*, 29: 1233-42. <https://doi.org/10.1080/08927014.2013.834050>

Chopra, B., and A. K. Dhingra. 2021. 'Natural products: A lead for drug discovery and development', *Phytother Res*, 35: 4660-702. <https://doi.org/10.1002/ptr.7099>

de Araujo, B. M. M., B. M. de Miranda, T. C. Kowaltschuk, F. M. Goncalves, A. G. D. Schroder, E. C. Kuchler, O. Guariza-Filho, E. Carneiro, C. M. de Araujo, and U. Xavier da Silva-Neto. 2024. 'Impact of chronic diseases on the periapical health of

endodontically treated teeth: A systematic review and meta-analysis', *PLoS One*, 19: e0297020. <https://doi.org/10.1371/journal.pone.0297020>

de Figueiredo, K. A., H. D. P. da Silva, S. L. F. Miranda, Fjds Goncalves, A. P. de Sousa, L. C. de Figueiredo, M. Feres, and B. Bueno-Silva. 2020. 'Brazilian Red Propolis Is as Effective as Amoxicillin in Controlling Red-Complex of Multispecies Subgingival Mature Biofilm In Vitro', *Antibiotics (Basel)*, 9. <https://doi.org/10.3390/antibiotics9080432>

de Freitas, M. C. D., M. B. de Miranda, D. T. de Oliveira, S. A. Vieira-Filho, R. B. Caligiorne, and S. M. de Figueiredo. 2017. 'Biological Activities of Red Propolis: A Review', *Recent Pat Endocr Metab Immune Drug Discov*, 11: 3-12. <https://doi.org/10.2174/1872214812666180223120316>

Del Rey, Y. C., H. Parize, S. Assar, G. Gostemeyer, and S. Schlafer. 2024. 'Effect of mutanase and dextranase on biofilms of cariogenic bacteria: A systematic review of in vitro studies', *Biofilm*, 7: 100202. <https://doi.org/10.1016/j.biofilm.2024.100202>

Dioguardi, M., V. Crincoli, L. Laino, M. Alovise, D. Sovereto, L. Lo Muzio, and G. Troiano. 2020. 'Prevalence of Bacteria of Genus Actinomyces in Persistent Extraradicular Lesions-Systematic Review', *J Clin Med*, 9. <https://doi.org/10.3390/jcm9020457>

Dos Santos, F. F., R. P. Morais-Urano, W. R. Cunha, S. G. de Almeida, Psdsr Cavallari, H. A. Manuquian, H. A. Pereira, R. Furtado, M. F. C. Santos, and E. Silva M. L. Amdrade. 2022. 'A review on the anti-inflammatory activities of Brazilian green, brown and red propolis', *J Food Biochem*, 46: e14350. <https://doi.org/10.1111/jfbc.14350>

Dutra, R. C., M. M. Campos, A. R. Santos, and J. B. Calixto. 2016. 'Medicinal plants in Brazil: Pharmacological studies, drug discovery, challenges and perspectives', *Pharmacol Res*, 112: 4-29. <https://doi.org/10.1016/j.phrs.2016.01.021>

Escobar-Arregoces, F., M. A. Eras, A. Bustos, A. Suarez-Castillo, D. A. Garcia-Robayo, and M. Del Pilar Bernal. 2024. 'Characterization of the oral microbiota and the relationship of the oral microbiota with the dental and periodontal status in children and adolescents with nonsyndromic cleft lip and palate. Systematic literature review and meta-analysis', *Clin Oral Investig*, 28: 245. <https://doi.org/10.1007/s00784-024-05624-3>.

Freires, I. A., S. M. de Alencar, and P. L. Rosalen. 2016. 'A pharmacological perspective on the use of Brazilian Red Propolis and its isolated compounds against human diseases', *Eur J Med Chem*, 110: 267-79. <https://doi.org/10.1016/j.ejmech.2016.01.033>

Furtado Junior, J. H. C., L. A. R. Valadas, Sgdc Fonseca, P. L. D. Lobo, L. H. M. Calixto, A. G. F. Lima, M. H. R. de Aguiar, I. S. Arruda, M. A. L. Lotif, E. M.

Rodrigues Neto, and M. M. F. Fonteles. 2020. 'Clinical and Microbiological Evaluation of Brazilian Red Propolis Containing-Dentifrice in Orthodontic Patients: A Randomized Clinical Trial', *Evid Based Complement Alternat Med*, 2020: 8532701. <https://doi.org/10.1155/2020/8532701>

Gluga, A., M. Sandulescu, O. Amza, R. Stanescu, and M. Imre. 2023. 'Dental pathologies of endodontic origin and subsequent bacterial involvement - a literature review', *Germs*, 13: 373-80. <https://doi.org/10.18683/germs.2023.1407>

Health, Ministry of. 2024. 'Chikungunya'.

Heasman, P. A. 2014. 'An endodontic conundrum: the association between pulpal infection and periodontal disease', *Br Dent J*, 216: 275-9. <https://doi.org/10.1038/sj.bdj.2014.199>

Hu, Y., B. Ren, L. Cheng, S. Deng, and Q. Chen. 2024. 'Candida species in periodontitis: A new villain or a new target?', *J Dent*, 148: 105138. <https://doi.org/10.1016/j.jdent.2024.105138>

Kalogeropoulos, D., H. Sakkas, B. Mohammed, G. Vartholomatos, K. Malamos, S. Sreekantam, P. Kanavaros, and C. Kalogeropoulos. 2022. 'Ocular toxoplasmosis: a review of the current diagnostic and therapeutic approaches', *Int Ophthalmol*, 42: 295-321. <https://doi.org/10.1007/s10792-021-01994-9>

Liu, S., S. Wang, N. Zhang, and P. Li. 2024. 'The oral microbiome and oral and upper gastrointestinal diseases', *J Oral Microbiol*, 16: 2355823. <https://doi.org/10.1080/20002297.2024.2355823>

Martins, D. O. S., I. A. Santos, D. M. de Oliveira, V. R. Grosche, and A. C. G. Jardim. 2020. 'Antivirals against Chikungunya Virus: Is the Solution in Nature?', *Viruses*, 12. <https://doi.org/10.3390/v12030272>

Mehrotra, Neha, and Saurabh Singh. 2019. 'Periodontitis'.

Mendez-Millan, J. A., M. Leon-Lopez, J. Martin-Gonzalez, J. J. Saucó-Marquez, D. Cabanillas-Balsera, and J. J. Segura-Egea. 2024. 'Antibiotic Over-Prescription by Dentists in the Treatment of Apical Periodontitis: A Systematic Review and Meta-Analysis', *Antibiotics (Basel)*, 13. <https://doi.org/10.3390/antibiotics13040289>

Ministério da Saúde Secretaria de Ciência, Tecnologia e Insumos, and Departamento de Assistência Farmacêutica Estratégicos, Ministério da Saúde. 2016. 'National Policy and Program of Medicinal Plants and Herbal Medicines'.

Miranda, S. L. F., J. T. Damasceno, M. Faveri, L. Figueiredo, H. D. da Silva, S. M. A. Alencar, P. L. Rosalen, M. Feres, and B. Bueno-Silva. 2019. 'Brazilian red propolis reduces orange-complex periodontopathogens growing in multispecies biofilms', *Biofouling*, 35: 308-19. <https://doi.org/10.1080/08927014.2019.1598976>

Moise, A. R., and O. Bobis. 2020. 'Baccharis dracunculifolia and Dalbergia ecastaphyllum, Main Plant Sources for Bioactive Properties in Green and Red Brazilian Propolis', *Plants (Basel)*, 9. <https://doi.org/10.3390/plants9111619>

Morrison, L., and T. R. Zembower. 2020. 'Antimicrobial Resistance', *Gastrointest Endosc Clin N Am*, 30: 619-35. <https://doi.org/10.1016/j.giec.2020.06.004>

Nani, B. D., J. C. O. Sardi, J. G. Lazarini, D. R. Silva, A. P. Massariolli, T. M. Cunha, S. M. de Alencar, M. Franchin, and P. L. Rosalen. 2020. 'Anti-inflammatory and anti-Candida Effects of Brazilian Organic Propolis, a Promising Source of Bioactive Molecules and Functional Food', *J Agric Food Chem*, 68: 2861-71. <https://doi.org/10.1021/acs.jafc.8b07304>

Newman, D. J., and G. M. Cragg. 2020. 'Natural Products as Sources of New Drugs over the Nearly Four Decades from 01/1981 to 09/2019', *J Nat Prod*, 83: 770-803. <https://doi.org/10.1021/acs.jnatprod.9b01285>

Nogueira, N. H., Dclh Nogueira, Apdf Machado, L. M. Reguengo, and R. P. D. Nascimento. 2024. 'Emerging berries from the Brazilian Amazon and Atlantic Forest biomes: new sources of bioactive compounds with potential health benefits', *Food Funct*, 15: 5752-84. <https://doi.org/10.1039/D4FO00182F>

Pereira, Alberto dos Santos, Fernando Rodrigues Mathias Silva Seixas, and Francisco Radler de Aquino Neto. 2002. 'Própolis: 100 anos de pesquisa e suas perspectivas futuras', *Química Nova*, 25: 321-26. <https://doi.org/10.1590/S0100-40422002000200021>

Regueira-Neto, M. D. S., S. R. Tintino, M. Rolon, C. Coronal, M. C. Vega, V. de Queiroz Balbino, and H. D. de Melo Coutinho. 2018. 'Antitrypanosomal, antileishmanial and cytotoxic activities of Brazilian red propolis and plant resin of *Dalbergia ecastaphyllum* (L) Taub', *Food Chem Toxicol*, 119: 215-21. <https://doi.org/10.1016/j.fct.2018.04.029>

Reilly, Jo Marie, Wenxue Xing, Vladimir Levicky, Sami Souccar, Christopher Rogers, Lakshmanan %J The American Journal of Forensic Medicine Sathyavagiswaran, and Pathology. 2020. 'Postmortem chikungunya diagnosis: a case report and literature review', 41: 48-51. <https://doi.org/10.1097/PAF.0000000000000519>

Ripari, N., A. F. M. Pereira, A. F. Junior, V. L. M. Rall, J. A. Aldana-Mejia, J. K. Bastos, and J. M. Sforcin. 2023. 'Brazilian red propolis in combination with beta-lactams exerts an efficient antibacterial action over methicillin-resistant *Staphylococcus aureus* (MRSA) strains', *J Appl Microbiol*, 134. <https://doi.org/10.1093/jambio/lxac080>

Santiago, M. B., L. F. Leandro, R. B. Rosa, M. V. Silva, S. C. Teixeira, J. P. S. Servato, S. R. Ambrosio, R. C. S. Veneziani, J. A. Aldana-Mejia, J. K. Bastos, and C. H. G. Martins. 2022. 'Brazilian Red Propolis Presents Promising Anti-H. pylori Activity in In

Vitro and In Vivo Assays with the Ability to Modulate the Immune Response', *Molecules*, 27. <https://doi.org/10.3390/molecules27217310>

Sen, T., and S. K. Samanta. 2015. 'Medicinal plants, human health and biodiversity: a broad review', *Adv Biochem Eng Biotechnol*, 147: 59-110. [https://doi.org/10.1007/10\\_2014\\_273](https://doi.org/10.1007/10_2014_273)

Shammaa, A. M., T. G. Powell, and I. Benmerzouga. 2021. 'Adverse outcomes associated with the treatment of Toxoplasma infections', *Sci Rep*, 11: 1035. <https://doi.org/10.1038/s41598-020-80569-7>

Silva-Beltran, N. P., A. P. Balderrama-Carmona, M. A. Umsza-Guez, and B. A. Souza Machado. 2020. 'Antiviral effects of Brazilian green and red propolis extracts on Enterovirus surrogates', *Environ Sci Pollut Res Int*, 27: 28510-17. <https://doi.org/10.1007/s11356-019-07458-z>

Silva-Beltran, N. P., J. C. Galvez-Ruiz, L. A. Ikner, M. A. Umsza-Guez, T. L. de Paula Castro, and C. P. Gerba. 2023. 'In vitro antiviral effect of Mexican and Brazilian propolis and phenolic compounds against human coronavirus 229E', *Int J Environ Health Res*, 33: 1591-603. <https://doi.org/10.1080/09603123.2022.2110576>

Silva, L. A., and T. S. Dermody. 2017. 'Chikungunya virus: epidemiology, replication, disease mechanisms, and prospective intervention strategies', *J Clin Invest*, 127: 737-49. <https://doi.org/10.1172/JCI84417>

Silva, M. P., T. M. Silva, A. C. Mengarda, M. C. Salvadori, F. S. Teixeira, S. M. Alencar, G. C. Luz Filho, B. Bueno-Silva, and J. de Moraes. 2021. 'Brazilian red propolis exhibits antiparasitic properties in vitro and reduces worm burden and egg production in an mouse model harboring either early or chronic *Schistosoma mansoni* infection', *J Ethnopharmacol*, 264: 113387. <https://doi.org/10.1016/j.jep.2020.113387>

Silva, Nagela Bernadelli Sousa, Jonathan Henrique de Souza, Mariana Brentini Santiago, Jhennyfer Rodrigues da Silva Aguiar, Daniel Oliveira Silva Martins, Rafael Alves da Silva, Igor de Andrade Santos, Jennyfer A Aldana-Mejía, Ana Carolina Gomes Jardim, and Reginaldo %J Scientific Reports dos Santos Pedroso. 2022. 'Potential in vitro anti-periodontopathogenic, anti-Chikungunya activities and in vivo toxicity of Brazilian red propolis', 12: 21165. <https://doi.org/10.1038/s41598-022-24776-4>

Sinott, F. A., A. Sena-Lopes, K. S. Leal, M. Thais de Oliveira Silva, M. Cardoso de Freitas, M. Quintana de Moura, M. E. Aires Berne, and S. Borsuk. 2019. 'Essential oil from Brazilian Red Propolis exhibits anthelmintic activity against larvae of *Toxocara cati*', *Exp Parasitol*, 200: 37-41. <https://doi.org/10.1016/j.exppara.2019.03.014>

Slavov, S. N., K. K. Otaguiri, M. L. Bianquini, H. T. O. Bitencourt, M. C. M. Chagas, D. S. S. Guerreiro, L. T. M. Figueiredo, D. T. Covas, and S. Kashima. 2018. 'Seroprevalence of Chikungunya virus in blood donors from Northern and Southeastern

Brazil', *Hematol Transfus Cell Ther*, 40: 358-62. <https://doi.org/10.1016/j.htct.2018.04.002>

Smith, N. C., C. Goulart, J. A. Hayward, A. Kupz, C. M. Miller, and G. G. van Dooren. 2021. 'Control of human toxoplasmosis', *Int J Parasitol*, 51: 95-121. <https://doi.org/10.1016/j.ijpara.2020.11.001>

Symeonidou, I., G. Sioutas, T. Lazou, A. I. Gelasakis, and E. Papadopoulos. 2023. 'A Review of *Toxoplasma gondii* in Animals in Greece: A FoodBorne Pathogen of Public Health Importance', *Animals (Basel)*, 13. <https://doi.org/10.3390/ani13152530>

Warschkau, D., and F. Seeber. 2023. 'Advances towards the complete in vitro life cycle of *Toxoplasma gondii*', *Fac Rev*, 12: 1. <https://doi.org/10.12703/r/12-1>

Yu, C., and P. V. Abbott. 2007. 'An overview of the dental pulp: its functions and responses to injury', *Aust Dent J*, 52: S4-16. <https://doi.org/10.1111/j.1834-7819.2007.tb00525.x>

Zaki, L., M. Olfatifar, F. Ghaffarifar, A. V. Eslahi, A. KarimiPourSaryazdi, A. Taghipour, N. Hamidianfar, M. Badri, and P. Jokelainen. 2024. 'Global prevalence of *Toxoplasma gondii* in birds: A systematic review and meta-analysis', *Parasite Epidemiol Control*, 25: e00350. <https://doi.org/10.1016/j.parepi.2024.e00350>

Zhang, L., J. Song, L. Kong, T. Yuan, W. Li, W. Zhang, B. Hou, Y. Lu, and G. Du. 2020. 'The strategies and techniques of drug discovery from natural products', *Pharmacol Ther*, 216: 107686. <https://doi.org/10.1016/j.pharmthera.2020.107686>

## CAPÍTULO II

**Potential *in vitro* anti-periodontopathogenic, anti-Chikungunya activities and *in vivo* toxicity of Brazilian red propolis**

Artigo publicado no periódico Scientific Reports em 2022

(<https://doi.org/10.1038/s41598-022-24776-4>)





OPEN

## Potential in vitro anti-periodontopathogenic, anti-*Chikungunya* activities and in vivo toxicity of Brazilian red propolis

Nagela Bernadelli Sousa Silva<sup>1</sup>, Jonathan Henrique de Souza<sup>1</sup>, Mariana Brentini Santiago<sup>1</sup>, Jhennyfer Rodrigues da Silva Aguiar<sup>1</sup>, Daniel Oliveira Silva Martins<sup>1,2</sup>, Rafael Alves da Silva<sup>3</sup>, Igor de Andrade Santos<sup>1</sup>, Jennyfer A. Aldana-Mejía<sup>4</sup>, Ana Carolina Gomes Jardim<sup>1,2</sup>, Reginaldo dos Santos Pedroso<sup>5</sup>, Sergio Ricardo Ambrósio<sup>6</sup>, Rodrigo Cássio Sola Veneziani<sup>6</sup>, Jairo Kenupp Bastos<sup>4</sup>, Regina Helena Pires<sup>7</sup> & Carlos Henrique Gomes Martins<sup>1</sup>✉

Bacterial and viral infections are serious public health issue. Therefore, this study aimed to evaluate the antibacterial, antibiofilm and antiviral potential of the Brazilian Red Propolis (BRP) crude hydroalcoholic extract, fractions, and isolated compounds, as well as their in vivo toxicity. The antibacterial activity was evaluated by determining the Minimum Inhibitory Concentration and the antibiofilm activity by determining the Minimum Inhibitory Concentration of Biofilm (MICB<sub>50</sub>). The viable bacteria count (Log<sub>10</sub> UFC/mL) was also obtained. The antiviral assays were performed by infecting BHK-21 cells with *Chikungunya* (CHIKV) *nanoluc*. The toxicity of the BRP was evaluated in the *Caenorhabditis elegans* animal model. The MIC values for the crude hydroalcoholic extract sample ranged from 3.12 to 100 µg/mL, while fractions and isolated compounds the MIC values ranged from 1.56 to 400 µg/mL. The BRP crude hydroalcoholic extract, oblongifolin B, and gutiferone E presented MICB<sub>50</sub> values ranging from 1.56 to 100 µg/mL against monospecies and multispecies biofilms. Neovestitol and vestitol inhibited CHIKV infection by 93.5 and 96.7%, respectively. The tests to evaluate toxicity in *C. elegans* demonstrated that the BRP was not toxic below the concentrations 750 µg/mL. The results constitute an alternative approach for treating various infectious diseases.

Despite important advances in the health area, infectious diseases have constituted a serious public health issue over time<sup>1</sup>. One example is periodontitis, an inflammatory disease that affects tooth-supporting apparatus and which is caused by microorganisms present in dysbiosis plaque biofilms<sup>2</sup>. According to Mehrotra and Singh<sup>3</sup>, about 2.6% of African Americans, 5% of Africans, 0.2% of Asians, 1% of North Americans, and 0.3% of South Americans have been diagnosed with periodontitis in its most severe form. Periodontal treatment is essential not only for dental parameters, but also to avoid other pathological conditions such as adverse reactions in pregnancy, cardiovascular and respiratory diseases, cancer, lupus, rheumatoid arthritis, diabetes mellitus, and chronic kidney disease<sup>4</sup>. Even if the illness can be treated with antibiotics, the infection can be aggravated in patients lacking treatment or in the presence of resistant periodontopathogenic bacteria<sup>5</sup>.

Viral diseases also burden the global health system due to lack of vaccines and approved antivirals to combat important human viruses, including the *Chikungunya* Fever, caused by the *Chikungunya* virus (CHIKV)<sup>6</sup>. CHIKV was identified in 2014 and has become hyperendemic in Brazil<sup>7</sup>. This virus causes dengue-like symptoms such

<sup>1</sup>Institute of Biomedical Sciences (ICBIM), Federal University of Uberlândia, Uberlândia, Brazil. <sup>2</sup>Institute of Biosciences, Letters and Exact Sciences (IBILCE), Sao Paulo State University, São José Do Rio Preto, Brazil. <sup>3</sup>Faculty of Medicine (FAMED), Federal University of Uberlândia, Uberlândia, Brazil. <sup>4</sup>Faculty of Pharmaceutical Sciences of Ribeirão Preto, University of São Paulo (USP), Ribeirão Preto, Brazil. <sup>5</sup>Technical School of Health (ESTES), Federal University of Uberlândia, Uberlândia, Brazil. <sup>6</sup>Exact and Technological Sciences Nucleus, University of Franca (UNIFRAN), Franca, Brazil. <sup>7</sup>Postgraduate Program in Health Promotion, University of Franca (UNIFRAN), Franca, Brazil. ✉email: carlos.martins2@ufu.br

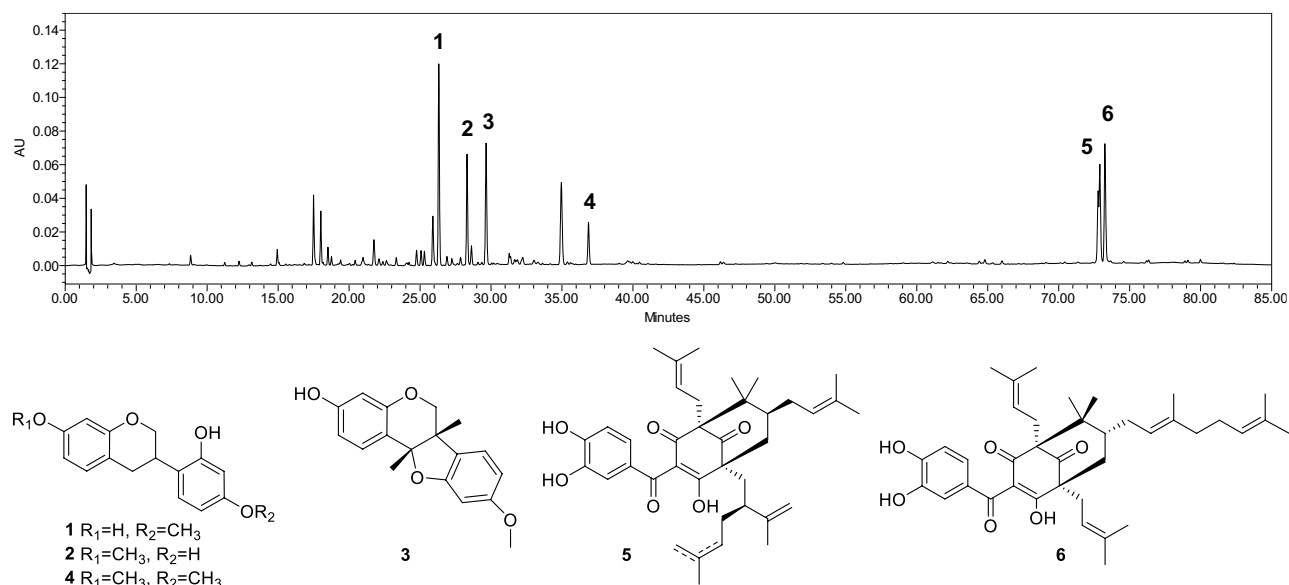


**Figure 1.** Chromatographic profile of Brazilian red propolis extract and chemical structures of their main compounds. Numbers correspond to: vestitol (1); neovestitol (2); medicarpin (3); 7-*O*-methylvestitol (4); guttiferone E/xanthochymol<sup>59</sup>; and oblongifolin B (6).

as fever, fatigue, arthralgia, and polyarthralgia<sup>8</sup>. By April 2022, 28,291 suspected cases of *Chikungunya Fever* had been registered and five deaths had been confirmed in Brazil; another eight deaths are under investigation<sup>9</sup>.

According to the World Health Organization, a considerable part of the worldwide population still depends on traditional medicine and employs natural products to treat several diseases<sup>10</sup>. Developing countries mainly use such products. In this scenario, Brazil is a valuable source of natural products given that it possesses diverse fauna and flora<sup>11</sup>. Brazilian Red Propolis (BRP), a resinous material produced by *Apis mellifera* bees through the collection of the exudates of two plant species: *Dalbergia ecastaphyllum*<sup>12,13</sup> and *Symphonia globulifera*<sup>14</sup> has excellent potential for developing new medicines. BRP is currently one of the most produced and commercialized types of Brazilian propolis. It is mainly found in the Brazilian mangroves of the Northeast, especially in Alagoas and Bahia states<sup>15</sup>.

BRP is composed of 50% resin, 30% wax, 10% essential oils, 5% pollen, and 5% other compounds, including secondary metabolites like flavonoids, isoflavonoids, cinnamic acid derivatives, esters, polyprenylated benzophenones, and some terpenes, which are considered the main biologically active constituents of this type of propolis<sup>16</sup>. The molecules isolated from BRP do not occur in any other type of propolis, which makes them rare and unique natural products<sup>17</sup>. Variations of this composition have been observed between locations. Some studies revealed that compounds such as formononetin and isoliquiritigenin are the most abundant in samples of Alagoas<sup>18</sup>. Instead, in “Canaveiras” sample, vestitol, neovestitol, medicarpin, and polyprenylated benzophenones have been identified as the main compounds and<sup>17</sup>. In this sense, BRP has been reported to possess antibacterial<sup>15,18–20</sup> antiparasitic<sup>21–27</sup>, and antiviral activities<sup>28</sup>.

Considering the lack of treatment options for periodontitis and CHIKV infection, we have hypothesized that BRP and its isolated compounds are a promising candidate for treating these diseases. To the best of our knowledge, there are no data on the BRP antiviral action against CHIKV, and few studies have reported on its antibacterial action against periodontopathogenic bacteria<sup>13,18,28–30</sup>. The use of BRP as a therapeutic option could reduce the use of antibiotics in periodontitis cases and become a novel antiviral strategy against CHIKV<sup>28</sup>.

This study aimed to evaluate the *in vitro* antibacterial, antibiofilm, and antiviral potential of the BRP crude hydroalcoholic extract, fractions, and isolated compounds, as well as their toxicity in an *in vivo* model.

## Results

**BRP crude extract characterization.** The chromatographic analysis revealed the presence of isoflavanes (vestitol, neovestitol, 7-*O*-methylvestitol), pterocarpans (medicarpin), and polyprenylated acylphloroglucinols (a mixture of guttiferone E/xanthochymol, and oblongifolin B) (Fig. 1), as main compounds of the BRP. The chromatographic profile of the fractions revealed the prominent presence of polyprenylated acylphloroglucinols on the hexane fraction, whereas the dichloromethane, ethyl acetate, and *n*-butanol fractions were composed mainly of isoflavanes (see Supplementary Figure S1).

**Minimum inhibitory concentration of the BRP crude hydroalcoholic extract, fractions, and isolated compounds.** Tables 1 and 2 show the MIC results for the crude hydroalcoholic extract, fractions and isolated compounds against periodontal bacteria included in the study. The MIC values for the crude hydroalcoholic extract sample ranged from 3.12 to 100  $\mu\text{g/mL}$ , for the dichloromethane fraction from 1.56 to 200  $\mu\text{g/mL}$ , ethyl acetate from 12.5 to 400  $\mu\text{g/mL}$ , hexane from 3.12 to 400  $\mu\text{g/mL}$ , and *n*-Butanol from 100 to 400  $\mu\text{g/mL}$  (Table 1).

Minimum Inhibitory Concentration ( $\mu\text{g/mL}$ )					
Crude extract		Fractions			
Bacteria		Dichloromethane	Ethyl acetate	Hexane	<i>n</i> -Butanol
<i>Porphyromonas gingivalis</i> (ATCC 49417)	3.12	1.56	12.5	3.12	100
<i>Porphyromonas gingivalis</i> (clinical isolate)	12.5	25	400	100	–
<i>Fusobacterium nucleatum</i> (ATCC 10953)	100	200	400	–	–
<i>Fusobacterium nucleatum</i> (clinical isolate)	12.5	12.5	–	400	–
<i>Prevotella intermedia</i> (ATCC 15033)	6.25	6.25	200	200	200
<i>Prevotella intermedia</i> (clinical isolate)	50	100	–	400	–
<i>Actinomyces naeslundii</i> (ATCC 19039)	25	25	–	400	–
<i>Actinomyces naeslundii</i> (clinical isolate)	100	100	400	400	400

**Table 1.** Minimum inhibitory concentration of the Brazilian Red Propolis crude hydroalcoholic extract, and fractions against periodontopathogenic bacteria. <sup>a</sup>Technique control strains: *Bacteroides fragilis* (ATCC 25285) and *Bacterioides thetaiotaomicron* (ATCC 29741)—Metronidazole: 1.47 and 2.95  $\mu\text{g/mL}$ , respectively.—> 400  $\mu\text{g/mL}$  was considered inactive.

Minimum Inhibitory Concentration ( $\mu\text{g/mL}$ )						
Isolated compounds						
Bacteria	Metilvestitol	Medicarpin	Vestitol	Neovestitol	Oblongifolin B	Guttiferone E
<i>Porphyromonas gingivalis</i> (ATCC 49,417)	25	50	12.5	12.5	50	1.56
<i>Porphyromonas gingivalis</i> (clinical isolate)	100	200	100	100	6.25	6.25
<i>Fusobacterium nucleatum</i> (ATCC 10,953)	50	50	25	12.5	50	200
<i>Fusobacterium nucleatum</i> (clinical isolate)	–	50	100	50	3.12	3.12
<i>Prevotella intermedia</i> (ATCC 15,033)	–	100	100	50	6.25	12.5
<i>Prevotella intermedia</i> (clinical isolate)	–	–	200	100	50	50
<i>Actinomyces naeslundii</i> (ATCC 19,039)	400	100	200	50	6.25	6.25
<i>Actinomyces naeslundii</i> (clinical isolate)	–	–	200	100	25	50

**Table 2.** Minimum inhibitory concentration of the BRP isolated compounds against periodontopathogenic bacteria. <sup>a</sup>Technique control strains: *Bacteroides fragilis* (ATCC 25285)—Metronidazole: 1.47  $\mu\text{g/mL}$  and *Bacterioides thetaiotaomicron* (ATCC 29741)—Metronidazole: 2.95  $\mu\text{g/mL}$ . – > 400  $\mu\text{g/mL}$  was considered inactive.

For the methylvestitol, the MIC values ranged from 25 to 400  $\mu\text{g/mL}$ , medicarpin from 50 to 400  $\mu\text{g/mL}$ , vestitol from 12.5 to 200  $\mu\text{g/mL}$ , neovestitol from 12.5 to 100  $\mu\text{g/mL}$ , oblongifolin B from 3.12 to 50  $\mu\text{g/mL}$ , and guttiferone E from 1.56 to 200  $\mu\text{g/mL}$  (Table 2).

**Antibiofilm activity of the BRP crude hydroalcoholic extract and isolated compounds.** The BRP crude hydroalcoholic extract reduced the monospecies biofilm formation of the standard strains (ATCC) and their clinical isolates (Fig. 2). Additionally, the number of viable cells in the monospecies biofilm expressed as  $\text{Log}_{10}$  CFU/mL decreased (Fig. 2). The lowest MIC<sub>50</sub> value obtained for the BRP crude hydroalcoholic extract against the monospecies biofilms was 3.12  $\mu\text{g/mL}$  against *A. naeslundii* (ATCC 19039) and *F. nucleatum* (clinical isolate) (Fig. 2e and f). Against the other evaluated monospecies biofilms, the BRP crude hydroalcoholic extract presented MIC<sub>50</sub> of 6.25  $\mu\text{g/mL}$ , except for *P. intermedia* (clinical isolate), against which MIC<sub>50</sub> was 12.5  $\mu\text{g/mL}$ . However, even at concentrations above MIC<sub>50</sub>, we detected viable biofilm cells (Fig. 2a–f).

As for the tested isolated compounds, they also reduced monospecies biofilm formation. In the presence of oblongifolin B (Fig. 3), the lowest MIC<sub>50</sub> was 0.78  $\mu\text{g/mL}$  against *A. naeslundii* (ATCC 19039) (Fig. 3c). Against the other evaluated monospecies biofilms, the MIC<sub>50</sub> values ranged from 1.56 to 6.25  $\mu\text{g/mL}$ . Oblongifolin B at 6.25  $\mu\text{g/mL}$  eliminated *P. gingivalis* (clinical isolate) viable cells and, at 12.5  $\mu\text{g/mL}$ , it eliminated *P. intermedia* (ATCC 15033) and *F. nucleatum* (clinical isolate) viable cells (Fig. 3a,b and d).

Guttiferone E presented low MIC<sub>50</sub> (0.78  $\mu\text{g/mL}$ ) against *A. naeslundii* (ATCC 19,039) (Fig. 4d). Against the other evaluated monospecies biofilms, MIC<sub>50</sub> ranged from 1.56 to 25  $\mu\text{g/mL}$  (Fig. 4a,b,c and e). Guttiferone E eliminated all the biofilm cells from a concentration of 3.12  $\mu\text{g/mL}$  against *P. gingivalis* (clinical isolate), 6.25  $\mu\text{g/mL}$  against *P. intermedia* (ATCC 15033), 25  $\mu\text{g/mL}$  against *F. nucleatum* (clinical isolate), and 1.56  $\mu\text{g/mL}$  against *A. naeslundii* (ATCC 19039). As for *P. gingivalis* (ATCC 49417), we verified the presence of viable biofilm cells even at concentrations above MIC<sub>50</sub> (Fig. 4a).

We also assessed the activity of the BRP crude hydroalcoholic extract and isolated compounds against multispecies biofilm formed by standard strains (group 1) and clinical isolates (group 2) (Fig. 5). The BRP crude

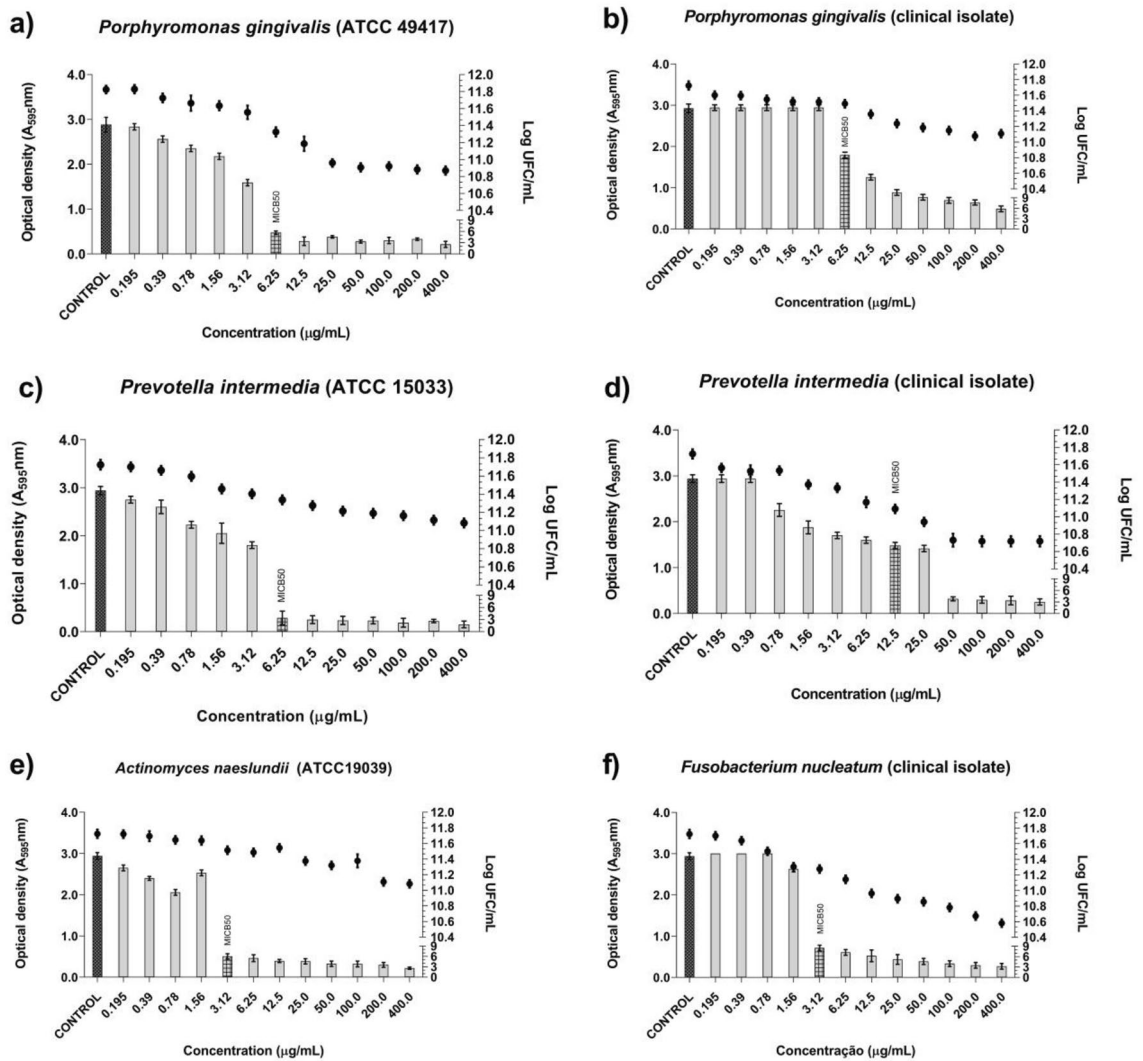


**Figure 2.** Antibiofilm activity of Brazilian Red Propolis crude hydroalcoholic extract samples and number of viable cells in monospecies biofilms formed by ATCC strains and clinical isolates included in the study. (a) *P. gingivalis* (ATCC 49417). (b) *P. gingivalis* (clinical isolate). (c) *P. intermedia* (ATCC 15033). (d) *P. intermedia* (clinical isolate). (e) *A. naeslundii* (ATCC 19039). (f) *F. nucleatum* (clinical isolate).

hydroalcoholic extract had MIC<sub>50</sub> of 6.25 µg/mL against the group 1 multispecies biofilm. However, even at higher concentrations, viable cells were still found in the biofilm. Similar results were found against the group 2 multispecies biofilm: MIC<sub>50</sub> was 6.25 µg/mL, and there also were viable biofilm cells above the MIC<sub>50</sub> concentration (Fig. 5A).

Concerning oblongifolin B, it had the lowest MIC<sub>50</sub> against the group 1 multispecies biofilm (1.56 µg/mL); however, at concentrations above MIC<sub>50</sub>, cells remained viable in the biofilm. Against the group 2 multispecies biofilm, oblongifolin B presented MIC<sub>50</sub> of 50 µg/mL and eliminated all the biofilm cells from the biofilm at this same concentration (Fig. 5B). On the other hand, guttiferone E showed MIC<sub>50</sub> of 3.12 µg/mL against the group 1 multispecies biofilm, and 6.25 µg/mL guttiferone E eliminated all the cells from the biofilm. Against the group 2 multispecies biofilm, guttiferone E had higher MIC<sub>50</sub> (100 µg/mL), but 50 µg/mL guttiferone E also eliminated all the viable cells from the biofilm (Figs. 5C).

Regarding the control (metronidazole), the MIC<sub>50</sub> of monospecies biofilms ranged from 2.95 to 5.9 µg/mL. As for the mixed biofilms, the MIC<sub>50</sub> was 2.95 µg/mL for both the biofilm formed by group 1 and the biofilm formed by group 2 (see supplementary material Figures S2 and S3).

**Effects of the BRP crude hydroalcoholic extract and isolated compounds on CHIKV replication.** To further evaluate the effects of BRP extract and its isolated compounds, BHK 21 cells were treated with each extract at 50, 10 and 2 µg/mL and cell viability was measured 16 h later. The results demonstrated that cells tolerated *n*-Butanol at 50 µg/mL (98.4%), ethyl acetate at 10 µg/mL (95.9%), while the crude extract, dichloromethane, and hexane at 2 µg/mL (99.3, 99.8, and 100%, respectively), (Table 3). Through the employment of BHK-21 cells infected with CHIKV-*nanoluc*, the anti-CHIKV activities of each sample were evaluated,

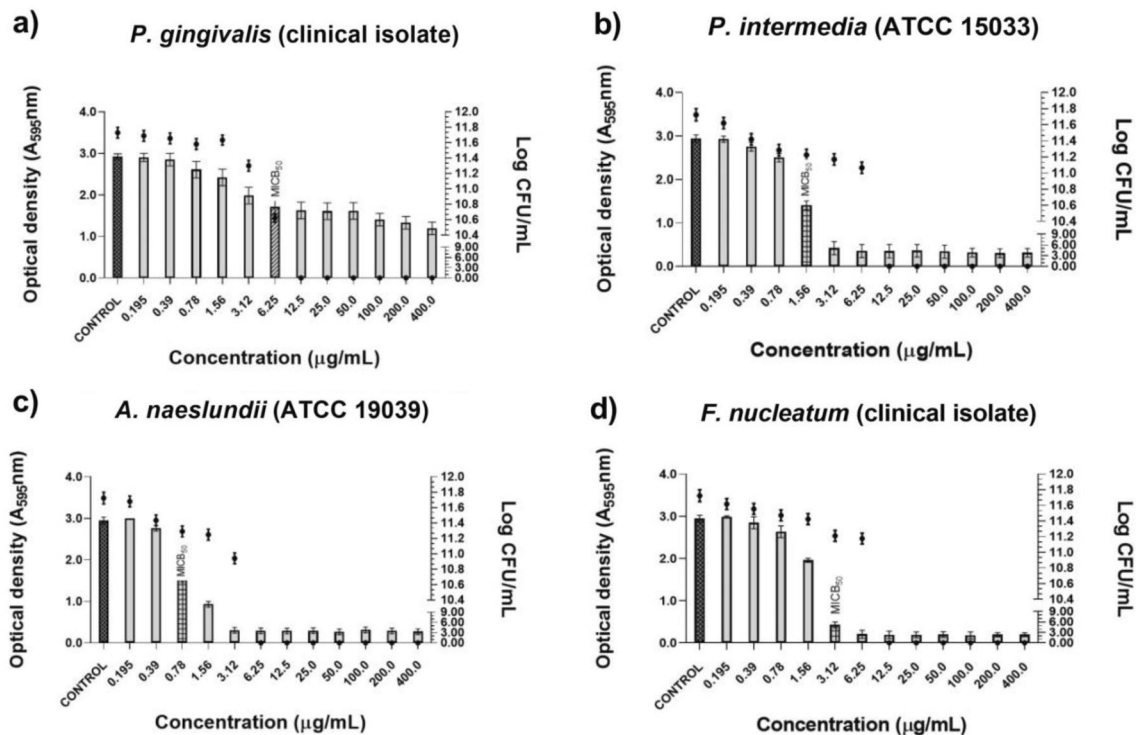


**Figure 3.** Antibiofilm activity of oblongifolin B and number of viable cells in monospecies biofilms formed by ATCC strains and clinical isolates included in the study. (a) *P. gingivalis* (clinical isolate) (b) *P. intermedia* (ATCC 15033). (c) *A. naeslundii* (ATCC 19039). (d) *F. nucleatum* (clinical isolate).

at the maximum non-cytotoxic concentrations selected through the viability assay. The results demonstrated that *n*-Butanol significantly inhibited 69% of CHIKV replication (Fig. 6). The other samples presented no effect on CHIKV infection (Fig. 6).

For the isolated substances (medicarpin, neovestitol, vestitol, oblongifolin B, methylvestitol and, guttiferone E), BHK-21 cells were treated with concentrations of each compound ranging from 32 to 0.5 µg/mL. As an outcome, the treatment with compounds in concentrations over 3 µg/mL presented cell viability rates higher than 80% (Table 4), and the highest non-cytotoxic concentration of each compound was selected for the antiviral assay. Since medicarpin, neovestitol and vestitol at 14 µg/mL presented cytotoxicity (Table 4), and at 3 µg/mL showed no antiviral activity (Supplementary Figure S4), the alternative concentration of 11 µg/mL was selected to the further assays. Therefore, the antiviral activity of medicarpin, neovestitol and vestitol was tested at 11 µg/mL, guttiferone E and oblongifolin B at 6 µg/mL, and methylvestitol at 14 µg/mL. The compounds medicarpin, neovestitol and vestitol inhibited CHIKV replication in vitro in 86%, 94%, and 97% respectively (Fig. 7).

**Toxicity assessment in *Caenorhabditis elegans*.** To assess the toxicity of the BRP crude hydroalcoholic extract and isolated compounds in an in vivo system, the technique for determining the lowest concentration capable of killing 50% (LC<sub>50</sub>) of the larvae in relation to the incubation time was employed. Figure 8 shows the toxicity evaluation of the BRP crude hydroalcoholic extract, oblongifolin B, and guttiferone E as a function of time and concentration. The LC<sub>50</sub> of the BRP crude hydroalcoholic extract and oblongifolin B was 1500 µg/mL, determined on the second day of incubation (Fig. 8A and B). On the other hand, guttiferone E had LC<sub>50</sub> of 750 µg/mL, determined on the last day of incubation (Fig. 8C).

## Discussion

For years, propolis has been used to treat infections in folk medicine, and its antimicrobial potential has been demonstrated by the scientific community<sup>15</sup>. This biological potential can be related to its differentiated chemical composition.

Sesquiterpenes, pterocarpan, and isoflavans characterize Brazilian red propolis. Red propolis chemical composition is much different from other propolis types, such as brown propolis, which is characterized by hydrocarbons, aldehydes, and monoterpenes; and green propolis, which is characterized by polycyclic aromatic hydrocarbons, sesquiterpenes, and naphthalene derivatives<sup>31</sup>.

Vestitol, neovestitol, and medicarpin have been reported as major compounds in red propolis from Canavieiras, Bahia State, Brazil. On the other hand, formononetin, calycosin, biochanin A, and isoliquiritigenin were detected at lower concentrations<sup>17</sup>. Guttiferone E and oblongifolin B were described as chemical markers of red propolis<sup>14</sup>, but they appear to be at lower concentrations in the studied sample compared to the isoflavans. The triterpenes β-amyrin and glutinol have also been described in BRP from this location<sup>14</sup>.

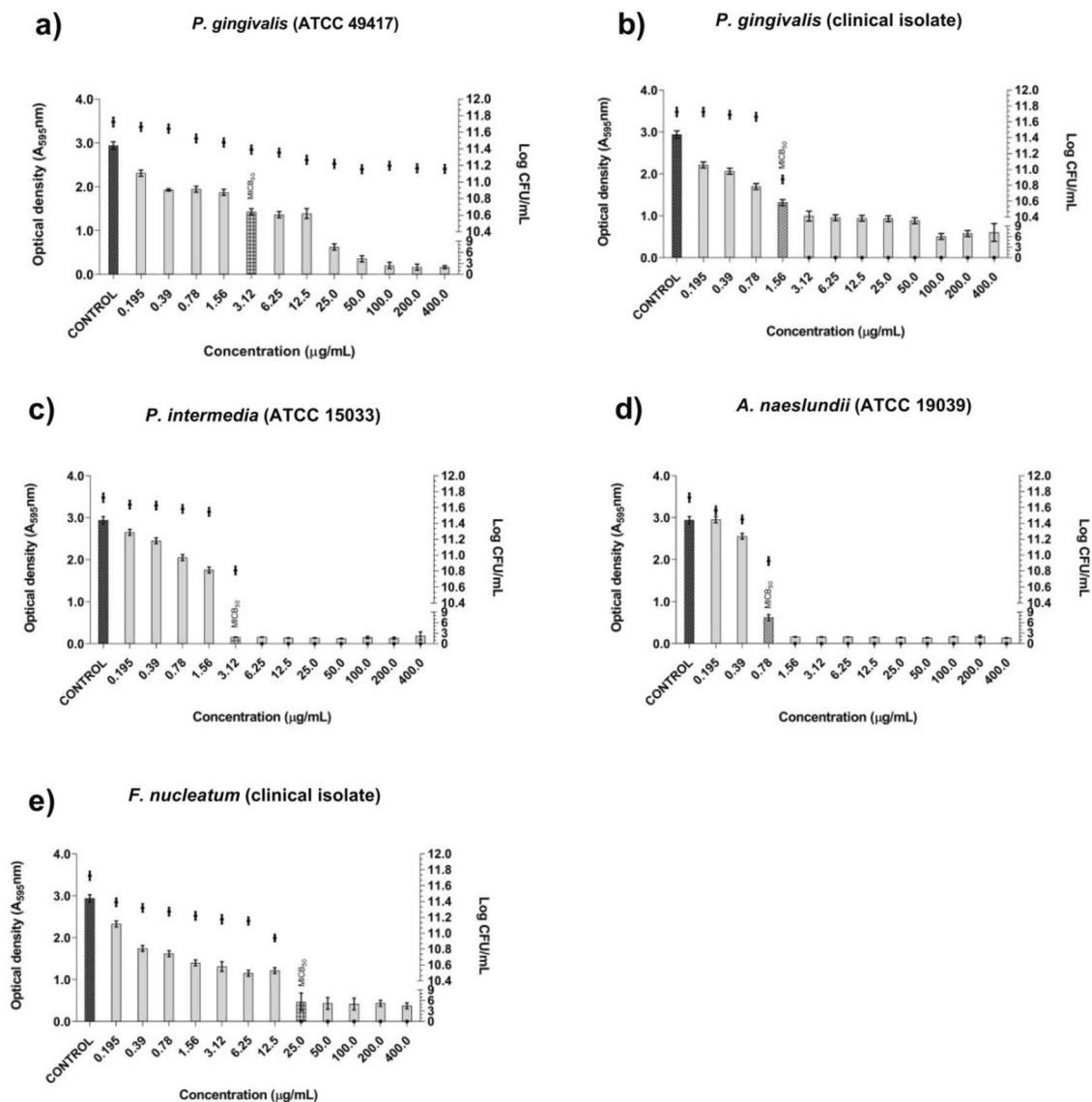


**Figure 4.** Antibiofilm activity of guttiferone E and number of viable cells in monospecies biofilms formed by ATCC strains and clinical isolates included in the study. (a) *P. gingivalis* (ATCC 49417). (b) *P. gingivalis* (clinical isolate). (c) *P. intermedia* (ATCC 15033). (d) *A. naeslundii* (ATCC 19039). (e) *F. nucleatum* (clinical isolate).

According to Rios and Recio<sup>32</sup> and Gibbons<sup>33</sup>, MIC values below 100  $\mu\text{g/mL}$  for crude hydroalcoholic extract or below 10  $\mu\text{g/mL}$  for isolated compounds are considered promising when evaluating the antibacterial activity of plant extracts, essential oils, and compounds isolated from natural sources. On the basis of these criteria and considering the MIC values presented here for all the evaluated BRP samples, the BRP crude hydroalcoholic extract and the isolated compounds guttiferone E and oblongifolin B displayed the best inhibition activity against most of the evaluated bacteria.

The red propolis dichloromethane fraction was not tested since the selection was based on the effect of the individual constituents of each fraction. The main compounds of hexane fraction, oblongifolin B and guttiferone E, displayed good activity at the individual testing, compared with the dichloromethane fraction individual compounds.

These samples showed antibacterial activity mainly against *P. gingivalis* (ATCC 49417), considered the most clinically important species in the development of periodontal disease<sup>34</sup> and *F. nucleatum* (clinical isolate) bacteria, also considered a relevant pathogen since it worsens gingival inflammation and tooth loss<sup>35</sup>. These results demonstrated the relevance of these natural products in periodontal disease control and treatment. In this paper, the BRP crude hydroalcoholic extract, fractions (*n*-hexane, dichloromethane, ethyl acetate, and *n*-butanol), and isolated compounds (methylvestitol, medicarpin, vestitol, neovestitol, oblongifolin B, and guttiferone E) were analyzed for their antibacterial activity against clinical isolates and the ATCC strains. The ATCC strains are more stable from a genetic viewpoint and would thus represent the bacterium species, thereby enabling comparison with other investigations. The in vitro assay furnishes a reliable indication of how the microorganism responds to the target agent, and extrapolation of the results for that species or even genus should be accepted. Clinical

### Crude extract

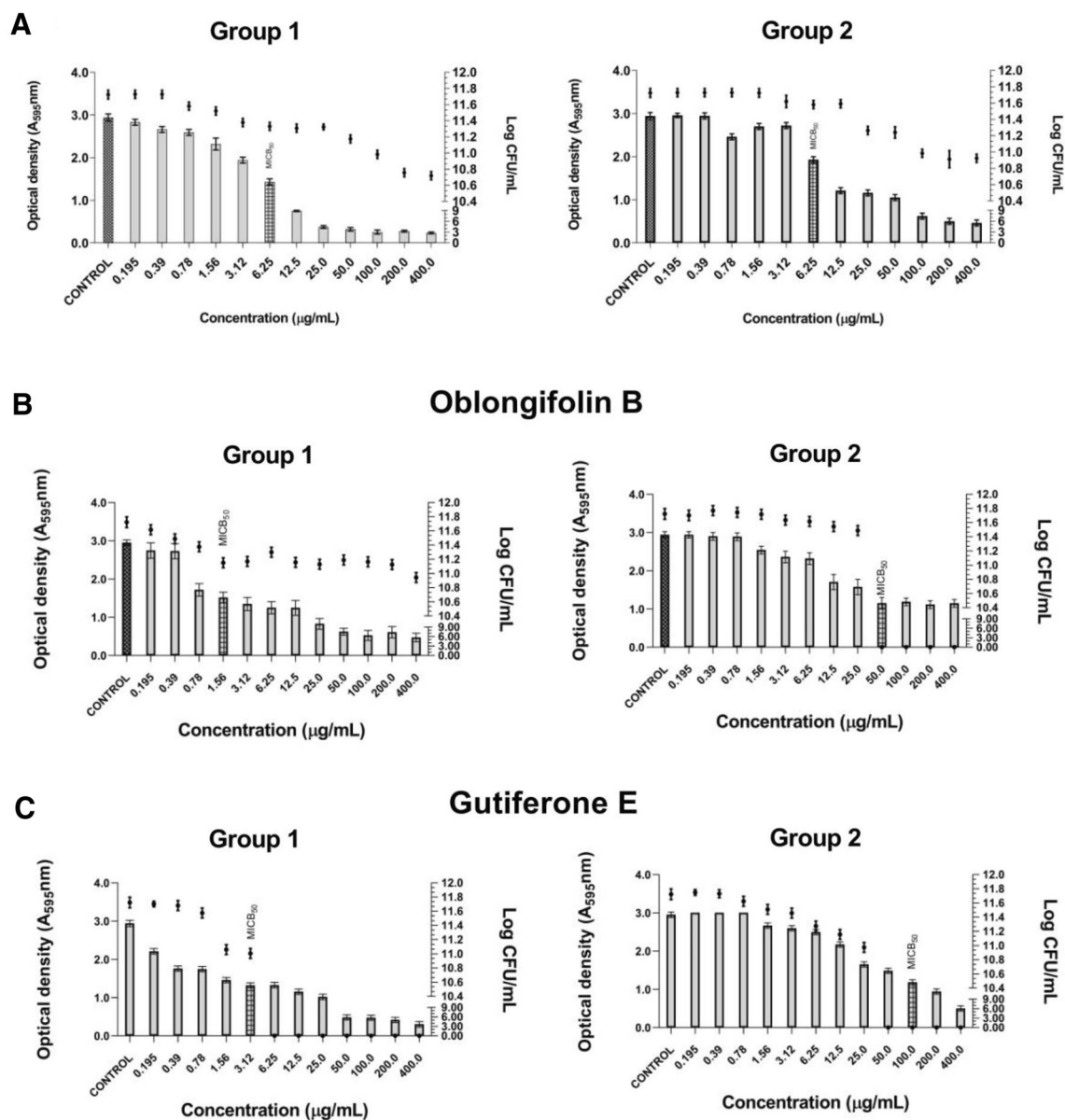


**Figure 5.** Antibiofilm activity of samples of Brazilian Red Propolis crude hydroalcoholic extract, oblongifolin B and guttiferone E and number of viable cells in multispecies biofilms formed by bacteria from groups 1 (standard strains) and 2 (clinical isolates). (A) Crude extract. (B) Oblongifolin B. (C) Guttiferone E.

Sample/concentration	50 µg/mL	10 µg/mL	2 µg/mL
Crude extract	57.3	83.2	99.3
<i>n</i> - Butanol	98.4	100.3	100.6
Dichloromethane	48.3	85.1	99.8
Hexane	45.7	83.3	100.0
Ethyl acetate	66.4	95.9	96.4

**Table 3.** Cell viability percentage in the presence of the BRP crude hydroalcoholic extract or fractions at 50, 10, and 2 µg/mL.

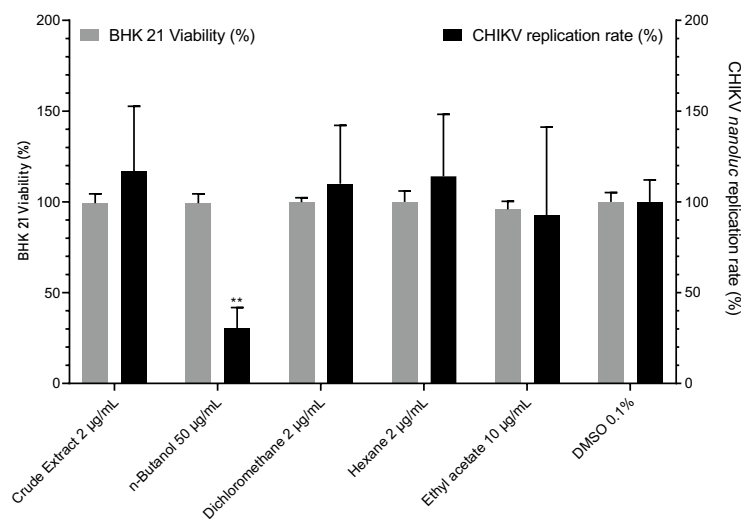


**Figure 6.** Cell viability and CHIKV replication rates in the presence of Brazilian Red Propolis crude hydroalcoholic extract and fractions.

Sample	Concentration (µg/mL)	Cell viability (%)
Medicarpin	14	84
	3	122
	0.5	113
Neovestitol	14	66
	3	110
	0.5	120
Vestitol	14	74
	3	117
	0.5	125
Oblongifolin B	32	72
	6	98
	1	99
Methylvestitol	14	108
	3	103
	0.5	103
Guttiferone E	32	15
	6	88
	1	90

**Table 4.** BHK-21 cell viability in the presence of the BRP isolated substances at concentrations ranging from 32 to 0.5 µg/mL.

isolates (also known as wild strains) are bacteria that can have their metabolism altered by environmental conditions and their genetics modified by circulation in the population, which would justify the relevance of evaluating these two types of strains.

The MIC values (1.56–400 µg/mL) for the other evaluated bacteria were significantly lower as compared to literature data. Bueno-Silva et al.<sup>29</sup> evaluated the antibacterial activity of the crude extract and isolated compounds neovestitol and vestitol obtained from BRP from the same botanical origin against *A. naeslundii* (ATCC 12104), and they reported MIC values of 25, 25, and 50 µg/mL, respectively. Here, neovestitol and vestitol were not promising against several of the evaluated periodontal bacteria. Another point to emphasize is that the MIC value for the crude extract reported by Bueno-Silva et al.<sup>29</sup> against *A. naeslundii* (ATCC 12104) resembled the value we obtained against *A. naeslundii* (ATCC 19039), suggesting a species susceptibility relation for the crude extract.

Santos et al.<sup>36</sup> evaluated the antibacterial activity of the aqueous hydroalcoholic extract and fractions (hexane, dichloromethane, and ethyl acetate) obtained from a different type of propolis, from the region of “Cachoeira da Prata”, Minas Gerais—Brazil, which is also collected from *Apis mellifera* bees. The tested bacteria were periodontal *F. nucleatum* (ATCC 10953), *P. gingivalis* (ATCC 33277), and *P. intermedia* (ATCC 25611). The extract gave MIC values of 1024, 256, and 256 µg/mL against *F. nucleatum* (ATCC 10953), *P. gingivalis* (ATCC 33277), and *P.*



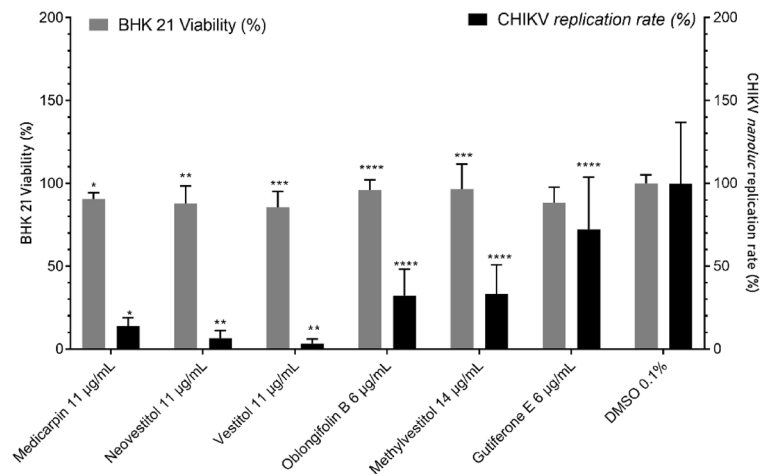


**Figure 7.** Effects of isolated compounds at on CHIKV infection and cell viability.

*intermedia* (ATCC 25611), respectively. As for the fractions, the MIC values ranged from 512 to > 1024 µg/mL. The MIC results against these bacteria were higher than those presented here for the BRP crude hydroalcoholic extract and fractions against the same bacterial species but from different strains: we found MIC values of 100, 3.12, and 6.25 µg/mL for the crude extract against *F. nucleatum* (ATCC 10953), *P. gingivalis* (ATCC 49417), and *P. intermedia* (ATCC 15033), respectively. As for the fractions, we found MIC values ranging from 12 to 400 µg/mL against the same bacteria. Therefore, compared to the results described by these authors, the BRP crude hydroalcoholic extract and fractions employed here were more effective against periodontal bacteria.

Additionally, these authors compared the MIC results they obtained with the crude extract and fractions by ANOVA analysis. They did not find any differences in the antibacterial activity of the fractions or extract against the evaluated bacteria. This corroborates our results: the BRP crude hydroalcoholic extract was more promising than the fractions and gave better values against all the evaluated bacteria, while the fractions presented antibacterial activity against only two bacteria (*P. gingivalis* ATCC 49417 and clinical isolate).

Shabbir et al.<sup>37</sup> evaluated the activity of the crude propolis extract collected in Skardu (Pakistan) originating from *Robinia pseudoacacia*, *Elegnus agustifolia* (Russian olive), and *Acacia modesta*, collected from *Apis mellifera* bees. The natural products afforded MIC values ranging from 64 to 512 µg/mL against *P. gingivalis* and *P. intermedia* clinical isolates. Our results suggested that BRP is more effective than the propolis used by Shabbir et al.<sup>37</sup> since the MIC values we obtained for the BRP crude hydroalcoholic extract against *P. gingivalis* and *P. intermedia* clinical isolates were lower (12.5 and 6.25 µg/mL, respectively). Therefore, BRP proved to have more promising activity than propolis from other countries given that it is composed of unique compounds that do not normally occur in other types of propolis<sup>15</sup>.

Inhibiting biofilm formation by these bacteria can contribute to reducing periodontitis. Indeed, Al-Ahmad et al.<sup>38</sup> described that *A. naeslundii* and *F. nucleatum* play the roles of initial colonizing bacterium and late colonizer, respectively. The latter bacterium was shown to be present at rates greater than 50% after 62 h of biofilm formation, contributing to increased inflammation and tooth loss<sup>38</sup>.

Other studies have evaluated the BRP monospecies antibiofilm activity against other types of bacteria. de Souza Silva et al.<sup>39</sup> evaluated the antibiofilm activity of the BRP crude hydroalcoholic extract (BRP collected in the same region as the BRP used in our study) coated on polymeric nanoparticles against *Staphylococcus aureus* (ATCC 25923), *Staphylococcus aureus* (ATCC 33591), *Staphylococcus aureus* (ATCC 43300), and *Pseudomonas aeruginosa* (ATCC 27853). The free BRP crude hydroalcoholic extract and the extract coated on nanoparticles inhibited the biofilm formed by the Gram-positive strains more effectively as compared to the biofilm formed by the Gram-negative strains, with biofilm inhibitory concentration values ranging from 15.6 to 125 µg/mL against the *S. aureus* strains and from 100 to 1560 µg/mL against the *P. aeruginosa* strain. These results corroborated our findings given that we verified the lowest MIC<sub>50</sub> values against the Gram-positive bacterium *A. naeslundii* (ATCC 19039) 3.12 µg/mL for the crude extract and 0.78 µg/mL for the isolated compounds oblongifolin B and guttiferone E.

Miranda et al.<sup>13</sup> evaluated the antibiofilm activity of the crude hydroalcoholic extract of BRP from the same botanical origin as the BRP used here. These authors divided the evaluated bacteria into complexes (*Actinomyces*, purple, yellow, green, orange, red, and others). At extract concentrations of 800 and 1,600 µg/mL, the authors showed a 40 and 45% decrease in the metabolic activity of the multispecies biofilms formed by these complexes, respectively. de Figueiredo et al.<sup>30</sup> also evaluated the antibiofilm activity of the BRP crude extract at 1600, 800, and 400 µg/mL and obtained 56, 56, and 57% reduction in the biofilm metabolic activity, respectively. Our study did not assess eradication, but it evaluated the ability of the BRP samples to inhibit biofilm formation. According to Wei et al.<sup>40</sup> inhibiting biofilm formation is much more important than eradicating it because biofilm formation inhibition prevents bacterial growth and, hence, bacterial maturation. The results presented here demonstrated that the BRP samples inhibited multispecies biofilm formation by periodontal bacteria by at least 50%. Oblongifolin B gave the lowest MIC<sub>50</sub> value (1.56 µg/mL) against the multispecies biofilm formed by the ATCC strains.

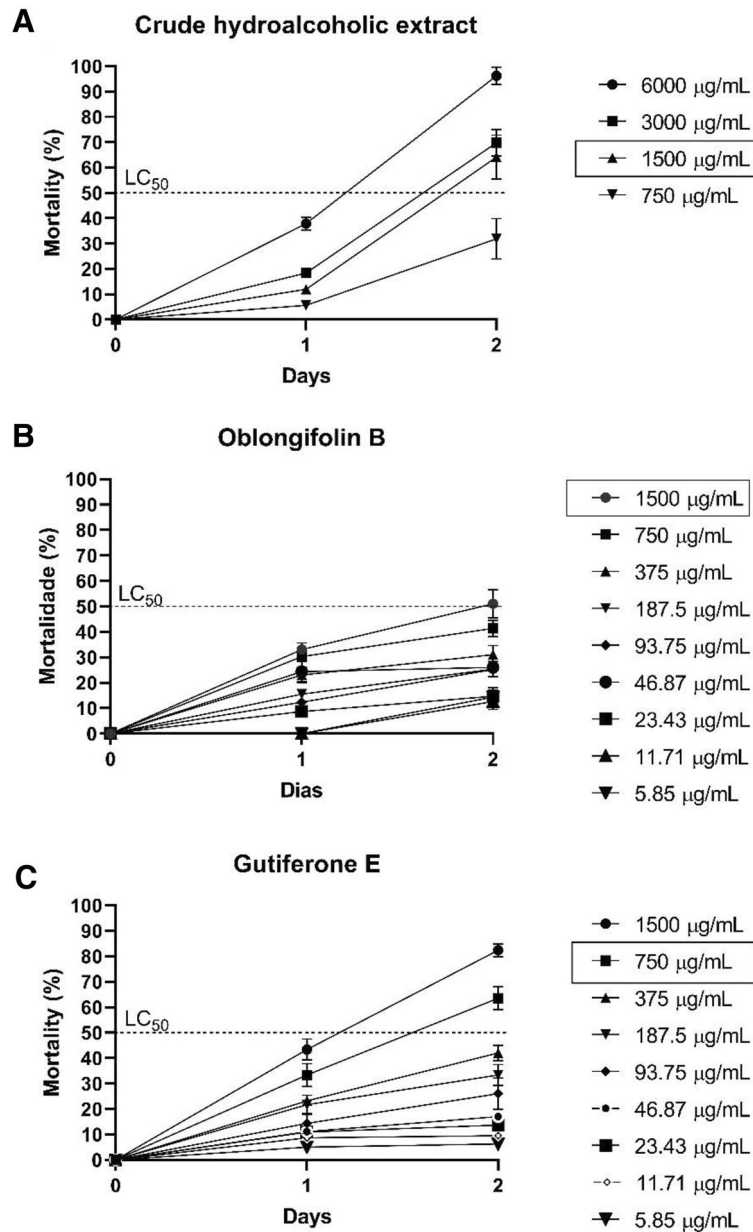


**Figure 8.** Evaluation of the toxicity of the Brazilian Red Propolis crude hydroalcoholic extract and isolated compounds guttiferone E and oblongifolin B in the *C. elegans* in vivo model. (A) Crude hydroalcoholic extract. (B) Oblongifolin B. (C) Guttiferone E.

As for the multispecies biofilm formed by the clinical isolates, the lowest MIC<sub>50</sub> value was 6.25  $\mu\text{g/mL}$ . These results suggested that the isolated compounds oblongifolin B and guttiferone E inhibited all the viable cells of most monospecies and multispecies biofilms formed by the bacteria included in this study. This pointed out that the BRP samples can inhibit biofilm formation and reach the cells within this bacterial community, eliminating them and leaving only the glycoprotein conjugate without live cells<sup>13</sup>.

It is worth mentioning that the MIC<sub>50</sub> values found in this paper are relatively low, especially for clinical isolates that are generally more resistant and demand higher concentrations. However, at the lowest concentration capable of inhibiting biofilm formation by at least 50%, the so-called MIC<sub>50</sub>, we demonstrated an inhibition of at least 50% of the biofilm. In other words, this did not correspond to total inhibition of the biofilm, which would probably require a higher concentration.

Propolis bioactive components such as flavonoids, esters, alcohols, essential oils, and other organic compounds have already been demonstrated to display antiviral activity against viruses such as herpes viruses (HSV-1 and HSV-2), sindbis virus, parainfluenza virus, cytomegalovirus, HIV, and *Varicella zoster* (HSV-1 and HSV-2), sindbis virus, parainfluenza virus, cytomegalovirus, HIV, and *Varicella zoster*<sup>41,42</sup>. In addition to the BRP antibacterial and antibiofilm activities demonstrated in this study, we evaluated the anti-CHIKV activity of the

BRP crude hydroalcoholic extract, fractions, and pure substances. We assessed the BHK-21 cell viability in the presence of the BRP samples by the MTT assay. In drug discovery, samples are considered non-toxic when the cell viability rate is above 50%, moderately cytotoxic when the cell viability rate varies between 25 and 50%, and highly cytotoxic when the cell viability rate is less than 25%<sup>43</sup>. In this study, all samples evaluated showed cell viability equal to or higher than 80% at a concentration of 50 µg/mL for the crude extract and fractions and 3 µg/mL for isolated compounds (Tables 3 and 4). All the BRP samples evaluated in this study provided BHK-21 cell viability equal to or higher than 80% (Tables 3 and 4), which was higher than the cell viability found by Rufatto et al.<sup>20</sup>, (between 14.5 and 46%).

Regarding the infection assays, the isolated compounds neovestitol and vestitol furnished the most promising results, with virus infection inhibition rates of 94 and 97%, respectively (Fig. 7). Even though several natural compounds with antiviral activity, including anti-CHIKV activity, have been described, neovestitol and vestitol have not had their antiviral potential screened. Our results showed higher inhibition rates than those reported in other studies with natural molecules, such as the study of Pohjala et al.<sup>44</sup>, who obtained an infection inhibition limit of at most 75% when they screened 356 compounds, being 123 of them natural compounds. To the best of our knowledge, there are no reports on the anti-CHIKV activity of BRP or isolated compounds. This shows the importance of capitalizing the BRP potential as candidate for antiviral treatment. Our study has pioneered evaluation of the BRP anti-CHIKV activity and has achieved expressive inhibition rates, paving the way for the development of antivirals against CHIKV as well as other viruses.

For BRP to be safely applicable, its toxicity must be evaluated in different experimental models. The murine model is the most used in vivo model to assess the toxicity of treatments, but it has disadvantages such as high cost, difficult maintenance, and delay in obtaining results, among others<sup>45</sup>. Therefore, here we evaluated toxicity by using another in vivo model, the nematode *C. elegans*, a complete animal with digestive, reproductive, endocrine, and neuromuscular systems. Apart from being small, having a short life cycle, and being easy to maintain, *C. elegans* possesses 60–80% genetic homology with humans<sup>46</sup>. In this context, we evaluated the most promising BRP samples for their toxicity against *C. elegans*. The lowest concentration capable of killing at least 50% of the larvae (LC<sub>50</sub>) was 1500 µg/mL for the BRP crude hydroalcoholic extract and oblongifolin B and 750 µg/mL for guttiferone E. These values were significantly higher than all the MIC and MICB<sub>50</sub> concentrations reported in this study.

Moreover, below this concentration, even after the larvae had been exposed to BRP samples for two days, LC<sub>50</sub> was not reached, demonstrating the non-toxic profile of these natural products. Interestingly, the LC<sub>50</sub> values of the BRP samples against *C. elegans* obtained in this study were higher than the LC<sub>50</sub> values of other types of Brazilian propolis evaluated against *C. elegans*. For example, Campos and collaborators (2015)<sup>47</sup> reported that propolis samples possessed LC<sub>50</sub> of 461.8 µg/mL. Here, the BRP concentrations determined as toxic were high, above the highest MIC value (400 µg/mL). Therefore, propolis is not toxic at the concentrations used in this study and can be safely employed at concentrations below 1500 and 750 µg/mL. The results obtained here are extremely relevant, because through different methodologies the antibacterial activity of Brazilian red propolis was demonstrated against a panel of periodontopathogenic bacteria. Another point to highlight is the anti-CHIKV activity of the BRP isolated compounds. *Chikungunya* infection has a high incidence and severity, therefore, the search for new treatment options is highly desirable. Our results constitute an initial step for further studies of BRP as an alternative approach for treating various infectious diseases.

## Conclusion

The Brazilian red propolis used in this study has antibacterial activity against a panel of periodontopathogenic bacteria. Furthermore, its crude extract and isolated compounds oblongifolin B and guttiferone E at concentrations similar to or slightly above the MIC concentrations inhibits monospecies and multispecies biofilms by over 50%. Medicarpin, neovestitol, and vestitol strongly inhibit CHIKV infection in vitro. Besides, toxicity tests on *C. elegans* demonstrated that the crude extract, oblongifolin B, and guttiferone E are non-toxic, proving to be safe and promising so that in the future, these samples of propolis can be used as medicine.

## Methods

**Crude hydroalcoholic extract, fractions, and isolated compounds.** BRP was collected in Canavieiras Bahia State, Brazil, in March 2019 at the Canavieiras Beekeepers Association (COAPER). BRP was frozen and extracted with 70% hydroalcoholic ethanol solution, as described by Santiago et al.<sup>48</sup>. The BRP crude hydroalcoholic extract was partitioned with organic solvents (hexane, dichloromethane, ethyl acetate, and *n*-butanol). Authentic standards from BRP (7-*O*-methylvestitol, medicarpin, vestitol, neovestitol, oblongifolin B, and guttiferone E) previously isolated by our research group were used to characterize the samples<sup>17</sup>.

Chromatographic analysis of BRP extract and its fractions were performed on a Waters 2695 HPLC instrument, coupled to a 2998 photodiode array detector (PDA), with Empower 3 software as a controller. Chromatographic profiles were carried out on a Supelco Ascentis Express C-18 (150 × 4.6 mm, 2.7 µm) column. Mobile phase with water (A) (0.1% formic acid) and acetonitrile (B) was used as follows: 10 → 100% of B until 80 min; 100% of B in 89 min; 100 → 10% in 90 min, maintaining the condition until 95 min. The injections were performed on a flow rate of 1 mL/min, a 40 °C, and an injection volume of 10 µL. Chromatograms were recorded at 275 nm.

For the antibacterial, antiviral, and toxicity assays were used the crude hydroalcoholic extract of BRP, fractions in dichloromethane, hexane, ethyl acetate, *n*-butanol, as well as the isolated compounds guttiferone E, oblongifolin B, methylvestitol, medicarpin, vestitol, and neovestitol.

**Bacterial strains, *Chikungunya* virus and animal model employed in the study.** The periodontopathogenic bacterial strains employed in the antibacterial and antibiofilm activity assays were obtained from the *American Type Culture Collection* (ATCC); their respective clinical isolates were obtained from human periodontal infections. The strains included *Porphyromonas gingivalis* (ATCC 49417 and clinical isolate), *Fusobacterium nucleatum* (ATCC 10953 and clinical isolate), *Prevotella intermedia* (ATCC 15033 and clinical isolate), and *Actinomyces naeslundii* (ATCC 19039 and clinical isolate). These bacteria are part of the collection of the Antimicrobial Assays Laboratory (LEA, abbreviation in Portuguese) of the Federal University of Uberlândia (UFU) and were cryopreserved at  $-20\text{ }^{\circ}\text{C}$ . For the in vivo toxicity assays, the mutant strain *Caenorhabditis elegans* AU37, obtained from the Genetics Center (CGC, University of Minnesota), was used.

For the antiviral assays, a CHIKV expressing the *Nanoluciferase* reporter (CHIKV-*nanoluc*) based on the CHIKV LR2006PYY1 strain (East/Central/South African genotype) was rescued<sup>49</sup>. The protocols were carried out as described previously<sup>50</sup>.

**Determination of the minimum inhibitory concentration<sup>51</sup>.** The antibacterial activity of the BRP crude hydroalcoholic extract, fractions, and isolated compounds were evaluated by the broth microdilution method, in triplicate. The assays were conducted in 96-well microplates; the methodology recommended by the Clinical and Laboratory Standards Institute<sup>52</sup>, with modifications, was followed. The inoculum was standardized to the McFarland 0.5 scale and diluted to a bacterial concentration of  $1.5 \times 10^6$  CFU/mL in the wells. To prepare the samples, the BRP crude hydroalcoholic extract, fractions, or isolated compounds were solubilized in 5% dimethyl sulfoxide (DMSO) and diluted in Brucella broth supplemented with hemin (5.0 mg/mL) and menadione (1.0 mg/mL); a twofold serial dilution with concentrations ranging from 0.195 to 400  $\mu\text{g/mL}$  was used. Control of 5% DMSO was performed, and the solvent did not interfere with bacterial growth at this concentration. It was also performed the following controls: inoculum (all the bacteria used in the test + the culture medium), to observe the viability of the bacteria; broth, to guarantee that the culture medium is sterile; and BRP sample, to guarantee that this solution is sterile. The microplates were incubated in an anaerobic chamber (Don Whitley Scientific, Bradford, U.K.) under anaerobic conditions (80%  $\text{N}_2$ , 10%  $\text{CO}_2$ , and 10%  $\text{H}_2$ ) at  $37\text{ }^{\circ}\text{C}$  for 72 h. Resazurin was used to reveal bacterial growth—the blue color indicated absence of bacterial growth, and the pink color indicated presence of bacteria<sup>53</sup>. As a control technique, metronidazole from 0.0115 to 5.9  $\mu\text{g/mL}$  was used against the control bacteria *Bacteroides fragilis* (ATCC 25285) and *Bacteroides thetaiotaomicron* (ATCC 29741)<sup>52</sup>.

**Evaluation of antibiofilm activity monospecies and multispecies by Minimum Inhibitory Concentration of Biofilm (MICB<sub>50</sub>).** To assess the antibiofilm activity, the BRP samples that presented the most promising MIC results against four or more bacteria were submitted to the Minimum Inhibitory Concentration of Biofilm (MICB<sub>50</sub>) assay. MICB<sub>50</sub> is defined as the lowest concentration of the microbial agent that can inhibit biofilm formation by at least 50%<sup>40</sup> and is calculated using the following equation:

$$1 - \frac{(\text{Absorbance (595nm) of the well containing the treated sample})}{\text{Absorbance (595nm) of the untreated control well}} \times 100$$

Here, MICB<sub>50</sub> was determined as described in the CLSI guidelines (2007)<sup>52</sup>, with modifications. First, the capacity of the analyzed strains to grow in the sessile mode was verified. All the strains at  $1.5 \times 10^6$  CFU/mL formed monospecies and multispecies biofilms after incubation at  $37\text{ }^{\circ}\text{C}$  for 72 h (data not shown).

For the monospecies biofilms, 100  $\mu\text{L}$  of each bacterium inoculum at  $1.5 \times 10^6$  CFU/mL was added to the well with the propolis samples to be evaluated at concentrations from 0.195 to 400  $\mu\text{g/mL}$  (crude hydroalcoholic extract, oblongifolin B and guttiferone E). The microplates were incubated in an anaerobic chamber at  $37\text{ }^{\circ}\text{C}$  for 72 h. For the multispecies biofilms, the main periodontopathogenic bacteria found in the oral biofilm were selected and divided into two groups: group 1 consisted only of the standard bacteria (*P. gingivalis* ATCC 49417, *P. intermedia* ATCC 15033, and *A. naeslundii* ATCC 19039), while group 2 was composed only by the *P. gingivalis*, *P. intermedia*, and *F. nucleatum* clinical isolates. The antibiofilm activity of the most promising BRP samples was evaluated against the multispecies biofilm formed by group 1 bacteria and against the multispecies biofilm composed by group 2 bacteria. For this purpose, 33.33  $\mu\text{L}$  of each evaluated bacterium, totaling 100  $\mu\text{L}$  of bacterial inoculum, at  $1.5 \times 10^6$  CFU/mL was added to the wells with the propolis samples to be evaluated at concentrations from 0.195 to 400  $\mu\text{g/mL}$  (crude hydroalcoholic extract, oblongifolin B and guttiferone E). The microplates were incubated under the same conditions as the monospecies biofilm microplates. The standard antibiotic metronidazole was used as a control at concentrations from 0.0115 to 5.9  $\mu\text{g/mL}$  with MIC<sub>50</sub> (see supplementary material, Figures S2 and S3). Control of 5% DMSO was performed, and the solvent did not interfere with bacterial growth at this concentration. It was also performed the following controls: inoculum (all the bacteria used in the test + the culture medium), to observe the viability of the bacteria; broth, to guarantee that the culture medium is sterile; and BRP sample, to guarantee that this solution is sterile. After incubation, the supernatant culture was withdrawn, and the planktonic cells were removed by washing the wells with ultrapure distilled water. Monospecies and multispecies biofilms were fixed with methanol and stained with 2% crystal violet<sup>54</sup>. The reading was performed in a microplate reader (GloMax<sup>®</sup>) at 595 nm. Reading was performed in a microplate reader (GloMax<sup>®</sup>) at 595 nm. The experiments were carried out in triplicate and independent events.

**Evaluation of the inhibition of biofilm formation by counting microorganism.** This assay was performed for monospecies and multispecies biofilms according to de Souza Silva et al.<sup>39</sup>, as described below. Two microplates were incubated, one for MICB<sub>50</sub> determination, and the other for microorganism count. After the microorganism count microplate was incubated, the supernatant was withdrawn, and the planktonic cells

were removed by washing the wells with ultrapure distilled water. Subsequently, supplemented Brucella broth was added to all the microplate wells, and the biofilm was detached from the well after an ultrasound bath. Then, tenfold serial dilutions were performed in each well of a 96-well microplate, and 50  $\mu\text{L}$  of each well, corresponding to each dilution available was placed on two plates of Brucella agar supplemented with horse blood (5%), hemin (5.0 mg/mL), and menadione (1.0 mg/mL). Each of the plates were fractionated into eight parts, as described by Harrison et al.<sup>55</sup> and incubated in an anaerobic chamber for 37 °C. After 72 h, the Colony Forming Units (CFU) count was performed in each plate. The results were expressed as  $\text{Log}_{10}$  (CFU/mL), and the assays were independently performed in triplicate.

**Mammalian cells for antiviral assays.** The BHK-21 cells (fibroblasts derived from Syrian golden hamster kidney; ATCC CCL-10) were maintained in Dulbecco's modified Eagle's medium (DMEM, Sigma-Aldrich) supplemented with 100 U/mL penicillin (Hyclone Laboratories), 100 mg/mL streptomycin (Hyclone Laboratories), 1% dilution of stock of non-essential amino acids (Hyclone Laboratories), and 1% fetal bovine serum (FBS, Hyclone Laboratories) in a humidified 5%  $\text{CO}_2$  incubator at 37 °C.

**Cell viability through MTT for antiviral assays.** BHK-21 cell viability in the presence of the tested BRP samples was measured by the MTT [3-(4,5-dimethylthiazol-2-yl)-2,5-diphenyl tetrazolium bromide] (Sigma-Aldrich) assay. BHK-21 cells were cultured in 48-well microplates and treated with different concentrations of the tested BRP sample at 37 °C for 16 h. Then, media containing the tested BRP sample was removed from the 48-well microplate. Next, 1 mg/mL MTT solution was added to each well, incubated for 30 min, and replaced with 300  $\mu\text{L}$  of DMSO to solubilize the formazan crystals. Absorbance was measured at 490 nm on a Glomax microplate reader (Promega). Cell viability was calculated according to the equation  $(T/C) \times 100\%$ , where T and C represent the optical density of the treated well and control groups, respectively. DMSO was used as untreated control<sup>50</sup>.

**Antiviral activity against CHIKV infection in vitro.** For initial screening of the anti-CHIKV activity of the BRP crude hydroalcoholic extract and isolated compounds, HK-21 cells were seeded at a density of  $5 \times 10^4$  cells per well in 48-well microplates 24 h before the infection. CHIKV-*nanoluc* at a multiplicity of infection<sup>56</sup> of 0.1 and the tested isolated compound or extract were simultaneously added to the cells. The cells were harvested in Renilla luciferase lysis buffer (Promega) 16 h post-infection (h.p.i.), and virus replication was quantified by measuring nanoluciferase activity with the Renilla luciferase Assay System (Promega). The CHIKV replication rates were calculated according to the equation  $(T/C) \times 100\%$ , where T and C represent the optical density of the treated well and control groups, respectively. DMSO 0.1% was used as untreated control.

**Toxicity assessment in *Caenorhabditis elegans*.** Toxicity evaluation was performed for the most promising BRP samples in the CIM, using the in vivo model of *C. elegans*, according to Andrade et al.<sup>57</sup> and Singulani et al.<sup>58</sup>. The *C. elegans* AU37 mutant strain was cultivated in Nematode Growth Medium (NGM) plates seeded with *Escherichia coli* OP50 and incubated at 16 °C for 72 h. After incubation, the NGM plates containing larvae and eggs were washed with M9 buffer, and the supernatant was placed in 15-mL conical tubes. A bleaching solution (hypochlorite + NaOH) was further added, to kill the adult larvae. The eggs were placed in NGM plates and incubated again at 15 °C for 24 h. Later, the NGM plates containing the larvae at the L1/L2 stages were washed with M9 buffer, and the supernatant was transferred to NGM plates seeded with *E. coli* OP50 and incubated at 16 °C for 24 h. After synchronization, 20  $\mu\text{L}$  of the NGM plate contents containing from 10 to 20 L4 stage larvae was added to each well of a 96-well flat-bottomed microplate and incubated at 16 °C for 72 h. The BRP crude hydroalcoholic extract was evaluated from 750 to 6000  $\mu\text{g}/\text{mL}$ , and the isolated compounds oblongifolin B and guttiferone E were evaluated from 5.85 to 1500  $\mu\text{g}/\text{mL}$ . DMSO was used as solvent (final concentration  $\leq 1\%$ ).

Larvae were counted every 24 h for three consecutive days under an inverted microscope. Larvae with movement were considered alive and static even after touching they were considered dead. For each sample, the lowest concentration that was able to kill 50% of the larvae, called Lethal Concentration ( $\text{LC}_{50}$ ), was determined according to time.

**Statistical analysis.** Individual experiments were performed in triplicate, and all the assays were performed a minimum of three times to confirm the reproducibility of the results. Differences between the means of the readings were compared by analysis of variance (one-way or two-way ANOVA) or Student's t-test conducted with the software Graph Pad Prism 8.0 (Graph Pad Software). The *p* values  $\leq$  than 0.05 were considered statistically significant.

### Data availability

All data generated or analysed during this study are included in this published article (and its Supplementary Information files).

Received: 22 August 2022; Accepted: 21 November 2022

Published online: 07 December 2022

### References

1. Ellwanger, J. H. et al. Beyond diversity loss and climate change: Impacts of Amazon deforestation on infectious diseases and public health. *An. Acad. Bras. Cienc.* **92**, e20191375. <https://doi.org/10.1590/0001-3765202020191375> (2020).

2. Papapanou, P. N. *et al.* Periodontitis: Consensus report of workgroup 2 of the 2017 World Workshop on the Classification of Periodontal and Peri-Implant Diseases and Conditions. *J. Clin. Periodontol.* **45**(Suppl 20), S162–S170. <https://doi.org/10.1111/jcpe.12946> (2018).
3. Mehrotra, N. & Singh, S. *Periodontitis* (StatPearls Publishing, 2020).
4. Slots, J. Periodontitis: Facts, fallacies and the future. *Periodontol.* **2000** **75**, 7–23. <https://doi.org/10.1111/prd.12221> (2017).
5. Cooley, L. & Teng, J. Anaerobic resistance: Should we be worried?. *Curr. Opin. Infect. Dis.* **32**, 523–530. <https://doi.org/10.1097/QCO.0000000000000595> (2019).
6. Silva, L. A. & Dermody, T. S. Chikungunya virus: Epidemiology, replication, disease mechanisms, and prospective intervention strategies. *J. Clin. Invest.* **127**, 737–749. <https://doi.org/10.1172/JCI84417> (2017).
7. Reilly, J. M. *et al.* Postmortem chikungunya diagnosis: A case report and literature review. *Am. J. Forensic Med. Pathol.* **41**, 48–51. <https://doi.org/10.1097/PAF.0000000000000519> (2020).
8. Vairo, F. *et al.* Chikungunya: Epidemiology, pathogenesis, clinical features, management, and prevention. *Infect. Dis. Clin. North Am.* **33**, 1003–1025. <https://doi.org/10.1016/j.idc.2019.08.006> (2019).
9. Department, H. S. Vol. 53 (ed Ministry of Health) (2022).
10. WHO. (World Health Organization, 2018).
11. Valli, M. *et al.* Development of a natural products database from the biodiversity of Brazil. *J. Nat. Prod.* **76**, 439–444. <https://doi.org/10.1021/np3006875> (2013).
12. Batista, L. L. *et al.* Comparative study of topical green and red propolis in the repair of wounds induced in rats. *Rev. Col. Bras. Cir.* **39**, 515–520. <https://doi.org/10.1590/s0100-69912012000600012> (2012).
13. Miranda, S. L. F. *et al.* Brazilian red propolis reduces orange-complex periodontopathogens growing in multispecies biofilms. *Biofouling* **35**, 308–319. <https://doi.org/10.1080/08927014.2019.1598976> (2019).
14. Ccana-Capatinta, G. V. *et al.* *Dalbergia ecastaphyllum* (L.) Taub. and *Symphonia globulifera* L.f.: The botanical sources of Isoflavonoids and Benzophenones in Brazilian Red Propolis. *Molecules* <https://doi.org/10.3390/molecules25092060> (2020).
15. Reis, J. H. O. *et al.* Evaluation of the antioxidant profile and cytotoxic activity of red propolis extracts from different regions of northeastern Brazil obtained by conventional and ultrasound-assisted extraction. *PLoS ONE* **14**, e0219063. <https://doi.org/10.1371/journal.pone.0219063> (2019).
16. Boeing, T. *et al.* The gastroprotective effect of red propolis extract from Northeastern Brazil and the role of its isolated compounds. *J. Ethnopharmacol.* **267**, 113623. <https://doi.org/10.1016/j.jep.2020.113623> (2021).
17. Aldana-Mejia, J. A. *et al.* A validated HPLC-UV method for the analysis of phenolic compounds in Brazilian red propolis and *Dalbergia ecastaphyllum*. *J. Pharm. Biomed. Anal.* **198**, 114029. <https://doi.org/10.1016/j.jpba.2021.114029> (2021).
18. Bueno-Silva, B., Marsola, A., Ikegaki, M., Alencar, S. M. & Rosalen, P. L. The effect of seasons on Brazilian red propolis and its botanical source: Chemical composition and antibacterial activity. *Nat. Prod. Res.* **31**, 1318–1324. <https://doi.org/10.1080/14786419.2016.1239088> (2017).
19. Freires, I. A., de Alencar, S. M. & Rosalen, P. L. A pharmacological perspective on the use of Brazilian Red Propolis and its isolated compounds against human diseases. *Eur. J. Med. Chem.* **110**, 267–279. <https://doi.org/10.1016/j.ejmech.2016.01.033> (2016).
20. Rufatto, L. C. *et al.* Brazilian red propolis: Chemical composition and antibacterial activity determined using bioguided fractionation. *Microbiol. Res.* **214**, 74–82. <https://doi.org/10.1016/j.micres.2018.05.003> (2018).
21. Ayres, D. C., Marcucci, M. C. & Giorgio, S. Effects of Brazilian propolis on *Leishmania amazonensis*. *Mem. Inst. Oswaldo Cruz* **102**, 215–220. <https://doi.org/10.1590/s0074-02762007005000020> (2007).
22. Dantas Silva, R. P. *et al.* Antioxidant, antimicrobial, antiparasitic, and cytotoxic properties of various Brazilian propolis extracts. *PLoS ONE* **12**, e0172585. <https://doi.org/10.1371/journal.pone.0172585> (2017).
23. do Nascimento, T. G. *et al.* Comprehensive multivariate correlations between climatic effect, metabolite-profile, antioxidant capacity and antibacterial activity of Brazilian red propolis metabolites during seasonal study. *Sci. Rep.* **9**, 18293. <https://doi.org/10.1038/s41598-019-54591-3> (2019).
24. Morsy, A. S. *et al.* Effect of Brazilian red propolis administration on hematological, biochemical variables and parasitic response of Santa Ines ewes during and after flushing period. *Trop. Anim. Health Prod.* **45**, 1609–1618. <https://doi.org/10.1007/s11250-013-0406-3> (2013).
25. Regueira-Neto, M. D. S. *et al.* Antitrypanosomal, antileishmanial and cytotoxic activities of Brazilian red propolis and plant resin of *Dalbergia ecastaphyllum* (L.) Taub. *Food Chem. Toxicol.* **119**, 215–221. <https://doi.org/10.1016/j.fct.2018.04.029> (2018).
26. Sena-Lopes, A. *et al.* Chemical composition, immunostimulatory, cytotoxic and antiparasitic activities of the essential oil from Brazilian red propolis. *PLoS ONE* **13**, e0191797. <https://doi.org/10.1371/journal.pone.0191797> (2018).
27. Sinott, F. A. *et al.* Essential oil from Brazilian Red Propolis exhibits anthelmintic activity against larvae of *Toxocara cati*. *Exp. Parasitol.* **200**, 37–41. <https://doi.org/10.1016/j.exppara.2019.03.014> (2019).
28. Silva-Beltran, N. P., Balderrama-Carmona, A. P., Umsza-Guez, M. A. & Souza Machado, B. A. Antiviral effects of Brazilian green and red propolis extracts on Enterovirus surrogates. *Environ. Sci. Pollut. Res. Int.* **27**, 28510–28517. <https://doi.org/10.1007/s11356-019-07458-z> (2020).
29. Bueno-Silva, B. *et al.* Anti-inflammatory and antimicrobial evaluation of neovestitol and vestitol isolated from Brazilian red propolis. *J. Agric. Food Chem.* **61**, 4546–4550. <https://doi.org/10.1021/jf305468f> (2013).
30. de Figueiredo, K. A. *et al.* Brazilian Red propolis is as effective as amoxicillin in controlling red-complex of multispecies subgingival mature biofilm in vitro. *Antibiotics (Basel)* <https://doi.org/10.3390/antibiotics9080432> (2020).
31. Ribeiro, V. P. *et al.* Chemical characterization of Brazilian propolis using automated direct thermal desorption-gas chromatography-mass spectrometry. *J. Sci. Food Agric.* **102**, 4345–4354. <https://doi.org/10.1002/jsfa.11788> (2022).
32. Rios, J. L. & Recio, M. C. Medicinal plants and antimicrobial activity. *J. Ethnopharmacol.* **100**, 80–84. <https://doi.org/10.1016/j.jep.2005.04.025> (2005).
33. Gibbons, S. Phytochemicals for bacterial resistance—strengths, weaknesses and opportunities. *Planta Med.* **74**, 594–602. <https://doi.org/10.1055/s-2008-1074518> (2008).
34. Yoshimasu, Y. *et al.* Rapid bactericidal action of propolis against porphyromonas gingivalis. *J. Dent. Res.* **97**, 928–936. <https://doi.org/10.1177/0022034518758034> (2018).
35. Han, Y. W. *Fusobacterium nucleatum*: A commensal-turned pathogen. *Curr. Opin. Microbiol.* **23**, 141–147. <https://doi.org/10.1016/j.mib.2014.11.013> (2015).
36. Santos, F. A. *et al.* Antibacterial activity of Brazilian propolis and fractions against oral anaerobic bacteria. *J. Ethnopharmacol.* **80**, 1–7. [https://doi.org/10.1016/s0378-8741\(02\)00003-x](https://doi.org/10.1016/s0378-8741(02)00003-x) (2002).
37. Shabbir, A., Rashid, M. & Tipu, H. N. Propolis, a hope for the future in treating resistant periodontal pathogens. *Cureus* **8**, e682. <https://doi.org/10.7759/cureus.682> (2016).
38. Al-Ahmad, A. *et al.* The in vivo dynamics of *Streptococcus* spp., *Actinomyces naeslundii*, *Fusobacterium nucleatum* and *Veillonella* spp. in dental plaque biofilm as analysed by five-colour multiplex fluorescence in situ hybridization. *J. Med. Microbiol.* **56**, 681–687. <https://doi.org/10.1099/jmm.0.47094-0> (2007).
39. de Souza Silva, T. *et al.* Green and Red Brazilian propolis: Antimicrobial potential and anti-virulence against ATCC and clinically isolated multidrug-resistant bacteria. *Chem Biodivers* **18**, e2100307. <https://doi.org/10.1002/cbdv.202100307> (2021).
40. Wei, G. X., Campagna, A. N. & Bobek, L. A. Effect of MUC7 peptides on the growth of bacteria and on Streptococcus mutans biofilm. *J. Antimicrob. Chemother.* **57**, 1100–1109. <https://doi.org/10.1093/jac/dkl120> (2006).

41. Gonzalez-Burquez, M. J. *et al.* Comparison between in vitro antiviral effect of Mexican propolis and three commercial flavonoids against canine distemper virus. *Evid. Based Complement Alternat. Med.* **2018**, 7092416. <https://doi.org/10.1155/2018/7092416> (2018).
42. Labska, K., Plodkova, H., Pumannova, M. & Sensch, K. H. Antiviral activity of propolis special extract GH 2002 against *Varicella zoster virus* in vitro. *Pharmazie* **73**, 733–736. <https://doi.org/10.1691/ph.2018.8672> (2018).
43. de Carvalho, F. M. A. *et al.* Brazilian red propolis: Extracts production, physicochemical characterization, and cytotoxicity profile for antitumor activity. *Biomolecules* <https://doi.org/10.3390/biom10050726> (2020).
44. Pohjala, L. *et al.* Inhibitors of alphavirus entry and replication identified with a stable *Chikungunya* replicon cell line and virus-based assays. *PLoS ONE* **6**, e28923. <https://doi.org/10.1371/journal.pone.0028923> (2011).
45. Hunt, P. R. & The, C. The *C. elegans* model in toxicity testing. *J Appl Toxicol* **37**, 50–59. <https://doi.org/10.1002/jat.3357> (2017).
46. Ruszkiewicz, J. A. *et al.* *C. elegans* as a model in developmental neurotoxicology. *Toxicol. Appl. Pharmacol.* **354**, 126–135. <https://doi.org/10.1016/j.taap.2018.03.016> (2018).
47. Campos, J. F. *et al.* Antimicrobial, antioxidant, anti-inflammatory, and cytotoxic activities of propolis from the stingless bee *Tetragonisca fiebrigi* (Jatai). *Evid. Based Complement Alternat. Med.* **2015**, 296186. <https://doi.org/10.1155/2015/296186> (2015).
48. Santiago, M. B. *et al.* Brazilian red propolis presents promising anti-*H. pylori* activity in in vitro and in vivo assays with the ability to modulate the immune response. *Molecules* <https://doi.org/10.3390/molecules27217310> (2022).
49. Matkovic, R. *et al.* The host DHX9 DExH-box helicase is recruited to *Chikungunya* virus replication complexes for optimal genomic RNA translation. *J. Virol.* <https://doi.org/10.1128/JVI.01764-18> (2019).
50. de Oliveira, D. M. *et al.* Organometallic complex strongly impairs *Chikungunya* virus entry to the host cells. *Front. Microbiol.* **11**, 608924. <https://doi.org/10.3389/fmicb.2020.608924> (2020).
51. Shaughnessy, M. K. *et al.* Evaluation of hospital room assignment and acquisition of *Clostridium difficile* infection. *Infect. Control Hosp. Epidemiol.* **32**, 201–206. <https://doi.org/10.1086/658669> (2011).
52. CLSI. Vol. Approved Standard M11-A7, CLSI (Clinical and Laboratory Standards Institute Wayne, PA, 2007).
53. Sarker, S. D., Nahar, L. & Kumarasamy, Y. Microtitre plate-based antibacterial assay incorporating resazurin as an indicator of cell growth, and its application in the in vitro antibacterial screening of phytochemicals. *Methods* **42**, 321–324. <https://doi.org/10.1016/j.ymeth.2007.01.006> (2007).
54. Stepanovic, S. *et al.* Quantification of biofilm in microtiter plates: overview of testing conditions and practical recommendations for assessment of biofilm production by staphylococci. *APMIS* **115**, 891–899. [https://doi.org/10.1111/j.1600-0463.2007.apm\\_630.x](https://doi.org/10.1111/j.1600-0463.2007.apm_630.x) (2007).
55. Harrison, J. J., Turner, R. J. & Ceri, H. High-throughput metal susceptibility testing of microbial biofilms. *BMC Microbiol.* **5**, 53. <https://doi.org/10.1186/1471-2180-5-53> (2005).
56. Moise, A. R. & Bobis, O. *Baccharis dracunculifolia* and *Dalbergia ecastophyllum*, main plant sources for bioactive properties in green and red Brazilian propolis. *Plants (Basel)* <https://doi.org/10.3390/plants9111619> (2020).
57. Andrade, G. *et al.* Brazilian *Copaifera* species: Antifungal activity against clinically relevant *Candida* species, cellular target, and in vivo toxicity. *J Fungi (Basel)* <https://doi.org/10.3390/jof6030153> (2020).
58. Singulani, J. L. *et al.* Activity of gallic acid and its ester derivatives in *Caenorhabditis elegans* and zebrafish (*Danio rerio*) models. *Future Med. Chem.* **9**, 1863–1872. <https://doi.org/10.4155/fmc-2017-0096> (2017).

## Author contributions

N.B.S.S. designed the experiments, functions/Writing—original draft; writing—proofreading and editing. J.H.S. designed the experiments and carried out the experiments. M.B.S. designed the experiments and carried out the experiments. J.R.S.A. designed the experiments and carried out the experiments. D.O.S.M. designed the experiments and analysed the results. R.A.S. designed the experiments and carried out the experiments. I.A.S. analysed the results and Writing—proofreading and editing. J.A.A. designed the experiments and carried out the experiments and analysed the results and Writing—proofreading and editing. A.C.J. analysed the results and Writing—proofreading and editing. R.P.S. Writing—proofreading and editing, methodology, supervision. S.R.A. Acquisition of financing, writing—proofreading and editing. R.C.S.V. Writing—proofreading and editing, acquisition of financing. J.K.B. Writing—proofreading and editing, acquisition of financing. R.H.P. Methodology. C.H.G.M. Conceptualization, formal analysis, methodology, supervision, validation; visualization, functions/Writing—original draft; writing—proofreading and editing. All authors gave the final approval for publication.

## Funding

This work was funded by Fundação de Amparo à Pesquisa do Estado de São Paulo (FAPESP Grant # 2017/04138–8), Fundação de Amparo à Pesquisa do Estado de Minas Gerais (FAPEMIG # 12138—Scholarship granted; APQ-03385–18 and APQ-01487–22), Coordenação de Aperfeiçoamento de Pessoal de Nível Superior (CAPES Finance Code 001—Scholarship granted and Prevention and Combat of Outbreaks, Endemics, Epidemics and Pandemics—Finance Code #88881.506794/2020–01) and Conselho Nacional de Desenvolvimento Científico e Tecnológico (CNPq Grant # 307974/2019–7).

## Competing interests

The authors declare no competing interests.

## Additional information

**Supplementary Information** The online version contains supplementary material available at <https://doi.org/10.1038/s41598-022-24776-4>.

**Correspondence** and requests for materials should be addressed to C.H.G.M.

**Reprints and permissions information** is available at [www.nature.com/reprints](http://www.nature.com/reprints).

**Publisher's note** Springer Nature remains neutral with regard to jurisdictional claims in published maps and institutional affiliations.



**Open Access** This article is licensed under a Creative Commons Attribution 4.0 International License, which permits use, sharing, adaptation, distribution and reproduction in any medium or format, as long as you give appropriate credit to the original author(s) and the source, provide a link to the Creative Commons licence, and indicate if changes were made. The images or other third party material in this article are included in the article's Creative Commons licence, unless indicated otherwise in a credit line to the material. If material is not included in the article's Creative Commons licence and your intended use is not permitted by statutory regulation or exceeds the permitted use, you will need to obtain permission directly from the copyright holder. To view a copy of this licence, visit <http://creativecommons.org/licenses/by/4.0/>.

© The Author(s) 2022



### **CAPÍTULO III**

#### **Brazilian red propolis reduces biomass and viable cells of oral biofilm cells and the *Toxoplasma gondii* intracellular proliferation**

Manuscrito que será submetido no periódico Biomedicine & Pharmacotherapy

## **Brazilian red propolis reduces biomass and viable cells of oral biofilm cells and the *Toxoplasma gondii* intracellular proliferation**

Nagela Bernadelli Sousa Silva<sup>a</sup>, Gabriel Guimarães Calefi<sup>a</sup>, Samuel Cota Teixeira<sup>b</sup>, Thales Alves de Melo Fernandes<sup>c</sup>, Natasha Marques Cassani<sup>d</sup>, Ana Carolina Gomes Jardim<sup>d</sup>, Sergio Ricardo Ambrósio<sup>e</sup>, Rodrigo Cássio Sola Veneziani<sup>e</sup>, Jairo Kenupp Bastos<sup>f</sup>, Bellisa de Freitas Barbosa<sup>b</sup>, Marcelo José Barbosa Silva<sup>g</sup>, Robinson Sabino Silva<sup>h</sup>, Carlos Henrique Gomes Martins<sup>a</sup>.

<sup>a</sup> Laboratory of Antimicrobial Testing, Institute of Biomedical Sciences (ICBIM), Federal University of Uberlândia, Uberlândia, Brazil

<sup>b</sup> Laboratory of Immunophysiology of Reproduction, Institute of Biomedical Science (ICBIM), Federal University of Uberlândia, Uberlândia, MG, Brazil

<sup>c</sup> Laboratory of Applied Toxinology, Butantan Institute, São Paulo, SP, Brazil

<sup>d</sup> Laboratory of Antiviral Research, Institute of Biomedical Science (ICBIM), Federal University of Uberlândia, Uberlândia, MG, Brazil

<sup>e</sup> University of Franca (UNIFRAN), Exact and Technological Sciences Nucleus, Franca, Brazil

<sup>f</sup> University of São Paulo (USP), Faculty of Pharmaceutical Sciences of Ribeirão Preto, Ribeirão Preto, Brazil

<sup>g</sup> Laboratory of Tumor Biomarkers, Institute of Biomedical Sciences (ICBIM), Federal University of Uberlândia, Uberlândia, Brazil

<sup>h</sup> Department of Physiology, Institute of Biomedical Sciences, Federal University of Uberlândia (UFU), Uberlândia, Minas Gerais, Brazil

**Emails:** nagela.silva@ufu.br; ggcalefi@ufu.br; samuel.teixeira@ufu.br; thales.fernandes.esib@esib.butantan.gov.br. natashacassani@gmail.com; jardim@ufu.br; sergio.ambrosio@unifran.edu.br; rodrigo.veneziani@unifran.edu.br; jkbastos@fcfrp.usp; eloisa.ferro@ufu.br; bellisafb@ufu.br; majbsilav@ufu.br; robinsonsabino@ufu.br; carlos.martins2@ufu.br.

### **Corresponding author**

Carlos Henrique Gomes Martins. Full Professor at the Institute of Biomedical Sciences (ICBIM) at the Federal University of Uberlândia (UFU). Institutional email: carlos.martins2@ufu.br. Address: Av. Pará Article 23.06.24 versão tese.pdfPage 11, 1720-Umuarama, Uberlândia, 38405-320, Brazil

## Abstract

Infectious diseases continue to be an important cause of thousands of deaths annually around the world. Therefore, this study aimed to evaluate the antimicrobial and antiparasitic activity of the crude hydroalcoholic extract and compounds isolated from Brazilian Red Propolis (BRP) against oral pathogens and *Toxoplasma gondii*, using *in vitro*, *in vivo* and *in silico* approaches. Antimicrobial activity was determined using the broth dilution method and synergistic activity using the checkerboard assay. Antibiofilm activity was evaluated by staining with 2% crystal violet and counting microorganisms. *In vivo* infection was carried out in *Caenorhabditis elegans* AU37 larvae and *in silico* analysis was performed using molecular docking. The effect on growth modulation of *T. gondii* were evaluate through a  $\beta$ -galactosidase colorimetric assay. Minimum Inhibitory Concentration values ranged from 3.12 to 400  $\mu\text{g/mL}$ . Biofilm Minimum Inhibitory Concentration (MICB<sub>50</sub>) values ranged from 6.25 to 375  $\mu\text{g/mL}$ , with a significant reduction in the number of viable cells. Furthermore, Gutiferone E and the crude extract reduced cell aggregation and caused damage to the biofilm cell wall. The highest concentrations of the crude extract and Gutiferone E increased the survival and reduced the risk of death of infected and treated larvae. Gutiferone E and Oblongifolin B inhibited the intracellular proliferation of *T. gondii* and demonstrated several targets of action against bacteria and *T. gondii* in *in silico* analysis. These data demonstrate that BRP has antimicrobial and antiparasitic activity against pathogens of clinical relevance, and can be used in the future as phytomedicines.

**Keywords:** Antimicrobial activity, antiparasitic activity, *C. elegans*, Brazilian Red Propolis

## 1. Introduction

Infectious diseases continue to be an important cause of thousands of deaths annually around the world. It is estimated that approximately 700.000 people die annually from these diseases, which could increase to ten million by 2050 [1]. In addition to posing a serious threat to human health, these infections also represent an economic burden on public health. [2]. Several bacterial infections still require interventions that are actually effective, such as endodontic infections. These infections are caused by a variety of microorganisms that infect dental pulp tissue and initiate a process of inflammation and necrosis and take advantage of this environmental condition to establish themselves. Although endodontic infections are caused by a wide variety of anaerobic bacteria, aerobic bacteria are also significantly important for the development of the infectious process, such as *Enterococcus faecalis* [3], *Streptococcus* spp., *Lactobacillus paracasei*, *Staphylococcus aureus*, among others and these bacteria may persist in the root canal even after endodontic treatment [4]. Yeasts such as *Candida albicans* and *C. glabrata* can also be found in this type of pathology, especially in immunocompromised individuals [5].

The persistence of microorganisms in root canals even after endodontic treatment is associated with the ability of these pathogens to form biofilms, as this microbial community protects them against factors from the external environment and favors their adhesion in the dental canal [6]. Furthermore, in biofilms, microorganisms become 10 to 1000 times more resistant to antimicrobials, increasing their persistence in the oral cavity, making the disinfection process difficult and reducing the chances of successful treatment [7, 8]. These pathogens can still spread to nearby tissues and cause systemic infections, which are often fatal [9].

Another infectious disease with high prevalence throughout the world, constituting a serious public health problem, is toxoplasmosis. Toxoplasmosis is a parasitic zoonosis caused by the intracellular parasite *Toxoplasma gondii*. It is estimated that one third of the global population is infected or has been exposed to this parasite, with a high prevalence in Africa, Southeast Asia, the Middle East, Central and Eastern Europe and Latin America [10, 11]. Unlike bacterial diseases, parasitic diseases such as toxoplasmosis are generally asymptomatic in immunocompetent individuals and rarely cause outbreaks, therefore being considered neglected diseases in the health sector [11]. In contrast, in immunocompromised patients, toxoplasmosis can cause systemic and fatal complications [12]. Furthermore, in pregnant women, this parasite can be transmitted to the fetus causing multisystem dysfunction, neural damage or fetal death [13].

The excessive use of antibiotics and antiparasitics, associated with virulence factors of microorganisms, contributed to the increase in drug resistance and difficult-to-treat infections [14, 15]. Therefore, many unconventional treatments have been a good option for these pathologies, such as natural products, due to their high safety, low cost and diverse biological properties [16]. Brazilian Red Propolis (BRP) is a resinous mixture collected by *Apis mellifera* bees from the trunk of *Dalbergia ecastophyllum* trees. It can be collected in several countries such as Cuba and Venezuela, but due to bioactive molecules never before described in the literature and with different biological potentials, BRP has stood out among the others. It has antimicrobial, anti-inflammatory, antioxidant, antiproliferative activity, among others [17]. Due to the multipotentiality of the bioactive components that BRP contains, propolis can be used as a promising therapeutic alternative against various microorganisms that cause human infections [18].

Therefore, the objective of this study was to evaluate the antimicrobial, antibiofilm, and antiparasitic activity of the crude hydroalcoholic extract and substances isolated from BRP against oral pathogens and *T. gondii* using *in vitro*, *in vivo* and *in silico* approaches.

## **2. Materials and methods**

### **2.1 Obtaining BRP samples**

BRP was collected in March 2019 at the Canavieiras Beekeepers Association (COAPER) in the state of Bahia, Brazil. The crude extract was extracted with 70% hydroalcoholic ethanol solution and partitioned with organic solvents in Oblongifolin B and Gutiferone E, as per district Aldana-Mejia, Ccana-Ccapatinta, Ribeiro, Arruda, Veneziani, Ambrosio and Bastos [19].

### **2.2 Bacterial and yeasts strains**

The bacteria used in this study include *Enterococcus faecalis* (ATCC 4082), *E. faecalis* (clinical isolate), *Streptococcus salivarius* (ATCC 25975), *S. salivarius* (clinical isolate), *Lactobacillus paracasei* (ATCC 11578) and *Staphylococcus aureus* (clinical isolate). The yeasts used were *Candida albicans* (ATCC 28366) and *C. glabrata* (ATCC MYA-276). These microorganisms were obtained from the American Type Culture Collection (ATCC) and the clinical isolates were obtained from human endodontic infections from previous work carried out by our research group, and are cryopreserved at

-80°C in the Antimicrobial Testing Laboratory (LEA) at the Federal University of Uberlândia (UFU).

## **2.3 Assessment of *in vitro* antimicrobial activity**

### **2.3.1 Determination of Minimum Inhibitory Concentration (MIC)**

The broth microdilution technique was used to determine the antibacterial activity of the crude extract and substances isolated from BRP, according to recommendations from the Clinical Laboratory Standards Institute (CLSI) [20], with modifications as described below. The crude extract and isolated substances were solubilized in 5% of dimethyl sulfoxide – DMSO (Sigma-Aldrich, San Luis, Missouri, USA) and diluted in Brain Heart Infusion broth - BHI (Kasvi, Pinhais, Paraná, Brazil). The samples were then pipetted into wells of 96-well microplates and diluted again to reach a concentration range that varied from 0.195 to 400 µg/mL. The inoculum was standardized to the McFarland 0.5 scale checked in densitometer (Biomérieux, Marcy-l'Étoile, Lyon, France) and diluted to a bacterial concentration of  $5 \times 10^5$  CFU/mL in the wells. The plates were then incubated at 37°C for 24h. Then, 30 µL of resazurin (Sigma-Aldrich) at a concentration of 0.02% was added to the wells for test interpretation. Resazurin is a reducing oxide that, in the presence of living metabolites, changes its original color (blue) to pink, indicating bacterial growth [21]. Sterility controls were carried out on the culture medium and BRP samples evaluated, 5% DMSO (the solvent did not interfere with bacterial growth at this concentration) and cell viability of the microorganisms. Chlorhexidine (Sigma-Aldrich) was used as a positive control at a concentration of 0.115 to 59.0 µg/mL against all bacteria included in the study. The tests were carried out in triplicate.

The MIC of the crude extract and substances isolated from BRP against yeast was determined following CLSI recommendations, with modifications as described below [22]. The BRP samples were diluted in Roswell Park Memorial Institute (RPMI) 1640 medium buffered with MOPS - [N-morpholino] propane sulfonic acid- (Sigma-Aldrich) and were evaluated at a concentration of 1.46 to 3000 µg/mL. Yeast-containing cell suspensions were prepared in the final concentration of  $0.5 \times 10^3$  to  $2.5 \times 10^3$  CFU/mL. The plates were then incubated at 37°C for 24h. After incubation, 30 µL of 0.01% resazurin was added to each well. The plate was then reincubated for 4 hours. The antifungal Amphotericin B (Sigma-Aldrich) was used as a test quality control at concentrations of 0.031 to 16 µg/mL

against *C. krusei* (ATCC 6258) and *C. parapsilosis* (ATCC 22019). The tests were performed independently in triplicate.

### **2.3.2 Determination of Minimum Bactericidal Concentration (MBC) and Minimum Fungicide Concentration (MFC)**

To evaluate whether propolis samples only inhibit microbial growth or completely eliminate the microorganism, before adding rezasurin to the MIC plates, 10  $\mu$ L from each well was aspirated and plated on BHI agar for bacteria (Kasvi) and Sabourad agar (Kasvi) for yeasts. After incubation for 24h at 37°C, MBC and MFC were defined as the lowest concentration of propolis that killed > 99.9% of the initial microbial population, where no visible growth of the microorganism was observed after subculture on the plates [23, 24].

### **2.3.3 Assessment of synergistic activity**

The most promising samples in the MIC were selected for the evaluation of synergistic activity through the checkerboard assay, according to Iten, Saller, Abel and Reichling [25], with modifications. Propolis and chlorhexidine (Sigma-Aldrich) samples were combined in standard MIC format against  $5 \times 10^5$  CFU/mL of bacterial inoculum of all bacteria included in the study. Amphotericin B (Sigma-Aldrich) was combined with propolis samples in the standard MIC format against  $0.5 \times 10^3$  to  $2.5 \times 10^3$  CFU/mL of the yeast inoculum. To evaluate synergism, the Fractional Inhibitory Concentration Index (FICI) values were calculated as follows:

$$\text{FICI} = 1 + 2$$

- (1) MIC value of the propolis sample alone/ combined MIC value
- (2) MIC value of the antimicrobial alone/ combined MIC value

The interpretation was made according to Iten, Saller, Abel and Reichling [25] this way:  $\text{FICI} \leq 0.5$  synergism;  $>0.5 \text{ FICI} < 1.0$  additive;  $\geq 1.0 \text{ FICI} \leq 4.0$  indifferent and  $\text{FICI} \geq 4.0$  antagonism. The assays were performed in triplicate.

## **2.4 Assessment of antibiofilm activity**

### **2.4.1 Determination of Biofilm Minimum Inhibitory Concentration (MICB<sub>50</sub>) and counting of viable microorganisms**

Prior to the antibiofilm activity tests, biofilm formation was standardized for all bacteria and yeasts evaluated in this study, to confirm whether these microorganisms were biofilm producers, what the inoculum concentration was and the ideal and incubation time for biofilm formation. For this, the microorganisms were incubated at a concentration of  $10^6$  to  $10^9$  cells/mL in 96-well plates with only broth for 24, 48 and 72h at 37°C. Biofilm formation was considered as absorbance in the spectrophotometer greater than or equal to 1. After standardization tests, it was determined that the ideal incubation time was 24h at 37°C, both for bacteria and yeasts. The inoculum of  $1 \times 10^6$  CFU/mL was determined to be the most suitable for bacteria and  $1 \times 10^8$  CFU/mL for yeasts (data not shown).

The most promising samples in MIC were selected to evaluate their ability to inhibit the biomass and reduce number of viable biofilm cells. To evaluate biomass inhibition, the bacteria were serially diluted in a 96-well microplate to be evaluated at a concentration of 0.195 to 400 µg/mL. The  $1 \times 10^6$  inoculum of each bacteria evaluated was pipetted into each well and the plates were incubated for 24h at 37°C. The wells were then washed with sterilized distilled water, fixed with methanol (Êxodo Científica, Sumaré, São Paulo, Brazil) and stained with 2% crystal violet (Sigma-Aldrich) [26]. The wells were then washed again to remove excess dye and solubilized with 33% acetic acid (Êxodo Científica). Biomass quantification was performed by reading the absorbance of each well at 595 nm on the SpectraMax microplate reader (Termo Fisher, Waltham, Massachusetts, USA). The biofilm formed by each microorganism evaluated without treatment was considered as control. Chlorhexidine (Sigma-Aldrich) was used as a positive control at a concentration of 0.115 to 59.0 µg/mL against all bacteria included in the study. Tests were performed in triplicate.

The quantification of biomass against yeasts was carried out according to Marcos-Zambrano, Escribano, Bouza and Guinea [27]. For this, the wells were washed, fixed with methanol and stained with 1% crystal violet. Reading was performed at 590 nm on the SpectraMax microplate reader (Termo Fisher). The biofilm formed by each microorganism evaluated without treatment was considered as control. Amphotericin B (Sigma-Aldrich) was evaluated against the yeasts tested at a concentration of 0.031 to 16 µg/mL, being considered as positive control.



The Minimum Inhibitory Concentration of Biofilm (MICB<sub>50</sub>) assay is defined as the lowest concentration of the microbial agent that can inhibit biofilm formation by at least 50%, and was determined for both bacteria and yeast, according to the equation below [28]:

$$\text{Inhibition} = 1 - \frac{\text{Absorbance (595 or 590 nm) of the sample treated well}}{\text{Absorbance (595 or 590 nm) of the untreated control well}} \times 100$$

Furthermore, the cellular viability of bacterial and yeast biofilms was assessed by counting microorganisms. In another 96-well microplate, the samples were diluted and the inoculum was prepared in the same way as described above. After incubation, the supernatant was withdrawn, and the planktonic cells were removed by washing the wells with ultrapure distilled water. RPMI broth (Sigma-Aldrich) for yeast and BHI broth (Kasvi) for bacteria were added to the wells and the biofilm was detached from the bottom of the well after 15 minutes in an ultrasound machine (Solidsteel, Piracicaba, São Paulo, Brazil). Each well was then serially diluted from 10<sup>0</sup> to 10<sup>-7</sup> and 50 µL of each dilution was pipetted onto plates containing BHI agar (Kasvi) for bacteria and Sabourad agar (Kasvi) for yeast, cut as described by Harrison, Turner and Ceri [29] and incubated for 24 hours at 37°C. After incubation, the number of microorganisms was counted and the results were expressed as Log<sub>10</sub> CFU/mL. The biofilm formed by each microorganism evaluated without treatment was considered as control. Chlorhexidine (Sigma-Aldrich) was used as a positive control at a concentration of 0.115 to 59.0 µg/mL against all bacteria included in the study and Amphotericin B (Sigma-Aldrich) was evaluated against the yeasts at a concentration of 0.031 to 16 µg/mL. The assays were performed in triplicate.

#### **2.4.2 Assessment of live and dead biofilm cells through Propidium Iodide (PI) and 4',6'-diamino-2-fenil-indol (DAPI) staining**

To obtain images of the cell viability of the biofilm treated with the most promising BRP samples, the wells were stained with DAPI (Termo Fisher) and PI (Sigma-Aldrich) as described by Williams, Hong, Danavall, Howard-Jones, Gibson, Frischer and Verity [30] with modifications. The yeasts were incubated at a concentration of 1x10<sup>8</sup> CFU/mL and the bacteria at a concentration of 1x10<sup>6</sup> CFU/mL together with the most promising propolis samples at the concentration determined as MICB<sub>50</sub> and stained with 30 µL of DAPI (1µg/mL) for 10 minutes under shaking in the dark and 30 µL of PI (10 µg/mL) for 30

minutes without shaking. After incubation, the dyes were removed and the wells were washed with Phosphate-buffered saline (PBS). Untreated biofilm was used as a control. Images were obtained using an EVOS M5000 Imaging System Microscope (Termo Fisher) fluorescence electron microscope.

### **2.4.3 Scanning Electron Microscopy (SEM)**

To evaluate the changes that most promising BRP samples cause in the morphology of bacterial and yeast cells, the biofilms were analyzed using images obtained by SEM, as already described by Melo, Mendonca, Monteiro, Siqueira, Pereira, Peres, Fernandez and Rossi [31], with modifications. The assay was conducted in 24-well plates and bacterial and yeast inoculum at concentrations of  $1 \times 10^6$  CFU/mL and  $1 \times 10^8$  CFU/mL, respectively, were pipetted into each well containing sterile PVC discs measuring 10 mm in diameter, along with the most promising propolis samples at MIC concentration of each microorganism. After 24 hours of incubation at 37°C, the discs were fixed in a solution of glutaraldehyde (Sigma-Aldrich) (2.5%) and paraformaldehyde (Sigma-Aldrich) (2%) in 0.15M sodium cacodylate buffer (pH 7.0) for two hours. Then, the discs were post-fixed in 1% osmium tetroxide solution (Sigma-Aldrich) for 2 hours and dehydrated in ethanol at the following concentrations: 30%, 50%, 70%, 90% and 100% at intervals of 20 minutes each. Subsequently, the discs were subjected to critical point drying (SPC), coated with gold (20-nm thickness) and analyzed using a Tescan scanning electron microscope, model VEGA 3 LMU at magnifications of 50x, 800x, 10,000x and 40,000x.

### **2.5 Assessment of *in vivo* antimicrobial activity**

*In vivo* assays were performed using the mutant strain of *Caenorhabditis elegans* AU37 according to Moy, Conery, Larkins-Ford, Wu, Mazitschek, Casadei, Lewis, Carpenter and Ausubel [32] and Singulani, Scorzoni, Gomes, Nazare, Polaquini, Regasini, Fusco-Almeida and Mendes-Giannini [33] with modifications. *C. elegans* AU37 was grown on Nematode Growth Medium (NGM) plates seeded with *Escherichia coli* OP50 and incubated at 16°C for three days. After incubation, the plates were washed with M9 buffer and the larvae were killed with the bleaching solution (sodium hypochlorite + NaOH) to synchronize the larvae at the L4 stage. After synchronization, larvae in the L4 phase were placed on BHI agar plates (Kasvi) containing the evaluated bacteria and on Sabourad plates (Kasvi) containing the evaluated yeasts. The plates were then incubated for 12 hours at 20°C under aerobic conditions, except for the plate containing larvae

infected with the bacteria *L. paracasei* (ATCC 11578), placed under microaerophilic conditions. After incubation, the larvae were washed with M9 buffer and placed in falcon tubes to be centrifuged in order to remove bacteria that may be attached to the worm's body. Subsequently, 20  $\mu$ L of the larval suspension (with approximately 20 larvae) was added to each well of a 96-well flat-bottom microplate, along with 80  $\mu$ L of BHI medium and 200 mg/mL of streptomycin (Sigma-Aldrich), 200 mg/mL of ampicillin (Sigma-Aldrich) and 90  $\mu$ g/mL kanamycin (Sigma-Aldrich) and 100  $\mu$ L of propolis samples at concentrations of 400  $\mu$ g/mL and MIC value (concentrations that are not toxic to worms as already demonstrated in previous studies by our group research [32]) and incubated for four days at 25°C. The number of living and dead cells were counted daily. Infected and untreated larvae were used as controls. As a positive control, larvae infected with the evaluated bacteria were treated with chlorhexidine (Sigma-Aldrich) at the MIC value. For larvae infected with yeast, treatment with amphotericin B (Sigma-Aldrich) at a concentration of 1  $\mu$ g/mL was used as a positive control. The assays were performed in duplicate.

## **2.6 *In silico* analysis of the antibacterial activity**

In order to gain insights into the antibacterial activity of Guttiferone E, we performed molecular docking simulations against bacterial targets. The targets (**Supplementary Table A1**) were obtained from AlphaFold-DB [34] and Protein Data Bank [35] retrieved from UniProt (The UniProt Consortium, 2023). The structure of Guttiferone E was obtained from PubChem [36] under accession code 5352088. The molecular docking simulations were performed using DockThor v.2 [37], a program that employs a multiple solution genetic algorithm and the MMFF94S molecular force field scoring function for pose prediction. The affinity and ranking of protein-ligand binding complexes takes into account intermolecular and intramolecular interactions, such as electrostatic, van der Waals, lipophilic contacts, polar and non-polar solvation contributions, and the ligand torsional entropy [37]. The default parameters of the search algorithm were 24 docking runs and 1,000,000 evaluations on each docking run, and a grid box of 20 Å was defined for atom selection from the binding sites obtained from UniProt and PDB annotations. The docking poses were clustered using a diversity criterion of 2.0 Å and ranked by the total energy from the MMFF94S force field. The docking results were visualized using the Python (<https://www.python.org/>) packages matplotlib [38] and

pandas [39]. The protein-ligand interactions were analyzed in Discovery Studio Visualizer v. 21.1.0 (BIOVIA, Dassault Systèmes).

## **2.7 Assessment of anti-*Toxoplasma gondii* activity**

### **2.7.1 Cell culture and parasite**

Human trophoblast cells (BeWo lineage) were commercially purchased from the American Type Culture Collection (CCL-98™, ATCC, Manassas, VA, USA) and maintained in Roswell Park Memorial Institute (RPMI)-1640 medium (Cultilab, Campinas, SP, Brazil) supplemented with 100 U/mL penicillin (Sigma Chemical Co., St. Louis, MO, USA), 100 µg/mL streptomycin (Sigma) and 10% heat-inactivated fetal bovine serum (FBS) (Cultilab) in a humidified incubator at 37 °C and 5% CO<sub>2</sub> [40].

*Toxoplasma gondii* tachyzoites (highly virulent RH strain, 2F1 clone) expressing the β-galactosidase gene were cultivated by serial passages in BeWo cells cultured in RPMI 1640 medium supplemented with 100 U/mL penicillin and 100 µg/mL streptomycin and 2% FBS at 37 °C and 5% CO<sub>2</sub> [41].

### **2.7.2 Host cell viability**

We evaluated the host cell viability in the presence of the Gutiferone E and Oblongifolin B to establish the non-toxic concentration of each compound. The viability of BeWo cells was assessed by MTT assay (Sigma-Aldrich) [(3-(4,5-dimethylthiazol-2-yl)-2,5-diphenyltertrazolin bromide)] [42]. In brief, BeWo cells ( $3 \times 10^4/200$  µL/well) were seeded in 96-well microplates in 10% FBS medium at 37 °C and 5% CO<sub>2</sub>. After adhesion, both compounds ranging from 256 to 4 µg/mL (twofold serial dilutions) diluted in 10% FBS medium were added to the microplate for 24 h. We also treated the cells with 1.2 % DMSO, which is the percentage used at the highest concentration of the compounds (256 µg/mL). Cells incubated with culture medium alone was considered to be 100% viable. Next, cells were submitted to MTT reagent (5 mg/mL, 10 µL) plus 90 µL of supplemented medium for 3 h at 37 °C and 5% CO<sub>2</sub>, followed by addition of 100 µL of 10% sodium dodecyl sulfate (SDS, Sigma) and 50% N,N-dimethyl formamide (Sigma-Aldrich). The MTT reduction was measured at 570 nm with a multi-well scanning spectrophotometer (VersaMax ELISA Microplate Reader, Molecular Devices, Sunnyvale, CA, USA). We showed cell viability in percentages (cell viability %), with the absorbance of cells incubated only with culture medium considered to be 100% viable.

### 2.7.3 *T. gondii* intracellular proliferation by $\beta$ -galactosidase assay

We screened different concentrations of Gutiferone E and Oblongifolin B to evaluate their effect on growth modulation of *T. gondii* through a  $\beta$ -galactosidase colorimetric assay. Briefly, BeWo cells ( $3 \times 10^4/200 \mu\text{L}/\text{well}$ ) were seeded in 96-well microplates in 10% FBS medium at 37 °C and 5% CO<sub>2</sub>. After 18 h, cells were infected with *T. gondii* tachyzoites at a multiplicity of infection (MOI) of 3:1 (parasite/host cell ratio) for 3 h in 2% FBS medium. Afterward, cells were washed with 1× sterile phosphate-buffered saline (1× PBS) to remove non-invaded parasites and then treated with a twofold serial dilution of Gutiferone E and Oblongifolin B (ranging from 256 to 4  $\mu\text{g}/\text{mL}$ ) for 24 h at 37 °C and 5% CO<sub>2</sub>. In addition, BeWo cells were treated with association of sulfadiazine plus pyrimethamine (SDZ+PYR, 200 + 8  $\mu\text{g}/\text{mL}$ , respectively), which are effective and safe concentrations for BeWo cells and considered the gold standard drugs for the treatment of congenital toxoplasmosis [43]. As negative control, infected cells were treated with 10% FBS medium. Parasite intracellular proliferation was analyzed using  $\beta$ -galactosidase assay using the chlorophenol red- $\beta$ -D-galactopyranoside reagent substrate (CPRG; Roche Diagnostics, Mannheim, Germany), as previously described [43]. We quantified *T. gondii* intracellular proliferation in percentage (% of *T. gondii* proliferation) and calculated the number of tachyzoites in comparison to a standard curve of free tachyzoites (ranging from  $1 \times 10^6$  to  $15.625 \times 10^3$  parasites). Infected BeWo cells treated with only culture medium (negative control) represented non-inhibited parasite growth. Dose-response inhibition curves (Log (inhibitor) vs. normalized response—Variable slope) were calculated as previously published. The selectivity index (SI) was determined based on the CC<sub>50</sub> BeWo cells/IC<sub>50</sub> *T. gondii* ratio [44]

### 2.7.4 *In silico* analysis of anti-*T. gondii* activity

To gain insights into the anti-*T. gondii* effects of Gutiferone E and Oblongifolin B isolated from BRP, we performed molecular docking simulations against the parasite targets. The targets (**Supplementary Table A1**) were obtained from PDB (Berman et al., 2000) and the structure of Oblongifolin B was collected from PubChem [36] under accession code 11570735. The molecular docking simulations and analysis were performed as described in the previous section (2.6).

### 2.7.5 Statistical analysis

Statistical analyses of biofilm were carried out using GraphPad Prism 5 (GraphPad Software Inc., CA, USA). Survival curves of *in vivo* assay were made using the Kaplan–Meier method. The cox regression model, also known as the proportional hazards model, was used to investigate the effect of the treatment on the outcome of death. The analysis of the Cox coefficients was based on the Wald statistics, and its p-value was analyzed. The treatment was considered relevant to the model if the Wald p-value was below the alpha threshold (0.05). The exponential of the coefficients (Exp(B)) was interpreted as the risk of larval death compared to the untreated infected larvae. This statistical method compared the survival distributions based on different treatments.

## 3. Results

### 3.1 Antimicrobial activity

#### 3.1.1 Determination of Minimum Inhibitory Concentration (MIC), Minimum Bactericidal Concentration (MBC) and Minimum Fungicide Concentration (MFC)

All BRP samples evaluated demonstrated antimicrobial activity, as shown in **Table 1**, with MIC values that ranged from 3.12 to 200 µg/mL against bacteria and 5.86 to 187.5 µg/mL against yeast. The isolated substances demonstrated the lowest MIC values, with emphasis on Gutiferone E presenting the lowest values (MIC values from 3.12 to 6.25 µg/mL for the bacteria). Regarding yeast, the crude extract demonstrated the best results, with MIC values from 5.86 to 46.8 µg/mL). Regarding MBC, the crude extract demonstrated bactericidal activity against *E. faecalis* (clinical isolate) and *S. salivarius* (ATCC 25975); Gutiferone E against *S. salivarius* (clinical isolate) and *L. paracasei* (ATCC 11578) and Oblongifolin B against *S. salivarius* (ATCC 29975), *S. salivarius* (clinical isolate) and *L. paracasei* (ATCC 11578). Regarding MFC values, Gutiferone E and Oblongifolin B demonstrated fungicidal activity against *C. glabrata* (ATCC MYA-276). The MIC values of the controls ranged from 0.92 to 3.68 µg/mL against bacteria and 0.25 to 2 µg/mL against yeast. Chlorhexidine demonstrated bactericidal activity against *S. salivarius* (ATCC 25975) and *L. paracasei* (ATCC 11578) and amphotericin B demonstrated fungicidal activity against the yeasts *C. parapsilosis* (ATCC 22019) and *C. Krusei* (ATCC 6258).

### 3.1.2 Synergistic activity

**Table 2** shows the results of the assay evaluating synergistic activity against the most promising BRP samples against the bacteria and yeasts included in the study. Gutiferone E and crude extract demonstrated indifferent activity combined to chlorhexidine and amphotericin B, respectively.

### 3.2 Antibiofilm activity

Gutiferone E demonstrated antibiofilm activity against all bacteria evaluated, as shown in Fig. **1A-1F**. MICB<sub>50</sub> values ranged from 0.195 to 12.5 µg/mL, with the lowest value demonstrated against *E. faecalis* (ATCC 4082) (**Fig 1B**). Regarding cell viability, above MICB<sub>50</sub>, there was a significant reduction in the number of viable biofilm cells against all bacteria compared to the control. The crude extract demonstrated a reduction in biofilm and the number of viable cells of both *C. albicans* (ATCC 28366) and *C. glabrata* (ATCC MYA-646), with MICB<sub>50</sub> values of 93.75 µg/mL and 375 µg/mL, respectively (**Fig. 1G and 1H**, respectively). In relation to controls, MICB<sub>50</sub> values ranged from 0.92 to 3.68 µg/mL against bacteria, reducing the number of viable cells significantly (**Fig. 2A-2F**). MICB<sub>50</sub> values against yeast ranged from 0.0625 to 0.125 µg/mL, with a significant reduction in the number of viable cells (**Fig. 2G-2H**).

#### 3.2.1 Propolis samples act on the integrity of the cell membrane of oral bacteria and fragment yeast DNA

The results of inhibition of biofilm formation and reduction in the number of viable biofilm cells can be visualized in fluorescence microscopy images after the use of cell viability marker fluorescent dyes (DAPI and PI). **Fig. 3** shows the control (untreated biofilm) and the biofilm treated at the concentration determined as MICB<sub>50</sub>, both stained with DAPI and PI of each microorganism evaluated. It is possible to observe that the treated biofilm has more dead cells (stained in red) than live cells (stained in blue) compared to the control, validating the cell viability tests previously carried out by counting microorganisms. Furthermore, the cells marked in red by the PI dye suggest that propolis acts on the cell membrane of these microorganisms, as these dye can only cross compromised membranes, staining the DNA or RNA inside dead cells or cells with damaged membranes. DAPI staining, in addition to staining viable cells, is also capable of binding to adenine and thymine in the smaller area of the DNA, making it possible to

visualize possible morphological changes in this structure. This change was observed in viable cells present in the *C. albicans* biofilm (ATCC 28366) after treatment with the crude extract at MICB<sub>50</sub> concentration, as shown in **Fig. 3Q and 3R**. After treatment, there was a fragmentation of the cell nucleus, as indicated by the red arrow in **Fig. 3R**.

### 3.2.2 Scanning Electron Microscopy (SEM)

To visualize possible morphological changes in the cells of the biofilm formed by the pathogens included in the study after treatment with the BRP samples, SEM images were analyzed and are shown in **Fig. 4**. There was a notable decrease in the biomass of all biofilms treated with the propolis samples compared to the control. In **Fig. 4A** it is possible to notice that the untreated biofilm of *E. faecalis* (ATCC 4082) had an extensive biomass represented by the formation of several bacterial plaques, with a large production of extracellular matrix, which favors this adhesion. After treatment with Gutiferone E, there was a significant decrease in biomass and low cell aggregation. In **Fig. 4B**, there was a decrease in the biomass of the biofilm formed by *E. faecalis* (clinical isolate) after treatment with Gutiferone E, and in addition it is possible to observe that the bacterial cells changed shape, acquiring an irregular morphology compared to the control.

### 3.3. Oral pathogen infection in an animal model

**Fig 5** shows the Kaplan-meier curve with survival curve of larvae infected with the oral pathogens included in the study treated with different concentrations of the most promising propolis samples. Larvae infected with the bacteria and yeasts evaluated in the study were treated with 400 µg/mL of Gutiferone E (against the bacteria) and the crude extract (against the yeasts) and at the concentration determined as the MIC. **Tables A2 and A3** in the **Supplementary material** present pairwise comparisons of infected and treated larvae compared to the control (infected and untreated larvae). The larvae infected with *E. faecalis* (ATCC 4082) and treated with 400 µg/mL of Gutiferone E demonstrate greater survival when compared to the untreated control ( $p=0.044$ ). For larvae infected with *E. faecalis* (clinical isolate), both the highest concentration evaluated (400 µg/mL) and the MIC value (6.25 µg/mL) of Gutiferone E demonstrated an effect on increasing the survival of larvae with compared to the untreated control ( $p=0.000$ ). Only the concentration of 400 µg/mL of Gutiferone E demonstrated a protective effect against *L. paracasei* (ATCC 11578) compared to larvae infected with this bacterium and not treated ( $p=0.044$ ). Both the highest evaluated concentration of Gutiferone E and the MIC value (3.12 µg/mL) were



capable of exerting a protective effect on larvae infected with *S. aureus* (clinical isolate) ( $p= 0.012$ ). The same happened with larvae infected with *C. albicans* compared to the untreated control ( $p=0.004$ ). **Table A4** shows the results of the Cox regression that evaluated the effect of treatments on the risk of death of larvae. The concentration of 400  $\mu\text{g/mL}$  of Gutiferone E reduced the risk of death in larvae infected with *E. faecalis* (ATCC 4082), *E. faecalis* (clinical isolate), *S. aureus* (clinical isolate), *L. paracasei* (ATCC 11578), *C. albicans* (ATCC 28366) and *C. glabrata* (ATCC MYA-276) with reduction rates that ranged from 36% to 64%, with the greatest reduction in the risk of death demonstrated against larvae infected with *E. faecalis* (ATCC 4082). MIC values reduced the risk of death by up to 46%, with the highest rate of reduction observed in larvae infected with *E. faecalis* (clinical isolate).

### 3.4 Molecular docking of Gutiferone E upon bacterial targets

The molecular docking results pointed out that Gutiferone E presented the best binding to *S. aureus* teichoic acid glycosyltransferase (tarP) and *L. paracasei* ribonuclease (rnz) (**Fig. 6A**), and *S. salivarius* urease accessory protein (ureG) and *E. faecalis* mevalonate diphosphate decarboxylase (mvaD) (**Fig. 7A**). Upon binding of *S. aureus* tarP, Gutiferone E forms hydrogen-bonds with Asp92 and Asp94, and hydrophobic interactions with Pro9, Thr10, Phe11, Asn13, Asp41, Gly70, Asn71, Ala72, Pro75, Arg76, Ser93, Asp95, Leu154, Asp178, Val203 and Asn205 (**Fig. 6B**). In parallel, Gutiferone E forms hydrogen-bonds with Gly11, Glu40 and Asp67, and hydrophobic interactions with Ser12, Pro13, Leu64, His65, Gly66, Ile69, Phe70, Arg142 and His248 with *L. paracasei* rnz (**Fig. 6C**). Also, Gutiferone binds *S. salivarius* ureG and interacts with Asp46 and Lys150 through hydrogen-bonds, and Leu20 and Ala127 through hydrophobic interactions (**Fig. 7B**). Lastly, Gutiferone forms hydrogen-bonds with Lys68 and Lys72, and hydrophobic interactions Phe58, Leu60, Ser107, Ala105 and Leu111 of *E. faecalis* mvaD (**Fig. 7C**).

### 3.5. Antiparasitic activity

#### 3.5.1 Gutiferone E and Oblongifolin B treatments promoted loss of cell viability

To determine the half-maximal cytotoxic concentration ( $\text{CC}_{50}$ ) of Gutiferone E and Oblongifolin B, BeWo cells were treated using twofold serial dilutions (ranging from 256 to 4  $\mu\text{g/mL}$ ) for 24 h. Our data demonstrated that all tested concentrations of Gutiferone E reduced cell viability compared to untreated BeWo cells (**Fig. 8A**;  $p < 0.0001$ ). In contrast,

Oblongifolin B promoted loss of cell viability only at higher dosages (256, 128, 64  $\mu\text{g}/\text{mL}$ ;  $p < 0.0001$ ) (**Fig. 8B**), when compared to control group (untreated cells). As control group, BeWo cells treated with 1.2% DMSO did not present loss of cell viability (**Fig. 8A-B**). As demonstrated in **Table 3**, the  $\text{CC}_{50}$  against BeWo cells was  $14.10 \mu\text{g}/\text{mL} \pm 0.635$  for Gutiferone E, while Oblongifolin B demonstrated a  $\text{CC}_{50}$  of  $54.08 \mu\text{g}/\text{mL} \pm 1.625$ .

### 3.5.2 Gutiferone E and Oblongifolin B strongly reduced *T. gondii* intracellular proliferation in BeWo cells

To assess the half-maximal inhibitory concentration ( $\text{IC}_{50}$ ) of Gutiferone E and Oblongifolin B, *T. gondii*-infected BeWo cells were treated using twofold serial dilutions (ranging from 256 to 4  $\mu\text{g}/\text{mL}$ ) for 24 h. Intracellular parasite growth (*T. gondii* proliferation %) was measured by the  $\beta$ -galactosidase activity. Both compounds in all tested concentrations strongly inhibited parasite proliferation in comparison with the infected/untreated cells ( $p < 0.0001$ ; **Fig. 8C-D**). As expected, SDZ+PYR treatment significantly controlled parasite growth compared to the control group ( $p < 0.0001$ ; **Fig. 8C-D**). Interestingly, both Gutiferone E and Oblongifolin B at higher dosages (256, 128 and 64  $\mu\text{g}/\text{mL}$ ) demonstrated to be more effective to inhibit parasite proliferation than the classical treatment ( $P < 0.0001$ ; **Fig. 8C-D**). As reported in **Table 3**, the  $\text{IC}_{50}$  against *T. gondii* in infected BeWo cells was  $0.27 \mu\text{g}/\text{mL} \pm 0.17$  for Gutiferone E, while Oblongifolin B demonstrated a  $\text{IC}_{50}$  of  $2.03 \mu\text{g}/\text{mL} \pm 0.21$ . Based on the  $\text{CC}_{50}$  BeWo cells/ $\text{IC}_{50}$  *T. gondii* ratio, Gutiferone E and Oblongifolin B had a selectivity index (SI) of 52.22 and 26.64, respectively.

### 3.5.3 *In silico* analysis of anti-*T. gondii* activity

The molecular docking simulations showed that Gutiferone E and Oblongifolin B exhibited the best binding to *T. gondii* uracil phosphoribosyltransferase (uprt) and prolyl tRNA synthetase (prs), respectively (**Fig. 9A**). Upon *T. gondii* uprt, Gutiferone E forms hydrogen-bonds with Arg117 and Asp215, and hydrophobic interactions with Val91, Arg92, Ala93, Ile115, Gln116, Ala122, Asp144, Pro145, Met146, Ala148, Thr149, Ser152, Arg206, Tyr207, Tyr208, Phe216, Gly217, Asp218 (**Fig. 9B**). In parallel, Oblongifolin B interacts with *T. gondii* prs Glu79 and Arg131 through hydrogen-bonds, and Pro78, Glu133, Arg142, Phe146, Trp148, Lys189, Glu193, Lys194, Phe195, Ala196, Gln216, Ala217, Ala218, Thr219, His221, Gly251, Cys252, Thr253, Arg255 and Lys455 (**Fig. 9C**).

#### 4. Discussion

BRP is the second most commercialized type of propolis in Brazil and has a wide range of chemical constituents such as chalcones, flavonoids, isoflavones, isoflavans, pterocarpanes and isoflavans. From its crude extract, various substances can be isolated such as vestitol, neovestitol, Oblongifolin B, Gutiferone E, medicarpine, among others. [45]. In the present study, two isolated substances were selected to carry out the tests due to the promising results of Gutiferone E and Oblongifolin B against other pathogens that cause oral infections, demonstrated in previous studies by our research group. [46]. According to Rios and Recio [47], the antimicrobial activity of a natural product is considered promising when the MIC value is  $<100 \mu\text{g/mL}$  for crude extract and  $< 10 \mu\text{g/mL}$  for isolated substances. According to this criterion, in the present study, Gutiferone E demonstrated promising results against all bacteria evaluated and the crude extract demonstrated promising antifungal activity against the yeasts evaluated. Several chemical constituents present in the crude extract of BRP have already been reported as potential antifungals, such as terpenes, isoflavonoids and pterocarpanes [48, 49]. Studies demonstrate that the substances isosativan and medicarpine have good antifungal activity [50]. Furthermore, the synergy of action between all the compounds present in the crude extract may explain the good antifungal activity exerted in this study. Gutiferone E is derived from benzophenones, a class known for its antibacterial activity, already demonstrated against *S. aureus* 209 (obtained from the Bulgarian Type Culture Collection, Institute for State Drug Control, Sofia) and other bacteria [49]. According to Conceicao, Beserra, Aldana Mejia, Caldas, Tanimoto, Luzenti, Gaspari, Evans, Bastos and Pellizzon [51], Gutiferone's action is greater on Gram-positive bacteria than Gram-negative bacteria, which may be the reason for the good antibacterial activity reported in the present study.

Some authors have already demonstrated the antibacterial activity of mouthwashes based on crude ethanolic extract of BRP against *S. salivarius* (ATCC 7073) and *L. paracasei* (ATCC 393) and demonstrated MIC values of 238 and 476 mg/mL, respectively [52]. The present study demonstrated that Gutiferone E demonstrates lower MIC values and bactericidal activity against *L. paracasei* (ATCC 11578) and *S. salivarius* (ATCC 25975), with MIC values of 3.12 and 6.25  $\mu\text{g/mL}$ , respectively. Mouthwash constantly undergoes changes in pH, which can degrade the organic acids present in BRP. Furthermore, the fluorine present in the mouthwash can chelate substances such as polyphenols, altering the antimicrobial activity of the product. More studies should be

conducted regarding the best formulation of propolis-based rinses, so that their antibacterial activity is not compromised.

Other authors evaluated the antibacterial activity of the crude ethanolic extract of BRP against *S. aureus* (ATCC 6538) demonstrating MIC from 64 µg/mL to ≥1024 µg/mL µg/mL, with variations in values in different months of the year [53]. The result of the crude hydroalcoholic extract of BRP demonstrated in the present study of MIC against *S. aureus* (clinical isolate) was higher than that reported by these authors, as it was a wild isolate collected from a patient with endodontic infection. However, Gutiferone E demonstrated better results than the crude extract for this bacteria in the present study (MIC of 31.2 µg/mL). The evaluation of the antibacterial activity of Gutiferone E against bacteria that cause endodontic infections is scarce in the literature, requiring further studies. Sokolonski, Fonseca, Machado, Deegan, Araujo, Umsza-Guez, Meyer and Portela [54] evaluated the antifungal activity of the ethanolic extract of BRP against isolates of *Candida* spp. causing oral pathologies and obtained MIC values that ranged from 1 to 4 mg/mL against *C. albicans*. In the present study, the hydroalcoholic extract demonstrated lower values compared to these authors, exerting fungicide activity against *C. albicans* (ATCC 28366).

In the present study, it was also evaluated whether propolis samples in combination with antibiotics and antifungals commonly used in the treatment of endodontic infections would have a synergistic action against the pathogens evaluated. Gutiferone E and the crude extract demonstrated indifferent activity against all microorganisms evaluated in combination with chlorhexidine and amphotericin B, respectively, indicating that propolis does not interfere with the action of antimicrobials. More studies are needed to understand the mechanism of action of combined therapies.

Endodontic infections can be treated to reduce the microbial load within the root canal system. However, biofilm formation impairs the disinfection process and contributes to a more persistent infection [7]. According to Er-Rahmani, Errabiti, Matencio, Trotta, Latrache, Koraichi and Elabed [55], The most promising natural products with antibiofilm activity are those that can disrupt or inhibit biofilm at low or sublethal concentrations. In the present study, the crude extract and Gutiferone E were able to inhibit biofilm formation by 50% or more and reduce the number of viable biofilm cells at concentrations equal to or lower than the MIC. The antibiofilm activity of Gutiferone E against *E. faecalis* deserves to be highlighted, as this bacterium is capable of surviving in the root canal even after endodontic treatment, withstanding pH variations, the presence of calcium hydroxide and

resisting antibiotics, a characteristic strongly associated with its ability to form biofilm [56]. In a study developed by Parolia, Kumar, Ramamurthy, Madheswaran, Davamani, Pichika, Mak, Fawzy, Daood and Pau [57], propolis collected from Malaysia was coated with gold nanoparticles and its antibiofilm activity against *E. faecalis* (clinical isolate) was evaluated. According to these authors, the nanoparticles significantly reduced the number of CFU/mL of the biofilm, leaving a number of viable cells of up to  $2.3 \times 10^6$  CFU/mL. In the present study, Gutiferone E was able to significantly reduce the number of viable cells, with a decrease of approximately four times compared to the control. Akca, Akca, Topcu, Macit, Pikdoken and Ozgen [58] evaluated the antibiofilm activity of the crude extract of a Turkish propolis against biofilms produced by *S. aureus* (ATCC 25923), *E. faecalis* (ATCC 29212) and *C. albicans* (ATCC 10231) demonstrating MIC values against these microorganisms of 128, 64 and 64  $\mu\text{g/mL}$ , respectively. In the present study, biofilm inhibition was evaluated based on the ability of the samples to inhibit biofilm by 50% or more, different from the methodology adopted by these authors, but the values demonstrated here are still lower (MIC<sub>B50</sub> of 12.5, 0.195 and 93.75  $\mu\text{g/mL}$  against *S. aureus* (clinical isolate), *E. faecalis* (ATCC 4082) and *C. albicans* ATCC 28366), respectively.

Biofilm cell viability assays play a crucial role in evaluating new agents with antibiofilm potential. The decrease in the number of viable cells after treatment with propolis samples can be visualized in fluorescence microscopy images using fluorescent dyes, as demonstrated in the present study. Propidium iodide is widely used for cell viability staining, staining cells with damaged or ruptured membranes, indicating cell death [59]. DAPI staining indicates live cells, as this dye can penetrate the cell membrane and bind to DNA. Murugan, Subramaniyan, Priya, Ragavendran, Arasu, Al-Dhabi, Choi, Guru and Arockiaraj [60] evaluated the antibacterial activity of Withaferin A against *S. aureus* (ATCC 700699) through staining with PI and DAPI and demonstrated an increase in PI-stained cells after treatment with Withaferin A compared to the control, which was also observed in the present study after treatment with propolis samples. The determination of biofilm cell viability should not be carried out exclusively by staining with fluorescent dyes such as PI, as it can emit underestimated signs of cell death, being considered complementary tests of microorganism count [59], as carried out in the present study. DAPI, in addition to playing an important role as an indicator of living cells, is also capable of binding to DNA, emitting fluorescence that is capable of detecting possible nuclear changes such as DNA fragmentation, which was observed in the nucleus of *C.*

*albicans* cells (ATCC 28366) after treatment with the crude extract of BRP in the present study. Hao, Cheng, Clancy and Nguyen [61] evaluated the effects of caspofungin on *C. albicans* (SC5314) and also observed fragmentation in the cell nucleus of these yeasts after treatment, as well as changes in chromatin morphology. This nuclear fragmentation may indicate that the cell is in the process of apoptosis, which indicates that in addition to acting on the cell membrane as observed after staining with PI, propolis samples can also act by inducing apoptosis in yeast cells.

In addition to visualizing the cell viability of biofilms, the present study demonstrated damage to the biofilm after treatment with propolis samples. In all biofilms, there was a decrease in biomass and cell aggregation. Furthermore, in the biofilm produced by *E. faecalis* (clinical isolate), after treatment with Gutiferone E, the morphology of the bacterial cells became irregular or possibly ruptured. According to Er-Rahmani, Errabiti, Matencio, Trotta, Latrache, Koraichi and Elabed [55], this change in morphology may be due to different mechanisms of action that several natural products present against biofilms, acting in interactions with bacterial proteins and cell walls, damage to the cytoplasmic membrane and inhibition of nucleic acid synthesis, among others. This change in the morphology of bacteria after treatment was also demonstrated by Moryl, Palatynska-Ulatowska, Maszewska, Grzejdziak, Dias de Oliveira, Pradebon, Steier, Rozalski and Poli de Figueiredo [62] after treating the biofilm produced by *E. faecalis* (ATCC 29212) with phages for 48h and Lange, Matuszewski, Kutwin, Ostrowska and Jaworski [63] after treatment of *E. faecalis* (ATCC 51299) and *S. aureus* (ATCC 25923) with fernosol.

In order to evaluate the antibacterial and antifungal activity of BRP samples against the pathogens included in the study in an animal model, *C. elegans* larvae were infected and treated with different concentrations of BRP for four days. Based on the literature, this is the first study that evaluated the antimicrobial activity of BRP against the microorganisms included in the study in *C. elegans* larvae. This animal model is commonly used to evaluate the toxicity of products and substances, by exposing the larvae to different concentrations of the sample, counting the number of live and dead larvae daily. This was previously carried out by our research group with the crude extract and substances isolated from BRP, which is why we used concentrations of BRP in the infection tests in the present study, which was already known as non-toxic to larvae [64]. The infection of pathogens in this type of *in vivo* model has been widely used to evaluate the antimicrobial activity of products. Ma, Yue, Liang, Gao, Wang, Cui, Li and Zhi [65] evaluated the antibacterial activity of Realgar, a type of arsenic sulfide, against *E. faecalis*

V583, infecting larvae of *C. elegans* N2 mutants for five days and demonstrated that realgar increased the defenses of *C. elegans* against this bacterium, inducing immune responses, leading to the elimination of the pathogen. Also according to these authors, realgar at a concentration of 7.5 µg/mL was able to increase the survival of larvae when infected with the bacteria evaluated, during five days of infection. In the present study, the concentration of 6.25 µg/mL of Gutiferone E exerted a protective effect against larvae infected with *E. faecalis* (clinical isolate) and reduced the risk of death, at a lower concentration than that reported by these authors, demonstrating the good antibacterial potential of Gutiferone E *in vivo*.

Other authors have already evaluated the antimicrobial activity in *C. elegans* larvae of different compounds against different microorganisms, such as the antivirulence potential of betulin (triterpenoid) against *S. pyogenes* (ATCC 700294D-5) [66], evaluation of the antibacterial activity of alkaloids against strains of *Staphylococcus aureus* resistant and sensitive to methicillin (obtained from Beijing University of Chinese Medicine) [67], antifungal activity of quinic acid derived from *Syzygium cumini* against *C. albicans* (ATCC 90028) and *C. glabrata* (MTCC3019) [68] and the antifungal activity of azoles and amphotericin B against *C. glabrata* (ATCC 90030 and NCPF 3203), *C. nivariensis* (CBS 9984 and CECT 11998) and *C. braccarensis* (NCYC 3397 and NCYC 3133) [69]. In the present study, Gutiferone E and the crude extract demonstrate their antibacterial and antifungal potential against the microorganisms evaluated *in vitro* and *in vivo* assays.

Most *in vivo* studies using *C. elegans* and *L. paracasei* have highlighted their importance as a probiotic bacterium and demonstrated how some strains such as *L. paracasei* subsp. *paracasei* 2004 improves the health of larvae and increases their life expectancy [70]. However, the present study demonstrated the pathogenicity of a strain of *L. paracasei* (ATCC 11578) isolated from the oral cavity, frequently associated with endodontic infections, demonstrating its potential to cause infections in *C. elegans* larvae. To our understanding, this is the first study that evaluated this type of *L. paracasei* infection in *C. elegans* larvae.

Considering the various chemical compounds present in BRP and their diverse biological activities, the isolated substances Gutiferone E and Oblongifolin B were evaluated for their antiparasitic activity against *T. gondii*. Regarding the treatment of BeWo cells with propolis samples, the therapeutic index was not higher than 100 µg/mL, demonstrating that a high dosage is not necessary for BRP samples to exert antiparasitic activity, demonstrating also relatively low IC<sub>50</sub> values (less than 3 µg/mL). The results

presented in the present study are promising as these samples were able to reduce the intracellular proliferation of these parasites more efficiently than classical therapy. This reduction in intracellular proliferation becomes extremely important since as part of the life cycle, *T. gondii* replicates within host cells, to later cause the lysis of these cells and infect new ones recently surrounded, causing new foci of infections [71]. This is the first study that evaluated the antiparasitic activity of BRP against *T. gondii*. Huang, Yao, He, Pan, Hou, Fan, Du and Tao [72] evaluated the anti-*T.gondii* activity of *Pelargonium X. asperum* essential oils in HFF cells infected with tachyzoites and demonstrated a promising inhibition of these parasites at a concentration of 1.42 µg/mL. In the present study, even at the lowest concentrations evaluated (4, 8, 16, 32 and 64 µg/mL) there was a decrease in the percentage of cell proliferation by *T. gondii*, demonstrating higher concentrations than those reported by these authors, but still below 100 µg/mL). Teixeira, Paschoalino, de Souza, Rosini, de Lima Junior, Luz, Fajardo Martinez, Alves, Almeida, Damasceno, Silva, Ietta, Barbosa, Ferro and Gomes Martins [44] evaluated the antiparasitic activity of Rottlerin and demonstrated that this compound decreased the intracellular proliferation at concentrations ranging from 0.625 to 20 µM, and resulted in the arrest of the parasites' cell cycle. Despite current efforts against toxoplasmosis, current therapy still has limitations. The present study demonstrated promising results and contributed to the advancement of knowledge in this area, contributing to the future use of propolis as the basis for antiparasitic medications.

Computational approaches have been applied in drug development due to the versatility to discover target and drug candidates [73]. In this context, the use of docking algorithms that evaluates the ligand-receptor binding and complementarity provides valuable insights into the mechanism of action of a given compound [74]. In view of this, we performed molecular docking simulations to evaluate the binding affinity of Guttiferone E and Oblongifolin B upon bacterial and *T. gondii* targets. Upon *S. aureus*, Guttiferone E exhibited the best binding to teichoic acid glycosyltransferase, which is crucial for *S. aureus* evasion of host defenses and considered as a druggable target against methicillin resistant *S. aureus* (MRSA) [75]. Against *L. paracasei*, Guttiferone E demonstrated the greatest binding to the bacterial ribonuclease, which is involved in tRNA maturation by the removal a 3'-trailer from precursor tRNA [76]. On *S. salivarius*, Guttiferone E displayed the best binding to the urease accessory protein, which is required for the production of active ureases through the incorporation of nickel ions into the apoenzyme, and the urea metabolism is thought to inhibit the initiation and progression of



dental caries [77]. Upon *E. faecalis*, Guttiferone E demonstrated the greatest affinity to the bacterial mevalonate diphosphate decarboxylase, which is final enzyme of the mevalonate pathway, crucial for the polyisoprenoid synthesis and bacterial growth [78]. In parallel, against *T. gondii*, the best binding of Guttiferone E and Oblongifolin B, respectively, was found to uracil phosphoribosyltransferase, which is involved in the biosynthesis of nucleotides and amino acids [79] and prolyl tRNA synthetase, which is essential for the binding of charged tRNA molecules into the protein synthesis machinery [80] and are recognized as druggable targets of *T. gondii*. In this sense, our analysis reveals that both Guttiferone E and Oblongifolin B bind to important bacterial and parasitic targets involved in crucial pathways. Although the exact target was not evidenced, our analysis provides valuable insights into the druggability of Guttiferone E and Oblongifolin B against the bacterial and parasitic pathogens.

## 5. Conclusion

The present study demonstrated the antibacterial and antifungal activity of the crude extract and the isolated substances Guttiferone E and Oblongifolin B against bacteria and yeasts that cause endodontic infections. Furthermore, these samples were able to reduce the biomass and number of viable cells in the biofilm produced by these microorganisms, in addition to reducing cell adhesion in sessile cells. The BRP samples evaluated increased the survival of *C. elegans* larvae infected with the oral pathogens included in the study, even after three days of infection. The substances Guttiferone E and Oblongifolin B demonstrated antiparasitic activity against *T. gondii*, significantly reducing the cellular proliferation of these parasites in BeWo cells. The molecular docking results pointed out that Guttiferone E presented the best binding to *S. aureus* teichoic acid glycosyltransferase (tarP) and *L. paracasei* ribonuclease (rnz) and *S. salivarius* urease accessory protein (ureG) and *E. faecalis* mevalonate diphosphate decarboxylase (mvaD). Regarding targets against *T. gondii*, Guttiferone E and Oblongifolin B exhibited the best binding to uracil phosphoribosyltransferase (uprt) and prolyl tRNA synthetase (prs), respectively. These data demonstrate that BRP has antibacterial and antiparasitic activity against pathogens of clinical relevance, and can be used in the future as phyto-medicines.

## **Funding**

This work was supported by Fundação de Amparo a Pesquisa do Estado de Minas Gerais (FAPEMIG - Scholarship grant number 12138) and National Council for Scientific and Technological Development (CNPq) n° 307 974/2019-7.

## **CRediT authorship contribution statement**

**N.B.S.S:** data curation, investigation, methodology and writing. **G.G.C:** data curation, investigation and methodology and writing **S.C.T:** data curation and methodology. **T.A.M.F:** data curation, Research; Methodology. **N.M.C:** data curation, Investigation; Methodology. **A.C.G.J:** formal analysis, validation. **S.R.A:** Formal analysis, Supervision, Validation, Acquisition of financing. **R.C.S.V:** formal analysis, Validation, Acquisition of financing. **J.K.B:** Formal analysis, validation, Acquisition of financing. **E.A.V.F:** data curation, Investigation. **B.F.B:** data curation, Investigation. **M.J.B.S:** data curation, Investigation and statistical analysis. **R.S.S:** data curation, Investigation. **C.H.G.M:** Conceptualization, Formal analysis, Supervision, Validation, Acquisition of financing, Supervision; Validation.

## **Declaration of Competing Interest**

None.

## **Data availability**

Data will be made available on request.

## **Acknowledgement**

The authors would like to thank the Federal University of Uberlândia for all their support, Support, Fundação de Amparo à Pesquisa do Estado de Minas Gerais (FAPEMIG) for granting the scholarship.

**Table 1:** Values of Minimum Inhibitory Concentration (MIC), Minimum Bactericidal Concentration (MBC) and Minimum Fungicide Concentration (MFC) of brazilian red propolis samples against oral pathogens.

<b>Bacteria</b>												
<b>Results in µg/mL</b>												
<b>Samples</b>	<i>Staphylococcus aureus</i> (clinical isolate)		<i>Enterococcus faecalis</i> (ATCC 4082)		<i>Enterococcus faecalis</i> (clinical isolate)		<i>Streptococcus salivarius</i> (ATCC 25975)		<i>Streptococcus salivarius</i> (clinical isolate)		<i>Lactobacillus paracasei</i> (ATCC 11578)	
	<b>MIC</b>	<b>MBC</b>	<b>MIC</b>	<b>MBC</b>	<b>MIC</b>	<b>MBC</b>	<b>MIC</b>	<b>MBC</b>	<b>MIC</b>	<b>MBC</b>	<b>MIC</b>	<b>MBC</b>
Crude extract	200	400	200	400	200	200	200	200	100	400	100	200
Gutiferone E	3.12	12.5	6.25	12.5	6,25	12.5	6,25	12.5	3.12	3.12	3.12	3.12
Oblongifolin B	12.5	50	25	100	25	12.5	12.5	12.5	12.5	12.5	12.5	12.5
Chlorhexidine	0.92	1.84	3.68	7.37	3.68	7.37	0.92	0.92	0.92	1.84	0.92	0.92
<b>Yeasts</b>												
<b>Results in µg/mL</b>												
<b>Samples</b>	<i>Candida albicans</i> (ATCC 28366)		<i>Candida glabrata</i> (ATCC MYA-276)		<i>Candida parapsilosis</i> (ATCC 22019)		<i>Candida Krusei</i> (ATCC 6258)					
	<b>MIC</b>	<b>MFC</b>	<b>MIC</b>	<b>MFC</b>	<b>MIC</b>	<b>MFC</b>	<b>MIC</b>	<b>MFC</b>	<b>MIC</b>	<b>MFC</b>		
Crude extract	46.87	46.87	5.86	46.87	-	-	-	-	-	-		
Gutiferone E	187.5	750	93.7	93.7	-	-	-	-	-	-		
Oblongifolin B	93.75	750	11.72	11.72	-	-	-	-	-	-		
Amphotericin B	-	-	-	-	0.25	0.25	2	2				

MIC range for *Candida parapsilosis* (ATCC 22019): 0.25-1.0 µg/mL and *Candida krusei* (ATCC 6258):0.25-2.0 µg/mL. - Not tested

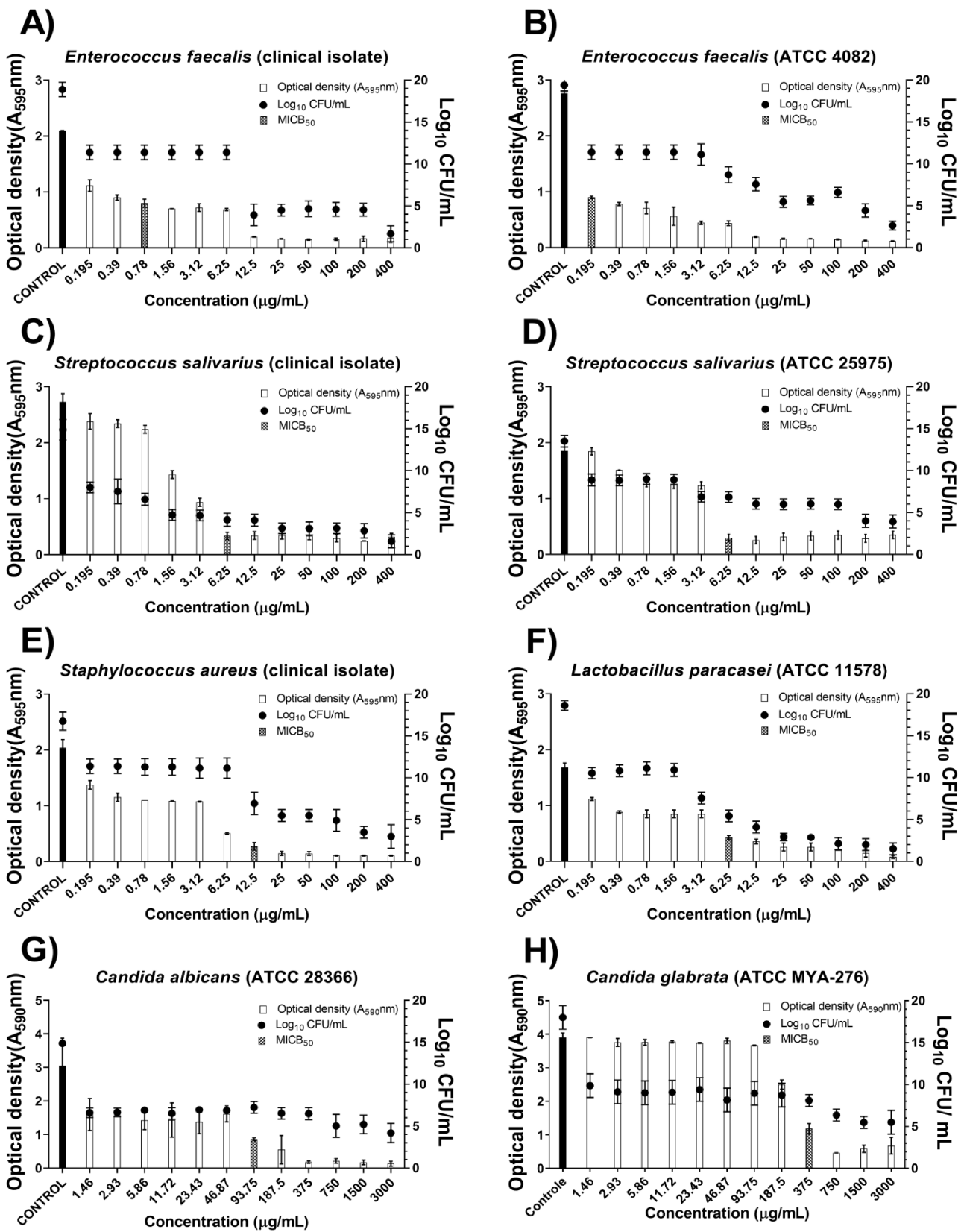
**Table 2:** FICI values of the BRP samples in combination with standard antimicrobials against oral pathogens.

Microorganism	BRP Sample	Antimicrobial	MICa (µg/mL)		MICb (µg/mL)		FIC		FICI	Result
			1	2	1	2	1	2		
<i>Staphylococcus aureus</i> (clinical isolate)	Gutiferone E	Chlorhexidine	3.12	0.92	3.12	0.92	1	1	2	Indifferent
<i>Streptococcus salivarius</i> ATCC (29975)	Gutiferone E	Chlorhexidine	12.5	0.92	6.25	0.92	0.5	1	1.5	Indifferent
<i>Streptococcus salivarius</i> (clinical isolate)	Gutiferone E	Chlorhexidine	6,25	0.92	12.5	0,92	2	1	3	Indifferent
<i>Enterococcus faecalis</i> (ATCC 4082)	Gutiferone E	Chlorhexidine	12,5	3,68	6,25	3,68	0.5	1	1.5	Indifferent
<i>Enterococcus faecalis</i> (clinical isolate)	Gutiferone E	Chlorhexidine	12.5	3,68	12,5	3,68	1	1	2	Indifferent
<i>Lactobacillus paracasei</i> (ATCC 11578)	Gutiferone E	Chlorhexidine	6.25	0.92	12.5	0.92	2	1	3	Indifferent
<i>Candida albicans</i> (ATCC 28366)	Crude extract	Amphotericin B	23,43	0,5	23,43	0,03	1	0,06	1,06	Indifferent
<i>Candida glabrata</i> (ATCC MYA-276)	Crude extract	Amphotericin B	5,86	0,5	5.86	0,5	1	1	2	Indifferent

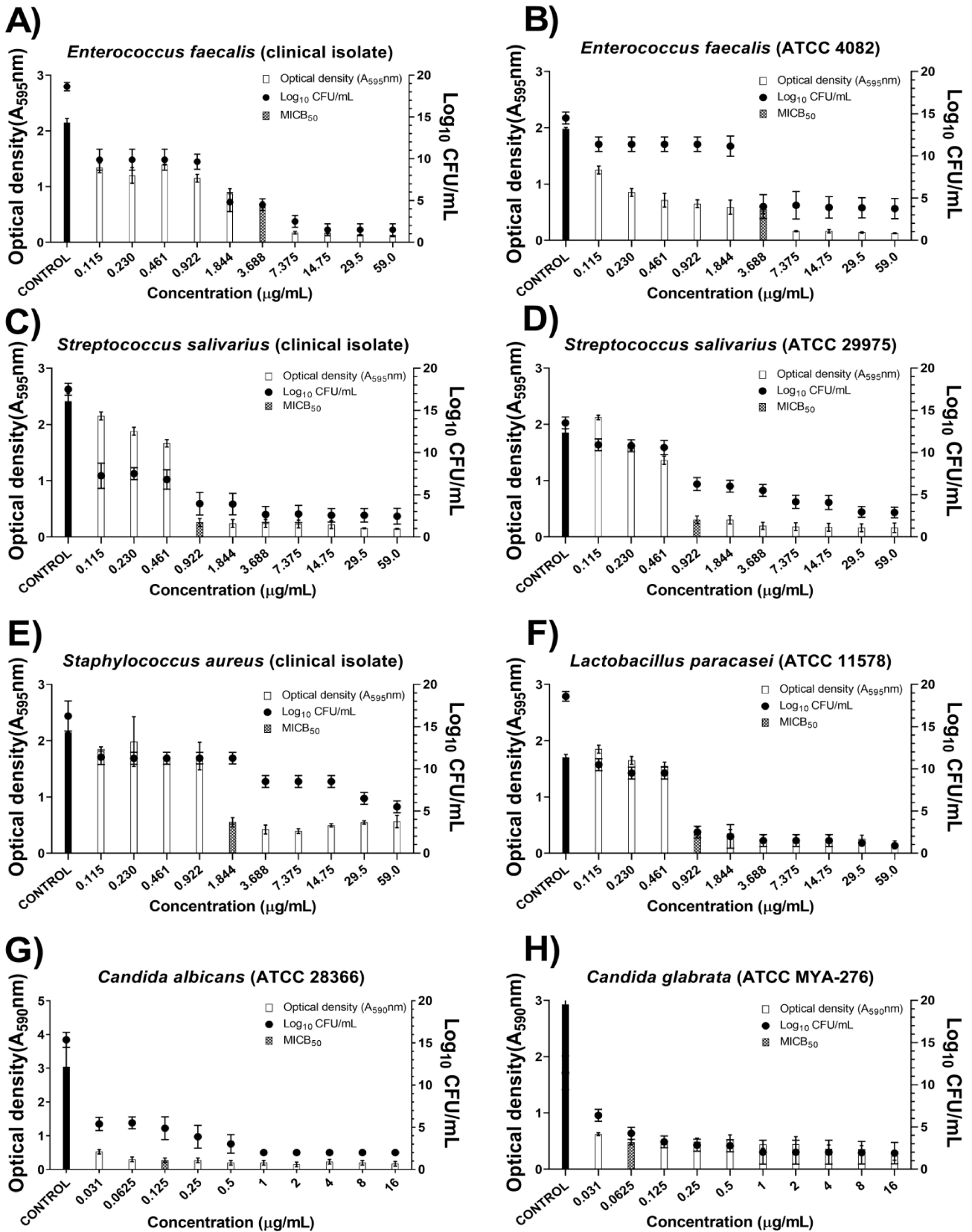
MICa—minimal inhibitory concentration alone. MICb- combined minimum inhibitory concentration. FIC- fractional inhibitory concentration. FICI- fractional inhibitory concentration index. (1)- BRP sample (2)- Antimicrobial FIC = MICb/MICa. FICI = FIC (1) + FIC (2).

**Table 3:** Evaluation of the cytotoxicity of the isolated substances Gutiferone E and Oblongifolin B in BeWo cells infected with *T. gondii*

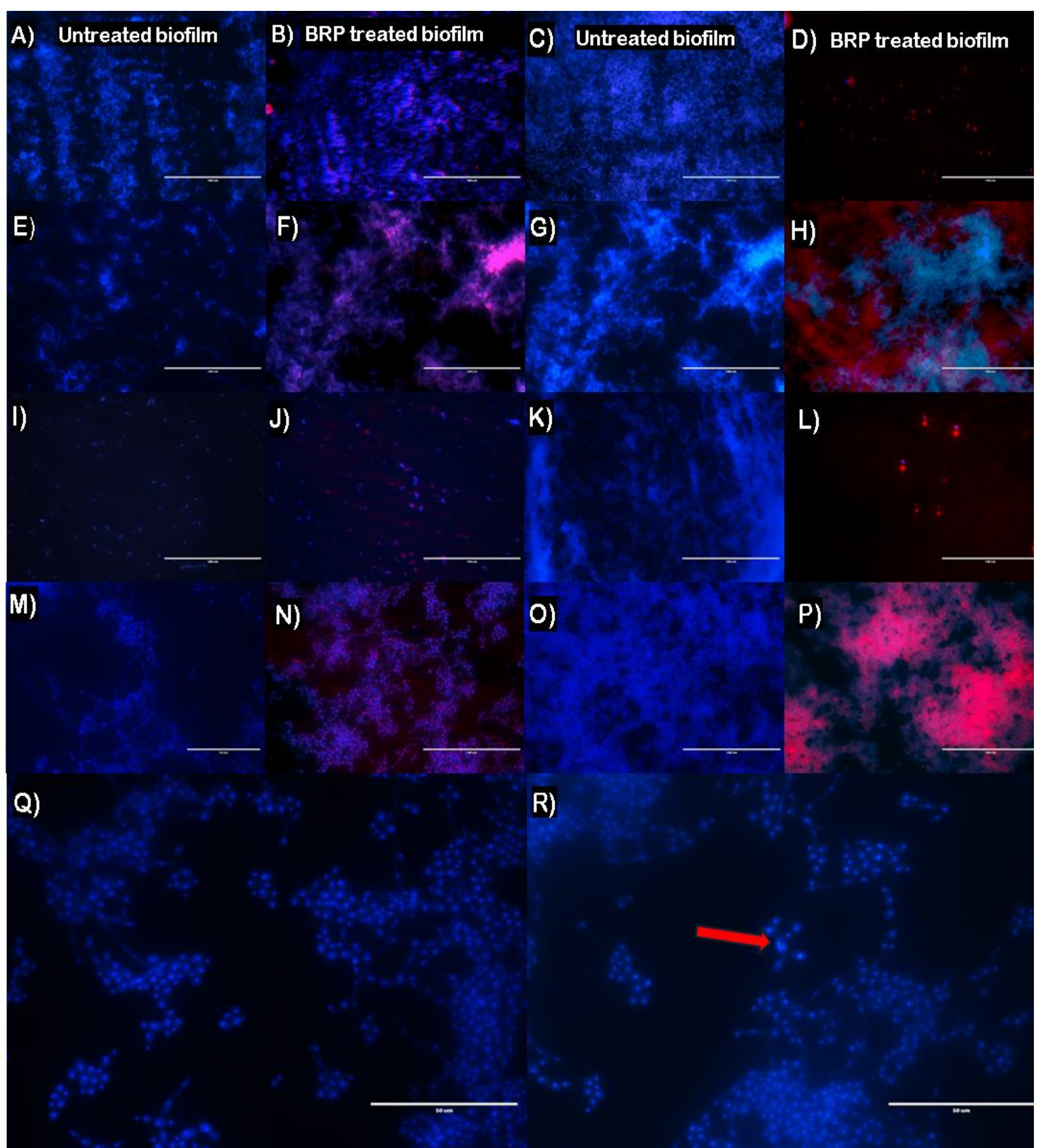
<b>Compounds</b>	<b>CC<sub>50</sub> (µg/mL)</b>	<b>IC<sub>50</sub> (µg/mL)</b>	<b>TI (CC<sub>50</sub>/IC<sub>50</sub>)</b>
<b>Gutiferone E</b>	14.10 ± 0.635	0.27 ± 0.17	52.22
<b>Oblongifolin B</b>	54.08 ± 1.625	2.03 ± 0.21	26.64



**Figure 1:** Antibiofilm activity of Gutiferone E and crude extract against bacteria and yeasts that causes oral infections. **A:** Antibiofilm activity of Gutiferone E against *E. faecalis* (clinical isolate). **B:** Antibiofilm activity of Gutiferone E against *Enterococcus faecalis* (ATCC 4082). **C:** Antibiofilm activity of Gutiferone E against *S. salivarius* (clinical isolate). **D:** Antibiofilm activity of Gutiferone E against *S. salivarius* (ATCC 25975). **E:** Antibiofilm activity of Gutiferone E against *S. aureus* (clinical isolate). **F:** Antibiofilm activity of Gutiferone E against *Lactobacillus paracasei* (ATCC 11578). **G:** Antibiofilm activity of crude extract against *Candida albicans* (ATCC 28366). **H:** Antibiofilm activity of crude extract against *Candida glabrata* (ATCC MYA-276).

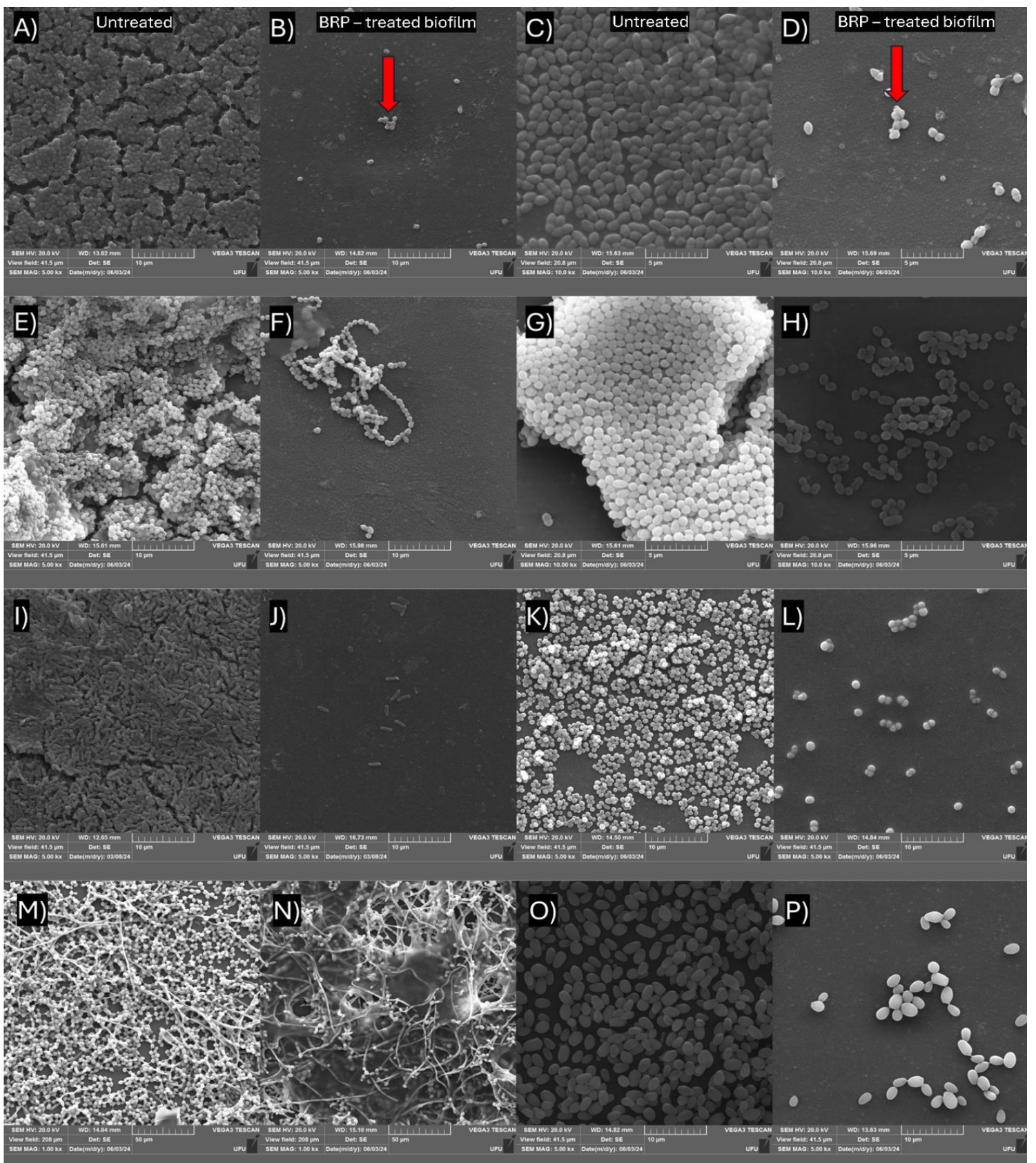


**Figure 2:** Antibiofilm activity of antibiotic and antifungal used as controls against bacteria and yeast included in the study. **A:** Antibiofilm activity of chlorhexidine against *E. faecalis* (clinical isolate). **B:** Antibiofilm activity of chlorhexidine against *Enterococcus faecalis* (ATCC 4082). **C:** Antibiofilm activity of chlorhexidine against *S. salivarius* (clinical isolate). **D:** Antibiofilm activity of chlorhexidine against *S. salivarius* (ATCC 25975). **E:** Antibiofilm activity of chlorhexidine against *S. aureus* (clinical isolate). **F:** Antibiofilm activity of chlorhexidine against *Lactobacillus paracasei* (ATCC 11578). **G:** Antibiofilm activity of amphotericin B against *Candida albicans* (ATCC 28366). **H:** Antibiofilm activity of amphotericin B against *Candida glabrata* (ATCC MYA-276).

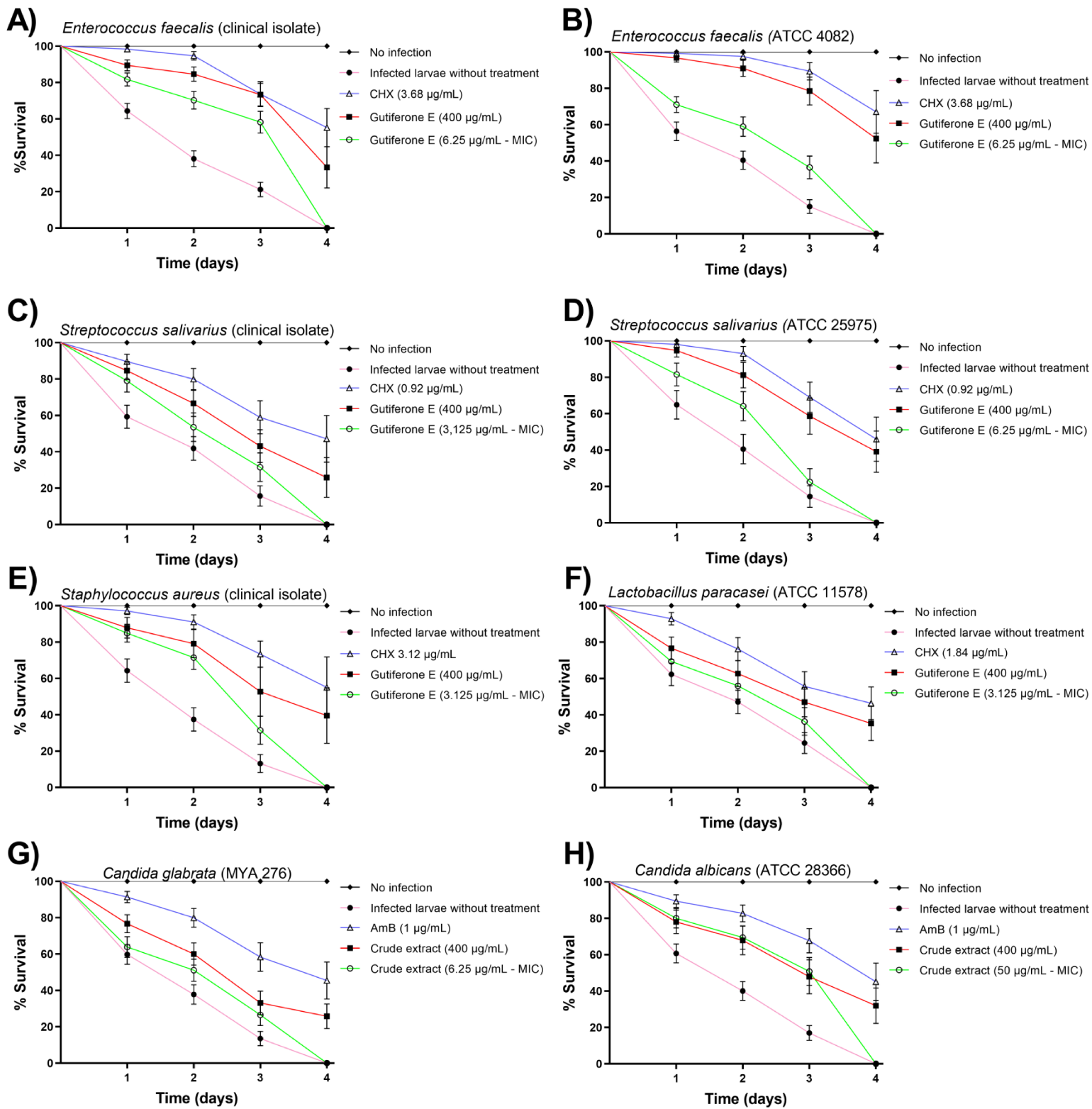


**Figure 3:** Fluorescence electron microscopy images of biofilms of oral pathogens included in the study, untreated and treated with BRP samples at MICB<sub>50</sub> concentration, stained with PI and DAPI solution. **A&B:** Biofilm of *E. faecalis* (ATCC 4082) untreated and treated with Gutiferone E, respectively. **C&D:** Biofilm of *E. faecalis* (clinical isolate) untreated and treated with Gutiferone E, respectively. **E&F:** Biofilm of *S. salivarius* (ATCC 25975) untreated and treated with Gutiferone E, respectively. **G&H:** Biofilm of *S. salivarius* (clinical isolate) untreated and treated with Gutiferone E, respectively. **I&J:** Biofilm of *L. paracasei* (ATCC 11578) untreated and treated with Gutiferone E, respectively. **K&L:** *S. aureus* biofilm (clinical isolate) untreated and treated with Gutiferone E, respectively. **M&N:** Biofilm of *C. albicans* (ATCC 28366) untreated and treated with BRP crude extract, respectively. **O&P:** Biofilm of *C. glabrata* (ATCC MYA-276) untreated and treated with BRP crude extract, respectively. **Q&R:** Biofilm of *C. albicans* (ATCC 28366) showing nuclear fragmentation after treatment with crude extract, indicated by the red arrow.

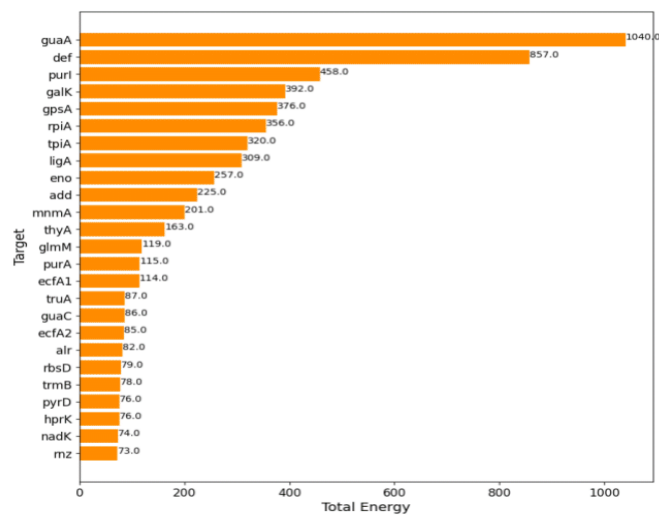
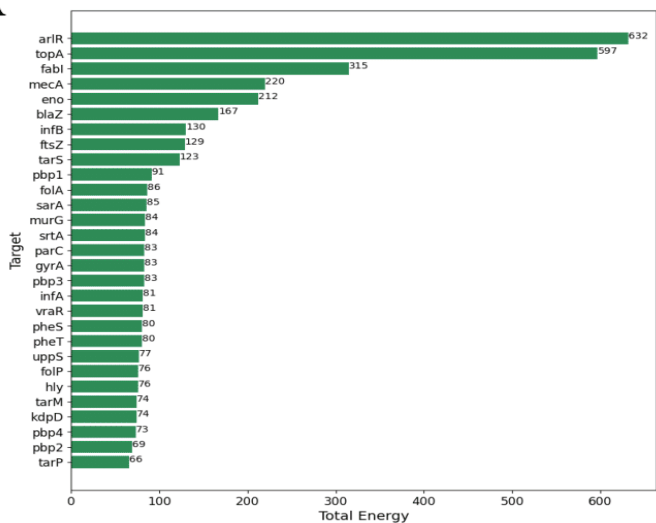
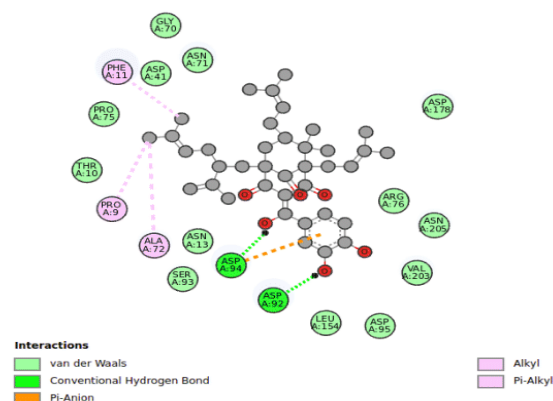
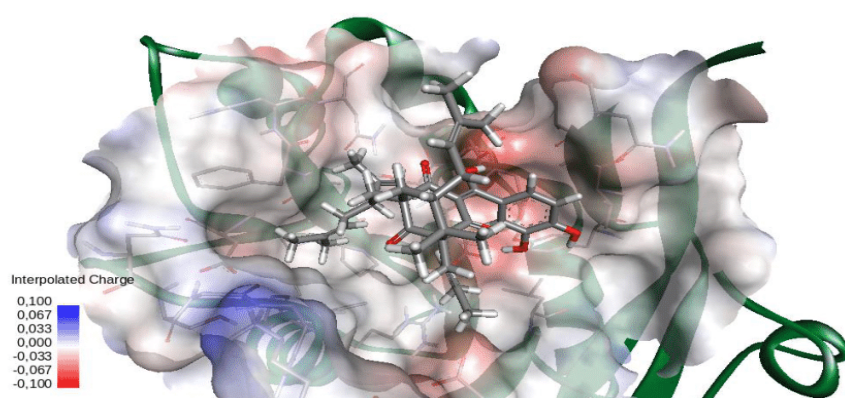
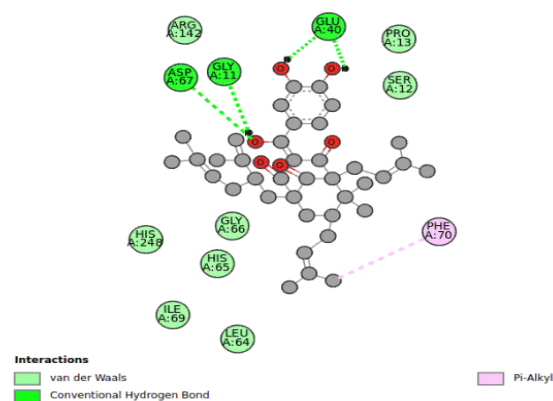
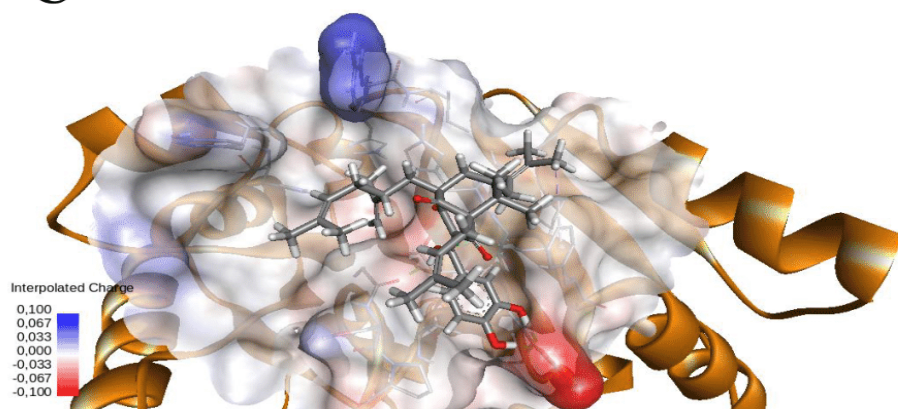




**Figure 4:** Scanning electron microscopy images of biofilms of oral pathogens untreated and treated with BRP samples. **A&B:** Biofilm of *E. faecalis* (ATCC 4082) untreated and treated with Gutiferone E, respectively. The red arrow shows the decrease in cell aggregation and biomass. **C&D:** *E. faecalis* biofilm (clinical isolate) untreated and treated with Gutiferone E, respectively. The red arrow highlights the change in the morphology of bacterial cells after treatment compared to the control. **E&F:** Biofilm of *S. salivarius* (ATCC 25975) untreated and treated with Gutiferone E, respectively. **G&H:** Biofilm of *S. salivarius* (clinical isolate) untreated and treated with Gutiferone E, respectively. **I&J:** Biofilm of *L. paracasei* (ATCC 11578) untreated and treated with Gutiferone E, respectively. **K&L:** *S. aureus* biofilm (clinical isolate) untreated and treated with Gutiferone E, respectively. **M&N:** Biofilm of *C. albicans* (ATCC 28366) untreated and treated with BRP crude extract, respectively. **O&P:** Biofilm of *C. glabrata* (ATCC MYA-276) untreated and treated with BRP crude extract, respectively.



**Figure 5:** Survival curve and concentration response of oral pathogen infection in *C. elegans* larvae. **A)** Larvae infected with *E. faecalis* (clinical isolate) and treated with different concentrations of Gutiferone E. **B)** Larvae infected with *E. faecalis* (ATCC 4082) and treated with different concentrations of Gutiferone E. **C)** Larvae infected with *S. salivarius* (clinical isolate) and treated with different concentrations of Gutiferone E. **D)** Larvae infected with *S. salivarius* (ATCC 25975) and treated with different concentrations of Gutiferone E. **E)** Larvae infected with *S. aureus* (clinical isolate) and treated with different concentrations of Gutiferone E. **F)** Larvae infected with *L. paracasei* (ATCC 11578) and treated with different concentrations of Gutiferone E. **G)** Larvae infected with *C. glabrata* (ATCC MYA-276) and treated with different concentrations of the crude BRP extract. **H)** Larvae infected with *C. albicans* (ATCC 28366) and treated with different concentrations of BRP crude extract. Survival curves were plotted using the Kaplan–Meier method, and survival curves were compared by log-rank test. CHX: Chlorhexidine; AmB: Amphotericin B.

**A****B****C**

**Figure 6.** Molecular docking simulations of Guttiferone E against *S. aureus* and *L. paracasei*. **A)** Binding affinity of Guttiferone E against *S. aureus* (left panel) and *L. paracasei* (right panel) ranked by the total energy. **B)** Best pose prediction of Guttiferone E upon *S. aureus* teichoic acid glycosyltransferase (tarP) colored in green. **C)** Best pose prediction of Guttiferone E against *L. paracasei* ribonuclease (rnz) colored in orange. The target surfaces are represented by the interpolated charge. The hydrophobic interactions, conventional hydrogen bond and carbon-hydrogen bond are colored in pink, green and blue, respectively. The carbon, oxygen and hydrogen atoms are shown in grey, red and black, respectively.

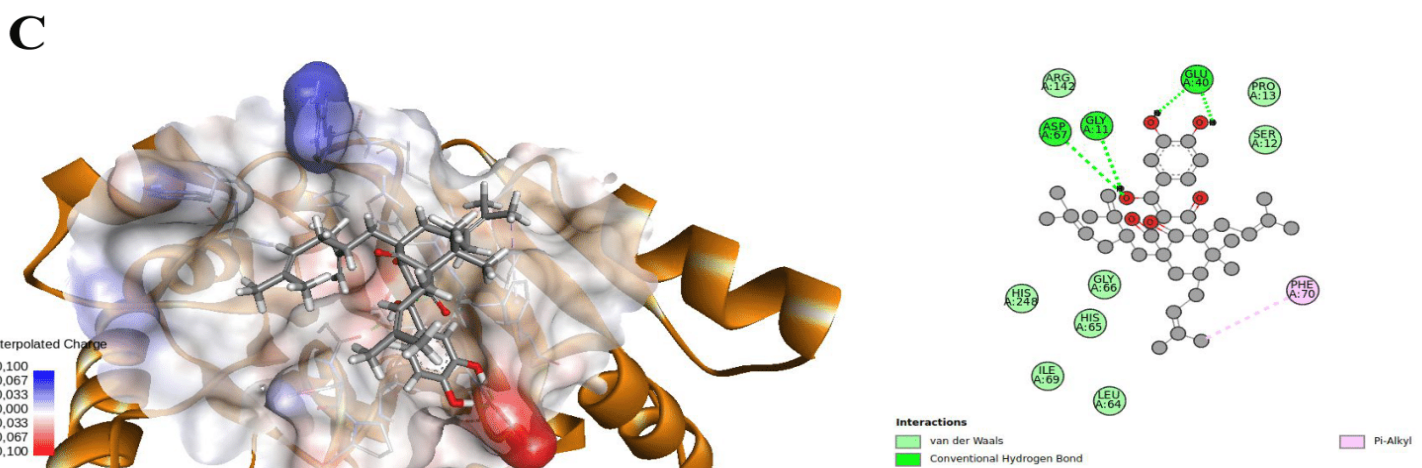
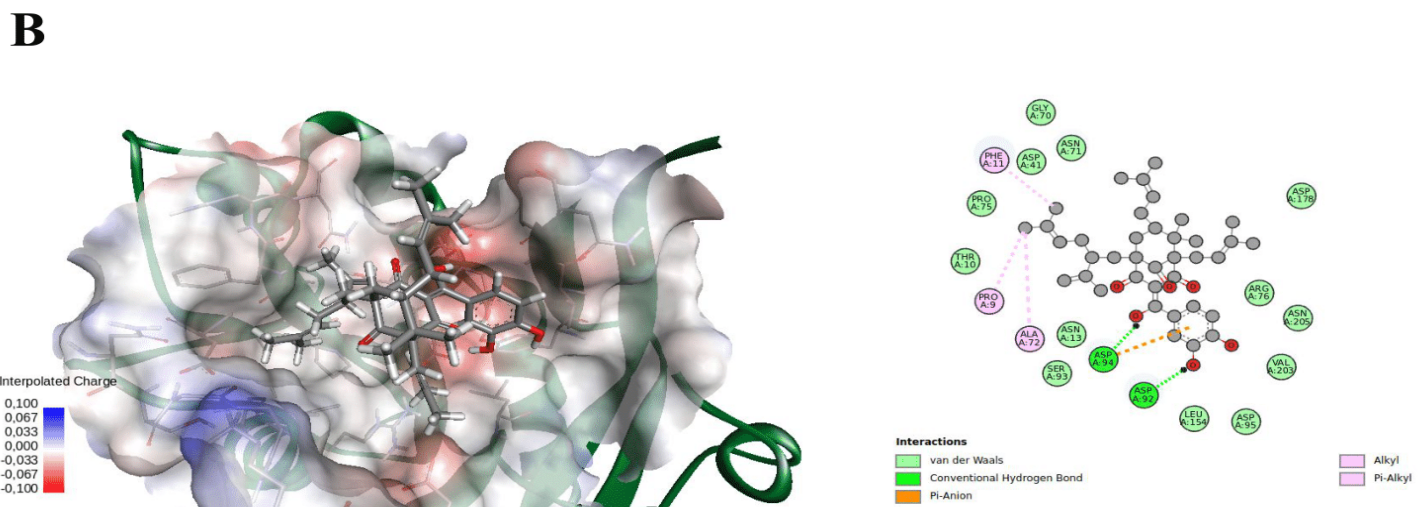
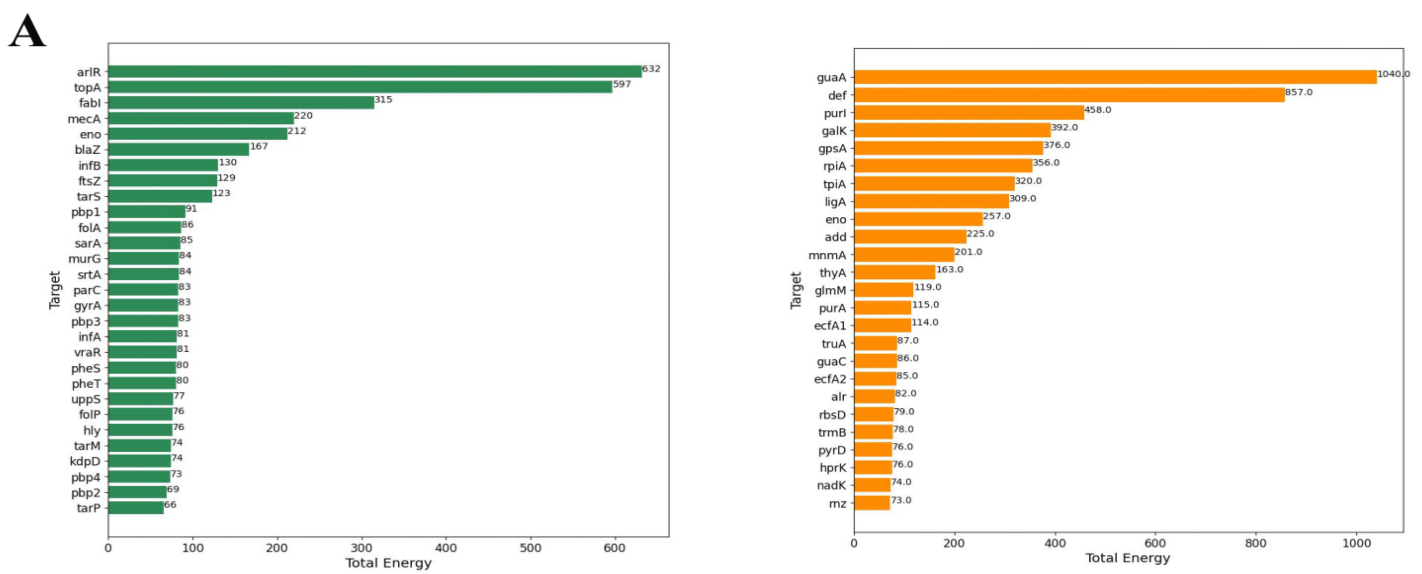
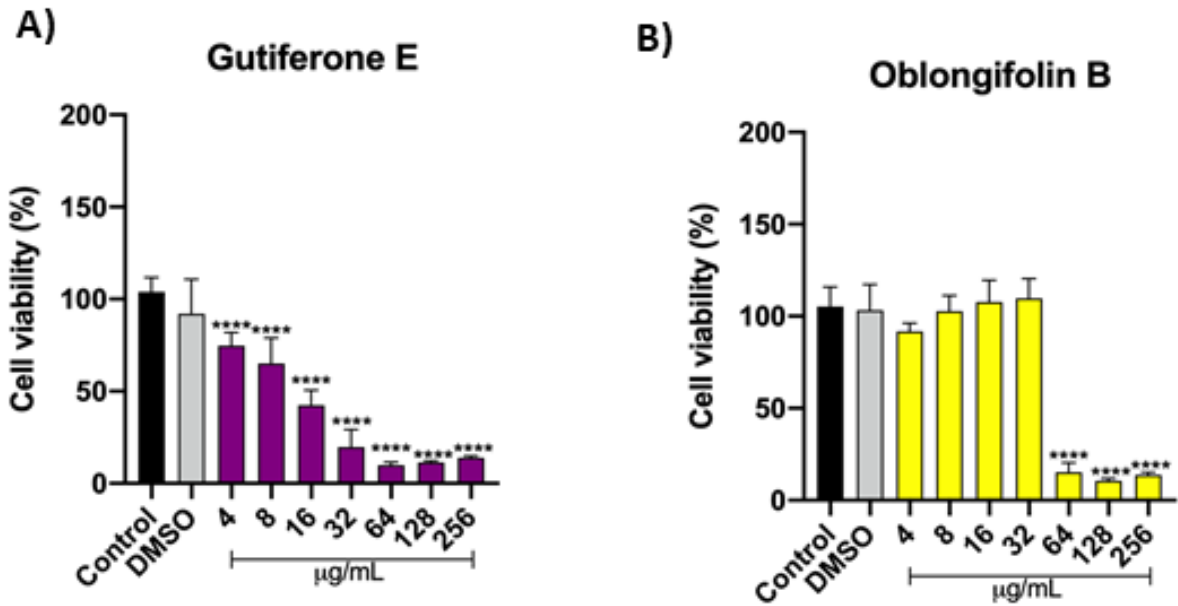
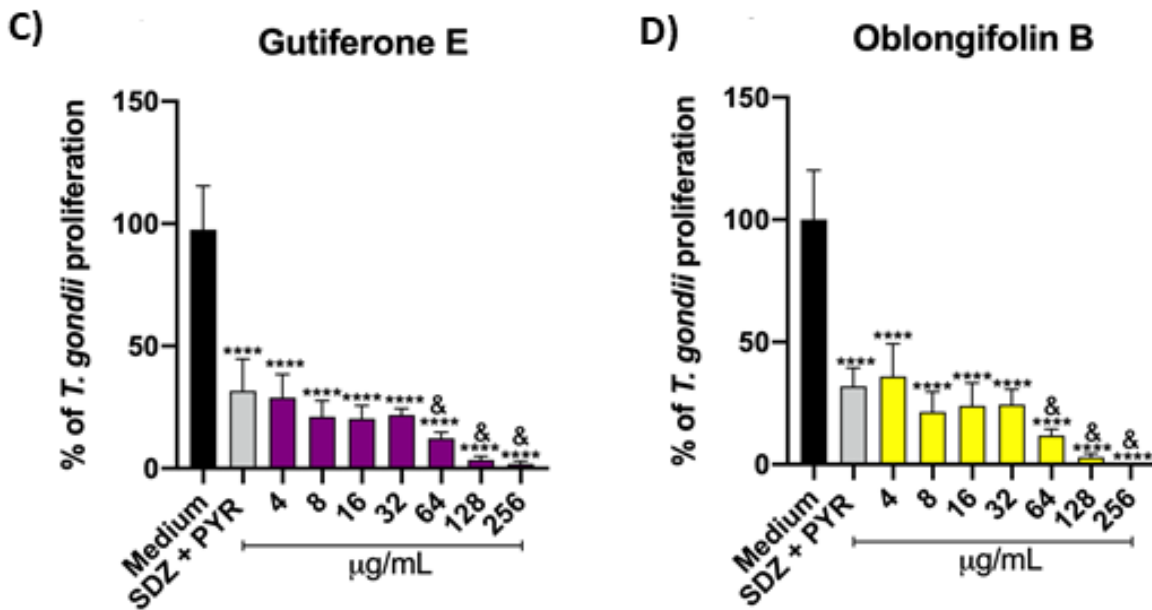


**Figure 7.** Molecular docking simulations of Guttiferone E against *S. salivarius* and *E. faecalis*. **A).** Binding affinity of Guttiferone E against *S. salivarius* (left panel) and *E. faecalis* (right panel) ranked by the total energy. **B).** Best pose prediction of Guttiferone E upon *S. salivarius* teichoic acid urase accessory protein (ureG) colored in magenta. **C).** Best pose prediction of Guttiferone E against *E. faecalis* mevalonate diphosphate decarboxylase (mvaD) colored in blue. The target surfaces are represented by the interpolated charge. The hydrophobic interactions, conventional hydrogen bond and carbon-hydrogen bond are colored in pink, green and blue, respectively. The carbon, oxygen and hydrogen atoms are shown in grey, red and black, respectively.

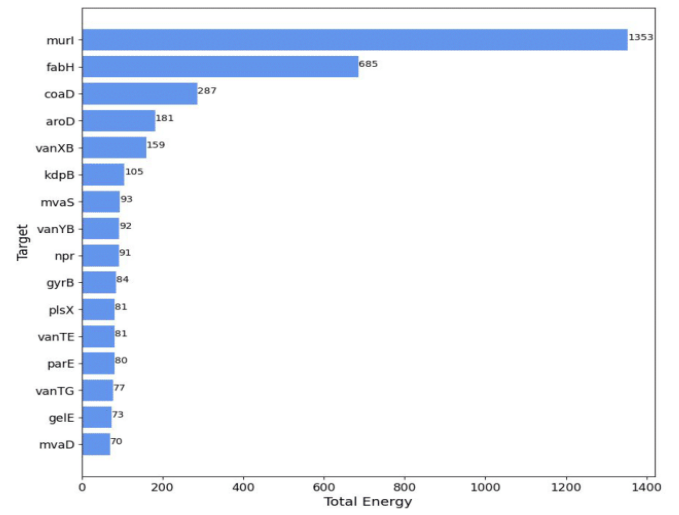
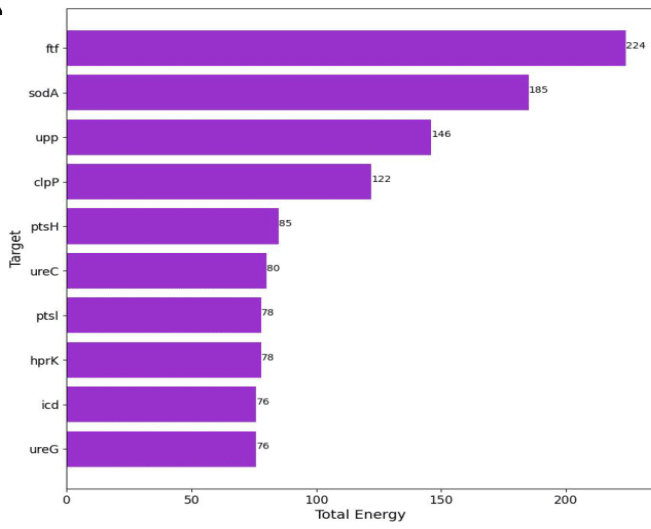
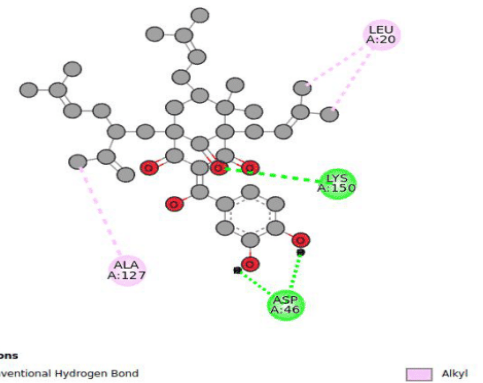
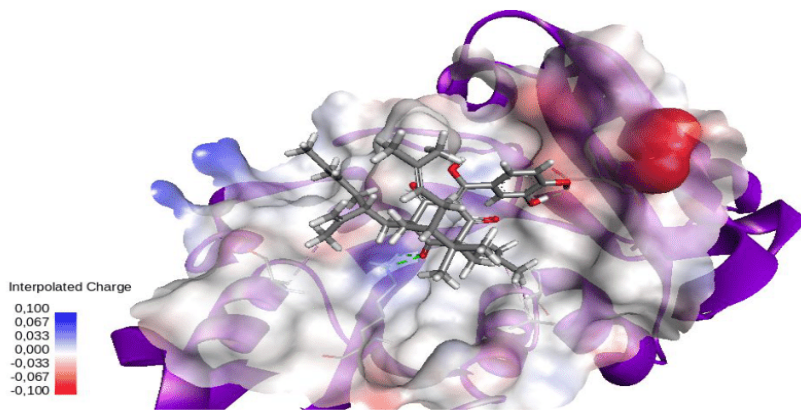
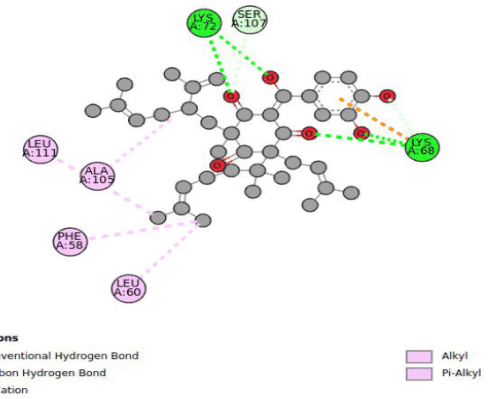
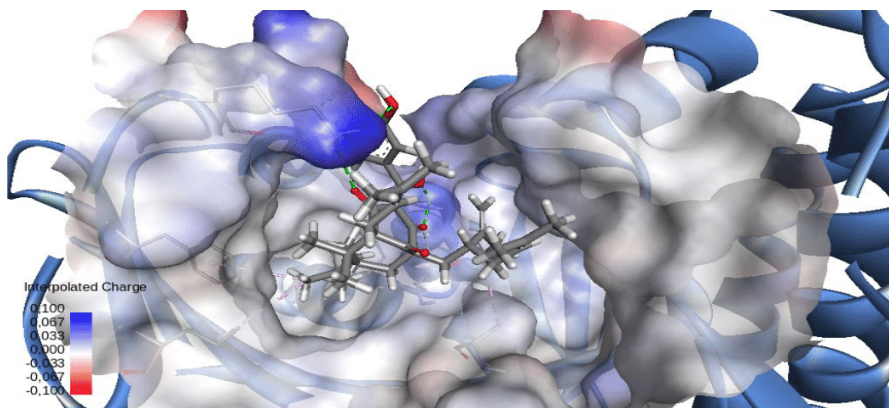
## Cell viability - MTT



## *T. gondii* Intracellular Proliferation Assay ( $\beta$ -galactosidase)



**Figure 8:** Host cell viability and *T. gondii* intracellular proliferation. BeWo cells were treated for 24 h in twofold serial dilutions (ranging from 256 to 4 µg/mL) with (A) Gutiferone E and (B) Oblongifolin B. Also, BeWo cells were treated with culture medium alone (control group), 1.2% DMSO (vehicle of compounds in the concentration of 256 µg/mL). Cell viability was expressed in percentages (Cell viability %), with the absorbance of cells incubated only with culture medium considered to be 100% viability. *T. gondii*-infected BeWo cells were exposed for 24 h to concentrations in twofold serial dilutions of (C) Gutiferone E and (d) Oblongifolin B (ranging from 256 to 4 µg/mL), sulfadiazine plus pyrimethamine (SDZ+PYR; 200 + 8 µg/mL, respectively) or culture medium only (control group - considered as 100% parasite proliferation). Parasite intracellular proliferation was analyzed using a colorimetric  $\beta$ -galactosidase assay and expressed in percentage change in comparison with control (*T. gondii* proliferation %). Data are shown as means  $\pm$  standard error of the means (SEM). \*Comparison between infected/untreated cells and infected/treated cells. &Comparison to SDZ+PYR-infected/treated cells. Significant differences were analyzed using one-way ANOVA test with Dunnett's multiple comparison post-test to evaluate significant differences ( $P < 0.05$ ).

**A****B****C**

**Figure 9.** Molecular docking simulations of Guttiferone E and Oblongifolin B against *T. gondii*. **A).** Binding affinity of Guttiferone E (left panel) and Oblongifolin B (right panel) ranked by the total energy. **B).** Best pose prediction of Guttiferone E upon *T. gondii* uracil phosphoribosyltransferase (uprT) colored in red. **C).** Best pose prediction of Oblongifolin B against *T. gondii* prolyl tRNA synthetase (prs) colored in yellow. The target surfaces are represented by the interpolated charge. The hydrophobic interactions, conventional hydrogen bond and carbon-hydrogen bond are colored in pink, green and blue, respectively. The carbon, oxygen and hydrogen atoms are shown in grey, red and black, respectively.

## References

- [1] P.R. Shankar, Book review: Tackling drug-resistant infections globally, 2016. <https://doi.org/10.4103/2045-080X.186181>.
- [2] Q. Yu, C. Wang, X. Zhang, H. Chen, M.X. Wu, M. Lu, Photochemical Strategies toward Precision Targeting against Multidrug-Resistant Bacterial Infections, *ACS Nano* (2024). <https://doi.org/10.1021/acsnano.3c12714>.
- [3] F. Alghamdi, M. Shakir, The Influence of *Enterococcus faecalis* as a Dental Root Canal Pathogen on Endodontic Treatment: A Systematic Review, *Cureus* 12(3) (2020) e7257. <https://doi.org/10.7759/cureus.7257>.
- [4] J.F. Siqueira, Jr., I.N. Rocas, Present status and future directions: Microbiology of endodontic infections, *Int Endod J* 55 Suppl 3 (2022) 512-530. <https://doi.org/10.1111/iej.13677>.
- [5] G. Mergoni, D. Percudani, G. Lodi, P. Bertani, M. Manfredi, Prevalence of *Candida* Species in Endodontic Infections: Systematic Review and Meta-analysis, *J Endod* 44(11) (2018) 1616-1625 e9. <https://doi.org/10.1016/j.joen.2018.07.016>.
- [6] K. Jhajharia, A. Parolia, K.V. Shetty, L.K. Mehta, Biofilm in endodontics: A review, *J Int Soc Prev Community Dent* 5(1) (2015) 1-12. <https://doi.org/10.4103/2231-0762.151956>.
- [7] A. Babeer, S. Bukhari, R. Alrehaili, B. Karabucak, H. Koo, Microrobotics in endodontics: A perspective, *Int Endod J* (2024). <https://doi.org/10.1111/iej.14082>.
- [8] J.A. Mooney, E.M. Pridgen, R. Manasherob, G. Suh, H.E. Blackwell, A.E. Barron, P.L. Bollyky, S.B. Goodman, D.F. Amanatullah, Periprosthetic bacterial biofilm and quorum sensing, *J Orthop Res* 36(9) (2018) 2331-2339. <https://doi.org/10.1002/jor.24019>.
- [9] J.J. Segura-Egea, J. Martin-Gonzalez, L. Castellanos-Cosano, Endodontic medicine: connections between apical periodontitis and systemic diseases, *Int Endod J* 48(10) (2015) 933-51. <https://doi.org/10.1111/iej.12507>.
- [10] D. Gonzalez-Barrio, A.J. Carpio, L. Preite, M. Miguel-Vicedo, R.M. Estevez-Reboredo, M. Gonzalez-Viadero, R. Barba-Sanchez, R. Calero-Bernal, D. Carmena, I. Fuentes, *Toxoplasma gondii* exposure in wildlife in Spain: Is there any predictable threat for humans and domestic animals?, *Sci Total Environ* 935 (2024) 173290. <https://doi.org/10.1016/j.scitotenv.2024.173290>.
- [11] A.M. Mares, C.I. Varlam, F.P. Iliuta, R.M. Lacau, M.C. Manea, A comprehensive assessment of toxoplasmosis and its dormant impact on psychotic disorders (Review), *Biomed Rep* 20(6) (2024) 86. <https://doi.org/10.3892/br.2024.1774>.
- [12] L. Zaki, M. Olfatifar, F. Ghaffarifar, A.V. Eslahi, A. KarimiPourSaryazdi, A. Taghipour, N. Hamidianfar, M. Badri, P. Jokelainen, Global prevalence of *Toxoplasma gondii* in birds: A systematic review and meta-analysis, *Parasite Epidemiol Control* 25 (2024) e00350. <https://doi.org/10.1016/j.parepi.2024.e00350>.
- [13] O. Fortin, R.L. DeBiasi, S.B. Mulkey, Congenital infectious encephalopathies from the intrapartum period to postnatal life, *Semin Fetal Neonatal Med* (2024) 101526. <https://doi.org/10.1016/j.siny.2024.101526>.
- [14] R.o.A.R. ., J. O'Neill, Grande-Bretagne, Antimicrobial Resistance: Tackling a Crisis for the Health and Wealth of Nations, *Review on Antimicrobial Resistance* 2014.

- [15] M. Montazeri, S. Mehrzadi, M. Sharif, S. Sarvi, A. Tanzifi, S.A. Aghayan, A. Daryani, Drug Resistance in *Toxoplasma gondii*, *Front Microbiol* 9 (2018) 2587. <https://doi.org/10.3389/fmicb.2018.02587>.
- [16] Y. Chi, Y. Wang, M. Ji, Y. Li, H. Zhu, Y. Yan, D. Fu, L. Zou, B. Ren, Natural products from traditional medicine as promising agents targeting at different stages of oral biofilm development, *Front Microbiol* 13 (2022) 955459. <https://doi.org/10.3389/fmicb.2022.955459>.
- [17] I.A. Freires, S.M. de Alencar, P.L. Rosalen, A pharmacological perspective on the use of Brazilian Red Propolis and its isolated compounds against human diseases, *Eur J Med Chem* 110 (2016) 267-79. <https://doi.org/10.1016/j.ejmech.2016.01.033>.
- [18] L.L. Batista, E.A. Campesatto, M.L. Assis, A.P. Barbosa, L.A. Grillo, C.B. Dornelas, Comparative study of topical green and red propolis in the repair of wounds induced in rats, *Rev Col Bras Cir* 39(6) (2012) 515-20. <https://doi.org/10.1590/s0100-69912012000600012>.
- [19] J.A. Aldana-Mejia, G.V. Ccana-Ccapatinta, V.P. Ribeiro, C. Arruda, R.C.S. Veneziani, S.R. Ambrosio, J.K. Bastos, A validated HPLC-UV method for the analysis of phenolic compounds in Brazilian red propolis and *Dalbergia ecastaphyllum*, *J Pharm Biomed Anal* 198 (2021) 114029. <https://doi.org/10.1016/j.jpba.2021.114029>.
- [20] CLSI, *Methods for Dilution Antimicrobial Susceptibility Tests for Bacteria That Grow Aerobically*, Wayne, PA: Clinical and Laboratory Standards Institute (2018).
- [21] S.D. Sarker, L. Nahar, Y. Kumarasamy, Microtitre plate-based antibacterial assay incorporating resazurin as an indicator of cell growth, and its application in the *in vitro* antibacterial screening of phytochemicals, *Methods* 42(4) (2007) 321-4. <https://doi.org/10.1016/j.ymeth.2007.01.006>.
- [22] CLSI, *Performance standards for antifungal susceptibility testing of yeasts*. CLSI supplement M60, Wayne, PA: Clinical and Laboratory Standards Institute (2017).
- [23] A. Nayak, B.R. Sowmya, H. Gandla, V. Kottrashetti, P. Ingalagi, V.S.C. Srinivas, Determination and comparison of antimicrobial activity of aqueous and ethanolic extracts of *Amorphophallus paeoniifolius* on periodontal pathogens: An *in vitro* study, *J Indian Soc Periodontol* 27(1) (2023) 40-44. [https://doi.org/10.4103%2Fjisp.jisp\\_182\\_22](https://doi.org/10.4103%2Fjisp.jisp_182_22).
- [24] Z.N. Siddiqui, F. Farooq, T.M. Musthafa, A. Ahmad, A.U.J.J.o.S.C.S. Khan, Synthesis, characterization and antimicrobial evaluation of novel halopyrazole derivatives, 17(2) (2013) 237-243. <https://doi.org/10.1016/j.jscs.2011.03.016>.
- [25] F. Iten, R. Saller, G. Abel, J. Reichling, Additive antimicrobial [corrected] effects of the active components of the essential oil of *Thymus vulgaris*--chemotype carvacrol, *Planta Med* 75(11) (2009) 1231-6. <https://doi.org/10.1055/s-0029-1185541>.
- [26] S. Stepanovic, D. Vukovic, V. Hola, G. Di Bonaventura, S. Djukic, I. Cirkovic, F. Ruzicka, Quantification of biofilm in microtiter plates: overview of testing conditions and practical recommendations for assessment of biofilm production by staphylococci, *APMIS* 115(8) (2007) 891-9. [https://doi.org/10.1111/j.1600-0463.2007.apm\\_630.x](https://doi.org/10.1111/j.1600-0463.2007.apm_630.x).
- [27] L.J. Marcos-Zambrano, P. Escribano, E. Bouza, J. Guinea, Production of biofilm by *Candida* and non-*Candida* spp. isolates causing fungemia: comparison of biomass production and metabolic activity and development of cut-off points, *Int J Med Microbiol* 304(8) (2014) 1192-8. <https://doi.org/10.1016/j.ijmm.2014.08.012>.



- [28] G.X. Wei, A.N. Campagna, L.A. Bobek, Effect of MUC7 peptides on the growth of bacteria and on *Streptococcus mutans* biofilm, *J Antimicrob Chemother* 57(6) (2006) 1100-9. <https://doi.org/10.1093/jac/dkl120>.
- [29] J.J. Harrison, R.J. Turner, H. Ceri, High-throughput metal susceptibility testing of microbial biofilms, *BMC Microbiol* 5 (2005) 53. <https://doi.org/10.1186/1471-2180-5-53>.
- [30] S.C. Williams, Y. Hong, D.C.A. Danavall, M.H. Howard-Jones, D. Gibson, M.E. Frischer, P.G. Verity, Distinguishing between living and nonliving bacteria: Evaluation of the vital stain propidium iodide and its combined use with molecular probes in aquatic samples, *Journal of Microbiological Methods* 32(3) (1998) 225-236. [https://doi.org/10.1016/S0167-7012\(98\)00014-1](https://doi.org/10.1016/S0167-7012(98)00014-1).
- [31] R.T. Melo, E.P. Mendonca, G.P. Monteiro, M.C. Siqueira, C.B. Pereira, P. Peres, H. Fernandez, D.A. Rossi, Intrinsic and Extrinsic Aspects on *Campylobacter jejuni* Biofilms, *Front Microbiol* 8 (2017) 1332. <https://doi.org/10.3389/fmicb.2017.01332>.
- [32] T.I. Moy, A.L. Conery, J. Larkins-Ford, G. Wu, R. Mazitschek, G. Casadei, K. Lewis, A.E. Carpenter, F.M. Ausubel, High-throughput screen for novel antimicrobials using a whole animal infection model, *ACS Chem Biol* 4(7) (2009) 527-33. <https://doi.org/10.1021/cb900084v>.
- [33] J.L. Singulani, L. Scorzoni, P.C. Gomes, A.C. Nazare, C.R. Polaquini, L.O. Regasini, A.M. Fusco-Almeida, M.J.S. Mendes-Giannini, Activity of gallic acid and its ester derivatives in *Caenorhabditis elegans* and zebrafish (*Danio rerio*) models, *Future Med Chem* 9(16) (2017) 1863-1872. <https://doi.org/10.4155%2Ffmc-2017-0096>.
- [34] J. Jumper, R. Evans, A. Pritzel, T. Green, M. Figurnov, O. Ronneberger, K. Tunyasuvunakool, R. Bates, A. Zidek, A. Potapenko, A. Bridgland, C. Meyer, S.A.A. Kohl, A.J. Ballard, A. Cowie, B. Romera-Paredes, S. Nikolov, R. Jain, J. Adler, T. Back, S. Petersen, D. Reiman, E. Clancy, M. Zielinski, M. Steinegger, M. Pacholska, T. Berghammer, S. Bodenstein, D. Silver, O. Vinyals, A.W. Senior, K. Kavukcuoglu, P. Kohli, D. Hassabis, Highly accurate protein structure prediction with AlphaFold, *Nature* 596(7873) (2021) 583-589. <https://doi.org/10.1038/s41586-021-03819-2>.
- [35] H.M. Berman, J. Westbrook, Z. Feng, G. Gilliland, T.N. Bhat, H. Weissig, I.N. Shindyalov, P.E. Bourne, The Protein Data Bank, *Nucleic Acids Res* 28(1) (2000) 235-42. <https://doi.org/10.1093/nar/28.1.235>.
- [36] S. Kim, J. Chen, T. Cheng, A. Gindulyte, J. He, S. He, Q. Li, B.A. Shoemaker, P.A. Thiessen, B. Yu, L. Zaslavsky, J. Zhang, E.E. Bolton, PubChem 2023 update, *Nucleic Acids Res* 51(D1) (2023) D1373-D1380. <https://doi.org/10.1093/nar/gkac956>.
- [37] I.A. Guedes, A.M.S. Barreto, D. Marinho, E. Krempser, M.A. Kuenemann, O. Sperandio, L.E. Dardenne, M.A. Miteva, New machine learning and physics-based scoring functions for drug discovery, *Sci Rep* 11(1) (2021) 3198. <https://doi.org/10.1038/s41598-021-82410-1>.
- [38] P. Dubois, Djangé Me, *Computing in Science and Engineering* 9(1) (2007) 96-97. <https://doi.org/10.1109/MM.2022.3160258>.
- [39] W. McKinney, *Data Structures for Statistical Computing in Python. Proceedings of the 9th Python in Science Conference, 2010*, pp. 56-61.
- [40] S.C. Teixeira, G. de Souza, B.C. Borges, T.E. de Araujo, A.M. Rosini, F.A. Aguila, S.R. Ambrosio, R.C.S. Veneziani, J.K. Bastos, M.J.B. Silva, C.H.G. Martins, B. de Freitas Barbosa, E.A.V. Ferro, *Copaifera* spp. oleoresins impair *Toxoplasma gondii* infection in both human trophoblastic cells and human placental explants, *Sci Rep* 10(1) (2020) 15158. <https://doi.org/10.1038/s41598-020-72230-0>.

- [41] B.F. Barbosa, J.B. Lopes-Maria, A.O. Gomes, M.B. Angeloni, A.S. Castro, P.S. Franco, M.L. Fermino, M.C. Roque-Barreira, F. Ietta, O.A. Martins-Filho, D.A. Silva, J.R. Mineo, E.A. Ferro, IL10, TGF beta1, and IFN gamma modulate intracellular signaling pathways and cytokine production to control *Toxoplasma gondii* infection in BeWo trophoblast cells, *Biol Reprod* 92(3) (2015) 82. <https://doi.org/10.1095/biolreprod.114.124115>.
- [42] T. Mosmann, Rapid colorimetric assay for cellular growth and survival: application to proliferation and cytotoxicity assays, *J Immunol Methods* 65(1-2) (1983) 55-63. [https://doi.org/10.1016/0022-1759\(83\)90303-4](https://doi.org/10.1016/0022-1759(83)90303-4).
- [43] R.J. da Silva, A.O. Gomes, P.S. Franco, A.S. Pereira, I.C.B. Milian, M. Ribeiro, P. Fiorenzani, M.C. Dos Santos, J.R. Mineo, N.M. da Silva, E.A.V. Ferro, B. de Freitas Barbosa, Enrofloxacin and Toltrazuril Are Able to Reduce *Toxoplasma gondii* Growth in Human BeWo Trophoblastic Cells and Villous Explants from Human Third Trimester Pregnancy, *Front Cell Infect Microbiol* 7 (2017) 340. <https://doi.org/10.3389/fcimb.2017.00340>.
- [44] S.C. Teixeira, M. Paschoalino, G. de Souza, A.M. Rosini, J.P. de Lima Junior, L.C. Luz, A.F. Fajardo Martinez, R.N. Alves, M.P.O. Almeida, J.L. Damasceno, M.J.B. Silva, F. Ietta, B.F. Barbosa, E.A.V. Ferro, C.H. Gomes Martins, Rottlerin impairs early and late steps of *Toxoplasma gondii* infection in human trophoblast cells and villous explants, *Chem Biol Interact* (2023) 110716. <https://doi.org/10.1016/j.cbi.2023.110716>.
- [45] G.V. Ccana-Ccapatinta, J.A.A. Mejia, M.H. Tanimoto, M. Groppo, J. Carvalho, J.K. Bastos, *Dalbergia ecastaphyllum* (L.) Taub. and *Symphonia globulifera* L.f.: The Botanical Sources of Isoflavonoids and Benzophenones in Brazilian Red Propolis, *Molecules* 25(9) (2020). <https://doi.org/10.3390/molecules25092060>.
- [46] N.B.S. Silva, J.H. de Souza, M.B. Santiago, J.R. da Silva Aguiar, D.O.S. Martins, R.A. da Silva, I. de Andrade Santos, J.A. Aldana-Mejia, A.C.G. Jardim, R. Dos Santos Pedroso, S.R. Ambrosio, R.C.S. Veneziani, J.K. Bastos, R.H. Pires, C.H.G. Martins, Potential *in vitro* anti-periodontopathogenic, anti-Chikungunya activities and *in vivo* toxicity of Brazilian red propolis, *Sci Rep* 12(1) (2022) 21165. <https://doi.org/10.1038/s41598-022-24776-4>.
- [47] J.L. Rios, M.C. Recio, Medicinal plants and antimicrobial activity, *J Ethnopharmacol* 100(1-2) (2005) 80-4. <https://doi.org/10.1016/j.jep.2005.04.025>.
- [48] L.C. Rufatto, D.A. dos Santos, F. Marinho, J.A.P. Henriques, M. Roesch Ely, S. Moura, Red propolis: Chemical composition and pharmacological activity, *Asian Pacific Journal of Tropical Biomedicine* 7(7) (2017) 591-598. <https://doi.org/10.1016/j.apjtb.2017.06.009>.
- [49] B. Trusheva, M. Popova, V. Bankova, S. Simova, M.C. Marcucci, P.L. Miorin, F. da Rocha Pasin, I. Tsvetkova, Bioactive constituents of brazilian red propolis, *Evid Based Complement Alternat Med* 3(2) (2006) 249-54. <https://doi.org/10.1093/ecam/nel006>.
- [50] J. Reynaud, D. Guilet, R. Terreux, M. Lussignol, N. Walchshofer, Isoflavonoids in non-leguminous families: an update, *Nat Prod Rep* 22(4) (2005) 504-15. <https://doi.org/10.1039/b416248j>.
- [51] M. Conceicao, F.P. Beserra, J.A. Aldana Mejia, G.R. Caldas, M.H. Tanimoto, A.M. Luzenti, P.D.M. Gaspari, N.D. Evans, J.K. Bastos, C.H. Pellizzon, Guttiferones: An insight into occurrence, biosynthesis, and their broad spectrum of pharmacological activities, *Chem Biol Interact* 370 (2023) 110313. <https://doi.org/10.1016/j.cbi.2022.110313>.
- [52] M.L. Martins, A.S.N. Monteiro, J.E.C. Guimaraes, M. Guimaraes, R.F. da Silva, L.M. Cabral, A. Farah, J. dePaula, M.T.V. Romanos, L.C. Maia, Y.W. Cavalcanti, A. Fonseca-Goncalves, Cytotoxic and

antibacterial effect of a red propolis mouthwash, with or without fluoride, on the growth of a cariogenic biofilm, *Arch Oral Biol* 107 (2019) 104512. <https://doi.org/10.1016/j.archoralbio.2019.104512>.

[53] M.S.N. Regueira, S.R. Tintino, A.R.P. da Silva, M.D.S. Costa, A.A. Boligon, E.F.F. Matias, V. de Queiroz Balbino, I.R.A. Menezes, H.D. Melo Coutinho, Seasonal variation of Brazilian red propolis: Antibacterial activity, synergistic effect and phytochemical screening, *Food Chem Toxicol* 107(Pt B) (2017) 572-580. <https://doi.org/10.1016/j.fct.2017.03.052>.

[54] A.R. Sokolonski, M.S. Fonseca, B.A.S. Machado, K.R. Deegan, R.P.C. Araujo, M.A. Umsza-Guez, R. Meyer, R.W. Portela, Activity of antifungal drugs and Brazilian red and green propolis extracted with different methodologies against oral isolates of *Candida* spp, *BMC Complement Med Ther* 21(1) (2021) 286. <https://doi.org/10.1186/s12906-021-03445-5>.

[55] S. Er-Rahmani, B. Errabiti, A. Matencio, F. Trotta, H. Latrache, S.I. Koraichi, S. Elabed, Plant-derived bioactive compounds for the inhibition of biofilm formation: a comprehensive review, *Environ Sci Pollut Res Int* 31(24) (2024) 34859-34880. <https://doi.org/10.1007/s11356-024-33532-2>.

[56] M.M. Elashiry, B.E. Bergeron, F.R. Tay, *Enterococcus faecalis* in secondary apical periodontitis: Mechanisms of bacterial survival and disease persistence, *Microb Pathog* 183 (2023) 106337. <https://doi.org/10.1016/j.micpath.2023.106337>.

[57] A. Parolia, H. Kumar, S. Ramamurthy, T. Madheswaran, F. Davamani, M.R. Pichika, K.K. Mak, A.S. Fawzy, U. Daood, A. Pau, Effect of Propolis Nanoparticles against *Enterococcus faecalis* Biofilm in the Root Canal, *Molecules* 26(3) (2021). <https://doi.org/10.3390/molecules26030715>.

[58] A.E. Akca, G. Akca, F.T. Topcu, E. Macit, L. Pikdoken, I.S. Ozgen, The Comparative Evaluation of the Antimicrobial Effect of Propolis with Chlorhexidine against Oral Pathogens: An *In Vitro* Study, *Biomed Res Int* 2016 (2016) 3627463. <https://doi.org/10.1155/2016/3627463>.

[59] M. Rosenberg, N.F. Azevedo, A. Ivask, Propidium iodide staining underestimates viability of adherent bacterial cells, *Sci Rep* 9(1) (2019) 6483. <https://doi.org/10.1038/s41598-019-42906-3>.

[60] R. Murugan, S. Subramaniyan, S. Priya, C. Ragavendran, M.V. Arasu, N.A. Al-Dhabi, K.C. Choi, A. Guru, J. Arockiaraj, Bacterial clearance and anti-inflammatory effect of Withaferin A against human pathogen of *Staphylococcus aureus* in infected zebrafish, *Aquat Toxicol* 260 (2023) 106578. <https://doi.org/10.1016/j.aquatox.2023.106578>.

[61] B. Hao, S. Cheng, C.J. Clancy, M.H. Nguyen, Caspofungin kills *Candida albicans* by causing both cellular apoptosis and necrosis, *Antimicrob Agents Chemother* 57(1) (2013) 326-32. <https://doi.org/10.1128/aac.01366-12>.

[62] M. Moryl, A. Palatynska-Ulatowska, A. Maszewska, I. Grzejdziak, S. Dias de Oliveira, M.C. Pradebon, L. Steier, A. Rozalski, J.A. Poli de Figueiredo, Benefits and Challenges of the Use of Two Novel vB\_Efa29212\_2e and vB\_Efa29212\_3e Bacteriophages in Biocontrol of the Root Canal *Enterococcus faecalis* Infections, *J Clin Med* 11(21) (2022). <https://doi.org/10.3390/jcm11216494>.

[63] A. Lange, A. Matuszewski, M. Kutwin, A. Ostrowska, S. Jaworski, Farnesol and Selected Nanoparticles (Silver, Gold, Copper, and Zinc Oxide) as Effective Agents Against Biofilms Formed by Pathogenic Microorganisms, *Nanotechnol Sci Appl* 17 (2024) 107-125. <https://doi.org/10.2147/nsa.s457124>.

[64] N.B.S. Silva, J.H. de Souza, M.B. Santiago, J.R. da Silva Aguiar, D.O.S. Martins, R.A. da Silva, I. de Andrade Santos, J.A. Aldana-Mejía, A.C.G. Jardim, R.J.S.R. dos Santos Pedroso, Potential *in vitro*

anti-periodontopathogenic, anti-Chikungunya activities and *in vivo* toxicity of Brazilian red propolis, 12(1) (2022) 21165. <https://doi.org/10.1038/s41598-022-24776-4>.

[65] W. Ma, J. Yue, S. Liang, M. Gao, X. Wang, N. Cui, H. Li, D. Zhi, Realgar increases defenses against infection by *Enterococcus faecalis* in *Caenorhabditis elegans*, *J Ethnopharmacol* 268 (2021) 113559. <https://doi.org/10.1016/j.jep.2020.113559>.

[66] D. Viszwapriya, G.A. Subramenium, U. Prithika, K. Balamurugan, S.K. Pandian, Betulin inhibits virulence and biofilm of *Streptococcus pyogenes* by suppressing ropB core regulon, sagA and dltA, *Pathog Dis* 74(7) (2016). <https://doi.org/10.1093/femspd/ftw088>.

[67] J. Qi, X. Zhang, X. Guo, Y. Yang, X. Fan, Y. Han, Y. Liu, Evaluation of the *in vitro* and *in vivo* antimicrobial activity of alkaloids prepared from *Chelidonium majus* L. using MRSA- infected *C. elegans* as a model host, *Fitoterapia* 175 (2024) 105944. <https://doi.org/10.1016/j.fitote.2024.105944>.

[68] S. Muthamil, B. Balasubramaniam, K. Balamurugan, S.K. Pandian, Synergistic Effect of Quinic Acid Derived From *Syzygium cumini* and Undecanoic Acid Against *Candida* spp. Biofilm and Virulence, *Front Microbiol* 9 (2018) 2835. <https://doi.org/10.3389/fmicb.2018.02835>.

[69] A. Hernando-Ortiz, E. Mateo, M. Ortega-Riveros, I. De-la-Pinta, G. Quindos, E. Eraso, *Caenorhabditis elegans* as a Model System To Assess *Candida glabrata*, *Candida nivariensis*, and *Candida bracarensis* Virulence and Antifungal Efficacy, *Antimicrob Agents Chemother* 64(10) (2020). <https://doi.org/10.1128/aac.00824-20>.

[70] S. Kishimoto, M. Nono, Y. Makizaki, Y. Tanaka, H. Ohno, E. Nishida, M. Uno, *Lactobacillus paracasei* subsp. *paracasei* 2004 improves health and lifespan in *Caenorhabditis elegans*, *Sci Rep* 14(1) (2024) 10453. <https://doi.org/10.1038/s41598-024-60580-y>.

[71] M.W. Black, J.C. Boothroyd, Lytic cycle of *Toxoplasma gondii*, *Microbiol Mol Biol Rev* 64(3) (2000) 607-23. <https://doi.org/10.1128/mubr.64.3.607-623.2000>.

[72] S.Y. Huang, N. Yao, J.K. He, M. Pan, Z.F. Hou, Y.M. Fan, A. Du, J.P. Tao, *In vitro* Anti-parasitic Activity of Pelargonium X. *asperum* Essential Oil Against *Toxoplasma gondii*, *Front Cell Dev Biol* 9 (2021) 616340. <https://doi.org/10.3389/fcell.2021.616340>.

[73] A.V. Sadybekov, V. Katritch, Computational approaches streamlining drug discovery, *Nature* 616(7958) (2023) 673-685. <https://doi.org/10.1038/s41586-023-05905-z>.

[74] D.B. Kitchen, H. Decornez, J.R. Furr, J. Bajorath, Docking and scoring in virtual screening for drug discovery: methods and applications, *Nat Rev Drug Discov* 3(11) (2004) 935-49. <https://doi.org/10.1038/nrd1549>.

[75] D. Gerlach, Y. Guo, C. De Castro, S.H. Kim, K. Schlatterer, F.F. Xu, C. Pereira, P.H. Seeberger, S. Ali, J. Codee, W. Sirisarn, B. Schulte, C. Wolz, J. Larsen, A. Molinaro, B.L. Lee, G. Xia, T. Stehle, A. Peschel, Methicillin-resistant *Staphylococcus aureus* alters cell wall glycosylation to evade immunity, *Nature* 563(7733) (2018) 705-709. <https://doi.org/10.1038/s41586-018-0730-x>.

[76] C. UniProt, UniProt: the Universal Protein Knowledgebase in 2023, *Nucleic Acids Res* 51(D1) (2023) D523-D531. <https://doi.org/10.1093/nar/gkac1052>.

[77] Y.Y. Chen, K.A. Clancy, R.A. Burne, *Streptococcus salivarius* urease: genetic and biochemical characterization and expression in a dental plaque streptococcus, *Infect Immun* 64(2) (1996) 585-92. <https://doi.org/10.1128/iai.64.2.585-592.1996>.

- [78] C.L. Chen, J.C. Mermoud, L.N. Paul, C.N. Steussy, C.V. Stauffacher, Mevalonate 5-diphosphate mediates ATP binding to the mevalonate diphosphate decarboxylase from the bacterial pathogen *Enterococcus faecalis*, *J Biol Chem* 292(52) (2017) 21340-21351. <https://doi.org/10.1074/jbc.m117.802223>.
- [79] M.A. Schumacher, D. Carter, D.M. Scott, D.S. Roos, B. Ullman, R.G. Brennan, Crystal structures of *Toxoplasma gondii* uracil phosphoribosyltransferase reveal the atomic basis of pyrimidine discrimination and prodrug binding, *EMBO J* 17(12) (1998) 3219-32. <https://doi.org/10.1093/emboj/17.12.3219>.
- [80] Y. Manickam, N. Malhotra, S. Mishra, P. Babbar, A. Dusane, B. Laleu, V. Bellini, M.A. Hakimi, A. Bougdour, A. Sharma, Double drugging of prolyl-tRNA synthetase provides a new paradigm for anti-infective drug development, *PLoS Pathog* 18(3) (2022) e1010363. <https://doi.org/10.1371/journal.ppat.1010363>.

**CAPÍTULO IV**  
**Considerações finais**

Esse trabalho teve como foco a avaliação da PVB demonstrando uma ampla gama de atividades farmacológicas relevantes. A elaboração de um novo fármaco a partir de um produto natural demanda investigações preliminares, incluindo a identificação das fontes botânicas, a caracterização dos componentes químicos, a padronização dos extratos, a avaliação da estabilidade, bem como a condução de pesquisas pré-clínicas para avaliar a eficácia e segurança. Os obstáculos residem na necessidade de preencher as lacunas essenciais para viabilizar o desenvolvimento de medicamentos, seja por meio da formulação utilizando tecnologias micro ou nanotecnológicas, empregando extratos padronizados, isolando substâncias *in natura* ou derivados semissintéticos.

Com relação ao primeiro estudo publicado no periódico *Scientific reports*, pode-se concluir que a PVB apresentou atividade antiperiodontopatogênica frente a todos os microrganismos avaliados, tanto as cepas padrão quanto clínicas. A atividade antiviral da PVB frente à CHIKV foi um resultado inédito e pioneiro, demonstrando a originalidade e inovação do estudo. A avaliação da toxicidade da PVB em *C. elegans* também foi inédita, sendo o primeiro artigo que avaliou sua toxicidade nesse tipo de animal. As concentrações que apresentaram atividade antibacteriana e antiviral podem ser futuramente utilizadas como parâmetro para testes clínicos.

Quanto ao segundo artigo submetido no mesmo periódico, foi demonstrado que a PVB possui atividade antibacteriana e antifúngica frente a todas as cepas avaliadas. Esse estudo ainda demonstrou a atividade antibiofilme da Gutiferona E e extrato bruto da PVB frente a esses microrganismos, analisando em imagens de microscopia a diminuição da viabilidade celular do biofilme após o tratamento e danos na parede celular desses microrganismos, bem como diminuição da adesão celular. Além disso, outra inovação desse estudo foi a avaliação da atividade antibacteriana da PVB *in vivo*, demonstrando que as concentrações determinadas como MIC exercem um efeito protetivo nas larvas infectadas e tratadas e diminuí o risco de morte em comparação com as larvas infectadas e não tratadas. Esses resultados são inéditos na literatura científica e mostram que a PVB exerce atividade antibacteriana e antifúngica tanto *in vitro* quanto *in vivo*, além de inibir a formação de biofilme.

As atividades antibiofilme da PVB apresentadas aqui são de extrema importância, pois a formação de biofilme pode resultar em infecções persistentes e resistentes a tratamentos convencionais, representando um desafio significativo na área

da saúde. Os estudos de toxicidade desempenham um papel crucial na avaliação da segurança dos produtos naturais, especialmente aqueles destinados a aplicações médicas ou terapêuticas. No entanto, é notável que na literatura científica, a quantidade de estudos de toxicidade, particularmente envolvendo organismos como *C. elegans* ainda é limitada. A falta de estudos de toxicidade pode representar uma lacuna significativa na compreensão abrangente dos efeitos adversos desses produtos.

Portanto, os resultados apresentados nos dois artigos são promissores e destacam a importância de explorar os produtos naturais, avaliando seus potenciais biológicos. A busca por alternativas terapêuticas derivadas da natureza não apenas enriquece nosso entendimento sobre as propriedades medicinais desses elementos, mas também aponta para um futuro promissor na descoberta de novos medicamentos e no aprimoramento das abordagens terapêuticas existentes.







## Quantification of biofilm produced by clinical, environment and hands' isolates *Klebsiella* species using colorimetric and classical methods

Nagela Bernadelli Sousa Silva<sup>a</sup>, Priscila Guerino Vilela Alves<sup>a</sup>, Lara de Andrade Marques<sup>a</sup>, Samuel Fernandes Silva<sup>b</sup>, Gabriel de Oliveira Faria<sup>a</sup>, Lúcio Borges de Araújo<sup>c</sup>, Reginaldo dos Santos Pedroso<sup>d</sup>, Mário Paulo Amante Penatti<sup>d</sup>, Ralciane de Paula Menezes<sup>d,\*</sup>, Denise von Dolinger de Brito Röder<sup>e</sup>

<sup>a</sup> Postgraduate Program in Health Sciences, Medicine, Federal University of Uberlândia (UFU), Brazil

<sup>b</sup> Institute of Biology, Federal University of Uberlândia (UFU), Brazil

<sup>c</sup> College of Mathematics, Federal University of Uberlândia (UFU), Brazil

<sup>d</sup> Technical School of Health (ESTES), Federal University of Uberlândia (UFU), Brazil

<sup>e</sup> Clinical Microbiology, Institute of Biomedical Sciences, Federal University of Uberlândia (UFU), Brazil

### ARTICLE INFO

#### Keywords:

Biofilm  
*Klebsiella oxytoca*  
*Klebsiella pneumoniae*  
Neonatal units

### ABSTRACT

Some species of *Klebsiella*, such as *Klebsiella pneumoniae* and *Klebsiella oxytoca*, are important nosocomial pathogens frequently involved in outbreaks in Neonatal Intensive Care Units (NICU) and have the ability to form a biofilm. This study aims to evaluate the biofilm production of *K. pneumoniae* and *K. oxytoca* isolates collected from the hands of health professionals, neonates' blood and the environment of a Brazilian NICU, using three colorimetric methods and a classical method of counting the colony-forming units and compare the analysis among these techniques. The biofilm formation was carried out by the microplate technique, using three colorimetric assays: crystal violet, safranin and 2,3-bis (2-methoxy-4-nitro-5-sulfophenyl) -5 [(phenylamino) arbonyl] - 2H-tetrazolium hydroxide (XTT). Also, colony-forming units were determined. Twenty-eight isolates of *K. pneumoniae* were collected from the blood, hands and environment and five of *K. oxytoca* from the hands and environment. All of them were strong biofilm producers, but *K. pneumoniae* isolates produced more biofilm than *K. oxytoca* when compared to the American Type Culture Collection (ATCC) strains used as positive controls. The number of viable cells in the biofilm produced by *K. pneumoniae* isolated from blood was significantly higher than in the control sample. Regarding the three colorimetric tests used in the study, the violet crystal obtained a higher absorbance average. The use of crystal-violet and XTT in the evaluation of biofilm *in vitro* make possible a complete analysis, since that it can quantify the total biomass (including the extracellular matrix) and evaluate the metabolic activity. In conclusion, this study identified isolates of *K. pneumoniae* and *K. oxytoca* that produce biofilms in the NICU and the bloodstream of neonates. This fact deserves attention since these patients are immunocompromised. The best methods will be chosen to answer research questions by always adopting more than one method so that more than one parameter or component of the biofilm is analyzed.

**Abbreviations:** ATCC, American Type Culture Collection; CAPES, Coordenação de Aperfeiçoamento de Pessoal de Nível Superior; CFU, colony-forming units; DNA, deoxyribonucleic acid; ESTES, Technical School of Health; FAPEMIG, Fundação de Amparo à Pesquisa do Estado de Minas Gerais; Ko, *Klebsiella oxytoca*; Kp, *Klebsiella pneumoniae*; MALDI TOF/MS, Matrix-Assisted Laser Desorption Ionization-Time of Flight; NaCl 0.9%, physiological saline; NICU, Neonatal Intensive Care Units; TSB, Trypticase Soy Broth; UFU, Federal University of Uberlândia; XTT, 2,3-bis (2-methoxy-4-nitro-5-sulfophenyl) -5 [(phenylamino) arbonyl] - 2H-tetrazolium hydroxide.

\* Corresponding author at: Federal University of Uberlândia (UFU), Av. Amazonas s/nº - Bloco 4K - 111, Campus Umuarama, Umuarama, Uberlândia, MG CEP 38400-902, Brazil.

E-mail address: [ralciane@ufu.br](mailto:ralciane@ufu.br) (R. de Paula Menezes).

<https://doi.org/10.1016/j.mimet.2021.106231>

Received 28 December 2020; Received in revised form 25 April 2021; Accepted 25 April 2021

Available online 28 April 2021

0167-7012/© 2021 Elsevier B.V. All rights reserved.

**Table 1**  
Biofilm production by *Klebsiella* species using three colorimetric methods and counting the number of colony-forming units.

Isolates	Site of isolation	Biomass mean OD	Extracellular matrix	Metabolic activity	Viable cells
			Mean OD	Mean OD	CFU/mL
Kp (ATCC)	–	1,97	1,59	0,44	$2.2 \times 10^8$
Kp 21	Environment	2,33*	1,51	0,60	$6.2 \times 10^8$
Kp 1	Blood	1,51	1,14*	0,64	$6.1 \times 10^8$
Kp 2	Blood	1,70	1,66	0,64	$7.2 \times 10^8$
Kp 3	Blood	1,30*	1,06*	0,63	$6.6 \times 10^8$
Kp 4	Blood	1,55*	1,22	0,84*	$8.2 \times 10^8$
Kp 1.1	Hand	2,49*	1,24	0,63	$5.4 \times 10^8$
Kp 9	Hand	2,59*	1,42	0,57	$4.3 \times 10^8$
Kp 10	Hand	2,77*	2,27*	0,55	$1.0 \times 10^8$
Kp 15	Hand	2,52*	1,43	0,38*	$3.7 \times 10^8$
Kp 17	Hand	2,35*	1,24*	0,55	$1.0 \times 10^8$
Kp 20	Hand	2,15	1,43	0,48	$5.1 \times 10^8$
Kp 40	Hand	1,83	1,13*	0,43	$6.6 \times 10^8$
Kp 46	Hand	2,25	1,57	0,55	$2.3 \times 10^9$
Kp 50	Hand	1,85	0,88*	0,46	$2.6 \times 10^9$
Kp 63	Hand	1,77	0,79*	0,27*	$2.9 \times 10^8$
Kp 68	Hand	2,19*	1,73	0,53	$5.0 \times 10^8$
Kp 72	Hand	1,81	1,99*	0,57	$4.3 \times 10^9$
Kp 73	Hand	2,09	1,69	0,85	$6.8 \times 10^8$
Kp 77	Hand	2,04	1,54	0,53	$4.8 \times 10^8$
Kp 85	Hand	2,59*	2,39*	1,01*	$8.0 \times 10^8$
Kp 92	Hand	1,50*	1,24*	0,53	$7.7 \times 10^8$
Kp 98	Hand	1,53*	1,03*	0,64	$6.3 \times 10^8$
Kp100	Hand	1,91	1,82*	0,59	$2.6 \times 10^8$
Kp126	Hand	1,68	1,65	0,36*	$1.3 \times 10^8$
Kp 137	Hand	1,60*	0,81*	0,56	$4.6 \times 10^8$
Kp 140	Hand	1,72	1,19*	0,46	$1.6 \times 10^8$
Kp 142	Hand	1,55*	0,96*	0,37*	$6.0 \times 10^8$
Kp 145	Hand	1,07*	1,04*	0,60	$1.3 \times 10^9$
Ko (ATCC)	–	1,90	0,95	0,68	$6.8 \times 10^8$
Ko 3.3	Environment	1,26*	0,79*	0,50	$5.8 \times 10^8$
Ko 35	Hand	1,38*	0,80*	0,54	$6.6 \times 10^8$
Ko 66	Hand	0,82*	0,68*	0,58*	$4.8 \times 10^8$
Ko125	Hand	1,86	1,18*	0,62*	$4.1 \times 10^9$
Ko143	Hand	1,84	1,29*	0,29*	$2.4 \times 10^8$

\* Statistically significant sample  $P < 0.05$  - All the statistically significant samples, produced more or less than the control. Kp: *Klebsiella pneumoniae*; Ko: *Klebsiella oxytoca*.

## 1. Introduction

Some *Klebsiella* species, such as *Klebsiella pneumoniae* and *Klebsiella oxytoca*, are important nosocomial pathogen frequently involved in Neonatal Intensive Care Units (NICU) outbreaks, with mortality around 30–40% (Cadot et al., 2019; Ruiz et al., 2019). Often these microorganisms show the ability to form biofilm on biotic and abiotic surfaces (Ghasemian et al., 2019). Biofilm structures protect the microorganism from commonly used disinfectants, antibiotics and attacks by the host immune response, increasing the permanence of pathogen on surfaces, which is directly associated with the infections (Poza, 2018).

Thus, this study aims to evaluate biofilm production by clinical, environment and hands *Klebsiella pneumoniae* and *K. oxytoca* isolates in a Brazilian NICU, using three colorimetric methods and counting of colony-forming units (CFU) count and compare these techniques.

## 2. Material and methods

### 2.1. Study design

The study was carried out at the Clinical Hospital NICU of the Federal University of Uberlandia. The hospital has 520 beds, of which 20 belong to the NICU. The samples were collected between March to December 2018 from blood cultures of neonates with infection, hands of healthcare workers and environment neonatal.

### 2.2. Sample collection

Blood cultures were collected based on clinical criteria established

by the hospital medical team and identification was performed by the BACT/Alert® system and Vitek® (bioMérieux-Durham, USA). The healthcare workers simulated hands washing in a sterile polypropylene bag containing 30 ml of sterile physiological saline (NaCl 0.9%). The material was placed in 15 ml sterile falcon tubes and was incubated at  $35 \pm 2^\circ \text{C}$  for 24 h (Ferg et al., 2014). The collections of environmental samples were made on surfaces of delimited areas with a sterile swab washed in 3 ml of 0.9% saline solution also sterilized and subjected to pressure and friction throughout the surface for 20 s. Finally, the swab with the sample was placed in the tube with Brain Heart Infusion (BHI) broth that was used to wash it (Meinke et al., 2012). The hands and environment samples were seeded in 5% sheep Blood Agar (HIMEDIA®, India), and Eosin-Methylene Blue Agar (HIMEDIA®, India) and incubated at  $35 \pm 2^\circ \text{C}$  for 18–24 h. Samples with the growth of one colony were considered positive and the identification was made by MALDI TOF/MS (Matrix-Assisted Laser Desorption Ionization-Time of Flight).

### 2.3. Biofilm formation

The research of biofilm formation was done using the microplate technique described by (Merritt et al., 2011). The samples were suspended from the stock BHI broth with 20% glycerol for  $4 \mu\text{l}$  of Trypticase Soy Broth (TSB) and incubated overnight at  $37^\circ \text{C}$ . Then the overnight cultures were diluted 1:100 into fresh medium to avoid the saturation of the medium. One hundred microliters of this dilution were added in the plates 96-well polystyrene and incubated at  $37^\circ \text{C}$  for 24 h. After incubation, the wells were washed with Phosphate Buffered Saline (PBS) to remove the non-adherent cells. For each type of colorimetric assay, one 96-well plate was used. For biomass quantification, each well

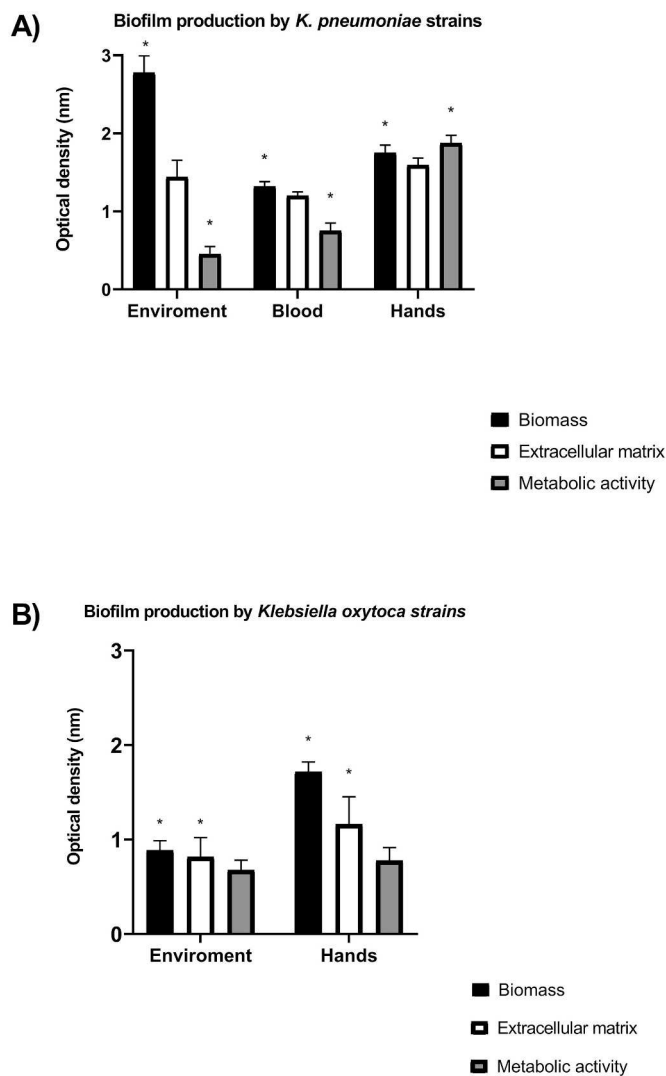


**Fig. 1.** Biofilm production according to the site collected.  
 \*Statistically significant samples ( $P \leq 0.05$ ).

was stained with 125  $\mu$ L of 0.1% Crystal Violet solution for 15 min and for extracellular matrix quantification 125  $\mu$ L of 0.1% Safranin was added in each well and incubated at room temperature for 15 min (Stepanović et al., 2007; O'Toole, 2011). To remove excess dye, the wells were rinsed three times with sterile distilled water. Then, a solution of 30% acetic acid was added to each well to solubilize the dyes and incubated at room temperature for 15 min. The wells were read in a microtiter plate reader at 595 and 530 nm, respectively. For the metabolic activity test, aliquots of 50  $\mu$ L of XTT salt solution (1 mg mL<sup>-1</sup> in PBS) and 4  $\mu$ L of menadione were added in each well and incubated at 37 °C for 3 h. The reading was made at 495 nm (Chandra et al., 2008). The quantification assays were done in triplicate and repeated three times independently. *Klebsiella pneumoniae* American Type Culture Collection (ATCC) 700,603 and *K. oxytoca* ATCC 13182 were used as a positive control.

Sterile TSB broth was used as a negative control. The interpretation of results was made according to Stepanović et al. (2007), being the isolates classified into the following categories:  $OD < OD_c$  = non-biofilm producer;  $OD_c < OD < 2 \times OD_c$  = weak biofilm producer;  $2 \times OD_c < OD < 4 \times OD_c$  = moderate biofilm producer;  $4 \times OD_c < OD$  = strong biofilm producer.

Besides that, the number of viable cells (CFU/mL) was determined by a classical method of counting, to assess cell viability (Melo et al., 2014).

After biofilm formation as described below, the biofilms were washed twice with PBS and after scraping the wells for 90s. The cell suspension obtained was plated onto the Trypticase Soy Agar (TSA) and incubated at 37 °C for 48 h. The CFU/mL were counted on each Petri dish (Melo et al., 2014).

Quantitative assays were compared using a *t*-test for isolates. For the comparison of the three tests, the ANOVA followed by the Tukey test was used. All tests were performed with a statistical significance of  $P < 0.05$ . The graphics were made using the Prism version 8. The study was conducted by the Commitment of ethics in research with human beings number n. 2.678.16.

### 3. Results

Twenty-eight isolates of *K. pneumoniae* were collected from the blood, hands and environment; and five *K. oxytoca* from the hands and environment. All of them were strong biofilm producers, but *K. pneumoniae* isolates produced more biofilm than *K. oxytoca* compared to the ATCC strains used as a positive control. *K. pneumoniae* biofilm production was significantly higher in nine (32%) isolates about biomass production, four (14%) about matrix evaluation and two (7%) when analyzing metabolic activity. In the five isolates of *K. oxytoca*, the production of biofilm was significantly lower than the control, by the three colorimetric techniques (Table 1).

Biofilm production was also compared in relation to the isolation site. Fig. 1A shows the production of biofilm by *K. pneumoniae*. Biomass production was statistically higher in isolates from the environment ( $OD = 2.83$ ) when compared to other sites and metabolic activity was higher in hand isolates ( $OD = 1.85$ ). Regarding the production of biofilm by the isolates of *K. oxytoca*, the production of biomass ( $OD = 1.75$ ) and extracellular matrix ( $OD = 1.25$ ) was statistically higher in the isolates of the hands when compared with those isolated from the environment (Fig. 1B).

In addition, the number of viable cells were counted manually and compared with the absorbance found in the XTT colorimetric assay. Fig. 2 shows the number of viable cells and the metabolic activity of the biofilm formed by *K. pneumoniae* and *K. oxytoca*. A correlation was observed between the two tests, since the samples that showed the highest absorbance of XTT also had a higher number of viable cells.

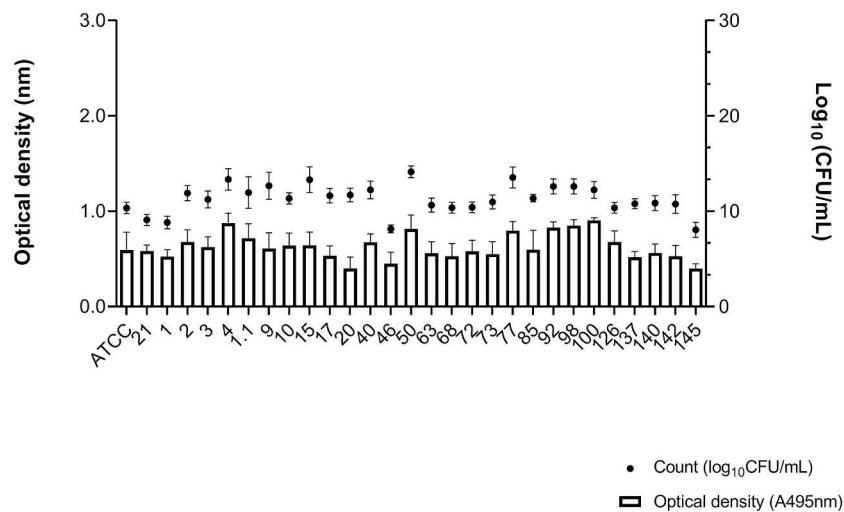
### 4. Discussion

In this study, all isolates from blood, health professionals' hands and the NICU environment were strong biofilm producers. It is already known that the production of biofilm makes bacteria more resistant to desiccation, to antimicrobials and more difficult to be removed during cleaning (Poza, 2018). The hospital environment constitutes an important reservoir of pathogens, remaining viable for a longer time due to the production of biofilm, especially on high-touch surfaces (Costa et al., 2019). The contact of health professionals with contaminated surfaces can contribute to the transmission of these pathogens in the unit, highlighting the importance of correct hand and surface hygiene (Chowdhury et al., 2018).

In this study, *K. pneumoniae* isolates showed significantly higher biofilm production compared to the control and with *K. oxytoca* isolates. The prerequisites for the ideal biofilm formation vary considerably among different species of bacteria, as well as the biofilm composition used to be different. Some intrinsic factors, such as pili, specific genes for the formation of biofilm, flagella, adhesins, fimbriae (that assist in the initial colonization of the host) and capsular polysaccharides (that protect the organism from phagocytosis) can be crucial for the production of a consistent biofilm (Singh et al., 2019; Payne and Boles, 2016; Maldonado et al., 2007).

Regarding collected sites, the sample that produced the most biomass was the environmental isolate for *K. pneumoniae* strains and for isolates of *K. oxytoca* the hands were the site with the highest production of both

**A)** Comparison between the number of viable cells (CFU / mL) and the absorbance of the XTT assay of *K. pneumoniae* isolates



**B)** Comparison between the number of viable cells (CFU / mL) and the absorbance of the XTT assay of *K. oxytoca* isolates

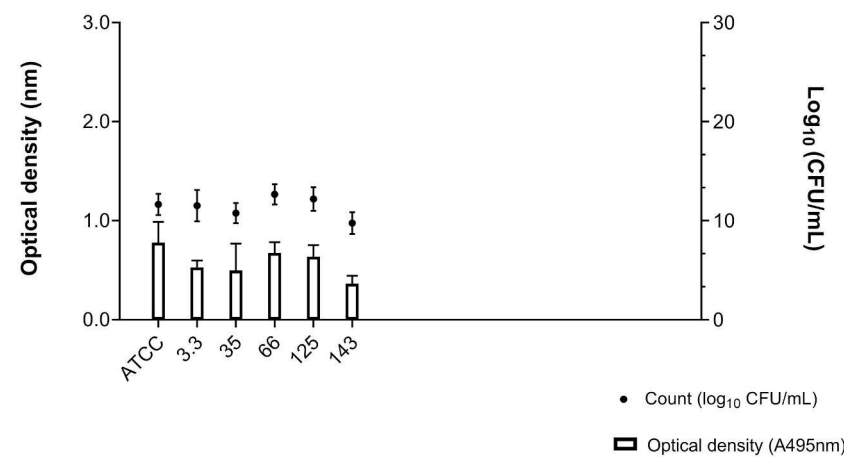


Fig. 2. Comparison of metabolic activity and viable cells according to the two methods used in the study.

biomass and extracellular matrix, compared to the other sites collected. It is estimated that environmental contamination is the source of pathogenic bacteria involved in 20% of infections associated with health-care. In addition, 25–79% of medical devices are contaminated, and these microorganisms can come from any part of the hospital environment (Chowdhury et al., 2018). In addition, it is estimated that 20–40% of pathogenic bacteria come from the hands of health professionals (Costa et al., 2019). Only contact of the gloved hand with a contaminated surface results in a variable degree of pathogen transfer, with planktonic bacterial transfer rates between 38 and 65% occurring from the surfaces to the hands. Blood is also a relevant site when it comes to the formation of biofilms, especially in the NICU, since the formation of *Klebsiella* biofilms in these immunocompromised patients often results in a worsening of the patient’s prognosis, since biofilms can protect bacterial cells against host immune responses and antimicrobial therapies (Wang et al., 2017).

In the last decades, several models for the *in vitro* study of the evaluation of biofilms were described (Peeters et al., 2008; Shukla and Rao, 2017; Veerachamy et al., 2014). Our study used three colorimetric methods for evaluate different parameters of the biofilm. This

evaluation is important since the biofilm is a complex structure and has several components to be analyzed, such as total biomass, extracellular matrix, metabolic activity and the number of viable cells. There is no method that is able for analyzing all of these biofilm parameters in a single trial, which would lead to loss of information about the biofilm. Crystal-violet is a basic protein-dye that stains the surface of negatively charged molecules and the biofilm extracellular matrix, therefore in a non-specific way, so that it doesn’t make possible the distinction of living or dead cells (Shukla and Rao, 2017). Also, XTT was used to evaluate the biofilm’s metabolic activity, since it is a tetrazolic salt capable of changing its chemical conformation in the presence of metabolites, changing its color from transparent to orange (Xu et al., 2016). The use of crystal-violet and XTT in the evaluation of biofilm *in vitro* complete the analysis, since that makes possible to quantify the total biomass (including the extracellular matrix) and evaluate the metabolic activity (production of metabolites by viable cells) of biofilm.

The number of viable cells in the biofilm was also counted. Thus, there was a greater metabolic activity and a greater number of viable cells among bloodstream isolates, suggesting a correlation between the two techniques. Although XTT has some disadvantages, such as the lack

of a linear relationship between the number of microorganisms present in the biofilm and the colorimetric signal, salt retention by these pathogens in planktonic and sessile form and a high cost (Costa-Orlandi et al., 2017), this trial it has high replicability and objectivity in the results provided. CFU counting, in addition to using many input materials, time and labor for the technique, is also subjective, dependent on the technical ability to count.

Safranin was another colorimetric method used to specifically quantify the extracellular matrix of the biofilm. Some researchers have said that safranin specifically stains the mucopolysaccharides of the biofilm due to the high affinity of the dye with these compounds (Stepanović et al., 2007). However, because some biofilms do not have polysaccharides in the matrix, which is replaced by deoxyribonucleic acid (DNA) and other compounds, that theory may be a limitation of the technique (Payne and Boles, 2016). Ommen et al. (2017) quantified biofilm biomass using different colorimetric techniques and found similar results in staining with safranin and crystal-violet, revealing the ability of safranin to not only stain the matrix but also the entire biofilm biomass. This finding is confirmed by the data of our study since the average absorbance found by the crystal-violet was close to the value of safranin. Then, this possible feature may limit its use in determining the matrix, what maybe makes the ideal method for the specific quantification of the extracellular matrix to be confocal microscopy, which allows visualization in real-time of all the different components of the matrix (Schlafer and Meyer, 2017).

## 5. Conclusions

This study identified isolates of *K. pneumoniae* and *K. oxytoca* that produces biofilms in the NICU and in the bloodstream of newborns, a fact that deserves attention since these patients are immunocompromised and highly susceptible to infections by these pathogens. Biofilms provide protection for microorganisms, making them resist longer in the unit and be more resistant to treatment, increasing the rates of morbidity and mortality. The epidemiological surveillance of these pathogens is therefore essential to explore and understand what type of pathogen is causing the infection in the unit, so that therapy is more targeted. Having this knowledge, it is possible to apply new or improved compounds to assist in the challenge of tartar and resolve biofilm infection in clinical settings.

For the evaluation of biofilm *in vitro*, each technique used in this study has advantages and disadvantages. It is up to the researcher, given the objective of the research, to choose the best methods that will safely answer the question of the research, always adopting more than one method, so that more than one parameter or component of the biofilm is analyzed.

## Funding sources

This study have received financial support from Coordenação de Aperfeiçoamento de Pessoal de Nível Superior (CAPES) and Fundação de Amparo à Pesquisa do Estado de Minas Gerais (FAPEMIG) (Process is APQ - 00965-18001/2018 Universal Demand).

## Declaration of Competing Interest

The authors declare that they have no known competing financial interests or personal relationships that could have appeared to influence the work reported in this paper.

## Acknowledgements

We would like to thank the Coordenação de Aperfeiçoamento de Pessoal de Nível Superior (CAPES) and code 001 CAPES, Fundação de Amparo à Pesquisa do Estado de Minas Gerais (FAPEMIG) for financial support and for granting the master's scholarship that was crucial for the

development of this study and the course on clinical analysis of the Technical School of Health (ESTES) for all their support and encouragement for this work.

## References

- Cadot, L., Bruguère, H., Jumas-Bilak, E., Didelot, M.N., Masnou, A., Barry, G., Cambonie, G., Parer, S., Romano-Bertrand, S., 2019. Extended spectrum beta-lactamase-producing *Klebsiella pneumoniae* outbreak reveals incubators as pathogen reservoir in neonatal care center. *Eur. J. Pediatr.* 178, 505–513. <https://doi.org/10.1007/s00431-019-03323-w>.
- Chandra, J., Mukherjee, P.K., Ghannoum, M.A., 2008. In vitro growth and analysis of *Candida* biofilms. *Nat Protoc* 3, 1909–1924. <https://doi.org/10.1038/nprot.2008.192>.
- Chowdhury, D., Tahir, S., Legge, M., Hu, H., Prvan, T., Johani, K., Whiteley, G.S., Glasbey, T.O., Deva, A.K., Vickery, K., 2018. Transfer of dry surface biofilm in the healthcare environment: the role of healthcare workers' hands as vehicles. *J. Hosp. Infect.* 100, e85–e90. <https://doi.org/10.1016/j.jhin.2018.06.021>.
- Costa, D.M., Johani, K., Melo, D.S., Lopes, L.K.O., Lima, L.K.O.L., Tipple, A.F.V., Hu, H., Vickery, K., 2019. Biofilm contamination of high-touched surfaces in intensive care units: epidemiology and potential impacts. *Lett. Appl. Microbiol.* 68, 269–276. <https://doi.org/10.1111/lam.13127>.
- Costa-Orlandi, C.B., Sardi, J.C.O., Pitangui, N.S., Oliveira, H.C., Scorzoni, L., Geleane, M. C., Medina-Alarcón, K.P., Melo, W.C.M.A., Marcelino, M.Y., Braz, J.D., Fusco-Almeida, A.M., Mendes-Giannini, M.J.S., 2017. Fungal biofilms and polymicrobial diseases. *J. Fungi* 3, 1–24. <https://doi.org/10.3390/jof3020022>.
- Ferng, Y.H., Clock, S.A., Wong-McLoughlin, J., DeLamora, P.A., Perlman, J.M., Gray, K.S., Paul, D.A., Prasad, P.A., Zauotis, T.E., Alba, L.R., Whittier, S., Larson, E.L., Saiman, L., 2014. Multicenter study of hand carriage of potential pathogens by neonatal ICU healthcare personnel. *J. Pediatric Infect. Dis. Soc.* 4, 276–279. <https://doi.org/10.1093/jpids/piu022>.
- Ghasemian, A., Mobarez, A.M., Peerayeh, S.N., Bezmin, A.T., 2019. The association of surface adhesin genes and the biofilm formation among *Klebsiella oxytoca* clinical isolates. *NMNI.* 27, 36–39. <https://doi.org/10.1080/10.1016/j.nmni.2018.07.001>.
- Maldonado, N.C., Ruiz, C.S., Cecilia, M., Macias, M.E.N., 2007. A simple technique to detect *Klebsiella* biofilm-forming-strains. In: *Inhibitory Potential of Lactobacillus fermentum* CRL 1058 Whole Cells and Products. Communicating Current Research and Educational Topics and Trends in Appl. Microbiol., pp. 52–59. <https://citeseerx.ist.psu.edu/viewdoc/download?doi=10.1.1.597.5733&rep=rep1&type=pdf>. Access: 03/12/2020.
- Meinke, R., Meyer, B., Frei, R., Passweg, J., Widmer, A.F., 2012. Equal efficacy of glucoprotamin and an aldehyde product for environmental disinfection in a hematologic transplant unit: a prospective crossover trial. *Infect. Control Hosp. Epidemiol.* 33, 1077–1180. <https://doi.org/10.1086/668028>.
- Melo, P.C., Sousa, C., Botelho, C., Oliveira, R., Nader-Filho, A., 2014. NaOCl effect on biofilm produced by *Staphylococcus aureus* isolated from the milking environment and mastitis infected cows. *Pesqui. Vet. Bras.* 34, 109–113. <https://doi.org/10.1590/S0100-736X2014000200002>.
- Merritt, J.H., Kadoori, D.E., O'toole, G.A., 2011. Growing and analyzing static biofilms. *Curr. Protoc. Microbiol.* 22, 1B.1.1–1B.1.18. <https://doi.org/10.1002/9780471729259.mc1b01s22>.
- Ommen, P., Zobek, N., Meyer, R.L., 2017. Quantification of biofilm biomass by staining: non-toxic safranin can replace the popular crystal violet. *J. Microbiol. Methods* 141, 87–89. <https://doi.org/10.1016/j.mimet.2017.08.003>.
- O'Toole, G.A., 2011. Microtiter dish biofilm formation assay. *J. Vis. Exp.* 47 <https://doi.org/10.3791/2437>.
- Payne, D.E., Boles, B.R., 2016. Emerging interactions between matrix components during biofilm development. *Curr. Genet.* 137–144. <https://doi.org/10.1007/s00294-015-0527-5>.
- Peeters, E., Nelis, H.J., Coenye, T., 2008. Comparison of multiple methods for quantification of microbial biofilms grown in microtiter plates. *J. Microbiol. Methods* 72, 157–165. <https://doi.org/10.1016/j.mimet.2007.11.010>.
- Pozo, J.L., 2018. Biofilm-related disease. *Expert Rev. Anti-Infect. Ther.* 16, 51–55. <https://doi.org/10.1080/14787210.2018.1417036>.
- Ruiz, J., Sanjuan, E., Amaro, C., Gordon, M., Villarreal, A., Castellanos-Ortega, A., Ramirez, P., 2019. *In vitro* study of antimicrobial activity on *Klebsiella pneumoniae* biofilms in endotracheal tubes. *J. Chemother.* 31, 1–7. <https://doi.org/10.1080/1120009X.2019.1601801>.
- Schlafer, S., Meyer, R.L., 2017. Confocal microscopy imaging of the biofilm matrix. *J. Microbiol. Methods* 138, 50–59. <https://doi.org/10.1016/j.mimet.2016.03.002>.
- Shukla, S.K., Rao, T.S., 2017. An improved crystal violet assay for biofilm quantification in 96-well microtitre plate. *Biorxiv.*, 100214 <https://doi.org/10.1101/100214>.
- Singh, A.K., Yadav, S., Chauhan, B.S., Nandy, N., Singh, R., Neogi, K., Roy, J.K., Srikrishna, S., Singh, R.K., Prakash, P., 2019. Classification of clinical isolates of *Klebsiella pneumoniae* based on their *in vitro* biofilm forming capabilities and elucidation of the biofilm matrix chemistry with special reference to the protein content. *Front. Microbiol.* 10, 669. <https://doi.org/10.3389/fmicb.2019.00669>.
- Stepanović, S., Vuković, D., Hola, V., Bonaventura, G., Djukić, S., Cirković, I., Ruzicka, F., 2007. Quantification of biofilm in microtiter plates: overview of testing conditions and practical recommendations for assessment of biofilm production by *Staphylococci*. *APMIS.* 115, 891–899. <https://doi.org/10.1111/j.1600-0463.2007.apm.630.x>.

- Veerachamy, S., Yarlagadda, T., Manivasagam, G., Yarlagadda, P.K., 2014. Bacterial adherence and biofilm formation on medical implants: a review. *Proc. Inst. Mech. Eng. H*. 228, 1083–1089. <https://doi.org/10.1177/0954411914556137>.
- Wang, H., Li, W., Gu, L., Gao, X., Ni, B., Deng, H., Yang, R., Han, Y., 2017. Emergence of two distinct subpopulations from *Klebsiella pneumoniae* grown in the stimulated microgravity environment. *Future Microbiol.* 12 (11), 939–951. <https://doi.org/10.2217/fmb-2017-0032>.
- Xu, Z., Liang, Y., Lin, S., Chen, D., Li, B., Li, L., Deng, Y., 2016. Crystal violet and XTT assays on *Staphylococcus aureus* biofilm quantification. *Curr. Microbiol.* 73, 474–482. <https://doi.org/10.1007/s00284-016-1081-1>.

## Article

# Combining Essential Oils with Each Other and with Clotrimazole Prevents the Formation of *Candida* Biofilms and Eradicates Mature Biofilms

Rafael Alves da Silva <sup>1</sup>, Nagela Bernadelli Sousa Silva <sup>2</sup>, Carlos Henrique Gomes Martins <sup>2,3</sup>, Regina Helena Pires <sup>4</sup>, Denise Von Dolinger de Brito Röder <sup>1,3,\*</sup> and Reginaldo dos Santos Pedroso <sup>5</sup>

- <sup>1</sup> Post-Graduation Program in Health Sciences, Federal University of Uberlândia (UFU), Uberlândia 38400-902, MG, Brazil
- <sup>2</sup> Post-Graduation Program in Applied Immunology and Parasitology (PIPA), Federal University of Uberlândia (UFU), Uberlândia 38400-902, MG, Brazil
- <sup>3</sup> Institute of Biomedical Sciences (ICBIM), Federal University of Uberlândia (UFU), Uberlândia 38400-902, MG, Brazil
- <sup>4</sup> Post-Graduation Program in Health Promotion, University of Franca (UNIFRAN), Franca 14404-600, SP, Brazil
- <sup>5</sup> Technical School of Health (ESTES), Federal University of Uberlândia (UFU), Uberlândia 38400-902, MG, Brazil
- \* Correspondence: denise.roder@ufu.br; Tel.: +55-34-3225-8670



**Citation:** Silva, R.A.d.; Silva, N.B.S.; Martins, C.H.G.; Pires, R.H.; Röder, D.V.D.d.B.; Pedroso, R.d.S. Combining Essential Oils with Each Other and with Clotrimazole Prevents the Formation of *Candida* Biofilms and Eradicates Mature Biofilms. *Pharmaceutics* **2022**, *14*, 1872. <https://doi.org/10.3390/pharmaceutics14091872>

Academic Editor: Francisco Javier De La Mata

Received: 5 July 2022

Accepted: 29 August 2022

Published: 5 September 2022

**Publisher's Note:** MDPI stays neutral with regard to jurisdictional claims in published maps and institutional affiliations.



**Copyright:** © 2022 by the authors. Licensee MDPI, Basel, Switzerland. This article is an open access article distributed under the terms and conditions of the Creative Commons Attribution (CC BY) license (<https://creativecommons.org/licenses/by/4.0/>).

**Abstract:** Fungal infections by *Candida* spp. are opportunistic and most often occur in individuals with some predisposing factor. Essential oils (EO) have anti-*Candida* potential, being a therapeutic alternative to be explored, especially for superficial and mucosal candidiasis. The objective was to analyze the synergistic potential between the EO of *Citrus limon*, *Cupressus sempervirens*, *Litsea cubeba* and *Melaleuca alternifolia*, and each of them with clotrimazole, to inhibit in vitro the formation and eradication of *Candida* spp. biofilms. Added to this, the survival of *Caenorhabditis elegans* was evaluated after exposure to EO, clotrimazole and their synergistic combinations. Anti-*Candida* activity was determined by microdilution for the substances alone and in EO–EO and EO–clotrimazole combinations. The combinations were performed by the checkerboard method, and the reduction in the metabolic activity of biofilms was determined by the viability of MTT/menadione. *C. elegans* larvae survival was evaluated after 24 h of exposure to EO, clotrimazole and synergistic combinations. The minimum inhibitory concentration (MIC) of EO ranged from 500 to >4000 µg/mL. The lowest MIC (500 µg/mL) was for *C. sempervirens* and *L. cubeba* on a *C. krusei* isolate; for clotrimazole, the MIC ranged from 0.015 to 0.5 µg/mL. Biofilm inhibition and eradication both ranged from 1000 to >4000 µg/mL. The lethal concentration (LC<sub>50</sub>) of *C. limon*, *L. cubeba* and *M. alternifolia* was 2000 µg/mL for *C. elegans*, while for *C. sempervirens* and clotrimazole, it was not determined within the concentration limits tested. In combination, more than 85% of the larvae survived *M. alternifolia*–clotrimazole, *M. alternifolia*–*L. cubeba*, *C. sempervirens*–clotrimazole and *C. sempervirens*–*C. limon* combinations. This study is the first, to our knowledge, to present a synergistic relationship of EO–EO and EO–clotrimazole combinations on *Candida* spp. biofilms.

**Keywords:** essential oils; clotrimazole; *Candida* spp.; synergy; biofilm; toxicity; *Caenorhabditis elegans*

## 1. Introduction

Infections caused by species of the genus *Candida* are opportunistic and more severe in immunocompromised, hospitalized individuals, using invasive devices and with comorbidities [1]. Superficial candidiasis affects the oral and vaginal mucosa, skin and nails; and factors external to the individual, such as climatic conditions in tropical and subtropical regions, and factors inherent to it, such as local humidity, use of immunosuppressive or antibacterial drugs and some comorbidities, such as diabetes, facilitate the development



of the disease [2]. In superficial infections, the most frequent *Candida* species is *C. albicans*; however, in recent years, *Candida non-albicans* species have shown relevance among the causative agents of vulvovaginal candidiasis (VVC) and recurrent VVC (RVVC), including the species *C. glabrata*, *C. krusei* and *C. tropicalis* [2–4].

The azole antifungals have been one of the therapeutic options for the treatment of superficial mycoses since the 1960s–1970s [5,6]. In this sense, topical formulations containing azoles are attractive for VVC and RVVC due to the lower incidence of adverse effects compared to the same drug class for oral use and systemic action [3]. Clotrimazole has a cure rate of between 73% and 100% of infections, similar to other topical antifungals such as nystatin [6,7].

In the last decades, the report of new *Candida* species and in vitro resistant isolates to traditional antifungals has been an incentive for the search and development of new ways of managing these infections [8]. Resistance is a result of multiple factors that include structural changes in the drug target and the ability of *Candida* spp. to form biofilms [9–11]. In this sense, the community structure and firm adherence between the microorganisms of the biofilm allow a barrier condition that makes penetration of drugs difficult and consequently reduces the effectiveness of the treatment [8,10,11].

Essential oils are plant-derived products with potential activity against microorganisms, attributable to the complex mixture of chemotypes [12–14]. Recently, combinations of multiple agents have optimized antifungal activity against clinically relevant fungi. Thus, a new therapeutic approach combining conventional antifungal drugs, such as clotrimazole, and natural products with antifungal activity may have the potential for clinical use [15–18].

The in vivo screening of compounds with proven in vitro antimicrobial action is one of the necessary steps within the current safety context to identify the toxicity of new anti-infective agents [19]. In this context, in vivo studies using alternative animal models such as *Drosophila melanogaster*, *Galleria mellonella* and *Caenorhabditis elegans* have been proposed to assess the preliminary toxicity of new health products [20,21]. Thus, the free-living nematode *C. elegans* can be an alternative predictive model option, being of low cost, fast cultivation and not very complex laboratory handling, and lending itself to the evaluation and screening of acute toxicity for use in animals, including humans, and contamination of the environment [11,19,22]. In this sense, the evident anti-*Candida* action of isolated essential oils could mean they present lower inhibitory values when combined with other essential oils or antifungal substances, such as clotrimazole, and its acute toxic repercussions.

Thus, in this study, the in vitro inhibitory activity of the essential oils of *Cupressus sempervirens*, *Citrus limon*, *Litsea cubeba* and *Melaleuca alternifolia*, alone and in combination, and associated with clotrimazole, against *Candida* species biofilms were analyzed. Furthermore, the in vivo toxicity of these essential oils against *C. elegans* was also evaluated.

## 2. Materials and Methods

### 2.1. Essential Oils and *Candida* Species

The essential oils (EO) of *Citrus limon*, *Cupressus sempervirens*, *Litsea cubeba* and *Melaleuca alternifolia* (FERQUIMA®; Vargem Grande Paulista, SP, Brazil) were included in this study. The analysis of the EO, carried out by chromatography, was informed by the supplier company and is shown in Table 1. Four reference strains, *Candida albicans* ATCC 90028, *Candida glabrata* ATCC 2001, *Candida krusei* ATCC 6258 and *Candida parapsilosis* ATCC 22019, and four clinical isolates from the vaginal mucosa (*Candida albicans* SV 01, *Candida glabrata* SV 02, *Candida krusei* SV 03 and *Candida parapsilosis* SV 04) obtained from previous studies were included in this study [23]. All microorganisms were stored in brain heart infusion (BHI)–glycerol broth at  $-20\text{ }^{\circ}\text{C}$  and subcultured on Sabouraud dextrose agar (SDA; Disco, Detroit, MI, USA) and CHROMagar *Candida* medium (Becton Dickinson and Company, Sparks, MD, USA), to evaluate the viability and purity, and even to confirm the identification of the species.

**Table 1.** Main components of essential oils from *Citrus limon*, *Cupressus sempervirens*, *Litsea cubeba* and *Melaleuca alternifolia*, according to the supplier company.

Essential Oil	Part of the Plant	Extraction Method	Main Components
<i>C. limon</i>	Fruit	Cold pressing	Limonene (65.6%), $\beta$ -pinene (15.06%), $\gamma$ -terpinene (7.93%), $\alpha$ -pinene (2.34%), sabinene (1.76%) and myrcene (1.55%)
<i>C. sempervirens</i>	Leaf	NI	$\alpha$ -Pinene (52.4%), $\delta$ -3-carene (22%), limonene (3.5%), terpinolene (3.4%), myrcene (2.4%), terpenyl acetate (1.7%), cedrol (1.4%), $\beta$ -pinene (1.2%) and terpinen-4-ol (1%)
<i>L. cubeba</i>	Fruit	Steam distillation	Geranyl acetate (42%), neral (30%) and limonene (13%)
<i>M. alternifolia</i>	Leaf	Steam distillation	Terpinen-4-ol (41%), $\gamma$ -terpinene (20.5%), $\alpha$ -terpinene (9.63%), $\alpha$ -terpinolene (3.37%), $\alpha$ -terpineol (2.78%), $\alpha$ -pinene (2.59%), $p$ -cymene (2.39%), aromadendrene (2%), vidiflorene (1.81%), $\delta$ -cadinene (1.54%) and 1,8-cineol (1.50%)

NI: not informed. Chemical analysis of the oils by chromatography was provided by the supplier company.

### 2.2. Determination of the Minimum Inhibitory Concentration (MIC) and Minimum Fungicidal Concentration (MFC)

To determine the MIC of EO and antifungal agents, the broth microdilution method was used [24], with some adaptations. Flat-bottomed 96-well plates (Kasvi, PR, Brazil) and RPMI-1640 broth with glutamine and without sodium bicarbonate (Corning Incorporated, Corning, NY, USA) were used, plus 18 g/L of glucose (Sigma-Aldrich, St. Louis, MO, USA), buffered with MOPS at pH 7 (Sigma-Aldrich, St. Louis, MO, USA) as a culture medium, and yeast suspension at a resulting final concentration of  $0.5\text{--}2.5 \times 10^3$  CFU/mL. The concentration ranges varied from 7.81 to 4000  $\mu\text{g/mL}$  for EO, from 0.03 to 16  $\mu\text{g/mL}$  for amphotericin B (Sigma-Aldrich, St. Louis, MO, USA) and from 0.125 to 64  $\mu\text{g/mL}$  for fluconazole and clotrimazole (Sigma-Aldrich, St. Louis, MO, USA). Amphotericin B and fluconazole were used as controls [24].

EO and amphotericin B were solubilized in DMSO (dimethyl sulfoxide; 2%), fluconazole and clotrimazole in water and later diluted in RPMI. *C. parapsilosis* ATCC 22019 and *C. krusei* ATCC 6258 strains were used to validate the tests [24]. The MIC was determined in a spectrophotometer at 490 nm [24]. The cut-off point for defining susceptibility was set at 80% inhibition of fungal growth compared to azole-free growth and 90% inhibition for amphotericin B [24] and EO [25]; cultures were incubated for 24 h at 35 °C. The tests were performed in triplicate.

The MFC was determined by transferring 5  $\mu\text{L}$  of cell suspension from each well to a plate containing SDA, followed by incubation for 48 h at 30 °C. The MFC was the one corresponding to the concentration of the well where the growth of yeast colonies was no longer evident [26]. The ratio of the MFC and MIC of EO and clotrimazole was used to interpret the results, defining the drug as fungistatic (MFC/MIC: >4) or fungicidal (MFC/MIC:  $\leq 4$ ) [27].

### 2.3. Evaluation of the Activity of EO and Clotrimazole against *Candida* spp. Biofilms

#### 2.3.1. Determination of the Minimum Biofilm-Inhibiting Concentration (MBIC)

Inhibition of biofilm formation was determined in 96-well, flat-bottomed plates [28], to which 100  $\mu\text{L}$  of cell suspension in RPMI-1640 was added ( $1$  to  $5 \times 10^6$  cells/mL, adjusted to a turbidity equivalent to 0.5 McFarland scale), as well as 100  $\mu\text{L}$  of the drug (EO and/or clotrimazole), at concentrations of  $4 \times \text{MIC}$ ,  $2 \times \text{MIC}$ ,  $1 \times \text{MIC}$ ,  $0.5 \times \text{MIC}$  and  $0.25 \times \text{MIC}$ . The culture was incubated at 35 °C for 48 h. Then, non-adherent cells were removed, and the wells were washed three times with PBS (10 mM phosphate buffer, 2.7 mM potassium chloride, 137 mM sodium chloride, pH 7.4). Then, 100  $\mu\text{L}$  of MTT solution (5 mg/mL; 3-(4,5-dimethyl-2-thiazolyl)-2,5-diphenyl-2H tetrazolium bromide; Sigma-Aldrich, St. Louis, MO, USA) plus 10  $\mu\text{L}$  of phytomenadione (1  $\mu\text{M}$ ; 2-methyl-3-[(E,7R,11R)-3,7,11,15-tetramethylhexadec-2-enyl]naphthalene-1, 4-dione; Sigma-Aldrich,

St. Louis, MO, USA) was added to each well. The plate was incubated at 35 °C for 24 h in the dark. Subsequently, the supernatant was removed, and 100 µL of DMSO was added to each well, and the plate was incubated at 35 °C for 15 min, protected from light. Then, 80 µL of solvent was removed from each well and transferred to another plate, and the reading was performed at 490 nm [29]. Growth and sterility controls were included for each plate in the experiment. The tests were performed in triplicate.

### 2.3.2. Determination of the Minimum Biofilm-Eradication Concentration (MBEC)

The biofilm was previously formed in 96-well, flat-bottomed plates. Two hundred microliters of the yeast cell suspension were added to each well (1 to 5 × 10<sup>6</sup> cells/mL, adjusted to 0.5 McFarland in RPMI-1640), and the plates were incubated at 35 °C for 48 h [28]. Then, non-adherent cells were removed, and the wells were washed three times with PBS. Then, 100 µL of the drug (EO and/or clotrimazole) was added at concentrations of 4 × MIC, 2 × MIC, 1 × MIC, 0.5 × MIC and 0.25 × MIC and incubated at 35 °C for 24 h in the dark. The procedures for revealing the biofilm were the same as described in the previous item.

### 2.4. Evaluation of the Synergistic Potential of EO–EO and EO–Clotrimazole Associations against Planktonic Growth and on Biofilms

To evaluate the combined effect of EO and clotrimazole on planktonic cells, the checkerboard technique was used [30,31]. The synergistic potential of the combination of the EO of *C. sempervirens*, *C. limon*, *L. cubeba* and *M. alternifolia* among themselves and of each one of them with clotrimazole on the *Candida* biofilm was made according to the results obtained for the MIC of the planktonic cells, as provided in the Supplementary Material (Table S1). Concentrations of 0.25 × MIC, 0.5 × MIC, 1 × MIC, 2 × MIC and 4 × MIC were used for drug testing. Then, 100 µL of drug A (EO) horizontal and 100 µL of drug B (EO/clotrimazole) vertical, and 100 µL of cell suspension (1 to 5 × 10<sup>3</sup> cells/mL) were added to all wells of a 96-well flat-bottomed plate. Growth (containing drug-free yeast suspension) and sterility (RPMI-1640) controls were included in each plate. The plates were incubated at 35 °C for 48 h, and the reading was performed at 490 nm; results were considered capable of reducing ≥ 90% of optical density (OD) in relation to the control free of EO and clotrimazole [30]. The results were interpreted according to the fractional inhibitory concentration index (FICI), determined as follows:

$$\text{FICI} : \left( \frac{\text{MIC "A" combined}}{\text{MIC "A" isolated}} \right) + \left( \frac{\text{MIC "B" combined}}{\text{MIC "B" isolated}} \right) \quad (1)$$

The interpretation was conducted according to the classification of the substance interaction score, where antagonism was considered when the score was greater than 4.0, indifference at a score greater than 1, additivity at a score between 0.5 and 1.0, and synergism at a score less than 0.5 [31]. One hundred microliters of the combined solution "A" (EO) and "B" (EO or clotrimazole) was added to each well, starting from column 11 and column 2. Briefly, the first and last wells received the highest concentrations of each of the two compounds evaluated, resulting in decreasing concentrations from one end of the plate to the other. Growth and sterility controls were included in each of the plates, and each experiment was conducted in triplicate.

### 2.5. Toxicity Assay for *Caenorhabditis elegans*

The toxicity test was performed by exposing *C. elegans* larvae (AU37 [glp-4 (bn2) I; mutant strain sek-1 (km4) X] to EO and clotrimazole [25].

*C. elegans* larvae were transferred to nematode growth medium (NGM), contained in Petri dishes, which contained a previous mat of *Escherichia coli* OP50 (*E. coli*). The plates were incubated at 16 °C for 72 h. Then, synchronization of the larvae in stage L2 was performed by treating the larvae with sodium hypochlorite. Then, the larvae were

transferred to another plate containing NGM medium without *E. coli* OP50 and incubated at 16 °C for 24 h [20,32].

For the experiment, a solution medium, composed of 40% BHI broth, plus cholesterol (10 µg/mL), kanamycin (90 µg/mL), ampicillin (200 µg/mL) and 60% 50 mM NaCl, was used. The assay was performed using 96-well flat-bottomed plates. Then, 180 µL of solution medium and 20 µL of the suspension of synchronized larvae in stage L4 were added to each well of the plate so that 10 to 20 *C. elegans* larvae were placed in each well, evaluated in final serial concentrations ranging from 4000 to 250 µg/mL diluted in solution medium. As a survival control, solution medium plus the larvae, without drug, was used, and as a test control, solution medium and DMSO were used. The plates were incubated for 24 h at 35 °C in a humid chamber.

The results were interpreted considering the survival rate of the larvae and the 50% lethal dose (LD<sub>50</sub>), determined by the concentration of the drug that was able to kill 50% of the larvae [33,34]. Each experiment was performed twice in triplicate.

### 3. Results

#### 3.1. Determination of the MIC and MFC of Essential and Antifungal Oils against Planktonic Growth

The lowest MIC (500 µg/mL) found was for *C. krusei* SV 03, with the EO of *C. sempervirens* and *L. cubeba*. The MIC of the EO ranged from 500 to >4000 µg/mL, considering the different oils and the eight isolates tested. The EO of *C. limon* presented an MIC that ranged from 1000 to 4000 µg/mL, *C. sempervirens* from 500 to >4000 µg/mL, *L. cubeba* from 500 to 2000 µg/mL and *M. alternifolia* from 1000 to 2000 µg/mL. For clotrimazole, the MIC ranged from 0.015 to 0.5 µg/mL (Table 1). The MIC of fluconazole and amphotericin B (test validation controls) were, respectively, 32 and 1 µg/mL; those for *C. krusei* ATCC 6258 and *C. parapsilosis* ATCC 2019 were 0.25 and 0.25 µg/mL, respectively.

The lowest fungicidal concentrations (1000 µg/mL) were found for the EO of *C. limon* against *C. albicans* ATCC 90028, *C. sempervirens* against *C. krusei* SV 03 and *L. cubeba* against *C. albicans* ATCC 90028 and *C. krusei* SV 03; for clotrimazole, the lowest fungicidal concentration (0.030 µg/mL) was found for the isolate of *C. glabrata* ATCC 2001.

Evaluation of the fungicidal activity (MFC/MIC: ≤4) showed that the EO of *L. cubeba* and the antifungal clotrimazole were fungicidal for all the tested isolates; however, all the other EO evaluated presented fungicidal activity dependent on the isolate, as can be seen in Table 2. Thus, fungicidal activity was found for the EO of *C. limon*, *M. alternifolia* and *C. sempervirens*, respectively, for four, five and six isolates.

**Table 2.** Minimum inhibitory concentration (µg/mL) and minimum fungicidal concentration (µg/mL) of essential oils and clotrimazole tested with *Candida* species.

<i>Candida</i> spp. Isolates	<i>C. limon</i>		<i>C. sempervirens</i>		<i>L. cubeba</i>		<i>M. alternifolia</i>		Clotrimazole	
	MIC	MFC	MIC	MFC	MIC	MFC	MIC	MFC	MIC	MFC
<i>C. albicans</i> ATCC 90028	<b>2000</b>	1000	<b>2000</b>	4000	<b>1000</b>	1000	<b>2000</b>	4000	<b>0.25</b>	0.25
<i>C. albicans</i> SV 01	4000	>4000	4000	>4000	<b>2000</b>	4000	4000	>4000	<b>0.125</b>	0.25
<i>C. glabrata</i> ATCC 2001	<b>4000</b>	4000	<b>2000</b>	4000	<b>2000</b>	4000	<b>4000</b>	4000	<b>0.015</b>	0.030
<i>C. glabrata</i> SV 02	4000	>4000	<b>1000</b>	4000	<b>2000</b>	4000	4000	>4000	<b>0.25</b>	0.5
<i>C. krusei</i> ATCC 6258	4000	>4000	<b>2000</b>	4000	<b>1000</b>	2000	<b>4000</b>	4000	<b>0.5</b>	1
<i>C. krusei</i> SV 03	<b>1000</b>	4000	<b>500</b>	1000	<b>500</b>	1000	<b>2000</b>	4000	<b>0.5</b>	1
<i>C. parapsilosis</i> ATCC 22019	<b>1000</b>	4000	<b>4000</b>	4000	<b>1000</b>	4000	<b>4000</b>	4000	<b>0.25</b>	0.5
<i>C. parapsilosis</i> SV 04	4000	>4000	>4000	>4000	<b>2000</b>	4000	4000	>4000	<b>0.125</b>	0.25

MIC: minimum inhibitory concentration (µg/mL); MFC: minimum fungicidal concentration (µg/mL). Fungicide: (MFC/MIC: <4) in **bold**.

### 3.2. Assessment of the Development of *Candida* spp. Biofilms

The activity of EO and clotrimazole to inhibit (MBIC) and eradicate (MBEC) the biofilm formed by *Candida* species is shown in Table 3. Most EO presented an MBIC greater than or equal to 4000 µg/mL. The lowest MBIC was 1000 µg/mL, found for *C. semperivirens* (*C. krusei* SV 03), *L. cubeba* (*C. albicans* ATCC 90028) and *M. alternifolia* (*C. krusei* SV 03). The lowest MBEC was 1000 µg/mL for *L. cubeba* (*C. albicans* ATCC 90028). Clotrimazole demonstrated MBIC and MBEC values ranging from 0.125 to 2 µg/mL and 0.25 to 4 µg/mL, respectively.

**Table 3.** Activity of essential oils and clotrimazole against the formation of biofilms and preformed biofilms of *Candida* species.

Species	<i>C. limon</i>			<i>C. semperivirens</i>			<i>L. cubeba</i>			<i>M. alternifolia</i>			Clotrimazole		
	MIC	MBIC	MBEC	MIC	MBIC	MBEC	MIC	MBIC	MBEC	MIC	MBIC	MBEC	MIC	MBIC	MBEC
<i>C. albicans</i> ATCC 90028	2000	4000	4000	2000	4000	>4000	<b>1000</b>	<b>1000</b>	<b>1000</b>	2000	2000	4000	0.25	1	1
<i>C. albicans</i> SV 01	4000	>4000	>4000	4000	4000	4000	2000	2000	4000	4000	4000	4000	0.125	0.5	1
<i>C. glabrata</i> ATCC 2001	4000	>4000	>4000	2000	>4000	4000	2000	2000	>4000	4000	4000	>4000	0.015	0.125	0.25
<i>C. glabrata</i> SV 02	4000	>4000	>4000	1000	>4000	>4000	2000	>4000	>4000	4000	4000	>4000	0.25	0.5	1
<i>C. krusei</i> ATCC 6258	4000	>4000	>4000	2000	2000	2000	<b>1000</b>	>4000	>4000	2000	4000	>4000	0.5	1	2
<i>C. krusei</i> SV 03	<b>1000</b>	2000	4000	<b>500</b>	<b>1000</b>	>4000	<b>500</b>	4000	>4000	<b>1000</b>	<b>1000</b>	>4000	0.5	1	1
<i>C. parapsilosis</i> ATCC 22019	<b>1000</b>	>4000	>4000	4000	4000	>4000	<b>1000</b>	4000	>4000	4000	4000	>4000	0.25	2	4
<i>C. parapsilosis</i> SV 04	4000	>4000	>4000	>4000	4000	>4000	2000	>4000	>4000	4000	>4000	>4000	0.125	0.25	0.5

Isolated MBIC and MBEC (µg/mL): capable of reducing  $\geq 90\%$  of optical density (OD) compared to control free of EO and clotrimazole. Results in **bold**:  $\leq 1000$  µg/mL.

### 3.3. Evaluation of Synergism of EO and Clotrimazole

The tests of EO–EO and EO–clotrimazole combinations resulted in 80 combinations; of these, 13 (16.25%) showed antagonism, 42 (52.5%) showed indifference, 17 (21.25%) had an additive effect and 8 (10%) showed synergism. The OE–OE and OE–clotrimazole combinations performed and their results related to inhibition of *Candida* spp. are provided in the Supplementary Materials (Table S1). The synergistic effect was variable, depending on the combination (EO–EO or EO–clotrimazole) and the *Candida* strain. The EO–EO and EO–clotrimazole combinations that showed synergism in the evaluation of MIC were selected for evaluation of inhibition (MBIC) and eradication (MBEC) of biofilms (Table 4).

**Table 4.** Minimum inhibitory, biofilm-inhibitory and biofilm-eradication concentrations of EO–EO and EO–clotrimazole combinations against *Candida* species.

Species	Combination	MIC (µg/mL)		Biofilm (µg/mL)			
		Isolated MIC *	Combined MIC **	Isolated MBIC *	Combined MBIC **	Isolated MBEC *	Combined MBEC **
<i>C. albicans</i> ATCC 90028	<i>M. alternifolia</i>	2000	250	2000	62.5	4000	62.5
	Clotrimazole	0.25	0.063	1	0.25	1	0.25
<i>C. albicans</i> SV 01	<i>L. cubeba</i>	2000	250	2000	125	4000	250
	<i>M. alternifolia</i>	4000	1000	4000	2000	4000	1000
<i>C. glabrata</i> ATCC 2001	<i>L. cubeba</i>	2000	500	2000	2000	>4000	2000
	<i>C. limon</i>	4000	1000	>4000	250	>4000	250
<i>C. glabrata</i> SV 02	<i>L. cubeba</i>	2000	250	>4000	1000	>4000	>1000
	<i>M. alternifolia</i>	4000	1000	4000	250	>4000	>250
	<i>C. limon</i>	4000	1000	>4000	4000	>4000	4000
	<i>M. alternifolia</i>	4000	1000	4000	250	>4000	250

Table 4. Cont.

Species	Combination	MIC ( $\mu\text{g/mL}$ )		Biofilm ( $\mu\text{g/mL}$ )			
		Isolated MIC *	Combined MIC **	Isolated MBIC *	Combined MBIC **	Isolated MBEC *	Combined MBEC **
<i>C. krusei</i> ATCC 6258	<i>C. sempervirens</i>	2000	1000	2000	4000	2000	>4000
	<i>C. limon</i>	4000	250	>4000	62.5	>4000	>250
	<i>C. limon</i>	1000	1000	>4000	4000	>4000	2000
	<i>M. alternifolia</i>	2000	1000	4000	250	>4000	500
<i>C. parapsilosis</i> SV 04	<i>C. sempervirens</i>	>4000	250	4000	500	>4000	125
	Clotrimazole	0.125	0.032	0.25	0.015	0.5	0.063

Isolated MBIC and MBEC ( $\mu\text{g/mL}$ ): able to reduce by  $\geq 90\%$  optical density (OD) compared to control free of EO and clotrimazole. \* Isolated: only one substance (EO or clotrimazole). \*\* Combined: MIC of the combination (EO–EO or EO–clotrimazole) that resulted in synergism.

### 3.4. In Vivo Assay in *Caenorhabditis elegans*

The test of acute toxicity of EO and clotrimazole against *C. elegans* showed average survival greater than 90% of larvae for the concentration of 250  $\mu\text{g/mL}$  of all tested EO; and for clotrimazole, 100% of *C. elegans* larvae survived at all concentrations within the evaluated range (0.125–4  $\mu\text{g/mL}$ ). It was not possible to determine the  $\text{LC}_{50}$  of *C. sempervirens* because at all concentrations evaluated, survival occurred in more than 90% of the larvae; the  $\text{LC}_{50}$  for the EO of *M. alternifolia* was 2000  $\mu\text{g/mL}$  and for *C. limon* and *L. cubeba* it was 4000  $\mu\text{g/mL}$  (Figure 1; Table 5). The test controls showed that DMSO concentrations  $\leq 5\%$  did not affect the survival of *C. elegans* larvae, and the untreated control showed a mean survival of 96% at 24 h.

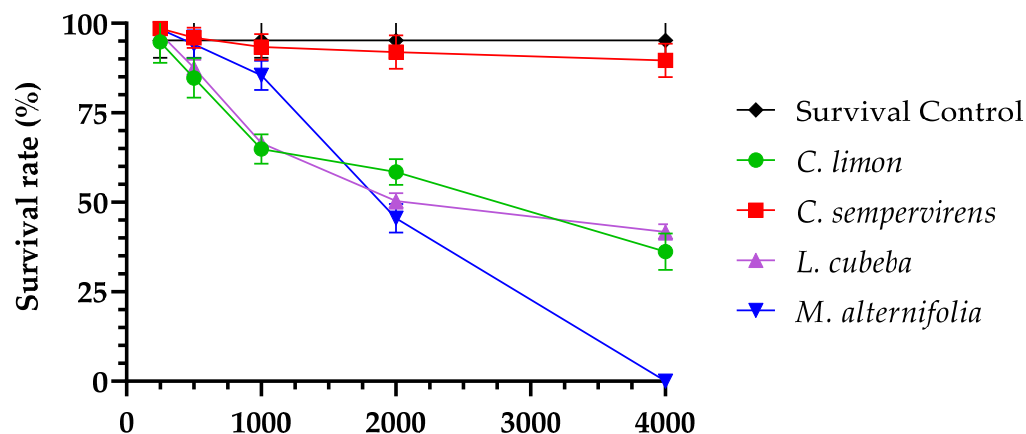


Figure 1. Survival rate (%) of *C. elegans* larvae in 24 h, evaluated at different concentrations of essential oils of *C. limon*, *C. sempervirens*, *L. cubeba* and *M. alternifolia*.

Table 5. Mean survival rate (%) of *C. elegans* tested at different concentrations of essential oils from *C. limon*, *C. sempervirens*, *L. cubeba* and *M. alternifolia*.

Concentration ( $\mu\text{g/mL}$ )	<i>C. limon</i>	<i>C. sempervirens</i>	<i>L. cubeba</i>	<i>M. alternifolia</i>
250	95.83	97.83	97.83	97.82
500	85.96	95.35	87.76	94.00
1000	64.58	93.48	67.50	85.11
2000	58.82	92.86	51.11 *	46.15 *
4000	37.25 *	88.64	40.43	0

\*  $\text{LC}_{50}$ : lethal concentration responsible for the mortality of 50% of *C. elegans* larvae.

The EO–EO and EO–clotrimazole combinations that showed synergism in the evaluation of the MIC were selected to evaluate the survival of *C. elegans* larvae. Overall, the combinations showed a mean survival of 90% of the larvae for the combinations *L. cubeba*–*M. alternifolia*, *C. sempervirens*–*C. limon*, *M. alternifolia*–clotrimazole and *C. sempervirens*–clotrimazole (Table 6). Survival of less than 20% of larvae, demonstrating greater acute toxicity, was found for the combinations *C. limon*–*M. alternifolia* and *L. cubeba*–*C. limon*.

**Table 6.** Survival rate (%) of *C. elegans* subjected to combinations of essential oil and clotrimazole after 24 h of exposure.

Compound "A"	Concentration (µg/mL)	Compound "B"	Concentration (µg/mL)	Survival (% Average)
<i>M. alternifolia</i>	250	Clotrimazole	0.063	88.89
<i>L. cubeba</i>	250	<i>M. alternifolia</i>	1000	93.3
<i>C. sempervirens</i>	250	Clotrimazole	0.032	100.00
<i>C. sempervirens</i>	1000	<i>C. limon</i>	250	90.00
<i>C. limon</i>	1000	<i>M. alternifolia</i>	1000	18.52
<i>L. cubeba</i>	500	<i>C. limon</i>	1000	13.79

#### 4. Discussion

EO have been extensively studied nowadays and can be a complementary alternative for the treatment of infections caused by *Candida* species, especially mucocutaneous infections. This study investigated the activity of the EO of *C. limon*, *C. sempervirens*, *L. cubeba* and *M. alternifolia*, alone and in combination with each other and with clotrimazole, on four species of the genus *Candida*, to determine in vitro the MIC, MBIC and MBEC; in addition to this, an in vivo toxicity assessment for the nematode *C. elegans* was performed.

The EO extracted from plants of the studied species are products that have a complex chemical composition and may have more than 20 identified compounds [12–15,18]. Our study used EO that presented limonene (65.6%),  $\alpha$ -pinene (52.4%), terpinen-4-ol (41%) and geranyl acetate (42%) as the main component, respectively, for *C. limon*, *C. sempervirens*, *M. alternifolia* and *L. cubeba*. These constituents are like those described for EO of these plants in other studies [15,18,29,35–41]. Terpene derivatives, a class that includes the mentioned constituents, are closely related to the antimicrobial biological action of these EO, as already demonstrated for *Candida* spp. in other studies [13,15,16,41–43].

In the present study, the MIC varied according to the isolate and according to the EO, but the EO of *C. sempervirens* and *L. cubeba* presented the lowest MIC (500 µg/mL) for the same species (*C. krusei* SV 03), while *M. alternifolia* and clotrimazole combined (62.5–0.25 µg/mL) inhibited *C. albicans* ATCC 90028 at lower concentrations than in isolation. In this sense, the ranges of results for the EO showed the effectiveness of plant-derived products in inhibiting microorganisms [42,43], a significant finding for the genus, given the recognized adaptive antifungal arsenal associated with *C. albicans* and the intrinsic fluconazole resistance of *C. krusei* [9,20,44].

This variability of MIC can be observed in the literature [9,18] and is due to the characteristics of each isolate, which may be related to virulence factors and the origin of the isolate (blood, feces, respiratory tract or environment). In addition to this, storage and the constant activation and reactivation of cells, which occur in repeated cultures, may have generated adaptive changes in the phenotypic profile of the reference strains [45].

The MFC were, on average, 2 × MIC for most isolates and EO, but for some, it was not possible to make this determination, as the values were greater than 4000 µg/mL, that is, greater than the limits of concentrations tested. Still, MIC and MFC of 2000 and 1000 µg/mL, respectively, were observed for *C. albicans* ATCC 90028 when evaluated for the EO of *C. limon*. This fact may be explained if the growth curve of cells in contact with this EO is evaluated, as it is possible that the fungicidal effect occurs through mechanisms that involve the depletion of some essential intracellular constituent for growth, such as ergosterol reserves, associated with other mechanisms of enzymatic inhibition, or action

on the membrane or cell wall [46] which is time-dependent, but other assays need to be performed to elucidate this finding.

The anti-*Candida* activity of EO may be a direct result of the interaction of the various chemical components present and the association of different mechanisms, which may explain the fungistatic and fungicidal effects. The characteristics common to EO, such as lipophilicity and ability to cause damage to vital structures, membrane, and cell wall, result in increased membrane permeability and release of intracellular contents, with consequent death of *Candida* spp. cells [13,37].

The fungistatic action of clotrimazole at low concentrations is due to structural changes in ergosterol; at high concentrations, it has a fungicidal effect [6]. Thus, it can be assumed that the potentiation of the effects, demonstrated by the synergism observed in the association of clotrimazole with different proportions of EO, is the result of the multiplicity of mechanisms resulting from the various constituents of the EO, leading to the fungicidal effect [47]. The activity of EO against biofilm [10,13,17,25,26,48–51] is another factor that contributes to the need for studies that evaluate the combination of other drugs and a greater number of EO [26,47,51,52].

The application of a product with simultaneous inhibition of microbial growth and biofilm is advantageous since it allows for more efficient satisfactory results in different structures of *Candida* spp. The present study demonstrated that there was inhibition of biofilm formation and a reduction in the viability of the cells of previously formed biofilm, with MIC up to five times lower for the synergistic combination when compared to the same MIC found for the drugs evaluated alone. This study is the first, to our knowledge, to present a synergistic relationship of EO–EO and EO–clotrimazole on *Candida* spp., evaluating their action on biofilms.

The initial assessment of a substance, such as toxicity and antifungal activity, is a preliminary step in the design of new drug and health product candidates [32]. Our study sought to evaluate the safety of EO and clotrimazole alone, as well as in combinations, exposed for 24 h to the in vivo model *C. elegans*. It was observed that more than 80% of *C. elegans* larvae survived at concentrations of 500 µg/mL for three of the evaluated EO. For *C. sempervirens*, 80% of the larvae survived at the concentration of 4000 µg/mL, and for clotrimazole, the survival of 100% of the larvae was observed at all concentrations.

Among the EO evaluated, the biological activity of the EO of *C. limon* and *M. alternifolia* is better known when compared with those of *L. cubeba* and *C. sempervirens* [18]. As observed in Table 4, the LC<sub>50</sub> was not determined for the EO of *C. sempervirens* (LC<sub>50</sub>: >4000 µg/mL), suggesting that it is the least toxic for *C. elegans* larvae among the four evaluated. Our study demonstrated that lethal toxicity of *L. cubeba* EO against *C. elegans* larvae was at 2000 µg/mL; however, lower concentrations such as 0.120–0.525 mg/mL (120–525 µg/mL) were found previously for the nematode *Bursaphelenchus xylophilus* [37]. In our study, we found lower toxicity of *C. sempervirens* EO alone; however, it was moderate and high for other combinations (OE–OE and OE–clotrimazole). Some studies have provided other models for assessing toxicity by evaluating different cell cultures, showing that in vitro inhibitory concentrations (IC<sub>50</sub>) for MCF-7 and MDA-MB-231 mammary tumor cells were lower than 34.5 and 65.2 µg/mL, respectively [53], and that *C. sempervirens* is lethal at higher concentrations in human promyelocytic leukemia strains (HL-60 and NB4) (LC<sub>50</sub>: 333.79 to 365.41 µg/mL) [38] and in experimental animal Ehrlich ascitic carcinoma (LC<sub>50</sub>: 372.43 µg/mL) [38]. In the larvae of *Culex quinquefasciatus*, a non-vertebrate model and vector of filariasis, the LC<sub>50</sub> was 16.1 µg/mL after 24 h of exposure [39].

The complexity of factors intrinsic to EO, such as the variability and concentration of chemotypes, which can vary in the same plant species according to the part of the plant used for extraction, region of cultivation and stage of development, may be, in part, responsible for the different results obtained in the same toxicity model used. In different models, this variability of constituents can be even greater, as can be seen in some studies [12,15,18,41,49,53]. Thus, it is suggested that toxicity is evaluated in different



models to obtain evidence of greater safety and definition of the best drug concentrations that may have biological action and an absence or reduction of damage.

Our study focused on the preliminary assessment of EO–EO and EO–clotrimazole combinations, using concentration ranges applied predictively to planktonic cells and subsequently to biofilm and *C. elegans* after 24 h. Therefore, the totality of combinations that the checkerboard provides for the biofilm was not explored, nor was the influence of different exposure times of the substances for inhibition, eradication and toxicity. Our study used evaluation in the *C. elegans* model; therefore, it is important to evaluate correlation with the results in other models for a better understanding of the mechanism related to toxicity, including the use of EO in biocompatible pharmaceutical applications in nanosystems to improve aspects of physicochemical and biological agents against *Candida* spp.

The complexity of the composition of EO allows wide use in alternative and complementary medicine. The exploration of antimicrobial activity may enable new strategies and therapeutic alternatives for infectious diseases, especially mucocutaneous ones, where topical application is possible. The association of EO makes it possible for some constituents, even though they are not in the majority, to interact, enhancing or evidencing biological effects and reducing toxicity. In this context, studies still need to be carried out to determine the practical relevance of the combinations, better concentrations of each one of them, and the economic and market viability, in addition to the advantages over existing products.

## 5. Conclusions

The EO–EO and EO–clotrimazole combinations showed synergistic activity in vitro, dependent on the isolate and on the *Candida* species, and of the combined drugs, when evaluating the inhibition of planktonic growth in vitro and the inhibition of biofilm formation and eradication. The combinations *M. alternifolia*–clotrimazole, *L. cubeba*–*M. alternifolia*, *C. semperovirens*–clotrimazole and *C. semperovirens*–*C. limon* were the most efficient against planktonic cells and biofilm. In addition, they demonstrated low or negligible toxicity to *C. elegans* larvae. Thus, our results suggest that the drug combinations evaluated here show promising activity in the control and treatment of vaginal infections caused by *Candida* species, for topical application through different devices, for example, local nanorelease systems, such as mucoadhesive formulations.

**Supplementary Materials:** The following supporting information can be downloaded at: <https://www.mdpi.com/article/10.3390/pharmaceutics14091872/s1>, Table S1: Combinations between OE–OE and OE–clotrimazole in *Candida* species.

**Author Contributions:** Concept, research, writing, review and editing, R.A.d.S., N.B.S.S., R.H.P., C.H.G.M., D.V.D.d.B.R. and R.d.S.P.; supervision, D.V.D.d.B.R. and R.d.S.P. All authors have read and agreed to the published version of the manuscript.

**Funding:** This study was financed in part by the Coordenação de Aperfeiçoamento de Pessoal de Nível Superior—Brasil (CAPES)—Finance Code 001.

**Institutional Review Board Statement:** Not applicable.

**Informed Consent Statement:** Not applicable.

**Data Availability Statement:** Not applicable.

**Acknowledgments:** To Coordenação de Aperfeiçoamento de Pessoal de Nível Superior (CAPES) for the master's scholarship awarded to R.A.S.

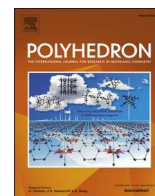
**Conflicts of Interest:** The authors declare no conflict of interest.

## References

1. Pfaller, M.A.; Diekema, D.J.; Turnidge, J.D.; Castanheira, M.; Jones, R.N. Twenty Years of the SENTRY Antifungal Surveillance Program: Results for *Candida* Species from 1997–2016. In *Open Forum Infectious Diseases*; Oxford University Press: Oxford, UK, 2019.
2. Silva-Rocha, W.P.; Azevedo, M.F.; Chaves, G.M. Epidemiology and fungal species distribution of superficial mycoses in Northeast Brazil. *J. Mycol. Méd.* **2017**, *27*, 57–64. [[CrossRef](#)] [[PubMed](#)]
3. Gonçalves, B.; Ferreira, C.; Alves, C.T.; Henriques, M.; Azeredo, J.; Silva, S. Vulvovaginal candidiasis: Epidemiology, microbiology and risk factors. *Crit. Rev. Microbiol.* **2016**, *42*, 905–927. [[CrossRef](#)]
4. Willems, H.M.E.; Ahmed, S.S.; Liu, J.; Xu, Z.; Peters, B.M. Vulvovaginal Candidiasis: A Current Understanding and Burning Questions. *J. Fungi* **2020**, *6*, 27. [[CrossRef](#)] [[PubMed](#)]
5. Denning, D.W.; Kneale, M.; Sobel, J.D.; Rautema-Richardson, R. Global burden of recurrent vulvovaginal candidiasis: A systematic review. *Lancet Infect. Dis.* **2018**, *18*, e339–e347. [[CrossRef](#)]
6. Soriano-Ruiz, J.L.; Calpena-Capmany, A.C.; Canadas-Enrich, C.; Febrer, N.B.; Suner-Carbo, J.; Souto, E.B.; Clares-Naveros, B. Biopharmaceutical profile of a clotrimazole nanoemulsion: Evaluation on skin and mucosae as anticandidal agent. *Int. J. Pharm.* **2019**, *554*, 105–115. [[CrossRef](#)]
7. Taudorf, E.H.; Jemec, G.B.E.; Hay, R.J.; Saunte, D.M.L. Cutaneous candidiasis—an evidence-based review of topical and systemic treatments to inform clinical practice. *J. Eur. Acad. Dermatol. Venereol.* **2019**, *33*, 1863–1873. [[CrossRef](#)]
8. Silva, S.; Rodrigues, C.F.; Araújo, D.; Rodrigues, M.; Henriques, M. *Candida* Species Biofilms' Antifungal Resistance. *J. Fungi* **2017**, *3*, 8. [[CrossRef](#)]
9. Santos, G.C.D.O.; Vasconcelos, C.C.; Lopes, A.J.O.; dos Cartágenes, M.; Filho, A.K.D.B.; do Nascimento, F.R.F.; Ramos, R.M.; Pires, E.R.R.B.; de Andrade, M.S.; Rocha, F.M.G.; et al. *Candida* Infections and Therapeutic Strategies: Mechanisms of Action for Traditional and Alternative Agents. *Front. Microbiol.* **2018**, *9W*, 1351. [[CrossRef](#)]
10. Sardi, J.C.O.; Scorzoni, L.; Bernardi, T.; Fusco-Almeida, A.M.; Giannini, M.M. *Candida* species: Current epidemiology, pathogenicity, biofilm formation, natural antifungal products and new therapeutic options. *J. Med. Microbiol.* **2013**, *62*, 10–24. [[CrossRef](#)]
11. Scorzoni, L.; de Paula e Silva, A.C.A.; Marcos, C.M.; Assato, P.A.; de Melo, W.C.M.A.; de Oliveira, H.C.; Costa-Orlandi, C.B.; Mendes-Giannini, M.J.S.; Fusco-Almeida, A.M. Antifungal Therapy: New Advances in the Understanding and Treatment of Mycosis. *Front. Microbiol.* **2017**, *8*, 36. [[CrossRef](#)]
12. Mutlu-Ingok, A.; Devecioglu, D.; Dikmetas, D.N.; Karbancioglu-Guler, F.; Capanoglu, E. Antibacterial, antifungal, antimycotoxic, and antioxidant activities of essential oils: An updated review. *Molecules* **2020**, *25*, 4711. [[CrossRef](#)] [[PubMed](#)]
13. Cannas, S.; Usai, D.; Tardugno, R.; Benvenuti, S.; Pellati, F.; Zanetti, S.; Molicotti, P. Chemical composition, cytotoxicity, antimicrobial and antifungal activity of several essential oils. *Nat. Prod. Res.* **2016**, *30*, 332–339. [[CrossRef](#)]
14. Tariq, S.; Wani, S.; Rasool, W.; Shafi, K.; Bhat, M.A.; Prabhakar, A.; Shalla, A.H.; Rather, M.A. A Comprehensive Review of the Antibacterial, Antifungal and Antiviral Potential of Essential Oils and Their Chemical Constituents Against Drug-Resistant Microbial Pathogens. *Microb. Pathog.* **2019**, *134*, 103580. [[CrossRef](#)] [[PubMed](#)]
15. Tungmunnithum, D.; Thongboonyou, A.; Pholboon, A.; Yangsabai, A. Flavonoids and other phenolic compounds from medicinal plants for pharmaceutical and medical aspects: An overview. *Medicines* **2018**, *5*, 93. [[CrossRef](#)] [[PubMed](#)]
16. El-Baz, A.; Mosbah, R.; Goda, R.; Mansour, B.; Sultana, T.; Dahms, T.; El-Ganiny, A. Back to Nature: Combating *Candida albicans* Biofilm, Phospholipase and Hemolysin Using Plant Essential Oils. *Antibiotics* **2021**, *10*, 81. [[CrossRef](#)]
17. Jafri, H.; Ahmad, I. Thymus vulgaris essential oil and thymol inhibit biofilms and interact synergistically with antifungal drugs against drug resistant strains of *Candida albicans* and *Candida Tropicalis*. *J. Mycol. Med.* **2020**, *30*, 100911. [[CrossRef](#)] [[PubMed](#)]
18. Silva, R.A.; Antonietti, F.M.P.M.; Röder, D.V.D.B.; Pedroso, R.S. Essential oils of *Melaleuca*, *Citrus*, *Cupressus*, and *Litsea* for the management of infections caused by *Candida* Species: A Systematic Review. *Pharmaceutics* **2021**, *13*, 1700. [[CrossRef](#)]
19. Elkabti, A.B.; Issi, L.; Rao, R.P. *Caenorhabditis elegans* as a Model Host to Monitor the *Candida* Infection Processes. *J. Fungi* **2018**, *4*, 123. [[CrossRef](#)]
20. Scorzoni, L.; de Lucas, M.P.; Mesa-Arango, A.C.; Fusco-Almeida, A.M.; Lozano, E.; Cuenca-Estrella, M.; Mendes-Giannini, M.J.; Zaragoza, O. Antifungal efficacy during *Candida krusei* infection in non-conventional models correlates with the yeast in vitro susceptibility profile. *PLoS ONE* **2013**, *8*, e60047. [[CrossRef](#)]
21. Segal, E.; Frenkel, M. Experimental in vivo models of candidiasis. *J. Fungi* **2018**, *4*, 21. [[CrossRef](#)]
22. Hernando-Ortiz, A.; Mateo, E.; Perez-Rodriguez, A.; de Groot, P.W.J.; Quindós, G.; Eraso, E. Virulence of *Candida auris* from different clinical origins in *Caenorhabditis elegans* and *Galleria mellonella* Host Models. *Virulence* **2021**, *12*, 1063–1075. [[CrossRef](#)]
23. Felix, T.C.; Araújo, L.B.; Brito Röder, D.V.D.; Pedroso, R.S. Evaluation of vulvovaginitis and hygiene habits of women attended in primary health care units of the Family. *Int. J. Women's Health* **2020**, *12*, 49–57. [[CrossRef](#)]
24. Clinical and Laboratory Standards Institute (CLSI). *M27-S4: Reference Method for Broth Dilution Antifungal Susceptibility Testing of Yeasts; Third Informational Supplement*, 3rd ed.; Clinical and Laboratory Standards Institute: Wayne, PA, USA, 2012.
25. Pedroso, R.S.; Balbino, B.L.; Andrade, G.; Dias, M.C.P.S.; Alvarenga, T.A.; Pedroso, R.C.N.; Pires, R.H. In Vitro and In Vivo Anti-*Candida* spp. Activity of plant-derived products. *Plants* **2019**, *11*, 494. [[CrossRef](#)]
26. Nikolić, M.M.; Jovanović, K.K.; Marković, T.L.; Marković, D.L.; Gligorijević, N.N.; Radulović, S.S.; Kostić, M.; Glamočlija, J.M.; Soković, M.D. Antimicrobial synergism and cytotoxic properties of *Citrus limon* L.; *Piper nigrum* L. and *Melaleuca alternifolia* (Maiden and Betche) Cheel essential oils. *J. Pharm. Pharmacol.* **2017**, *69*, 1606–1614. [[CrossRef](#)]

27. Siddiqui, Z.N.; Farooq, F.; Musthafa, T.N.M.; Ahmad, A.; Khan, A.U. Synthesis, characterization and antimicrobial evaluation of novel halopyrazole derivatives. *J. Saudi Chem. Soc.* **2013**, *17*, 237–243. [[CrossRef](#)]
28. Pierce, C.G.; Uppuluri, P.; Tristan, A.R.; Wormley, F.L., Jr.; Mowat, E.; Ramage, G.; Lopez-Ribot, J.L. A simple and reproducible 96-well plate-based method for the formation of fungal biofilms and its application to antifungal susceptibility testing. *Nat. Prot.* **2008**, *3*, 1494–1500. [[CrossRef](#)]
29. Cota, B.B.; Oliveira, D.B.C.; Borges, T.C.; Catto, A.C.; Serafim, C.V.; Rodrigues, A.R.A.; Kohlhoff, M.; Zani, C.L.; Andrade, A.A. Antifungal activity of extracts and purified saponins from the rhizomes of *Chamaecostus cuspidatus* against *Candida* and *Trichophyton* species. *J. Appl. Microbiol.* **2020**, *130*, 61–75. [[CrossRef](#)]
30. American Society for Microbiology. Synergism testing: Broth microdilution checkerboard and broth macrodilution methods. In *Clinical Microbiology Procedures Handbook*; Isenberg, H.D., Ed.; ASM Press: Washington, DC, USA, 1992; pp. 1–28.
31. Odds, F.C. Synergy, antagonism, and what the checkerboard puts between them. *J. Antimicrob. Chemother.* **2003**, *52*, 1. [[CrossRef](#)]
32. Tampakakis, E.; Okoli, I.; Mylonakis, E.A. *C. elegans*-based, whole animal, in vivo screen for the identification of antifungal compounds. *Nat. Protoc.* **2008**, *3*, 1925–1931. [[CrossRef](#)]
33. Lu, L.; Shu, C.; Chen, L.; Yang, Y.; Ma, S.; Zhu, K.; Shi, B. Insecticidal activity and mechanism of cinnamaldehyde in *C. elegans*. *Fitoterapia* **2020**, *146*, 104687. [[CrossRef](#)]
34. Medina-Alarcón, K.P.; Singulani, J.L.; Voltan, A.R.; Sardi, J.C.; Petrônio, M.S.; Santos, M.B.; Polaquini, C.R.; Regasini, L.O.; Bolzani, V.S.; da Silva, D.H.; et al. Alkyl Protocatechuate loaded nanostructured lipid systems as a treatment strategy for *Paracoccidioides brasiliensis* and *Paracoccidioides litizii* in vitro. *Front. Microbiol.* **2017**, *8*, 1048. [[CrossRef](#)]
35. Luo, M.; Jiang, L.K.; Zou, G.L. Acute and genetic toxicity of essential oil extracted from *Litsea cubeba* (Lour.) Pers. *J. Food Prot.* **2005**, *68*, 581–588. [[CrossRef](#)]
36. Hammer, K.A.; Carson, C.F.; Riley, T.V. Antifungal effects of *Melaleuca alternifolia* (tea tree) oil and its components on *Candida albicans*, *Candida glabrata* and *Saccharomyces cerevisiae*. *J. Antimicrob. Chemother.* **2004**, *12*, 1081–1085. [[CrossRef](#)]
37. Park, I.K.; Kim, J.; Lee, S.G.; Shin, S.C. Nematicidal activity of plant essential oils and components from ajowan (*Trachyspermum ammi*), allspice (*Pimenta dioica*) and litsea (*Litsea cubeba*) essential oils against pine wood nematode (*Bursaphelenchus xylophius*). *J. Nematol.* **2007**, *39*, 275–279.
38. Fayed, S.A. Chemical Composition, Antioxidant, Anticancer Properties and Toxicity Evaluation of Leaf Essential Oil of *Cupressus sempervirens*. *Not. Bot. Horti Agrobot. Cluj-Napoca* **2015**, *43*, 320–326. [[CrossRef](#)]
39. Almadiy, A.A.; Nenaah, G.E. Bioactivity and safety evaluations of *Cupressus sempervirens* essential oil, its nanoemulsion and main terpenes against *Culex quinquefasciatus* Say. *Environ. Sci. Pollut. Res.* **2022**, *29*, 13417–13430. [[CrossRef](#)]
40. Swamy, M.K.; Akhtar, M.S.; Sinniah, U.R. Antimicrobial properties of plant essential oils against human pathogens and their mode of action: An updated review. *Evid.-Based Complement. Altern. Med.* **2016**, *2016*, 3012462. [[CrossRef](#)]
41. Mahizan, N.A.; Yang, S.-K.; Moo, C.-L.; Song, A.A.-L.; Chong, C.-M.; Chong, C.-W.; Abushelaibi, A.; Lim, S.-H.E.; Lai, K.-S. Terpene Derivatives as a Potential Agent against Antimicrobial Resistance (AMR) Pathogens. *Molecules* **2019**, *24*, 2631. [[CrossRef](#)]
42. Algiannis, N.; Kalpotzakis, K.; Mitaku, S.; Chinou, L.B. Composition and antimicrobial of essential oils two *Origanum* species. *J. Agric. Food Chem.* **2001**, *49*, 4168–4170. [[CrossRef](#)]
43. Holetz, F.B.; Pessini, G.L.; Sanches, N.R.; Cortez, D.A.; Nakamura, C.V.; Filho, B.P. Screening of some plants used in the Brazilian folk medicine for the treatment of infectious diseases. *Mem. Inst. Oswaldo Cruz* **2002**, *97*, 1027–1031. [[CrossRef](#)]
44. Jamiu, A.T.; Albertyn, J.; Sebolai, O.M.; Pohl, C.H. Update on *Candida krusei*, a potential multidrug-resistant pathogen. *Med. Mycol.* **2020**, *59*, 14–30. [[CrossRef](#)]
45. Bacelo, K.L.; Costa, K.R.C.; Ferreira, J.C.; Candido, R.C. Biotyping stability of *Candida albicans* isolates after culture storage determined by randomly amplified polymorphic DNA and phenotypical methods. *Mycoses* **2010**, *53*, 468–474. [[CrossRef](#)]
46. Mukherjee, P.K.; Chandra, J.; Kuhn, D.M.; Ghannoum, M.A. Mechanism of fluconazole resistance in *Candida albicans* biofilms: Phase-specific role of efflux pumps and membrane sterols. *Infect. Immun.* **2003**, *71*, 4333–4340. [[CrossRef](#)]
47. Carbone, C.; Teixeira, M.D.C.; Sousa, M.D.C.; Martins-Gomes, C.; Silva, A.M.; Souto, E.M.B.; Musumeci, T. Clotrimazole-Loaded Mediterranean Essential Oils NLC: A Synergic Treatment of *Candida* Skin Infections. *Pharmaceutics* **2019**, *11*, 231. [[CrossRef](#)] [[PubMed](#)]
48. Palmeira-de-Oliveira, A.; Gaspar, C.; Palmeira-de-Oliveira, R.; Silva-Dias, A.; Salgueiro, L.; Cavaleiro, C.; Pina-Vaz, C.; Martinez-de-Oliveira, J.; Queiroz, J.A.; Rodrigues, A.G. The anti-*Candida* activity of *Thymbra capitata* essential oil: Effect upon pre-formed biofilm. *J. Ethnopharmacol.* **2012**, *140*, 379–383. [[CrossRef](#)]
49. Ahmad, A.; Khan, A.; Manzoor, N. Reversal of efflux mediated antifungal resistance underlies synergistic activity of two monoterpenes with fluconazole. *Eur. J. Pharm. Sci.* **2013**, *48*, 80–86. [[CrossRef](#)]
50. Abdullahi, T.J.; Jacobus, A.; Olihile, S.; Onele, G.; Carolina, H.P. Inhibitory effect of polyunsaturated fatty acids alone or in combination with fluconazole on *Candida krusei* biofilms in vitro and in *Caenorhabditis elegans*. *Med. Myc.* **2021**, *59*, 1225–1237.
51. Stringaro, A.; Vavala, E.; Colone, M.; Pepi, F.; Mignogna, G.; Garzoli, S.; Cecchetti, S.; Ragno, R.; Angiolella, L. Effects of *Mentha suaveolens* essential oil alone or in combination with other drugs in *Candida albicans*. *Evid. Based Complement. Altern. Med.* **2014**, *2014*, 12590. [[CrossRef](#)]

52. Pires, R.H.; Montanari, L.B.; Martins, C.H.; Zaia, J.E.; Almeida, A.M.; Matsumoto, M.T.; Mendes-Giannini, M.J. Anticandidal efficacy of cinnamon oil against planktonic and biofilm cultures of *Candida parapsilosis* and *Candida orthopsilosis*. *Mycopathologia* **2011**, *172*, 453–464. [[CrossRef](#)]
53. Powers, C.N.; Osier, J.L.; McFeeters, R.L.; Brazell, C.B.; Olsen, E.L.; Moriarity, D.M.; Satyal, P.; Setzer, W.N. Antifungal and cytotoxic activities of sixty commercially-available essential oils. *Molecules* **2018**, *23*, 1549. [[CrossRef](#)]



## Antibacterial and antifungal activities *in vitro* of a novel silver(I) complex with sulfadoxine-salicylaldehyde Schiff base

Igor Santos Oliveira<sup>a</sup>, Carlos Marrote Manzano<sup>a</sup>, Douglas Hideki Nakahata<sup>a,b</sup>, Mariana Brentini Santiago<sup>c</sup>, Nagela Bernadelli Sousa Silva<sup>c</sup>, Carlos Henrique Gomes Martins<sup>c</sup>, Fernando Pimentel Respíndula<sup>d</sup>, Douglas Henrique Pereira<sup>d</sup>, Pedro Paulo Corbi<sup>a,\*</sup>

<sup>a</sup> Institute of Chemistry, University of Campinas – UNICAMP, PO Box 6154, 13083-970 Campinas, SP, Brazil

<sup>b</sup> Instituto de Química, Universidade Federal de Goiás – UFG, 74690-900 Goiânia, GO, Brazil

<sup>c</sup> Laboratory of Antimicrobial Testing, Institute of Biomedical Sciences, Federal University of Uberlândia – UFU, 38405-302 Uberlândia, MG, Brazil

<sup>d</sup> Chemistry Collegiate, Federal University of Tocantins – UFT, PO Box 66, 77402-970 Gurupi, TO, Brazil

### ARTICLE INFO

#### Keywords:

Silver(I)  
Sulfadoxine  
Schiff base  
DFT studies  
Antimicrobial activity

### ABSTRACT

Skin wound infections can be considered one of the most common causes of death in burned patients. The raising reports of multidrug resistant microorganisms reveals a complicated condition for the treatment of burn wound injuries, establishing urgency in the development of novel antimicrobial agents. Considering this scenario, the present work describes the synthesis, antibacterial and antifungal activities of a sulfadoxine-salicylaldehyde Schiff base (SFX-SL), and of its novel dimeric silver(I) complex (AgSFX-SL). Elemental analysis indicated a 1:1 metal:ligand molar composition for the AgSFX-SL complex, with the minimum formula  $\text{AgC}_{19}\text{H}_{17}\text{N}_4\text{O}_5\text{S}$ . Mass spectrometric (HRMS) data reveal the existence of dimeric species of the complex in solution. Infrared (FT-IR) and nuclear magnetic resonance (NMR) spectroscopic studies suggest coordination of the Schiff base to silver(I) by the nitrogen and oxygen atoms of the sulfonamide group. The structure of the SFX-SL Schiff base was determined by single crystal X-ray diffraction. Molecular modeling confirms the proposition of a dimeric structure for the AgSFX-SL complex as early indicated by mass spectrometric data. The AgSFX-SL complex showed an effective antimicrobial activity over pathogens including Gram-positive *Staphylococcus aureus* (multidrug resistant), *S. epidermidis*, *Cutibacterium acnes*, and Gram-negative *Pseudomonas aeruginosa* and *Burkholderia cepacia*, with minimum inhibitory concentration (MIC) values in the range 12.0–48.0  $\mu\text{mol}\cdot\text{L}^{-1}$ . Additionally, the AgSFX-SL complex was active against *Candida albicans* with a MIC value of 2.8  $\mu\text{mol}\cdot\text{L}^{-1}$ . Electrophoresis assays showed that the AgSFX-SL complex does not interact with protein models lysozyme and bovine serum albumin (BSA).

### 1. Introduction

Burn wounds in their diverse forms are characterized by the accumulation of injured tissues and cells, becoming a potential target for infections by pathogenic microorganisms such as Gram-negative *Pseudomonas aeruginosa* and Gram-positive methicillin-resistant *Staphylococcus aureus* (MRSA) bacterial strains, and fungi [1]. These infections can complicate the treatment process and, consequently, the recovery of affected individuals, increasing time, cost of treatment and mortality [2]. The World Health Organization (WHO) estimates >180,000 deaths annually due to burns, establishing itself as a global public health issue.

With the increasing reports of resistant microorganisms, this scenario

could be aggravated, since the development of new antimicrobial agents is much slower than the emergence of new resistant microorganisms [3]. In this case, metallodrugs have demonstrated potential as novel antimicrobial agents exhibiting a multitarget mode of action on different cellular structures. The metal-based agents act by promoting membrane disruption, formation of reactive oxygen species (ROS), denaturation of essential proteins and enzymes, and interruption on cell division process. This set of possible cellular targets can overcome the resistance mechanisms in emerging microorganisms and thus promote patient recovery [4,5].

One of the strategies for metallodrug design is based on the combination of bioactive molecules with well-established activities, such as

\* Corresponding author.

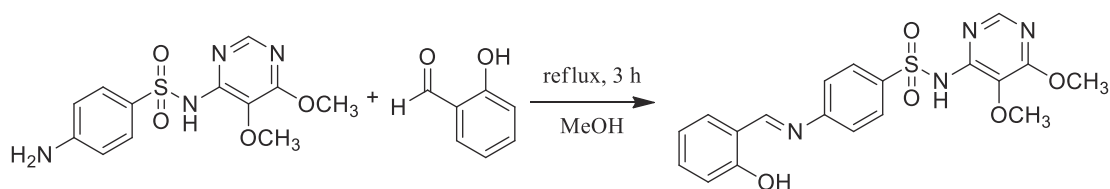
E-mail address: [deposit@ccdc.cam.ac.uk](mailto:deposit@ccdc.cam.ac.uk) (P. Paulo Corbi).

<https://doi.org/10.1016/j.poly.2022.116073>

Received 8 May 2022; Accepted 27 July 2022

Available online 2 August 2022

0277-5387/© 2022 Elsevier Ltd. All rights reserved.



**Scheme 1.** Reactional scheme of sulfadoxine-salicylaldehyde Schiff base formation (SFX-SL).

antibacterial and anti-inflammatory ones, with metals such as silver, platinum and copper, among others. Silver, for example, can be considered as one of the most studied metals over the centuries due to its antimicrobial activities. The literature describes several applications of silver during the history of science as in the maintenance of purity of beverages for long periods, and the use of silver wires in surgical sutures. Silver salts, on the other hand, were used mostly empirically for a long time for the treatment of several human disorders as conjunctivitis, gastroenteritis, skin lesions and *ophthalmia neonatorum* [6,7].

The sulfa drugs, or sulfonamides, represent a good example of a class of bioactive molecules which has been considered in the synthesis of new metallodrugs. Sulfonamides are considered as an important mark in antimicrobial chemotherapy since the discovery of Prontosil's antibacterial effects [8]. In special, silver sulfadiazine (SSD) is probably the most notable example of the success of combination of sulfonamides and metal ions in the search of antibacterial agents for skin infections. According to the literature, SSD is included in the list of essential medicines of the World Health Organization (WHO) and used typically in the form of a 1 % cream to treat second and third-degree burns. Although used for >50 years, SSD is still considered in many cases for topical treatment to avoid infections in the cases of skin lesions in burn patients [1,6].

Nowadays, the sulfonamide moiety plays an important role in drug design, giving rise to anti-inflammatory, antibacterial, antifungal and antiparasitic compounds [9]. However, microbial resistance is a strong factor for restricted use of sulfonamides, diminishing its application range. Structural modifications in such compounds, including the synthesis of sulfonamide-Schiff base derivatives, have been employed for bioactivity enhancement seeking to overcome bacterial resistance. Mondal et al. [10] published the synthesis of Schiff bases of several sulfonamides that exhibited inhibitory action against resistant microorganisms, while the former sulfonamides were inactive. Also, the synthesis of Schiff bases derivatives from sulfadiazine with activity and selectivity for Staphylococci and fungi were described. These compounds presented minimum inhibitory concentration (MIC) values lower than those of sulfadiazine [11]. Other Schiff bases from sulfonamides presented antifungal activity against fluconazole-resistant *Candida auris* strains [12]. Such data reinforces the potential of application of sulfonamide derived Schiff bases in medicine.

Sulfadoxine (SFX) is a sulfonamide that is used in combination with pyrimethamine as antiparasitic drug. It is commercialized as Fansidar®,

used in chloroquine-resistant malaria diseases treatment [13]. The SFX molecule acts as a folate antagonist, promoting inhibition of dihydrofolate reductase enzyme and disturbing the essential parasite's folate biosynthetic pathway [14]. However, mutations in the genes of this enzyme can cause the emergence of sulfadoxine-resistant parasites [15].

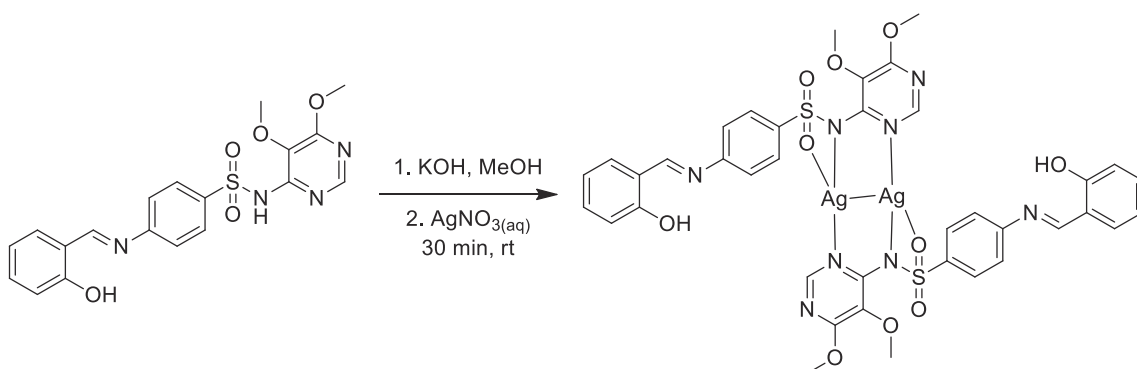
Chellan et al. [16] published the synthesis of metal complexes with sulfadoxine Schiff base derivatives with good responses *in vitro* against sulfadoxine-resistant strains of *Plasmodium* parasites, evidencing an enhancement in antimicrobial activity of this drug when associated with metal ions. In a similar approach, our research group has dedicated efforts in the development of novel antimicrobial agents based in the combination of metal complexes with sulfonamides [17–24]. The silver (I) and copper(II) complexes with sulfadoxine [14], mafenide [15], sulfathiazole and sulfamethoxazole [17], and sulfadimethoxine [18], as examples, exhibited *in vitro* antibacterial activities over Gram-positive and Gram-negative bacterial strains, including those related to skin infections as *Pseudomonas aeruginosa*. In the case of the silver complex with mafenide, the minimum inhibitory concentration (MIC) of the compound over *P. aeruginosa* was at least two times lower than SSD [15].

In this work we describe the synthesis and structural characterization of a sulfadoxine-salicylaldehyde Schiff base (SFX-SL) and its new silver (I) complex. Spectroscopic and theoretical studies of the complex and the evaluation of its antibacterial and antifungal activities are also provided in this article.

## 2. Experimental section

### 2.1. Reagents and equipment

Sulfadoxine, salicylaldehyde, silver nitrate and bovine serum albumin (BSA) were purchased from Sigma-Aldrich/Merck. Elemental analyses of the compounds were carried out in a CHNS/O Analyzer 2400, Perkin-Elmer. Nuclear magnetic resonance (NMR) data for SFX and SFX-SL in dimethylsulfoxide solution (DMSO- $d_6$ ) were obtained by using a Bruker AVANCE III 400 MHz spectrometer operating at temperature of 298 K. The  $^{13}\text{C}$  nuclear magnetic resonance (NMR) spectra for the Ag(I) complex and the Schiff base were acquired in a Bruker 400 MHz spectrometer, with combination of magic angle spinning (MAS) and cross-polarization (CP). Infrared (FTIR) absorption spectra were recorded in an Agilent FTIR spectrometer, model Cary 630. The spectra were



**Scheme 2.** Synthetic route of the silver(I) sulfadoxine-salicylaldehyde Schiff base (AgSFX-SL) complex.

obtained by attenuated total reflectance (ATR) method, from 4000 to 400  $\text{cm}^{-1}$  with 4  $\text{cm}^{-1}$  of resolution. The mass spectra were obtained using an Orbi-trap Thermo Q-Exactive equipment, using electrospray ionization (ESI-MS) method. Samples were prepared in a methanol: water solution containing 0.1 % of formic acid. The final solutions of the compounds were infused directly into the instrument's ESI source. The samples were analyzed in the positive mode with flow rate of 200  $\mu\text{L}\cdot\text{min}^{-1}$  and cone voltage of 3.5 kV.

## 2.2. Synthesis of SFX-SL Schiff base

Sulfadoxine (1.0 mmol) was added into a flask with salicylaldehyde (1.0 mmol) and methanol. The reaction (Scheme 1) was taken under reflux and magnetic stirring over 3 h, resulting in a yellow precipitate. After cooling, the precipitate was separated by vacuum filtration, washed with few portions of methanol and dried with  $\text{P}_2\text{O}_5$  in a desiccator. Single-crystals of SFX-SL were obtained by slow crystallization of reactional supernatant stored in  $-4^\circ\text{C}$  after few days. Calculated (%): C, 55.06; H, 4.38; N, 13.52; Found (%): C, 54.39; H, 4.00; N 13.54. Yield 86 %.

## 2.3. Synthesis of the silver complex with sulfadoxine Schiff base (AgSFX-SL)

The silver(I) complex was synthesized according to the following procedure (Scheme 2): first, the Schiff base SFX-SL (0.25 mmol) and potassium hydroxide (0.30 mmol) were added in a round flask with 5.0 mL of methanol. Then, after the Schiff base partial solubilization, a freshly prepared solution of silver nitrate (0.25 mmol) was slowly added and the reaction was kept on stirring for 30 min, at room temperature, and under light protection. A bright yellow precipitate was formed and separated by filtration, washed with methanol, and dried in a desiccator with  $\text{P}_2\text{O}_5$ . Based on the elemental analysis, the minimum formula  $\text{AgC}_{19}\text{H}_{17}\text{N}_4\text{O}_5\text{S}$  was proposed for the complex. Calculated (%): C, 43.78; H, 3.29; N, 10.75; Found (%): C, 43.17; H, 3.20; N 10.20. Yield 94 %. No single crystals of this compound were obtained, despite several attempts, for a detailed X-ray diffraction analysis.

## 2.4. Structure determination

Crystal data of SFX-SL Schiff base were collected on a Bruker APEX II Duo diffractometer using  $\text{Mo K}\alpha$  radiation ( $\lambda = 0.71073 \text{ \AA}$ ) from a fine-focus sealed tube with a curved graphite monochromator and at 150 K. For all data sets, SAINT and SADABS [25,26] were used for data integration and multi-scan absorption correction. Using Olex2 [27], the structure was solved with the ShelXT [28] structure solution program using Intrinsic Phasing and refined with the ShelXL [29] refinement package using Least Squares minimization. All non-hydrogen atoms were refined anisotropically, while hydrogen atoms were refined according to the riding model. The complete crystallographic data are presented in Supplementary Material. Figures were generated using Olex2 [27] and Mercury [30].

## 2.5. Molecular modeling

For theoretical studies, the density functional theory (DFT) was used and all molecules were optimized to the minimum energy using the hybrid functional  $\omega\text{B97XD}$  [31]. For carbon, hydrogen, oxygen, sulfur and nitrogen the 6-31G(d,p) [32,33] basis set was used and for the silver atom LANL2DZ effective core potential basis set was selected [34]. Frequency calculations were performed to confirm that the structures optimized were at their minimum energy. All optimization and frequency calculations were performed using the Gaussian 09 program [35]. The structures were constructed using the GaussView program [36]. The binding energy ( $\Delta E_{\text{Bind}}$ ), Gibbs energy and the enthalpy of the coordination process was quantified by the equations 1–3.

$$\Delta E_{\text{Bind}} = E_{\text{complex}} - [E_{\text{ligand}} + E_{\text{metal}}] \quad (1)$$

$$\Delta G = G_{\text{complex}} - [G_{\text{ligand}} + G_{\text{metal}}] \quad (2)$$

$$\Delta H = H_{\text{complex}} - [H_{\text{ligand}} + H_{\text{metal}}] \quad (3)$$

where  $\Delta E_{\text{Bind}}$  corresponds to binding energy,  $E_{\text{complex}}$  is the energy of the complex,  $E_{\text{ligand}}$  and  $E_{\text{metal}}$  correspond to the electronic energies of SFX-SL and the silver atom, respectively [37–39]. The zero-point energy (ZPE) was added in the electronic energy ( $E + \text{ZPE}$ ). The Gibbs energy and the enthalpy of the process were also calculated in an analogous way.

The energies of the HOMO (Highest Occupied Molecular Orbital) and LUMO (Lowest Unoccupied Molecular Orbital) were used to obtain chemical hardness ( $\eta$ ), chemical softness ( $S$ ), chemical potential ( $\mu$ ), electronegativity ( $\chi$ ) and electrophilicity index ( $\omega$ ) [40,41] taking into account the Koopmans theorem [42], equations 4–7:

$$\eta = \frac{(E_{\text{HOMO}} - E_{\text{LUMO}})}{2} \quad (4)$$

$$S = \frac{1}{\eta} \quad (5)$$

$$\mu = \frac{(E_{\text{HOMO}} + E_{\text{LUMO}})}{2} = -\chi \quad (6)$$

$$\omega = \frac{\mu^2}{2\eta} \quad (7)$$

The AIMALL package [43] was selected and applied to characterize the interactions or bonds using the Quantum Theory of Atoms in Molecules (QTAIM) [44–48].

## 2.6. Antibacterial activity studies

To determine the minimum inhibitory concentration (MIC) of the selected bacterial strains, the microdilution method was applied following the recommendation of the Clinical and Laboratory Standards Institute (CLSI) [49,50]. For the aerobic bacteria, the selected compounds were first dissolved in dimethylsulfoxide (DMSO, Merck®) and distilled water and diluted with Mueller Hinton broth (Kasvi®). For the anaerobic strain, the compounds were diluted with Schaedler broth (Difco®) supplemented with hemin (5  $\text{mg}\cdot\text{mL}^{-1}$ , Sigma®) and menadione (1  $\text{mg}\cdot\text{mL}^{-1}$ , Sigma®). After that, 12 concentrations of the compounds in the range 0.195–400  $\mu\text{g}\cdot\text{mL}^{-1}$  in a 96-well microplate were examined.

All bacterial strains evaluated in this research were from the American Type Culture Collection (ATCC). The aerobic bacterial strains used were *S. aureus* (ATCC BA-44), *B. cepacia* (ATCC 25416), *S. epidermidis* (ATCC 12228) and *P. aeruginosa* (ATCC 15442), while *C. acnes* (ATCC 11827) was the only anaerobic bacteria selected. Such strains were chosen based on their presence in community and hospital acquired infections, including skin wounds. The inoculums were adjusted to the final cell concentration of  $5\cdot 10^5 \text{ CFU}\cdot\text{mL}^{-1}$  for the aerobic and  $1\cdot 10^6 \text{ CFU}\cdot\text{mL}^{-1}$  for the anaerobic bacterial strains, where CFU means colony forming unity.

The 96-well microplates containing the aerobic bacterial strains were incubated for 24 h at  $37^\circ\text{C}$ , while the microplate containing the anaerobic bacterial strain was incubated for 72 h at  $37^\circ\text{C}$  in an anaerobic chamber (Don Whitley Scientific, Bradford, U.K.). After, 30  $\mu\text{L}$  of 0.02 % aqueous resazurin (Sigma®) solution was added to each well of the plates to show bacterial growth [51]. The blue and red colors of this colorimetric assay characterize the absence and the presence of microbial growth, respectively. As positive controls, gentamicin (0.0115 to 5.9  $\mu\text{g}\cdot\text{mL}^{-1}$ ), vancomycin (0.0115 to 5.9  $\mu\text{g}\cdot\text{mL}^{-1}$ ) and chloramphenicol (7.198 to 5000  $\mu\text{g}\cdot\text{mL}^{-1}$ ) were employed, while dimethylsulfoxide (5 %, v/v) was employed as negative control. Silver nitrate was used for

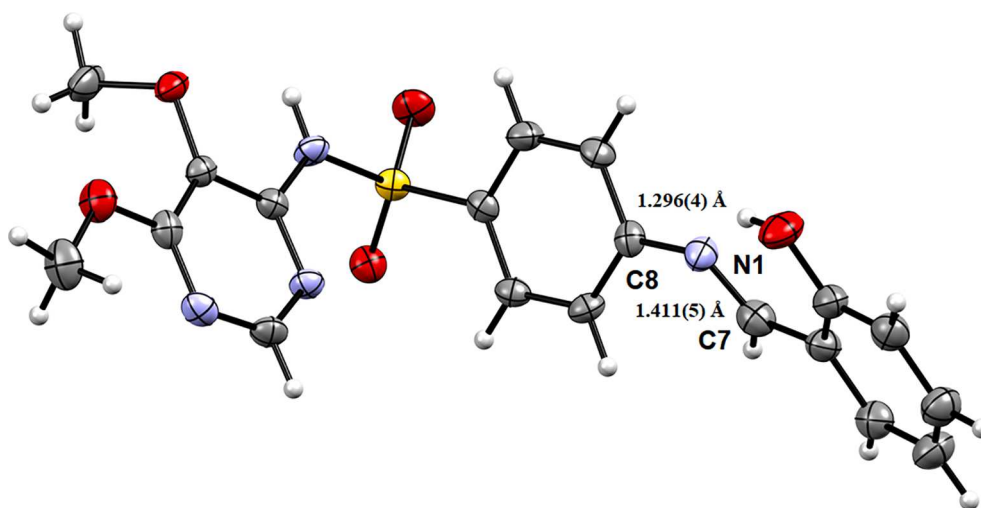


Fig. 1. Molecular representation of SFX-SL. Ellipsoids are drawn at 50% probability level.

comparative studies, considering its well-established antimicrobial activity although toxic to humans in concentrations higher than 1 %. An inoculum was included to examine bacterial cell growth. All experiments were conducted in triplicate.

### 2.7. Antifungal activity assays

The antifungal activity studies of the compounds were conducted by using the broth microdilution method as recommended by CLSI (2008). Strains of *Candida albicans* used in this work were acquired from the American Type Culture Collection (ATCC 90028 and 64550, Rockville MD, USA).

Stock solutions were initially prepared by dissolving the samples in DMSO (Sigma-Aldrich, Co) at a concentration of  $192,000 \mu\text{g}\cdot\text{mL}^{-1}$ . Dilutions with the stock solutions were carried out in RPMI 1640 culture medium buffered at pH 7.2 with  $0.165 \text{ mol}\cdot\text{L}^{-1}$  of 3-*N*-morpholinopropanesulfonic acid (MOPS, Acros Organics, Geel, Turnhout, Belgium) at  $12,000 \mu\text{g}\cdot\text{mL}^{-1}$  and these are the working solutions. The inoculum was prepared using a spectrophotometric method and compared to a 0.5 McFarland scale to obtain the value of  $6 \times 10^6 \text{ CFU}\cdot\text{mL}^{-1}$ . Then, the dilutions recommended by CLSI (2008) [52] were performed in RPMI broth until the inoculum reached  $1.2 \times 10^3 \text{ CFU}\cdot\text{mL}^{-1}$ .

The determination of MIC values was conducted in microdilution plates with 96 wells, in which serial dilutions were made with the final concentrations of the samples ranging from 1.46 to  $3,000 \mu\text{g}\cdot\text{mL}^{-1}$ . The culture medium used was MOPS-buffered RPMI broth with a final pH of 7.2. Each well received 100  $\mu\text{L}$  of the inoculum suspension and the final volume in each well was 200  $\mu\text{L}$ . The positive control used was the drug amphotericin B, which was diluted in broth to obtain concentrations from 0.031 to  $16 \mu\text{g}\cdot\text{mL}^{-1}$ . Dimethylsulfoxide was used as the negative control with concentrations from 10 % to 1 % (v/v). The inoculum-added culture medium was used as a growth control. The microplate was incubated at 37 °C for 24 h.

After incubation, 30  $\mu\text{L}$  of an aqueous solution of resazurin (Sigma) at 0.02 % was added to each well, the microplate was reincubated for another 3 h, the reading was performed visually and analyzed descriptively. The blue and red colors characterize the absence and presence of microbial growth, respectively [53], thus, the minimum inhibitory concentration (MIC) was evaluated, which corresponds to the minimum concentration of the sample capable of inhibiting the growth of yeasts. The tests were performed in triplicate.

### 2.8. Gel electrophoresis analysis (SDS-PAGE)

Lysozyme and BSA were chosen to evaluate possible protein

interactions of the compounds considered in this work. Solutions of the SFX-SL Schiff base and silver nitrate ( $1.0 \text{ mmol}\cdot\text{L}^{-1}$ ) were prepared in water with 1 % of dimethylsulfoxide (v/v), while the AgSFX-SL complex was suspended in water with 1 % of dimethylsulfoxide (v/v). Then, 5  $\mu\text{L}$  of the samples were mixed with 10  $\mu\text{L}$  of BSA or lysozyme solutions ( $250 \mu\text{mol}\cdot\text{L}^{-1}$  in phosphate buffer  $\text{HPO}_4^{2-}/\text{H}_2\text{PO}_4^-$ , pH = 7.4) followed by the addition of 35  $\mu\text{L}$  of phosphate buffer and incubated for 3 h at temperature of 37 °C. After that, 50  $\mu\text{L}$  of loading buffer (Tris/HCl  $100 \text{ mmol}\cdot\text{L}^{-1}$ , pH 6.8, SDS 4.0 %, bromophenol blue 0.2 % and glycerol 20.0 %) were added to each sample for a final concentration of  $50 \mu\text{mol}\cdot\text{L}^{-1}$  and  $25 \mu\text{mol}\cdot\text{L}^{-1}$  of compound and protein, respectively.

The mixtures were subsequently heated in a water bath for 5 min at 96 °C. The samples (10  $\mu\text{L}$ ) were then added to the sodium dodecyl sulfate polyacrylamide gel (SDS-PAGE) and electrophoresed for 2 h at 100 V. Finally, each gel was washed accordingly and dyed using Coomassie blue [18]. Samples with only BSA or lysozyme were used as control; Precision Plus Protein™ Dual Color Standard was used as weight marker.

## 3. Results and discussion

### 3.1. X-ray diffraction

The Schiff base SFX-SL crystallized in the monoclinic  $P2_1/c$  space group and it is a polymorph (CSD entry GUVQOE) of a crystal structure obtained for this compound [54]. The obtained crystal structure confirms the formation of the imine due to the 1.296(4) Å C8-N1 bond length, which is consistent with a double bond, although longer than the average value of 1.279(8) Å [55]. This value is also consistent with the polymorph of this compound, which showed a value of 1.275(3) Å [54]. When comparing the present structure with data from sulfadoxine [56], there is a difference between the C8-N1 bond length in sulfadoxine (1.355(4) Å) and SFX-SL (1.411(5) Å). This may be related to the  $\text{sp}^3$  hybridization on the N atom of sulfadoxine and  $\text{sp}^2$  hybridization in SFX-SL. Fig. 1 presents the asymmetric unit representation of SFX-SL.

The crystal structure of SFX-SL shows a network of hydrogen bonds, which is very distinct from the one shown by CSD entry GUVQOE [55] (see Figure S1). The sulfonamide group of SFX-SL participates in hydrogen bonds to the hydroxyl group of the phenol. Meanwhile, the nitrogen atoms from the pyrimidine ring are not involved in hydrogen bonding. Contrastingly, the GUVQOE polymorph presents a  $R_2^2(8)$  hydrogen bonding pattern involving one of the N atoms from the pyrimidine group and the nitrogen from the sulfonamide (see Figure S2).



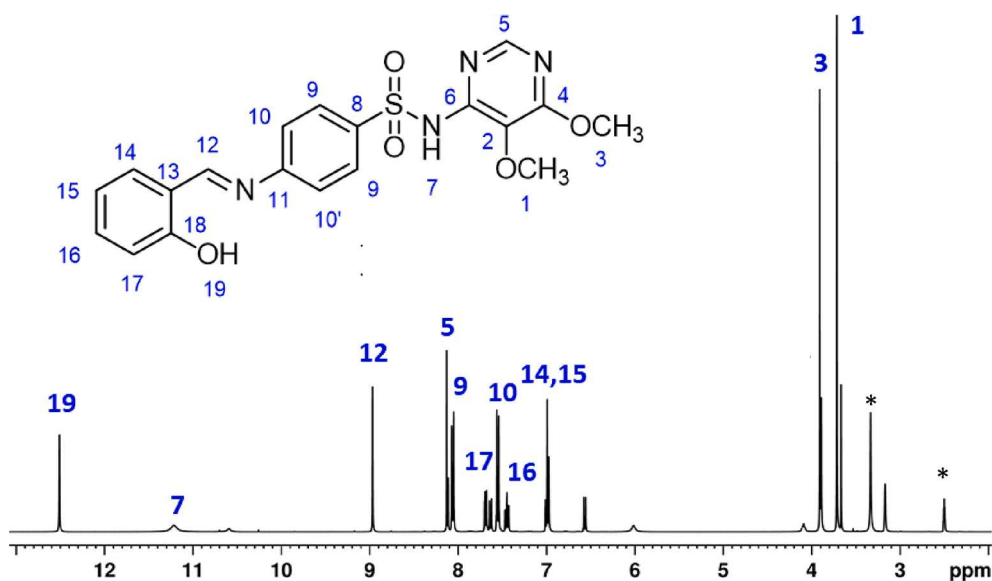


Fig. 2.  $^1\text{H}$  NMR spectra of SFX-SL. The asterisk at 2.50 denotes the presence of  $\text{CHD}_2(\text{SO})\text{CD}_3$  residual peak, while the peak at 3.30 ppm refers to  $\text{H}_2\text{O}$  from the  $\text{DMSO}-d_6$  used as solvent in the experiment.

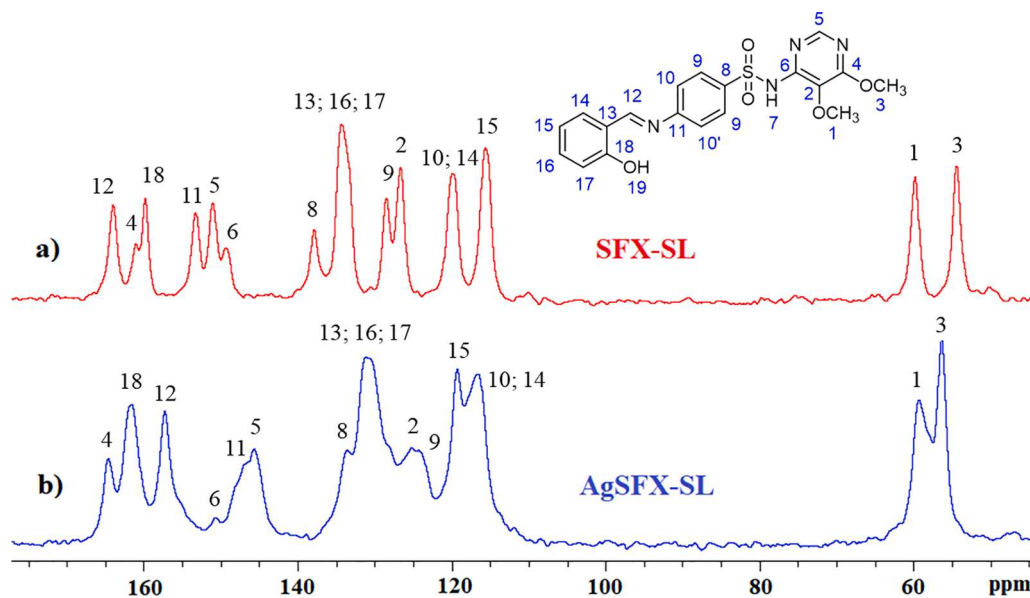


Fig. 3.  $^{13}\text{C}$  NMR CPMAS spectra of (a) SFX-SL and (b) AgSFX-SL.

### 3.2. Infrared spectroscopic data (FT-IR)

Comparing the FT-IR spectra data of SFX and SFX-SL (Figure S3) it is possible to notice the disappearance of the bands related to asymmetric and symmetric stretching modes of the amino group ( $-\text{NH}_2$ ) of SFX, at  $3461$  and  $3374\text{ cm}^{-1}$ , respectively. Such results are an important indicative for Schiff base formation from SFX and salicylaldehyde. The FT-IR spectrum of AgSFX-SL complex shows the main bands from the ligand SFX-SL. The stretching bands of sulfone group ( $\text{O}=\text{S}=\text{O}$ ) are shifted to  $1262$  and  $1153\text{ cm}^{-1}$  in the spectrum of the complex, indicating that this group is one of the possible coordination sites of the ligand to silver. Moreover, the absence of the stretching mode of the  $\text{N}-\text{H}$  group from the  $\text{SO}_2\text{N}-\text{H}$  moiety of SFX-SL in the complex evidence that the sulfonamide group is deprotonated and coordinated to silver by its nitrogen atom [17].

### 3.3. $^1\text{H}$ and $^{13}\text{C}$ NMR spectroscopic data

The  $^1\text{H}$  and  $^{13}\text{C}$  NMR spectroscopic studies of Schiff base SFX-SL were performed in solution state using  $\text{DMSO}-d_6$  as solvent. For comparative purposes, SFX was analyzed in the same conditions. In the  $^1\text{H}$  NMR spectrum of the Schiff base SFX-SL (Fig. 2) it is possible to observe signals related to the methoxy groups in the pyrimidine ring at  $3.72$  and  $3.91\text{ ppm}$  and the presence of the singlet related to the azomethine moiety ( $-\text{HC}=\text{N}-$ ) at  $8.97\text{ ppm}$ . The signals observed at  $6.99$ ,  $7.45$  and  $7.69\text{ ppm}$  corresponded to the aromatic hydrogens and a singlet at  $11.22\text{ ppm}$  corresponds to the hydroxyl group derivate from salicylaldehyde. There are also other signals with low intensity present in the aliphatic region of the SFX-SL  $^1\text{H}$  NMR spectrum centered at  $3.16$  and  $4.01\text{ ppm}$  which match with residual methanol used in the synthesis of the compound. The asterisks (\*) at  $2.50$  and  $3.30\text{ ppm}$  in Fig. 2 refers to  $\text{CHD}_2(\text{SO})\text{CD}_3$  residual peak and  $\text{H}_2\text{O}$ , respectively, from the  $\text{DMSO}-d_6$  used in the experiment. Additional unlabeled and low-

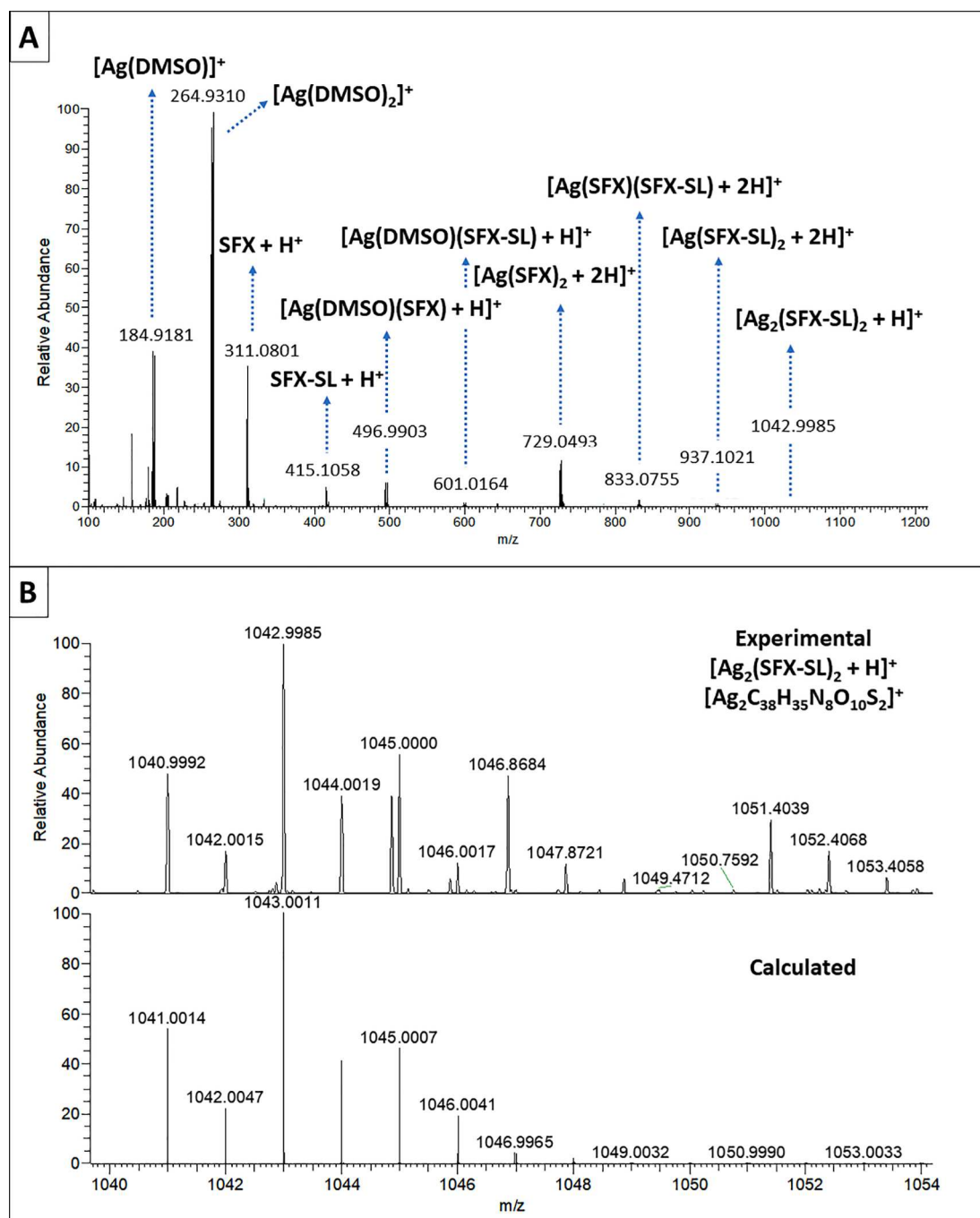


**Fig. 4.** Mass spectrum of AgSFX-SL from 100 to 1500 m/z with assigned signals in A. Expanded spectra and calculated isotopic pattern of  $[\text{Ag}_2(\text{SFX-SL})_2 + \text{H}]^+$  molecular ion in B.

intensity signals can be attributed to some residual SFX [17] present in the sample.

The AgSFX-SL complex demonstrated low solubility in DMSO and in other solvents. Considering this, the  $^{13}\text{C}$  NMR spectroscopic experiments of SFX-SL and AgSFX-SL were performed in solid state for comparative analysis. The spectra of SFX-SL and AgSFX-SL with carbon atoms assignments are shown in Fig. 3. The two signals observed in the spectrum of SFX-SL and AgSFX-SL in the range 50–60 ppm are attributed to the carbon atoms of  $-\text{OCH}_3$  groups in the pyrimidine ring. The solid-state  $^{13}\text{C}$  NMR data indicates the maintenance of the Schiff base integrity and its coordination to silver. The chemical shifts in signals related to carbon nuclei C5, C6 and C8 at 150.99, 149.29 and 137.87 ppm in the ligand spectrum to 145.65, 150.62 and 133.53 ppm in the spectrum of

the AgSFX-SL complex, respectively, suggest nitrogen coordination of the  $\text{SO}_2\text{N}$ -group to Ag(I). The observed data reinforce the coordination of the ligand to silver by the sulfonamide moiety as indicated by FT-IR spectrum of the AgSFX-SL complex. Nevertheless, chemical shifts were also observed for carbon atoms C12, C13 and C18 when the ligand and silver complex  $^{13}\text{C}$  NMR spectra are compared. So, ligand interaction with Ag(I) by the oxygen atom of the salicylic moiety and the imine nitrogen atom cannot be totally discarded considering this technique.

#### 3.4. High resolution mass spectrometric studies (HRMS)

The spectrum of the AgSFX-SL complex is presented in Fig. 4. Peaks at 833.0755 m/z and 729.0493 m/z were detected and assigned to  $[\text{Ag}$

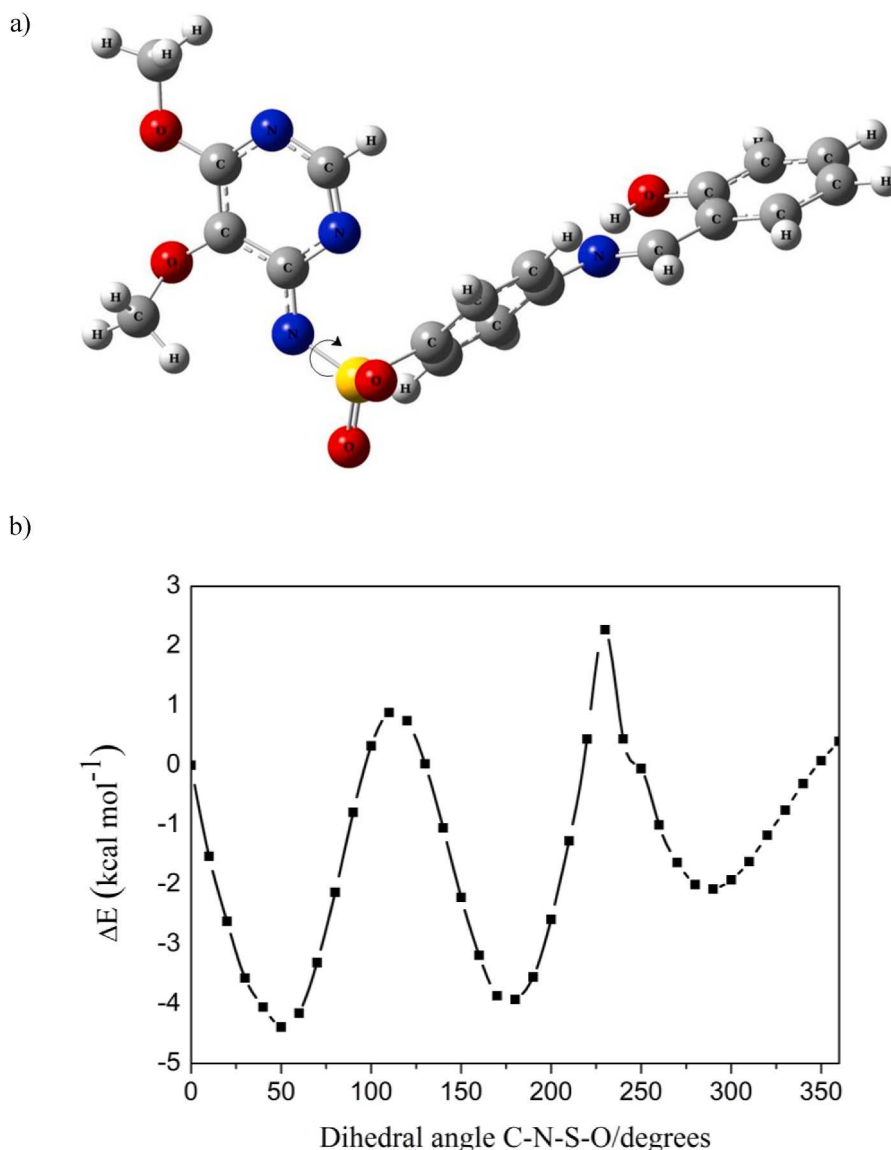


Fig. 5. a) Optimized structure of the SFX-SL anion and b) internal rotational barrier for the C-N-S-O dihedral.

(SFX-SL)(SFX) + H<sup>+</sup> and [Ag(SFX)<sub>2</sub> + 2H]<sup>+</sup> species. These peaks correspond to successive loss of salicyl groups of the Schiff base ligand. Peaks at  $m/z$  601.0164 and at 264.9310  $m/z$  were also observed, being attributed to ligand scrambling in the gas phase and formation of [Ag(SFX-SL)(DMSO) + H]<sup>+</sup> and [Ag(DMSO)<sub>2</sub>]<sup>+</sup> species. The DMSO comes from sample preparation before HRMS analysis. The presence of the [Ag<sub>2</sub>(SFX-SL)<sub>2</sub> + H]<sup>+</sup> ion at 1042.9985  $m/z$  indicates a dimeric structure for the AgSFX-SL complex as already observed for similar silver complexes with sulfa drugs [17,20,22–24]. The peak at 937.0121  $m/z$  is related to the fragmentation of the [Ag<sub>2</sub>(SFX-SL)<sub>2</sub> + H]<sup>+</sup> ion with the loss of one silver ion thus corroborating the dimeric form of the complex. The full spectrum of the silver complex with expanded regions can be found at the [supplementary material \(Figure S4\)](#).

### 3.5. Molecular modeling

For the theoretical study of the AgSFX-SL complex, the SFX-SL ligand was considered in its anionic form by deprotonation of the nitrogen atom of the sulfonamide group. The loss of the hydrogen of the SO<sub>2</sub>N-H moiety of the ligand was confirmed by considering the experimental FT-IR spectrum of the AgSFX-SL complex, as discussed in section 3.2. The anionic structure was generated from the neutral molecule obtained

from the crystal, according to the crystallographic data described in section 3.1.

Considering the FT-IR and NMR spectroscopic data, oxygen coordination from the sulfonamide group to Ag(I) was also proposed. With the experimental data, the lower energy conformers were elucidated and consequently the most stable ones for the AgSFX-SL complex. In Fig. 5a the torsion dihedral is shown in detail and Fig. 5b presents the internal rotational barrier determined for the deprotonated SFX-SL ligand, where the torsion angle varied in 360° with 10° intervals.

From the results obtained in the rotational barrier for the SFX-SL anion, it is possible to observe two more stable conformers at 50° and 180°. The 50° conformation is the structure shown in Fig. 5a, in which the –OCH<sub>3</sub> group is in the C–N–S–O dihedral plane. At 180° the nitrogen of the pyrimidine ring is oriented towards one of the oxygens of the –SO<sub>2</sub> group. The third conformer at 290° presents the least possibility to coordinate the metal, as it presents steric hindrances.

The possibility of formation of monomeric or dimeric species involving silver complexes with sulfonamides is well established in the literature. In this context, and taking into account the 1:1 metal:ligand molar composition found from elemental analysis, monomeric and dimeric forms for the silver(I) complex with SFX-SL were considered [17,20]. Fig. 6 shows the dimeric structure of the complex with

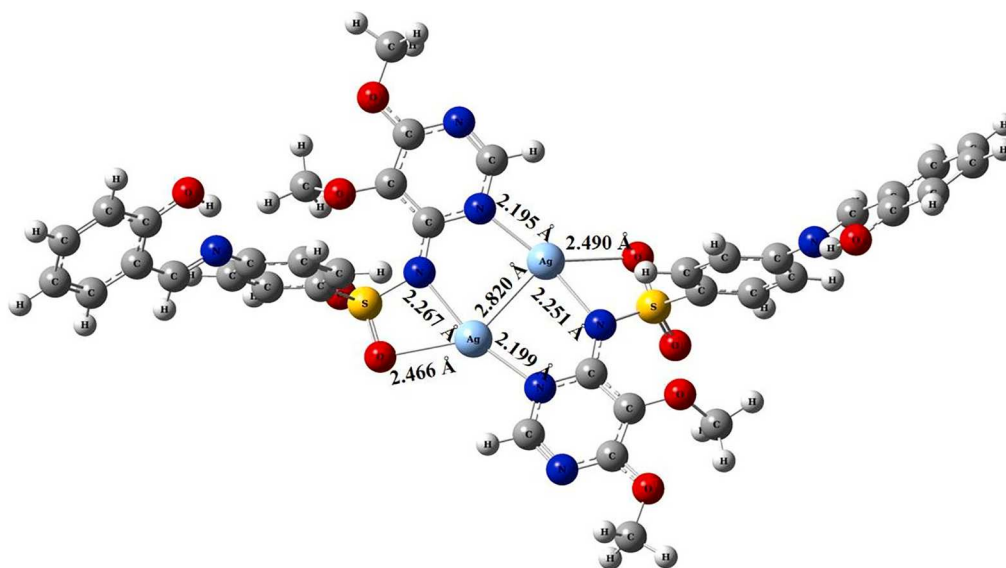


Fig. 6. Structural formula for the AgSFX-SL complex.

Table 1

Main bond length values calculated for AgSFX-SL and reported values for other silver-sulfonamide complexes.

Compound	Ag – N (Å)*	Ag – O (Å)*	Ag...Ag (Å)	Reference
AgSFX-SL	2.195 – 2.267	2.466 – 2.490	2.820	This work
Ag(I)-sulfadoxine	2.26(2) – 2.53(1)	2.60(2) – 2.71(2)	2.744(6)	[17]
Ag(I)-sulfameter	2.192(6) – 2.267(5)	2.662(2)	2.901(1)	[22]
Ag(I)-sulfadimethoxine	2.235(6) – 2.408(6)	2.806(7) – 2.899(6)	2.737(9)	[23]
Ag(I)- sulfachloropyridazine	2.105(6)	–	2.8897(3)	[59]
Ag(I)-sulfamoxole	2.122(5) – 2.152(4)	–	2.8957(10)	[60]

\* Ranges of bond-length values found in the crystal structures. For the specific case of Ag-O bonds, they may be absent altogether, depending on the crystal structure.

respective bond length between metal and donor atoms of the SFX-SL ligand. The coordination mode proposed here for AgSFX-SL is consistent with one of the common geometrical motifs reported for silver(I)-sulfonamide complexes, forming an eight-membered ring where each two nitrogen atoms (from the sulfonamide group and from the pyrimidine ring) of the ligand bind to a particular silver(I) ion [57]. Additional binding to oxygen atoms of the sulfonamide group was also observed in crystal structures of silver(I)-sulfonamide complexes reported by our group [17,22,23]. The monomeric structural proposition for the complex is presented at the [supplementary material \(Figure S5\)](#) for comparative purposes.

Table 1 presents a comparison of the main calculated bond lengths for AgSFX-SL and values reported for crystal structures of other silver-sulfonamide complexes. After the formation of the dimer depicted in Fig. 6, the bond lengths between oxygen and silver presented the values of 2.466 Å and 2.490 Å. The calculated Ag-O bond lengths are slightly shorter with the values of 2.60(2) Å and 2.662(2) Å reported for the silver(I)-sulfadoxine [17] and of the silver(I)-sulfameter [22] complexes, respectively. The calculated Ag-N bond lengths of the nitrogen atoms of SFX-SL and silver are consistent with the mean value of 2.24(12) Å reported in the Cambridge Structural Database [58]. Finally, the theoretical model of AgSFX-SL proposed here accounts for the formation of an argentophilic interaction Ag-Ag (2.820 Å), similar to what was

Table 2

Binding energy ( $\Delta E_{\text{Bind}}$ ) at zero Kelvin, Gibbs energy ( $\Delta G$ ) and enthalpy at 298 Kelvin for the complexes.

Complex	$E_{\text{Bind}}$ Kcal mol <sup>-1</sup>	$\Delta G$	$\Delta H$
AgSFX-SL (monomer)	-141.97	-133.48	-142.16
AgSFX-SL (dimer)	-357.99	-317.62	-348.08

observed in crystal structures of silver-sulfonamide complexes [17,22,59].

To observe the magnitude of the coordination of the metal with the SFX-SL ligand and the formation of the dimeric structure, the binding energies ( $E_{\text{Bind}}$ ), Gibbs energies ( $\Delta G$ ) and enthalpies ( $\Delta H$ ) involved in the coordination were calculated for the monomeric and dimeric species and are represented in Table 2.

Analyzing the results in Table 1, it is possible to infer that  $E_{\text{Bind}}$  values are  $< 0$ , showing that the coordination is effective in both species. The values of  $\Delta G$  and  $\Delta H$  are also  $< 0$ , so coordination is spontaneous, and energy is released in the process.

Comparing the energy values between the monomer and the dimer, it is evident that the dimer formation favors complexation due to the significant increase in binding energy, Gibbs and enthalpy. Since the existence of a dimeric species was also corroborated by experimental HRMS data, the proposed structure presented in Fig. 6 is the most probable one for the AgSFX-SL complex.

As the dimer is the most probable species, the FTIR spectrum, the reactivity indices, and topological properties were evaluated for the AgSFX-SL complex. Theoretical results of the FTIR spectra were calculated for the anionic SFX-SL and for AgSFX-SL, Figure S6. The results show that all vibrational frequencies of the bonds in the complex spectrum were altered when compared to the vibrational frequencies of the isolated ligand, thus confirming that the interaction occurred. The spectra follow the same trend as the experimental results and it is worth noting that for the theoretical simulations all peaks are determined and that no scale factor was used to perform the calculations.

The reactivity indices, Energy gap ( $E_g$ ), chemical hardness ( $\eta$ ), chemical softness ( $S$ ), chemical potential ( $\mu$ ), electronegativity ( $\chi$ ) and electrophilicity index ( $\omega$ ) were calculated for the AgSFX-SL complex and for SFX-SL. The results are presented in Table S2 at the [supplementary material](#). The hardness determinant ( $\eta$ ) is a property that measures the stability of the molecule. Electronegativity ( $\chi$ ) measures the strength of

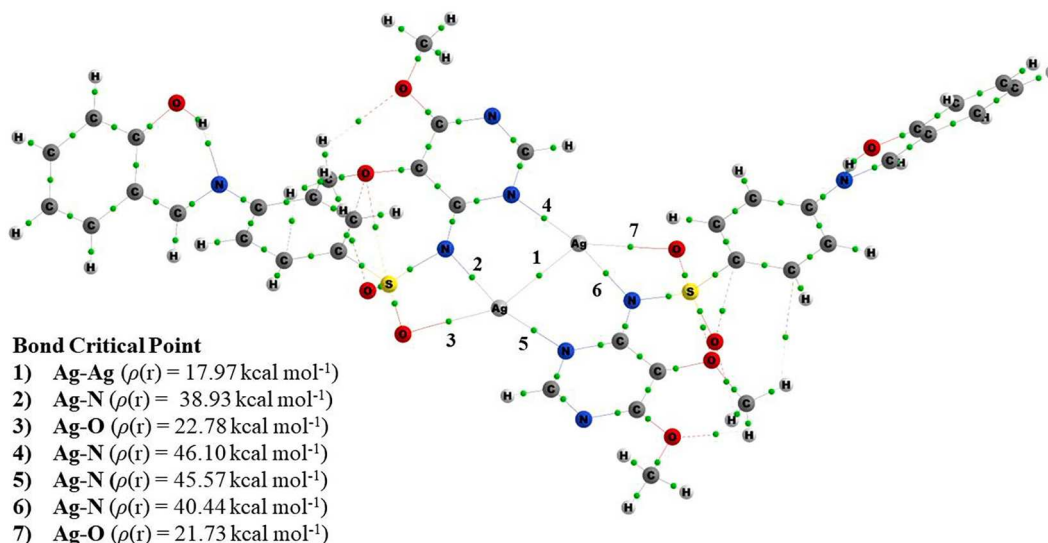


Fig. 7. Molecular graph for the AgSFX-SL complex and topological parameter  $\rho(r)$  generated by QTAIM.

Table 3

MIC values of the compounds over bacteria and yeasts. Values are given in  $\mu\text{g}\cdot\text{mL}^{-1}$  and ( $\mu\text{mol}\cdot\text{L}^{-1}$ ).

Compounds	Aerobic bacteria				Anaerobic bacteria <i>C. acnes</i> ATCC 11,827	Yeasts	
	<i>S. aureus</i> ATCC BA44	<i>B. cepacia</i> ATCC 25,416	<i>S. epidermidis</i> ATCC 12,228	<i>P. aeruginosa</i> ATCC 15,442		<i>C. albicans</i> ATCC 90,028	<i>C. albicans</i> ATCC 64,550
SFX	>400 (>1288.9)	>400 (>1288.9)	>400 (>1288.9)	>400 (>1288.9)	200 (644.5)	3000 (9667.1)	3000 (9667.1)
AgSFX	50 (59.9)	12.5 (15.0)	25 (29.9)	12.5 (15.0)	200 (239.5)	2.93 (3.5)	2.93 (3.5)
SFX-SL	>400 (>965.2)	400 (965.2)	>400 (>965.2)	>400 (>965.2)	200 (482.6)	375 (904.8)	187.5 (452.4)
AgSFX-SL	50 (48.0)	12.5 (12.0)	25 (24.0)	12.5 (12.0)	200 (191.8)	2.93 (2.8)	2.93 (2.8)
AgNO <sub>3</sub>	12.5 (73.6)	3.12 (18.4)	3.12 (18.4)	3.12 (18.4)	100 (587)	2.93 (17.25)	5.86 (34.50)
Gentamicin	–	–	0.05	1.5	0.4	–	–
Vancomycin	0.7	–	–	–	–	–	–
Chloramphenicol	–	14.4	–	–	–	–	–
Amphotericin	–	–	–	–	–	1.0	1.0

attracting electrons. The electrophilicity index ( $\omega$ ) measures the electrophilic power of the molecules and can be classify as strong ( $\omega > 1.5$  eV), moderate ( $\omega$  between 0.9 and 1.4) and very small ( $\omega < 0.8$  eV). The chemical potential ( $\mu$ ) is usually associated with the charge transfer ability of the system in its ground state. Alternatively,  $\mu$  is the index of escaping tendency of electrons from an equilibrium system [61–63].

Analyzing the results for the reactivity indices at Table S2, it is possible to infer that the results between the ligand and the complex are very close for all properties, which allows to infer that the complex formed has practically the same reactivity, stability and electrophilic characteristics and strength of attracting electrons as the ligand.

The results for QTAIM analysis aimed at the characterization of the nature of the chemical bonds of the dimer. The obtained data for AgSFX-SL are shown at the supplementary material (Table S3).

The molecular graph for the AgSFX-SL is shown in Fig. 7 and the Critical Binding Points (CBP) prove that the complex is formed. The electron density ( $\rho(r)$ ) values are also represented in Fig. 7 and as observed, the  $\rho(r)$  values follow the same trend found for the structural parameters, where for smaller bond lengths, the electron density is greater.

Another way to classify the interactions is by the Laplacian of electron density ( $\nabla^2\rho(r)$ ) and total energy density ( $H(r)$ ). When  $\nabla^2\rho(r) > 0$  and  $H(r) < 0$  the interaction is partially covalent and for  $\nabla^2\rho(r) > 0$  and  $H(r) > 0$  are electrostatic. The results show that all electron density Laplacian ( $\nabla^2\rho(r)$ ) are positive and that all total energy densities are negative. The values of  $H(r)$  and  $\nabla^2\rho(r)$  show that the character of all interactions of the metal with the SFX-SL ligand is partially covalent.

### 3.6. Antibacterial and antifungal activity studies

The MIC values of the compounds against bacteria and yeasts associated to skin wound infections are shown in Table 3. The bacterial strains selected are pathogens that commonly cause burn wound infections and skin lesions. These bacterial strains are resistant to some antibiotics, which represent a challenge for treatment [64–66]. Also, the bacterial strains used in this study have shown to be resistant to sulfadoxine in the considered conditions.

The AgSFX complex described in an earlier work by our research group was repurposed as described in reference [17] and used for comparative studies in the MIC assays. The AgSFX and AgSFX-SL complexes presented the lowest MIC values for aerobic bacteria in the range from 12.5 to 59.9  $\mu\text{mol}\cdot\text{L}^{-1}$ . All the tested compounds presented relative low activities and high MIC values for *C. acnes* (anaerobic strain). The obtained MIC values for AgSFX and AgSFX-SL complexes were lower than those found in the literature for silver sulfadiazine (SSD), a commercial antibacterial agent. For *P. aeruginosa*, the MIC value found for SSD was 56  $\mu\text{mol}\cdot\text{L}^{-1}$ , while for *S. epidermidis*, the MIC value for SSD was 224  $\mu\text{mol}\cdot\text{L}^{-1}$  [67].

Sulfadoxine (SFX) and its respective Schiff base (SFX-SL) showed no significant activity against the tested bacterial strains. Meanwhile, the SFX-SL species demonstrated a moderate activity against yeast in comparison to SFX, showing an enhancement of activity after the modification of the sulfa drug in its Schiff base form.

The MIC values of the AgSFX and AgSFX-SL complexes were much lower than the values found for SFX and SFX-SL against bacteria and

fungi as can be seen in Table 2. The antimicrobial activities presented by the metal complexes are probably due to the presence of silver ions, with emphasis on a superior efficacy in the inhibition of aerobic microorganisms' growth. Although AgNO<sub>3</sub> presented low MIC values in this experiment, it is important to emphasize that this compound exhibits toxicity to cells and tissues at concentrations >1 %. This effect can be attributed to the fast release of Ag(I) ions [68].

### 3.7. Polyacrylamide gel electrophoresis assays (SDS-PAGE)

Considering the antibacterial and antifungal activities exhibited for SFX-SL and the AgSFX-SL complex as presented in Table 3, biophysical assays based on sodium dodecyl sulfate polyacrylamide gel electrophoresis (SDS-PAGE) were conducted. Such technique is an important tool to further investigate the possible biomolecular targets for several classes of drugs and correlate it with their activities. Lysozyme and bovine serum albumin (BSA) are commonly used to examine if the compounds are able to interact with proteins in biological medium. As early reported, albumins are the most abundant proteins in plasma and drug interaction with albumin can be considered as a key factor for the pharmacokinetics and pharmacodynamics of such compounds [16]. Lysozyme is a protein of approximately 12 kDa also commonly used in the evaluation of proteins and drug interactions. By the evaluation of the influence of the SFX-SL and AgSFX-SL on the electrophoretic mobility of the chosen proteins, it is possible to evaluate the selectivity of the compounds for this class of biomolecules and correlate it with its antimicrobial activities [16]. No evidence of interaction was found for the compounds in this preliminary approach with the model proteins bovine serum albumin (BSA) and lysozyme. Figure S7 at the supplementary material presents the pattern of the bands obtained after incubation of the compounds with the selected proteins. Further investigations of interaction mode with other possible targets, such as DNA or even with proteins by using other techniques, are envisaged and will be performed in the future.

## 4. Conclusions

The Schiff base of sulfadoxine with salicylaldehyde (SFX-SL) and its respective silver(I) complex (AgSFX-SL) were obtained. The experimental and computational studies revealed coordination of the Schiff base to Ag(I) by the oxygen and deprotonated nitrogen atoms from sulfonamide group, and by the nitrogen atom from pyrimidine ring forming a dimeric structure. The AgSFX complex formerly described in the literature and the novel AgSFX-SL complex presented MIC values from 2.8 to 59.9 μmol·L<sup>-1</sup> for the selected bacterial strains. The obtained results were comparable to the activity of the commercial drug SSD for *P. aeruginosa* and *S. epidermidis* species that participate in skin wound infections. The complexes were also active over *C. albicans* with concentration values in the micromolar range. Preliminary biophysical assays suggest no interaction of the compounds with the selected model proteins albumin and lysozyme.

### CRediT authorship contribution statement

**Igor Santos Oliveira:** Conceptualization, Methodology, Investigation, Writing – review & editing. **Carlos Marrote Manzano:** Methodology, Investigation. **Douglas Hideki Nakahata:** Methodology, Investigation, Writing – review & editing. **Mariana Brentini Santiago:** Investigation. **Nagela Bernadelli Sousa Silva:** Investigation. **Carlos Henrique Gomes Martins:** Methodology, Investigation, Supervision, Funding acquisition. **Fernando Pimentel Respíndula:** Investigation. **Douglas Henrique Pereira:** Conceptualization, Investigation, Supervision, Writing – review & editing, Funding acquisition. **Pedro Paulo Corbi:** Conceptualization, Investigation, Writing – review & editing, Project administration, Supervision, Funding acquisition.

## Declaration of Competing Interest

The authors declare that they have no known competing financial interests or personal relationships that could have appeared to influence the work reported in this paper.

## Data availability

Additional research data can be found at the [supplementary material](#) of the manuscript

## Acknowledgements

This work was financed by FAPESP (São Paulo State Research Council, grant# 2021/08717-8, 2018/12062-4 and 17/25995-6), CNPq (National Research Council Brazil, Grant # 407012/2018-4) and CAPES-Print 2464/2018 (Coordination for the Improvement of Higher Education, Grant # 88881.310539/2018-01) and CAPES-Finance Code 001. The authors dedicate this work to the memory of Professor Ademir Neves from Federal University of Santa Catarina, Brazil.

## Appendix A. Supplementary data

The crystallographic data can be obtained free of charge at the Cambridge Crystallographic Data Centre, with CCDC 2163975, or from Cambridge Crystallographic Data Centre (CCDC), 12 Union Road, Cambridge CB2 1EZ, UK; email: [deposit@ccdc.cam.ac.uk](mailto:deposit@ccdc.cam.ac.uk). Supplementary data to this article can be found online at <https://doi.org/10.1016/j.poly.2022.116073>.

## References

- [1] J.S. Glasser, C.H. Guymon, K. Mende, S.E. Wolf, D.R. Hospenthal, C.K. Murray, Activity of topical antimicrobial agents against multidrug-resistant bacteria recovered from burn patients, *Burns*. 36 (2010) 1172–1184, <https://doi.org/10.1016/j.burns.2010.05.013>.
- [2] S. Zhang, J. Ye, Y. Sun, J. Kang, J. Liu, Y. Wang, Y. Li, L. Zhang, G. Ning, Electrospun fibrous mat based on silver (I) metal-organic frameworks-poly(lactic acid) for bacterial killing and antibiotic-free wound dressing, *Chem. Eng. J.* 390 (2020), 124523, <https://doi.org/10.1016/j.cej.2020.124523>.
- [3] Z. Xu, C. Zhang, X. Wang, D. Liu, Release Strategies of Silver Ions from Materials for Bacterial Killing, *ACS Appl. Bio Mater.* 4 (2021) 3985–3999, <https://doi.org/10.1021/acsabm.0c01485>.
- [4] E.J. Anthony, E.M. Bolitho, H.E. Bridgewater, O.W.L. Carter, J.M. Donnelly, C. Imberti, E.C. Lant, F. Lermyte, R.J. Needham, M. Palau, P.J. Sadler, H. Shi, F. X. Wang, W.Y. Zhang, Z. Zhang, Metalloids are unique: Opportunities and challenges of discovery and development, *Chem. Sci.* 11 (2020) 12888–12917, <https://doi.org/10.1039/d0sc04082g>.
- [5] A. Frei, J. Zuegg, A.G. Elliott, M. Baker, S. Braese, C. Brown, F. Chen, C.G. Dowson, G. Dujardin, N. Jung, A.P. King, A.M. Mansour, M. Massi, J. Moat, H.A. Mohamed, A.K. Renfrew, P.J. Rutledge, P.J. Sadler, M.H. Todd, C.E. Willans, J.J. Wilson, M. A. Cooper, M.A.T. Blaskovich, Metal complexes as a promising source for new antibiotics, *Chem. Sci.* 11 (2020) 2627–2639, <https://doi.org/10.1039/c9sc06460e>.
- [6] S. Medici, M. Peana, V.M. Nurchi, M.A. Zoroddu, Medical uses of silver: history, myths, and scientific evidence, *J. Med. Chem.* 62 (2019) 5923–5943, <https://doi.org/10.1021/acs.jmedchem.8b01439>.
- [7] S. Medici, M. Peana, G. Crisponi, V.M. Nurchi, J.I. Lachowicz, M. Remelli, M. A. Zoroddu, Silver coordination compounds: A new horizon in medicine, *Coord. Chem. Rev.* 327–328 (2016) 349–359, <https://doi.org/10.1016/j.ccr.2016.05.015>.
- [8] A. Tacic, V. Nikolic, L. Nikolic, I. Savic, Antimicrobial sulfonamide drugs, *Adv. Technol.* 6 (2017) 58–71, <https://doi.org/10.5937/savteh1701058t>.
- [9] Y. Chen, Recent functionalizations of primary sulfonamides, *Synth.* 48 (2016) 2483–2522, <https://doi.org/10.1055/s-0035-1562503>.
- [10] S. Mondal, S.M. Mandal, T.K. Mondal, C. Sinha, Spectroscopic characterization, antimicrobial activity, DFT computation and docking studies of sulfonamide Schiff bases, *J. Mol. Struct.* 1127 (2017) 557–567, <https://doi.org/10.1016/j.molstruc.2016.08.011>.
- [11] M. Krátký, M. Dzurková, J. Janoušek, K. Konečná, F. Trejtnar, J. Stolaríková, J. Vinšová, Sulfadiazine salicylaldehyde-based schiff bases: Synthesis, antimicrobial activity and cytotoxicity, *Molecules*. 22 (2017) 1–15, <https://doi.org/10.3390/molecules22091573>.
- [12] A. Hamad, Y. Chen, M.A. Khan, S. Jamshidi, N. Saeed, M. Clifford, C. Hind, J. M. Sutton, K.M. Rahman, Schiff bases of sulphonamides as a new class of antifungal agent against multidrug-resistant *Candida auris*, *Microbiologyopen*. 10 (2021) 1–8, <https://doi.org/10.1002/mbo3.1218>.

- [13] J.G. Kublin, F.K. Dzinjalama, D.D. Kamwendo, E.M. Malkin, J.F. Cortese, L. M. Martino, R.A.G. Mukadam, S.J. Rogerson, A.G. Lescano, M.E. Molyneux, P. A. Winstanley, P. Chimpeni, T.E. Taylor, C.V. Plowe, Molecular markers for failure of sulfadoxine-pyrimethamine and chloroquine-dapsone treatment of *Plasmodium falciparum* malaria, *J. Infect. Dis.* 185 (2002) 380–388, <https://doi.org/10.1086/338566>.
- [14] A. Nzila, S.A. Ward, K. Marsh, P.F.G. Sims, J.E. Hyde, Comparative folate metabolism in humans and malaria parasites (part I): Pointers for malaria treatment from cancer chemotherapy, *Trends Parasitol.* 21 (2005) 292–298, <https://doi.org/10.1016/j.pt.2005.04.002>.
- [15] J.A. Francis, M. Shalauddin, N.F.W. Ridzwan, S.B. Mohamad, W.J. Basirun, S. Tayyab, Interaction mechanism of an antimalarial drug, sulfadoxine with human serum albumin, *Spectrosc. Lett.* 53 (2020) 391–405, <https://doi.org/10.1080/00387010.2020.1764588>.
- [16] P. Chellan, V.M. Avery, S. Duffy, J.A. Triccas, G. Nagalingam, C. Tam, L.W. Cheng, J. Liu, K.M. Land, G.J. Clarkon, I. Romero-Canelón, P.J. Sadler, Organometallic conjugates of the drug sulfadoxine for combatting antimicrobial resistance, *Chem. - A Eur. J.* 24 (2018) 10078–10090, <https://doi.org/10.1002/chem.201801090>.
- [17] N.T. Zanvetto, C. Abbehaio, W.R. Lustrí, A. Cuin, N. Masciocchi, P.P. Corbi, Silver sulfadoxinate: Synthesis, structural and spectroscopic characterizations, and preliminary antibacterial assays in vitro, *J. Mol. Struct.* 1082 (2014) 180–187, <https://doi.org/10.1016/j.molstruc.2014.11.004>.
- [18] P.G. Esqueizaro, C.M. Manzano, D.H. Nakahata, I.A. Santos, U.E.A. Ruiz, M. B. Santiago, N.B.S. Silva, C.H.G. Martins, D.H. Pereira, F.R.G. Bergamini, A.C. G. Jardim, P.P. Corbi, Synthesis, spectroscopic characterization and in vitro antibacterial and antiviral activities of novel silver(I) complexes with mafenide and ethyl-mafenide, *J. Mol. Struct.* 1246 (2021), 131261, <https://doi.org/10.1016/j.molstruc.2021.131261>.
- [19] D.H. Nakahata, R.E.F. De Paiva, W.R. Lustrí, P.P. Corbi, Sulfonamide-containing copper(II) complexes: New insights on biophysical interactions and antibacterial activities, *New J. Chem.* 44 (2020) 17236–17244, <https://doi.org/10.1039/d0nj01889a>.
- [20] J.H. Bormio Nunes, R.E.F. De Paiva, A. Cuin, W.R. Lustrí, P.P. Corbi, Silver complexes with sulfathiazole and sulfamethoxazole: Synthesis, spectroscopic characterization, crystal structure and antibacterial assays, *Polyhedron.* 85 (2015) 437–444, <https://doi.org/10.1016/j.poly.2014.09.010>.
- [21] D.H. Nakahata, R.E.F. de Paiva, W.R. Lustrí, C.M. Ribeiro, F.R. Pavan, G.G. da Silva, A.L.T.G. Ruiz, J.E. de Carvalho, P.P. Corbi, Sulfonamide-containing copper (II) metallonucleases: Correlations with in vitro antimycobacterial and antiproliferative activities, *J. Inorg. Biochem.* 187 (2018) 85–96, <https://doi.org/10.1016/j.jinorgbio.2018.07.011>.
- [22] D.H. Nakahata, W.R. Lustrí, A. Cuin, P.P. Corbi, Crystal structure, spectroscopic characterization and antibacterial activities of a silver complex with sulfamer, *J. Mol. Struct.* 1125 (2016) 609–615, <https://doi.org/10.1016/j.molstruc.2016.07.049>.
- [23] A.T.M. Fiori, D.H. Nakahata, A. Cuin, W.R. Lustrí, P.P. Corbi, Synthesis, crystallographic studies, high resolution mass spectrometric analyses and antibacterial assays of silver(I) complexes with sulfisoxazole and sulfadimethoxine, *Polyhedron.* 121 (2017) 172–179, <https://doi.org/10.1016/j.poly.2016.09.046>.
- [24] A.T. Fiori-Duarte, R.E.F. de Paiva, C.M. Manzano, W.R. Lustrí, P.P. Corbi, Silver(I) and gold(I) complexes with sulfasalazine: Spectroscopic characterization, theoretical studies and antiproliferative activities over Gram-positive and Gram-negative bacterial strains, *J. Mol. Struct.* 1214 (2020), 128158, <https://doi.org/10.1016/j.molstruc.2020.128158>.
- [25] Bruker (2012). SAINT, APEXII. Bruker AXS Inc., Madison, Wisconsin, USA., (2012).
- [26] Bruker (2001). SADABS, APEXII. Bruker AXS Inc., Madison, Wisconsin, USA., (2001).
- [27] O.V. Dolomanov, L.J. Bourhis, R.J. Gildea, J.A.K. Howard, H. Puschmann, OLEX2: a complete structure solution, refinement and analysis program, *J. Appl. Crystallogr.* 42 (2009) 339–341, <https://doi.org/10.1107/S0021889808042726>.
- [28] G.M. Sheldrick, SHELXT – Integrated space-group and crystal-structure determination, *Acta Crystallogr. A* 71 (2015) 3–8, <https://doi.org/10.1107/S2053273314026370>.
- [29] G.M. Sheldrick, Crystal structure refinement with SHELXL, *Acta Crystallogr. Sect. C Struct. Chem.* 71 (2015) 3–8, <https://doi.org/10.1107/S2053296140242118>.
- [30] C.F. Macrae, I.J. Bruno, J.A. Chisholm, P.R. Edgington, P. McCabe, E. Pidcock, L. Rodriguez-Monge, R. Taylor, J. van de Streek, P.A. Wood, Mercury CSD 2.0 – new features for the visualization and investigation of crystal structures, *J. Appl. Crystallogr.* 41 (2008) 466–470, <https://doi.org/10.1107/S0021889807067908>.
- [31] J. Da Chai, M. Head-Gordon, Long-range corrected hybrid density functionals with damped atom-atom dispersion corrections, *Phys. Chem. Chem. Phys.* 10 (2008) 6615–6620, <https://doi.org/10.1039/b810189b>.
- [32] R. Ditchfield, W.J. Hehre, J.A. Pople, Self-consistent molecular-orbital methods. IX. An extended gaussian-type basis for molecular-orbital studies of organic molecules, *J. Chem. Phys.* 54 (1971) 720–723, <https://doi.org/10.1063/1.16774902>.
- [33] W.J. Hehre, K. Ditchfield, J.A. Pople, Self-consistent molecular orbital methods. XII. Further extensions of gaussian-type basis sets for use in molecular orbital studies of organic molecules, *J. Chem. Phys.* 56 (1972) 2257–2261, <https://doi.org/10.1063/1.1677527>.
- [34] P.J. Hay, W.R. Wadt, Ab initio effective core potentials for molecular calculations. Potentials for the transition metal atoms Sc to Hg, *J. Chem. Phys.* 82 (1985) 270–283, <https://doi.org/10.1063/1.448799>.
- [35] J. Frisch, G. W. Trucks, H.B. Schlegel, G.E. Scuseria, M.A. Robb, J.R. Cheeseman, G. Scalmani, V. Barone, B. Mennucci, G.A. Petersson, H. Nakatsuji, M. Caricato, X. Li, H.P. Hratchian, A.F. Izmaylov, J. Bloino, G. Zheng, J.L. Sonnenberg, M. Hada, M. Ehara, K. Toyota, R. Fukuda, J. Hasegawa, M. Ishida, T. Nakajima, Y. Honda, O. Kitao, H. Nakai, T. Vreven, J.A. Montgomery, J.E. Peralta, F. Ogliaro, M. Bearpark, J.J. Heyd, E. Brothers, K. N. Kudin, V. N. Staroverov, R. Kobayashi, J. Normand, K. Raghavachari, A. Rendell, J. C. Burant, S.S. Iyengar, J. Tomasi, M. Cossi, N. Rega, J.M. Millam, M. Klene, J.E. Knox, J.B. Cross, V. Bakken, C. Adamo, J. Jaramillo, R. Gomperts, R.E. Stratmann, O. Yazyev, A.J. Austin, R. Cammi, C. Pomelli, J.W. Ochterski, R.L. Martin, K. Morokuma, V.G. Zakrzewski, G.A. Voth, P. Salvador, J.J. Dannenberg, S. Dapprich, A.D. Daniels, Ö. Farkas, J.B. Foresman, J.V. Ortiz, J. Cioslowski, D.J. Fox, Gaussian09, Revision D.1, Gaussian, Inc., Wallingford, CT, 2009.
- [36] Dennington, R., Keith, T. and Millam, J. Gauss View, Version 5. Semicem Inc., Shawnee Mission.
- [37] A.N. Mallya, S. Panda, DFT study of iminodiacetic acid functionalised polyaniline copolymer interaction with heavy metal ions through binding energy, stability constant and charge transfer calculations, *Comput. Theor. Chem.* 1202 (2021), 113288, <https://doi.org/10.1016/j.comptc.2021.113288>.
- [38] A.M.F. Costa, S.Q. de Aguiar Filho, T.J. Santos, D.H. Pereira, Theoretical insights about the possibility of removing Pb<sup>2+</sup> and Hg<sup>2+</sup> metal ions using adsorptive processes and matrices of carboxymethyl diethylaminoethyl cellulose and cellulose nitrate biopolymers, *J. Mol. Liq.* 331 (2021), <https://doi.org/10.1016/j.molliq.2021.115730>.
- [39] A.N. Mallya, M.K. Poduval, P.C. Ramamurthy, Design, synthesis, fabrication and simulation of conjugated molecule for detection of lithium ions, *Mater. Res. Express.* 6 (2019), <https://doi.org/10.1088/2053-1591/aaef1>.
- [40] R.G. Parr, R.A. Donnelly, M. Levy, W.E. Palke, Electronegativity: The density functional viewpoint, *J. Chem. Phys.* 68 (1977) 3801–3807, <https://doi.org/10.1063/1.436185>.
- [41] H.A. Duarte, Chemical reactivity indexes from density functional theory: Formalism and perspectives, *Quim. Nova.* 24 (2001) 501–508, <https://doi.org/10.1590/s0100-40422001000400011>.
- [42] T. Koopmans, Über die Zuordnung von Wellenfunktionen und Eigenwerten zu den Einzelnen Elektronen Eines Atoms, *Physica* 1 (1934) 104–113, [https://doi.org/10.1016/S0031-8914\(34\)90011-2](https://doi.org/10.1016/S0031-8914(34)90011-2).
- [43] AIMAll (Version 17,11,14), Keith TA, (2017) TK Gristmill Software, Overland Park KS, USA (aim.tkgristmill.com).
- [44] R.F.W. Bader, H. Essén, The characterization of atomic interactions, *J. Chem. Phys.* 80 (1983) 1943–1960, <https://doi.org/10.1063/1.446956>.
- [45] T.A. Keith, R.F.W. Bader, Y. Aray, Structural homeomorphism between the electron density and the virial field, *Int. J. Quantum Chem.* 57 (1996) 183–198, [https://doi.org/10.1002/\(SICI\)1097-461X\(1996\)57:2<183::AID-QUA4>3.0.CO;2-U](https://doi.org/10.1002/(SICI)1097-461X(1996)57:2<183::AID-QUA4>3.0.CO;2-U).
- [46] I.H.S. Ribeiro, D.T. Reis, D.H. Pereira, A DFT-based analysis of adsorption of Cd<sup>2+</sup>, Cu<sup>2+</sup>, Zn<sup>2+</sup>, Hg<sup>2+</sup>, Pb<sup>2+</sup>, and Zn<sup>2+</sup>, on vanillin monomer: a study of the removal of metal ions from effluents, *J. Mol. Model.* 25 (2019), <https://doi.org/10.1007/s00894-019-4151-z>.
- [47] D.T. Reis, I.H.S. Ribeiro, D.H. Pereira, DFT study of the application of polymers cellulose and cellulose acetate for adsorption of metal ions (Cd<sup>2+</sup>, Cu<sup>2+</sup> and Cr<sup>3+</sup>) potentially toxic, *Polym. Bull.* 77 (2020) 3443–3456, <https://doi.org/10.1007/s00289-019-02926-5>.
- [48] D.T. Reis, S.Q. de Aguiar Filho, C.G.L. Grotto, M.F.R. Bihain, D.H. Pereira, Carboxymethylcellulose and cellulose xanthate matrices as potential adsorbent material for potentially toxic Cu<sup>2+</sup>, Cd<sup>2+</sup> and Pb<sup>2+</sup> metal ions: a theoretical study, *Theor. Chem. Acc.* 139 (2020) 1–8, <https://doi.org/10.1007/s00214-020-02610-2>.
- [49] CLSI Methods for Antimicrobial Susceptibility Testing of Anaerobic Bacteria; Approved Standard-Seventh Edition Volume 27 Number 2 Methods for Antimicrobial Susceptibility Testing of Anaerobic Bacteria; Approved Standard- Seventh Edition, Replace. M11-A6, 27 (2007).
- [50] CLSI Methods for Dilution Antimicrobial Susceptibility Tests for Bacteria That Grow Aerobically; Approved Standard – Ninth Edition Performance Standards for Antimicrobial Susceptibility Testing; Twenty-second Informational Supplement (2012).
- [51] S.D. Sarker, L. Nahar, Y. Kumarasamy, Microtitre plate-based antibacterial assay incorporating resazurin as an indicator of cell growth, and its application in the in vitro antibacterial screening of phytochemicals, *Methods* 42 (2007) 321–324, <https://doi.org/10.1016/j.ymeth.2007.01.006>.
- [52] Clinical and Laboratory Standards Institute. Reference method for broth dilution antifungal susceptibility testing of yeasts. CLSI document M 27–A3, 34th ed. Wayne: Wayne, Pennsylvania, USA, 2008.
- [53] K.D. Goughenour, J.-M. Balada-Llasat, C.A. Rappleye, D.W. Warnock, Quantitative microplate-based growth assay for determination of antifungal susceptibility of *histoplasma capsulatum* yeasts, *J. Clin. Microbiol.* 53 (10) (2015) 3286–3295.
- [54] Y.-H. Tang, Yun-Zhi; Wen, He-Rui; Zhang, Jian; Tan, CCDC 717094: Experimental Crystal Structure Determination, (2010). 10.5517/ccs2623.
- [55] F.H. Allen, D.G. Watson, L. Brammer, A.G. Orpen, R. Taylor, International tables for crystallography. Volume C: mathematical physical and chemical tables, *Acta Crystallogr. Sect. A Found. Crystallogr.* 49 (1993) 371–373, <https://doi.org/10.1107/S0108767393099969>.
- [56] S. SeethaLekshmi, M.S.R.N. Kiran, U. Ramamurthy, S. Varughese, Molecular basis for the mechanical response of sulfa drug crystals, *Chem. - A Eur. J.* 25 (2019) 526–537, <https://doi.org/10.1002/chem.201803987>.
- [57] I. Beloso, J. Castro, J.A. García-Vázquez, P. Pérez-Lourido, J. Romero, A. Sousa, Electrochemical synthesis and structural characterization of silver(I) complexes of N-2-pyridyl sulfonamide ligands with different nuclearity: Influence of the steric hindrance at the pyridine ring and the sulfonamide group on the structure of the complexes, *Inorg. Chem.* 44 (2005) 336–351, <https://doi.org/10.1021/ic0490268>.
- [58] C.R. Groom, I.J. Bruno, M.P. Lightfoot, S.C. Ward, The Cambridge structural database, *Acta Crystallogr. Sect. B Struct. Sci. Cryst. Eng. Mater.* 72 (2016) 171–179, <https://doi.org/10.1107/S2052520616003954>.

- [59] N. Mosconi, C. Giuidori, F. Velluti, E. Hure, A. Postigo, G. Borthagaray, D.F. Back, M.H. Torre, M. Rizzotto, Antibacterial, antifungal, phytotoxic, and genotoxic properties of two complexes of AgI with sulfachloropyridazine (SCP): X-ray diffraction of  $[Ag(SCP)]_n$ , *ChemMedChem*. 9 (2014) 1211–1220, <https://doi.org/10.1002/cmdc.201400071>.
- [60] F. Velluti, N. Mosconi, A. Acevedo, G. Borthagaray, J. Castiglioni, R. Faccio, D. F. Back, G. Moyna, M. Rizzotto, M.H. Torre, Synthesis, characterization, microbiological evaluation, genotoxicity and synergism tests of new nano silver complexes with sulfamoxole: X-ray diffraction of  $[Ag_2(SMX)_2] \cdot DMSO$ , *J. Inorg. Biochem.* 141 (2014) 58–69, <https://doi.org/10.1016/j.jinorgbio.2014.08.007>.
- [61] L.R. Domingo, P. Pérez, The nucleophilicity N index in organic chemistry, *Org. Biomol. Chem.* 9 (2011) 7168–7175, <https://doi.org/10.1039/c1ob05856h>.
- [62] R.A. Costa, J.N. da Silva, V.G. Oliveira, L.M. Anselmo, M.M. Araújo, K.M.T. Oliveira, R. de C.S. Nunomura, New insights into structural, electronic, reactivity, spectroscopic and pharmacological properties of Bergenin: Experimental, DFT calculations, MD and docking simulations, *J. Mol. Liq.* 330 (2021). 10.1016/j.molliq.2021.115625.
- [63] A. Bhattacharya, J.P. Naskar, P. Saha, R. Ganguly, B. Saha, S.T. Choudhury, S. Chowdhury, A new oxorhenium(V) complex with benzothiazole derived ligand: Relative stability and global chemical reactivity indices, *Inorg. Chim. Acta.* 447 (2016) 168–175, <https://doi.org/10.1016/j.ica.2016.04.002>.
- [64] D. Church, S. Elsayed, O. Reid, B. Winston, R. Lindsay, *Burn Wound Infections* 19 (2006) 403–434, <https://doi.org/10.1128/CMR.19.2.403>.
- [65] W. Norbury, D.N. Herndon, J. Tanksley, M.G. Jeschke, C.C. Finnerty, *Infect. Burns* 17 (2016), <https://doi.org/10.1089/sur.2013.134>.
- [66] Y. Wang, J. Beekman, J. Hew, S. Jackson, A.C. Issler-fisher, R. Parungao, S. S. Lajevardi, Z. Li, P.K.M. Maitz, *Burn injury : Challenges and advances in burn wound healing, infection, pain and scarring*, *Adv. Drug Deliv. Rev.* 123 (2018) 3–17, <https://doi.org/10.1016/j.addr.2017.09.018>.
- [67] U. Kalinowska-Lis, A. Felczak, L. Checińska, K. Zawadzka, E. Patyna, K. Lisowska, J. Ochocki, Synthesis, characterization and antimicrobial activity of water-soluble silver(I) complexes of metronidazole drug and selected counter-ions, *Dalt. Trans.* 44 (2015) 8178–8189, <https://doi.org/10.1039/c5dt00403a>.
- [68] B.S. Atiyeh, M. Costagliola, S.N. Hayek, S.A. Dibo, Effect of silver on burn wound infection control and healing: Review of the literature, *Burns*. 33 (2007) 139–148, <https://doi.org/10.1016/j.burns.2006.06.010>.





## Article

# Inanimate Surfaces and Air Contamination with Multidrug Resistant Species of *Staphylococcus* in the Neonatal Intensive Care Unit Environment

Ralciane de Paula Menezes <sup>1,†</sup>, Lara de Andrade Marques <sup>2,†</sup>, Felipe Flávio Silva <sup>2</sup>, Nagela Bernadelli Sousa Silva <sup>2</sup>, Priscila Guerino Vilela Alves <sup>2</sup> , Meliza Arantes de Souza Bessa <sup>3</sup> , Lúcio Borges de Araújo <sup>4,5</sup> , Mário Paulo Amante Penatti <sup>1</sup>, Reginaldo dos Santos Pedroso <sup>1</sup> and Denise Von Dolinger de Brito Röder <sup>6,\*</sup>

- <sup>1</sup> Technical Course in Clinical Analysis, Technical School of Health (ESTES), Federal University of Uberlândia (UFU), Uberlândia 38400-320, MG, Brazil; ralciane@ufu.br (R.d.P.M.); mario.penatti@ufu.br (M.P.A.P.); rpedroso@ufu.br (R.d.S.P.)
- <sup>2</sup> Postgraduate Program in Health Sciences, Faculty of Medicine, Federal University of Uberlândia (UFU), Uberlândia 38400-320, MG, Brazil; lara.marques@ufu.br (L.d.A.M.); felipeflavio21@hotmail.com (F.F.S.); nagela\_bernadelli.mg@hotmail.com (N.B.S.S.); priscilaguerinoalves@gmail.com (P.G.V.A.)
- <sup>3</sup> Institute of Biology, Federal University of Uberlândia (UFU), Uberlândia 38400-320, MG, Brazil; melizaarantes@gmail.com
- <sup>4</sup> Faculty of Medicine, Federal University of Uberlândia (UFU), Uberlândia 38400-320, MG, Brazil; lucio.araujo@ufu.br
- <sup>5</sup> Faculty of Mathematics, Federal University of Uberlândia (UFU), Uberlândia 38400-320, MG, Brazil
- <sup>6</sup> Institute of Biomedical Sciences, Federal University of Uberlândia (UFU), Uberlândia 38400-320, MG, Brazil
- \* Correspondence: denise.roder@ufu.br; Tel.: +55-(34)991-854-234
- † These authors contributed equally to this work.



**Citation:** Menezes, R.d.P.; Marques, L.d.A.; Silva, F.F.; Silva, N.B.S.; Alves, P.G.V.; Bessa, M.A.d.S.; Araújo, L.B.d.; Penatti, M.P.A.; Pedroso, R.d.S.; Brito Röder, D.V.D.d. Inanimate Surfaces and Air Contamination with Multidrug Resistant Species of *Staphylococcus* in the Neonatal Intensive Care Unit Environment. *Microorganisms* **2022**, *10*, 567.

<https://doi.org/10.3390/microorganisms10030567>

Academic Editors: Célia F. Rodrigues, Vineet K. Singh and Natália Cruz-Martins

Received: 8 November 2021

Accepted: 27 January 2022

Published: 5 March 2022

**Publisher's Note:** MDPI stays neutral with regard to jurisdictional claims in published maps and institutional affiliations.



**Copyright:** © 2022 by the authors. Licensee MDPI, Basel, Switzerland. This article is an open access article distributed under the terms and conditions of the Creative Commons Attribution (CC BY) license (<https://creativecommons.org/licenses/by/4.0/>).

**Abstract:** Background: Contamination of the hospital environment with multi-resistant (MDR) *Staphylococcus* increases the risk of infection. The aim of this study is to identify the MDR species of *Staphylococcus* on inanimate surfaces, in air, and in clinical samples, and analyze the risk factors that correlate with the occurrence of infections in a Neonatal Intensive Care Unit. Methods: Samples of inanimate surfaces and air were taken using a premoistened swab (0.9% sodium chloride) and spontaneous air sedimentation, respectively. The clinical isolates were recovered from infected neonates. The isolates (environmental and clinical) were identified by matrix-assisted laser desorption ionization-time of flight and the resistance profile was calculated using the disk diffusion agar technique. Results: In total, 181 isolates were obtained, 93 from (surfaces), 18 from the air, and 70 clinical samples. *S. epidermidis* was the most frequent species (66.8%), and the failure rate in air cleaning was 100%. More than 60% of the isolates were MDR, and the majority of clinical isolates (60.4%) had a resistance profile identical to that of the environmental isolates. Conclusion: *Staphylococcus* spp. were found in most of the analyzed samples, with a high frequency of MDR isolates, demonstrating the importance of the hospital environment as a reservoir, and the need for infection control measures, and rational use of antimicrobials.

**Keywords:** *Staphylococcus*; environmental contamination; air; neonatal intensive care unit; antimicrobial resistance

## 1. Introduction

The microbial contamination of the hospital environment plays an important role in the development of Healthcare Associated Infections (HAI) and contributes to the increase in morbidity and mortality of patients admitted to the Neonatal Intensive Care Unit (NICU) [1]. It is estimated that more than 25% of the cases of HAIs are triggered by microorganisms present in the environment, for example high touch surfaces, which lead to a greater risk of the transmission of infections in healthcare services [2–6].

During hospitalization, patients spread bacteria capable of surviving for long periods on inanimate surfaces and in the air, including Gram-positive bacteria, which are one of the main etiological agents of HAI in the NICU [3,7]. Coagulase-negative *Staphylococcus* (CoNS) are responsible for up to 40% of these infections, with emphasis on *Staphylococcus epidermidis* and *Staphylococcus haemolyticus*, while *Staphylococcus aureus* is responsible for up to 25% of HAIs [8–14].

*Staphylococcus* spp. multidrug resistance (MDR) is responsible for 2% to 5% of HAIs in the NICU and causes significant neonatal morbidity and mortality (20–35%) [11,15,16]. These microorganisms can survive for long periods on inanimate surfaces and in the air [3,15,17]. Studies have shown that the persistence of MDR isolates in the environment can vary from 7 days to 5 years, depending on the type of surface, humidity, and temperature, persisting longer on dry surfaces [3,18].

The transfer of these microorganisms between the environment and patients has been demonstrated in the literature [3,7,17], and emphasizes the importance of knowing the reservoirs of hospital microbiota. Despite the relevance of the subject, studies of this type in the NICU are scarce; therefore, the purpose of this study was to identify the MDR species of *Staphylococcus* on inanimate surfaces, in air, and in clinical samples and analyze the risk factors that correlate with the occurrence of infections caused by these microorganisms in an NICU.

## 2. Materials and Methods

### 2.1. Studied NICU

The study was performed in a 20-bed NICU of the Uberlândia University Hospital.

Disinfection of the NICU surfaces is performed using Glucoprotamin™ with 0.5% quarternary ammonium compound by rubbing with the product at least three times a day, at the beginning of each work shift (6:00 a.m., 1:00 p.m., and 6:00 p.m.).

### 2.2. Sampling

#### 2.2.1. Surface Screening

Environmental samples were collected in March, June, and August 2018, always on the same day of the week and two hours before unit disinfection. High-touch surfaces were considered to be those with frequent contact with the hands and that provide the greatest risk of transmission of microorganisms [3].

Samples were collected from the surface of 20 baby incubators, 20 monitor tables, 20 respirator monitor, 20 infusion pumps, 20 vital sign monitors, six NICU access doors, five soap dishes, five paper towel holders, five faucet spouts, three cabinet drawers, three light switches, three medicine storage refrigerators' doors, three medication preparation tables, and three bath sink drains, totaling 136 collection points per month and 408 samples.

The sampling sites were sampled using swabs (Plastlabor, Rio de Janeiro, Brazil) pre-moistened with 0.9% sodium chloride and vigorously wiped over approximately 6 cm<sup>2</sup>. Swabs were vortexed in 2 mL of neutralizing solution (Hexis Científica, Jundiaí, Brazil), and 0.2 mL was plated on nutrient and *Staphylococcal* selective agars (Oxoid Ltd., Basingstoke, UK). Growth on nutrient agar was assessed and aerobic colony counts per cm<sup>2</sup> were calculated and classified as: no growth; scanty growth (<2.5 colony-forming unit [CFU]/cm<sup>2</sup>); light growth (≥2.5–12 CFU/cm<sup>2</sup>); moderate growth (>12–40 CFU/cm<sup>2</sup>); and heavy growth (>40 CFU/cm<sup>2</sup>), according to the number of CFU counted. Hygiene failure was considered to have occurred for those samples that showed growth ≥2.5 CFU/cm<sup>2</sup> [7].

#### 2.2.2. Air

The air sample was collected as follows: three Petri dishes containing nutrient and staphylococcal selective agar were exposed at each timepoint, totaling nine plates, in the center of the NICU III and II by the spontaneous sedimentation method, 1 m from the ground, 1 m from any obstacle, for 1 h [19]. Healthcare workers were allowed to freely enter the rooms when the sampling was on-going, however the movements were

not recorded. Samples that showed the growth of at least one colony were considered positive. The samples that showed growth of colonies with different characteristics were classified as having multiple growths and the identification and susceptibility test for staphylococci was carried out. The plates were incubated for 24 h at 37 °C and the CFU count was calculated, being classified as no growth, scanty growth (1 or 2 CFU/plate), light growth ( $\geq 2$ –10 CFU/plate), moderate growth ( $>10$ –40 CFU/plate), and heavy growth ( $>40$  CFU/plate). Hygiene failure was considered to have occurred for those samples that showed growth  $\geq 2$  CFU/plate/hour [19]. These air samplings were performed at the same times as the surface samplings.

### 2.2.3. Clinical Samples of Neonates and Epidemiological Surveillance

The clinical isolates included in the study from the bloodstream and ocular secretions were laboratory confirmed and obtained between the months of January and December 2018. The medical team established the parameters for the collection of biological samples and sent them to the Clinical Analysis Laboratory, where they were processed and identified.

In addition, neonates admitted to the NICU in 2018 were followed up daily through the “National Healthcare Safety Network” (NHSN) system [20], from admission to discharge or death, to check for the presence of clinical characteristics that are considered risk factors for the occurrence of infections, including birth weight, gestational age, use of a drain, use of a bladder catheter, use of invasive procedures such as the insertion of a central venous catheter (CVC), peripherally inserted central catheter (PICC), umbilical venous catheter, phlebotomy and intracath, total parenteral nutrition, mechanical ventilation, use of antimicrobial prior to infection, length of hospital stay, and outcome of hospitalization (discharge or death). Only neonates with *Staphylococcus* spp. infection were included in the study.

Neonates who had more than one positive culture were considered to have a new episode of infection when the isolation of the microorganisms occurred more than 14 days apart and showed different resistance profiles [21].

### 2.3. Identification and Antimicrobial Susceptibility Testing

All isolates were identified using matrix-assisted laser desorption ionization-time of flight (MALDI-TOF MS, Bruker Daltonik, Germany) [22] and the susceptibility to the antimicrobials: penicillin (10 µg), oxacillin (1 µg), cefoxitin (30 µg), gentamicin (10 µg), sulfazotrim (25 µg), erythromycin (15 µg), and clindamycin (2 µg) was evaluated following the methodology proposed by the Clinical and Laboratory Standards Institute document M07-A9 [23]. Bacterial isolates were classified as susceptible, intermediate, or resistant according to the Clinical and Laboratory Standards Institute (CLSI) document M100 [24]. MDR was defined as acquired non-susceptibility to at least one agent in three or more antimicrobial categories [25].

### 2.4. Detection of Methicillin-Resistant *Staphylococcus* (MRS)

The methicillin-resistant *Staphylococcus* test (MRS) was performed using a diffusion disk with cefoxitin (30 µg). Isolates of *S. aureus* and CoNS were considered resistant to methicillin when they presented an inhibition halo  $\leq 21$  mm and  $\leq 24$  mm, respectively [25]. For quality control, the reference strains *S. aureus* American Type Culture Collection (ATCC) 25,923 (methicillin-susceptible) and ATCC 43,300 (methicillin-resistant) were used.

### 2.5. Resistance to Macrolides, Lincosamides, and Streptogramin B (MLSB)

The isolates that were initially susceptible to clindamycin (2 µg) and resistant to erythromycin (15 µg) were examined for inducible clindamycin resistance using the D-test according to CLSI recommendations [24]. Briefly, erythromycin (15 µg) and clindamycin (2 µg) disks were placed 15–20 mm apart (edge to edge) and then incubated at 35–37 °C for 18 h. Isolates showing resistance to erythromycin but susceptibility to clindamycin and

producing a D-shaped zone of inhibition around the clindamycin disk on the side facing the erythromycin disk were considered to show an iMLS resistance phenotype. Moreover, resistance to both erythromycin and clindamycin was taken to indicate a cMLS resistance phenotype. Isolates showing resistance to erythromycin while being susceptible to clindamycin with no blunting zone were classified as showing an MS resistance phenotype. *S. aureus* ATCC 25923, *S. aureus* ATCC BAA-976 (Test D negative), and *S. aureus* ATCC BAA-977 (Test D positive) were used as controls.

### 2.6. Statistical Analysis

The mean time of hospitalization was described within each group of neonates (with or without infection) using the means and standard deviations. The other variables were described using double-entry tables. The risk factors for the occurrence of infection in neonates were assessed by univariate and multiple logistic regression, followed by the selection of variables using the stepwise method [26]. The chi-square test was used for analyzing categorical variables. All tests were performed using the Statistical Package for the Social Sciences (SPSS v.20) software and a significance level of 5% was applied.

### 2.7. Research Ethics

This research was approved by the Human Research Ethics Committee of the Federal University of Uberlândia (Approval N°. 2.173,884) and performed following the ethical precepts of the Declaration of Helsinki.

## 3. Results

### 3.1. Microbial Load of Inanimate Surfaces and Air

*Staphylococcus* spp. were isolated in 93 (22.8%) of the 408 samples from inanimate surfaces, with an average number of colonies of 8.5 CFU/cm<sup>2</sup>, ranging from 1 to >40 CFU/cm<sup>2</sup>; the average hygiene failure rate was equal to 10.6%. Regarding the samples collected from the air, all exposed plates showed growth of *Staphylococcus* spp., totaling 18 isolates, 16 (88.9%) of which were *S. epidermidis* and two (11.1%) *S. aureus*. Colony counts ranged from 2 to 40 CFU/plate, with an average of 10.1 CFU/plate. The analysis of the air samples indicated 100% hygiene failure (Table 1).

**Table 1.** Categories of microbial load for inanimate surfaces, air, and hygiene failure in the Neonatal Intensive Care Unit.

Inanimate Surfaces	No Growth	Scanty Growth <2.5 cfu/cm <sup>2</sup>	Light Growth ≥2.5–12 cfu/cm <sup>2</sup>	Moderate Growth >12–40 cfu/cm <sup>2</sup>	Heavy Growth >40 cfu/cm <sup>2</sup>	Hygiene Fails (≥2.5 cfu/cm <sup>2</sup> )	
						n	%
Light switches (n = 9)	4	2	3	0	0	3	33.3
Monitors table (n = 60)	34	11	8	2	5	15	25.0
Baby incubators (n = 60)	34	12	11	3	0	14	23.3
Door handle (n = 18)	11	3	3	1	0	4	22.2
Medication preparation table (n = 9)	7	1	0	1	0	1	11.1
Drawer (n = 9)	8	0	0	0	1	1	11.1
Respirators monitors (n = 60)	49	5	5	1	0	6	10.0
Towel paper holder (n = 15)	12	2	1	0	0	1	6.6
Vital sign monitors (n = 60)	55	3	2	0	0	2	3.3
Infusion pumps (n = 60)	56	2	2	0	0	2	3.3
Soap dish (n = 15)	13	2	0	0	0	0	0
Facet spout (n = 15)	14	1	0	0	0	0	0
Sink drains (n = 9)	9	0	0	0	0	0	0
Medicine storage refrigerator's door (n = 9)	9	0	0	0	0	0	0

Table 1. Cont.

Air	No Growth	Scanty Growth <2 cfu/plate	Light Growth ≥2–10 cfu/plate	Moderate Growth >10–40 cfu/plate	Heavy Growth >40 cfu/plate	Hygiene Fails (≥2 cfu/plate/hour)	
						n	%
N = 9	0	0	3	5	1	9	100

### 3.2. Surfaces and Isolated Species

In the samples from surfaces, CoNS was isolated from incubators ( $n = 26$ ; 28.9%), monitor tables ( $n = 25$ ; 27.8%), respirator monitors ( $n = 10$ ; 11.2%), door handles ( $n = 7$ ; 7.7%), vital signs monitors ( $n = 5$ ; 5.5%), paper towel holders ( $n = 5$ ; 5.5%), infusion pumps ( $n = 4$ ; 4.4%), light switches ( $n = 4$ ; 4.4%), medication preparation tables ( $n = 2$ ; 2.2%), faucet spouts ( $n = 1$ ; 1.2%), and drawers ( $n = 1$ ; 1.2%). *S. epidermidis* was the most commonly isolated species in the samples from inanimate surfaces (71%) and other CoNS represented 25.8% of the total. On the other hand, *S. aureus* represented 3.2% of the total isolates, being recovered from incubators ( $n = 1$ ; 33.3%), light switches ( $n = 1$ ; 33.3%), and monitor tables ( $n = 1$ ; 33.3%) (Table 2).

**Table 2.** *Staphylococcus* spp isolated from inanimate surfaces, air, and neonatal infection in the Neonatal Intensive Care Unit.

Microorganisms	Samples
<i>Staphylococcus aureus</i>	Inanimate surfaces ( $n = 3$ ) Air ( $n = 2$ ) Neonates ( $n = 14$ )
<i>Staphylococcus epidermidis</i>	Inanimate surfaces ( $n = 66$ ) Air ( $n = 16$ ) Neonates ( $n = 39$ )
<i>Staphylococcus capitis</i>	Inanimate surfaces ( $n = 7$ ) Neonates ( $n = 10$ )
<i>Staphylococcus haemolyticus</i>	Inanimate surfaces ( $n = 6$ ) Neonates ( $n = 3$ )
<i>Staphylococcus warneri</i>	Inanimate surfaces ( $n = 4$ ) Neonates ( $n = 1$ )
<i>Staphylococcus xylosum</i>	Inanimate surfaces ( $n = 4$ ) Neonates ( $n = 1$ )
<i>Staphylococcus hominis</i>	Inanimate surfaces ( $n = 3$ ) Neonates ( $n = 2$ )

### 3.3. Clinical Samples

Between January and December 2018, 284 newborns were admitted to the NICU. Of these, 48 (16.9%) had *Staphylococcus* spp. infection. In 34 (70.8%) of the newborns, the isolation occurred from the bloodstream, in 10 (20.8%) from ocular secretions, and in four (8.4%) patients, *Staphylococcus* spp. were isolated from both sites. A total of sixteen (33.3%) newborns had mixed infection with the isolation of different species of *Staphylococcus* from the same site. In total, 70 isolates were recovered; however, the majority ( $n = 53$ ; 75.7%) were from the bloodstream, followed by ocular secretions ( $n = 17$ ; 24.3%). Of these 70 isolates recovered from clinical samples, 39 (55.7%) were *S. epidermidis*, 17 (24.3%) other CoNS, and 14 (20%) *S. aureus*.

### 3.4. Multidrug Resistance

Of the 181 isolates (environmental and clinical), 132 (72.9%) were MRS, (including seven MRSA), with 48.5% from inanimate surfaces, 10.6% from the air, and 40.9% from

clinical isolates. Erythromycin and clindamycin resistance was seen in 56.4% (102/181) and 54.1% (98/181) of the isolates, respectively. Resistance to erythromycin and clindamycin were more frequent in MRS compared to methicillin-susceptible *Staphylococcus* (MSS) (E-R: 59.1% vs. 49.1% and Clin-R: 62.9% vs. 30.6%). Erythromycin susceptibility and clindamycin resistance was detected in 34 MRS isolates. The overall prevalence of iMLSB, cMLSB and MS phenotypes was 12.7% (23/181), 35.4% (64/181), and 8.3% (15/181), respectively. Both iMLSB and cMLSB phenotypes predominated in MRS strains ( $p$ -value = 0.002) (Table 3).

**Table 3.** Clindamycin susceptibility patterns among MRS and MSS.

		MRS (%) N = 132	MSS (%) N = 49	Total (%) N = 181
E-S (n = 79)	E-S, CL-S	20 (15.2)	25 (51.0)	45 (24.9)
	E-S, CL-R	34 (25.8)	x	34 (18.8)
E-R (n = 102)	E-R, CL-S (iMLSB)	19 (14.4)	4 (8.2)	23 (12.7)
	E-R, CL-R (cMLSB)	49 (37.1)	15 (30.6)	64 (35.4)
	E-R, CL-S (MS Phenotype)	10 (7.6)	5 (10.2)	15 (8.3)

S: susceptible.

A total of twenty-nine (60.4%) neonates presented infection with *Staphylococcus* spp., with a resistance profile identical to that of some environmental isolates, 11 (30.5%) from baby incubators, eight (22.2%) from the air, seven (19.4%) from monitor tables, four (11.1%) from respirator monitors, one (2.8%) from a vital sign monitor, one (2.8%) from a switch, one (2.8%) from a paper towel holder, and one (2.8%) from a cabinet drawer. In three of these neonates (10.3%), there was more than one episode of infection, totaling 36 MRS clinical isolates with a profile identical to that presented by isolates from the environment, 29 (54.7%) coming from the bloodstream and six (35.3%) from eye discharge. Figure 1 shows the design of the unit with the layout of the beds (23 to 42) and the environmental and clinical isolates that presented an identical resistance profile.

### 3.5. Risk Factors

Independent risk factors for the occurrence of *Staphylococcus* spp. infection were the use of antimicrobials prior to infection (RR = 6.68;  $p$  = 0.0045), use of more than three antimicrobials (RR = 4.01;  $p$  = 0.0024), and hospital stay length (RR = 1.03;  $p$  = 0.0013). Mortality was twice as high (RR = 2.24;  $p$  = 0.0490) in neonates infected by *Staphylococcus* spp. as in un-infected neonates (Table 4).

**Table 4.** Clinical characteristics and evolution of neonates admitted to the Neonatal Intensive Care Unit.

Characteristics	<i>Staphylococcus</i> Infection N = 48		Without Infection N = 196		Univariate Analysis		Multivariate Analysis	
	N	%	N	%	RR (IC <sub>95%</sub> )	p	RR (IC <sub>95%</sub> )	p
Weight (g)								
<750	14	29.2	12	6.1	-	-	-	-
751–1000	5	10.4	8	4.1	0.54 (0.14–2.08)	0.3675	-	-
1001–1500	11	22.9	36	18.4	0.26 (0.09–0.73)	0.0104	-	-
1501–2500	11	22.9	86	43.9	0.11 (0.04–0.30)	0.0000	-	-
>2500	7	14.6	54	27.5	0.11 (0.04–0.33)	0.0001	-	-
Gestational Age (weeks)								
<34	33	68.8	91	46.4	-	-	-	-
34 a 37	5	10.4	58	29.6	0.24 (0.09–0.64)	0.0047	-	-
>37	10	20.8	47	24.0	0.59 (0.27–1.29)	0.1860	-	-
Use of drain	4	8.3	13	6.6	1.28 (0.40–4.11)	0.6790	-	-
Use of bladder catheter	10	20.8	15	7.7	3.18 (1.33–7.60)	0.0095 *	-	-



▲: *S. epidermidis* (clinical samples); ●: *S. epidermidis* (environment); ▲: *S. epidermidis* (clinical samples). Resistance: Green:  $\beta$ -lactams, CLI, GEN, SUT, ERI; Red:  $\beta$ -lactams, GEN, SUT, ERI; Blue:  $\beta$ -lactams, CLI, GEN, SUT, ERI; Yellow:  $\beta$ -lactams, ERI; Black:  $\beta$ -lactams, GEN, SUT; Grey:  $\beta$ -lactams, CLI, GEN, SUT; Pink:  $\beta$ -lactams, CLI, ERI; Orange:  $\beta$ -lactams, GEN, ERI;  $\beta$ -lactams Penicillin, Oxacillin and Cefoxitin; CLI: Clindamycin; GEN: Gentamicin; SUT: Sulfazotrim; ERY: Erythromycin.

#### 4. Discussion

This study investigated MDR *Staphylococcus* spp. on inanimate surfaces and environmental air in the NICU of a tertiary hospital and the risk factors for the occurrence of infections in critically ill neonates. This is an important way to evaluate the efficiency of surface cleaning and its impact on HAI, because simple measures, such as the correct sanitization of the environment and health care personnel hand washing, have a significant impact on the reduction of neonatal morbidity and mortality, bearing in mind that the environment is a reservoir of microorganisms that can be transmitted to neonates via the hands and invasive devices [3].

Previous studies conducted in the intensive care unit (ICU) of a Scottish hospital that accounted for CFU of inanimate surfaces showed that, of the 500 “high-touch” surfaces analyzed, 414 (82.8%) showed a count of  $>1$  CFU/cm<sup>2</sup>, with a hygiene failure rate of 47% [7]. This discrepancy in percentages can be explained by the difference in collection techniques, as Smith and collaborators [7] used double-sided dip slides coated with selective nutrient agar, as well as different methods of cleaning and disinfecting the ICU, which is performed twice a day with detergent and sodium hypochlorite solution.

The CFU count of the air samples showed a 100% hygiene failure rate. It is noteworthy that the unit’s ventilation system is central and does not have EPA (high efficiency particulate air) filters. At all times when the air was sampled, the unit was 100% occupied. Active air sampling was performed; however, the movements were not recorded. Increased people-traffic and a positive correlation with active air sampling at higher bed occupancy levels is also unsurprising [27]. These results are worrying, because the air conditioning system at the NICU is central, and there are many invasive procedures, performed in the unit, such as bladder catheterization, CVC insertion, PICC, and umbilical venous catheterization. In addition, extremely premature newborns are admitted to the unit, who have immature immune systems, favoring infections by environmental microorganisms. Therefore, it is recommended that the unit’s environment be as clean as possible to minimize contamination by pathogenic microorganisms.

This failure rate of air cleaning is higher than that found by Adams and Dancer [17], who evaluated the contamination of a hospital environment that used mechanically ventilated air, with 10 air changes per hour, and constant temperature, and humidity. In their study, half of the exposed plates produced counts of  $>1$  CFU/plate and the hygiene failure rate was 50%. These results confirm that air sampling can be used as a routine monitoring strategy for these units.

MDR microorganisms in the hospital environment are a public health problem, especially in critical patient units, because infections caused by these microorganisms usually have limited therapeutic options, and are associated with treatment failures and higher rates of morbidity and mortality [28]. In our study, more than half of the isolates were MDR, as has been observed in other studies carried out in Brazil, Colombia, and Kuwait. Those studies reported MDR *S. epidermidis* on “high-touch” surfaces, in NICU environmental air, and in clinical samples (52.7%, 33.9%, and 61.8%, respectively) [28–30]. Our study revealed the presence of *S. epidermidis* MDR in much higher percentages (81%), 72.7% of inanimate surfaces, 68.8% of air, and 100% of clinical isolates, which alerts us to the need for urgent measures to minimize the risk of proliferation of these microorganisms in the NICU.

Neonates with MDR infection stayed for longer in the NICU (average 50.6 days) and are more likely to die (25.0%) than those infected with non-MDR bacteria (36.8 days and 20.0%, respectively). In addition, MDR isolates from the bloodstream and ocular secretion (54.7% and 35.3%, respectively) presented a resistance profile identical to those recovered



from environmental samples. These findings reinforce the importance of the rational use of antimicrobials and the appropriate and efficient cleaning of the environment to reduce the persistence and spread of MDR microorganisms.

According to our study, previous antibiotic therapy, use of more than three antimicrobials, and the mean hospital stay were considered independent risk factors for the occurrence of *Staphylococcus* spp. infection. Similar findings have been reported by researchers from other countries, such as Japan and China [31–34].

The previous use of antimicrobials, usually broad-spectrum, increases hospital costs and drives the emergence of resistant microorganisms, as it exerts a selective pressure in the ICU environment, selecting MDR isolates. It is also associated with death as a consequence of inadequate therapy [35,36]. Thus, we can observe the occurrence of a cycle, as MDR microorganisms from neonatal infections are deposited on surfaces exposed to air or directly by the hands of health professionals. In this way, they can be transmitted to other patients who have risk factors for *Staphylococcus* infections, resulting in increased rates of morbidity and mortality [37]. In this study, mortality was twice as high in neonates infected with *Staphylococcus* spp. compared to those hospitalized in the same period and who did not develop an infection.

There are many variables involved in newborn ICU infection, many of which we address in this study. There are many risk factors, and the microorganisms involved are quite variable. *Staphylococcus* spp. colonize human skin, and spread through the environment, and thus are most commonly involved in infection. The route of infection can be the environment, or the hands of health professionals; however, the true involvement of these routes of infection needs to be deeply investigated in order for consistent conclusions to be drawn. CoNS were isolated concomitantly from environmental samples and neonatal infections, including *S. capitis*, *S. haemolyticus*, *S. warneri*, *S. xylosus*, and *S. hominis*, emphasizing the importance of the environment as an infection route that can also worsen clinical outcomes. Our results can be improved with the use of molecular analysis to assess the genetic similarity between isolates from the environment and infections cases, so that cases where this shows an identical resistance profile and the presence of resistance genes that are prevalent in the NICU can be identified. However, our results demonstrate the importance of the environment as a reservoir of MDR isolates, data which are scarce in the literature. Other studies in the future may provide the comparison of isolates from the environment with those isolated from cases of bacteremia, using techniques based on molecular biology or proteomics, and also investigate the occurrence of cross-infection. This will certainly contribute to a better understanding of infection routes and reservoirs of *Staphylococcus* species in the NICU.

## 5. Conclusions

The NICU environment acts as an important reservoir of potentially pathogenic microorganisms, because *Staphylococcus* spp. were recovered from all surveyed sites, with *S. epidermidis* being the most frequent species. In addition, it was found that most isolates were MDR, and the use of antimicrobials prior to infection, the use of more than three antimicrobials, and length of stay in the unit were risk factors for the occurrence of infection.

These findings call attention to the need for both the rational use of antimicrobials in the unit and for the constant and rigorous cleaning of the environment and the hands of professionals before and after handling neonates. This will minimize the chances of contamination and dissemination of MDR isolates in the NICU and, consequently, contribute to reducing infection and morbidity and mortality rates.

**Author Contributions:** Conceptualization, L.d.A.M., F.F.S. and D.V.D.d.B.R.; methodology, L.d.A.M., F.F.S., N.B.S.S., P.G.V.A. and M.A.d.S.B.; validation, R.d.P.M., M.P.A.P., R.d.S.P. and D.V.D.d.B.R.; formal analysis, L.B.d.A., M.P.A.P., R.d.S.P. and D.V.D.d.B.R.; investigation, L.d.A.M., F.F.S., N.B.S.S., P.G.V.A. and M.A.d.S.B.; resources, M.P.A.P., R.d.S.P. and D.V.D.d.B.R.; data curation, L.d.A.M., F.F.S. and D.V.D.d.B.R.; writing—original draft preparation, L.d.A.M. and R.d.P.M.; writing—review and editing, L.d.A.M., R.d.P.M., R.d.S.P. and D.V.D.d.B.R.; visualization, R.d.P.M., L.d.A.M., F.F.S., N.B.S.S.,

P.G.V.A., M.A.d.S.B., L.B.d.A., M.P.A.P., R.d.S.P. and D.V.D.d.B.R.; supervision, M.P.A.P., R.d.S.P. and D.V.D.d.B.R.; funding acquisition, D.V.D.d.B.R. All authors have read and agreed to the published version of the manuscript.

**Funding:** This research was funded by FAPEMIG, grant number APQ-00965-18.

**Institutional Review Board Statement:** The study was conducted according to the guidelines of the Declaration of Helsinki, and approved by the Ethics Committee of Uberlândia Federal University, protocol code 2.173,884.

**Informed Consent Statement:** Informed consent was obtained from all subjects involved in the study.

**Data Availability Statement:** Not applicable.

**Acknowledgments:** To CAPES for the availability of journals and scholarships for master's and scientific initiation. We also thank the Technical School of Health at the Federal University of Uberlândia, and Maria Gabriela Ferreira, Sávnia Gonçalves Oliveira Melo, and Paula Augusta Fogaça Aguiar for their support.

**Conflicts of Interest:** The authors declare no conflict of interest.

## References

- Russotto, V.; Cortegiani, A.; Raineri, S.M.; Giarratano, A. Bacterial contamination of inanimate surfaces and equipment in the intensive care unit. *J. Intensive Care* **2015**, *3*, 54. [CrossRef] [PubMed]
- Costa, D.M.; Johani, K.; Melo, D.S.; Lopes, L.K.O.; Lima, L.K.O.L.; Tipple, A.F.V.; Hu, H.; Vickery, K. Biofilm contamination of high-touched surfaces in intensive care units: Epidemiology and potential impacts. *Lett. Appl. Microbiol.* **2019**, *68*, 269–276. [CrossRef] [PubMed]
- Suleyman, G.; Alangaden, G.; Bordossy, A.C. The role of environmental contamination in the transmission of nosocomial pathogens and healthcare-associated infections. *Curr. Infect. Dis. Rep.* **2018**, *20*, 12. [CrossRef] [PubMed]
- Huslage, K.; Rutala, W.A.; Sickbert-Bennett, E.; Weber, D.J. A quantitative approach to defining “high-touch” surfaces in hospitals. *Infect. Control Hosp. Epidemiol.* **2010**, *31*, 850–853. Available online: [https://scholar.google.com.br/scholar?hl=pt-BR&as\\_sdt=0%2C5&q=Huslage+K%2C+Rutala+WA%2C+Sickbert-Bennett+E%2C+Weber+DJ.+A+quantitative+approach+to+defining+%E2%80%9Chigh-touch%E2%80%9D+surfaces+in+hospitals.+Infect+Control+Hosp+Epidemiol+2010%3B+31+%288%29%3A+850%E2%80%93853.&btnG=](https://scholar.google.com.br/scholar?hl=pt-BR&as_sdt=0%2C5&q=Huslage+K%2C+Rutala+WA%2C+Sickbert-Bennett+E%2C+Weber+DJ.+A+quantitative+approach+to+defining+%E2%80%9Chigh-touch%E2%80%9D+surfaces+in+hospitals.+Infect+Control+Hosp+Epidemiol+2010%3B+31+%288%29%3A+850%E2%80%93853.&btnG=) (accessed on 10 October 2020). [CrossRef] [PubMed]
- Dancer, S.J. The role of environmental cleaning in the control of hospital-acquired infection. *J. Hosp. Infect.* **2009**, *73*, 378–385. [CrossRef]
- Shams, A.M.; Rose, L.J.; Edwards, J.R.; Cali, S.; Harris, A.D.; Jacob, J.T.; LaFae, A.; Pineles, L.L.; Thom, K.A.; McDonald, L.C.; et al. Assessment of the overall and multidrug-resistant organism bioburden on environmental surfaces in healthcare facilities. *Infect. Control Hosp. Epidemiol.* **2016**, *37*, 1426–1432. [CrossRef]
- Smith, J.; Adams, C.E.; King, M.F.; Noakes, C.J.; Robertson, C.; Dancer, S.J. Is there an association between airborne and surface microbes in the critical care environment? *J. Hosp. Infect.* **2018**, *100*, 123–129. [CrossRef]
- Salgueiro, V.C.; Seixas, M.D.L.; Guimarães, L.C.; Ferreira, D.D.C.; Da Cunha, D.C.; Nouér, S.A.; Dos Santos, K.R.N. High rate of neonates colonized by methicillin-resistant *Staphylococcus* species in an Intensive Care Unit. *J. Infect. Dev. Ctries.* **2019**, *13*, 810–816. [CrossRef]
- Reich, P.J.; Boyle, M.G.; Hogan, P.G.; Johnson, A.J.; Wallace, M.A.; Elward, A.M.; Warner, B.B.; Burnham, C.-A.D.; Fritz, S.A. Emergence of community-associated methicillin-resistant *Staphylococcus aureus* strains in the neonatal intensive care unit: An infection prevention and patient safety challenge. *Clin. Microbiol. Infect.* **2016**, *22*, 645–648. [CrossRef]
- Jamal, M.; Ahmad, W.; Andleeb, S.; Jalil, F.; Imran, M.; Nawaz, M.A.; Hussain, T.; Ali, M.; Rafiq, M.; Kamil, M.A. Bacterial biofilm and associated infections. *J. Chin. Med. Assoc.* **2018**, *81*, 7–11. [CrossRef]
- Mohsen, L.; Ramy, N.; Saied, D.; Akmal, D.; Salama, N.; Haleim, M.M.A.; Aly, H. Emerging antimicrobial resistance in early and late-onset neonatal sepsis. *Antimicrob. Resist. Infect. Control* **2017**, *6*, 63. [CrossRef] [PubMed]
- Polin, R.A.; Denson, S.; Brady, M.T.; Papile, L.-A.; Baley, J.E.; Carlo, W.A.; Cummings, J.J.; Kumar, P.; Tan, R.C.; Watterberg, K.L.; et al. Epidemiology and diagnosis of health care-associated infections in the NICU. *Pediatrics* **2012**, *129*, e1104–e1109. [CrossRef] [PubMed]
- Brito, D.V.; Brito, C.S.; Resende, D.S.; Moreira, Ó.J.; Abdallah, V.O.; Gontijo Filho, P.P. Nosocomial infections in a Brazilian neonatal intensive care unit: A 4-year surveillance study. *Rev. Soc. Bras. Med. Trop.* **2010**, *43*, 633–637. [CrossRef] [PubMed]
- Marra, A.R.; Camargo, L.F.A.; Pignatari, A.C.C.; Sukiennik, T.; Behar, P.R.P.; Medeiros, E.A.S.; Ribeiro, J.; Girão, E.; Correa, L.; Guerra, C.; et al. Nosocomial bloodstream infections in Brazilian hospitals: Analysis of 2563 cases from a prospective nationwide surveillance study. *J. Clin. Microbiol.* **2011**, *49*, 1866–1871. [CrossRef]
- Chen, Y.-C.; Lin, C.-F.; Rehn, Y.-J.F.; Chen, J.-C.; Chen, P.-Y.; Chen, C.-H.; Wang, T.-M.; Huang, F.-L. Reduced nosocomial infection rate in a neonatal intensive care unit during a 4-year surveillance period. *J. Chin. Med. Assoc.* **2017**, *80*, 427–431. [CrossRef]

16. O'Reilly, D.; O'Connor, C.; McCallion, N.; Drew, R.J. A retrospective study (2001–2017) of acute and chronic morbidity and mortality associated with *Staphylococcus aureus* bacteraemia in a tertiary neonatal intensive care unit. *Ir. J. Med. Sci.* **2019**, *188*, 1297–1301. [CrossRef]
17. Adams, C.E.; Dancer, S.J. Dynamic transmission of *Staphylococcus aureus* in the intensive care unit. *Int. J. Environ. Res. Public Health* **2020**, *17*, 2109. [CrossRef]
18. Dancer, S.J. Controlling hospital-acquired infection: Focus on the role of the environment and new technologies for decontamination. *Clin. Microbiol. Rev.* **2014**, *27*, 665–690. [CrossRef]
19. Pasquarella, C.; Pitzurra, O.; Savino, A. The index of microbial air contamination. *J. Hosp. Infect.* **2000**, *46*, 241–256. [CrossRef]
20. Dudeck, M.A.; Horan, T.C.; Peterson, K.D.; Allen-Bridson, K.; Morrell, G.; Anttila, A.; Pollock, D.A.; Edwards, J.R. National Healthcare Safety Network report, data summary for 2011, device-associated module. *Am. J. Infect. Control* **2013**, *41*, 286–300. [CrossRef]
21. Barnes, S.; Olmsted, R.N.; Monsees, E. *Guide to Preventing Central Line-Associated Bloodstream Infections*; Association for Professionals in Infection Control and Epidemiology (APIC): Washington, DC, USA, 2015. Available online: [http://apic.org/Resource\\_/TinyMceFileManager/2015/APIC\\_CLABSI\\_WEB.pdf](http://apic.org/Resource_/TinyMceFileManager/2015/APIC_CLABSI_WEB.pdf) (accessed on 10 October 2020).
22. Kassim, A.; Pflüger, V.; Premji, Z.; Daubenberger, C.; Revathi, G. Comparison of biomarker based Matrix Assisted Laser Desorption Ionization-Time of Flight Mass Spectrometry (MALDI-TOF MS) and conventional methods in the identification of clinically relevant bacteria and yeast. *BMC Microbiol.* **2017**, *17*, 128. [CrossRef] [PubMed]
23. Clinical and Laboratory Standards Institute (CLSI). *Metodologia dos Testes de Sensibilidade a Agentes Antimicrobianos por Diluição para Bactéria de Crescimento Aeróbico*; Norma Aprovada—Sexta Edição; CLSI: Wayne, PA, USA, 2012; Volume 23. Available online: [http://www.anvisa.gov.br/servicosauade/manuais/clsi/clsi\\_opasm7\\_a6.pdf](http://www.anvisa.gov.br/servicosauade/manuais/clsi/clsi_opasm7_a6.pdf) (accessed on 10 October 2020).
24. Clinical and Laboratory Standards Institute (CLSI). *Performance Standards for Antimicrobial Susceptibility Testing*, 28th ed.; CLSI: Wayne, PA, USA, 2018. Available online: [https://clsi.org/media/1930/m100ed28\\_sample.pdf](https://clsi.org/media/1930/m100ed28_sample.pdf) (accessed on 10 October 2020).
25. Magiorakos, A.-P.; Srinivasan, A.; Carey, R.B.; Carmeli, Y.; Falagas, M.E.; Giske, C.G.; Harbarth, S.; Hindler, J.F.; Kahlmeter, G.; Olsson-Liljequist, B.; et al. Multidrug-resistant, extensively drug-resistant and pandrug-resistant bacteria: An international expert proposal for interim standard definitions for acquired resistance. *Clin. Microbiol. Infect.* **2012**, *18*, 268–281. [CrossRef] [PubMed]
26. Hosmer, D.W.; Lemeshow, S. *Applied Logistic Regression*, 2nd ed.; John Wiley & Sons: New York, NY, USA, 2004; p. 392. Available online: [http://resource.heartonline.cn/20150528/1\\_3kOQSTg.pdf](http://resource.heartonline.cn/20150528/1_3kOQSTg.pdf) (accessed on 10 October 2020).
27. Hiwar, W.; King, M.; Shuweihi, F.; Fletcher, L.A.; Dancer, S.J.; Noakes, C.J. What is the relationship between indoor air quality parameters and airborne microorganisms in hospital environments? A systematic review and meta-analysis. *Indoor Air* **2021**, *31*, 1308–1322. [CrossRef] [PubMed]
28. Rodrigues, D.O.; da Paixao Peixoto, L.; Mourao Barros, E.T.; Guimarães, J.R.; Gontijo, B.C.; Almeida, J.L.; Guimaraes de Azevedo, L.; Oliveira e Lima, J.C.; Camara, D.S. Epidemiology of bacterial contamination of inert hospital surfaces and equipment in critical and non-critical care units: A Brazilian multicenter study. *Microbiol. Res. J. Int.* **2019**, *13*, 1–25. [CrossRef]
29. Morgado-Gamero, W.B.; Hernandez, M.M.; Ramirez, M.C.; Medina-Altahona, J.; De La Hoz, S.; Mendoza, H.P.; Parody, A.; Teixeira, E.C.; Agudelo-Castañeda, D.M. Antibiotic resistance of airborne viable bacteria and size distribution in neonatal intensive care units. *Int. J. Environ. Res. Public Health* **2019**, *16*, 3340. [CrossRef]
30. Al-Haqan, A.; Boswihi, S.S.; Pathan, S.; Udo, E.E. Antimicrobial resistance and virulence determinants in coagulase-negative *Staphylococci* isolated mainly from preterm neonates. *PLoS ONE* **2020**, *15*, e0236713. [CrossRef]
31. Shirai, Y.; Arai, H.; Tamaki, K.; Konishi, H.; Kawase, Y.; Shimizu, N.; Tateda, K.; Yoda, H. Neonatal methicillin-resistant *Staphylococcus aureus* colonization and infection. *J. Neonatal. Perinatal. Med.* **2017**, *10*, 439–444. [CrossRef]
32. Zhang, L. Meta analysis on related risk factors of nosocomial infection for premature infants with critical illness. *Nurs. Rehabil. J.* **2016**, *15*, 819–823. Available online: <http://www.zjhlykf.com/ch/index.aspx> (accessed on 10 October 2020).
33. Wang, L.; Du, K.-N.; Zhao, Y.-L.; Yu, Y.-J.; Sun, L.; Jiang, H.-B. Risk factors of nosocomial infection for infants in neonatal intensive care units: A systematic review and meta-analysis. *Med. Sci. Monit.* **2019**, *25*, 8213. [CrossRef]
34. Li, X.; Ding, X.; Shi, P.; Zhu, Y.; Huang, Y.; Li, Q.; Lu, J.; Li, Z.; Zhu, L. Clinical features and antimicrobial susceptibility profiles of culture-proven neonatal sepsis in a tertiary children's hospital, 2013 to 2017. *Medicine* **2019**, *98*, e14686. [CrossRef]
35. Bonjean, M.; Hodille, E.; Dumitrescu, O.; Dupieux, C.; Mongo, C.N.; Allam, C.; Beghin, M.; Paris, M.; Borrel, O.; Chardon, H.; et al. Disk diffusion testing for detection of methicillin-resistant *Staphylococci*: Does moxalactam improve upon cefoxitin? *J. Clin. Microbiol.* **2016**, *54*, 2905–2909. [CrossRef] [PubMed]
36. Tziialla, C.; Borghesi, A.; Serra, G.; Stronati, M.; Corsello, G. Antimicrobial therapy in neonatal intensive care unit. *Ital. J. Pediatr.* **2015**, *41*, 27. [CrossRef] [PubMed]
37. Sharma, A.; Kalita, J.M.; Nag, V.L. Screening for methicillin-resistant *Staphylococcus aureus* carriage on the hands of healthcare workers: An assessment for hand hygiene practices. *Indian J. Crit. Care Med.* **2019**, *23*, 590. [CrossRef] [PubMed]

## Impact of alcohol gel on hand bacteria in healthcare professionals

*Impacto del gel de alcohol en las bacterias de las manos en los profesionales sanitarios*

*Impacto do álcool gel nas bactérias das mãos de profissionais de saúde*

<https://doi.org/10.17058/reci.v11i3.16493>

Received: 20/05/2020











Accepted: 18/09/2020

Available online: 20/01/2022

**Corresponding Author:**

Ralciane Menezes  
ralciane@ufu.br

Av. Amazonas s/no - Bloco 4K - 111 - Campus  
UmuaramaUberlândia, Minas Gerais, Brasil.

Gabriel Faria<sup>1</sup> ;  
Ralciane Menezes<sup>1</sup> ;  
Priscila Alves<sup>1</sup> ;  
Lara Marques<sup>1</sup> ;  
Nagela Silva<sup>1</sup> ;  
Meliza Bessa<sup>1</sup> ;  
Felipe Silva<sup>1</sup> ;  
Denise Röder<sup>1</sup> ;  
Reginaldo Pedroso<sup>1</sup> ;  
Mario Penatti<sup>1</sup> 

<sup>1</sup> Universidade Federal de Uberlândia, Minas Gerais, Brasil.

### ABSTRACT

**Background and objectives:** Healthcare-Associated Infections are a problem reported by hospitals worldwide, increasing patient morbidity and mortality, prolonging hospitalization, and increasing health care costs. The hands of health professionals are still the main source of infections, making hand hygiene extremely important for spreading infection control. The objective of this study was to analyze the presence of bacteria on the hands of health professionals after hygiene with alcohol gel in a Neonatal Unit and describe the resistance of microorganisms to antimicrobials.

**Methods:** Hand samples were collected using the modified glove-juice method on both occasions, before and after hand hygiene with alcohol gel. Bacteria were identified by MALDI-TOF and susceptibility tests according to Clinical and Laboratory Standards Institute document M100-E29. **Results:** A total of 214 samples were obtained, of which 104 (48.6%) showed bacterial growth before hand hygiene and 52 (24.3%) after hand hygiene with alcohol gel. There were 217 isolates from the cultures, of which coagulase-negative *Staphylococcus* was the most frequent with 41 (27.2%) and 24 (36.4%) positive cultures, respectively before and after hand hygiene. The second most frequent microorganism was *Klebsiella pneumoniae* with 32 (21.2%) and 16 (24.2%), respectively before and after hand hygiene. Multidrug resistance to antimicrobials was detected in 58.1% of gram-positive bacteria and in 34.3% of gram-negative bacteria.

**Conclusion:** A decrease was observed, but not an elimination of the microbial load after hand hygiene with alcohol gel, demonstrating the need for improvements in hand hygiene.

**Keywords:** Hand Hygiene. Health Personnel. Neonatal Intensive Care Units. Drug Resistance, Microbial.

### RESUMO

**Justificativa e objetivos:** As Infecções Relacionadas à Assistência à Saúde são um problema relatado por hospitais em todo o mundo, aumentando a morbimortalidade dos pacientes, prolongando a hospitalização e aumentando os custos dos cuidados de saúde. As mãos dos profissionais de saúde ainda são a principal fonte de infecções, tor-

nando a higienização das mãos extremamente importante para a disseminação do controle de infecções. O objetivo deste estudo foi analisar a presença de bactérias nas mãos de profissionais de saúde após higienização com álcool gel em uma Unidade Neonatal e descrever a resistência dos microrganismos aos antimicrobianos. **Métodos:** Amostras de mãos foram coletadas pelo método luva-suco modificado em ambas as ocasiões, antes e após a higienização das mãos com álcool gel. As bactérias foram identificadas por MALDI-TOF e testes de suscetibilidade de acordo com o documento M100-E29 do Clinical and Laboratory Standards Institute. **Resultados:** Obteve-se um total de 214 amostras, das quais 104 (48,6%) apresentaram crescimento bacteriano antes da higienização das mãos e 52 (24,3%) após a higienização das mãos com álcool gel. Foram 217 isolados das culturas, sendo *Staphylococcus coagulase-negativo* o mais frequente com 41 (27,2%) e 24 (36,4%) culturas positivas, respectivamente antes e após a higienização das mãos. O segundo microrganismo mais frequente foi *Klebsiella pneumoniae* com 32 (21,2%) e 16 (24,2%), respectivamente antes e após a higienização das mãos. A multirresistência aos antimicrobianos foi detectada em 58,1% das bactérias gram-positivas e em 34,3% das bactérias gram-negativas. **Conclusão:** Observou-se diminuição, mas não eliminação da carga microbiana após higienização das mãos com álcool gel, demonstrando a necessidade de melhorias na higienização das mãos.

**Palavras-chave:** Higiene das Mãos. Pessoal de Saúde. Unidades de Terapia Intensiva Neonatal. Resistência a Medicamentos, Microbiana.

## RESUMEN

**Justificación y objetivos:** Las Infecciones Asociadas a la Atención de la Salud son un problema reportado por los hospitales a nivel mundial, aumentando la morbimortalidad de los pacientes, prolongando la hospitalización y aumentando los costos de la atención médica. Las manos de los profesionales de la salud siguen siendo la principal fuente de infecciones, por lo que la higiene de manos es extremadamente importante para el control de infecciones. El objetivo de este estudio fue analizar la presencia de bacterias en las manos de los profesionales de la salud después de la higiene con alcohol en gel en una Unidad Neonatal y describir la resistencia de los microorganismos a los antimicrobianos. **Métodos:** Se recogieron muestras de manos mediante el método guante-jugo modificado en ambas ocasiones, antes y después de la higiene de manos con alcohol en gel. Las bacterias se identificaron mediante MALDI-TOF y pruebas de susceptibilidad de acuerdo con el documento M100-E29 del Clinical and Laboratory Standards Institute. **Resultados:** Se obtuvieron un total de 214 muestras, de las cuales 104 (48,6%) presentaron crecimiento bacteriano antes de la higiene de manos y 52 (24,3%) después de la higiene de manos con alcohol en gel. Hubo 217 aislamientos de los cultivos, de los cuales el *Staphylococcus coagulasa negativo* fue el más frecuente con 41 (27,2%) y 24 (36,4%) cultivos positivos, respectivamente antes y después de la higiene de manos. El segundo microrganismo más frecuente fue *Klebsiella pneumoniae* con 32 (21,2%) y 16 (24,2%), respectivamente antes y después de la higiene de manos. Se detectó multirresistencia a los antimicrobianos en el 58,1% de las bacterias grampositivas y en el 34,3% de las bacterias gramnegativas. **Conclusión:** Se observó una disminución, pero no una eliminación de la carga microbiana después de la higiene de manos con alcohol en gel, lo que demuestra la necesidad de mejoras en la higiene de manos.

**Palabras clave:** Higiene de manos. Personal sanitario. Unidades de Cuidados Intensivos Neonatales. Farmacorresistencia Microbiana.

## INTRODUCTION

Healthcare-associated Infections (HAI) are responsible for higher morbidity and mortality, longer length of hospital stay and greater health care costs.<sup>1</sup> Reducing HAI rates has become a challenge to be overcome by hospitals worldwide.

Neonatal Intensive Care Units (NICU) have had high HAI rates, especially because babies have different characteristics, with immature immune systems and low birth weight. In addition, in most cases, they depend on parenteral nutrition and often undergo invasive procedures, such as central venous catheters and orotracheal intubation, as well as broad-spectrum antimicrobial therapy.<sup>2,3</sup>

The reduction of the HAI rates is possible through early identification of risk factors, for instance through health surveillance, staff training, antimicrobial therapy

management and especially, correct hand hygiene.<sup>3,4</sup> The hands of healthcare professionals are one of the main vehicles for the transmission of microorganisms between professionals and patients, especially because they are in frequent contact with the potentially contaminated surfaces.<sup>4,5</sup> Furthermore, a premature newborn is handled about 200 times in 24 hours, which increases the risk of infection.<sup>6</sup>

Bacteria present on hands include *Staphylococcus aureus*, *Staphylococcus epidermidis*, *Enterococcus* spp., *Pseudomonas aeruginosa*, *Klebsiella* spp., *Enterobacter* spp., *Pantoea* spp. and yeast belonging to the *Candida* genus. Some of these microorganisms are resistant to antimicrobials. For example, *S. aureus* and *S. epidermidis* were found to be resistant to oxacillin/methicillin, *Enterococcus* to vancomycin and *Enterobacteriaceae* and *P. aeruginosa*, to carbapenems.<sup>1,7</sup>

Conventional hand hygiene (soap and water) is poorly performed among health professionals, especially those working in hospitals.<sup>6,8,9</sup> This is due to a gap in practice, perception and knowledge about the importance of hand hygiene and its impact on the occurrence of HAI. The difficulty in accessing places to perform this procedure or lack thereof, the prolonged time required for hand hygiene, as well as dermatological issues, such as dryness and/or hypersensitivity caused by the substances used in the cleaning process induce many professionals to not adopt the conventional appropriate cleaning processes.<sup>8</sup>

An alternative to conventional hand hygiene is hand hygiene with alcohol hand-rub (at concentration 60-80%, depending on the type of alcohol used),<sup>7,8</sup> which promotes hygiene without loss of effectiveness in removing and/or inactivating microorganisms. The use of this product is indicated when hands are not visibly dirty, it requires less time for hygiene, is easy to obtain and available, and can be arranged on the bedside, with less occurrence of hypersensitivity. Among the many products on the market for hand hygiene, alcohol gel is well accepted by health professionals.<sup>10</sup>

The aim of this study is to analyze the bacteria on the hands of healthcare professionals of a Neonatal Unit before and after using alcohol gel, and evaluate the susceptibility of microorganisms to antimicrobials.

## METHODS

The study was carried out in the Neonatal Unit of the Hospital University of Uberlândia. The Neonatal Unit contains a total of 42 beds, 20 for intensive care, 16 for semi-intensive care and six for intermediate care in the "Kangaroo Care" model.

The Neonatal Unit has a multidisciplinary team composed of approximately 120 professionals who work directly with patients, including nurses, nursing technicians, physicians and physiotherapists.

### Sample Collection

Three hand washing samples were collected during three work shifts (morning, afternoon and night), on three occasions; the first in April, the second in June and the third in September 2018, representing different seasonal periods.

Collections were performed according to the glove-juice modified technique.<sup>11</sup> Briefly, the research participant put both hands at the same time in a polypropylene bag containing 10 mL of BHI broth (*Brain Heart Infusion*, HIMEDIA®, India), bathing them in the broth for one minute. Then, the bag was sealed and the sample identified as "Before". Subsequently, the participant dried his/her hands with a sterile surgical dressing and performed hand hygiene with alcohol gel, according to the institution's protocol. After complete drying of the alcohol, about one minute, a second collection was performed in another bag identified as "After".

The alcohol gel brand was the same as the one available at the Neonatal Unit (Hydrated Alcohol Gel 70%

v/v, Rioquímica®, Brazil).

### Culture and bacterial identification

The samples (BHI in bags) were first incubated in a bacteriological incubator at  $35 \pm 2$  °C for 18-24 hours. Subsequently, aliquots (10 µL) were taken and analyzed by Gram staining, seeded in 5% Sheep Blood Agar (HIMEDIA®, India), Mannitol-Salted Agar (HIMEDIA®, India) and Eosin-Methylene Blue Agar (HIMEDIA®, India), and incubated at  $35 \pm 2$  °C for 18-24 hours. Microorganisms were identified by the analytical technique of mass spectrometry: Matrix Associated Laser Desorption-Ionization - Time of Flight (MALDI-TOF), which separates atoms or molecules according to their mass/charge ratio. MALDI-TOF has been recognized as a fast and reliable tool to identify bacteria, once mass spectra can be viewed as species-specific fingerprints, allowing for accurate identification of purified strains at the genus and species level.<sup>12,13</sup>

### Antimicrobial susceptibility testing

The antibacterial susceptibility profile was determined by agar disk diffusion method, according to Clinical and Laboratory Standards Institute document M100-E29.<sup>14</sup>

Gram-negative bacteria were tested for the following (DME®, Brazil): amikacin (30 µg); amoxicillin and clavulanic acid (20/10 µg); ampicillin and sulbactam (10/10 µg), cefepime (30 µg), cefoxitin (30 µg), ceftriaxone (30 µg), ciprofloxacin (05 µg), gentamycin (10 µg), meropenem (10 µg), piperacillin and tazobactam (100/10 µg), sulfazotrim (25 µg), ceftazidime (30 µg), aztreonam (30 µg). Susceptibility of *Acinetobacter baumannii* and *Stenotrophomonas maltophilia* to antimicrobials was assessed by the Minimum Inhibitory Concentration (MIC), as recommended by CLSI.<sup>14</sup>

Gram-positive bacteria (DME®, Brazil) were tested for the following: tetracycline (30 µg), ciprofloxacin (05 µg), chloramphenicol (30 µg), erythromycin (15 µg), clindamycin (02 µg), penicillin (10 µg), gentamycin (10 µg); sulfazotrim (25 µg), cefoxitin (30 µg) (also checking resistance to oxacillin), and vancomycin (30 µg) (only for *Enterococcus* spp.).

Microorganisms resistant to three or more classes of the tested antimicrobials were considered Multi-drug-Resistant (MDR).<sup>15</sup>

### Statistical analyses

Results were tabulated and expressed as relative and absolute frequencies. McNemar's test was performed to assess the effect of alcohol on hand bacteria. The level of statistical significance was set at  $P < 0.05$ . The IBM SPSS Statistics for Windows, version 21.0 was used.

### Study ethics

This study was approved by the Research Ethics Committee of the Federal University of Uberlândia, under no. CAAE 82191417.6.0000.5152. This research was conducted according to ethical standards required by Resolutions 466/2012 - 510/2016 - 580/2018 of the Brazilian Ministry of Health.

**RESULTS**

A total of 214 samples were collected, comprising before and after hand hygiene, with 48.6% (n = 104) displaying bacterial growth before hand hygiene with alcohol gel, decreasing to 24.3% after hand hygiene with alcohol gel. Table 1 displays the results in each

collection period.

The study identified 217 microorganisms; 151 in the “Before” samples, and 66 in the “After” samples, as exhibited in Figures 1 and 2, respectively. Coagulase negative *Staphylococcus* (CoNS) was the most frequent, followed by *Klebsiella pneumoniae*.

**Table 1.** Results of the microbiological analyses of health professional hands from the Neonatal Unit, before and after hand hygiene with alcohol gel, by collection period.

Year	Professionals n	Positive cultures for bacteria				Reduction after Hand Hygiene (%)	P value
		Before*		After**			
		n	%	n	%		
First Collection (April)	80	37	46.2	20	25	45.9	< 0.001
Second Collection (June)	63	37	58.7	20	31.7	45.9	< 0.001
Third Collection (September)	71	30	42.3	12	16.9	60	< 0.001
TOTAL	107	104	48.6	52	24.3	50	< 0.001

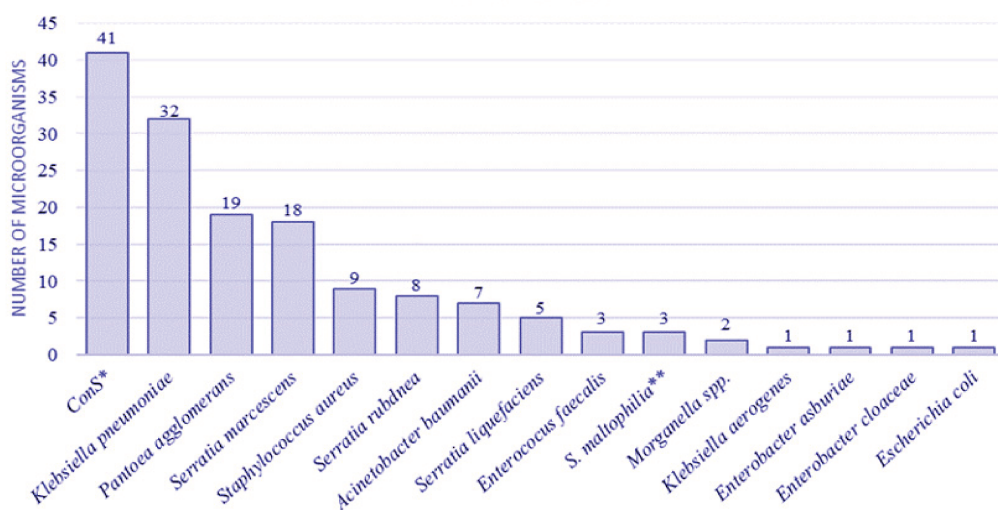


**Figure 1.** Frequency of microorganisms isolated from healthcare professional hands before hand hygiene in the studied Neonatal Unit. (Note: \*= coagulase-negative Staphylococcus; \*\*= Stenotrophomonas maltophilia).

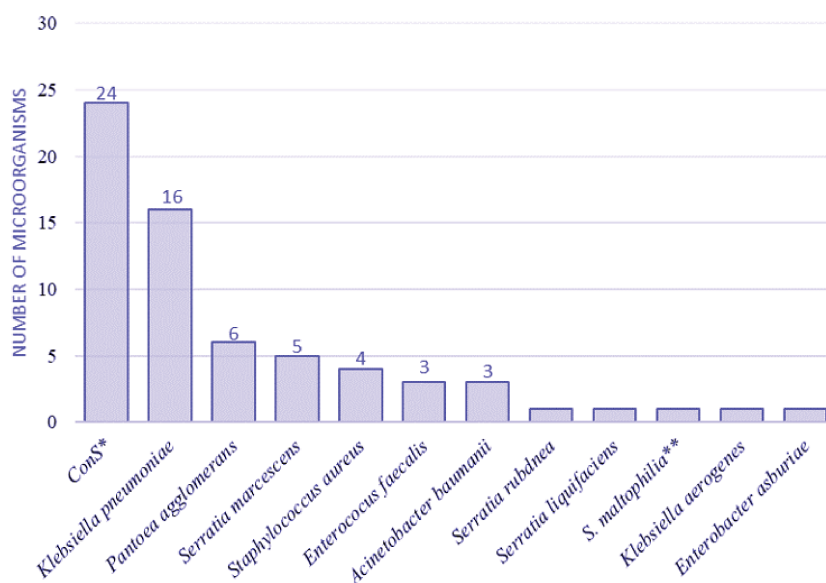


**Figure 2.** Frequency of microorganisms isolated from healthcare professional hands after hand hygiene in the studied Neonatal Unit (Note: \*= coagulase-negative Staphylococcus; \*\*= Stenotrophomonas maltophilia).

Tables 2 and 3 show the results obtained in the antimicrobial susceptibility testing of isolates after alcohol gel hygiene. In total, 18 (58.1%) gram-positive bacteria and 12 (34.3%) gram-negative bacteria were MDR. Furthermore, four (50%) of *Staphylococcus aureus* were

MRSA (Methicillin-resistant *Staphylococcus aureus*).

Only one *A. baumannii* isolate was resistant to ampicillin and sulbactam, while one *S. maltophilia* was resistant only to ceftazidime, and one *Enterococcus* spp. to vancomycin.

**Table 2.** Antimicrobial resistance of gram-positive bacteria isolated from healthcare professional hands after hand hygiene in the studied Neonatal Unit.

Antimicrobial	Genus / Species					
	CoNS (n=24)		<i>Staphylococcus aureus</i> (n=4)		<i>Enterococcus faecalis</i> (n=3)	
	n	%	n	%	n	%
Ciprofloxacin	5	20.8	0	0.0	3	100.0
Clindamycin	7	29.2	2	50.0	*	*
Chloramphenicol	8	33.3	2	50.0	0	0.0
Erythromycin	12	50.0	3	75.0	3	100.0
Gentamicin	8	33.3	2	50.0	*	*
Oxacillin	9	37.5	2	50.0	*	*
Penicillin	21	87.5	3	75.0	0	0.0
Sulfazotrim	8	33.3	4	100.0	*	*
Tetracycline	7	29.2	3	75.0	1	33.3
MDR	14	58.3	3	75.0	1	33.3

MDR= Multidrug Resistant; CoNS= coagulase negative *Staphylococcus*; \*= cutoff points not defined by CLSI for bacterial species / genus. Oxacillin resistance determined by resistance to Cefoxitin.

**Table 3.** Antimicrobial resistance of gram-negative bacteria isolated from healthcare professional hands after hand hygiene in the studied Neonatal Unit.

Antimicrobial	Genus / Species							
	<i>P. agglomerans</i> (n=6)		<i>K. pneumoniae</i> (n=16)		<i>Serratia</i> spp. (n=7)		Other (n=2)	
	n	%	n	%	n	%	n	%
Amikacin	2	33.3	1	6.3	1	14.3	0	0.0
Amox/Clav Ac.	4	66.7	5	31.3	4	57.1	2	100.0
Amp/Sulbactam	2	33.3	3	18.8	2	28.6	2	100.0
Aztreonam	3	50.0	1	6.3	1	14.3	0	0.0
Cefepime	4	66.7	1	6.3	1	14.3	0	0.0
Cefoxitin	6	100.0	15	93.8	7	100.0	2	100.0
Ceftazidime	3	50.0	1	6.3	0	0.0	0	0.0
Ceftriaxone	3	50.0	2	12.5	2	28.6	0	0.0
Ciprofloxacin	3	50.0	3	18.8	1	14.3	1	50.0
Gentamicin	3	50.0	0	0.0	1	14.3	0	0.0
Meropenem	2	33.3	1	6.3	0	0.0	0	0.0
Pipe/Tazo	0	0.0	1	6.3	0	0.0	1	50.0
Sulfazotrim	1	16.7	1	6.3	1	14.3	0	0.0
MDR	5	83.3	2	12.5	3	42.9	2	100.0

Amox/Clav Ac= Amoxicillin and Clavulanic Acid; Amp/Sulbactam = Ampicillin and Sulbactam; Pipe/Tazo = Piperacillin and Tazobactam; MDR = Multidrug Resistant; Others = *Klebsiella aerogenes* (1) and *Enterobacter asburiae* (1) *P. agglomerans* = *Pantoea agglomerans*; *K. pneumoniae* = *Klebsiella pneumoniae*

## DISCUSSION

The Centers for Disease Control and Prevention (CDC) have recognized the importance of hand hygiene in reducing HAI rates since 1974.<sup>9</sup> Studies indicate that this practice is still underestimated by healthcare professionals worldwide, with adoption rates ranging from 30% to 60%.<sup>8,9</sup>

Studies assessing the presence of microorganisms on healthcare professionals' hands during their work shifts have reported different results. In India,<sup>16</sup> 42.7%

of healthcare professionals' hands displayed bacterial growth, while in Italy,<sup>17</sup> only 5.41% healthcare professionals' hands showed positive culture for bacteria. In another study<sup>18</sup> was demonstrated that the hands of 97% of professionals in the United States exhibited bacterial growth. In Greece,<sup>19</sup> all professionals participating in the study displayed contaminated hands. These differences found in results of many studies may be due to the sample collection method (fingerprint, glove-juice or contact



plates), and especially, what each author considers as a positive sample. Herein, in our study all bacterial growth was considered positive, since premature newborns are extremely vulnerable to infections.<sup>20</sup>

In the present study, professionals were asked to clean their hands with alcohol gel to check for reduction of microbial load on hands after the hygiene process. The results indicate that 48.6% of professionals still had their hands contaminated to some degree with bacteria. Coagulase-negative *Staphylococcus* were the most frequent isolates, as described in the literature.<sup>19,20</sup> These microorganisms compose the skin microbiome, but are also opportunistic agents of infection in neonates, as demonstrated by Sanderson et al., in which 71% of cases of bloodstream infection in neonates were caused by CoNS.<sup>21</sup> In a study reporting the incidence of nosocomial infections in the same Neonatal Unit of this study, CoNS and *Staphylococcus aureus* were the most frequently causative agents of infections in neonates, representing 36.5% and 23.6% of total infections, respectively.<sup>22</sup>

Gram-negative bacteria are less common on hands compared to gram-positive cocci, but they are important infection agents in neonates. In the present study, *Klebsiella pneumoniae* was the most common gram-negative bacteria. Chen and colleagues reported *Klebsiella pneumoniae* as responsible for 16% of neonatal infections, followed by *Staphylococcus aureus* (12.3%).<sup>3</sup> In Egypt, the most frequent microorganism was also *Klebsiella pneumoniae*, present in 41.6% of infections, followed by CoNS, present in 22.8% of cases.<sup>23</sup>

A total of 24.3% of the samples from professional hands analyzed after hand hygiene with alcohol gel did not show any reduction in microbial load. Studies evaluating alcoholic preparations (gel, foam, liquid) demonstrate effectiveness in reducing microbial loads by up to 99.9%.<sup>8,24</sup>

In a study conducted in India, 35% of healthcare professionals displayed bacterial growth on their hands, becoming non-detected after hygiene with alcohol-based hand rub.<sup>25</sup> Similar results were reported in another study in which only 5% of hands showed bacterial growth after hand hygiene with alcohol-based handrub.<sup>26,27</sup>

The discrepancies between the literature and the present study may be related to the fact that in studies evaluating the effectiveness of alcoholic preparations, participants were trained so everyone could perform the proper hand hygiene technique. The effectiveness of these preparations has been proven under these conditions.<sup>25</sup> In this study, participants were instructed to perform hand hygiene with alcohol gel as usual, thus evidencing a possible deficiency in the way they usually perform hand hygiene, since part of participants (24.3%) exhibited bacterial growth after the hand hygiene procedure.

Concerning MDR bacteria, 58.1% of gram-positive bacteria and 34.3% of gram-negative bacteria were considered as multidrug-resistant in this study, while 50% of isolated *Staphylococcus aureus* were MRSA. Several studies have demonstrated that MDR bacteria are found on the hands of healthcare professionals, including MRSA,

ranging from 1.3% to 1.6%. However, when evaluating only *Staphylococcus* spp., in general, 39% are categorized as MDR. Regarding gram-negative bacteria, frequencies range between 3.2% to 56% concerning the presence of MDR on health professionals' hands.<sup>16,17,19</sup> For example, in China, 7.3% of positive samples were reported when assessing the presence of gram-negative bacilli from the hands of health professionals in an intensive care unit, among which *Klebsiella pneumoniae* was the most common, and 50% were MDR.<sup>4</sup>

Working in Intensive Care Units increases the risk of carrying potential microorganisms that cause HAIs in neonates, including MDR.<sup>22</sup> Concerning NICUs, hand hygiene habits become extremely important, as most patients are premature and extremely vulnerable to infections, remain in the hospital for long periods and receive various essential life-sustaining procedures.<sup>20</sup>

The presence of bacteria on hands before hand hygiene indicates which pathogens may be spreading in the unit, and a key point is noted after hygiene, since hands should be cleaned before contact with any medical devices and patients, providing safe care according to World Health Organization guidelines. Successful hand hygiene must take into account two factors, namely the quality of the product used in the process and quality/effectiveness of the performed hygiene.<sup>10</sup>

This study has limitations, including the technique used for collection ("modified glove-juice"), as well as hand drying with towels, which may have reduced the microbial load on hands. In addition, the non-evaluation of the hand hygiene technique performed by the assessed professionals was to ensure that professionals whose samples tested positive after the hygiene procedure resulted from inadequate technique, amount of product or even insufficient hygiene time, which may be evaluated in future studies.

The persistence of these bacteria even after hand hygiene seems to demonstrate a failure in the hygiene process, either due to the applied methodology or the alcohol gel time of action. The most frequent microorganisms found before and after hand hygiene, were Coagulase Negative *Staphylococcus*, *Klebsiella pneumoniae* and *Pantoea agglomerans*. Multidrug resistance to antimicrobials was evaluated, revealing that most of gram-positive (58.1%) and many gram-negative (34.3%) bacteria are multidrug-resistant.

This study revealed the need for improvements concerning the hand hygiene process performed by healthcare professionals in the studied unit in order to reduce the microbial load on hands. Further studies may be conducted in an attempt to better determine the most important variables involved in this process, such as the alcohol gel amount, hygiene process and product efficiency (alcohol content, composition and gel alcohol presentation, among others). Thus, efforts are required to improve both hygiene adherence and quality, which can be demonstrated and proven by epidemiological studies involving *in vitro* experiments.

## ACKNOWLEDGEMENTS

The authors are grateful to the Technical Course in Clinical Analysis of the Technical School of Health - UFU for providing the material and allowing the use of the microbiology laboratory to carry out this study. Thanks are also due to the Neonatal HC-UFU Unit, especially Dr. Daniela Marques de Lima Mota Ferreira and Nurse Walska Cristina Gomes da Silva, to *Conselho Nacional de Desenvolvimento Científico e Tecnológico* (CNPq) and to *Fundação de Amparo à Pesquisa do Estado de Minas Gerais* (FAPEMIG) for financial support (grant number APQ-00965-18). In addition, thanks are also due to Com. Dr<sup>a</sup> Ana Lúcia Ribeiro Gonçalves for her assistance in the statistical analysis, and a special thanks is in order for Dr. Paula Augusta Dias Fogaça Aguiar for her assistance in carrying out bacterial identifications by MALDI-TOF analyses.

## REFERENCES

- Tajeddin E, Rashidan M, Razaghi M, et al. The role of the intensive care unit environment and health-care workers in the transmission of bacteria associated with hospital acquired infections. *J Infect Public Health*. 2016; 9:13-23. doi: 10.1016/j.jiph.2015.05.010
- Bowen JR, Callander I, Richards R, et al. Decreasing infection in neonatal intensive care units through quality improvement. *Arch Dis Child Fetal Neonatal Ed*. 2017; 102: F51-F57. doi: 10.1136/archdischild-2015-310165
- Chen YC, Lin CF, Rehn YF, et al. Reduced nosocomial infection rate in a neonatal intensive care unit during a 4-year surveillance period. *J Chin Med Assoc*. 2017; 80: 427-31. doi: 10.1016/j.jcma.2017.02.006
- Wang HP, Zhang HJ, Liu J, et al. Antimicrobial resistance of 3 types of gram-negative bacteria isolated from hospital surfaces and the hands of health care workers. *Am J Infect Control*. 2017; 45: e143-7. doi: 10.1016/j.ajic.2017.06.002
- Wolfensberger A, Clack L, Kuster SP, et al. Transfer of pathogens to and from patients, healthcare providers, and medical devices during care activity—a systematic review and meta-analysis. *Infect. Control Hosp. Epidemiol*. 2018; 39:1093-107. doi: 10.1017/ice.2018.156
- Hor SY, Hooker C, Iedema R, et al. Beyond hand hygiene: a qualitative study of the everyday work of preventing cross-contamination on hospital wards. *BMJ Qual Saf*. 2016; 26:1-7. doi: 10.1136/bmjqs-2016-005878
- Brasil. Agência Nacional De Vigilância Sanitária - ANVISA. 2007. Segurança do Paciente: Higienização das mãos. [http://www.anvisa.gov.br/servicos/audite/manuais/paciente\\_hig\\_maos.pdf](http://www.anvisa.gov.br/servicos/audite/manuais/paciente_hig_maos.pdf)
- Greenaway RE, Ormandy K, Fellows C, et al. Impact of hand sanitizer format (gel/foam/liquid) and dose amount on its sensory properties and acceptability for improving hand hygiene compliance. *J Hosp Infect*. 2018; 100:195-201. doi: 10.1016/j.jhin.2018.07.011
- Vermeil T, Peters A, Kilpatrick C, et al. Hand hygiene in hospitals: anatomy of a revolution. *J Hosp Infect*. 2019; 101:383-392. doi: 10.1016/j.jhin.2018.09.003
- World Health Organization. WHO guidelines on hand hygiene in health care 2009. WHO Press, Geneva, Switzerland. 2009.
- American Society for Testing and Materials International. "ASTM E 1174-06: Standard test method for evaluation of the effectiveness of healthcare personnel handwash formulations". West Conshohocken, PA: American Society for Testing and Materials; 2006.
- Pellegrino FLPC, Chagas TPG, Alves MS, et al. Matrix-Assisted Laser Desorption Ionization-Time of Flight Mass Spectrometry (MALDI-TOF MS) Applications in Bacteriology: Brazilian Contributions. *HU Rev*. 2017; 43: 285-294. doi: 10.34019/1982-8047.2017.v43.2859
- Mortier T, Wieme AD, Vandamme P, Waegeman W. Bacterial species identification using MALDI-TOF mass spectrometry and machine learning techniques: A large-scale benchmarking study. *Comput. Struct. Biotechnol. J*. 2021; 19: 6157-6168. doi: 10.1016/j.csbj.2021.11.004
- Clinical and Laboratory Standards Institute (CLSI). Performance Standards for Antimicrobial Testing: Twenty-ninth Edition Informational Supplement M100-E29. 2019. <http://em100.edaptivedocs.net/dashboard.aspx>
- Magiorakos AP, Srinivasan A, Carey RB, et al. Multidrug-resistant, extensively drug-resistant and pandrug-resistant bacteria: an international expert proposal for interim standard definitions for acquired resistance. *CMI*. 2012; 18:268-81. doi: 10.1111/j.1469-0691.2011.03570.x
- Visalacha S, Palraj KK, Kopula SS, et al. Carriage of multidrug resistant bacteria on frequently contacted surfaces and hands of health care workers. *JCDR*. 2016; 10:DC18-DC20. doi: 10.7860/JCDR/2016/19692.7772
- La Fauci V, Costa GB, Genovese C, et al. Drug-resistant bacteria on hands of healthcare workers and in the patient area: an environmental survey in Southern Italy's hospital. *Rev Esp Quimioter*. 2019; 32:303-10. <https://www.ncbi.nlm.nih.gov/pmc/articles/PMC6719646/>
- Ferng YH, Clock SA, Wong-McLoughlin J, et al. Multicenter study of hand carriage of potential pathogens by neonatal ICU healthcare personnel. *J Pediatric Infect Dis Soc*. 2014; 4:276-9. doi: 10.1093/jpids/piu022
- Tselebonis A, Nena E, Nikolaidis C, et al. Monitoring of Frequency and Antimicrobial Susceptibility of Pathogens on the hands of Healthcare Workers in a Tertiary Hospital. *Folia medica*. 2016; 58:200-5. doi: 10.1515/folmed-2016-0028
- Medeiros FDVA, Herdy Alves V, Ortiz Sobrinho Valetre C, et al. A correlação entre procedimentos assistenciais invasivos e a ocorrência de sepse neonatal. *Acta paul. Enferm*. 2016; 29:573-8. doi: 10.1590/1982-0194201600079
- Sanderson E, Yeo KT, Wang AY, et al. Dwell time and risk of central-line-associated bloodstream infection in neonates. *J Hosp Infect*. 2017; 97:267-74. doi: 10.1016/j.jhin.2017.06.023
- Brito DVD, Brito CS, Resende DS, et al. Nosocomial infections in a Brazilian neonatal intensive care unit: a 4-year surveillance study. *Rev Soc Bras Med Trop*. 2010; 43:633-7. doi: 10.1590/S0037-86822010000600006
- Gadallah MAH, Fotouh AMA, Habil IS, et al. Surveillance of

health care-associated infections in a tertiary hospital neonatal intensive care unit in Egypt: 1-year follow-up. *Am J Infect Control*. 2014; 42:1207-11. doi: 10.1016/j.ajic.2014.07.020

24. Pires D, Soule H, Bellissimo-Rodrigues F, et al. Hand hygiene with alcohol-based hand rub: how long is long enough? *Infect. Control Hosp. Epidemiol*. 2017; 38:547-52. doi: 10.1017/ice.2017.25
25. Kapil R, Bhavsar HK, Madan M. Hand hygiene in reducing transient flora on the hands of healthcare workers: an educational intervention. *Indian J Med Microbiol*. 2015; 33:125-128. doi: 10.4103/0255-0857.148409
26. Singh S, Singh AK. Prevalence of bacteria contaminating the hands of healthcare workers during routine patient care: A hospital-based study. *Journal of The Academy of Clinical Microbiologists*. 2016; 18:60-2. doi: 10.4103/0972-1282.184764
27. Zubair M, Zafar A, Yaqoob A, et al. Comparison of Different Hand Washing Techniques to Control Transmission of Microorganisms. *PJMHS*. 2017; 11:1118-20.

## AUTHOR'S CONTRIBUTION

**Gabriel de Oliveira Faria:** study conception and design, data collection, data analysis and interpretation, article writing, critical review of the content and final approval of the version to be submitted

**Priscila Guerino Vilela Alves:** data collection, data analysis and interpretation, critical review of the content and final approval of the version to be submitted

**Lara de Andrade Marques:** data collection, data analysis and interpretation, critical review of the content

and final approval of the version to be submitted

**Nagela Bernadelli Sousa Silva:** data collection, data analysis and interpretation, critical review of the content and final approval of the version to be submitted

**Meliza Arantes de Souza Bessa:** data collection, data analysis and interpretation, critical review of the content and final approval of the version to be submitted

**Felipe Flávio Silva:** data collection, data analysis and interpretation, critical review of the content and final approval of the version to be submitted

**Denise von Dolinger de Brito Röder:** study conception and design, data collection, data analysis and interpretation, article writing, critical review of the content and final approval of the version to be submitted

**Ralciane de Paula Menezes:** study conception and design, data collection, data analysis and interpretation, article writing, critical review of the content and final approval of the version to be submitted






**Reginaldo dos Santos Pedroso:** conception and design of the study, analysis and interpretation of data, critical review of the content and final approval of the submitted version

**Mário Paulo Amante Penatti:** study conception and design, data collection, data analysis and interpretation, article writing, critical review of the content and final approval of the version to be submitted

All authors have approved the final version to be published and are responsible for all aspects of the work, including ensuring its accuracy and integrity.

## Article

# Polyalthic Acid from *Copaifera lucens* Demonstrates Anticariogenic and Antiparasitic Properties for Safe Use

Mariana B. Santiago <sup>1</sup>, Vinicius Cristian O. dos Santos <sup>1</sup>, Samuel C. Teixeira <sup>2</sup>, Nagela B. S. Silva <sup>1</sup>, Pollyanna F. de Oliveira <sup>3</sup>, Saulo D. Ozelin <sup>3</sup>, Ricardo A. Furtado <sup>3</sup>, Denise C. Tavares <sup>3</sup>, Sergio Ricardo Ambrósio <sup>3</sup>, Rodrigo Cassio S. Veneziani <sup>3</sup>, Eloisa Amália V. Ferro <sup>2</sup>, Jairo K. Bastos <sup>4</sup> and Carlos Henrique G. Martins <sup>1,\*</sup>

- <sup>1</sup> Laboratory of Antimicrobial Testing, Institute of Biomedical Sciences, Federal University of Uberlândia, Uberlândia 38405318, MG, Brazil; mariana.brentini@ufu.br (M.B.S.); drsantos.vco@hotmail.com (V.C.O.d.S.); nagela\_bernadelli.mg@hotmail.com (N.B.S.S.)
- <sup>2</sup> Laboratory of Immunophysiology of Reproduction, Institute of Biomedical Science, Federal University of Uberlândia, Uberlândia 38405318, MG, Brazil; samuctx@gmail.com (S.C.T.); eloisa.ferro@ufu.br (E.A.V.F.)
- <sup>3</sup> Nucleus of Research in Sciences and Technology, University of Franca, Franca 14404600, SP, Brazil; pollyanna.oliveira@unifal-mg.edu.br (P.F.d.O.); sauloozelin@hotmail.com (S.D.O.); ricardo.furtado@unifran.edu.br (R.A.F.); denisecrispim2001@yahoo.com (D.C.T.); sergio.ambrosio@unifran.edu.br (S.R.A.); rodrigo.veneziani@unifran.edu.br (R.C.S.V.)
- <sup>4</sup> Faculty of Pharmaceutical Sciences of Ribeirão Preto, University of São Paulo, Ribeirão Preto 14040900, SP, Brazil; jkbastos@fcfrp.usp.br
- \* Correspondence: carlos.martins2@ufu.br; Tel.: +55-343-239-1363

**Abstract:** This study aimed at evaluating the potential of *Copaifera lucens*, specifically its oleoresin (CLO), extract (CECL), and the compound *ent*-polyalthic acid (PA), in combating caries and toxoplasmosis, while also assessing its toxicity. The study involved multiple assessments, including determining the minimum inhibitory concentration (MIC) and minimum bactericidal concentration (MBC) against cariogenic bacteria. CLO and PA exhibited MIC and MBC values ranging from 25 to 50 µg/mL, whereas CECL showed values equal to or exceeding 400 µg/mL. PA also displayed antibiofilm activity with minimum inhibitory concentration of biofilm (MIC<sub>B50</sub>) values spanning from 62.5 to 1000 µg/mL. Moreover, PA effectively hindered the intracellular proliferation of *Toxoplasma gondii* at 64 µg/mL, even after 24 h without treatment. Toxicological evaluations included in vitro tests on V79 cells, where concentrations ranged from 78.1 to 1250 µg/mL of PA reduced colony formation. Additionally, using the *Caenorhabditis elegans* model, the lethal concentration (LC<sub>50</sub>) of PA was determined as 1000 µg/mL after 48 h of incubation. Notably, no significant differences in micronucleus induction and the NDI were observed in cultures treated with 10, 20, or 40 µg/mL of CLO. These findings underscore the safety profile of CLO and PA, highlighting their potential as alternative treatments for caries and toxoplasmosis.

**Keywords:** *Copaifera lucens*; *ent*-polyalthic acid; antibacterial; antibiofilm; antiparasitic; toxicity



**Citation:** Santiago, M.B.; dos Santos, V.C.O.; Teixeira, S.C.; Silva, N.B.S.; de Oliveira, P.F.; Ozelin, S.D.; Furtado, R.A.; Tavares, D.C.; Ambrósio, S.R.; Veneziani, R.C.S.; et al. Polyalthic Acid from *Copaifera lucens* Demonstrates Anticariogenic and Antiparasitic Properties for Safe Use. *Pharmaceuticals* **2023**, *16*, 1357. <https://doi.org/10.3390/ph16101357>

Academic Editors: Chung-Yi Chen, Shengbao Cai and Jiangbo He

Received: 16 August 2023

Revised: 6 September 2023

Accepted: 22 September 2023

Published: 26 September 2023



**Copyright:** © 2023 by the authors. Licensee MDPI, Basel, Switzerland. This article is an open access article distributed under the terms and conditions of the Creative Commons Attribution (CC BY) license (<https://creativecommons.org/licenses/by/4.0/>).

## 1. Introduction

The oral cavity comprises various microenvironments such as tooth surfaces and mucosal epithelium. In each of these oral cavity sites, one can find about fifty species of microorganism, each of these locations in the oral cavity will be inhabited by different bacterial species, due to the cellular tropism of each microbe, there are around a thousand species that are capable of colonizing and integrating the microbiota of the oral cavity. Changes in the resident microbial community lead to dysbiosis, affecting the composition of the community [1,2].

In the case of dental caries, a diet with excess carbohydrates and sugars promotes the production of extracellular polymeric substances (EPS), the matrix that integrates the

bacterial biofilm. As a result, saliva cannot neutralize the pH, and the bacteria in the formed and strengthened biofilm by a rich matrix of EPS produce acids that demineralize the tooth enamel, leading to dental caries [2]. Bacteria belonging to the lactobacillus and mutans streptococci groups, such as *Streptococcus mutans*, *S. mitis*, *S. salivarius*, and *Lactobacillus paracasei*, are directly responsible for the development of caries [3,4].

In 2019, according to the Global Burden of Disease, Injuries and Risk Factors Study, caries in permanent teeth were the most prevalent health condition in adults, with an estimated 2 billion cases. In the same year, caries in deciduous teeth were also the condition that most affected children (aged 0 to 14 years old), with an estimated 0.5 billion cases [5].

Chlorhexidine has been used as a gold-standard antimicrobial agent against cariogenic bacteria. Still, its long-time use can cause undesirable side effects such as taste change, the greenish-brown coloration of the teeth, mucosal peeling, and stone formation, in addition to the development of antimicrobial resistance in the oral microbiota [6]. That is the reason why developing new therapeutic alternatives with biological properties, capable of combating these diseases safely, becomes important and necessary.

Toxoplasmosis, caused by the protozoa *Toxoplasma gondii*, is an endemic disease that affects both humans and warm-blooded animals worldwide [7,8]. Its transmission occurs horizontally, involving the ingestion of food or water contaminated with infective oocysts, as well as the consumption of infected raw food among intermediate hosts, or through blood transfusion and organ donation from infected patients; it can also occur vertically which happens during pregnancy. The infection is usually asymptomatic or with mild flu-like symptoms in healthy humans. However, cases of clinical importance occur in immunosuppressed and pregnant individuals [7–9].

Even though approximately 30% of the world's population is infected with *T. gondii* [10,11], toxoplasmosis is considered a neglected tropical disease [12,13], mainly because its higher incidence occurs in developing countries such as Brazil [7,8,11]. The gold-standard treatment against toxoplasmosis uses the drugs pyrimethamine (PYR) and sulfadiazine (SDZ). However, the therapy requires the prolonged use of the drugs which can increase toxicity and present significant failure rates in treatment [14]. Therefore, developing new therapeutic agents capable of safely combating the disease is also necessary.

To this end, natural products have been sourced to develop new drugs [15]. Trees belonging to the *Copaifera* genus are native to tropical regions of Latin America and West Africa. The genus *Copaifera* belongs to the Fabaceae family and includes 72 species. More than 20 *Copaifera* spp. exist in the Brazilian territory, where they are popularly called “copaibeiras”, “pau d’oleo”, or “copaibas” [16,17].

The scientific literature contains numerous reports on the pharmacological activities of *Copaifera* species, such as their anti-inflammatory potential, antitumor, antiproliferative, anthelmintic, antituberculosis, gastroprotective, chemopreventive, immunomodulatory, and other antibacterial actions [16,17]. Although natural compounds have been traditionally employed, their use ought to occur safely; many studies have reported that several plant species applied in herbal medicine exhibit mutagenic, carcinogenic, or toxic effects [18].

The literature has widely described the chemical composition of different oleoresins [19,20]. In general, oleoresin is a natural product of secondary metabolism and consists mainly of a mixture of diterpene acids (resin fraction) and sesquiterpenes (volatile fraction) [16]. Although significant differences in the chemical profile of the oleoresin are observed between different species and various individuals of the same taxon, the diterpenes belonging to the types of skeleton caurano, clerodano, and labdano can be identified in all oleoresins [21], such as copalic, hardwickiic, kaurenoic, and polyalthic acids [22,23]. Specifically, for *C. lucens*, it was found that *ent*-polyalthic acid is the main constituent of this class of metabolites [24].

The diterpene *ent*-polyalthic acid, *ent*-15,16-epoxy-8(17),13(16),14-labdatrien-19-oic acid, is known for its biological properties, including gastroprotective [25], anti-inflammatory [26], antibacterial [27,28], antifungal [27], antitumor [29], and muscle relaxant actions [30]. Con-

sequently, this molecule demonstrates potential to assist in the development of alternative therapies capable of addressing significant clinical conditions.

With the purpose of bringing scientific evidence to inform these health issues, the present study aimed to evaluate the potential anticariogenic properties of the crude extract of *C. lucens* (CECL), *C. lucens* oleoresin (CLO), and its major compound *ent*-polyalthic acid (PA). Additionally, the potential antiparasitic properties of PA were studied and the toxicity of the samples CLO and PA was assessed.

## 2. Results

### 2.1. Anticariogenic Activity

The anticariogenic evaluation of planktonic cells from CLO, CECL and PA was performed by determining the minimal inhibitory concentration (MIC) and minimal bactericidal concentration (MBC). The results are shown in Table 1.

**Table 1.** Minimal Inhibitory Concentration (MIC) and Minimal Bactericidal Concentration (MBC) of *Copaifera lucens* oleoresin (CLO), crude extract of *Copaifera lucens* (CECL) an *ent*-polyalthic acid (PA) against cariogenic strains.

Cariogenic Strains	CLO ( $\mu\text{g/mL}$ )		CECL ( $\mu\text{g/mL}$ )		PA ( $\mu\text{g/mL}$ )		Chlorhexidine ( $\mu\text{g/mL}$ )	
	MIC	MBC	MIC	MBC	MIC	MBC	MIC	MBC
<i>Enterococcus faecalis</i> (ATCC 4082)	25	25	>400	>400	25	25	7.37	7.37
<i>Lactobacillus paracasei</i> (ATCC 11578)	25	50	>400	>400	25	50	3.68	3.68
<i>Streptococcus mitis</i> (ATCC 49456)	25	50	400	400	25	50	3.68	3.68
<i>Streptococcus mutans</i> (ATCC 25175)	25	50	>400	>400	50	50	0.92	0.92
<i>Streptococcus salivarius</i> (ATCC 25975)	25	50	400	400	50	50	0.92	0.92
<i>Streptococcus sanguinis</i> (ATCC 10556)	25	50	400	400	25	50	7.37	7.37
<i>Streptococcus sobrinus</i> (ATCC 33478)	25	25	400	>400	25	25	0.92	0.92

CLO—*Copaifera lucens* oleoresin. CECL—crude extract of *Copaifera lucens*. PA—*ent*-polyalthic acid. MIC—Minimal Inhibitory Concentration. MBC—Minimal Bactericidal Concentration.

The CLO and PA values ranged from 25 to 50  $\mu\text{g/mL}$ , while the CECL values were higher or equal to the highest evaluated concentration of 400  $\mu\text{g/mL}$ . CLO showed bactericidal activity against *Enterococcus faecalis* and *S. sobrinus*, PA showed bactericidal activity against *E. faecalis*, *S. mutans*, *S. salivarius*, and *S. sobrinus*, whereas CECL showed bactericidal activity against *S. mitis*, *S. salivarius*, and *S. sanguinis*. The positive control chlorhexidine presented MIC/MBC ranging from 0.92 to 7.37  $\mu\text{g/mL}$ .

It was observed that the isolated compound PA presented the same bactericidal results as CLO; as it is also one of the major compounds present in CLO, it was considered that the anticariogenic activity presented by CLO is due to PA, and this compound was chosen for the continuation of the assessment of inhibition activity in biofilm formation.

To evaluate the anticariogenic activity of PA in bacterial communities, the biofilm formation inhibition assay was performed. Thus, the minimum inhibitory concentration of biofilm (MIC<sub>B50</sub>) and cell viability (Log<sub>10</sub> CFU/mL) were determined. The cariogenic strains were capable of forming biofilms at 10<sup>7</sup> CFU/mL after 24 h of incubation in a suitable atmosphere.

The PA antibiofilm activity (Figure 1) presented MIC<sub>B50</sub> values that ranged from 62.5 to 1000  $\mu\text{g/mL}$ , and it was able to completely eliminate cell viability for the strains *S. salivarius* (500  $\mu\text{g/mL}$ ), *S. sobrinus* (1000  $\mu\text{g/mL}$ ), *S. mitis* (250  $\mu\text{g/mL}$ ), *S. mutans* (125  $\mu\text{g/mL}$ ), and *L. paracasei* (500  $\mu\text{g/mL}$ ). The antibiofilm activity of the drug chlorhexidine, the standard drug used in the treatment of caries, against the strains used in the present study was also evaluated. The results are shown in Figure 2.

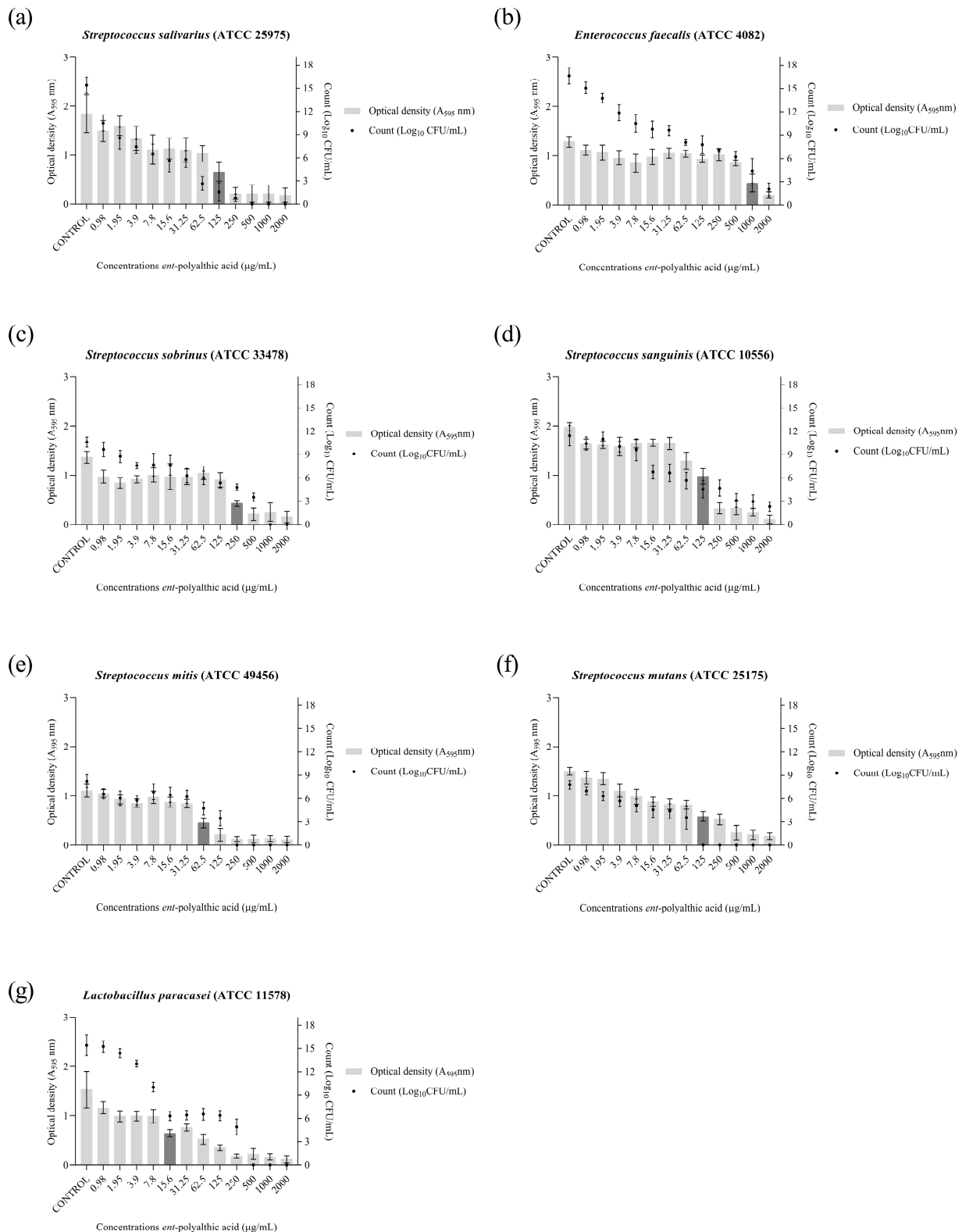


**Figure 1.** Graphical representation of antibiofilm activity as demonstrated by optical density (O.D.) and number of microorganisms ( $\text{Log}_{10}\text{CFU/mL}$ ) of the ent-polyalthic acid against cariogenic bacteria. (a) *Streptococcus salivarius* (ATCC 25975); (b) *Enterococcus faecalis* (ATCC 4082); (c) *Streptococcus sobrinus* (ATCC 33478); (d) *Streptococcus sanguinis* (ATCC 10556); (e) *Streptococcus mitis* (ATCC 49456); (f) *Streptococcus mutans* (ATCC 25175); (g) *Lactobacillus paracasei* (ATCC 11578). The MIC<sub>50</sub> value is represented in dark gray.

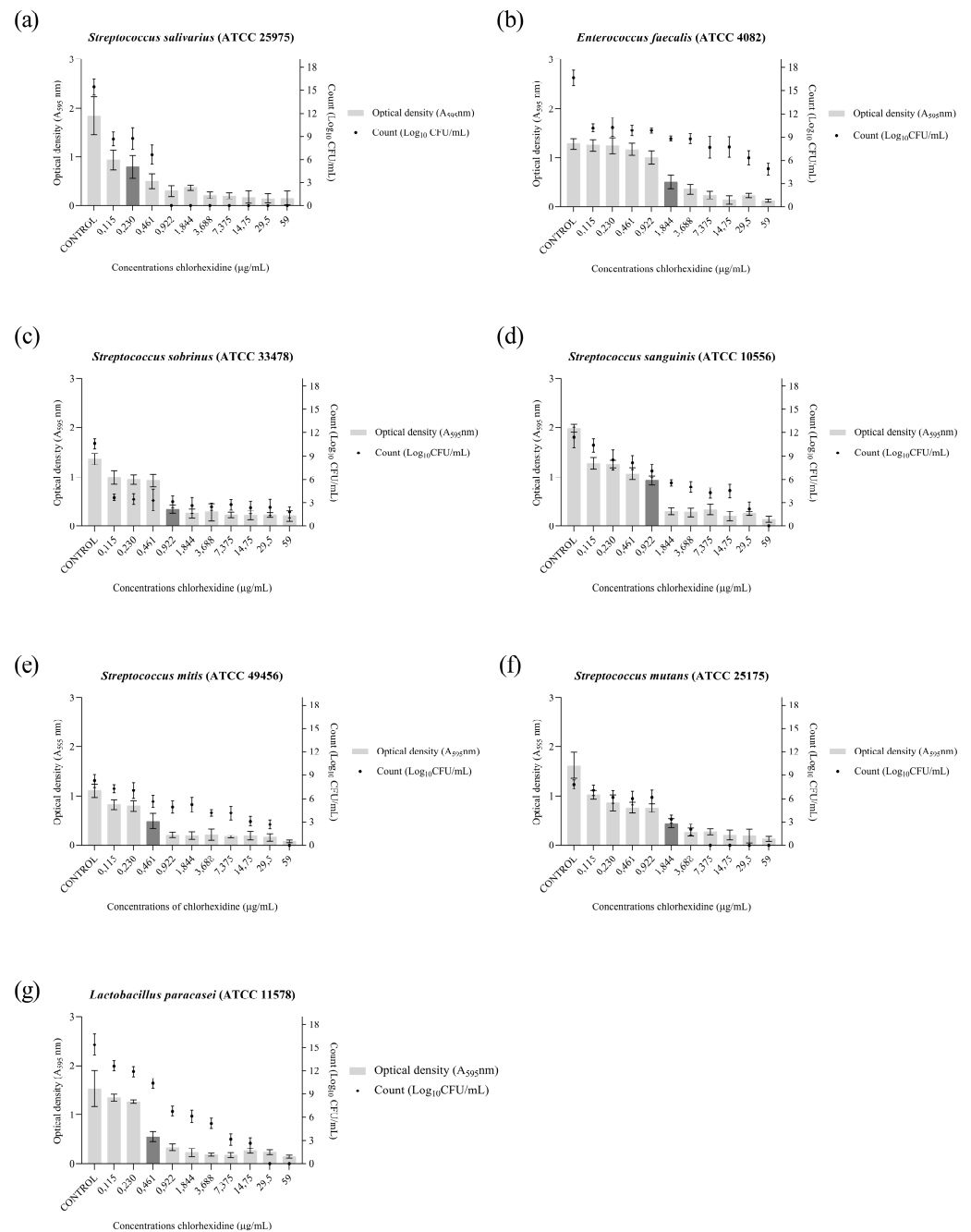


**Figure 2.** Graphical representation of the antibiofilm activity as demonstrated by optical density (O.D.) and number of microorganisms (Log<sub>10</sub> CFU/mL) of the chlorhexidine against cariogenic bacteria. (a) *Streptococcus salivarius* (ATCC 25975). (b) *Enterococcus faecalis* (ATCC 4082). (c) *Streptococcus sobrinus* (ATCC 33478). (d) *Streptococcus sanguinis* (ATCC 10556). (e) *Streptococcus mitis* (ATCC 49456). (f) *Streptococcus mutans* (ATCC 25175). (g) *Lactobacillus paracasei* (ATCC 11578). The MIC<sub>50</sub> value is represented in dark gray.

## 2.2. Antiparasitic Activity

For the antiparasitic evaluation assays, PA did not interfere with the cell viability of BeWo cells at concentrations of 64 µg/mL and lower, only losing viability at high doses of 128 µg/mL and 256 µg/mL (Figure 3a). In the assay for the evaluation of intracellular proliferation of *T. gondii*, the percentage was quantified through the activity of β-galactosidase in viable parasites. The inhibitory potential of compound PA was assessed at concentrations ranging from 4 to 256 µg/mL, and the combination of SDZ (200 µg/mL) and PYR



(8 µg/mL) was also tested. The percentages of proliferation observed in the treatments described were compared with the negative control, which consisted of only infected BeWo cells. The data were graphically represented (Figure 3b), and after analysis, it was possible to identify that compound PA at concentrations of 32 ( $p < 0.01$ ), 64 ( $p < 0.01$ ), 128 ( $p < 0.0001$ ), and 256 µg/mL ( $p < 0.0001$ ), as well as SDZ + PYR ( $p < 0.0001$ ), significantly inhibited the intracellular proliferation of *T. gondii* compared to the negative control. PA obtained a cytotoxicity concentration of 50% (CC<sub>50</sub>) of  $171.76 \pm 7.725$ , and inhibition concentration of 50% (IC<sub>50</sub>) of  $93.24 \pm 1.395$ .

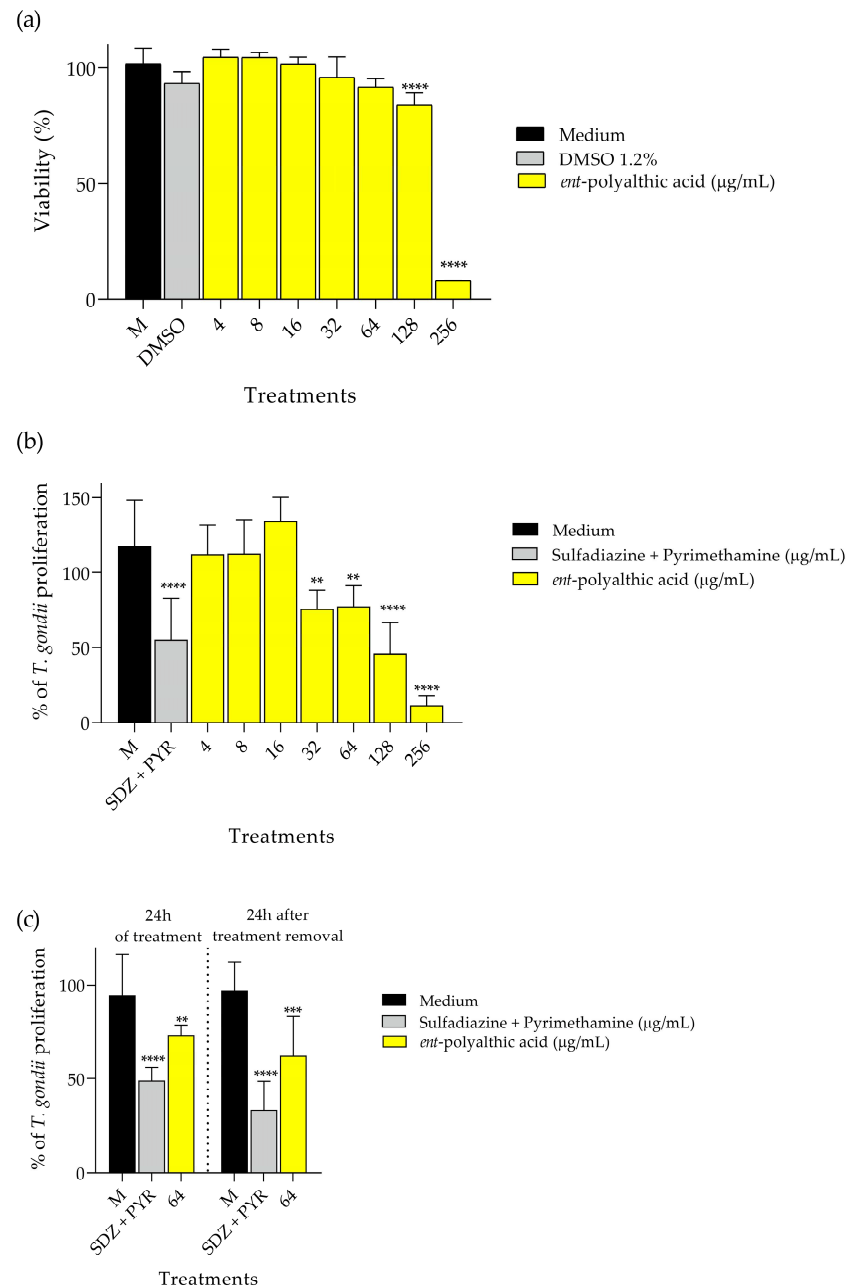


**Figure 3.** Graphical demonstration of the antiparasitic activity of the *ent*-polyalthic acid. (a) Viability of BeWo cells after 24 h of treatments. (b) *Toxoplasma gondii* intracellular proliferation after treatments. (c) Evaluation of the irreversibility antiparasitic action after treatment removal. \*\* Statistical significance with  $p < 0.01$  when compared with the control (medium). \*\*\* Statistical significance with  $p < 0.001$  when compared with the control (medium). \*\*\*\* Statistical significance with  $p < 0.0001$  when compared with the control (medium).

Because of the promising anti-*T. gondii* activities exhibited by PA, a reversibility test was conducted to evaluate the maintenance of the antiparasitic effects. The assay was also performed on BeWo cells to quantify the intracellular proliferation of *T. gondii* through  $\beta$ -galactosidase activity. As expected, PA at 64  $\mu\text{g}/\text{mL}$  ( $p < 0.01$ ) and SDZ + PYR at 200  $\mu\text{g}/\text{mL}$  and 8  $\mu\text{g}/\text{mL}$ , respectively ( $p < 0.0001$ ), reduced intracellular parasite proliferation at 24 h of treatment (Figure 3c). Interestingly, PA ( $p < 0.001$ ) and SDZ + PYR ( $p < 0.0001$ ) treatments maintained their ability to control parasite growth even after 24 h of treatment removal in comparison with the control group (infected cells incubated with RPMI 1640 medium only) (Figure 3c).

### 2.3. Toxicity Assessment

The toxicity evaluation of the survival fraction of V79 cells after treatment with different concentrations of CLO are shown in Figure 4. A significant reduction in colony formation was shown in concentrations ranging from 78.1 to 1250  $\mu\text{g}/\text{mL}$  when compared to the group negative control. There was no significant difference in colony formation at the lowest concentrations tested (from 4.88 to 39.0  $\mu\text{g}/\text{mL}$ ). Therefore, the concentrations of 10, 20, and 40  $\mu\text{g}/\text{mL}$  were chosen for the genotoxicity assessment.

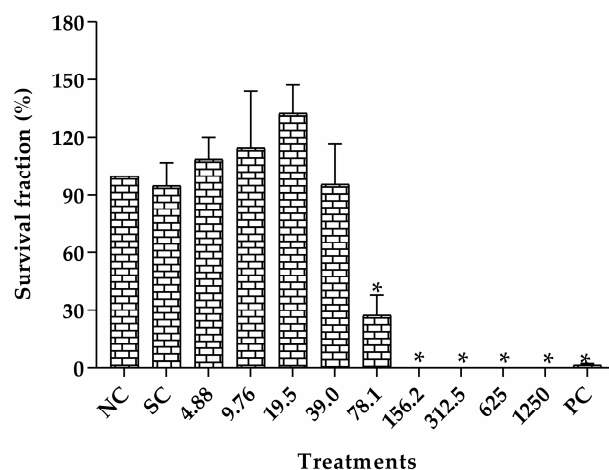


**Figure 4.** Survival fraction of V79 cells after the treatment with *Copaifera lucens* oleoresin. CLO (*Copaifera lucens* oleoresin), NC (negative control, without treatment), SC (solvent control, Tween 80, 1%), PC (positive control, methyl methanesulfonate, 110  $\mu\text{g}/\text{mL}$ ). \* Significantly different from the negative control ( $p < 0.05$ ).

The binucleated micronucleated V79 cell frequencies and nuclear division indexes (NDI) after treatment with CLO are shown in Figure 5. No significant difference in micronucleus induction and in the NDI were observed between cultures treated with 10, 20, or 40  $\mu\text{g}/\text{mL}$  of CLO compared to the negative control group, revealing absence of genotoxicity and cytotoxicity, respectively.

Table 2 shows the results obtained from the in vivo evaluation in Swiss mice of the genotoxic potential of CLO and PA. No significant differences in the frequencies of micronucleated poly-chromatic erythrocytes (MNPCEs) were observed between animals treated with the different doses of CLO or PA and the negative control, demonstrating the absence of genotoxic activity. No significant reduction in the percentage of polychromatic erythrocyte (PCEs) in total red blood cells was observed in any of the treatment groups compared to the negative control, demonstrating the absence of cytotoxicity of the different treatments under the conditions tested.

The in vivo toxicity assessment using the *C. elegans* model was employed to determine the lowest concentration capable of killing 50% ( $\text{LC}_{50}$ ) of the larvae over time. Figure 6 shows the toxicity evaluation of different concentrations of PA over a 72-h period. The  $\text{LC}_{50}$  of PA was determined at 1000  $\mu\text{g}/\text{mL}$  after 48 h of incubation.

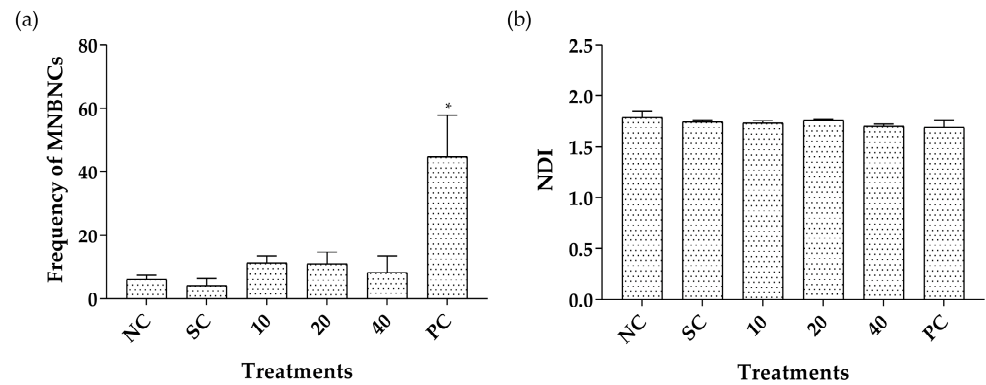


**Figure 5.** Binucleated micronucleated V79 cell frequency (a) and NDI (b) after treatment with *Copaifera lucens* oleoresin. CLO (*Copaifera lucens* oleoresin), NC (negative control, without treatment), SC (solvent control, Tween 80, 1%), PC (positive control, methyl methanesulphonate, 110 µg/mL). \* Significantly different from the negative control ( $p < 0.05$ ).

**Table 2.** Frequencies of MNPCEs and PCE/PCE + NCE ratio in the bone marrow of Swiss mice observed after the treatment with different doses of *Copaifera lucens* oleoresin, *ent*-polyalthic acid, and in respective controls.

Treatments (mg/kg)	MNPCEs	PCE/(PCE + NCE)
	Mean ± SD	Mean ± SD
Negative control	2.60 ± 1.34	0.59 ± 0.13
Tween 80	2.40 ± 1.14	0.72 ± 0.10
DMSO	1.60 ± 0.55	0.69 ± 0.02
CLO 125	5.00 ± 4.58	0.54 ± 0.04
CLO 250	9.60 ± 2.88	0.57 ± 0.07
CLO 500	6.80 ± 3.56	0.53 ± 0.07
PA 1	4.00 ± 0.55	0.56 ± 0.05
PA 10	3.60 ± 0.89	0.54 ± 0.02
PA 20	2.80 ± 1.79	0.56 ± 0.03
Positive control	34.60 ± 1.82 *	0.67 ± 0.14

MNPCEs—micronucleated polychromatic erythrocytes; PCE—polychromatic erythrocyte; NCE—normochromatic erythrocyte; Negative control—water; Tween 80, 5%; DMSO—dimethylsulfoxide, 5%; CLO—*Copaifera lucens* oleoresin; PA—*ent*-polyalthic acid; Positive control—methyl methanesulphonate, 40 mg/kg. \*—Significantly different from the negative control group ( $p < 0.05$ ).

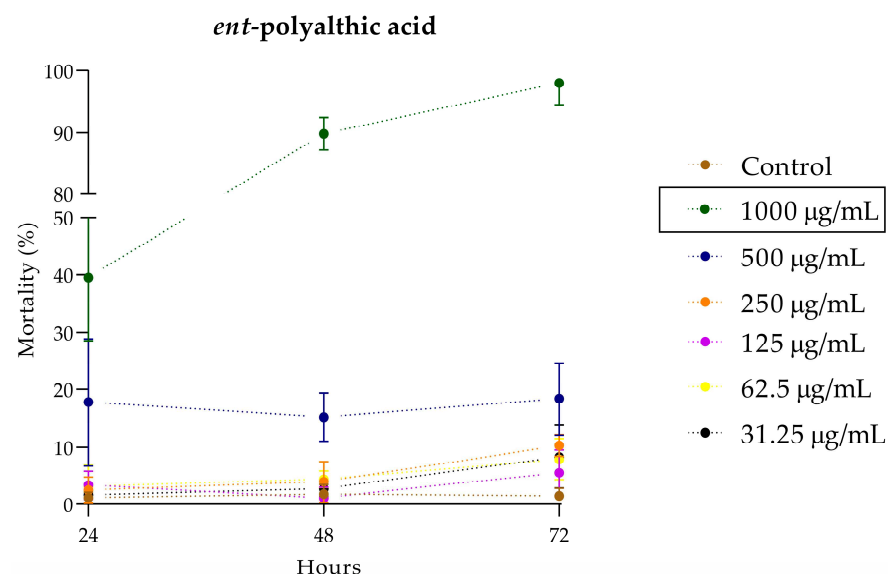


**Figure 6.** Evaluation of the toxicity of the *ent*-polyalthic acid in the *Caenorhabditis elegans* in vivo model.

### 3. Discussion

To date, no article has been found in the literature that evaluated the anticariogenic activity of *C. lucens*. Therefore, this study was the first to address this topic.

Holetz, et al. [31] consider that an extract exhibits good antibacterial activity at concentrations below 100 µg/mL, moderate activity between 100 and 500 µg/mL, and weak activity between 500 and 1000 µg/mL; above 1000 µg/mL, the extract antibacterial activity is considered inactive. Based on the authors' criteria, it can be concluded that CECL showed moderate antibacterial activity against the strains *S. mitis*, *S. salivarius*, *S. sanguinis*, and *S. sobriunus* (MIC 400 µg/mL). On the other hand, CLO displayed good antibacterial activity against all seven cariogenic strains (MIC 25 µg/mL) evaluated in the present study.

Nevertheless, because of the lack of studies evaluating the anticariogenic potential of *C. lucens*, it is not possible to directly compare the data obtained in the present study with other authors. There are reports of the same biological property in other *Copaifera* species. Abrão et al. [32] evaluated the anticariogenic potential of the oleoresin of *C. duckei* and found MIC values between 25 and 50 µg/mL against the same strains. All of these aforementioned data indicate that *Copaifera* spp. is a source with active antibacterial potential, specifically against cariogenic bacteria. Furthermore, they validate the results obtained in the present study, as the MIC values found for CLO fall within the concentration range reported in the literature for other oleoresins of *Copaifera* spp.

Abrão et al. [32] evaluated the antibacterial activity of *ent*-polyalthic acid isolated from *C. duckei* against the cariogenic bacteria used in the present study, and the authors reported MIC and MBC values ranging from 25 to 50 µg/mL. The PA isolated from *C. lucens* used in the present study also exhibited MIC and MBC values within the same concentration range as reported by the authors. Despite the differences in the source of origin and extraction method, the compound used by the authors and in the present study refers to the same molecule, and therefore shares the same chemical composition. As previously mentioned, PA is the major compound in CLO, representing approximately 69.8% of the total oleoresin composition [24]. Regarding the oleoresin of *C. duckei*, the scientific literature reports values ranging from 6.9% to 40.86% [33–35] of *ent*-polyalthic acid in its composition. Therefore, CLO appears to be a source where a higher concentration of PA can be obtained.

When analyzing the MIC and MBC results of CLO and PA, it is observed that both samples exhibit identical results against the same strains with the exception of *S. mutans* and *S. salivarius* bacteria. For CLO, the MIC value was 25 µg/mL, while PA showed an MIC of 50 µg/mL against these particular strains. However, it is important to note that the bactericidal concentration was found to be the same for both samples. Based on these results, it may be suggested that the antibacterial activity exhibited by CLO is attributed to its compound PA. Therefore, since PA has been shown as a promising active compound, the experiments were pursued using it.

Bacterial biofilms exhibit high resistance to antibiotics, and the way it embeds within its EPS matrix is considered a virulence factor associated with the development of chronic infections which can affect even immunocompetent individuals [36]. Studies estimate that the treatment required for effective elimination of these bacterial communities needs to be administered at concentrations 10- to 1000-fold higher than those needed to eliminate the bacteria in their planktonic form [37–39]. This propensity was confirmed in the present study, where the concentrations of PA required to inhibit 50% of biofilm formation by cariogenic bacteria ranged from 15.6 to 1000 µg/mL, while the MIC to inhibit planktonic bacteria was 25 to 50 µg/mL. Even at the highest concentration evaluated (2000 µg/mL), it was not possible to completely eliminate the cell viability of the *E. faecalis* and *S. sanguinis* strains within the biofilm.

Abrão et al. [32] evaluated the activity of *ent*-polyalthic acid in inhibiting biofilm formation by *L. paracasei* (ATCC 11578), *S. mutans* (ATCC 25275), and *S. sobriunus* (ATCC 33478) strains, with a standardized bacterial inoculum concentration of  $1 \times 10^6$  CFU/mL. They obtained MIC<sub>50</sub> value of 3.12 µg/mL against *L. paracasei* and 50 µg/mL against *S. mutans* and *S. sobriunus*, completely inhibiting cell viability at concentrations of 50 µg/mL

(*L. paracasei*) and 200 µg/mL (*S. mutans* and *S. sobrinus*). In the present study, using the same strains, PA exhibited MIC<sub>B50</sub> of 15.6 µg/mL against *L. paracasei*, 125 µg/mL against *S. mutans* and 250 µg/mL against *S. sobrinus*, with complete inhibition of cell viability observed at concentrations of 500, 125, and 1000 µg/mL, respectively. It is important to note that in the present study, the inoculum concentration used was  $1 \times 10^7$  CFU/mL, which is higher than that used by Abrão et al. [32]. This difference in inoculum concentration may explain the data obtained in the present study.

Considering neglected diseases, *Copaifera* spp. can be a source with biological properties against parasites. Santos et al. [24] evaluated the activity against the promastigote form of *Leishmania amazonensis* of nine oleoresins from *Copaifera* spp. and all samples showed significant differences in parasite inhibition. One of the species evaluated by the authors was the oleoresin of *C. lucens* (containing 69.8% of PA in its composition), which exhibited IC<sub>50</sub> of  $20 \pm 0.9$  µg/mL against *L. amazonensis* [24]. Izumi, et al. [40] evaluated the oleoresin of *C. lucens* in the inhibition of *Trypanosoma cruzi* in three different forms of the parasite. They found IC<sub>50</sub> value of  $10.0 \pm 2$  µg/mL against the amastigote form,  $51.0 \pm 1.4$  µg/mL against the epimastigote form and  $215.0 \pm 21.2$  µg/mL against the trypomastigote form. Mizuno, et al. [41] evaluated the antileishmanial and antitrypanosomal activity of polyalthic acid. The authors found IC<sub>50</sub> values of  $8.68 \pm 0.33$  µg/mL against *L. donovani* amastigotes and  $3.87 \pm 0.28$  µg/mL against *T. brucei* [41].

The initial findings presented in the current investigation indicate that a significant portion of the antimicrobial properties exhibited by CLO may potentially be ascribed to the bioactive constituent PA. Moreover, the current literature has demonstrated the promising antiparasitic effects of CLO [24] and PA against protozoan parasites [41]. Considering all the aforementioned points and taking into account that CLO consists of an approximate 69.8% composition of PA [24], we decided to exclusively employ PA for evaluating its anti-*T. gondii* efficacy within the BeWo cell model, which serves as the host cell model for this assessment.

In this context, Teixeira, et al. [42] evaluated the inhibitory activity of *ent*-polyalthic acid from *Copaifera* spp. against *T. gondii* tachyzoites using human villous explants as an experimental model. The PA used by the authors reduced the viability of villous explant at concentrations of 256 and 512 µg/mL. Furthermore, the compound was able to significantly inhibit the proliferation of tachyzoites at concentrations of 64 and 128 µg/mL. In addition to the inhibitory capacity at these concentrations (64 and 128 µg/mL), the compound also maintained its antiparasitic action even upon the removal of the treatment after 24 h of incubation [42]. In the present study, conducted in BeWo cells, the antiparasitic activity was similar, where the reduction in cell viability occurred at concentrations of 128 and 256 µg/mL, and the inhibitory action on *T. gondii* tachyzoites proliferation was significantly lower at non-cytotoxic concentrations of 32 and 64 µg/mL. At a concentration of 64 µg/mL, the antiparasitic activity of PA was maintained after 24 h of withdrawal of treatment. Taken together, using a different experimental model, our data are in agreement with the current literature that has demonstrated the prominent anti-*T. gondii* activity of PA, highlighting the potential of this bioactive compound.

As already mentioned, *C. lucens* oleoresin is rich in diterpenes, especially PA and copalic acid (CA), which are the major compounds [16]. Considering the popular use and the region of occurrence, CLO can be useful against tropical diseases and bacteria, so further studies could help to understand the effectiveness and possible human use. Furtado, et al. [43] carried out an extensive work, aiming to investigate the genotoxic potential of oleoresin from six different species of the *Copaifera* genus in mouse bone marrow. As a result, the absence of cytotoxicity and genotoxicity were found, even at the maximum limits recommended by OECD guidelines (2000 mg/kg) [44]. These results taken together with those obtained in the present study demonstrate the absence of significant genotoxic risk of oleoresin in these species of *Copaifera*.

The literature is scant regarding bioassays using PA in isolate form although it is known to be highly cytotoxic in human tumor cells [45] and antimutagenic against 3-

amino-1,4-dimethyl-5H-pyrido(4,3-B)indole (Trp-P-1) genetic damage by Ames test [46]. In addition, PA had a considerable antibacterial and antifungal effect in vitro owing to cytotoxicity, including a greater effect than most of its semi-synthetic derivatives with extra carboxyl groups which were also tested [27].

CA is considered one of the biomarkers for *Copaifera* genus and represents up to 11% of the constitution of the CLO, but it is still considered as the second most abundant compound [24].

Another novel finding presented in our study is the toxicity evaluation using the *C. elegans* model. The use of the nematode model for toxicity assessment has been implemented satisfactorily as it provides an in vivo system with low maintenance requirements and expresses homologs of approximately 80% of human genes, despite some limitations such as evolutionary distance from humans and lack of organs [47]. The toxicity of PA was evaluated over a period of 72 h, and it showed good performance. Below the LC<sub>50</sub> value (1000 µg/mL), even after 72 h of exposure, the compound exhibited a non-toxic profile to *C. elegans*.

All the toxicity evaluation data presented here, both for CLO and PA, indicate that they have the potential to become alternatives in the fight against cariogenic bacteria and *T. gondii*, as they did not show toxicity at the concentrations where they exhibited these biological properties.

## 4. Materials and Methods

### 4.1. Plant Material and Polyalthic Acid

*Copaifera lucens* Dwyer oleoresin (CLO) and crude extract of *Copaifera lucens* (CECL), obtained from the leaves of the tree, were collected in Rio de Janeiro, Brazil, between August 2012 and May 2014; this was authorized by the Brazilian government through SISBIO (35143-1) and CGEN (010225/2014-5). The plant material was identified by Haroldo Cavalcante de Lima at the Rio de Janeiro Botanical Garden Herbarium (JBRJ) and is deposited there under identification number 474304. Pure *ent*-polyalthic acid (PA) was obtained according to the methodology reported by our research group [35].

#### 4.1.1. Obtainment of CECL

The leaves of *C. lucens* were subjected to a dehydration process in a circulating air oven maintained at 40 °C and subsequently comminuted using a knife mill. One hundred grams of the resulting powder was subjected to a maceration process using a solvent consisting of ethanol and water in a 7:3 ratio (1 L). The solvent was systematically percolated, filtered, and then replaced, with this sequence being repeated every 48 h for a total of three cycles. The residual aqueous-enriched extract was preserved at a temperature of −80 °C and subsequently subjected to lyophilization in a Liobras Inc. apparatus until complete desiccation, yielding a total of 28 grams of the crude extract.

#### 4.1.2. Obtainment of CLO and Isolation of PA

The oleoresin was acquired through the process of perforating the trunk using an auger. The harvested oleoresin underwent filtration and was subsequently subjected to various chromatographic procedures. The methods employed for the isolation of PA were based on previously established procedures as described by our research group [35]. In summary, a quantity of 10 grams of oleoresin was subjected to vacuum liquid chromatography using organic solvents, leading to the generation of seven distinct fractions. PA was selectively eluted in fractions 2 and 3 which were subsequently combined and subjected to crystallization in a hexane-acetone mixture, resulting in the isolation of 1.2 g of pure compound. The chemical structure of PA was elucidated through the utilization of <sup>1</sup>H and <sup>13</sup>C Nuclear Magnetic Resonance in CDCl<sub>3</sub>, and its structural characteristics were compared to existing literature data [48].

## 4.2. Anticariogenic Activity

### 4.2.1. Bacteria Used

The strains used in the study came from the American Type Culture Collection (ATCC, Manassas, VA, USA). The cariogenic strains used were *Streptococcus mutans* (ATCC 25175), *S. mitis* (ATCC 49456), *S. sanguinis* (ATCC 10556), *S. sobrinus* (ATCC 33478), *Lactobacillus paracasei* (ATCC 11578), *Enterococcus faecalis* (ATCC 4082), and *S. salivarius* (ATCC 25975). For all assays performed the bacteria were incubated in Brain Heart Infusion agar (BHI), added with defibrinated sheep blood (5%) in a microaerophilia incubator for 24 h at 37 °C with 10% CO<sub>2</sub>, except for *E. faecalis* and *S. salivarius* which were incubated aerobically at 37 °C for 24 h.

### 4.2.2. Minimal Inhibitory Concentration (MIC) and Minimal Bactericidal Concentration (MBC)

MIC was determined by the microdilution technique in 96-well microplates following the recommendations of the Clinical and Laboratory Standards Institute [49], with adaptations using resazurin to reveal bacterial growth [50]. Briefly, solutions of the CLO, CECL, and PA in a concentration of 1.0 mg/mL were prepared in dimethylsulfoxide (DMSO, Sigma Chemical Co., St. Louis, MO, USA) followed by dilution in broth until concentrations ranging from 0.195 to 400 µg/mL were obtained, with a final DMSO content of 5% (v/v).

The inoculum concentration was adjusted to each microorganism. For cariogenic bacteria, the final concentration was  $5 \times 10^5$  CFU/mL. The positive control used was chlorhexidine (Sigma) at concentrations ranging from 0.115 to 59 µg/mL. The bacteria were incubated under the conditions described above. After the period of incubation, a 10-µL aliquot was removed from each well of the microplate and seeded on agar for the evaluation of MBC. The agar was incubated under appropriate conditions and, afterwards, the presence and/or absence of bacterial growth was verified to determine the MBC. Then, 30 µL of an aqueous solution of resazurin (0.02%) was added to each microplate to verify the microbial viability. Resazurin serves as an oxidation-reduction indicator, facilitating the real-time assessment of microbial viability. In this context, the blue hue indicates the absence of microbial viability, while the red color signifies the presence of microbial viability, therefore determining the value of MIC [50]. The sample evaluated was considered as bactericidal when it exhibited the same value in both the MIC and MBC assays. In cases where the MIC value was lower than the MBC value, the samples were considered bacteriostatic [51]. The experiments were carried out in triplicate.

### 4.2.3. Antibiofilm Activity

The antibiofilm activity was evaluated by determination of the MIC<sub>B50</sub> which was the lowest concentration of the sample that inhibited the formation of 50% or more of the biofilm [52]. The method used was microplate dilution, a methodology similar to that used for determining MIC [49], with modifications. The experiments were carried out for the strains that showed better MIC results, performed in triplicate, with results demonstrated graphically.

The method used to inhibit the formation of biofilm was similar to the MIC assay conducted for planktonic cells. Serial dilutions of the samples were prepared in the wells of a 96-well microplate, the final concentration ranging from 0.98 to 2000 µg/mL. Chlorhexidine at concentrations between 0.115 to 59 µg/mL was assessed as negative control. The inoculum was added with 100 µL of each strain at a concentration of  $10^7$  CFU/mL; the bacterial strains in the absence of chlorhexidine or PA were used as positive control. The bacteria were incubated under the conditions described above. Subsequently, following the incubation period, the contents within each well were carefully aspirated and each well underwent a series of three washes using 200 µL of sterile Milli-Q water to eliminate any planktonic cells. The biofilm adhered to the wells was fixed by exposing it to 150 µL of methanol for a period of 20 min. Antibiofilm activity was measured by MIC<sub>B50</sub> de-

terminated by optical density (OD) and by counting the number of colony-forming units ( $\text{Log}_{10}$  CFU/mL).

Based on the procedures described by Sandberg et al. [53], OD was quantified in the biofilm by adding 200  $\mu\text{L}$  of crystal violet (0.2%) to the microplate wells. After 15 min at room temperature, excess dye was removed with tap water and dried in air at room temperature. Next, 200  $\mu\text{L}$  of acetic acid at 33% (*v/v*) was added to each well to re-solubilize the dye bound to the cells. After 30 min, the OD of the microplates was measured at 595 nm using a microtiter plate reader (GloMax<sup>®</sup>, Promega, Madison, WI, USA). The percentage of inhibition was calculated using the equation:

$$1 - \left( \frac{\text{At595nm}}{\text{Ac595nm}} \right) \times 100$$

where At595nm and Ac595nm are the absorbance values of the wells treated with the samples and the control, respectively [52].

The antibiofilm activity measured by counting the numbers of CFU was performed to assess cell viability. Briefly, after the incubation period, the entire volume was carefully aspirated from the wells of the microplate and washed with water to completely remove the non-adherent cells. Then, 200  $\mu\text{L}$  of broth was added to each well and the microplate went through the sonication process so that the adhered cells are released by the vibrations. Dilutions of  $10^{-1}$  to  $10^{-7}$  were performed for all wells and 50  $\mu\text{L}$  of each dilution was plated in BHI agar added with defibrinated sheep blood (5%), which were incubated as already described. After incubation, the colonies were counted and the results were expressed in  $\text{Log}_{10}$  CFU/mL and shown graphically. Selection of the best inoculum concentration and incubation time for the antibiofilm activity assay was accomplished by standardizing biofilm formation.

### 4.3. Antiparasitic Activity

#### 4.3.1. Cell Culture and Parasite Maintenance

Human trophoblast cells were purchased commercially from the ATCC and were maintained following the protocols previously described by Drewlo, et al. [54]. In brief, cell culture maintenance was carried out employing RPMI 1640 medium (Cultilab, Campinas, SP, Brazil), supplemented with 100 U/mL penicillin (Sigma), 100  $\mu\text{g}/\text{mL}$  streptomycin (Sigma), and 10% fetal bovine serum (FBS) (Cultilab). The cultures were incubated at a temperature of 37 °C in a humidified environment containing CO<sub>2</sub> (5%).

Tachyzoites of *Toxoplasma gondii* (virulent RH strain, 2F1 clone), which consistently expressed the  $\beta$ -galactosidase gene, were cultivated following established protocols as described elsewhere [55]. Briefly, tachyzoites were maintained by serial passages in BeWo cells cultured in a RPMI 1640 medium containing 2% FBS, 100 U/mL penicillin, and 100  $\mu\text{g}/\text{mL}$  streptomycin under controlled conditions of 37 °C and 5% CO<sub>2</sub>.

#### 4.3.2. Viability of the Host Cell

The viability of the host cell in the presence of PA was evaluated to determine the non-toxic concentration of the compound. The viability of BeWo cells treated with different concentrations of PA was assessed by MTT colorimetric test as described by Mosmann [56]. Briefly, in a 96-well plate, BeWo cells were placed at a concentration of  $3.0 \times 10^4$  cells/well for adhesion, after PA solutions were added at concentrations ranging from 4 to 256  $\mu\text{g}/\text{mL}$ . Tests using the solvent DMSO at 1.2% (percentage present in the highest concentration used) was also performed. Also, cells incubated with only culture medium were used as a positive control of cell viability.

Microplates were incubated for 24 h at 37 °C under a humidified atmosphere and 5% CO<sub>2</sub>. After this period, the supernatant was removed and 10  $\mu\text{L}$  of MTT (5 mg/mL) plus 90  $\mu\text{L}$  of supplemented RPMI 1640 was added; the microplates were again incubated as described above for 4 h, followed by the addition of 10% sodium dodecyl sulfate (SDS, Sigma) and 50% N,N-dimethyl formamide (Sigma) with further incubation for 30 min. MTT reduc-



tion was measured at 570 nm absorbance using a multi-well scanning spectrophotometer (Titertek Multiskan Plus, Flow Laboratories, McLean, VA, USA). The values obtained were expressed in percentage of cell viability (cell viability %), where the absorbance of cells incubated only with culture medium were considered 100% viable. Assays were performed with eight replicates and demonstrated graphically.

#### 4.3.3. Evaluation of Intracellular Proliferation of *Toxoplasma gondii*: $\beta$ -Galactosidase Activity

Concentrations of PA were used to evaluate its effect modulating the growth of a highly virulent strain of *T. gondii* (RH strain, 2F1 clone), using BeWo cells as a host, and the  $\beta$ -galactosidase colorimetric assay as previously described [57]. For this purpose, BeWo cells at a concentration of  $3.0 \times 10^4$  cells per well were placed in a 96-well microplate and infected with *T. gondii* tachyzoites at a multiplicity of infection (MOI) of 3:1 (ratio of parasites per cell). After three hours of infection, the medium was removed and the washing process was performed to remove excess parasites that did not infect the cells; afterwards, PA was added in concentrations ranging from 4 to 256  $\mu\text{g}/\text{mL}$ . The association of sulfadiazine (SDZ—Sigma) plus pyrimethamine (PYR—Sigma) was used, as gold-standard drugs, at concentrations of 200  $\mu\text{g}/\text{mL}$  and 8  $\mu\text{g}/\text{mL}$ , respectively. The concentrations of SDZ + PYR used have been reported as non-toxic to BeWo cells, but efficiently control the parasitism [58]. Infected BeWo cells were incubated with RPMI 1640 medium in the absence of any drug and used as negative control. The plates were then incubated for 24 h at 37 °C and 5%  $\text{CO}_2$ . To quantify the intracellular proliferation of *T. gondii*, the colorimetric  $\beta$ -galactosidase assay was used. The number of intracellular tachyzoites was calculated in comparison with the standard production of free tachyzoites (ranging from  $15.625 \times 10^3$  parasites to  $1 \times 10^6$ ). The percentage of proliferation (% *T. gondii* proliferation) was performed in comparison with the negative control (which shows 100% proliferation). Assays were performed with eight replicates and demonstrated graphically.

#### 4.3.4. Reversibility Assay

To assess the maintenance of the antiparasitic effects of PA, the reversibility assay was carried out as previously described [59,60], with the modifications described below. In brief, *T. gondii* tachyzoites were inoculated into BeWo cells at a MOI of 3:1. After 3 h of invasion, the cells were washed to eliminate the unattached parasites and used this basic experimental design to test the following situations: (1) following a 3-h invasion period, the intracellular parasites were permitted to proliferate under the influence of PA (at a concentration of 64  $\mu\text{g}/\text{mL}$ ) and SDZ + PYR (at concentrations of 200  $\mu\text{g}/\text{mL}$  and 8  $\mu\text{g}/\text{mL}$ , respectively), or in the absence of treatment, with only the culture medium (referred to as the untreated group) for a duration of 24 h. (2) the intracellular parasites were cultivated under identical conditions as described in (1), and after a 24-h treatment period, the cells were subjected to a thorough washing process, the culture medium was replaced, and the parasites were allowed to continue proliferating for an additional 24 h, this time in the absence of any treatment.

Subsequently, the reversibility rate was quantified as a percentage (reversibility of treatment %) at the 24-h mark after discontinuation of the treatment, with reference to both the untreated group (considered as 100% reversibility) and the corresponding treatment condition at the initial 24-h treatment period (utilized as the baseline for comparison). The assessment of *T. gondii* intracellular proliferation was conducted through the employment of the  $\beta$ -galactosidase assay. Assays were performed with eight replicates and demonstrated graphically.

### 4.4. Toxicity Assessment

#### 4.4.1. In Vitro System-Test

To carry out the cytotoxicity and genotoxicity experiments, Chinese hamster lung fibroblasts (V79 cells) were used. The cells were maintained in monolayer in plastic culture flasks (25  $\text{cm}^2$ ) with Eagle's minimal essential medium (DMEM) plus Nutrient Mixture F-10

(HAM-F10) 1:1 (Sigma) supplemented with 10% FBS, antibiotics (0.01 mg/mL streptomycin and 0.005 mg/mL penicillin; Sigma), and 2.38 mg/mL HEPES (Sigma), at 37 °C with 5% CO<sub>2</sub> atmosphere. Under these conditions, the average cell cycle time was 12 h and the cell line was used after the 4th passage. All the experiments were performed in triplicate.

The cytotoxicity was evaluated by the in vitro cell survival assay based on the ability of a single cell to grow into a colony. The clonogenic efficiency assay was used according to the protocol described by Franken, et al. [61]. The cells ( $5 \times 10^5$ ) were treated with CLO concentrations ranging from 4.88 to 1250 µg/mL for 3 h. In addition, a positive (methyl methanesulfonate, MMS, 110 µg/mL; Sigma), a negative (without treatment) and a solvent control (Tween 80 1%; Synth) were included.

The cytotoxicity results obtained by clonogenic efficiency assay led to the selection of three CLO concentrations (10, 20 and 40 µg/mL), which were used in the evaluation of the genotoxic potential by the micronucleus assay. The positive (MMS, 44 µg/mL), negative and solvent controls (Tween 80, 1%) were included.

Cytotoxicity was assessed using the IC<sub>50</sub> value (50% cell growth inhibition) as a response parameter, which was calculated with the GraphPad Prism program by plotting cell survival against the respective concentrations of the test compound. All experiments were repeated independently at least three times.

#### 4.4.2. In Vivo System-Test

For the experiment, male and heterogenic Swiss mice (*Mus musculus*), weighing 30–40 g, obtained from the central house of animals of the University of São Paulo, Ribeirão Preto, Brazil, were used. Animals were maintained in ventilated cages under controlled conditions of temperature ( $23 \pm 2$  °C), humidity ( $50 \pm 10\%$ ), light/dark cycle (12/12 h), food and water *ad libitum*. The study protocol was approved by the Ethics Committee for Animal Care of the University of Franca (process no. 2014/014).

In vivo studies were conducted to assess the genotoxicity of CLO and PA by micronucleus test in mouse bone marrow [44]. Animals were randomly divided in groups containing five animals each. For the treatments, CLO samples were diluted in 5% Tween 80, and PA samples were diluted in 5% DMSO (Sigma). Single doses of CLO (125, 250 and 500 mg/kg) and PA (1, 10 and 20 mg/kg) were administered by gavage in corresponding groups. Negative (water), Tween 80 (5%), DMSO (5%), and positive (MMS, 40 mg/kg, intraperitoneal) controls were included. The procedures and analyses were performed according to MacGregor, et al. [62].

#### 4.4.3. Toxicity Assessment in *Caenorhabditis elegans*

The in vivo model using *C. elegans* was used to assess the toxicity of PA; the procedure was performed as previously described in the literature [63]. The mutant strain *C. elegans* AU37 was used, the nematodes were cultivated in plates containing Nematode Growth Medium (NGM) and *Escherichia coli* OP50 kept in biochemical oxygen demand (BOD) at 16 °C for 72 h to obtain nematode eggs. After obtaining the eggs, the NGM plates were washed with M9 buffer to remove the larvae and eggs from the plates and transferred to tubes. A bleaching solution (hypochlorite + NaOH) was added to kill the adult larvae to obtain only the eggs. The eggs were added to a new NGM plate and incubated in BOD for 24 h at 16 °C. After this period, the eggs developed to the L1/L2 larval stage, the NGM plate was washed again, and the supernatant was then added to a new NGM plate containing *E. coli* OP50 and incubated in BOD for 24 h at 16 °C, for the larvae to synchronize to the L4 stage.

Toxicity assessment was performed in flat-bottomed 96-well microplates. Briefly, about 10 to 20 larvae of *C. elegans* in larval stage L4 were added to each well containing PA concentrations ranging from 31.25 to 1000 µg/mL. Toxicity control of the solvent used (1% DMSO) and positive control of larvae (larvae + culture medium) were carried out. The microplates were incubated in BOD at 25 °C for 72 h. Toxicity assessment was performed by counting live and/or dead larvae every 24 h under an inverted microscope. Larvae that

showed movement were considered as alive, and those that remained static after being touched were considered as dead. The lethal concentration (LC) capable of killing 50% of the larvae was calculated. Assays were performed in triplicate and demonstrated graphically.

#### 4.5. Statistical Analysis

The antiparasitic results were demonstrated as means  $\pm$  standard deviations (S.Ds.). All data were checked first for normal distribution. Significance differences were assessed by comparison with controls by use of either one-way analysis of variance (ANOVA), Tukey's or Dunnett's multiple comparisons post-tests for the parametric data. Statistical differences were considered significant at  $p < 0.05$ .

The results of the micronucleus assays were analyzed statistically by analysis of variance for completely randomized experiments, with calculation of F statistics and respective  $p$  values. In cases where  $p < 0.05$ , treatment means were compared with Tukey's test, the minimum significant difference was calculated for  $\alpha = 0.05$ .

## 5. Conclusions

Based on the results obtained in the present study, it can be concluded that CECL exhibits moderate anticariogenic activity, while CLO demonstrates good anticariogenic activity, possibly due to the presence of the active compound PA which shows similar MIC/MBC results against the evaluated bacteria. PA also exhibits antibiofilm properties, being able to inhibit 50% of biofilm formation at low concentrations and completely eliminate cells at higher concentrations. The compound (PA) also shows antiparasitic properties, inhibiting the *T. gondii* intracellular proliferation and maintaining its action even after treatment removal. Furthermore, the absence of genotoxicity and cytotoxicity of CLO and its major compound, PA, was revealed under experimental conditions.

**Author Contributions:** Conceptualization, M.B.S. and C.H.G.M.; methodology, M.B.S., V.C.O.d.S., S.C.T., N.B.S.S., P.F.d.O., S.D.O. and R.A.F.; validation, D.C.T., S.R.A., R.C.S.V., E.A.V.F., J.K.B. and C.H.G.M.; formal analysis, D.C.T., J.K.B. and C.H.G.M.; investigation, M.B.S., V.C.O.d.S., S.C.T., N.B.S.S., P.F.d.O., S.D.O. and R.A.F.; resources, J.K.B. and C.H.G.M.; data curation, D.C.T., S.R.A., R.C.S.V., E.A.V.F., J.K.B. and C.H.G.M.; writing—original draft preparation, M.B.S.; writing—review and editing, S.C.T., D.C.T., E.A.V.F., J.K.B. and C.H.G.M.; visualization, M.B.S. and C.H.G.M.; supervision, C.H.G.M.; project administration, J.K.B. and C.H.G.M.; funding acquisition, J.K.B. and C.H.G.M. All authors have read and agreed to the published version of the manuscript.

**Funding:** This work was funded by Fundação de Amparo à Pesquisa do Estado de São Paulo (FAPESP grant 2011/13630-7 and 2016/23012-2; FAPESP Scholarship 2016/20589-7), Coordenação de Aperfeiçoamento de Pessoal de Nível Superior (CAPES finance code 001, scholarship granted), and Conselho Nacional de Desenvolvimento Científico e Tecnológico (CNPq 310632/2013-7 and 307387/2016-0).

**Institutional Review Board Statement:** The animal study protocol was approved by the Ethics Committee for Animal Care of the University of Franca (process no. 2014/014).

**Informed Consent Statement:** Not applicable.

**Data Availability Statement:** All data generated and analyzed during this study are available from the corresponding author upon reasonable request.

**Conflicts of Interest:** The authors declare no conflict of interest.

## References

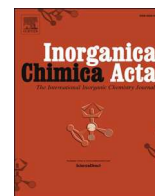
1. Arweiler, N.B.; Netuschil, L. The Oral Microbiota. *Adv. Exp. Med. Biol.* **2016**, *902*, 45–60. [[CrossRef](#)] [[PubMed](#)]
2. Lamont, R.J.; Koo, H.; Hajishengallis, G. The oral microbiota: Dynamic communities and host interactions. *Nat. Rev. Microbiol.* **2018**, *16*, 745–759. [[CrossRef](#)] [[PubMed](#)]
3. Valm, A.M. The Structure of Dental Plaque Microbial Communities in the Transition from Health to Dental Caries and Periodontal Disease. *J. Mol. Biol.* **2019**, *431*, 2957–2969. [[CrossRef](#)] [[PubMed](#)]
4. Lu, Y.; Lin, Y.; Li, M.; He, J. Roles of Streptococcus mutans-Candida albicans interaction in early childhood caries: A literature review. *Front. Cell. Infect. Microbiol.* **2023**, *13*, 1151532. [[CrossRef](#)]

5. Wen, P.Y.F.; Chen, M.X.; Zhong, Y.J.; Dong, Q.Q.; Wong, H.M. Global Burden and Inequality of Dental Caries, 1990 to 2019. *J. Dent. Res.* **2022**, *101*, 392–399. [[CrossRef](#)]
6. Choo, A.; Delac, D.M.; Messer, L.B. Oral hygiene measures and promotion: Review and considerations. *Aust. Dent. J.* **2001**, *46*, 166–173. [[CrossRef](#)]
7. Dubey, J.P.; Lago, E.G.; Gennari, S.M.; Su, C.; Jones, J.L. Toxoplasmosis in humans and animals in Brazil: High prevalence, high burden of disease, and epidemiology. *Parasitology* **2012**, *139*, 1375–1424. [[CrossRef](#)]
8. Dubey, J.P.; Murata, F.H.A.; Cerqueira-Cezar, C.K.; Kwok, O.C.H.; Villena, I. Congenital toxoplasmosis in humans: An update of worldwide rate of congenital infections. *Parasitology* **2021**, *148*, 1406–1416. [[CrossRef](#)]
9. Uddin, A.; Hossain, D.; Ahsan, M.I.; Atikuzzaman, M.; Karim, M.R. Review on diagnosis and molecular characterization of *Toxoplasma gondii* in humans and animals. *Trop. Biomed.* **2021**, *38*, 511–539. [[CrossRef](#)]
10. Abdelbaset, A.E.; Abushahba, M.F.N.; Igarashi, M. *Toxoplasma gondii* in humans and animals in Japan: An epidemiological overview. *Parasitol. Int.* **2022**, *87*, 102533. [[CrossRef](#)]
11. Robert-Gangneux, F.; Darde, M.L. Epidemiology of and diagnostic strategies for toxoplasmosis. *Clin. Microbiol. Rev.* **2012**, *25*, 264–296. [[CrossRef](#)] [[PubMed](#)]
12. Mrzljak, A.; Novak, R.; Pandak, N.; Tabain, I.; Franusic, L.; Barbic, L.; Bogdanic, M.; Savic, V.; Mikulic, D.; Pavicic-Saric, J.; et al. Emerging and neglected zoonoses in transplant population. *World J. Transplant.* **2020**, *10*, 47–63. [[CrossRef](#)] [[PubMed](#)]
13. Milne, G.; Webster, J.P.; Walker, M. *Toxoplasma gondii*: An Underestimated Threat? *Trends Parasitol.* **2020**, *36*, 959–969. [[CrossRef](#)] [[PubMed](#)]
14. Dunay, I.R.; Gajurel, K.; Dhakal, R.; Liesenfeld, O.; Montoya, J.G. Treatment of Toxoplasmosis: Historical Perspective, Animal Models, and Current Clinical Practice. *Clin. Microbiol. Rev.* **2018**, *31*, e00057-17. [[CrossRef](#)]
15. Newman, D.J.; Cragg, G.M. Natural Products as Sources of New Drugs over the Nearly Four Decades from 01/1981 to 09/2019. *J. Nat. Prod.* **2020**, *83*, 770–803. [[CrossRef](#)]
16. Arruda, C.; Aldana Mejía, J.A.; Ribeiro, V.P.; Gambeta Borges, C.H.; Martins, C.H.G.; Sola Veneziani, R.C.; Ambrósio, S.R.; Bastos, J.K. Occurrence, chemical composition, biological activities and analytical methods on *Copaifera* genus—A review. *Biomed. Pharmacother.* **2019**, *109*, 1–20. [[CrossRef](#)]
17. Da Trindade, R.; da Silva, J.K.; Setzer, W.N. *Copaifera* of the Neotropics: A Review of the Phytochemistry and Pharmacology. *Int. J. Mol. Sci.* **2018**, *19*, 1511. [[CrossRef](#)]
18. Mohd-Fuat, A.R.; Kofi, E.A.; Allan, G.G.C. Mutagenic and cytotoxic properties of three herbal plants from Southeast Asia. *Trop. Biomed.* **2007**, *24*, 49–59.
19. Lemos, M.; Santin, J.R.; Mizuno, C.S.; Boeing, T.; de Sousa, J.P.B.; Nanayakkara, D.; Bastos, J.K.; de Andrade, S.F. *Copaifera langsdorffii*: Evaluation of potential gastroprotective of extract and isolated compounds obtained from leaves. *Rev. Bras. Farmacogn.* **2015**, *25*, 238–245. [[CrossRef](#)]
20. Veiga Junior, V.F.; Pinto, A.C. O GÊNERO *Copaifera* L. *Química Nova* **2002**, *25*, 273–286. [[CrossRef](#)]
21. Pieri, F.A.; Mussi, M.C.; Moreira, M.A.S. Óleo de copaiba (*Copaifera* sp.): Histórico, extração, aplicações industriais e propriedades medicinais. *Rev. Bras. Plantas Med.* **2009**, *11*, 465–472. [[CrossRef](#)]
22. De Souza, P.A.; Rangel, L.P.; Oigman, S.S.; Elias, M.M.; Ferreira-Pereira, A.; De Lucas, N.C.; Leitão, G.G. Isolation of two bioactive diterpenic acids from *Copaifera glycyarpa* oleoresin by high-speed counter-current chromatography. *Phytochem. Anal.* **2010**, *21*, 539–543. [[CrossRef](#)] [[PubMed](#)]
23. Leandro, L.M.; Vargas, F.d.S.; Barbosa, P.C.S.; Neves, J.K.O.; da Silva, J.A.; da Veiga-Junior, V.F. Chemistry and biological activities of terpenoids from copaiba (*Copaifera* spp.) oleoresins. *Molecules* **2012**, *17*, 3866–3889. [[CrossRef](#)]
24. Santos, A.O.; Ueda-Nakamura, T.; Dias Filho, B.P.; Veiga Junior, V.F.; Pinto, A.C.; Nakamura, C.V. Effect of Brazilian copaiba oils on *Leishmania amazonensis*. *J. Ethnopharmacol.* **2008**, *120*, 204–208. [[CrossRef](#)] [[PubMed](#)]
25. Reyes-Trejo, B.; Sanchez-Mendoza, M.E.; Becerra-Garcia, A.A.; Cedillo-Portugal, E.; Castillo-Henkel, C.; Arrieta, J. Bioassay-guided isolation of an anti-ulcer diterpenoid from *Croton reflexifolius*: Role of nitric oxide, prostaglandins and sulfhydryls. *J. Pharm. Pharmacol.* **2008**, *60*, 931–936. [[CrossRef](#)] [[PubMed](#)]
26. Rodriguez-Silverio, J.; Sanchez-Mendoza, M.E.; Rocha-Gonzalez, H.I.; Reyes-Garcia, J.G.; Flores-Murrieta, F.J.; Lopez-Lorenzo, Y.; Quinonez-Bastidas, G.N.; Arrieta, J. Evaluation of the Antinociceptive, Antiallodynic, Antihyperalgesic and Anti-Inflammatory Effect of Polyalthic Acid. *Molecules* **2021**, *26*, 2921. [[CrossRef](#)] [[PubMed](#)]
27. Cicek, S.S.; Wenzel-Storjohann, A.; Girreser, U.; Tasdemir, D. Biological Activities of Two Major Copaiba Diterpenoids and Their Semi-synthetic Derivatives. *Rev. Bras. Farmacogn.* **2020**, *30*, 18–27. [[CrossRef](#)]
28. Pfeifer Barbosa, A.L.; Wenzel-Storjohann, A.; Barbosa, J.D.; Zidorn, C.; Peifer, C.; Tasdemir, D.; Cicek, S.S. Antimicrobial and cytotoxic effects of the *Copaifera reticulata* oleoresin and its main diterpene acids. *J. Ethnopharmacol.* **2019**, *233*, 94–100. [[CrossRef](#)]
29. Huang, D.; Qing, S.; Zeng, G.; Wang, Y.; Guo, H.; Tan, J.; Zhou, Y. Lipophilic components from *Fructus Viticis Negundo* and their anti-tumor activities. *Fitoterapia* **2013**, *86*, 144–148. [[CrossRef](#)]
30. Sánchez-Mendoza, M.E.; Reyes-Trejo, B.; de la Rosa, L.; Rodríguez-Silverio, J.; Castillo-Henkel, C.; Arrieta, J. Polyalthic Acid Isolated from *Croton reflexifolius* has Relaxing Effect in Guinea Pig Tracheal Smooth Muscle. *Pharm. Biol.* **2009**, *46*, 800–807. [[CrossRef](#)]
31. Holetz, F.B.; Pessini, G.L.; Sanches, N.R.; Cortez, D.A.; Nakamura, C.V.; Filho, B.P. Screening of some plants used in the Brazilian folk medicine for the treatment of infectious diseases. *Mem. Inst. Oswaldo Cruz* **2002**, *97*, 1027–1031. [[CrossRef](#)] [[PubMed](#)]

32. Abrão, F.; Alves, J.A.; Andrade, G.; de Oliveira, P.F.; Ambrosio, S.R.; Veneziani, R.C.S.; Tavares, D.C.; Bastos, J.K.; Martins, C.H.G. Antibacterial Effect of *Copaifera duckei* Dwyer Oleoresin and Its Main Diterpenes against Oral Pathogens and Their Cytotoxic Effect. *Front. Microbiol.* **2018**, *9*, 201. [[CrossRef](#)] [[PubMed](#)]
33. Carvalho, J.C.; Cascon, V.; Possebon, L.S.; Morimoto, M.S.; Cardoso, L.G.; Kaplan, M.A.; Gilbert, B. Topical antiinflammatory and analgesic activities of *Copaifera duckei* dwyer. *Phytother. Res.* **2005**, *19*, 946–950. [[CrossRef](#)] [[PubMed](#)]
34. Cascon, V.; Gilbert, B. Characterization of the chemical composition of oleoresins of *Copaifera guianensis* Desf., *Copaifera duckei* Dwyer and *Copaifera multijuga* Hayne. *Phytochemistry* **2000**, *55*, 773–778. [[CrossRef](#)]
35. Carneiro, L.; Bianchi, T.; da Silva, J.; Oliveira, L.; Borges, C.; Lemes, D.; Bastos, J.; Veneziani, R.; Ambrósio, S. Development and Validation of a Rapid and Reliable RP-HPLC-PDA Method for the Quantification of Six Diterpenes in *Copaifera duckei*, *Copaifera reticulata* and *Copaifera multijuga* Oleoresins. *J. Braz. Chem. Soc.* **2017**, *29*, 729–737. [[CrossRef](#)]
36. Stewart, P.S.; Costerton, J.W. Antibiotic resistance of bacteria in biofilms. *Lancet* **2001**, *358*, 135–138. [[CrossRef](#)]
37. Fux, C.A.; Stoodley, P.; Hall-Stoodley, L.; Costerton, J.W. Bacterial biofilms: A diagnostic and therapeutic challenge. *Expert. Rev. Anti Infect. Ther.* **2003**, *1*, 667–683. [[CrossRef](#)]
38. Richards, J.J.; Melander, C. Controlling bacterial biofilms. *ChemBiochem* **2009**, *10*, 2287–2294. [[CrossRef](#)]
39. Mooney, J.A.; Pridgen, E.M.; Manasherob, R.; Suh, G.; Blackwell, H.E.; Barron, A.E.; Bollyky, P.L.; Goodman, S.B.; Amanatullah, D.F. Periprosthetic bacterial biofilm and quorum sensing. *J. Orthop. Res.* **2018**, *36*, 2331–2339. [[CrossRef](#)]
40. Izumi, E.; Ueda-Nakamura, T.; Veiga-Junior, V.F.; Nakamura, C.V. Toxicity of oleoresins from the genus *Copaifera* in *Trypanosoma cruzi*: A comparative study. *Planta Med.* **2013**, *79*, 952–958. [[CrossRef](#)]
41. Mizuno, C.S.; Souza, A.B.; Tekwani, B.L.; Ambrosio, S.R.; Veneziani, R.C. Synthesis and biological evaluation of polyalthic acid derivatives for the treatment of neglected diseases. *Bioorg. Med. Chem. Lett.* **2015**, *25*, 5529–5531. [[CrossRef](#)]
42. Teixeira, S.C.; Rosini, A.M.; de Souza, G.; Martinez, A.F.; Silva, R.J.; Ambrosio, S.R.; Veneziani, R.C.; Bastos, J.K.; Martins, C.H.; Barbosa, B.F.; et al. Polyalthic acid and oleoresin from *Copaifera trapezifolia* Hayne reduce *Toxoplasma gondii* growth in human villous explants, even triggering an anti-inflammatory profile. *Exp. Parasitol.* **2023**, *250*, 108534. [[CrossRef](#)] [[PubMed](#)]
43. Furtado, R.A.; de Oliveira, P.F.; Senedese, J.M.; Ozelin, S.D.; de Souza, L.D.R.; Leandro, L.F.; de Oliveira, W.L.; da Silva, J.J.M.; Oliveira, L.C.; Rogez, H.; et al. Assessment of genotoxic activity of oleoresins and leaves extracts of six *Copaifera* species for prediction of potential human risks. *J. Ethnopharmacol.* **2018**, *221*, 119–125. [[CrossRef](#)] [[PubMed](#)]
44. OECD. Test No. 474: Mammalian Erythrocyte Micronucleus Test; OECD: Paris, France, 2014.
45. Sanchez-Me, M.E.; Garcia-Tap, M.; Garcia San, J.R.; Arrieta, J.; Olivares-C, I.M.; Santiago-C, J.A.; Ahumada-An, A.K. Effects of Polyalthic Acid from *Croton reflexifolius* on Viability of Cancerous Cells. *Int. J. Pharmacol.* **2017**, *13*, 286–291. [[CrossRef](#)]
46. Miyazawa, M.; Shimamura, H.; Nakamura, S.-I.; Kameoka, H. Antimutagenic Activity of (+)-Polyalthic Acid from *Vitex rotundifolia*. *J. Agric. Food Chem.* **1995**, *43*, 3012–3015. [[CrossRef](#)]
47. Ruszkiewicz, J.A.; Pinkas, A.; Miah, M.R.; Weitz, R.L.; Lawes, M.J.A.; Akinyemi, A.J.; Ijomone, O.M.; Aschner, M. *C. elegans* as a model in developmental neurotoxicology. *Toxicol. Appl. Pharmacol.* **2018**, *354*, 126–135. [[CrossRef](#)] [[PubMed](#)]
48. Carreras, C.R.; Rossomando, P.C.; Giordano, O.S. Ent-labdanes in eupatorium buniifolium. *Phytochemistry* **1998**, *48*, 1031–1034. [[CrossRef](#)]
49. CLSI. *Methods for Dilution Antimicrobial Susceptibility Tests for Bacteria That Grow Aerobically*. Document, 9th ed.; M7-A9; Clinical and Laboratory Standards Institute: Wayne, PA, USA, 2012.
50. Sarker, S.D.; Nahar, L.; Kumarasamy, Y. Microtitre plate-based antibacterial assay incorporating resazurin as an indicator of cell growth, and its application in the in vitro antibacterial screening of phytochemicals. *Methods* **2007**, *42*, 321–324. [[CrossRef](#)]
51. Nayak, A.; Sowmya, B.R.; Gandla, H.; Kottrashetti, V.; Ingalagi, P.; Srinivas, V.S.C. Determination and comparison of antimicrobial activity of aqueous and ethanolic extracts of *Amorphophallus paeoniifolius* on periodontal pathogens: An in vitro study. *J. Indian Soc. Periodontol.* **2023**, *27*, 40–44. [[CrossRef](#)]
52. Wei, G.X.; Campagna, A.N.; Bobek, L.A. Effect of MUC7 peptides on the growth of bacteria and on *Streptococcus mutans* biofilm. *J. Antimicrob. Chemother.* **2006**, *57*, 1100–1109. [[CrossRef](#)]
53. Sandberg, M.; Maattanen, A.; Peltonen, J.; Vuorela, P.M.; Fallarero, A. Automating a 96-well microtitre plate model for *Staphylococcus aureus* biofilms: An approach to screening of natural antimicrobial compounds. *Int. J. Antimicrob. Agents* **2008**, *32*, 233–240. [[CrossRef](#)] [[PubMed](#)]
54. Drewlo, S.; Baczyk, D.; Dunk, C.; Kingdom, J. Fusion assays and models for the trophoblast. *Methods Mol. Biol.* **2008**, *475*, 363–382. [[CrossRef](#)] [[PubMed](#)]
55. Chen, Q.W.; Dong, K.; Qin, H.X.; Yang, Y.K.; He, J.L.; Li, J.; Zheng, Z.W.; Chen, D.L.; Chen, J.P. Direct and Indirect Inhibition Effects of Resveratrol against *Toxoplasma gondii* Tachyzoites In Vitro. *Antimicrob. Agents Chemother.* **2019**, *63*, e01233-18. [[CrossRef](#)] [[PubMed](#)]
56. Mosmann, T. Rapid colorimetric assay for cellular growth and survival: Application to proliferation and cytotoxicity assays. *J. Immunol. Methods* **1983**, *65*, 55–63. [[CrossRef](#)]
57. Teo, C.F.; Zhou, X.W.; Bogyo, M.; Carruthers, V.B. Cysteine protease inhibitors block *Toxoplasma gondii* microneme secretion and cell invasion. *Antimicrob. Agents Chemother.* **2007**, *51*, 679–688. [[CrossRef](#)]
58. Da Silva, R.J.; Gomes, A.O.; Franco, P.S.; Pereira, A.S.; Milian, I.C.B.; Ribeiro, M.; Fiorenzani, P.; Dos Santos, M.C.; Mineo, J.R.; da Silva, N.M.; et al. Enrofloxacin and Toltrazuril Are Able to Reduce *Toxoplasma gondii* Growth in Human BeWo Trophoblastic Cells and Villous Explants from Human Third Trimester Pregnancy. *Front. Cell. Infect. Microbiol.* **2017**, *7*, 340. [[CrossRef](#)]

59. Adeyemi, O.S.; Murata, Y.; Sugi, T.; Kato, K. Inorganic nanoparticles kill *Toxoplasma gondii* via changes in redox status and mitochondrial membrane potential. *Int. J. Nanomed.* **2017**, *12*, 1647–1661. [[CrossRef](#)]
60. Kamau, E.T.; Srinivasan, A.R.; Brown, M.J.; Fair, M.G.; Caraher, E.J.; Boyle, J.P. A focused small-molecule screen identifies 14 compounds with distinct effects on *Toxoplasma gondii*. *Antimicrob. Agents Chemother.* **2012**, *56*, 5581–5590. [[CrossRef](#)]
61. Franken, N.A.; Rodermond, H.M.; Stap, J.; Haveman, J.; van Bree, C. Clonogenic assay of cells in vitro. *Nat. Protoc.* **2006**, *1*, 2315–2319. [[CrossRef](#)]
62. MacGregor, J.T.; Heddle, J.A.; Hite, M.; Margolin, B.H.; Ramel, C.; Salamone, M.F.; Tice, R.R.; Wild, D. Guidelines for the conduct of micronucleus assays in mammalian bone marrow erythrocytes. *Mutat. Res.* **1987**, *189*, 103–112. [[CrossRef](#)]
63. Singulani, J.L.; Scorzoni, L.; Gomes, P.C.; Nazare, A.C.; Polaquini, C.R.; Regasini, L.O.; Fusco-Almeida, A.M.; Mendes-Giannini, M.J.S. Activity of gallic acid and its ester derivatives in *Caenorhabditis elegans* and zebrafish (*Danio rerio*) models. *Future Med. Chem.* **2017**, *9*, 1863–1872. [[CrossRef](#)] [[PubMed](#)]

**Disclaimer/Publisher’s Note:** The statements, opinions and data contained in all publications are solely those of the individual author(s) and contributor(s) and not of MDPI and/or the editor(s). MDPI and/or the editor(s) disclaim responsibility for any injury to people or property resulting from any ideas, methods, instructions or products referred to in the content.



Research paper

## Crystal design, spectroscopic analyses and antibacterial study of new carbazate ligands and their Cu(II) complexes

Eduardo de A. Duarte<sup>a</sup>, Mariana B. Santiago<sup>b</sup>, Nagela B.S. Silva<sup>b</sup>, Carlos H.G. Martins<sup>b</sup>,  
Claudia C. Gatto<sup>a,\*</sup>

<sup>a</sup> Laboratory of Inorganic Synthesis and Crystallography, Institute of Chemistry, University of Brasilia, Campus Darcy Ribeiro, Brasilia-DF 70904-970, Brazil

<sup>b</sup> Laboratory of Antimicrobial Testing, Institute of Biomedical Sciences, University of Uberlândia, Campus Umuarama, Uberlândia-MG 38405-320, Brazil



## ARTICLE INFO

## Keywords:

Carbazates  
Copper complexes  
Crystal structures  
Hirshfeld surface  
Antibacterial activity

## ABSTRACT

The current work reports the synthesis and crystal structures of two carbazate ligands, 2-hydroxyacetophenone-methylcarbazate (HL<sup>1</sup>) and 2-hydroxyacetophenone-benzylcarbazate (HL<sup>2</sup>), and their Cu(II) complexes [Cu(L<sup>1</sup>)(CH<sub>3</sub>OH)]<sub>2</sub> (1) and [Cu(L<sup>2</sup>)<sub>n</sub>] (2). All compounds were characterized by X-ray single-crystal analysis, spectroscopic and physicochemical methods. Intermolecular interactions were analyzed quantitatively with the 3D Hirshfeld surface and the 2D fingerprint plots. The dimeric complex (1) exhibits a μ<sub>2</sub>-oxo group located between the two metal ions, an ONO-donor system, and a coordinated methanol molecule with a square-pyramidal geometry to the metal ions. The polymeric complex (2) shows the Cu(II) atom tetracoordinate, bonded to two anionic carbazate, through the ONO-donor system of one molecule, and to a deprotonated nitrogen atom from the second molecule of the ligand. This one-dimensional network shows the metal center with a square planar geometry. The antibacterial properties of the free ligands and metal complexes have been evaluated against periodontopathogenic bacterial strains and were observed to increase the activity after the complexation of the carbazates.

## 1. Introduction

Studies of Schiff bases transition metal complexes are in constant evolution due to the several possibilities of applications. The preparation of the metal complexes is via the addition of the precursor metal salt and the Schiff base in appropriate and suitable experimental conditions. The Schiff bases are an important class of organic compounds widely studied due to their biological and pharmaceutical properties, such as antimicrobial, antifungal, and antimalarial activity.<sup>1–5</sup>

The carbazates are Schiff bases that have the potential to coordinate and form stable transition metal complexes with different geometries. They are obtained through a condensation reaction between an aldehyde or ketone and a primary amine. Generally, the donor atoms can coordinate with several different metal ions. There are many reported studies in the literature with similar Schiff bases, such as hydrazones, semicarbazones, dithiocarbazates and their Ni(II), Cu(II), Co(II), Zn(II) complexes.<sup>6–8</sup> However, carbazate ligands and their metal complexes are not yet expansively explored. There are very few recent papers in the

literature on this type of ligand.<sup>9,10</sup>

There is great interest in carbazate and its complexes due to its pharmacological and biological applications. These compounds also show cytotoxic potential against different cancer cells and are successful when tested against Gram-positive and Gram-negative bacteria.<sup>1–3</sup>

Anaerobic bacteria such as *Porphyromonas gingivalis*, *Actinomyces naeslundii*, and *Fusobacterium nucleatum* are part of the oral microbiota, which can be permanent or resident in the oral environment. When dysbiosis occurs in this system, bacteria proliferate and can cause infections, the most commonly associated with these bacteria being gingivitis, periodontitis, and endodontic infection. However, oral microorganisms are also associated with other chronic diseases e.g. inflammatory bowel disease, cancers, cardiovascular diseases, Alzheimer's disease, diabetes, rheumatoid arthritis, and preterm birth.<sup>11</sup>

In this sense, this work reports the study of new carbazate ligands and their dimeric and polymeric Cu(II) complexes. The compounds were analyzed by single crystal X-ray diffraction, FT-IR, UV-vis, NMR, Mass

\* Corresponding author at: Laboratory of Inorganic Synthesis and Crystallography, University of Brasilia (IQ-UnB), Campus Universitário Darcy Ribeiro, Brasília-DF CEP 70904-970, Brazil.

E-mail address: [cggatto@gmail.com](mailto:cggatto@gmail.com) (C.C. Gatto).

<https://doi.org/10.1016/j.ica.2023.121421>

Received 26 October 2022; Received in revised form 10 January 2023; Accepted 31 January 2023

Available online 2 February 2023

0020-1693/© 2023 Elsevier B.V. All rights reserved.

spectrometry, and Hirshfeld surfaces. Furthermore, the biological activity was evaluated against periodontopathogenic bacteria strains. The results of the study of the antibacterial activity of bacteria related to periodontal infections evaluated show an interesting comparison between the complexes and the free ligands.

## 2. Experimental section

### 2.1. Materials, methods and instruments

All reagents and solvents used were obtained from commercial sources and used as received. Elemental analyses were performed with Perkin Elmer/Series II 2400 analyzer. The infrared spectra were recorded from KBr pellets (4000–400  $\text{cm}^{-1}$ ) using FT-IR Varian 640. UV–vis-NIR Varian Cary 5000 spectrophotometer and the concentration used for all analyses was 2  $\mu\text{M}$  and 20  $\mu\text{M}$  in methanol (MeOH), N, N-dimethylformamide (DMF) and dimethylsulfoxide (DMSO). The ESI-MS and ESI-MS/MS spectra were obtained from the AB Sciex TripleTOF 5600+ spectrometer equipment, in positive mode, 5500 V and 200  $^{\circ}\text{C}$ .  $^1\text{H}$  nuclear magnetic resonance spectra were collected on a Varian Mercury plus (300 MHz), with TMS as an internal reference and DMSO- $d_6$  as solvent. Electrospray ionization mass spectrometry analysis (ESI-MS) was performed on an AB Sciex Triple TOF 5600+ mass spectrometer in positive mode, with a voltage of 5500 V and source temperature of 200  $^{\circ}\text{C}$ .

### 2.2. Synthesis of 2-hydroxyacetophenone N(4)-methylcarbazate ( $\text{HL}^1$ )

The synthesis of  $\text{HL}^1$  was prepared similarly to the literature procedure.<sup>12–13</sup> 1 mmol (90.7 mg) of methylcarbazate was solubilized in 20 mL of ethanol and 1 mmol (136.15 mg, 0.12 mL) of 2-hydroxyacetophenone was added. The reaction was carried out under reflux conditions for 3 h. Colorless crystals were obtained directly from the mother solution by slow evaporation of solvent after a few days. Yield: 81.16 % (168.87 mg) Melting point: 166–168  $^{\circ}\text{C}$ . Elemental analysis calculated for  $\text{C}_{10}\text{H}_{12}\text{N}_2\text{O}_3$ : C, 57.69; H, 5.81; N, 13.45 and found: C, 57.48; H, 6.22; N, 13.43. Selected IR bands (KBr,  $\nu/\text{cm}^{-1}$ ):  $\nu(\text{N—H})$  3292,  $\nu(\text{O—H})$  3224,  $\nu(\text{C=O})$  1712,  $\nu(\text{C=N})$  1611,  $\nu(\text{C—O})$  1380,  $\nu(\text{N—N})$  1174,  $\delta(\text{phenol})$  762.  $^1\text{H}$  RMN (DMSO- $d_6$   $\delta$ , ppm): 2.31 (s, 3H,  $\text{CH}_3$ ), 3.76 (s, 3H,  $\text{CH}_3$ ), 6.87 (t, 1H, Ar), 7.26 (t, 1H, Ar), 7.53 (d, 1H, Ar), 7.95 (d, 1H, Ar) e 10.78 (s, 1H, N—H). ESI(+)-MS/MS ( $m/z$ ): 219.0464; 209.0917; 141.0876; 100.0758; 74.0614.

### 2.3. Synthesis of 2-hydroxyacetophenone N(4)-benzylcarbazate ( $\text{HL}^2$ )

In a round bottom flask containing 20 mL of ethanol, 1 mmol (167.8 mg) of benzylcarbazate was added, followed by 1 mmol (136.15 mg, 0.12 mL) of 2-hydroxyacetophenone. The reaction was carried out under heating, stirring and refluxing for 3 h. Colorless crystals were obtained after a few days directly from the mother solution. Yield: 92.75 % (263.70 mg) Melting range: 132–133  $^{\circ}\text{C}$ . Elemental analysis calculated for  $\text{C}_{16}\text{H}_{16}\text{N}_2\text{O}_3$ : C, 67.59; H, 5.67; N, 9.85 and found: C, 67.93; H, 5.95; N, 9.96. Selected IR bands (KBr,  $\nu/\text{cm}^{-1}$ ):  $\nu(\text{N—H})$  3236,  $\nu(\text{O—H})$  3164,  $\nu(\text{C=O})$  1707,  $\nu(\text{C=N})$  1620,  $\nu(\text{C—O})$  1353,  $\nu(\text{N—N})$  1150,  $\delta(\text{phenol})$  756. RMN  $^1\text{H}$  (DMSO- $d_6$   $\delta$ , ppm): 2.31 (s, 3H,  $\text{CH}_3$ ), 5.25 (s, 2H,  $\text{CH}_2$ ), 6.88–7.56 (m, 9H, Ar), 10.90 (s, 1H, N—H) e 12.89 (s, 1H, O—H). ESI (+)-MS/MS ( $m/z$ ): 285.1227; 219.0464; 100.0762; 79.0240; 74.0615.

### 2.4. Synthesis of the ( $\mu_2$ -phenoxo)bis(2-hydroxyacetophenone-methylcarbazate) bis(methanol)dicopper(II), $[\text{Cu}(\text{L}^1)(\text{CH}_3\text{OH})]_2$ (1)

The complex (1) was obtained by reaction of 0.1 mmol (20.81 mg) of the  $\text{HL}^1$  and 0.05 mmol (9.08 mg) of  $\text{Cu}(\text{CH}_3\text{COO})_2 \cdot x\text{H}_2\text{O}$ . The salt was solubilized in 5 mL of methanol and the ligand was solubilized in 5 mL of acetonitrile. The mixture was kept under heat and reflux for 2 h. The final green solution was left at room temperature for the slow

evaporation of the solvent. After two weeks green suitable to single crystal X-ray analysis were obtained directly from the mother solution. Yield: 47.38 % (14.30 mg). Melting range: 238–240  $^{\circ}\text{C}$ . Elemental analysis calculated for  $\text{C}_{11}\text{H}_{14}\text{CuN}_2\text{O}_4$ : C, 43.78; H, 4.68; N, 9.28 and found: C, 43.38; H, 4.71; N, 9.23. Selected IR bands (KBr,  $\nu/\text{cm}^{-1}$ ):  $\nu(\text{O—H})$  3292 ( $\text{CH}_3\text{OH}$ ) e 3414 ( $\text{H}_2\text{O}$ ),  $\nu(\text{C=N})$  1598,  $\nu(\text{C—O})$  1365,  $\nu(\text{N—N})$  1172,  $\delta(\text{phenol})$  756. ESI(+)-MS/MS ( $m/z$ ): 457.2725; 343.0576; 270.0056; 231.0730; 217.1041; 209.0909; 173.9835; 137.5457; 74.0611.

### 2.5. Synthesis of the catena-(2-hydroxyacetophenone-benzylcarbazate) copper(II), $[\text{Cu}(\text{L}^2)]_n$ (2)

The complex (2) was synthesized by a reaction between 0.1 mmol (28.43 mg) of the  $\text{HL}^2$  dissolved in 5 mL of acetonitrile and 0.1 mmol (18.16 mg) of  $\text{Cu}(\text{CH}_3\text{COO})_2 \cdot x\text{H}_2\text{O}$  dissolved in 5 mL of methanol. The reaction was under stirring, heating and reflux for 2 h. Green solution and a dark green precipitate were obtained which was filtered and recrystallized from DMF. After three weeks, green crystals suitable for X-ray diffraction were obtained. Yield: 78.53 % (27.16 mg). Melting range: 208–210  $^{\circ}\text{C}$ .  $\text{C}_{16}\text{H}_{14}\text{CuN}_2\text{O}_3$ : C, 55.57; H, 4.08; N, 8.10 and found: C, 55.18; H, 4.05; N, 8.56. Selected IR bands (KBr,  $\nu/\text{cm}^{-1}$ ):  $\nu(\text{O—H})$  3421 ( $\text{H}_2\text{O}$ ),  $\nu(\text{C=N})$  1599,  $\nu(\text{C—O})$  1339,  $\nu(\text{N—N})$  1121,  $\delta(\text{phenol})$  757. ESI (+)-MS/MS ( $m/z$ ): 419.0899; 346.0366; 307.1047; 285.1225; 137.5453; 74.0610.

### 2.6. Crystal structure determination

The X-ray diffraction data were collected at room temperature (296 K) on a Bruker CCD SMART APEX II single crystal diffractometer with Mo  $\text{K}\alpha$  radiation (0.71073  $\text{\AA}$ ). SADABS<sup>14</sup> was used to scale the data and perform the multi-scan absorption correction. The structures were solved by direct methods using SHELXS-97<sup>15</sup> and subsequent Fourier-difference map analyses yielded the positions of the non-hydrogens atoms, the refinement was performed using SHELXL-2018<sup>16</sup>. The hydrogen atoms of the amino and hydroxyl group of  $\text{HL}^1$  and  $\text{HL}^2$  and the methyl group of  $\text{HL}^2$  were localized in the Fourier-difference map. The other hydrogen atoms were placed in idealized positions and refined with riding models. Molecular graphics were generated via OLEX2 software.<sup>17</sup> Crystal data, experimental details and refinement results are summarized in Table 1.

### 2.7. Computational details

The software CrystalExplorer 17.5<sup>18</sup> was used to calculate the Hirshfeld surfaces (HS) and related 2D-fingerprint plots<sup>18–20</sup>, using the Crystallographic Information Files (CIFs) obtained by single-crystal X-ray. A fixed color scale of  $-0.4277$  (red) to 1.1543 (blue) was used to map the 3D  $d_{\text{norm}}$  surfaces (normalized contact distances) for the ligands and complexes. A 2D-fingerprint plot of  $d_i$  versus  $d_e$  was used to identify and quantify in percentages the intermolecular interactions of the compounds. The full interaction maps were produced using the software Mercury<sup>21</sup>. The interaction maps are indicative of hydrogen bond acceptors (red), donors (blue), and hydrophobic interactions (brown), respectively.

### 2.8. Antibacterial activity

#### 2.8.1. Tested bacteria

The bacteria assessed in the present work were obtained from the American Type Culture Collection (ATCC) and were maintained in the culture collection of the Laboratory of Antimicrobial Testing (LEA) of the Federal University of Uberlândia, State of Minas Gerais, Brazil: *Actinomyces naeslundii* (ATCC 19039), *Peptostreptococcus anaerobius* (ATCC 27337), *Veillonella parvula* (ATCC 17745), *Porphyromonas gingivalis* (ATCC 49417), and *Fusobacterium nucleatum* (ATCC 10953).



**Table 1**  
X-ray structure data collection and refinement parameters for compounds HL<sup>1</sup>, HL<sup>2</sup>, (1) and (2).

	HL <sup>1</sup>	HL <sup>2</sup>	(1)	(2)
Empirical formula	C <sub>10</sub> H <sub>12</sub> N <sub>2</sub> O <sub>3</sub>	C <sub>16</sub> H <sub>16</sub> N <sub>2</sub> O <sub>3</sub>	C <sub>11</sub> H <sub>14</sub> CuN <sub>2</sub> O <sub>4</sub>	C <sub>16</sub> H <sub>14</sub> CuN <sub>2</sub> O <sub>3</sub>
Formula weight (g/mol)	208.08	284.31	301.78	345.83
Crystal System	Monoclinic	Monoclinic	Monoclinic	Monoclinic
Space group	P2 <sub>1</sub> /c	P2 <sub>1</sub> /n	P2 <sub>1</sub> /c	P2 <sub>1</sub> /c
a (Å)	5.589(18)	6.288(6)	9.116(5)	14.071(2)
b (Å)	16.820(5)	15.873(16)	19.962(11)	11.444(17)
c (Å)	11.132(4)	14.540(13)	6.837(4)	9.218(14)
β (°)	94.778(6)	95.087(7)	107.748(10)	104.848(3)
V (Å <sup>3</sup> )	1042.8(6)	1445.5(2)	1185.1(11)	1434.8(4)
Z	4	4	4	4
Reflections collected	21,815	12,105	22,373	31,697
Independent reflections /R(int)	1841/0.0719	2753/0.1320	2087/0.0869	2525/0.0592
Absorption correction	multi-scan	multi-scan	multi-scan	multi-scan
Max/min transmission	0.979/0.952	0.990/0.830	0.539/0.745	0.649/0.745
Final R indices [I > 2σ(I)]	0.049/0.113	0.061/0.122	0.053/0.104	0.029/0.067
Goof	1.039	0.919	1.123	1.050
Largest diff.peak and hole (eÅ <sup>-3</sup> )	0.171/-0.183	0.164/-0.170	0.380/-0.477	0.270/-0.301

### 2.8.2. Minimal Inhibitory concentration (MIC) and minimal bactericidal concentration (CBM)

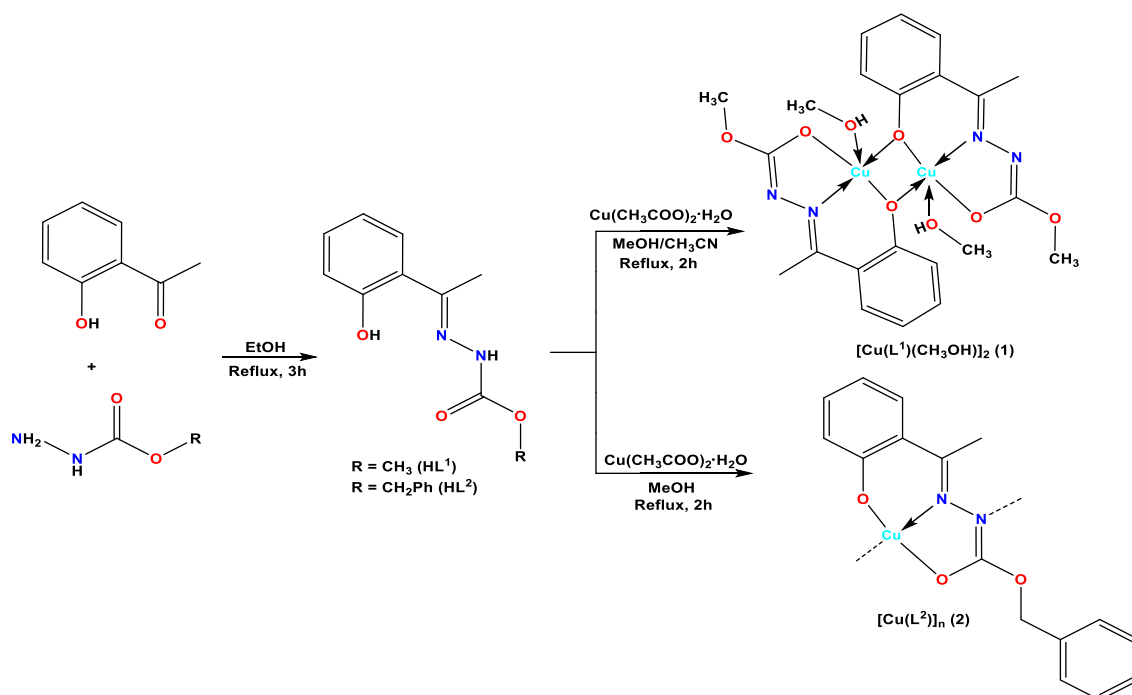
The microdilution method was used to determine the minimal inhibitory concentration (MIC) values in triplicate by using the 96-well microplates, adopted from the Clinical and Laboratory Standards Institute.<sup>22</sup> The compounds were dissolved in dimethyl sulfoxide (DMSO) at 1.0 mg mL<sup>-1</sup>, followed by dilution in Brucella broth (DIFCO, Kansas City, MO, USA) supplemented with hemin (5.0 mg mL<sup>-1</sup>, Sigma, St. Louis, MO, USA) and menadione (1 mg mL<sup>-1</sup>, Sigma); concentrations ranging from 0.195 to 400.0 μg mL<sup>-1</sup> were achieved. The inoculum was adjusted to give a cell concentration of 1 × 10<sup>6</sup> CFU mL<sup>-1</sup>. DMSO 5% (v/v) was used as the negative control, and a chlorhexidine (Sigma) was used as the positive control. The microplates containing anaerobic bacteria were incubated at 36 °C for 72 h in an anaerobic chamber containing 5–10 % H<sub>2</sub>, 10 % CO<sub>2</sub>, and 80–85 % N<sub>2</sub> (Don Whitley Scientific, Bradford, UK). After incubation, 30 μL of a 0.02 % aqueous resazurin (Sigma) solution was added to each well.<sup>23</sup> Resazurin is an oxidation probe that allows immediate microbial growth observation. The blue and red colors represent microbial growth absence and

presence, respectively.

To determine the minimum bactericidal concentration (MBC), a 10 μL aliquot of the inoculum was removed from each well before resazurin (Sigma) was added, and the aliquot was seeded in Schaedler agar (DIFCO) supplemented with hemin (5 mg mL<sup>-1</sup>, Sigma), menadione (1 mg mL<sup>-1</sup>, Sigma) and 5 % defibrinated horse blood was used. The agar plates were incubated at 36 °C for 72 h under gaseous conditions appropriate. The MBC assays were performed in triplicate. After incubation, MBC was defined as the lowest sample concentration that killed >99.9 % of the initial bacterial population, where no visible bacterial growth was observed.<sup>22</sup>

### 3. Results and discussion

The condensation reactions between 2-hydroxyacetophenone with methylcarbazate and benzylcarbazate produced respectively, two tridentate ONO ligands HL<sup>1</sup> and HL<sup>2</sup>. The complexation reactions of Cu(II) with HL<sup>1</sup> and HL<sup>2</sup> yielded two metal complexes, a dimeric complex [Cu(L<sup>1</sup>)(CH<sub>3</sub>OH)]<sub>2</sub> (1), and a polymeric complex [Cu(L<sup>2</sup>)]<sub>n</sub> (2), represented



**Scheme 1.** Synthesis of the carbazate ligands HL<sup>1</sup>, HL<sup>2</sup> and their copper(II) complexes (1) and (2).

in Scheme 1. The compounds were characterized by X-ray diffraction, physicochemical and spectroscopic analysis.

### 3.1. Crystal structures

The crystal structures of the carbazates **HL**<sup>1</sup> and **HL**<sup>2</sup> were elucidated by single crystal X-ray diffraction analysis, the ORTEP illustrations are shown in Fig. 1. The X-ray analysis showed **HL**<sup>1</sup> and **HL**<sup>2</sup> with an *E* configuration concerning the priority of the substituent bonded to C6–N2. Carbazates can exhibit keto-enol tautomerism in the –HN–C=O group, however, the IR spectrum shows a strong band of  $\nu(\text{C}=\text{O})$  at 1712 and 1707  $\text{cm}^{-1}$  for **HL**<sup>1</sup> and **HL**<sup>2</sup>. The compounds crystallized in keto form, comparing the bond lengths of C9–O2 and C9–N2 is found respectively 1.213(3) Å and 1.350(3) Å for **HL**<sup>1</sup> and 1.219(4) Å and 1.353(5) Å for **HL**<sup>2</sup>. The bond length of the C9–O2 is characteristic of a C=O double bond, while in C9–N2 case, it is verified that is a single bond. The <sup>1</sup>H NMR spectrum also presents only one signal to OH due to the phenol group. The evidence is also suggesting the presence of the keto form in the solid state and solution. The bond distances N1–N2, C9–N2 and C9–O3 show some electron delocalization throughout the carbazate function. This result is in agreement with other carbazates already described in the literature.<sup>13,24–27</sup> Table 2 shows the most relevant bond lengths and angles for **HL**<sup>1</sup> and **HL**<sup>2</sup>.

The two carbazates exhibit intramolecular hydrogen bond between the phenolic oxygen atom and the azomethine nitrogen atom with a distance of 2.565(3) Å and 2.559(5) Å for **HL**<sup>1</sup> and **HL**<sup>2</sup>, respectively. Intermolecular hydrogen bonds between N2–H2...O2' are observed bonding two molecules like a dimer (Fig. S1 in SI), with distances of 3.012(3) Å and 2.896(5) Å for **HL**<sup>1</sup> and **HL**<sup>2</sup> (with symmetry operations:  $-x + 1, -y + 1, -z$  and  $-x - 1, -y, -z + 2$ ), respectively. The interactions also can be observed at the full interactions maps around the molecules of the molecular crystal structures of the carbazate ligands. The intense red regions near the NH are indicative of hydrogen bond acceptors and hydrogen bond donors are marked in the intense blue regions near the OH of the phenol group. The hydrophobic regions in brown can be found above and below the phenyl rings of the ligands Fig. 2, Fig. 3.

The crystal structure determination of **(1)** revealed a dinuclear centrosymmetric copper(II) complex with a doubly deprotonated molecule of the **HL**<sup>1</sup> with an *ONO* chelating system. The metal centers

**Table 2**

Selected bond lengths (Å) and bond angles (°) for the carbazate ligands **HL**<sup>1</sup>, **HL**<sup>2</sup> and their copper(II) complexes **(1)** and **(2)**.

Bond lengths (Å)			Bond angles (°)		
	<b>HL</b> <sup>1</sup>	<b>(1)</b>		<b>HL</b> <sup>1</sup>	<b>(1)</b>
C1–O1	1.355(3)	1.355(3)	C9–O3–C10	115.6(2)	117.5(4)
C9–O2	1.213(3)	1.275(6)	C7–N1–N2	119.3(2)	117.6(4)
C9–O3	1.331(3)	1.339(6)	C9–N2–N1	120.9(2)	108.2(4)
N1–N2	1.382(3)	1.404(5)	O2–C9–O3	124.7(2)	119.0(5)
N1–C7	1.284(3)	1.289(6)	C6–C7–N1	116.5(2)	120.5(4)
O3–C10	1.449(3)	1.423(6)	O1–C1–C6	122.8(2)	123.2(5)
Cu1–O1	–	1.898(3)	N2–C9–O2	–	127.2(5)
Cu1–O1'	–	2.013(3)	O1–Cu1–O2	–	171.55(15)
Cu1–N1	–	1.933(4)	O1–Cu1–O4	–	91.32(14)
Cu1–O2	–	1.923(4)	O1–Cu1–N1	–	93.56(16)
Cu1–O4	–	2.354(4)	N1–Cu1–O1'	–	165.70(16)
Cu1'–O4'	–	2.354(4)	O1–Cu1–O1'	–	80.34(14)
	<b>HL</b> <sup>2</sup>	<b>(2)</b>		<b>HL</b> <sup>2</sup>	<b>(2)</b>
C9–O3	1.331(5)	1.342(2)	C9–O3–C10	115.1(3)	115.67(18)
C9–O2	1.219(4)	1.260(3)	C9–N2–N1	120.2(4)	109.31(18)
N1–N2	1.376(4)	1.407(3)	O2–C9–O3	124.8(4)	120.8(2)
N1–C7	1.290(4)	1.301(3)	O3–C9–N2	112.8(4)	112.93(19)
C1–O1	1.362(5)	1.314(3)	C7–N1–N2	119.1(4)	119.20(19)
C9–N2	1.353(5)	1.322(3)	O2–C9–N2	122.4(4)	126.3(2)
Cu1–O1	–	1.846(2)	O1–Cu1–O2	–	175.05(7)
Cu1–N1	–	1.951(2)	O1–Cu1–N2'	–	90.89(8)
Cu1–O2	–	1.950(2)			
Cu1–N2'	–	2.005(2)			
Cu1–N1	–	1.951(2)			

are pentacoordinate with  $\mu_2$ -oxo group located between the two copper atoms. Each copper atom is bonded to a methanol molecule, a ligand molecule by the oxygen atom of the phenol ring (O1), imine nitrogen (N1), carbonyl oxygen (O2), and the bridge by the oxygen of the phenol ring (O1) of a second ligand molecule. The metal centers exhibit a distorted geometry with bond distance Cu–O of 1.898(3) Å and 1.923(4) Å. The distance Cu–Cu' of 2.9901(17) Å is too long to present any interaction between the metal ions.

The best geometry of **(1)** can be indicated by Addison's parameter ( $\tau_5$ ), where  $\tau_5 = (\beta - \alpha)/60$  ( $\alpha$  and  $\beta$  are the largest coordination angles).<sup>28</sup> The value of  $\tau = 0$  is for a perfect square pyramidal geometry and  $\tau = 1$  is for a perfect trigonal bipyramidal geometry. In complex **(1)** the found  $\tau$

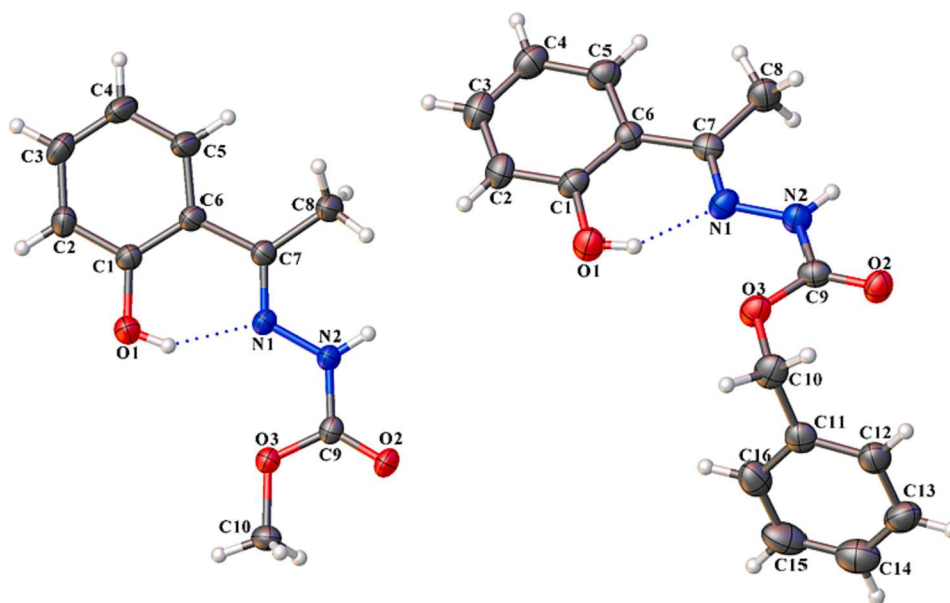


**Fig. 1.** Molecular structures of **HL**<sup>1</sup> and **HL**<sup>2</sup> with crystallographic labeling (30% probability displacement ellipsoids). Intramolecular hydrogen bonds are shown as dashed lines.

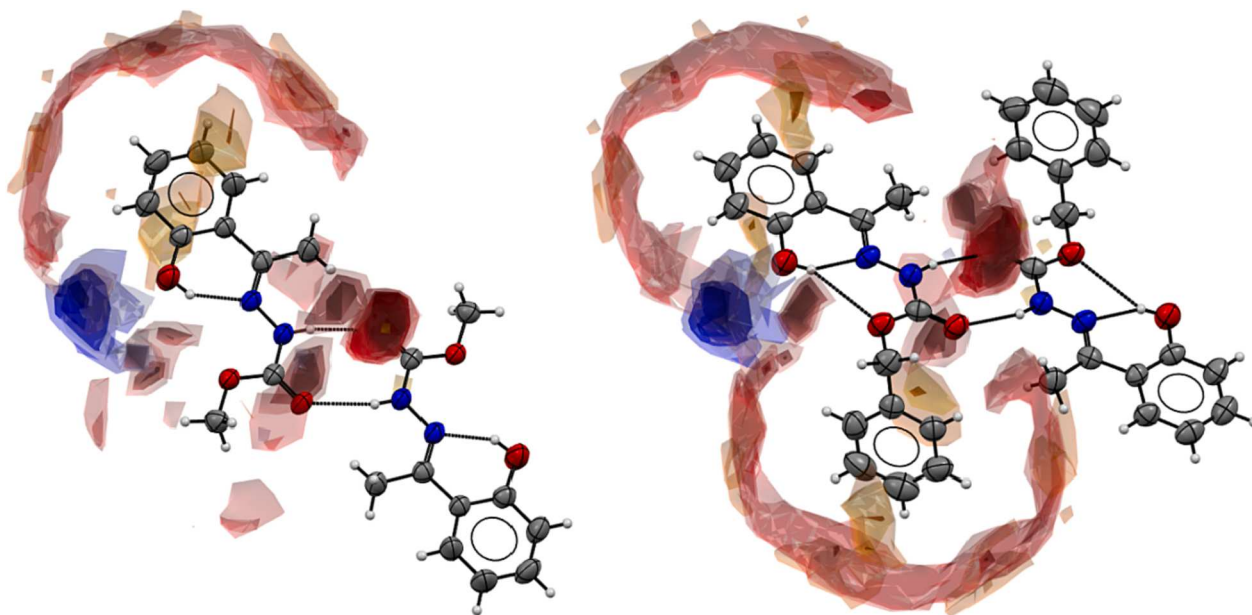


Fig. 2. Full interactions maps for HL<sup>1</sup> and HL<sup>2</sup> showing the acceptor and donor likelihood regions, and hydrophobic groups.

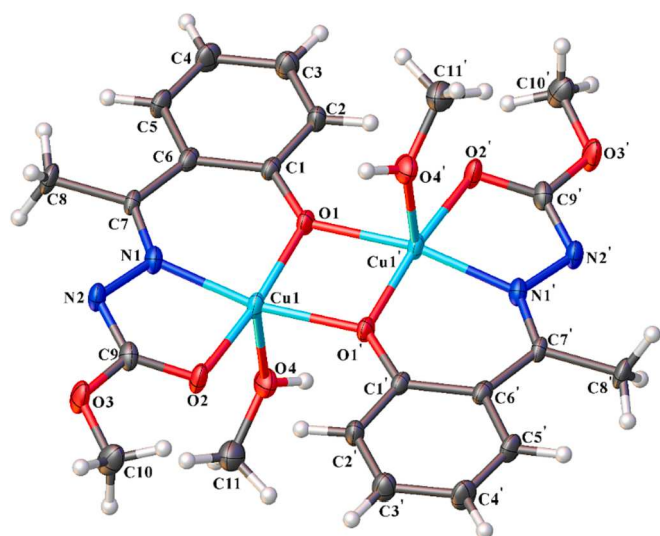


Fig. 3. Molecular structure of (1) with crystallographic labeling (30% probability displacement ellipsoids).

= 0.0973, calculated with the angles O1–Cu1–O2 of 171.55(15)° and N1–Cu1–O1' of 165.71(16)°, suggesting a distorted square-based pyramid for the metal ions, with the ligand forming the base of this pyramid and the methanol in the apical position of the pyramid.

The distortion observed in the coordination geometry was probably caused by the bridge  $\mu_2$ -oxo and the rigidity of the carbazate ligand in the environment around the copper(II) atoms. The angles found in the coordination polyhedron are between 80.34(14)° and 171.55(15)°. The results obtained for bond lengths and angles are consistent with similarly reported carbazate complexes<sup>29</sup>, and also with dinuclear copper(II) complexes with 2-hydroxyacetophenone-dithiocarbazate<sup>23</sup>.

A one-dimensional chain is observed in the complex (1) formed by intermolecular hydrogen bonds between the hydrogen of the coordinated methanol molecules and the deprotonated nitrogen of the carbazate ligand, O4–H4A...N2' [d(O...N) = 2.916(5) Å,  $\angle$ (O4–H4...N2') = 151(5)° with symmetry operator ('): x, y, z + 1], Fig. S2 in SI.

The compound (2) crystallized as a coordination polymer,

represented in Fig. 4. Each copper atom is coordinated to a deprotonated HL<sup>2</sup> molecule through the oxygen atom (O1) of the phenol ring, imine nitrogen (N1), and carbonyl oxygen (O2). The nitrogen atom (N2) of a second molecule of the ligand occupies the fourth position of the coordination polyhedron. The copper ions are tetracoordinate with a distorted square planar geometry.

The copper(II) atom with a 4-fold coordinative environment could be classified through Okuniewski's parameter ( $\tau_4$ ) which is used to predict the coordination polyhedron of tetracoordinate complexes.<sup>30</sup> The  $\tau_4$  value closer to zero indicates a square geometry, while a  $\tau_4$  value of one suggests a tetrahedral geometry. The  $\tau_4$  value for (2) was calculated using the N1–Cu1–N2' of 175.48(8)° and O1–Cu1–O2 of 175.08(7)° with a value of 0.0657, close to zero and an indication of a distorted square planar geometry for (2).

Comparing the complex (2) with the free ligand HL<sup>2</sup> it was observed a major contribution of the enol tautomer with C9–O2 bond distance of 1.261(3) Å in the complex (2) and a major character of a C9–N2 single bond of 1.322(3) Å. This behavior is according to similar bond lengths in previously reported complexes.<sup>26,31</sup> The polyhedron positions are occupied by atoms from the carbazate ligand, with distances Cu1–N1' of 1.950(2) Å, Cu1–O1 of 1.846(2) Å, and Cu1–O2 of 1.949(2) Å. The bond distance Cu1–N2' of 2.005(2) Å (symmetry operator: x, –y + 3/2, z – 1/2) enables the formation of a one-dimensional polymeric chain. Selected bond lengths and angles are summarized in Table 2 and agree with results obtained in similar complexes previously published.<sup>26–27</sup>

### 3.2. Infrared spectroscopy

In an attempt to certify the coordination modes of the free carbazates and their copper(II) complexes, the vibrational infrared spectra were collected (Figs. S3–S6 in Supporting Information). The bands attributed to  $\nu$ (O–H) appear around 3224 cm<sup>-1</sup> for HL<sup>1</sup> and 3418 cm<sup>-1</sup> for HL<sup>2</sup>, while  $\nu$ (N–H) is attributed in 3292 cm<sup>-1</sup> for HL<sup>1</sup> and 3236 cm<sup>-1</sup> for HL<sup>2</sup>. The infrared spectra of HL<sup>1</sup> and HL<sup>2</sup> show respectively, the  $\nu$ (N–H) bands at 3292 cm<sup>-1</sup> and 3236 cm<sup>-1</sup> and  $\nu$ (C=O) at 1712 and 1707 cm<sup>-1</sup>, indicating the predominance of keto tautomer for the carbazate ligands.

The  $\nu$ (N–H) and  $\nu$ (C=O) vibrational mode does not appear in the spectra of the complexes, indicating the coordination of the deprotonated carbazate and through the enol tautomer in (1) and (2). The bands assigned to  $\nu$ (C=N) at 1611 cm<sup>-1</sup> for HL<sup>1</sup> and 1620 cm<sup>-1</sup> for HL<sup>2</sup>

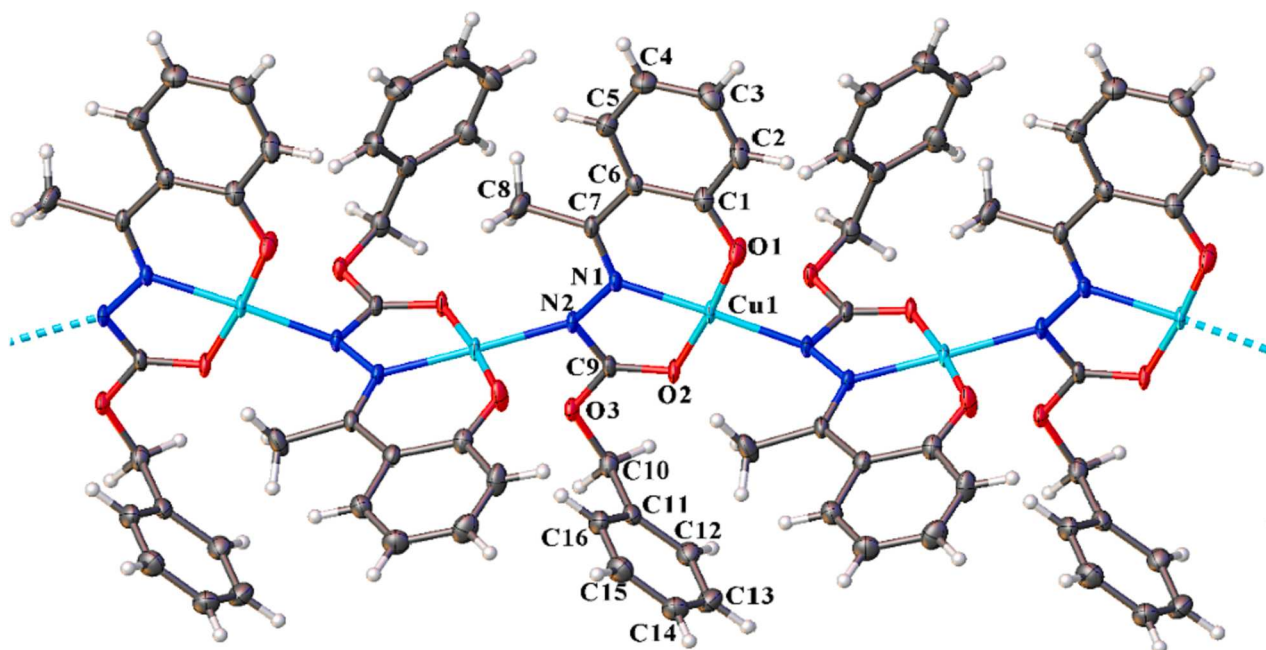


Fig. 4. Molecular structure of (2) with crystallographic labeling (30% probability displacement ellipsoids).

undergo a shift to lower values of the wavelength, 1598 and 1599  $\text{cm}^{-1}$  in the spectra of the complexes (1) and (2) respectively, suggesting the coordination of the carbazate to the copper(II) atoms through the *N*-imino atom.

The same behavior happened to  $\nu(\text{N}-\text{N})$  bands, a shift to smaller values, 1172 and 1121  $\text{cm}^{-1}$  to (1) and (2), respectively. This phenomenon is due to the weakening of the bonds with the coordination of the carbazate used in the formation of complexes. The  $\nu(\text{O}-\text{H})$  for (1) appears at 3292  $\text{cm}^{-1}$  due to the methanol molecule coordinated with the metal ions. The infrared analysis that was carried out supports the crystal data analysis and is according to similar complexes described previously.<sup>31–34</sup>

### 3.3. Electronic spectroscopy

The Schiff bases studied have chromophore groups that allow the investigation of some electronic transitions. In this way, it is possible a better understanding of their structures and resonance forms. The electronic spectra of **HL**<sup>1</sup>, **HL**<sup>2</sup>, and their copper(II) complexes in the region of UV–vis are shown in Figs. S7 and S8. The UV–vis experiment was made at room temperature, using three different solvents (MeOH, DMF and DMSO), for organic ligands and copper complexes. The solutions were prepared at  $2 \times 10^{-5}$  mol L<sup>-1</sup> concentration, to see the electronic transitions  $\pi \rightarrow \pi^*$ ,  $n \rightarrow \pi^*$ , LMCT and CTLM. Complexes solutions were also prepared at  $1 \times 10^{-3}$  mol L<sup>-1</sup> concentration, which made it possible to see d–d transition bands in their spectra. The results are summarized in Table S1.

In the **HL**<sup>1</sup> and **HL**<sup>2</sup> spectra, a strong absorption can be verified in the region between 269 and 272 nm, depending on the solvent. This band is characterized by  $\pi \rightarrow \pi^*$  orbitals transitions that occur between the azomethine group and a small contribution from the aromatic rings. In the region between 301 and 316 nm, the  $n \rightarrow \pi^*$  transitions are found, to a lesser extent, from the transition of non-bonding electrons to the  $\pi^*$  orbitals of the heteroatoms that constitute the carbazate.<sup>25</sup>

It is observed that there is a bathochromic displacement in the first absorption band. The absorption band shifts to longer wavelengths, 269–272 nm in the ligands to 280–295 nm in the complexes.<sup>35,36</sup> There is a decrease in the energy gap between the HOMO and LUMO, in such a way that when the complexation occurs, there is a decrease in the energy that

promotes an electron from the HOMO orbital to the LUMO.<sup>35</sup> In addition, another evidence of the complexation is the appearance of a strong band in the region of 345–364 nm, this absorption is due to a charge transfer that exists from the *NO* sites of the ligand to the metal.

The d–d transition bands were also observed at the complexes' spectra. It is possible to observe that the absorption wavelength of the d–d transition occurs in the red region and the color that is emitted by the product is its complementary, green, which is the color of both complexes.<sup>35</sup> The results discussed here are in agreement with previously published works of other copper(II) complexes.<sup>32,33,37</sup>

### 3.4. <sup>1</sup>H NMR spectra

The characterization by NMR spectroscopy was of great importance to carry out the study of the free carbazate ligands. The <sup>1</sup>H NMR spectra in DMSO-*d*<sub>6</sub> and the data referring to chemical shifts of these spectra are found in Supporting Information (Figs. S9 and S10, Tables S2 and S3).

At the <sup>1</sup>H NMR spectrum for the **HL**<sup>1</sup> ligand were verified seven resonance signals. After the integration of the signals, 11 hydrogen atoms of the molecule were obtained in their characteristic chemical shifts. Only the hydrogen atom from the phenol could not be observed due to its high lability that failed to produce a measurable and quantifiable resonance signal. The signal in the spectrum at 2.31 ppm, with integration equal to 3, appears as a singlet and it corresponds to the methyl hydrogen atoms marked 2 in the ligand structure. This signal appears at this chemical shift value because the H atoms are close to the C=N bond of the imino group. The signal at 3.76 ppm integrated to 3, is referring to the other methyl of the structure, marked as 1 and this signal appears in a greater displacement because this methyl is directly linked to nearby oxygen. In these two cases, the nearby groups, the C=N bond, and the oxygen atom of the ester act as electron drawing groups causing a deshielding of the analyzed hydrogen atoms.

The range from 6.87 ppm to 7.95 ppm is characterized by the signals of the four hydrogen atoms of the phenol aromatic ring, each one with an integration equal to 1. The ortho hydrogen atoms couple in the range of 3J – 7 – 10 Hz, the meta ones couple in the range of 4J – 2 – 3 Hz, and the couple in the range 5J – 0 – 1 Hz.<sup>35</sup> The triplet signal observed at 6.87 ppm is attributed to H(4), it has 3J = 6.8 Hz, ortho coupling with H (3) and H(5). At 7.26 ppm, there is H(5), also in the form of a triplet

signal, with  $3J = 7.7$  Hz. At 7.53 ppm there is a signal with a lot of interference, so it is not possible to identify each one of its couplings individually. The last signal at 7.95 ppm with  $3J = 7.8$  Hz coupling is a doublet referring to H(3), the fact that it is a doublet shows that this hydrogen has only one other vicinal hydrogen, and it is more deshielded than the others due to their proximity to the OH of the phenolic ring.<sup>38,39</sup>

Finally, at 10.78 ppm, there is a signal with integration equal to 1. This is a very deshielded signal that is due to the hydrogen atom of the N—H bond, given that this hydrogen is bonded to a nitrogen atom and is a neighbor of a carbonyl group. It is one of the most labile hydrogen atoms in the molecule and is eventually lost in complexations, so it makes sense if its signal is far from the others.

At the  $^1\text{H}$  NMR spectrum of the  $\text{HL}^2$  ligand is possible to observe the signal at 2.31 ppm integrated to 3, attributed to the methyl group close to the C=N bond. The signal at 5.25 ppm can be attributed to the methylene group, and due to the methylene being directly linked to an oxygen atom, is undergoing deshielding. The multiplets in the region between 6.88 and 7.56 ppm correspond to the hydrogen atoms of the two aromatic rings, integrated to 9. There are two aromatic rings and an overlap between the signals. For this reason, it was not possible to obtain the coupling constants of each hydrogen atom.<sup>40</sup>

The integral signal equal to 1 verified at 10.90 ppm is characteristic of the N—H bond, this signal is very deshielded because it is directly linked to a nitrogen atom and also because it is a neighbor of a carbonyl group. Finally, the signal at 12.89 ppm, integrated to 1, is characterized by the hydrogen atom attached to the oxygen atom of the phenol ring. Based on its higher acidity and therefore its high lability, it produced a signal of very low intensity. The results corroborate the other analytical methods used and were consistent with other previously published ligands.<sup>3,38,40–42</sup>

### 3.5. Mass spectrometry

The mass spectrometry was used in positive mode electrospray ionization form (ESI(+)-MS/MS) with a concentration of 50  $\mu\text{M}$  (methanol/dimethylformamide, 99/1% ratio) in an acid medium (0.1 % acetic acid) to evaluate the real species present in the compounds solutions. The spectra containing the fragmentations are shown in Figs. 5 and 6, Figs. S11 and S12.

Signals with  $m/z$  209.0917 (calcd = 209.0841) and 285.1227 (calcd = 285.1135) were observed in the mass spectra of the  $\text{HL}^1$  and  $\text{HL}^2$  ligands, respectively and they are in agreement with the monoisotopic mass plus one hydrogen for each molecular. It is also possible to observe that several fragmentations are common to the two ligands due to the similarity in their structures and are in agreement with the data obtained in the structural characterization by X-ray of single crystals and other techniques employed.

In the case of the complexes, due to their more complex chemical structures, fragments of their molecular ions were not obtained, as in the case of ligands. However, several other fragments that derive were verified, corroborating the data obtained in the other analyses. In addition, fragments of the ligands were observed in the spectra of their derivative complexes. Since the complexes were dissolved in DMF, the ESI(+)-MS/MS spectrum showed the presence of the specie  $[\text{Cu}(\text{L}^1)(\text{DMF})\text{H}^+]$  in  $m/z = 343.0576$  for the complex (1). And the specie  $[\text{Cu}(\text{L}^2)(\text{DMF})\text{H}^+]$  in  $m/z = 419.0899$  for the complex (2), and also peaks which can be attributed to the formation of the  $[\text{Cu}(\text{L})\text{H}^+]$  species after the loss of DMF molecule.

### 3.6. Hirshfeld surface

The Hirshfeld surface (HS) was used to analyze and quantify non-covalent interactions existing in a crystal lattice using the crystallographic information files (CIF) of the synthesized compounds. Based on

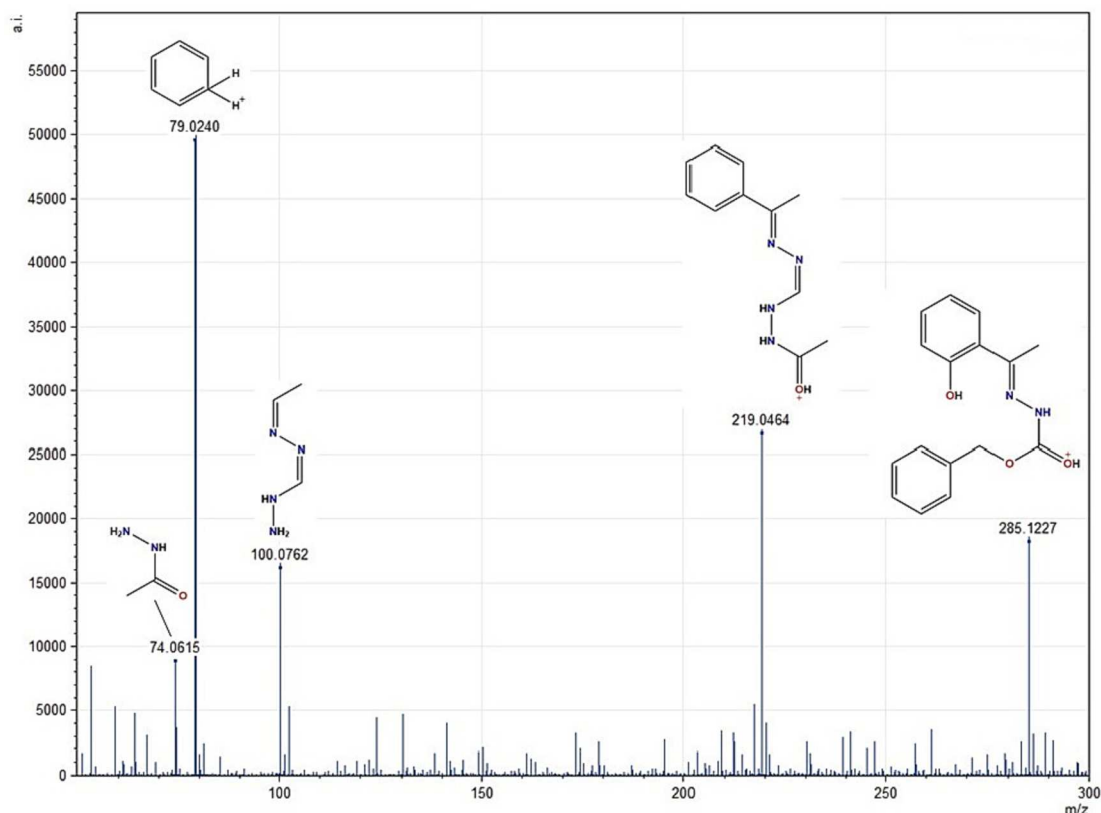


Fig. 5. Mass Spectra for ligand  $\text{HL}^2$ .

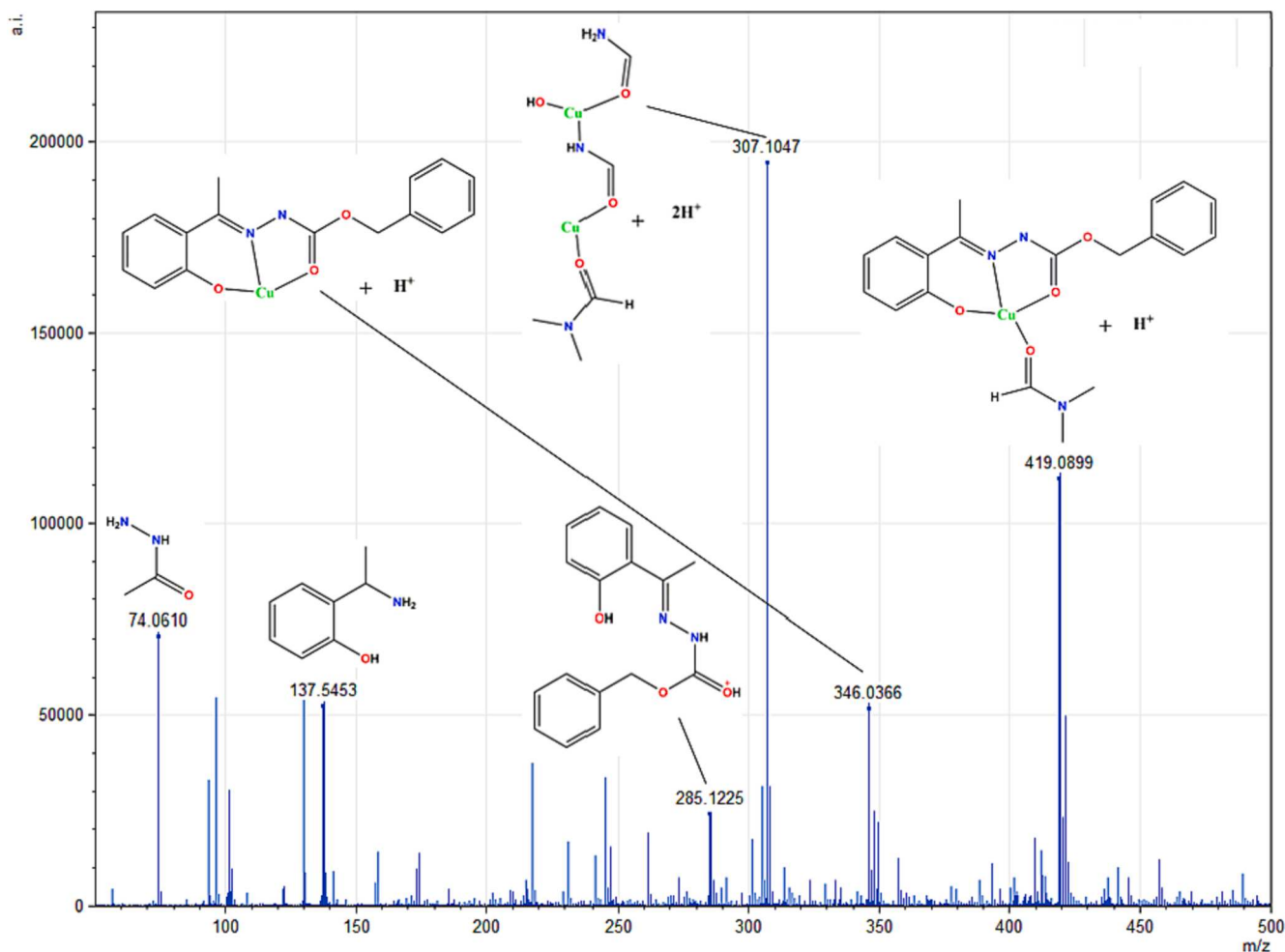


Fig. 6. Mass Spectra for complex (2).

the HS, distance functions can be drawn, the main ones being  $d_i$  and  $d_e$ . From the normalization of these two functions, taking into account the van der Waals radii of the atoms, the  $d_{\text{norm}}$  function is obtained, that is the normalized contact distance.<sup>18–20</sup> The red regions represent contacts at a distance smaller than the sum of the van der Waals radii of the atoms, the white regions show close contacts and the blue represents contacts at a distance greater than the sum of the van der Waals radii of the atoms.<sup>18–20</sup> The  $d_{\text{norm}}$  surfaces of **HL**<sup>1</sup>, **HL**<sup>2</sup>, (1), and (2) can be seen in Fig. 7. The interactions represented in red are the most representative and of greater interest. The more intense the color, the stronger the interaction. Red regions are related to the N—H...O and C—H...O hydrogen bonds and agree with the observed single-crystal X-ray diffraction.

The two-dimensional graph was obtained with the combination of the functions  $d_i$  and  $d_e$ . This graph is the Fingerprint of the molecule and takes into account all the contacts present in its crystal structure, from the closest contacts to those at greater distances. Decomposing the functions in this two-dimensional graph, each type of contact existing in the crystal lattice can be quantified in percentage.<sup>18–20</sup> The fingerprint plots for the four compounds are shown in the Supplementary Material, Figs. S17 – S20. Fig. 8 represents the contribution of close contacts for the synthesized compounds. Fingerprint plots of the compounds indicate that the H...H, C...H and O...H interactions are the most significant for the ligands and complexes, their contribution varies between 10,7% and 56,3%.

### 3.7. Antibacterial activity

To investigate the antibacterial activity of the synthesized compounds, the free ligands and the copper(II) complexes were tested against *A. naeslundii*, *P. anaerobius*, *V. parvula*, *P. gingivalis* and *F. nucleatum* strains. The anaerobic bacterial strains causing periodontal infection were used. The results are expressed as the minimum inhibitory concentration (MIC) and minimum bactericidal concentration (MBC), defined as the lowest concentration of the interest compound that does not occur during the growth of the microorganism, and are listed in Table 3.

Complexes (1) and (2) exhibited good antimicrobial activity and were more pronounced when compared to free ligands **HL**<sup>1</sup> and **HL**<sup>2</sup>. The obtained results were according to other similar published works.<sup>29,42,43</sup> The two complexes showed antibacterial activity against the tested microorganisms, but, in general, complex (2) showed better MIC and MBC values than complex (1), including a MIC/MBC of 1.56/1.56  $\mu\text{g mL}^{-1}$  in the inhibition in the growth of *P. anaerobius* and *P. anaerobius* with 3.12/3.12  $\mu\text{g mL}^{-1}$ , with the bactericidal effect. Another interesting finding is the MIC/MBC of 12.5/25  $\mu\text{g mL}^{-1}$  of the inhibition in the growth of *P. gingivalis* and bacteriostatic effect, this pathogen is responsible for the chronic periodontitis, but recent studies present the relation between this bacteria strain and Alzheimer Disease since *P. gingivalis* colonies were found in the brain of Alzheimer's patients.<sup>44,45</sup>

It is clear that there is a relationship between oral microbes and human health, in addition to affecting their site, these microbes are related to several systemic diseases.<sup>11</sup> There is a link between oral

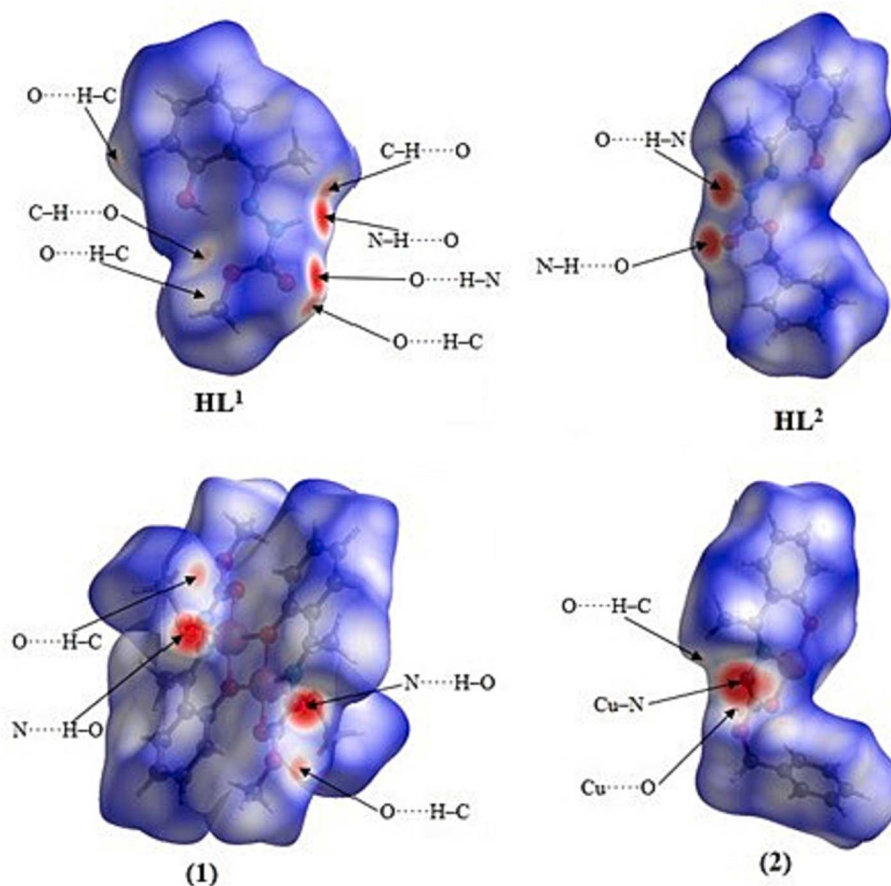


Fig. 7. Hirshfeld surface of HL<sup>1</sup>, HL<sup>2</sup>, (1) and (2).

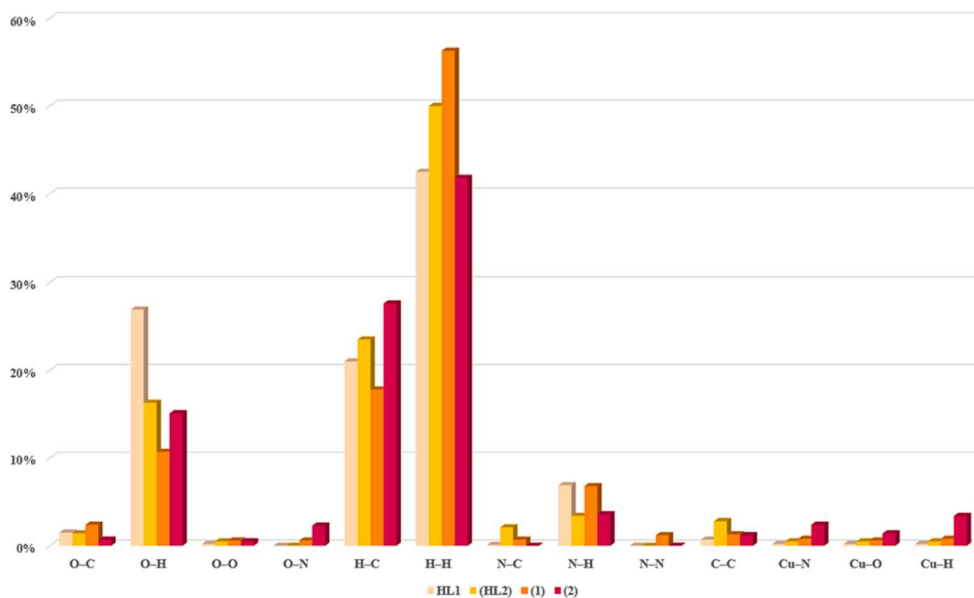


Fig. 8. Percentage contribution of close contacts for HL<sup>1</sup>, HL<sup>2</sup>, (1) and (2).

bacteria and the development of carcinomas, more specifically *P. gingivalis* and *F. nucleatum* are oral pathogens that use pathways that can trigger the development of tumors.<sup>46</sup> The understanding of oral microbes is no longer limited to the investigation of oral diseases, due to the human microbiome project, since the oral microbiota is one of the project's five priority research sites (oral cavity, nasal cavity, vagina,

intestine and skin).<sup>47</sup>

Taking into account the results presented, it can be seen that the metal complexes were more efficient than their free carbazate ligands. Among the possible explanations for this phenomenon, it is worth mentioning the lipophilicity necessary to permeate the cell membrane, as suggested by Tweed's Chelation Theory. The presence of the metallic

**Table 3**  
Minimum Inhibitory Concentration and Minimum Bactericidal Concentration (MIC/MBC).

Compounds	<i>Actinomyces naeslundii</i> ATCC 19039	<i>Peptostreptococcus anaerobius</i> ATCC 27337	<i>Veillonella parvula</i> ATCC 17745	<i>Porphyromonas gingivalis</i> ATCC 49417	<i>Fusobacterium nucleatum</i> ATCC 10953
HL <sup>1</sup>	>400/>400	>400/>400	>400/>400	>400/>400	>400/>400
HL <sup>2</sup>	>400/>400	>400/>400	>400/>400	>400/>400	>400/>400
(1)	25/50	3.12/3.12	200/400	25/50	50/50
(2)	25/25	1.56/1.56	50/50	12.5/25	25/25
Chlorhexidine	1.844/1.844	0.230/0.230	0.922/0.922	0.922/0.922	1.844/1.844

center increases the lipophilicity of the molecule, since there is an overlap in the orbitals of the ligand and metal, promoting electron delocalization throughout the structure, and facilitating the passage through the lipid membrane of the bacteria.<sup>48</sup>

The complexation of the carbazate ligands to the copper(II) ion increases lipophilicity, resulting in an improvement in the penetration power of the complexes inside the lipid membrane and blocking cellular enzymatic activity. Coordination compounds also can impede the growth of microorganisms by disrupting the process of cellular respiration and blocking protein synthesis. Differences in the structure of the ligands and complexes can improve the permeability capacity of the cells of the microorganisms tested and influence the results, as observed for compounds (1) and (2).<sup>49</sup>

Analyzing related publications is possible to see that the presented result is in line with what was found for similar compounds published before. In general, the trend of similar compounds previously published showed greater activity of the metal complexes compared with the free Schiff bases and the amoxicillin as a control.<sup>50</sup> Additionally, antimicrobial tests performed on metal complexes derived from carbazate ligands showed greater activity against Gram-positive bacteria when compared to their free ligands.<sup>51</sup> In a comparison with one of our previous works involving carbazates, in the present one, we achieved better results comparing the MIC values for the Cu(II) complexes.<sup>34</sup>

#### 4. Conclusions

In the present study, we have described the crystal structures of two carbazate ligands derived from 2-hydroxyacetophenone and their Cu(II) complexes. The ligands HL<sup>1</sup> and HL<sup>2</sup> are capable of forming dimeric structures by noncovalent interactions. The binuclear complex (1) also formed a one-dimensional arrangement through their intermolecular interactions. Nitrogen atoms of the deprotonated HL<sup>2</sup> link the polymeric complex (2). Moreover, the spectroscopic and structural analysis revealed that the Cu(II) ions coordinated with the ligands in different geometries, forming a square-based pyramid dimer and a square geometry polymer. The single crystal X-ray diffraction followed by the study of the Hirshfeld surfaces evidenced the most important non-covalent interactions in the compounds. Evaluating antibacterial activity verified great activity for the complexes against the tested periodontopathogenic bacteria when compared with the free ligands.

#### Declaration of Competing Interest

The authors declare that they have no known competing financial interests or personal relationships that could have appeared to influence the work reported in this paper.

#### Data availability

No data was used for the research described in the article.

#### Acknowledgments

All funding agencies are acknowledged for partial financial support.

#### Funding

We gratefully acknowledge the financial support of FAPDF, CNPq, Coordenação de Aperfeiçoamento de Pessoal de Nível Superior - Brasil (CAPES) - Finance Code 001, FINEP/CTINFRA and UnB.

#### Appendix A. Supplementary data

Supplementary data to this article can be found online at <https://doi.org/10.1016/j.ica.2023.121421>.

#### References

- [1] M. Milenković, A. Bacchi, G. Cantoni, S. Radulović, N. Gligorijević, S. Arandelović, D. Sladić, M. Vujčić, D. Mitić, K. Anđelković, *Inorganica Chim. Acta* 395 (2013) 33.
- [2] M.A. Rodrigues, I.M. Marzano, G.H. Ribeiro, L. Colina-Vegas, M. Pivatto, A.P. S. Fontes, C.M. Ribeiro, F.R. Pavan, K.J. De Almeida, A.A. Batista, E.C. Pereira-Maia, W. Guerra, *Polyhedron* 98 (2015) 146.
- [3] M. Milenković, G. Cantoni, A. Bacchi, V. Spasojević, M. Milenković, D. Sladić, N. Krstić, D. Ancrossed, K. Signelković, *Polyhedron* 80 (2014) 47.
- [4] A. Kryshchshyn, D. Kaminsky, P. Grellier, R. Lesyk, J. Eur. Med. Chem. 85 (2014) 51.
- [5] C. Nie, Q. Zhang, H. Ding, B. Huang, X. Wang, X. Zhao, S. Li, H. Zhou, J. Wu, Tian Y. 43 (2014) 599.
- [6] M.B. Zivković, I.T. Novaković, I.Z. Matic, D.M. Sladić, N.M. Krstić, *Steroids* 148 (2019) 36.
- [7] E.A. Saad, M.M. Hassanien, F.W. El-Iban, *Biochem. Biophys. Res. Commun.* 484 (2017) 579.
- [8] M.A. Malik, S.A. Lone, M.Y. Wani, M.I.A. Talukdar, O.A. Dar, A. Ahmad, A. Hashmi, *Bioorg. Chem.* 98 (2020), 103771.
- [9] İşler, E.; Zülfişkaroğlu, A.; Vural, H.; Dege, N. ;*Mol. Cryst. Liq. Cryst.* 2021.
- [10] Vinaya; Basavaraju, Y. B.; Lakshmana, B.; Yathirajan, H. S.; Parkin, S. ;*Acta Crystallogr. Sect. E Crystallogr. Commun.* 2022. 78.
- [11] X. Peng, L. Cheng, Y. You, C. Tang, B. Ren, Y. Li, X. Xu, X. Zhou, *J. Int. Oral Sci.* 14 (2022) 1.
- [12] B. Zhu, X.W. Cheng, *Acta Crystallogr. Sect. E Struct. Reports Online* (2008) 64.
- [13] L.P. Lv, W.W. Li, W.B. Yu, T.M. Yu, X.C. Hu, *Acta Crystallogr. Sect. E Struct. Reports Online* 65 (2009), o1896.
- [14] Sheldrick, G. M. SADABS. Program for Empirical Absorption Correction of Area Detector Data. 1997.
- [15] G.M. Sheldrick, SHELXS-97, Program for Structure Refinement, 1997.
- [16] G.M. Sheldrick, *Acta Crystallogr. Sect. C* 71 (2015) 3.
- [17] O.V. Dolomanov, L.J. Bourhis, R.J. Gildea, J.A.K. Howard, H. Puschmann, *J. Appl. Crystallogr.* 42 (2009) 339.
- [18] McKinnon, J. J.; Spackman, M. A.; Mitchell, A. S. *Novel tools for visualizing and exploring intermolecular interactions in molecular crystals.* 2004. Vol. 60.
- [19] M.A. Spackman, D. Jayatilaka, *CrystEngComm* 11 (2009) 19.
- [20] K. Azouzi, B. Hamdi, R. Zouari, A. Salah, Ben. Bull. Mater. Sci. 40 (2017) 289.
- [21] S. Martínez-Fernández, X. Franch, J. Bisbal, *Sci. Comput. Program.* 134 (2017) 61.
- [22] CLSI *Methods for Antimicrobial Susceptibility Testing of Anaerobic Bacteria*; Clinical and Laboratory Standards Institute, Ed.; 9th ed.; CLSI standard M11-A7.: Wayne, PA. 2018.
- [23] F.C. Lima, T.S. Silva, C.H.G. Martins, C.C. Gatto, *Inorganica Chim. Acta* 483 (2018) 464.
- [24] P. Nithya, R. Rajamanikandan, J. Simpson, M. Ilanchelian, S. Govindarajan, *Polyhedron* 145 (2018) 200.
- [25] S. Poornima, S. Packiaraj, A. Pushpaveni, S. Govindarajan, R.J. Butcher, J. P. Jasinski, M. Zeller, *Inorganica Chim. Acta* 497 (2019), 119072.
- [26] A.D. Khalaji, K. Fejfarova, M. Dusek, D. Das, *Monatshfte fur Chemie* 143 (2012) 753.
- [27] S. Jana, S. Khan, A. Bauzá, A. Frontera, S. Chattopadhyay, *J. Mol. Struct.* 1127 (2017) 355.
- [28] A.W. Addison, T.N. Rao, J. Reedijk, J. van Rijn, G.C. Verschoor, *J. Chem. Soc. Dalton Trans.* (1984) 1349.
- [29] Knoll, S.; Tschwatschal, F.; Gelbrich, T.; Ristau, T.; Borsdorf, R.; Zinnatons, È.; Sn, O.; Sn, O. 1998. 624. 1015.
- [30] A. Okuniewski, D. Rosiak, J. Chojnacki, B. Becker, *Polyhedron* 90 (2015) 47.
- [31] P. Pattanayak, J.L. Pratihar, D. Patra, C.H. Lin, P. Brandão, D. Mal, V. Felix, *J. Coord. Chem.* 66 (2013) 568.



- [32] S. Poornima, T. Premkumar, R.J. Butcher, S. Govindarajan, J. Therm. Anal. Calorim. 138 (2019) 3925.
- [33] Gatto C. C., Duarte E. de A., Liarte G. S., Silva T. S., Santiago M. B., Martins C. H. G. *J. Coord. Chem.* 2020. 8972.
- [34] S. Kim, H. Lee, H. So, H. Lee, K.T. Kim, C. Kim, *Spectrochim. Acta - Part A Mol. Biomol. Spectrosc.* 228 (2020), 117787.
- [35] Pavia, D. L.; Lampman, G. M.; Kriz, G. S.; Vyvyan, J. R. *Introduction to Spectroscopy; Fourth.*; Cengage Learning: Belmont, CA – USA. 2008.
- [36] R.N. Patel, A. Singh, V.P. Sondhiya, Y. Singh, K.K. Shukla, D.K. Patel, R. Pandey, *J. Coord. Chem.* 65 (2012) 795.
- [37] F.C. Lima, Y.A.O. Só, R. Gargano, M. Fujimori, E.L. França, A.C. Honorio-França, C. C. Gatto, *J. Mol. Struct.* 1212 (2020), 128083.
- [38] C.D.Q.O. Cavalcante, D.D.S. Arcanjo, G.G.D. Silva, D.M.D. Oliveira, C.C. Gatto, *New J. Chem.* 43 (2019) 11209.
- [39] A.A. Recio Despaigne, J.G. Da Silva, A.C.M. Do Carmo, O.E. Piro, E.E. Castellano, H. Beraldo, *J. Mol. Struct.* 920 (2009) 97.
- [40] S. Savir, Z.J. Wei, J.W.K. Liew, I. Vythilingam, Y.A.L. Lim, H.M. Saad, K.S. Sim, K. W. Tan, *J. Mol. Struct.* 1211 (2020), 128090.
- [41] K. Srinivasan, S. Poornima, S. Govindarajan, W.T.A. Harrison, *J. Mol. Struct.* 1184 (2019) 519.
- [42] T. Rosu, E. Pahontu, C. Maxim, R. Georgescu, N. Stanica, A. Gulea, *Polyhedron* 30 (2011) 154.
- [43] M.L. Low, L. Maigre, P. Dorlet, R. Guillot, J.M. Pagès, K.A. Crouse, C. Policar, N. Delsuc, *Bioconjug. Chem.* 25 (2014) 2269.
- [44] S. Kanagasigam, S.S. Chukkapalli, R. Welbury, S.K. Singhrao, *J. Alzheimer's Dis. Reports* 4 (2020) 501.
- [45] S.S. Dominy, C. Lynch, F. Ermini, M. Benedyk, A. Marczyk, A. Konradi, M. Nguyen, U. Haditsch, D. Raha, C. Griffin, L.J. Holsinger, S. Arastu-Kapur, S. Kaba, A. Lee, M. I. Ryder, B. Potempa, P. Mydel, A. Hellvard, K. Adamowicz, H. Hasturk, G. D. Walker, E.C. Reynolds, R.L.M. Faull, M.A. Curtis, M. Dragnow, J. Potempa, *Sci. Adv.* 5 (2019) 1.
- [46] H. Tuominen, J. Rautava, *Pathobiology* 88 (2021) 116.
- [47] P.J. Turnbaugh, R.E. Ley, M. Hamady, C.M. Fraser-Liggett, R. Knight, J.I. Gordon, *Nature* 449 (2007) 804.
- [48] A.A. Al-Amiery, A.A.H. Kadhun, A.B. Mohamad, *Bioinorg., Chem. Appl.* (2012).
- [49] A.Z. El-Sonbati, W.H. Mahmoud, G.G. Mohamed, M.A. Diab, S.M. Morgan, S. Y. Abbas, *Appl. Organomet. Chem.* 33 (2019) 1.
- [50] T.M.A. Al-Shboul, M. El-khateeb, Z.H. Obeidat, T.S. Ababneh, S.S. Al-Tarawneh, M. S. Al Zoubi, W. Alshaer, A. Abu Seni, T. Qasem, H. Moriyama, Y. Yoshida, H. Kitagawa, T.M.A. Jazzazi, *Inorganics* (2022) 10.
- [51] P. Nithya, J. Simpson, S. Govindarajan, *Inorganica Chim. Acta* 467 (2017) 180.



ELSEVIER

Contents lists available at ScienceDirect

## Journal of Medical Mycology

journal homepage: [www.elsevier.com](http://www.elsevier.com)Journal of Medical Mycology  
Journal de Mycologie Médicale

## Research Paper

# Virulence factors, antifungal susceptibility and molecular profile in *Candida* species isolated from the hands of health professionals before and after cleaning with 70% ethyl alcohol-based gel



Priscila Guerino Vilela Alves<sup>a</sup>, Ralciane de Paula Menezes<sup>b</sup>, Nagela Bernadelli Sousa Silva<sup>c</sup>, Gabriel de Oliveira Faria<sup>d</sup>, Meliza Arantes de Souza Bessa<sup>e</sup>, Lúcio Borges de Araújo<sup>f</sup>, Paula Augusta Dias Fogaça Aguiar<sup>d</sup>, Mário Paulo Amante Penatti<sup>b</sup>, Reginaldo dos Santos Pedroso<sup>b,\*</sup>, Denise von Dolinger de Brito Röder<sup>g</sup>

<sup>a</sup> Postgraduate Program in Health Sciences, Medicine, Federal University of Uberlândia (UFU), Uberlândia, Minas Gerais, Brazil

<sup>b</sup> Technical School of Health, Federal University of Uberlândia (UFU), Uberlândia, Minas Gerais, Brazil

<sup>c</sup> Postgraduate Program in Applied Immunology and Parasitology, Federal University of Uberlândia (UFU), Uberlândia, Minas Gerais, Brazil

<sup>d</sup> Clinical Hospital, Federal University of Uberlândia (UFU), Uberlândia, Minas Gerais, Brazil

<sup>e</sup> Biologist, Federal University of Uberlândia, Uberlândia, Minas Gerais, Brazil

<sup>f</sup> Faculty of Mathematics, Federal University of Uberlândia (UFU), Uberlândia, Minas Gerais, Brazil

<sup>g</sup> Institute of Biomedical Sciences, Federal University of Uberlândia (UFU), Uberlândia, Minas Gerais, Brazil

## ARTICLE INFO

## Article History:

Received 10 July 2023

Revised 10 February 2024

Accepted 6 May 2024

Available online 9 May 2024

## Keywords:

Candida

Hands

Virulence factors

Biofilm

NICU

Healthcare professionals

## ABSTRACT

Fungal infections in neonatal intensive care units (NICU) are mainly related to *Candida* species, with high mortality rates. They are predominantly of endogenous origin, however, cross-infection transmitted by healthcare professionals' hands has occurred. The aim of this study was to identify *Candida* species isolated from the hands of healthcare professionals in a NICU before and after hygiene with 70% ethanol-based gel and evaluate virulence factors DNase, phospholipase, proteinase, hemolysin, biofilm biomass production, and metabolic activity. In vitro antifungal susceptibility testing and similarity by random amplified polymorphic DNA (RAPD) were also performed. *C. parapsilosis* complex was the most frequent species (57.1%); all isolates presented at least one virulence factor; three isolates (*Candida parapsilosis* complex) were resistant to amphotericin B, two (*Candida famata* [currently *Debaryomyces hansenii*] and *Candida guilliermondii* [currently *Meyerozyma guilliermondii*]) was resistant to micafungin, and six (*Candida parapsilosis* complex, *Candida guilliermondii* [= *Meyerozyma guilliermondii*], *Candida viswanathi*, *Candida catenulata* [currently *Diutina catenulata*] and *Candida lusitanae* [currently *Clavispora lusitanae*]) were resistant to fluconazole. Molecular analysis by RAPD revealed two clusters of identical strains that were in the hands of distinct professionals. *Candida* spp. were isolated even after hygiene with 70% ethanol-based gel, highlighting the importance of stricter basic measures for hospital infection control to prevent nosocomial transmission.

© 2024 Published by Elsevier Masson SAS on behalf of SFMM.

## Introduction

Fungal infections that occur in Neonatal Intensive Care Units (NICU) are mainly related to *Candida* species, which is the seventh

**Abbreviations:** NICU, neonatal intensive care units; RAPD, random amplified polymorphic DNA; BrSCOPE, Brazilian surveillance and control of pathogens of epidemiologic importance; HCW, healthcare professionals; ABHSs, alcohol-based hand antiseptics; LBP, low biomass production; MBP, moderate biomass production; HBP, high biomass production; LMA, low metabolic activity; MMA, moderate metabolic activity; HMA, high metabolic activity

\* Corresponding author at: Campus Umuarama, Bloco 4k - Sala 5° piso. Av. Professor José Inácio de Souza - s/n - Bloco 4K - 5° piso, Bairro Umuarama, 38.402-018, Uberlândia, MG.

E-mail address: [rpedroso@ufu.br](mailto:rpedroso@ufu.br) (R.d.S. Pedroso).

<https://doi.org/10.1016/j.mycmed.2024.101482>

1156-5233/© 2024 Published by Elsevier Masson SAS on behalf of SFMM.

most prevalent cause (5.6%) of bloodstream nosocomial infections (BSI) among all pathogens included in the Brazilian Surveillance and Control of Pathogens of Epidemiologic Importance (BrSCOPE) [1,2]. Invasive *Candida* infections can be fatal, especially in hospitalized newborns in NICU, due to an immature immune system influenced by healthcare, such as central venous catheters, broad-spectrum antibiotics, and parenteral nutrition [3].

The hospital environment is a large reservoir of opportunistic pathogens, which can be transmitted to individuals in many ways [4]. The modes of transmission and portals of entry for hospital fungal infections vary according to the pathogen involved [4]. *Candida* spp. infections are predominantly of endogenous origin [4], but cross-infection transmitted by healthcare professionals' hands (HCWs) has

been reported in 20–40% of healthcare-associated infections (HAIs) [4,5] and is considered one of the main sources of candidemia outbreaks in NICU [6,7]. The ability of *Candida* isolates to adhere and grow as biofilms in internal medical devices and intravascular catheters, for example, has been associated with higher mortality [5,8–10], since from these reservoirs, persistent *Candida* cells (tolerant to antifungals) tend to migrate to the bloodstream [11–14].

Hand hygiene and antiseptic practices for *Candida* infection control, according to the main world health organizations, are hand-washing with soap and water, especially with dirt, followed by using alcohol-based hand antiseptics (ABHSs) [10–13,15–17]. In this context, the aim of this study was to evaluate the presence of *Candida* spp. before and after hand hygiene of healthcare professionals in a NICU with 70% ethanol-based gel, as well as to phenotypically characterize the isolates and determine their genetic similarity.

## Materials and methods

### Study site, participant selection, and sample collection

This prospective cohort study was carried out in the NICU of a tertiary teaching hospital in Brazil with 514 beds and a multidisciplinary team of 120 healthcare professionals, including nurses, nursing technicians, doctors, and physiotherapists. Of these, 107 (89.1%) professionals participated in the study. Hand samples were collected from HCWs before and after disinfection with 70% ethyl alcohol-based gel (Hydrated 70% v/v Ethanol Gel, Rioquímica®, Brazil), which is used in the unit. HCWs were instructed to immerse both hands in a sterile polypropylene bag containing 30 mL of Brain Heart Infusion (BHI) broth (HIMEDIA®, India) and rub their hands in the broth. The bag was sealed and labeled as the "before" group. Afterward, the professionals dried their hands with a sterile surgical compress and disinfected their hands with alcohol gel according to the institution's protocol. They then introduced both hands into another sterile polypropylene bag containing 30 mL of BHI broth and rubbed their hands in the broth. The bag was sealed and labeled as the "after" group [17].

### Isolation and identification of species

The entire sample obtained was transferred to sterile Falcon tubes and centrifuged at 4000 g for 10 min. Subsequently, the supernatant was discarded, and the sediment was resuspended in 0.9% saline at a 1:1 ratio. 0.1 mL was inoculated in plates containing Sabouraud Dextrose Agar (SDA; Isofar, Duque de Caxias, RJ, Brazil) supplemented with chloramphenicol and chromogenic agar (Himedia, Mumbai, India) and incubated at 30 °C for up to 72 h [18]. The SDA plates were used for enumerating colony-forming units per milliliter (CFU/mL). The count was performed on plates that showed growth from a single colony to evaluate the efficacy of 70% ethanol-based gel.

The yeast species were identified by matrix-assisted laser desorption/ionization time-of-flight (MALDI-TOF) mass spectrometry (Bruker MALDI Biotyper 4.0).

### Evaluation of in vitro virulence factors

#### Extracellular enzymatic activity

The production of phospholipase, proteinase, hemolysin, and DNase was determined according to the methods described by Rorig et al. [19], with adaptations. Briefly, yeast colonies were suspended in 0.9% saline solution with turbidity equivalent to tube two of the McFarland scale ( $3 \times 10^8$  to  $6 \times 10^8$  CFU/mL). Subsequently, five  $\mu$ L aliquots of each suspension were deposited at equidistant points on Petri dishes (90 × 15 mm) containing egg yolk agar for phospholipase, bovine albumin agar for proteinase, 7% sheep blood agar for hemolysin, and DNase agar (Hexis, São Paulo, Brazil). Incubation was performed at 30 °C for four days for phospholipase, seven days for

proteinase and DNase, and 48 h for hemolysin. Tests were performed in duplicate and on two different occasions. The interpretation was carried out according to Menezes et al. [20].

#### Biofilm formation

Biofilm production was detected according to Pierce et al. [21] and Costa-Orlandi et al. [22], with modifications. Briefly, 10  $\mu$ L of a 24-hour culture in SDA from each isolate was inoculated into 20 mL of Yeast Extract Peptone-Dextrose (YPD) broth and incubated overnight at  $35 \pm 2$  °C. After incubation, the tubes were centrifuged at 5000 rpm for five minutes, the supernatant was removed, and the pellet was resuspended in 20 mL of phosphate-buffered saline (PBS), a process that was repeated three times. Then, 1 mL of 0.9% saline was added to the remaining pellet, 20  $\mu$ L of this suspension was pipetted into a Neubauer chamber, and the cell density was adjusted to  $1.0 \times 10^6$  cells/mL. After counting, 10–100  $\mu$ L of the inoculum was added to 900–1000  $\mu$ L of Roswell Park Memorial Institute (RPMI) 1640 broth (Himedia, Mumbai, India) supplemented with glucose and MOPS buffer (Hexis, São Paulo, Brazil) and deposited 100  $\mu$ L into flat-bottom 96-well plates and incubated for 24 h at  $35 \pm 2$  °C.

For biofilm quantification, two plates were incubated, one for biomass production quantification and the other for metabolic activity evaluation, following Pierce et al. [21] and Costa-Orlandi et al. [22]. After 24 h incubation, the supernatant was gently removed, and the wells of both plates were washed three times with PBS to remove planktonic cells. Biofilm biomass production quantification was performed by adding 100  $\mu$ L of 0.5% Crystal Violet and incubating at room temperature for five minutes. Then, the wells were washed with sterile distilled water to remove the excess dye, and 100  $\mu$ L of 33% acetic acid was added after washing. The reading was done in a plate reader (Epoch-Biotek) at a wavelength of 570 nm.

For metabolic activity evaluation, 50  $\mu$ L of the 2,3-bis(2-methoxy-4-nitro-5-sulfophenyl)-5-[carbonyl(phenylamino)]-2H-151 tetrazolium hydroxide-XTT (1 mg mL<sup>-1</sup> of PBS) and menadione (1 mM in ethanol) solution were added to the wells and incubated for 3 h. After incubation, the reading was done in a plate reader (Epoch-Biotek) at a wavelength of 490 nm. Results were classified according to the Optical Density (OD) of each sample [23]: Crystal Violet (staining low biomass production (LBP) < 0.44; moderate biomass production (MBP) = 0.44–1.17; high biomass production (HBP) > 1.17). XTT reduction (low metabolic activity (LMA) < 0.097; moderate metabolic activity (MMA) = 0.097–0.2; high metabolic activity (HMA) > 0.2) [23]. Wells containing only RPMI were the negative control. *Candida albicans* ATCC 90,028 was used as the test control. Tests were done in quadruplicate and repeated three times independently.

#### Antifungal susceptibility testing

The susceptibility test to fluconazole (Fluoxol, La Paz, Bolivia), amphotericin B (Cristalia, São Paulo, Brazil), and micafungin (Raffo, Buenos Aires, Argentina) was performed by the broth microdilution method as described in document M27-S4 [24]. *Candida parapsilosis* ATCC 22019 and *Candida albicans* ATCC 90028 were used as the test control. The assay was performed in duplicate, and the reading was done at 490 nm.

The minimum inhibitory concentration (MIC) was defined as the lowest concentration of the antifungal capable of promoting 50% reduction in yeast growth for fluconazole and micafungin and 90% for amphotericin B [24]. The MIC<sub>50</sub> represents the value of the MIC at which at least 50% of the strains were inhibited. The MIC<sub>50</sub> was considered the value at position  $n \times 0.5$  when  $n$  was an even number of strains. For an odd  $n$ , the value at position  $(n + 1) \times 0.5$  represented the MIC<sub>50</sub> value. The MIC<sub>90</sub> represents the value of the MIC at which at least 90% of the strains were inhibited. The MIC<sub>90</sub> was calculated using  $n \times 0.9$ . When the result was an integer, that number

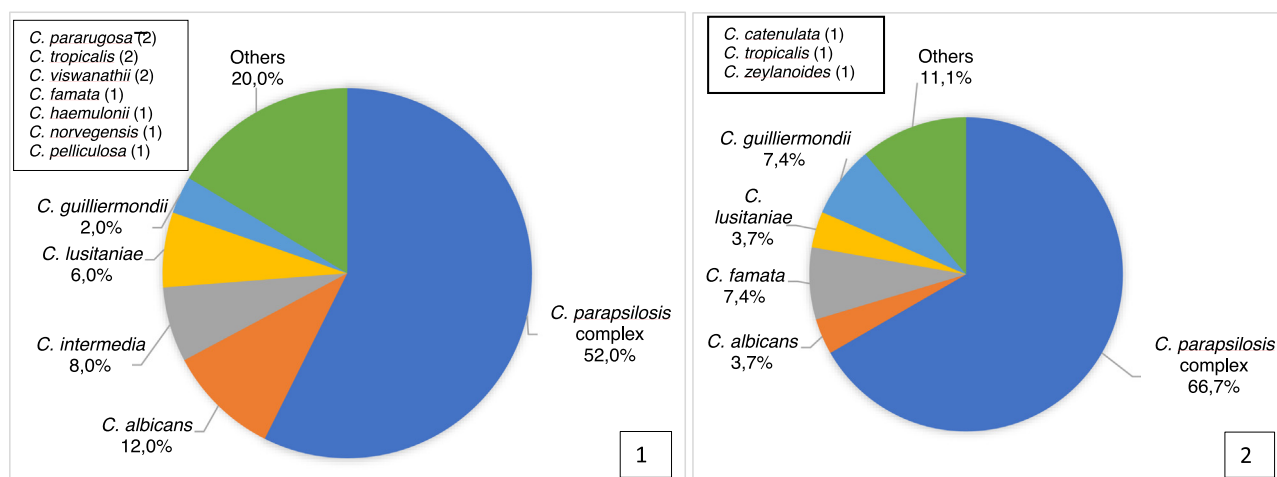


Fig. 1. *Candida* species isolated from the hands of healthcare professionals 1 - before and 2 - after cleaning with 70% ethyl alcohol-based gel.

represented the MIC<sub>90</sub>; for a result where the number was not an integer, the next integer after the respective value represented the MIC<sub>90</sub> [25]. MIC<sub>50</sub> and MIC<sub>90</sub> were calculated only for *C. parapsilosis* isolates, as they had an  $n > 10$ . The interpretation of MIC and the cutoffs for each antifungal were considered according to the CLSI M27-S4, M60, and M59 documents [24,26,27]. Due to the lack of clinical breakpoint (CBPs) or epidemiological cutoff values (ECVs) by CLSI for amphotericin B, micafungin, and fluconazole regarding *C. catenulata* (= *Diatina catenulata*), *C. intermedia*, *C. pararugosa* (currently *Wickerhamiella pararugosa*), *C. lusitaniae* (= *Clavispora lusitaniae*), *C. norvegensis* (currently *Pichia norvegensis*), *C. famata* (= *Debaryomyces hansenii*), *C. pelliculosa* (currently *Wickerhamomyces anomalus*), *C. haemulonii* (currently *Candida haemuli*), *C. viswanathii*, and *C. zeylanoides* species, isolates with MIC for amphotericin B  $\leq 2 \mu\text{g}/\text{mL}$  were considered low MIC and MIC  $> 2 \mu\text{g}/\text{mL}$  high MIC; isolates with MIC for fluconazole  $\leq 8 \mu\text{g}/\text{mL}$  were considered low MIC and MIC  $> 8 \mu\text{g}/\text{mL}$  was considered high MIC, and MIC for micafungin  $\leq 1.0 \mu\text{g}/\text{mL}$  were considered low MIC and those with MIC of  $\geq 2 \mu\text{g}/\text{mL}$  were considered high MIC [28].

#### RAPD (random amplified polymorphic DNA)

Genomic DNA extraction was performed for all isolates obtained from SDA media (24 h) at 35 °C according to Bolano et al. [29]. For RAPD-PCR analysis, the primers OPA9 (5'-GGGTAACGCC-3'), OPA18 (5'-AGCTGACCGT-3'), OPB11 (5'-GTAGACCCGT-3'), and OPG17 (5'-ACGACCGACA-3') (Operon Technologies Inc.) were used. Reactions and amplification products were carried out according to the protocol of Riceto et al. [30]. The gels were observed under ultraviolet light (L-Pix HE, Loccus Brasil, Cotia, SP, Brazil) and images were captured using the photodocumentation system (Image Lab-1D Loccus Brasil, Cotia, SP, Brazil). Bands were represented as present (1) or absent (0) and analyzed using the Multivariate Statistical Package (MVSP) version 3.21 statistical program (Kovach Computing Services, UK). Genetic relationships were calculated using the Jaccard coefficient (Sj). Sj values of 1.00 and 0.99 represent the same genotype, values between 0.80 and 0.99 represent highly similar but not identical samples and values below 0.80 represent distinct samples [30]. Dendrograms based on Sj values were generated by the UPGMA method (Unweighted Pair-Group Method with Arithmetical Averages).

#### Statistical analysis

Quantitative variables were described within the group before and after hand hygiene with 70% ethyl alcohol-based gel, using mean, median, maximum, and minimum standard deviation.

Additionally, the Shapiro-Wilk normality test was applied. For variables that showed normal distribution in both groups, the t-Student test was used to compare them; for those that did not show normal distribution, the Mann-Whitney test was applied [31].

Qualitative variables were described (frequency and percentage) through two-way tables. The associations of qualitative variables were evaluated using the likelihood ratio test/G-test [32]. P values  $< 0.05$  were considered significant. All analyses were performed using SPSS software for Windows (version 20.0; IBM Corp., Armonk, NY, USA).

#### Results

Of the 107 HCWs who participated in the study, *Candida* species were isolated from the hands of 46 (43.0%) in the before a group and 24 (22.4%) in the after group. Regarding CFU, the before group ranged from 0.6 – 60.8  $\times 10^4$  CFU/mL, and the after group ranged from 0.0 – 30.0  $\times 10^4$  CFU/mL, with a 94.1% reduction after the use of 70% ethyl alcohol-based gel and a  $p < 0.001$ .

Seventy-seven *Candida* isolates from 14 distinct species were analyzed, with 50 (64.9%) from the before a group and 27 (35.1%) from the after group (Fig 1). In the before a group, seven rare/atypical species were isolated (14.0% - *C. haemulonii* [= *C. haemuli*], *C. intermedia*, *C. lusitaniae* [= *Clavispora lusitaniae*], *C. norvegensis* [= *Pichia norvegensis*], *C. viswanathii*, *C. pararugosa* [= *Wickerhamiella pararugosa*] and *C. pelliculosa* [= *Wickerhamomyces anomalus*], and three (11.1% - *C. catenulata* [= *Diatina catenulata*], *C. lusitaniae* [= *Clavispora lusitaniae*], and *C. zeylanoides*) were isolated in the after group.

Fig. 1 *Candida* species isolated from the hands of healthcare professionals before and after cleaning with 70% ethyl alcohol-based gel.

All isolates from both groups were able to form biofilms, in addition to producing at least one exoenzyme (Table 1). Of the 50 isolates from the before a group, 49 (98.0%) had HMA and 41 (82.0%) had HBP, nine (18.0%) had MBP, and one (2.0%) had MMA. Fifteen (30.0%) were positive for DNase, eight (16.0%) had phospholipase activity (five moderate and three high), six (12.0%) had proteinase activity (three high and three moderate), and two (4.0%) had hemolytic activity (moderate).

All 27 isolates from the after the group had HBP, 20 (74.1%) had HMA, five (18.5%) had MMA, and two (7.4%) had LMA. Twelve (44.4%) were positive for DNase, four (14.8%) had proteinase activity (high), two (7.4%) had hemolytic activity (moderate), and two (7.40%) had phospholipase activity (moderate).

When the two groups were compared, there was no statistically significant difference in virulence factors (Table 2).

**Table 1**  
Phenotypic and genotypic characteristics of *Candida* spp. isolated from the hands of healthcare professionals in a neonatal intensive care unit, before and after hand hygiene with 70% ethyl alcohol-based gel.

Sample	Hemolytic activity	DNase	Proteinase	Phospholipase	Biofilm		Antifungal susceptibility profile			Genotypic profile
					CV	XTT	Ampho B	Fluco	Mica	
<b>Before (50)</b>										
C. pa 2	Neg	Neg	Neg	Neg	HBP	HMA	S	S	S	M*
C. pa 4	Neg	Neg	Neg	Neg	HBP	HMA	S	S	S	M
C. pa 10	Neg	Neg	Neg	Neg	HBP	HMA	S	S	S	M
C. pa 13	Neg	Neg	Neg	Neg	HBP	HMA	S	S	S	M*
C. pa 15	Neg	Neg	Neg	High	HBP	HMA	S	S	S	M
C. pa 16	Neg	Neg	Neg	Neg	HBP	MMA	R	S	S	M
C. pa 30	Neg	Pos	Neg	Neg	HBP	HMA	R	S	S	–
C. pa 38	Neg	Neg	Neg	Neg	HBP	HMA	S	SDD	S	–
C. pa 39	Neg	Neg	Neg	Neg	HBP	HMA	S	S	S	F
C. pa 40	Neg	Neg	Neg	Neg	HBP	HMA	S	S	S	F
C. pa 52	Neg	Pos	Neg	Neg	HBP	HMA	S	S	S	L
C. pa 62	Neg	Neg	Neg	Neg	HBP	HMA	S	S	S	–
C. pa 64	Neg	Neg	Neg	Neg	HBP	HMA	S	S	S	L
C. pa 69	Neg	Neg	Neg	Neg	HBP	HMA	S	S	S	L
C. pa 74	Neg	Neg	Neg	Neg	MBP	HMA	S	S	S	–
C. pa 75	Neg	Neg	Neg	Neg	HBP	HMA	S	SDD	S	–
C. pa 88	Neg	Pos	Neg	Neg	HBP	HMA	S	SDD	S	–
C. pa 92	Neg	Neg	Neg	Neg	HBP	HMA	S	S	S	M
C. pa 98	Neg	Pos	Neg	Neg	HBP	HMA	S	S	S	K
C. pa 100	Neg	Neg	Neg	Neg	HBP	HMA	S	S	S	M
C. pa 101	Neg	Pos	Neg	Neg	MBP	HMA	S	S	S	–
C. pa 102	Neg	Pos	Neg	Neg	HBP	HMA	S	S	S	–
C. pa 111	Neg	Pos	Neg	Neg	MBP	HMA	S	R	S	–
C. pa 119	Neg	Pos	High	Neg	MBP	HMA	S	S	S	L
C. pa 139	Mod	Neg	Neg	Neg	HBP	HMA	S	S	S	J
C. pa 149	Neg	Neg	Neg	Neg	HBP	HMA	S	S	S	J
C. al 31	Neg	Neg	Neg	Neg	HBP	HMA	S	S	S	B
C. al 91	Mod	Neg	High	Neg	HBP	HMA	S	SDD	S	B
C. al 95	Neg	Neg	Neg	Neg	HBP	HMA	S	S	S	B
C. al 96	Neg	Neg	Neg	High	HBP	HMA	S	S	S	–
C. al 115	Neg	Neg	Neg	High	HBP	HMA	S	S	S	B*
C. al 143	Neg	Neg	Neg	High	HBP	HMA	S	S	S	B*
C. in 8	Neg	Neg	Neg	Neg	HBP	HMA	L	L	L	A
C. in 43	Neg	Pos	Mod	Mod	HBP	HMA	L	L	L	–
C. in 48	Neg	Neg	Mod	Neg	MBP	HMA	L	L	L	A
C. in 97	Neg	Pos	Neg	Neg	HBP	HMA	L	L	L	A
C. lu 37	Neg	Neg	Neg	Neg	HBP	HMA	L	L	L	E
C. lu 83	Neg	Pos	Neg	Neg	HBP	HMA	L	L	L	–
C. lu 140	Neg	Neg	Neg	Neg	HBP	HMA	L	L	L	E
C. gui 133	Neg	Neg	Neg	Neg	HBP	HMA	S	R	S	C
C. para 12	Neg	Neg	Neg	Neg	HBP	HMA	L	L	L	D
C. para 49	Neg	Neg	Neg	Neg	HBP	HMA	L	L	L	D
C. tro 44	Neg	Neg	Neg	Neg	HBP	HMA	S	S	S	–
C. tro 53	Neg	Neg	Neg	Neg	HBP	HMA	S	S	S	–
C. vis 82	Neg	Neg	Neg	Neg	MBP	HMA	L	H	L	–
C. vis 109	Neg	Pos	Neg	Neg	MBP	HMA	L	L	L	–
C. nor 26	Neg	Neg	Neg	Neg	HBP	HMA	L	L	L	–
C. fa 27	Neg	Neg	Neg	Neg	MBP	HMA	S	S	S	–
C. pe 50	Neg	Neg	Neg	Neg	HBP	HMA	L	L	L	–
C. hae 77	Neg	Neg	Mod	Mod	MBP	HMA	L	L	L	–
<b>After (27)</b>										
C. pa 3	Neg	Neg	Neg	Neg	HBP	LMA	S	S	S	–
C. pa 11	Neg	Neg	High	Neg	HBP	MMA	S	S	S	I
C. pa 21	Neg	Pos	High	Neg	HBP	HMA	R	SDD	I	H
C. pa 23	Neg	Pos	Neg	Neg	HBP	HMA	S	S	S	G
C. pa 33	Neg	Pos	Neg	Neg	HBP	HMA	S	S	S	G
C. pa 51	Neg	Pos	Neg	Neg	HBP	HMA	S	S	S	G
C. pa 55	Neg	Pos	Neg	Neg	HBP	HMA	S	S	S	–
C. pa 60	Neg	Pos	Neg	Neg	HBP	HMA	S	S	S	–
C. pa 61	Neg	Neg	Neg	Neg	HBP	LMA	S	S	S	I
C. pa 66	Neg	Pos	Neg	Neg	HBP	HMA	S	S	S	I
C. pa 73	Neg	Pos	Neg	Neg	HBP	HMA	S	S	S	I
C. pa 89	Neg	Neg	Neg	Neg	HBP	HMA	S	R	S	–
C. pa 94	Neg	Pos	Neg	Neg	HBP	HMA	S	S	S	K
C. pa 106	Neg	Neg	Neg	Neg	HBP	MMA	S	S	S	H
C. pa 108	Neg	Pos	Neg	Neg	HBP	HMA	S	SDD	S	–
C. pa 110	Neg	Neg	Neg	Neg	HBP	HMA	S	S	S	H
C. pa 118	Neg	Pos	High	Neg	HBP	HMA	S	S	S	G
C. pa 120	Neg	Neg	High	Neg	HBP	AAM	S	S	S	H
C. fa 20	Neg	Neg	Neg	Neg	HBP	AAM	S	S	S	–

(continued)

**Table 1** (Continued)

Sample	Hemolytic activity	DNase	Proteinase	Phospholipase	Biofilm		Antifungal susceptibility profile			Genotypic profile
					CV	XTT	Ampho B	Fluco	Mica	
C. fa 135	Neg	Neg	Neg	Neg	HBP	MMA	S	S	S	–
C. gui 93	Mod	Neg	Neg	Neg	HBP	MMA	S	S	S	C
C. gui 146	Mod	Neg	Neg	Neg	HBP	AAM	S	S	S	–
C. al 107	Neg	Neg	Neg	Mod	HBP	AAM	S	SDD	S	B
C. ca 46	Neg	Pos	Neg	Neg	HBP	AAM	L	H	L	–
C. lu 134	Neg	Neg	Neg	Neg	HBP	AAM	L	H	L	E
C. tro 117	Neg	Neg	Neg	Mod	HBP	AAM	L	L	L	–
C. zey 150	Neg	Neg	Neg	Neg	HBP	MMA	L	L	L	–

Note: ampho, amphotericin B; fluco, fluconazole; mica, micafungin; C.al, *Candida albicans*; C. ca, *C. catenulata* (= *Diutina cetmulata*); C. pa, *C. parapsilosis*; C. para, *C. pararugosa* (= *Wickerhamiella pararugosa*); C. lu, *C. lusitaniae* (= *Clavispora lusitaniae*); C. in, *C. intermedia*; C. nor, *C. norvegensis* (= *Pichia norvegensis*); C. fa, *C. famata* (= *Debaryomyces hansenii*); C. tro, *C. tropicalis*; C. pe, *C. pelliculosa* (= *Wickerhamomyces anomalus*); C. hae, *C. haemulonii* (*C. haemuli*); C. vis, *C. viswanathi*; C. gui, *C. guilliermondii* (= *Meyerozyma guilliermondii*); C. zey, *C. zeylanoides*; pos, positive; neg, negative; mod, moderate; XTT, tetrazolium salt; CV, crystal violet; MBP, moderate biomass production; HBP, high biomass production; LMA, low metabolic activity; MMA, moderate metabolic activity; HMA, high metabolic activity; S, susceptible; SDD susceptibility dose dependent; I, intermediate susceptibility; R, resistant; L, low MIC; H, high MIC \* same genotype; - did not form genotypic profiles.

**Table 2**

Comparison of samples from groups before and after hand hygiene by healthcare professionals in a neonatal intensive care unit with 70% ethyl alcohol-based gel in relation to virulence factors and susceptibility profile to antifungal agents.

Classification		Before 50 (%)	After 27 (%)	Total 77 (%)	Valor p
<b>Virulence factors</b>					
<b>Biomass production (CV)</b>	MBP	1 (2.0)	0 (0.0)	1 (1.3)	2.165
	HBP	49 (98.0)	27 (100.0)	76 (98.7)	
<b>Metabolic activity (XTT)</b>	LMA	0 (0.0)	2 (7.4)	2 (2.3)	0.115
	MMA	9 (18.0)	5 (18.5)	14 (18.2)	
	HMA	41 (82.0)	20 (74.1)	61 (79.2)	
<b>DNase</b>	positive	15 (30.0)	12 (44.4)	27 (30.7)	0.208
	negative	35 (70.0)	15 (55.6)	50 (64.9)	
<b>Hemolytic activity</b>	moderate	2 (4.0)	2 (7.4)	4 (5.2)	0.529
	negative	48 (96.0)	25 (92.6)	73 (94.8)	
<b>Proteinase</b>	high	3 (6.0)	4 (14.8)	7 (9.1)	0.134
	moderate	3 (6.0)	0 (0.0)	3 (3.9)	
	negative	44 (88.0)	23 (85.2)	67 (87.0)	
<b>Phospholipase</b>	high	3 (6.0)	1 (3.7)	4 (5.2)	0.511
	moderate	5 (10.0)	1 (3.7)	6 (7.8)	
	negative	42 (84.0)	25 (92.6)	67 (87.0)	
<b>Antifungal susceptibility profile</b>					
<b>MIC Anfotericina B</b>	susceptible	47 (94.0)	26 (96.3)	73 (94.8)	0.656
	resistant**	3 (6.0)	1 (3.7)	4 (5.2)	
<b>MIC Fluconazol</b>	susceptible	43 (86.0)	21 (77.8)	64 (83.1)	0.642
	SDD	4 (8.0)	3 (11.1)	7 (9.1)	
	resistant**	3 (6.0)	3 (11.1)	6 (7.8)	
<b>MIC Micafungina</b>	susceptible	49 (98.0)	26 (96.3)	75 (97.4)	0.227
	I	0 (0.0)	1 (3.7)	1 (1.3)	
	resistant**	1 (2.0)	0 (0.0)	1 (1.3)	

MIC, minimum inhibitory concentration; SDD, susceptibility dose dependent; I, intermediate susceptibility; MPB, moderate biomass production; HBP, high biomass production; LMA, low metabolic activity; MMA, moderate metabolic activity; HMA, high metabolic activity. \* p values < 0.05 were considered significant; \*\*samples classified as high MIC were analyzed as resistant.

**Table 1** Phenotypic and genotypic characteristics of *Candida* spp. isolated from the hands of HCWs in a NICU, before and after hand hygiene with 70% ethyl alcohol-based gel

**Table 2** Comparison of samples from groups before and after hand hygiene of HCWs from a NICU with 70% ethyl alcohol-based gel in relation to virulence factors and antifungal susceptibility profile

**Table 3** shows the MIC range values for the three antifungal agents tested. In the before a group, three (6.0%) isolates were resistant to amphotericin B, two (4.0%) were resistant, and one (2.0%) presented high MIC to fluconazole, and one (2.0%) isolate presented high MIC to micafungin (Tables 1 and 3). Isolates of *C. parapsilosis* complex presented a MIC50 of 0.50 µg/mL and MIC90 of 2.00 µg/mL for amphotericin B, for fluconazole they presented a MIC50 of 2.00 µg/mL and MIC90 of 4.00 µg/mL, and for micafungin they presented a MIC50 of 1.00 µg/mL and MIC90 of 2.00 µg/mL.

In the after group, one (3.7%) isolate was resistant to fluconazole and two (7.4%) presented high MIC. One (3.7%) isolate was resistant to amphotericin B (Table 1 and 3). Isolates of *C. parapsilosis* complex presented a MIC50 of 0.50 µg/mL and MIC90 of 2.00 µg/mL for amphotericin B, for fluconazole they presented a MIC50 of 1.00 µg/mL and MIC90 of 4.00 µg/mL, and for micafungin they presented a MIC50 of 1.0 µg/mL and MIC90 of 2.0 µg/mL.

There was no statistically significant difference in antifungal resistance between the two groups (Table 2).

**Table 3** MIC values presented by *Candida* species on the hands of HCWs in a NICU, before and after cleaning with a 70% ethyl alcohol-based gel

Molecular analysis of the 77 isolates revealed the presence of two clusters of identical strains, represented by genotypes B\* and M\*, totaling four isolates, two of *C. albicans* (B\* - 115 and 143) and two of

**Table 3**  
Minimum inhibitory concentration values presented by *Candida* species in the hands of healthcare professionals in a neonatal intensive care unit, before and after cleaning with gel based on 70% ethyl alcohol.

Species (n) [currently name]	Amphotericin B MIC range ( $\mu\text{g/mL}$ )	Fluconazole MIC range ( $\mu\text{g/mL}$ )	Micafungin MIC range ( $\mu\text{g/mL}$ )
<b>Before (50)</b>			
<i>C. parapsilosis</i> complex (26)	0.125 – 4.00	0.50 – 8.00	0.015 – 2.00
<i>C. pararugosa</i> (2) [=Wickerhamiella pararugosa]	0.25 – 0.50	2.00 – 4.00	0.125 – 0.125
<i>C. albicans</i> (6)	0.125 – 0.50	0.50 – 4.00	0.015 – 0.03
<i>C. famata</i> (1) [=Debaryomyces hansenii]	1.00	1.00	2.00
<i>C. guilliermondii</i> (1) [=Meyerozyma guilliermondii]	0.50	8.00	1.00
<i>C. haemulonii</i> (1) [=C. haemulii]	4.00	4.00	0.125
<i>C. intermedia</i> (4)	0.06 – 0.25	1.00 – 4.00	0.03 – 0.25
<i>C. lusitaniae</i> (3) [=Clavispora lusitaniae]	0.50 – 1.00	0.50 – 1.00	0.25 – 0.50
<i>C. tropicalis</i> (2)	0.25 – 0.25	1.00 – 1.00	0.125 – 0.125
<i>C. norvegensis</i> (1) [=Pichia norvegensis]	1.00	1.00	0.015
<i>C. pelliculosa</i> (1) [=Wickerhamomyces anomalus]	0.25	0.125	0.50
<i>C. viswanathii</i> (2)	0.25 – 1.00	1.00 – 16.00	0.06 – 0.50
<b>After (27)</b>			
<i>C. parapsilosis</i> complex (18)	0.125 – 4.00	0.50 – 16.00	0.125 – 4.00
<i>C. albicans</i> (1)	0.50	4.00	0.015
<i>C. catenulata</i> (1) [=Ditina catenulata]	1.00	16.00	0.03
<i>C. famata</i> (2)	0.25 – 1.00	1.00 – 4.00	0.03 – 0.06
<i>C. guilliermondii</i> (2)	0.50 – 1.00	1.00 – 8.00	0.03 – 1.00
<i>C. lusitaniae</i> (1)	1.00	4.00	0.06
<i>C. tropicalis</i> (1)	0.25	0.50	0.015
<i>C. zeylanoides</i> (1)	0.50	0.50	1.00

MIC, minimum inhibitory concentration.

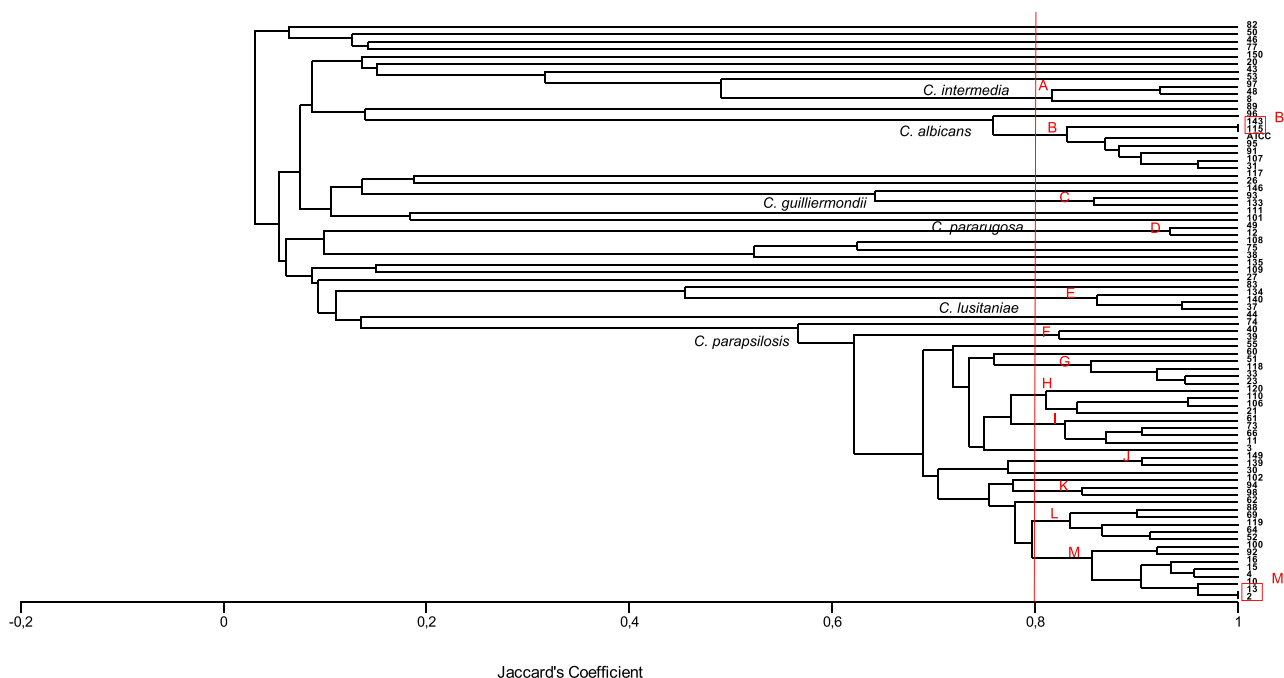


**Fig. 2.** RAPD dendrogram of the 77 hand samples of health professionals before and after cleaning with a 70% ethyl alcohol-based gel.

*C. parapsilosis* complex (M\* - 2 and 13), all from the before a group and from different HCWs. The remaining isolates that showed high similarity were grouped into 13 clusters, i.e., 13 identified profiles from A to M (47/77 – 61.0%). These and other results are presented in Fig 2 and Table 1.

Cluster B is composed of six isolates of *C. albicans*, two of which (31 and 107) are highly similar and come from different groups and HCWs (Fig. 2 and Table 1).

Cluster C, formed by two *C. guilliermondii* (=Meyerozyma guilliermondii) isolates (93 and 133), showed high similarity, and came from different groups and professionals.

In cluster E, two *C. lusitaniae* (=Clavispora lusitaniae) isolates (37 and 140) found in the before a group and from different professionals, showed high similarity with *C. lusitaniae* 134, isolated from the hands of another professional in the after group (Fig. 2 and Table 1).

In cluster K, two *C. parapsilosis* complex isolates (94 and 98) were found in the hands of two HCWs and different groups (before and after, respectively). The other *C. parapsilosis* complex isolates that showed high similarity at the before moment (17/26, 65.4%) were grouped into clusters F, J, L, and M, while the remaining *C. parapsilosis* complex isolates from the after a moment (12/18, 67.0%) were grouped into clusters G, H, and I (Fig. 2 and Table 1).

## Discussion

*Candida* spp. related HAIs are a public health problem due to their severity and high morbidity and mortality rates [33–35]. Lack of hand hygiene or inadequate hand hygiene by HCWs has been reported as one of the main reasons for the horizontal transmission of virulent *Candida* species, responsible for invasive infections in critical patients such as neonates [35,36]. Despite the importance of *Candida* species in the occurrence of HAIs, only two studies in Brazil [10,11], one in the UK [36], and two in India [8,37] have evaluated the action of alcohol-based gel in the inactivation of these species on the hands of HCWs.

This is the first study to investigate the presence of *Candida* spp. on the hands of HCWs in a NICU before and after hand hygiene with 70% ethyl alcohol-based gel. Of the 107 HCWs who participated in the study, 70 (65.4%) had contaminated hands, with 24 (34.3%) positive after hand hygiene. The 70% ethyl alcohol-based gel used in this study was able to reduce the number of CFUs, demonstrating the efficacy of its use in hand hygiene. This technique is easy to use and handle, requires less time for application, and can be used at the bedside. However, *Candida* samples were isolated from the after group, and this could have happened due to factors such as the amount of product versus friction time, which may not have been sufficient for the elimination of yeasts [15,16,34], and whether hands were wet at the time of application [15,16] or greater resistance to the antiseptic [13]. In addition, biofilm production present in all isolates in this study may have contributed to a greater permanence of yeasts in the environment, allowing them to adhere to biomedical devices and making it difficult to remove these microorganisms from hands [8,33].

In this study, *C. parapsilosis* complex and *C. albicans* were the most isolated species from the hands of HCWs, followed by rare species such as *C. guilliermondii* (= *Meyerozyma guilliermondii*), *C. famata* (= *Debaryomyces hansenii*), *C. haemulonii* (= *C. haemuli*), *C. intermedia*, and *C. lusitaniae* (= *Clavispora lusitaniae*). In the last decade, emerging and atypical yeasts have been reported as a cause of increased fungal infections in immunocompromised and/or hospitalized patients, and these pathogens in some cases have been reported with an important profile of resistance to antifungal drugs, especially azoles, and increased resistance to polyenes and echinocandins [38].

The evaluation of the virulence factors of microorganisms on the hands of HCWs is crucial, as these microorganisms can be responsible for triggering invasive infections in critical patients such as neonates. This was observed in our study published in 2018 [20], in which a case of candidemia caused by *C. albicans* in the NICU showed similarities with the other *C. albicans* isolates collected from the hands of HCWs. Other studies conducted in NICUs in Brazil [39], Mexico [40], and Portugal [41] have also identified *C. parapsilosis* species in the hands of HCWs, and these isolates were responsible for outbreaks of candidemia in neonates.

In this study, all isolates had at least one virulence factor among those analyzed. DNase, an extracellular hydrolytic enzyme that contributes to microbial pathogenicity by enhancing its adhesion, tissue damage, and evasion of the immune system, as well as its dissemination [42], was present in almost all species isolated from the hands of HCWs. *C. catenulata* (= *Diatina catenulata*) was the only species that did not produce any enzymes, but it was a strong producer of biomass, showed high metabolic activity, and was high MIC to fluconazole (MIC 16  $\mu\text{g}/\text{mL}$ ). The study by Chen et al. [43] showed a high MIC of this species for fluconazole (>8  $\mu\text{g}/\text{mL}$ ) in invasive infection samples, mainly in ICU patients. Candidemia caused by unusual species seems to have a poorer response to antifungal treatment due to MIC values above the epidemiological cutoff and a longer duration of candidemia [34].

All samples were able to form a biofilm, 87.5% with HBP and 90.9% with HMA. These data corroborate the fact that even after hand hygiene with 70% ethyl alcohol-based gel, *Candida* species were still

isolated. The persistence of pathogens in biofilm in the hospital environment or in living tissues can be a source of cross-transmission with a marked clinical impact, leading to hospital-acquired infections that are more difficult to treat and have a higher chance of recurrence [44,45].

The majority (88.3%) of isolates were susceptible to the tested antifungals (amphotericin B, fluconazole, and micafungin). However, *C. parapsilosis* complex isolates showed resistance to amphotericin B and fluconazole and exhibited intermediate susceptibility to micafungin. Although resistance to echinocandins is generally low among *C. parapsilosis* complex, the increased use of this class of antifungals has resulted in changes in species prevalence and a gradual increase in minimum inhibitory concentrations of echinocandins among several species [46]. In our study, *C. haemulonii* (= *C. haemuli*) presented a high MIC (4  $\mu\text{g}/\text{mL}$ ) for amphotericin B. This yeast is a rare subtype, reported as an emerging and virulent pathogen, difficult to identify due to its phenotypic similarity with other *Candida* subtypes, which may increase the risk of inadequate antimicrobial administration and worsening of emerging resistance patterns [47].

Forty-six (59.8%) isolates were highly similar ( $S_j > 80\%$ ) in the four primers tested. Two isolates of *C. albicans* (*C. al* 115 and 143) and two isolates of *C. parapsilosis* complex (*C. pa* 2 and 13) showed genetic similarities between different HCWs in the group before hand hygiene, and these isolated, despite not producing any extracellular hydrolytic enzymes and being sensitive to the tested antifungals, presented HBP and HMA. *C. albicans* is the main pathogenic species and the most frequent cause of candidiasis in humans [48], and *C. parapsilosis* complex is a major concern because it is a frequent colonizer of human skin and hospital environments [13] and is the main *Candida* species responsible for a significant proportion of nosocomial fungemia outbreaks, particularly in NICUs [4,5,13].

*C. intermedia* showed similarity between two HCWs in the group before hand hygiene and had virulence factors such as moderate production of proteinase, DNase, and HBP formation. *C. intermedia* is an unusual species found in the microbiota of the human oropharyngeal cavity, and although there are no reports of infection by this species in neonates, has been isolated from the bloodstream of pediatric [49] and adults [50,51] patients with infections associated with the presence of intravenous catheters.

In this study, *C. lusitaniae* (= *Clavispora lusitaniae*) was found to have similarities between isolates of HCWs before and after hand hygiene, with the presence of virulence factors such as HBP and HMA, and the isolate after hand hygiene also showed high MIC (4  $\mu\text{g}/\text{mL}$ ) to fluconazole. However, *C. lusitaniae* is another rare species, only occasionally related to episodes of candidemia, corresponding to 0.2–9.4% of all *Candida* isolates in blood or other sterile sites [37,52], and unlike our results, in other studies [37,52] this species showed resistance to amphotericin B and sensitivity to fluconazole and was able to produce phospholipase, hemolysin, and proteinase enzymes.

This study has some limitations. Materials were not collected from the hands of the same HCWs in different groups, and genetic sequencing of the *Candida* isolates was not performed to confirm cross-transmission. A suggestion for future studies would be molecular analysis of isolates that showed resistance to the antifungals tested to characterize the mechanisms of resistance.

It is important to note that HCWs have a wide possibility of hand contamination during routine activities, and when not properly sanitized, increase the possibility of cross-transmission of pathogens between patients and/or professionals, with a negative impact on the entire healthcare system [15,16,53] including NICU.

In conclusion, *Candida* species were isolated from the hands of most HCWs in a tertiary hospital's NICU in Brazil in both groups (before and after), but the 70% ethyl alcohol-based gel sanitizer used in this study was effective in reducing the isolates. The most frequent species was the *C. parapsilosis* complex. All isolates produced at least



one virulence factor, with biofilm being present in all species, showing HBP and HMA. Some isolates showed high genetic similarity and were in different HCWs and groups, highlighting the importance of hand hygiene to minimize the risk of cross-contamination in NICUs.

## Glossary

NICU, neonatal intensive care units; RAPD, random amplified polymorphic DNA; BrSCOPE, Brazilian surveillance and control of pathogens of epidemiologic importance; HCW, healthcare professionals; ABHSS, alcohol-based hand antiseptics; BHI, Brain Heart Infusion; SDA, Sabouraud Dextrose Agar; CFU, colony forming units; MALDI-TOF, matrix-assisted laser desorption/ionization time-of-flight; YPD, Yeast Extract Peptone-Dextrose; PBS, phosphate-buffered saline; RPMI, Roswell Park Memorial Institute; LBP, low biomass production; MBP, moderate biomass production; HBP, high biomass production; LMA, low metabolic activity; MMA, moderate metabolic activity; HMA, high metabolic activity; MIC, minimum inhibitory concentration.

## Author contributions

All authors contributed to the study conception and design. Material preparation, data collection and analysis were performed by [Priscila Guerino Vilela Alves], [Nagela Bernadelli Sousa e Silva], [Meliza Arantes de Souza Bessa], [Gabriel de Oliveira Faria], [Ralciane de Paula Menezes], [Lúcio Borges de Araújo] and [Mário Paulo Amante Penatti]. The first draft of the manuscript was written by [Priscila Guerino Vilela Alves], [Denise Von Dolinger de Brito Röder] and [Reginaldo dos Santos Pedrosa] and all authors commented on previous versions of the manuscript. All authors read and approved the final manuscript.

## Informed consent

Informed consent was obtained from all study participants.

## Ethics approval

This study was performed in line with the principles of the Declaration of Helsinki. Approval was granted by the Ethics Committee of the Federal University of Uberlândia (document 2.173.884/2018).

## Consent to participate

Informed consent was obtained from all individual participants included in the study.

## Funding

This study was supported by [Fundação de Amparo à Pesquisa do Estado de Minas Gerais](#) (FAPEMIG) [grant number [APQ-00965, 2018](#)]; and [Coordenação de Aperfeiçoamento de Pessoal de Nível Superior](#) (CAPES) [one a research grant].

## Declaration of competing interest

none.

## Acknowledgments

The authors would like to thank the Neonatal Intensive Care Unit of the University Hospital of Uberlândia, especially Dr. Daniela Marques de Lima Mota Ferreira and Nurse Waleska Cristina Gomes da Silva, the Curso Técnico em Análises Clínicas and the Escola Técnica de Saúde of the University of Uberlândia (ESTES-UFU) for the

research space, and [Fundação de Amparo à Pesquisa do Estado de Minas Gerais](#) (FAPEMIG) and [Coordenação de Aperfeiçoamento de Pessoal de Nível Superior](#) (CAPES) for funding (APQ-00965–18), research grants for PGVA and NBSS, respectively, and CAPES for providing access to article databases. Special thanks to Murilo de Oliveira Brito for his work support.

## References

- [1] Doi AM, Pignatari ACC, Edmond MB, Marra AR, Camargo LFA, Siqueira RA, et al. Epidemiology and microbiologic characterization of nosocomial candidemia from a Brazilian national surveillance program. *PLoS One* 2016;11:e0146909. doi: [10.1371/journal.pone.0146909](#).
- [2] McCarty TP, White CM, Pappas PG. Candidemia and invasive candidiasis. *Infect Dis Clin North Am* 2021;35:389–413. doi: [10.1016/j.idc.2021.03.007](#).
- [3] da Silva CM, de Carvalho AMR, Macêdo DPC, Jacá MB, Amorim R de JM, Neves RP. Candidemia in Brazilian neonatal intensive care units: risk factors, epidemiology, and antifungal resistance. *Braz J Microbiol* 2023. doi: [10.1007/s42770-023-00943-1](#).
- [4] Savastano C, De Oliveira Silva E, Gonçalves LL, Nery JM, Silva NC, Dias ALT. *Candida glabrata* among *Candida* spp. from environmental health practitioners of a Brazilian Hospital. *Brazil J Microbiol* 2016;47:367–72. doi: [10.1016/j.bjm.2015.05.001](#).
- [5] Suleyman G, Alangaden G, Bardossy AC. The role of environmental contamination in the transmission of nosocomial pathogens and healthcare-associated infections. *Curr Infect Dis Rep* 2018;20:12. doi: [10.1007/s11908-018-0620-2](#).
- [6] Wang H, Zhang L, Kudinha T, Kong F, Ma X-J, Chu Y-Z, et al. Investigation of an unrecognized large-scale outbreak of *Candida parapsilosis* sensu stricto fungaemia in a tertiary-care hospital in China. *Sci Rep* 2016;6:27099. doi: [10.1038/srep27099](#).
- [7] Qi L, Fan W, Xia X, Yao L, Liu L, Zhao H, et al. Nosocomial outbreak of *Candida parapsilosis* sensu stricto fungaemia in a neonatal intensive care unit in China. *Journal of Hospital Infection* 2018;100:e246–52. doi: [10.1016/j.jhin.2018.06.009](#).
- [8] Keri V, Kumar A, Singh G, Xess I, Khan MA, Rastogi N, et al. Fungal carriage on healthcare workers' hands, clothing, stethoscopes and electronic devices during routine patient care: a study from a tertiary care center. *J Prev Med Hyg* 2021; E170. Pages. doi: [10.15167/2421-4248/JPMH2021.62.1.1645](#).
- [9] Kratzel A, Todt D, V'kovski P, Steiner S, Gultom M, Thao TTN, et al. Inactivation of severe acute respiratory syndrome coronavirus 2 by who-recommended hand rub formulations and alcohols. *Emerg Infect Dis* 2020;26:1592–5. doi: [10.3201/eid2607.200915](#).
- [10] Hernández-Castro R, Arroyo-Escalante S, Carrillo-Casas EM, Moncada-Barrón D, Álvarez-Verona E, Hernández-Delgado L, et al. Outbreak of *Candida parapsilosis* in a neonatal intensive care unit: a health care workers source. *Eur J Pediatr* 2010;169:783–7. doi: [10.1007/s00431-009-1109-7](#).
- [11] Guilhermetti M, Marques Würlzler LA, Castanheira Facio B, Da Silva Furlan M, Campo Meschial W, Bronharo Tognim MC, et al. Antimicrobial efficacy of alcohol-based hand gels. *Journal of Hospital Infection* 2010;74:219–24. doi: [10.1016/j.jhin.2009.09.019](#).
- [12] Fallica F, Leonardi C, Toscano V, Santonocito D, Leonardi P, Puglia C. Assessment of alcohol-based hand sanitizers for long-term use, formulated with addition of natural ingredients in comparison to WHO Formulation 1. *Pharmaceutics* 2021;13:571. doi: [10.3390/pharmaceutics13040571](#).
- [13] Thomaz DY, Del Negro GMB, Ribeiro LB, Da Silva M, Carvalho GOMH, Camargo CH, et al. A Brazilian Inter-Hospital Candidemia Outbreak Caused by Fluconazole-Resistant *Candida parapsilosis* in the COVID-19 Era. *JoF* 2022;8:100. doi: [10.3390/jof8020100](#).
- [14] Soldini S, Posteraro B, Vella A, De Carolis E, Borghi E, Falleni M, et al. Microbiologic and clinical characteristics of biofilm-forming *Candida parapsilosis* isolates associated with fungaemia and their impact on mortality. *Clin Microbiol Infect* 2018;24:771–7. doi: [10.1016/j.cmi.2017.11.005](#).
- [15] Boyce JM, Pittet D. Guideline for hand hygiene in health-care settings: recommendations of the healthcare infection control practices advisory committee and the HICPAC/SHEA/APIC/IDSA Hand Hygiene Task Force. *Infect Control Hosp Epidemiol* 2002;23:S3–40. doi: [10.1086/503164](#).
- [16] World Health Organization. WHO guidelines on hand hygiene in health care. *WHO Patient Safety*; 2009. p. 262.
- [17] American Society for Testing and Materials International. ASTM e 1174-06: standard test method for evaluation of the effectiveness of healthcare personnel handwash formulations. West Conshohocken, PA: American Society for Testing and Materials; 2006.
- [18] Orozco PA, Cortés JA, Parra CM. Colonización por levaduras en recién nacidos y personal de salud en la unidad de cuidados intensivos neonatales de un hospital universitario en Bogotá, Colombia. *Revista Iberoamericana de Micología* 2009;26:108–11. doi: [10.1016/S1130-1406\(09\)70020-8](#).
- [19] Rörig KCO, Colacite J, Abegg MA. Produção de fatores de virulência in vitro por espécies patogênicas do gênero *Candida*. *Rev Soc Bras Med Trop* 2009;42:225–7. doi: [10.1590/S0037-86822009000200029](#).
- [20] De Paula Menezes R, Silva FF, Melo SGO, Alves PGV, Brito MO, De Souza Bessa MA, et al. Characterization of *Candida* species isolated from the hands of the healthcare workers in the neonatal intensive care unit. *Med Mycol* 2019;57:588–94. doi: [10.1093/mmy/myy101](#).

- [21] Pierce CG, Uppuluri P, Tristan AR, Wormley FL, Mowat E, Ramage G, et al. A simple and reproducible 96-well plate-based method for the formation of fungal biofilms and its application to antifungal susceptibility testing. *Nat Protoc* 2008;3:1494–500. doi: [10.1038/nprot.2008.141](https://doi.org/10.1038/nprot.2008.141).
- [22] Costa-Orlandi CB, Sardi JCO, Santos CT, Fusco-Almeida AM, Mendes-Giannini MJS. In vitro characterization of *Trichophyton rubrum* and *T. mentagrophytes* biofilms. *Biofouling* 2014;30:719–27. doi: [10.1080/08927014.2014.919282](https://doi.org/10.1080/08927014.2014.919282).
- [23] Marcos-Zambrano LJ, Escribano P, Bouza E, Guinea J. Production of biofilm by *Candida* and non-*Candida* spp. isolates causing fungemia: comparison of biomass production and metabolic activity and development of cut-off points. *Int J Medical Microbiol* 2014;304:1192–8. doi: [10.1016/j.ijmm.2014.08.012](https://doi.org/10.1016/j.ijmm.2014.08.012).
- [24] Clinical and Laboratory Standards Institute, CLSI. Reference method for broth dilution antifungal susceptibility testing of yeasts; fourth informational supplement. Document M27-S4. Clinical and Laboratory Standards Institute; 2012.
- [25] Schwarz S, Silley P, Simjee S, Woodford N, Van Duijkeren E, Johnson AP, et al. Assessing the antimicrobial susceptibility of bacteria obtained from animals. *Vet Microbiol* 2010;141:1–4. doi: [10.1016/j.vetmic.2009.12.013](https://doi.org/10.1016/j.vetmic.2009.12.013).
- [26] Clinical and Laboratory Standards Institute (CLSI). Performance Standards for antifungal susceptibility testing of yeasts. Approved standard–M-60, 1. Clinical and Laboratory Standards Institute, 2017.
- [27] Clinical and Laboratory Standards Institute (CLSI). Epidemiological Cutoff Values for Antifungal susceptibility testing. Approved standard–M59, 2. Clinical and Laboratory Standards Institute, 2018.
- [28] Pfaller MA, Diekemab DJ. Progress in Antifungal Susceptibility Testing of *Candida* spp. by Use of Clinical and Laboratory Standards Institute Broth Microdilution Methods, 2010 to 2012. *J Clin Microbiol* 2012;50(9):2846–56. doi: [10.1128/jcm.01901-07](https://doi.org/10.1128/jcm.01901-07).
- [29] Bolano A, Stinchi S, Preziosi R, Bistoni F, Allegrucci M, Baldelli F, et al. Rapid methods to extract DNA and RNA from *Cryptococcus neoformans*. *FEMS Yeast Res* 2001;1:221–4. doi: [10.1111/j.1567-1364.2001.tb00037.x](https://doi.org/10.1111/j.1567-1364.2001.tb00037.x).
- [30] Riceto EBM, Menezes RP, Röder DVDB, Pedroso RS. Molecular profile of oral *Candida albicans* isolates from HIV-infected patients and healthy persons. *International journal of development research* 2017;7:14432–6.
- [31] Zar JH. *Biostatistical analysis*. 4th ed. Prentice Hall; 1999. p. 663.
- [32] Agresti A. *An introduction to categorical data analysis*. 2nd ed. New York: John Wiley & Sons; 2007. p. 400.
- [33] Brühwasser C, Hinterberger G, Mutschlechner W, Kaltseis J, Lass-Flörl C, Mayr A. A point prevalence survey on hand hygiene, with a special focus on *Candida* species. *Am J Infect Control* 2016;44:71–3. doi: [10.1016/j.ajic.2015.07.033](https://doi.org/10.1016/j.ajic.2015.07.033).
- [34] Sakita KM, Faria DR, Silva EMD, Tobaldini-Valério FK, Kioshima ES, Svidzinski TIE, et al. Healthcare workers' hands as a vehicle for the transmission of virulent strains of *Candida* spp.: a virulence factor approach. *Microb Pathog* 2017;113:225–32. doi: [10.1016/j.micpath.2017.10.044](https://doi.org/10.1016/j.micpath.2017.10.044).
- [35] De Rose D, Santisi A, Ronchetti M, Martini L, Serafini L, Betta P, et al. Invasive *Candida* Infections in Neonates after Major Surgery: current Evidence and New Directions. *Pathogens* 2021;10:319. doi: [10.3390/pathogens10030319](https://doi.org/10.3390/pathogens10030319).
- [36] Moore G, Schelenz S, Borman AM, Johnson EM, Brown CS. Yeastcidal activity of chemical disinfectants and antiseptics against *Candida auris*. *J Hospital Infection* 2017;97:371–5. doi: [10.1016/j.jhin.2017.08.019](https://doi.org/10.1016/j.jhin.2017.08.019).
- [37] Biswal M, Rudramurthy SM, Jain N, Shamanth AS, Sharma D, Jain K, et al. Controlling a possible outbreak of *Candida auris* infection: lessons learnt from multiple interventions. *J Hospital Infection* 2017;97:363–70. doi: [10.1016/j.jhin.2017.09.009](https://doi.org/10.1016/j.jhin.2017.09.009).
- [38] Kumar S, Kumar A, Roudbary M, Mohammadi R, Černáková L, Rodrigues CF. Overview on the Infections Related to Rare *Candida* Species. *Pathogens* 2022;11:963. doi: [10.3390/pathogens11090963](https://doi.org/10.3390/pathogens11090963).
- [39] Miranda L das N, Rodrigues ECA, Costa SF, van der Heijden IM, Dantas KC, Lobo RD, et al. *Candida parapsilosis* candidaemia in a neonatal unit over 7 years: a case series study. *BMJ Open* 2012;2:e000992. doi: [10.1136/bmjopen-2012-000992](https://doi.org/10.1136/bmjopen-2012-000992).
- [40] Vaz C, Sampaio P, Clemons KV, Huang Y-C, Stevens DA, Pais C. Microsatellite multilocus genotyping clarifies the relationship of *Candida parapsilosis* strains involved in a neonatal intensive care unit outbreak. *Diagn Microbiol Infect Dis* 2011;71:159–62. doi: [10.1016/j.diagmicrobio.2011.05.014](https://doi.org/10.1016/j.diagmicrobio.2011.05.014).
- [41] Hernández-Castro R, Arroyo-Escalante S, Carrillo-Casas EM, Moncada-Barrón D, Álvarez-Verona E, Hernández-Delgado L, et al. Outbreak of *Candida parapsilosis* in a neonatal intensive care unit: a health care workers source. *Eur J Pediatr* 2010. doi: [10.1007/s00431-009-1109-7](https://doi.org/10.1007/s00431-009-1109-7).
- [42] Pandey N, Gupta MK, Tilak R. Extracellular hydrolytic enzyme activities of the different *Candida* spp. isolated from the blood of the Intensive Care Unit-admitted patients. *J Lab Physicians* 2018;10:392–6. doi: [10.4103/JLP.JLP\\_81\\_18](https://doi.org/10.4103/JLP.JLP_81_18).
- [43] Chen X-F, Zhang W, Fan X, Hou X, Liu X-Y, Huang J-J, et al. Antifungal susceptibility profiles and resistance mechanisms of clinical *diutina catenulata* isolates with high MIC Values. *Front Cell Infect Microbiol* 2021;11:739496. doi: [10.3389/fcimb.2021.739496](https://doi.org/10.3389/fcimb.2021.739496).
- [44] Silva S, Rodrigues C, Araújo D, Rodrigues M, Henriques M. *Candida* Species Biofilms' Antifungal Resistance. *JoF* 2017;3:8. doi: [10.3390/jof3010008](https://doi.org/10.3390/jof3010008).
- [45] Pierantoni DC, Corte L, Casadevall A, Robert V, Cardinali G, Tascini C. How does temperature trigger biofilm adhesion and growth in *Candida albicans* and two non-*Candida albicans* *Candida* species? *Mycoses* 2021;64:1412–21. doi: [10.1111/myc.13291](https://doi.org/10.1111/myc.13291).
- [46] Castanheira M, Deshpande LM, Messer SA, Rhomberg PR, Pfaller MA. Analysis of global antifungal surveillance results reveals predominance of Erg11 Y132F alteration among azole-resistant *Candida parapsilosis* and *Candida tropicalis* and country-specific isolate dissemination. *Int J Antimicrob Agents* 2020;55:105799. doi: [10.1016/j.ijantimicag.2019.09.003](https://doi.org/10.1016/j.ijantimicag.2019.09.003).
- [47] Coles M, Cox K, Chao A. *Candida haemulonii*: an emerging opportunistic pathogen in the United States? *IDCases* 2020;21:e00900. doi: [10.1016/j.idcr.2020.e00900](https://doi.org/10.1016/j.idcr.2020.e00900).
- [48] Riera FO, Caeiro JP, Angiolini SC, Vigezzi C, Rodriguez E, Icelly PA, et al. Invasive Candidiasis: update and Current Challenges in the Management of This Mycosis in South America. *Antibiotics* 2022;11:877. doi: [10.3390/antibiotics11070877](https://doi.org/10.3390/antibiotics11070877).
- [49] Charsizadeh A, Mirhendi H, Nikmanesh B, Eshaghi H, Rahmani M, Farhang A, et al. Candidemia in Children Caused by Uncommon Species of *Candida*. *Arch Pediatr Infect Dis* 2018;6. doi: [10.5812/pedinfect.11895](https://doi.org/10.5812/pedinfect.11895).
- [50] Ruan S-Y, Chien J-Y, Hou Y-C, Hsueh P-R. Catheter-related fungemia caused by *Candida* intermedia. *Int J Infect Dis* 2010;14:e147–9. doi: [10.1016/j.ijid.2009.03.015](https://doi.org/10.1016/j.ijid.2009.03.015).
- [51] Hasejima N, Matsubayashi M, Kawabe R, Shimura C, Hijikata N, Oda T, et al. The first case of bloodstream infection by *Candida intermedia* in Japan: the importance of molecular identification. *J Infect Chemotherapy* 2011;17:555–8. doi: [10.1007/s10156-011-0215-4](https://doi.org/10.1007/s10156-011-0215-4).
- [52] de Melo APV, Zuza-Alves DL, Silva-Rocha WP, Souza LBFC, Francisco EC, Melo ASA, Chaves GM. Virulence factors of *Candida* spp. obtained from blood cultures of patients with candidemia attended at tertiary hospitals in Northeast Brazil. *J de Mycologie Médicale* 2019;29:132–9. doi: [10.1016/j.mycmed.2019.02.002](https://doi.org/10.1016/j.mycmed.2019.02.002).
- [53] Silva NS, Macedo LJD, Mouta AAN, Souza SKMD, Silva ACBD, Beltrão RPL. Hand hygiene by health professionals: a literature review. *RSD* 2021;10:e462101119446. doi: [10.33448/rsd-v10i11.19446](https://doi.org/10.33448/rsd-v10i11.19446).



OPEN

## Exploring the antifungal, antibiofilm and antienzymatic potential of Rottlerin in an in vitro and in vivo approach

Nagela Bernadelli Sousa Silva<sup>1</sup>, Ralciane Paula Menezes<sup>2</sup>, Daniela Silva Gonçalves<sup>1</sup>, Mariana Brentini Santiago<sup>1</sup>, Noemi Chagas Conejo<sup>1</sup>, Sara Lemes Souza<sup>1</sup>, Anna Lívia Oliveira Santos<sup>1</sup>, Robinson Sabino da Silva<sup>3</sup>, Salvador Boccaletti Ramos<sup>4</sup>, Eloisa Amália Vieira Ferro<sup>5</sup> & Carlos Henrique Gomes Martins<sup>1</sup>✉

*Candida* species have been responsible for a high number of invasive infections worldwide. In this sense, Rottlerin has demonstrated a wide range of pharmacological activities. Therefore, this study aimed to evaluate the antifungal, antibiofilm and antivirulence activity of Rottlerin in vitro against *Candida* spp. and its toxicity and antifungal activity in vivo. Rottlerin showed antifungal activity against all yeasts evaluated, presenting Minimum Inhibitory and Fungicidal Concentration (MIC and MFC) values of 7.81 to > 1000 µg/mL. Furthermore, it was able to significantly inhibit biofilm production, presenting Biofilm Inhibitory Concentration (MICB<sub>50</sub>) values that ranged from 15.62 to 250 µg/mL and inhibition of the cell viability of the biofilm by 50% (IC<sub>50</sub>) from 2.24 to 12.76 µg/mL. There was a considerable reduction in all hydrolytic enzymes evaluated, with emphasis on hemolysis where Rottlerin showed a reduction of up to 20%. In the scanning electron microscopy (SEM) analysis, Rottlerin was able to completely inhibit filamentation by *C. albicans*. Regarding in vivo tests, Rottlerin did not demonstrate toxicity at the therapeutic concentrations demonstrated here and was able to increase the survival of *C. elegans* larvae infected. The results herein presented are innovative and pioneering in terms of Rottlerin's multipotentiality against these fungal infections.

**Keywords** Rottlerin, Antifungal activity, Antibiofilm, Hydrolytic enzymes, *Caenorhabditis elegans*

Infections caused by yeasts of the genus *Candida* have increased significantly over the years, being identified as the fourth leading cause of healthcare-related bloodstream infections in the United States and the seventh cause in Brazil, impacting morbidity and mortality rates<sup>1,2</sup>. In association with that, there is the fact that resistant isolates are increasingly linked to outbreaks, especially by *C. parapsilosis* and *C. auris*<sup>3,4</sup>. The isolation of these species is worrying due to the fact that they are less susceptible to the antifungals of choice for the treatment of fungal Healthcare-associated Infections (HAI)<sup>5</sup>. These infections are influenced by several factors, with the production of biofilm and hydrolytic enzymes being the main ones<sup>6</sup>. The biofilm is a form of protection against the cells of the host's immune system and antifungal agents and the hydrolytic enzymes act in the invasion of host tissues, evasion of the immune system and in the maintenance of the viability and multiplication of yeast in the host<sup>7-9</sup>.

Despite the four classes of antifungals available on the market for the treatment of these invasive fungal infections, mortality remains high and the toxicity of these medications continues to be a relevant problem. Additionally, the mechanism of action of these antifungals is limited, demonstrating the urgency of discovering a new antifungal agent<sup>10</sup>.

In this sense, the molecule called Rottlerin, a red polyphenol powder produced from the fruits of *Mallotus philippinensis* Muell. Arg (Euphorbiaceae), stands out as an important source of relevant bioactive molecules,

<sup>1</sup>Laboratory of Antimicrobial Testing, Institute of Biomedical Sciences (ICBIM), Federal University of Uberlândia (UFU), Av. Pará, 1720 - Umuarama, Uberlândia 38405-320, Brazil. <sup>2</sup>Technical School of Health (ESTES), Federal University of Uberlândia (UFU), Uberlândia, Brazil. <sup>3</sup>Innovation Center in Salivary Diagnostic and Nanotheranostics, Institute of Biomedical Sciences (ICBIM), Federal University of Uberlândia (UFU), Uberlândia, Brazil. <sup>4</sup>Department of Engineering and Exact Sciences, Faculty of Agricultural and Veterinary Sciences - Jaboticabal (FAV), São Paulo State University (UNESP), Jaboticabal, Brazil. <sup>5</sup>Laboratory of Immunophysiology of Reproduction, Institute of Biomedical Sciences (ICBIM), Federal University of Uberlândia, Uberlândia, Brazil. ✉email: carlos.martins2@ufu.br

which has demonstrated a wide range of pharmacological activities<sup>11</sup>. Although known mainly for its anthelmintic activity<sup>12</sup>, other pharmacological potentials of Rottlerin are found in the literature, even less explored to date, as an anti-inflammatory<sup>13</sup>, antibacterial<sup>14</sup> antioxidant<sup>11</sup> and antiparasitic<sup>15,16</sup>.

In light of that and the need to discover effective compounds against fungal specimens, this study aimed to evaluate *in vitro* the antifungal, antibiofilm and antienzymatic activities of Rottlerin against the main yeasts of the genus *Candida*. Furthermore, the *Caenorhabditis elegans* model was used to evaluate the toxicity of Rottlerin and its antifungal efficacy during infection of *Candida* species.

## Results

### Minimum inhibitory concentration (MIC) and minimum fungicide concentration (MFC) of Rottlerin

Rottlerin showed antifungal activity against all yeasts evaluated, with MIC and MFC values varying between 7.81 and > 1000 µg/mL (Table 1). The best Rottlerin MIC results were observed for *C. guilliermondii* ATCC 6260 (7.81 µg/mL), *C. dubliniensis* ATCC MYA-646 (31.25 µg/mL), *C. orthopsilosis* ATCC 96141 (31.25 µg/mL), *C. albicans* ATCC 90028 (62.5 µg/mL), *C. metapsilosis* ATCC 96143 (62.5 µg/mL) and *C. auris* (clinical isolate) (62.5 µg/mL), demonstrating fungicidal action against the majority of yeasts evaluated.

### Antienzymatic activity of Rottlerin

Table 2 shows the mean values of the dc/dcp ratio of the positive control of each yeast tested and the mean values of the dc/dcp ratio of the yeasts treated with Rottlerin as well as with Amphotericin B. In addition, the percentage of inhibition of hydrolytic enzymes produced by each yeast when treated with Rottlerin or Amphotericin was calculated. There was a significant reduction in the size of the halo of enzymes treated with Rottlerin, especially in some yeasts. Without treatment, *C. guilliermondii* (ATCC 6260), *C. metapsilosis* (ATCC 96143) and *C. krusei* (ATCC 6258) showed strong hemolytic activity, showing moderate activity after treatment with Rottlerin. Regarding the percentages of reduction in enzyme production, there was a significant reduction for some yeasts evaluated, for at least one enzyme tested. For the phospholipase enzyme, Rottlerin showed an inhibition percentage of 7% and rates that ranged from 4 to 29% for the hemolysin enzyme, with emphasis on *C. galabrata* (ATCC 2001) with a 29% and *C. dubliniensis* (ATCC MYA-646) with an 18% of reduction. One can observe that for some yeasts, Rottlerin was more efficient in reducing the production of these enzymes when compared to Amphotericin B. As an example, there is the production of proteinase by *Candida parapsilosis* (ATCC 22019) where Rottlerin presented 20% of reduction of these enzyme, compared to Amphotericin B, where there was no reduction. Regarding the production of DNase, Rottlerin was able to completely inhibit the production of this enzyme against the yeasts *C. guilliermondii* (ATCC 6260), *C. orthopsilosis* (ATCC 96141) and *C. krusei* (ATCC 6258).

### Antibiofilm activity

Rottlerin demonstrated significant inhibition of the biofilm formed against *C. albicans* (ATCC 90028), *C. dubliniensis* (ATCC MYA-646) and *C. auris* (clinical isolate). MIC<sub>50</sub> values ranged from 15.62 to 250 µg/mL for Rottlerin, with the lowest value observed for the clinical isolate in *C. auris*, with biomass inhibition at concentrations above MIC<sub>50</sub>. Regarding cell viability, Rottlerin IC<sub>50</sub> values ranged from 2.24 to 12.76 µg/mL, with the lowest value observed against *C. albicans* (ATCC 90028) with a significant decrease in viable cells (Fig. 1A–C). At the concentration of 15.62 µg/mL, Rottlerin showed inhibition of biomass, even at concentrations lower than MIC<sub>50</sub>, as well as inhibition of cell viability from that same concentration, compared to the three yeasts evaluated.

The MIC<sub>50</sub> and IC<sub>50</sub> values of Amphotericin B against the yeasts are shown in Fig. 1D–F.

Rottlerin (µg/mL)		
Yeasts	MIC	MFC
<i>Candida albicans</i> (ATCC 900028)	62.5	62.5
<i>Candida dubliniensis</i> (ATCC MYA-646)	31.25	31.25
<i>Candida tropicalis</i> (ATCC 13803)	125	> 1000
<i>Candida glabrata</i> (ATCC 2001)	125	125
<i>Candida guilliermondii</i> (ATCC 6260)	7.81	7.81
<i>Candida metapsilosis</i> (ATCC 96143)	62.5	62.5
<i>Candida orthopsilosis</i> (ATCC 96141)	31.25	125
<i>Candida auris</i> (clinical isolate)	62.5	125
Control technique (µg/mL)—Amphotericin B		
<i>Candida krusei</i> (ATCC 6258)	1	1
<i>Candida parapsilosis</i> (ATCC 22019)	0.5	0.5

**Table 1.** MIC and MFC results obtained from the Rottlerin molecule against the yeasts evaluated in the study. MIC range for *Candida parapsilosis* (ATCC 22019): 0.25–1.0 µg/mL and *Candida krusei* (ATCC 6258): 0.25–2.0 µg/mL<sup>47</sup>.

	Positive control	Rottlerin		Amphotericin B	
	Mean (dc/dcp)	Mean (dc/dcp)	Reduction (%)	Mean (dc/dcp)	Reduction (%)
Hemolysin					
<i>Candida albicans</i> (ATCC 900028)	0.51	0.62	-21.56	0.51	0
		*p value: 0.0389		*p value: 0.7575	
<i>Candida dubliniensis</i> (ATCC MYA- 646)	0.65	0.53	18.46	0.55	15.39
		*p value: 0.0019		*p value: 0.0007	
<i>Candida tropicalis</i> (ATCC 13803)	0.37	0.62	-67	0.65	-75
		*p value: 0.0260		*p value: 0.0006	
<i>Candida glabrata</i> (ATCC 2001)	0.52	0.37	29	0.47	9.61
		*p value: 0.0022		*p value: 0.0299	
<i>Candida guilliermondii</i> (ATCC 6260)	0.63	0.71	-12.69	0.71	-12
		*p value:0.0077		*p value:0.0077	
<i>Candida metapsilosis</i> (ATCC 96143)	0.57	0.65	-14	0.62	-8
		p value:0.0769		p value:0.1195	
<i>Candida orthopsilosis</i> (ATCC 96141)	0.55	0.53	4	0.83	-50.9
		p value: 0.6094		*p value: 0.0035	
<i>Candida auris</i> (clinical isolate)	0.69	0.61	12	0.64	8
		*p value: 0.0101		p value: 0.3037	
<i>Candida krusei</i> (ATCC 6258)	0.44	0.67	-52	0.66	-50
		*p value: 0.0009		*p value: 0.0010	
<i>Candida parapsilosis</i> (ATCC 22019)	0.64	0.65	-1	0.66	-3
		p value: 0.2929		p value: 0.6094	
Proteinase					
<i>Candida dubliniensis</i> (ATCC MYA- 646)	0.77	0.86	-11.68	0.47	39
		*p value: 0.0061		*p value: 0.0006	
<i>Candida tropicalis</i> (ATCC 13803)	0.89	0.74	17	0.66	26
		*p value: 0.0019		*p value: 0.0010	
<i>Candida parapsilosis</i> (ATCC 22019)	0.65	0.52	20	0.65	0
		*p value: 0.0029		p value: 0.1010	
Phospholipase					
<i>Candida albicans</i> (ATCC 900028)	0.8	0.75	7	0.56	30
		*p value: 0.0194		*p value: 0.0009	
DNase					
<i>Candida guilliermondii</i> (ATCC 6260)	Positive	Negative		Negative	
<i>Candida orthopsilosis</i> (ATCC 96141)	Positive	Negative		Negative	
<i>Candida krusei</i> (ATCC 6258)	Positive	Negative		Negative	

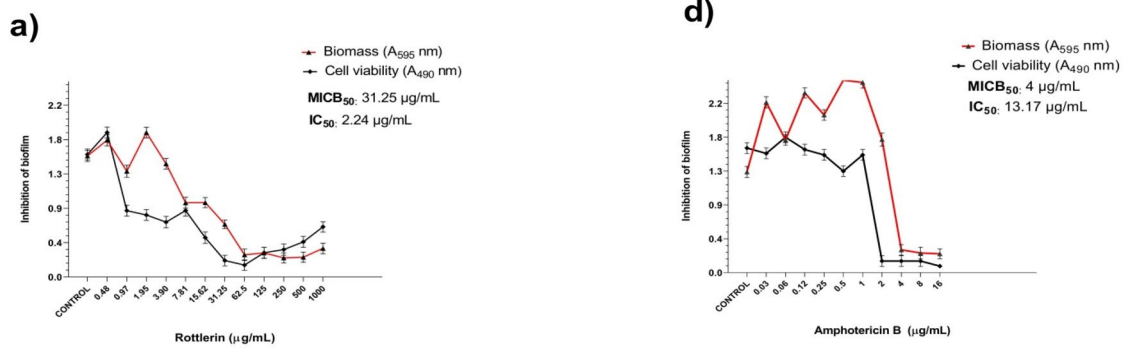
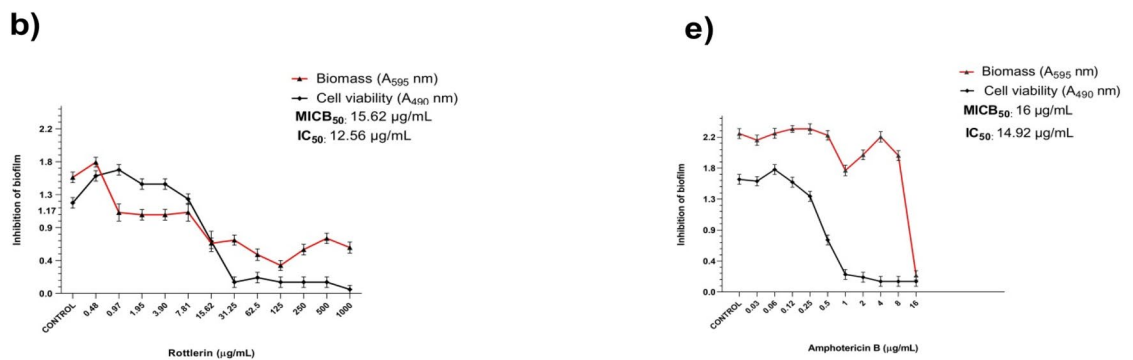
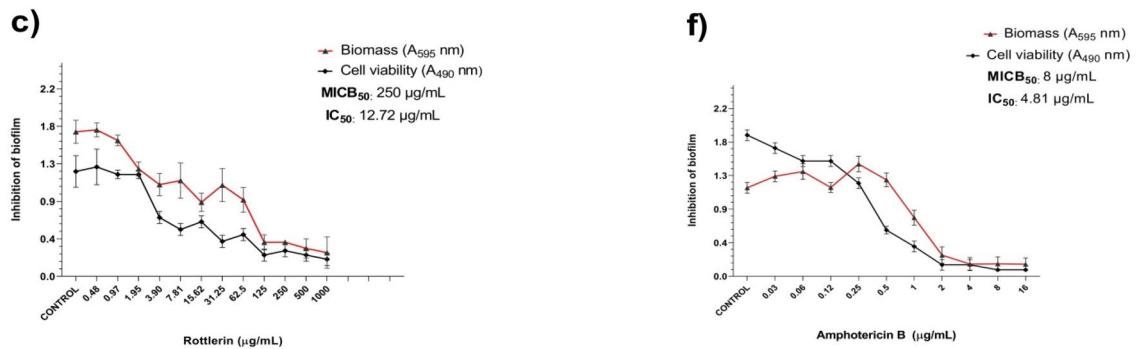
**Table 2.** Analysis of the inhibition of the production of hydrolytic enzymes by yeasts included in the study exposed to a concentration of ½ MIC of Rottlerin. \*p value: statistically significant value.

### Scanning electron microscopy (SEM)

Figure 2 shows the changes in the structure of the biofilm of *C. albicans* (ATCC 90028), *C. auris* (clinical isolate) and *C. dubliniensis* (MYA-646) caused by the concentration of ½MIC of Rottlerin. The effect of the sample on the *C. albicans* (ATCC 90028) biofilm stands out, as it was able to completely inhibit the formation of hyphae (Fig. 2A). In relation to *C. auris* (clinical isolate), Rottlerin promoted a decrease in the amount of microbial aggregates, in addition to a change in the shape of these yeasts (Fig. 2B—black circle). It was also possible to observe lesions in the cell wall in addition to the change in appearance (blue arrow). In relation to the *C. dubliniensis* (ATCC MYA-646) biofilm, Rottlerin reduced both cell aggregation and the production of extracellular matrix, indicated by the red arrow (Fig. 2C). Furthermore, damage to the cell wall was identified, with holes in the central region of the cell (blue arrow). The black circle shows a change in the surface of the yeast, which has become rough.

### In vivo toxicity and infection in the *C. elegans* model

Rottlerin demonstrated toxicity at the highest concentration evaluated as shown in Fig. 3. The lowest concentration capable of killing 50% or more of the larvae (LC<sub>50</sub>) was 1000 µg/mL, accounting for 68%. After toxicity assay, concentrations of 500 to 31.25 µg/mL were selected for the in vivo infection assay, as they did not present toxicity against *C. elegans* larvae.

***C. albicans* (ATCC 90028)*****C. auris* (clinical isolate)*****C. dubliniensis* (ATCC MYA-646)**

**Figure 1.** Antibiofilm activity against the three yeasts included in the tests. (a–c) Antibiofilm activity of the Rottlerin molecule against *C. albicans* (ATCC 90028), *C. auris* (clinical isolate) and *C. dubliniensis* (ATCC MYA-646), respectively. (d–f) Antibiofilm activity of Amphotericin B against *C. albicans* (ATCC 90028), *C. auris* (clinical isolate) and *C. dubliniensis* (ATCC MYA-646), respectively.

*C. elegans* larvae were infected with the tested yeasts and Rottlerin was evaluated for its antifungal activity. Figure 4 shows larvae infected with *C. albicans* (ATCC 90028), *C. dubliniensis* (ATCC MYA-646) and *C. auris* (clinical isolate) and treated with Rottlerin and Amphotericin B. All concentrations of Rottlerin evaluated increased larvae survival on the first day of incubation, presenting survival rates above 50% ( $p < 0.001$ ). The survival rates of larvae infected with *C. albicans* (ATCC 90028) ranged from 80 to 95% (Fig. 4A), those infected with *C. auris* (clinical isolate) from 60 to 85% (Fig. 4C) and those infected with *C. dubliniensis* (ATCC MY-646) from 80 to 100% (Fig. 4E). There were statistically significant differences regarding the survival of infected yeasts and the concentration of treatment (see Supplementary Material, Table S1). Amphotericin B also increased the survival rates of infected larvae on the first day of incubation. Survival rates of larvae infected with *C. albicans*

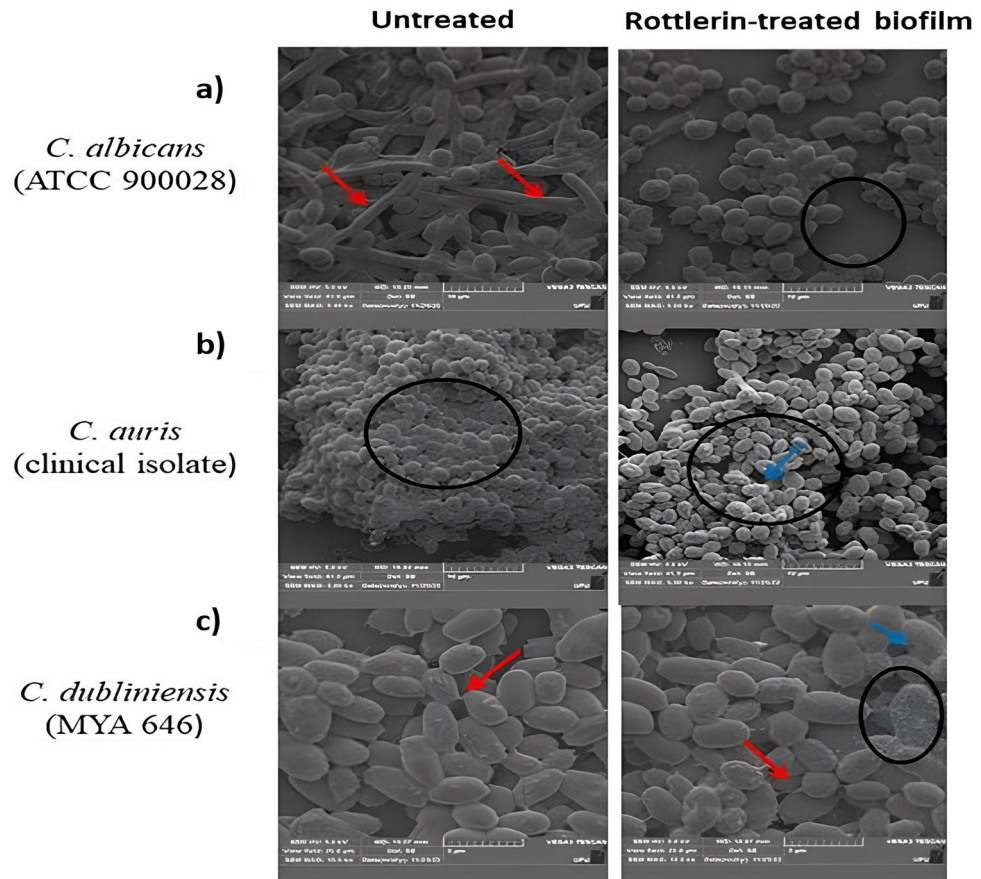


**Figure 2.** Scanning electron microscopy images of biofilms formed in vitro. (a) *C. albicans* biofilm without Rottlerin treatment, (to the left) and *C. albicans* biofilm with Rottlerin treatment (on the right). Red arrows indicate yeast filamentation and the black circle indicates inhibition of yeast filamentation. (b) *C. auris* biofilm without Rottlerin treatment (to the left) and *C. auris* biofilm with Rottlerin treatment (on the right). The black circle on the left shows the dense layer of adherent cells and the circle on the right shows a decrease in this aggregation. The blue arrow shows the change in yeast shape as well as the holes in the center of the yeast. (c) *C. dubliniensis* biofilm without Rottlerin treatment, (to the left) *C. dubliniensis* biofilm with Rottlerin treatment (on the right). Arrows to the left show the extensive polymeric extracellular matrix produced by yeasts, joining one yeast cell to another. The blue arrow on the right shows the damage in the central region of the yeast and the red arrow shows the reduction in the extracellular matrix, with a visible distancing of one yeast cell from the other, decreasing cell adhesion.

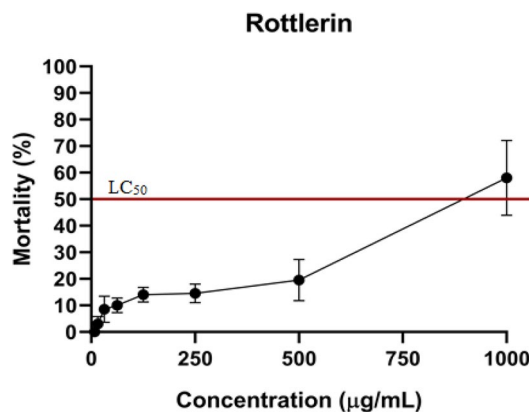


**Figure 3.** Evaluation of Rottlerin toxicity using *C. elegans* larvae as an in vivo model.

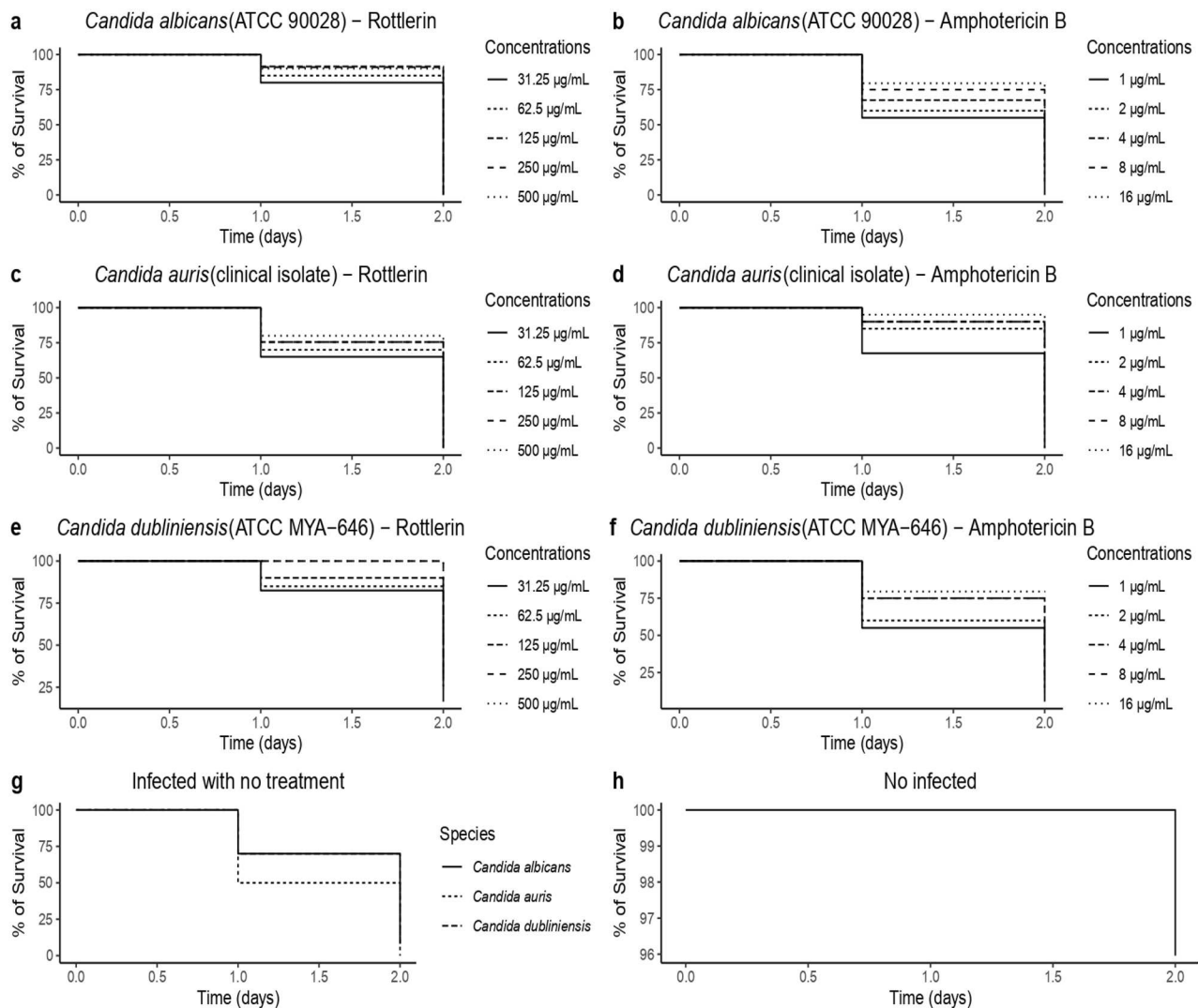


**Figure 4.** Survival curves and concentration responses of Rottlerin and Amphotericin B from the *C. elegans* infected with *Candida* species. (a) Survival curves and concentration responses of Rottlerin from the *C. elegans* infected with *C. albicans*. (b) Survival curves and concentration responses of Amphotericin B from the *C. elegans* infected with *C. albicans*. (c) Survival curves and concentration responses of Rottlerin from the *C. elegans* infected with *C. auris*. (d) Survival curves and concentration responses of Amphotericin B from the *C. elegans* infected with *C. auris*. (e) Survival curves and concentration responses of Rottlerin from the *C. elegans* infected with *C. dubliniensis*. (f) Concentration responses of Amphotericin B from the *C. elegans* infected with *C. dubliniensis*. (g) Infected larvae without any treatment. (h) Uninfected larvae.

(ATCC 90028) ranged from 60 to 80% (Fig. 4B), those infected with *C. auris* (clinical isolate) survived at rates of 70 to 95% (Fig. 4D) and those infected with *C. dubliniensis* (ATCC MYA-646) survived at 60% to 80% (Fig. 4F). Regarding the incubation time, the larvae infected with the yeasts evaluated, even when treated with Rottlerin and Amphotericin B, died mostly on the second day of incubation. It is possible to see that the survival rate of larvae infected with the yeasts and not treated was lower than the survival rate of larvae infected and treated with Rottlerin (Fig. 4G). The negative control is shown in Fig. 4H.

Regarding the two treatments used on infected larvae, the larvae had a higher survival rate when treated with Rottlerin than with Amphotericin B, on the first day of incubation, as shown in Tables S2 and S3 (see Supplementary Material).

The larvae infected with *C. albicans* (ATCC 90028), *C. dubliniensis* (ATCC MYA-646) and *C. auris* (clinical isolate) treated with the highest concentration of Rottlerin evaluated and incubated for 24 h are shown in Fig. 5. Even in the face of infection, treatment with Rottlerin managed to increase the survival of these larvae, constituting a protective factor against infection (Fig. 5A–C), that also happened when treated with Amphotericin B, yet with lower survival rates than when treated with Rottlerin (Fig. 5D–F). When untreated, most larvae died after 24 h of incubation (Fig. 5G–L).



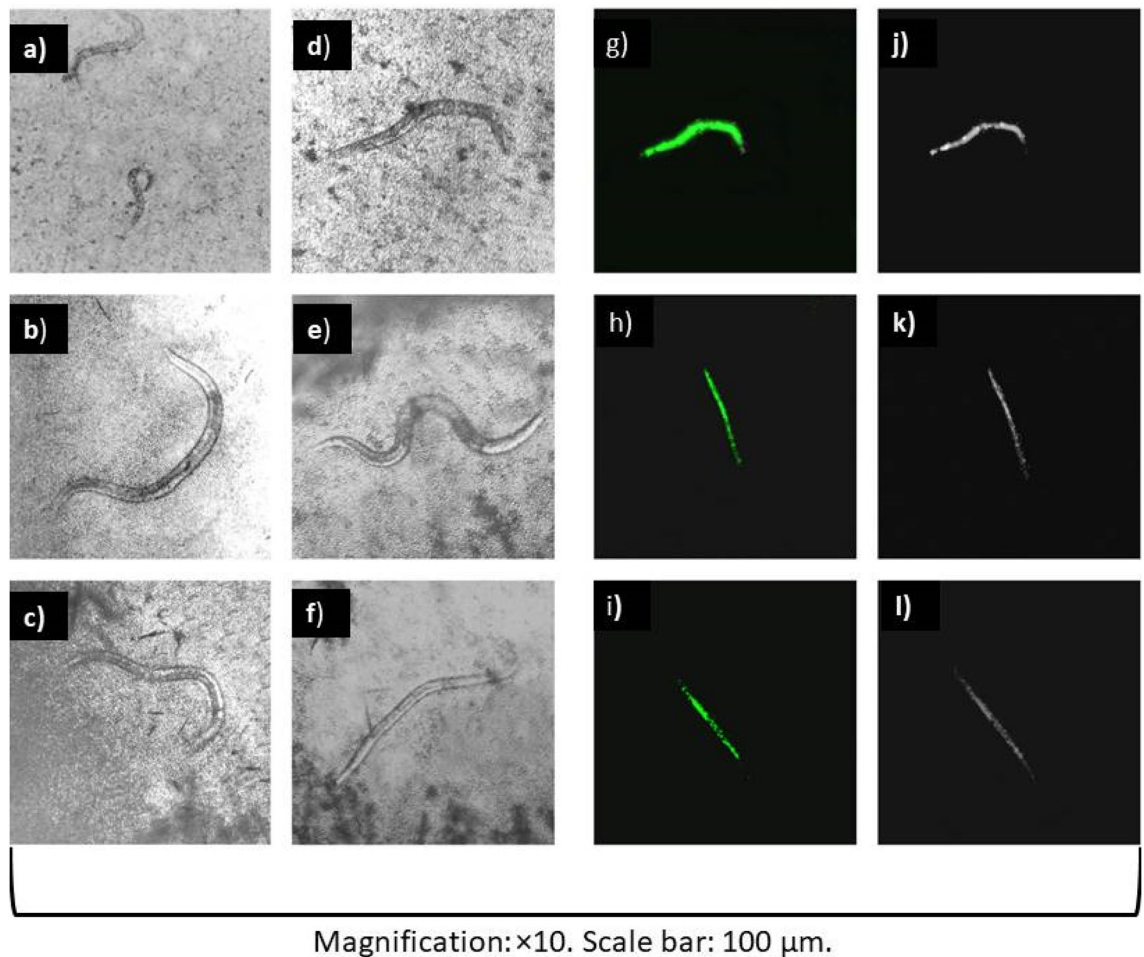


**Figure 5.** Transmittance and fluorescence images of *C. elegans* worms treated and untreated with Rottlerin and Amphotericin B after 24 h of incubation. (a–c) Transmittance images of *C. elegans* larvae infected with *C. albicans*, *C. dubliniensis* and *C. auris*, respectively, treated with the highest concentration of Rottlerin evaluated. (d–f) Transmittance images of *C. elegans* larvae infected with *C. albicans*, *C. dubliniensis* and *C. auris*, respectively, treated with the highest concentration of Amphotericin B evaluated. (g–i) Fluorescence images of larvae infected with *C. albicans*, *C. dubliniensis* and *C. auris* and untreated stained with SYTOX Green. (j–l) Transmittance images of larvae infected with *C. albicans*, *C. dubliniensis* and *C. auris* and not treated.

## Discussion

In recent decades, the number of microorganisms resistant to various classes of antimicrobials has increased. In the field of fungi, *C. auris* is a multi-resistant pathogen similar to superbugs and commonly isolated in hospitals, being able to persist in the environment for a long time and standing out as a global threat<sup>17</sup>. Although there are antifungals available to treat these infections, such as azoles, polyenes and echinocandins, the excessive and long-term use of these medications has already resulted in 34,800 cases of infection and 1700 deaths caused by drug-resistant *Candida* yeasts. Furthermore, these medications, when administered over a long period, have been shown to be highly toxic<sup>18</sup>. Therefore, the discovery of new antifungal agents becomes extremely important. Natural products are a rich source of metabolites with therapeutic properties, and are currently of great interest in this era of multidrug resistance. It is therefore of great interest to identify new natural products and their structural scaffolds that act on new targets and can escape cross-resistance mechanisms<sup>19</sup>.

Rottlerin has several pharmacological properties, many recently discovered, such as its antitumor activity, for example in tumor suppression through inhibition of EZH2 expression in prostate cancer cells, antitumor activity by inhibiting protein C kinase, tumor suppressor function by inhibiting the Cdc20 pathway in glioma cells, among others. Studies regarding this molecule also address its ability to promote cellular autophagy, modulate protein synthesis and inhibit enzymes such as PKC $\delta$ <sup>20–24</sup>. The antibacterial action of Rottlerin has already been demonstrated against isolates of *Mycobacterium tuberculosis*-H37Ra (MIC 11.56  $\mu\text{g/mL}$ )<sup>25</sup> and potent bactericidal activity against the clinical isolate of *Helicobacter pylori* (MIC 8–256  $\text{mg/L}$ )<sup>14</sup>. Gangwar, et al.<sup>26</sup> identified the presence of alkaloids, phenolic groups, steroids, flavones, saponins, steroids, sugars, tannins and triterpenes in the methanolic extract of *M. philippinensis* fruits and demonstrated that these classes were responsible for its antibacterial activity against several Gram-positive bacteria and Gram-negative, but no antifungal activity.

This is the first study that evaluated the antifungal and antivirulence activity of the Rottlerin molecule against *Candida* spp. The antifungal activity described in the present study can be explained by the influence of chalcones on pathogenic fungi, since Rottlerin is a chalcone derivative. Antifungal activity of chalcone derivatives against *C. albicans* LABMIC 0107 (MIC: 0.31 mg/mL) e *C. albicans* LABMIC 0105 (MIC: 0.62 mg/mL). Some studies have already been carried out to investigate the mechanism of action of chalcones in fungi<sup>27</sup>. Mellado, et al.<sup>28</sup> demonstrated the antifungal action of chalcones against phytopathogens *Botrytis cinerea* e *Monilinia fructicola* and identified the antifungal action mediated by the C1 and C5 charge and by the hydrogen acceptor and donor. More studies are needed to investigate the mechanism of action of Rottlerin against pathogenic fungi to better understand which region in its molecular structure is responsible for the inhibitory action.

Other molecules derived from *Mallotus philippensis* have already been evaluated for their antifungal potential, such as kamalachalcone E, against *C. albicans* (ATCC 10231 and ATCC 24433), *C. glabrata* (NCYC 388) and *C. tropicalis* (ATCC 750), presenting  $IC_{50} > 256 \mu\text{g/mL}$ <sup>29</sup>. In the present study, Rottlerin showed antifungal activity against all species evaluated, with MIC values lower than those presented by the author above (7.81 to 125  $\mu\text{g/mL}$ ), being more promising against these yeasts (Table 1).

*Candida* species produce several virulence factors that give these microorganisms the ability to colonize and invade host tissue, such as adhesins and thigmotropism (contact sensing)<sup>30</sup>. Despite being relatively simple tests, this is the first study that evaluated the antienzymatic activity of Rottlerin against *Candida* species. The production of these enzymes is little studied, and more studies are needed on the interference of this type of virulence factor against this species. In this study, Rottlerin was able to reduce the production halo of most enzymes in relation to the control (Table 2). Rottlerin showed an inhibition percentage of 7% in the production of phospholipase, demonstrating a statistically significant reduction in relation to the control. Phospholipase is an enzyme related to host cell invasion, through the hydrolysis of phospholipids and proteins present in the envelope of the host cell<sup>31</sup>. By reducing this enzyme, the invasiveness of this yeast becomes impaired.

The hemolytic activity of the yeasts included in the study was also evaluated in the present study. Menezes et al.<sup>32</sup> also evaluated the hemolytic activity of *C. glabrata* (ATCC 2001) and demonstrated that capsaisin and pepper extracts were able to inhibit the hemolysin enzyme by up to 48.6%. In the present study, the Rottlerin molecule was not able to reduce the hemolytic activity of *C. glabrata* (ATCC 2001). However, an inhibition rate of up to 20% was demonstrated here for other yeasts evaluated and also clinically important, such as *Candida dubliniensis* (ATCC MYA-646) and *Candida glabrata* (ATCC 2001). Hemolysin degrades the host's red blood cells and extracts iron for yeast nutrition, which ensures greater persistence in the host<sup>7</sup>. Reducing this enzyme implies a reduction in the survival of these pathogens in the human body.

Regarding the production of the DNase enzyme, in this study, Rottlerin was able to completely inhibit the production of this enzyme. The role of DNase in increasing the virulence and pathogenicity of *Candida* species has not yet been fully elucidated, but it is believed that it contributes to the evasion of the immune system or degrades the DNA of other microorganisms, facilitating the colonization microenvironment, as a competitive strategy<sup>33</sup>. Most studies on DNase focus on identifying the production of this enzyme in *Candida* strains and do not evaluate compounds that can inhibit its production, especially molecules isolated from plants such as Rottlerin, evaluated in the present study. It is important to highlight that Rottlerin was evaluated as an antienzymatic substance at a subinhibitory concentration ( $\frac{1}{2}$ MIC), being a non-toxic concentration according to the results shown in the present study.

Biofilm is considered as one of the most important virulence factors, being responsible for the increase in antifungal resistance and recurrence of infections<sup>34</sup>. In a study published by Larkin et al.<sup>4</sup>, it was demonstrated that caspofungin does not have inhibitory activity against *C. auris* (clinical isolate) biofilm, and the antifungals fluconazole and azoles, commonly used in the treatment of fungal infections, are less active. The results shown in the present study revealed that Rottlerin was able to inhibit in vitro the biofilm of three species of clinical importance, including *C. auris* (clinical isolate), considered as an emerging species that has generated global concern due to its high resistance to antifungals. The literature has few studies that evaluated the antifungal activity of natural products against *C. auris*, especially isolated molecules such as Rottlerin. In the present study, Rottlerin was able to inhibit the biomass production of this pathogen by at least 50% at a concentration of 15.62  $\mu\text{g/mL}$  (Fig. 1B), lower than the MIC concentration, inhibiting its cell viability at an even lower concentration (12.56  $\mu\text{g/mL}$ ). Inhibiting the production of biofilm by this species is extremely important, as this pathogen is associated with hospital outbreaks and its widespread dissemination throughout the environment is mainly due to its long residence on surfaces (animate and inanimate) due to its ability to aggregate. Therefore, inhibiting biofilm by this pathogen implies controlling its spread and consequently reducing cases of infections<sup>35</sup>.

Tsang et al.<sup>36</sup> evaluated the ability of purpurin, a natural pigment isolated from madder root, to reduce the cell viability of biofilms of *C. dubliniensis* (MYA-646) demonstrating a 45% reduction at a concentration of 1  $\mu\text{g/mL}$  and a 65% reduction at a concentration of 3  $\mu\text{g/mL}$ . In the present study, Rottlerin was able to inhibit cell viability by 50% or more at a concentration higher than that reported by these authors (12.72  $\mu\text{g/mL}$ ) against the same strain (Fig. 1C). However, it is worth mentioning that in the present study, Rottlerin was able to inhibit biofilm by this yeast at a concentration lower than its MIC concentration (31.25  $\mu\text{g/mL}$ ). Inhibiting this yeast biofilm is mainly relevant for oral health. *C. dubliniensis* is related to oral candidiasis, especially in immunocompromised individuals, such as HIV-infected individuals<sup>37</sup>. Furthermore, this yeast has already been isolated from periodontal pockets of adolescents<sup>38</sup>. In the biofilm, many metabolites are produced, which may be associated with worsening cases of periodontitis caries<sup>39</sup>. Initial adhesion is the first step towards the development of infection in host tissue by *Candida* species. If this process is interrupted, these yeasts are unable to adhere to or even colonize the tissue<sup>40</sup>. Therefore, inhibiting biofilm formation is much more effective than treating it after it is formed.

The in vitro antibiofilm activity of Rottlerin was confirmed by scanning electron microscopy. After treatment with Rottlerin, *C. albicans* (ATCC 90028) was unable to produce hyphae and pseudohyphae, important virulence structures of this species (Fig. 2A). Similar results were found by El-Houssaini et al.<sup>41</sup>. These authors, after treating

the biofilm formed by *C. albicans* (clinical isolate) with micafungin, showed the absence of filamentation in the biofilm. Filamentation is a characteristic of the initial adhesion and proliferative phase of biofilm. It is through hyphae and pseudohyphae that these yeasts are able to develop and maintain the biofilm structure. Furthermore, hyphae are related to the production of several virulence factors such as adhesins, tissue-degrading enzymes, defense proteins and extracellular cytosolic peptide<sup>30</sup>. Therefore, the findings of the present study are encouraging as the Rottlerin molecule was able to reduce one of the most important structures of the biofilm of this species, contributing to the reduction of virulence and adhesion capacity of these microorganisms.

In the present study, Rottlerin was able to reduce the amount of microorganisms aggregated in the biofilm produced by *C. auris*-clinical isolate (Fig. 2B). Vazquez-Munoz et al.<sup>42</sup> evaluated the antibiofilm potential of bismuth nanoantibiotics against *C. auris* (0381) and obtained similar results to those found in the present study, demonstrating a slight reduction in biofilm. However, bismuth nanoantibiotics did not demonstrate changes in cell morphology. Here, it was demonstrated that Rottlerin changed the cell shape of these yeasts and made the yeast surface rougher. Hao, et al.<sup>43</sup> also demonstrated this type of structural change in biofilms of *C. auris* (CBS10913) and *C. auris* (CBS12373), when treated with fluconazole in combination and chlorhexidine acetate. The control group of these authors had an oval shape and a smooth surface. After treatment, the cells were flattened and became swollen, corroborating the results of the present study, where Rottlerin was able to cause damage to this yeast, making it shriveled and flat. Furthermore, one can observe a reduction in one of the main biofilm substances, the extracellular polymeric matrix (EPS), in the biofilm by *C. dubliniensis* (Fig. 2C). In addition to being responsible for the adhesion and cohesion of microorganisms to each other, the matrix is mainly responsible for tolerance to antifungals and evasion of the host's immune system. The rupture of this matrix leads to the destruction of the biofilm<sup>44</sup>. In the SEM images shown here, the reduction of the extracellular matrix is evident, as well as how much the yeasts detached from each other after the treatment with Rottlerin.

In this study, the toxicity of Rottlerin was evaluated in *C. elegans* larvae, demonstrating that this molecule was toxic at concentrations much higher than the concentrations of MIC, MIC<sub>50</sub>, IC<sub>50</sub> and concentrations with antienzymatic action (Fig. 3). Crisford et al.<sup>45</sup> also evaluated the toxicity of Rottlerin against *C. elegans* larvae that express *slo-1* (a family of channels that regulate hormone release, among other functions) or *kcnma1* (mammalian ortholog), evaluating the effect of short-term exposure (3 h) and long-term (24 h) in the locomotion of these larvae. These authors demonstrated that in wild-type *slo-1* larvae, short-term exposure did not inhibit the locomotion of these nematodes. However, larvae expressing *kcnma1* had their movement slowed down after 3 h of exposure to 10 µM Rottlerin. Long-term exposure affected wild strains. In this present study, the effect of Rottlerin on larvae locomotion was not evaluated, but no changes or inhibition of movement were observed in larvae after exposure to Rottlerin at the concentrations evaluated here. More studies are needed on the toxicity of this molecule against other types of animals to confirm the toxicity presented in this study. It is hoped that the results found here will encourage other authors on this topic.

Furthermore, in the present study, *C. elegans* was used as an animal model, used for testing infection by *Candida* spp. Rottlerin was able to protect *C. elegans* larvae infected with the yeasts evaluated, demonstrating more than 50% survival (Fig. 4A), even at the lowest concentration evaluated (31.25 µg/mL). The data on the in vitro antifungal activity of Rottlerin were confirmed by in vivo assays, as the MIC values for the three yeasts tested were similar or close (*C. albicans*—MIC of 62.5 µg/mL, *C. auris*—MIC of 62.5 µg/mL and *C. dubliniensis*—MIC of 31.25 µg/mL).

Other authors have also demonstrated the antifungal activity of several compounds in *C. elegans* larvae infected with *Candida* spp. Singulani et al.<sup>46</sup> evaluated the antifungal activity of gallic acid against larvae infected with *C. albicans* (ATCC 90028) and demonstrated a 46% increase in larvae survival at a concentration of 30 µg/mL. The concentration capable of increasing the survival of these larvae in this study was lower than that found in the present study. However, a higher survival rate was demonstrated here for the same strain when compared to those authors.

Regarding the incubation time of the worms, even after treatment with Rottlerin, there was a drop in survival after 48 h and the majority of larvae died in the present study. This was also demonstrated by Singulani et al.<sup>46</sup>. The explanation for that may be related to the pathogenesis of *Candida* in *C. elegans* and how these yeasts affect the development of worms. Furthermore, it is still not known exactly how Rottlerin exerts its antifungal activity or its therapeutic window. Therefore, more studies are needed on its pharmacological action in different models to better evaluate its antifungal action against these yeasts.

More studies are needed to understand Rottlerin's mechanism of action and what its targets are in the demonstrated antifungal activity. Furthermore, the toxicity of Rottlerin must be evaluated against a murine model to confirm the data presented here.

## Conclusion

This study demonstrated the in vitro and in vivo antifungal potential of Rottlerin, as well as its antibiofilm and antienzymatic potential against *Candida* spp. of clinical relevance, in subinhibitory concentrations (½MIC). Additionally, the toxicity of Rottlerin was evaluated, showing no toxicity at the concentrations determined in the tests carried out in the study. Furthermore, Rottlerin was able to increase the survival of *C. elegans* larvae infected with the *Candida* species evaluated. The results presented here are innovative and unprecedented and are encouraging regarding the multipotentiality of Rottlerin against these fungal infections, which may be relevant in the clinical environment, especially in this era of multidrug resistance that the world is facing. In this sense, Rottlerin may be a promising therapeutic alternative in the future against these microorganisms.

## Materials and methods

### Chemical compound—Rottlerin

Rottlerin (1-[6-[(3-Acetyl-2,4,6-trihydroxy-5-methylphenyl)methyl]-5,7-dihydroxy-2,2-dimethyl-2H-1-benzopyran-8-yl]3phenyl-2-propen-1-one)—AdipoGen, AG-CN2-0526, Batch no A01432, was solubilized in dimethyl sulfoxide—DMSO (Sigma-Aldrich—St. Louis, MO, USA) to form a stock solution of 20 mM. Before each experiment, the stock solution of Rottlerin was always freshly diluted in appropriate liquid culture medium.

### Microorganisms used in the study

The following standard strains were used: *C. albicans* (ATCC 90028), *C. dubliniensis* (ATCC MYA-646), *C. guilliermondii* (ATCC 6260), *C. glabrata* (ATCC 2001), *C. krusei* (ATCC 6258), *C. metapsilosis* (ATCC 96143), *C. orthopsilosis* (ATCC 96141), *C. parapsilosis* (ATCC 22019) and *C. tropicalis* (ATCC 13803), obtained from American Type Culture Collection (ATCC). In addition, a clinical isolate of *C. auris* was used, kindly provided by Hospital das Clinicas, Faculty of Medicine of Ribeirao Preto, University of Sao Paulo (HCFMRP/USP), isolated from the blood of a patient. All yeasts used in this study are part of the culture collection of the Laboratory of Antimicrobial Testing of the Federal University of Uberlândia (LEA/UFU), preserved in deep freezing at  $-80^{\circ}\text{C}$  until the start of tests.

### Assessment of antifungal activity

To determine the antifungal activity of Rottlerin, broth microdilution methodology was used to determine the Minimum Inhibitory Concentration (MIC), defined as the lowest concentration of the antimicrobial agent capable of inhibiting microbial growth, which was carried out in accordance with the recommendations of the Clinical and Laboratory Standards Institute<sup>47</sup>, in document M27-A2, with modifications, described below. Rottlerin was solubilized in DMSO (5% v/v) and diluted in Roswell Park Memorial Institute (RPMI) 1640 medium buffered with MOPS—[N-morpholino] propane sulfonic acid—(Sigma-Aldrich—St. Louis, MO, USA) until reaching the final concentration in the well between 1.46 and 1000  $\mu\text{g}/\text{mL}$ . Yeast-containing cell suspensions were prepared in the final concentration of  $0.5 \times 10^3$  to  $2.5 \times 10^3$  CFU/mL, checked in densitometer (Densimat<sup>®</sup>, Biomérieux). After preparing the plates and incubating them for 24 h at  $37^{\circ}\text{C}$ , 30  $\mu\text{L}$  of 0.01% aqueous resazurin solution (Sigma-Aldrich—St. Louis, MO, USA) was added to observe microbial growth. The plate was then reincubated for 4 h. The blue and pink color change indicated the absence and presence of growth, respectively. The interpretation of the MIC is carried out by observing the lowest concentration that remained blue in the supernatant medium of the microplate<sup>48</sup>. The antifungal Amphotericin B (Sigma-Aldrich—St. Louis, MO, USA) was used as a test quality control at concentrations of 0.031 to 16  $\mu\text{g}/\text{mL}$  against *C. krusei* (ATCC 6258) and *C. parapsilosis* (ATCC 22019). The MIC endpoint was considered as 100% growth inhibition. Control of 5% DMSO was performed, and the solvent did not interfere with bacterial growth at this concentration. It was also performed the following controls: inoculum (all the bacteria used in the test + the culture medium), to observe the viability of the bacteria; broth, to guarantee that the culture medium is sterile; and Rottlerin sample, to guarantee that this solution is sterile. The tests were performed independently in triplicate.

### Determination of the fungicidal or fungistatic action of the sample

In order to evaluate whether Rottlerin demonstrates a fungicidal (complete elimination of yeast) or fungistatic (only growth inhibition) action, the Minimum Fungicide Concentration (MFC) was determined, defined as the lowest concentration of the test sample without any microbial growth, such as described below. Before the addition of resazurin, 10  $\mu\text{L}$  of the inoculum was removed from each well and deposited on Sabouraud Dextrose Agar—SDA (Difco Laboratories, Detroit, USA), incubated at  $37^{\circ}\text{C}$  for 24 h and then the presence or absence of growth was observed. The relationship between MFC and MIC was used to interpret the results, defining the molecule as fungistatic (MFC/MIC:  $\geq 4$ ) or fungicidal (MFC/MIC  $\leq 4$ )<sup>49</sup>.

### Assessment of antienzymatic activity

Prior to the testing to reduce the production of hydrolytic enzymes, all yeasts included in the study were tested for their ability to produce hemolysin, proteinase, phospholipase and DNase. As a result, it was observed that all of them produced hemolysin, only *C. albicans* (ATCC 90028) produced phospholipase, *C. tropicalis* (ATCC 13803), *C. parapsilosis* (ATCC 22019) and *C. dubliniensis* (ATCC MYA-646) produced proteinase and *C. guilliermondii* (ATCC 6260), *C. orthopsilosis* (ATCC 96141) and *C. krusei* (ATCC 6258) produced DNase. Therefore, tests to reduce enzymatic activity using Rottlerin and Amphotericin B were carried out only with yeasts that produce these enzymes.

Rottlerin was evaluated for its ability to inhibit or reduce the production of phospholipase, proteinase, DNase and hemolysin enzymes at concentrations  $\frac{1}{2}$  MIC, according to El-Houssaini et al.<sup>41</sup> with adaptations. Initially, 500  $\mu\text{L}$  of a yeast suspension at turbidity equivalent to 0.5 on the McFarland scale was pipetted into a tube containing 500  $\mu\text{L}$  of RPMI broth buffered with MOPS ([N-morpholino] propane sulfonic acid) and supplemented with 2% glucose, in order to reach a final concentration of microorganisms of  $1 \times 10^6$ – $1 \times 10^7$  cells/mL in each tube. The material was incubated at  $37^{\circ}\text{C}$  for 24 h. Subsequently, the tubes were centrifuged at 3000 RPM for 10 min, with the supernatant discarded and the pellet resuspended in Phosphate Buffered Saline (PBS), repeating this procedure three times. Finally, 5  $\mu\text{L}$  of this suspension was deposited at equidistant points on plates containing SDA supplemented with 7% horse blood<sup>50</sup>, as well as in proteinase agar (yeast extract 11.7 g; bovine albumin 2 g; 3 drops of protovit; bacteriological agar 18 g and  $\text{H}_2\text{O}$  1000 mL)<sup>51</sup>, egg yolk agar (Agar Sabouraud 65 g; NaCl 57.3 g;  $\text{CaCl}_2$  0.55 g; egg yolk 40 g and  $\text{H}_2\text{O}$  1000 mL)<sup>52</sup> and DNase (Laborclin, Brazil)<sup>53</sup>, to evaluate hemolytic activity and proteinase, phospholipase and DNase enzymes, respectively. The SDA plates were incubated for

48 h, the phospholipase plates for 96 h and the proteinase and DNase plates for 7 days at 37 °C. Amphotericin B was used as test quality control. Tests were performed in triplicate in independent experiments.

The enzymes were named Pz (phospholipase zone), Prz (proteinase zone) and Hi (hemolysis index). After incubation, the colony diameter (dc) and zone precipitation (dcp) were measured and the ratio of dc/dcp was calculated and classified as negative (Pz or Prz or Hi = 1), moderate ( $0.63 < \text{Pz or Prz or Hi} < 1$ ) and sharp (Pz or Prz or  $\text{Hi} \leq 0.63$ )<sup>52</sup>. As a positive control, yeast in RPMI broth without any treatment was used. The mean dc/dcp ratio of the positive control was compared with the mean dc/dcp ratio of yeast treated with Rottlerin and Amphotericin B.

The reduction in enzyme production was expressed as a percentage, applying the following formula<sup>41</sup>:

$$\text{Reduction(\%)} = 1 - [(\text{Pz or Prz or Hi assay} / \text{Pz or Prz or Hi control})] \times 100.$$

The inhibition of the enzymes hemolysis, phospholipase and proteinase were compared using the Student's t-test for independent and heteroscedastic samples.

The DNA is the substrate for the DNase enzyme and is already present in the medium. Toluidine blue forms a complex with DNA, responsible for the blue color of the agar medium. Enzymatic action of DNase, breaks this complex, depolymerizing and breaking the DNA-dye complex, resulting in a color change, identified by pinkish to red colored areas around the growth of the yeast. A negative test is indicated when the medium remains blue, as there is no breakdown of the complex by absence of the enzyme.

### Assessment of antibiofilm activity

Before starting tests to evaluate the inhibition of biofilm formation, standardization was carried out, evaluating whether the yeasts included in the study formed biofilms. For so, the microorganisms were incubated at a concentration of  $1 \times 10^6$  cell/mL checked in densitometer, in 96-well plates with only RPMI broth for 24, 48 and 72 h at 37 °C. Biofilm formation was considered as absorbance in the spectrophotometer greater than or equal to 1 and the best incubation time of 48 h (data not shown). After standardization, yeasts that presented  $\text{OD} > 1$  were selected for further testing. Rottlerin's ability to inhibit biofilm was evaluated in terms of biomass production and cell viability. For so, the samples were diluted in 5% DMSO. The inoculum was prepared as Pierce et al.<sup>54</sup> at the concentration  $1 \times 10^6$  CFU/mL. Therefore, aliquots of the sample were pipetted into microplates and diluted in RPMI-1640 with 2% glucose and buffered with MOPS ([N-morpholino] propane sulfonic acid) in order to yield a final sample concentration of 1.46 to 1000 µg/mL.

Two plates were prepared, one for evaluating biomass and another one for evaluating cell viability. The plates were incubated for 48 h at 37 °C. After incubation, biomass assessment was carried out, according to O'Toole<sup>55</sup>, with modifications. Briefly, the contents of the wells were removed and washed with PBS (pH: 7.2) to remove non-adherent cells, followed by fixation with methanol for 15 min. Then, the wells were stained with 1% crystal violet (Sigma-Aldrich—St. Louis, MO, USA) for 20 min and washed with PBS to remove excess dye. Finally, 200 µL of 33% acetic acid were added to the wells for 30 min. The reading was performed on a spectrophotometer at a wavelength of 595 nm. The antifungal Amphotericin B was evaluated against the yeasts tested at a concentration of 0.031 to 16 µg/mL, being considered as test quality control.

Furthermore, the Minimum Inhibitory Concentration of Biofilm (MICB<sub>50</sub>) assay was determined. MICB<sub>50</sub> is defined as the lowest concentration of the microbial agent that can inhibit biofilm formation by at least 50%<sup>56</sup>, according to the equation below:

$$1 - \frac{(\text{Absorbance (595 nm) of the sample treated well})}{\text{Absorbance (595 nm) of the untreated control well}} \times 100.$$

The evaluation of the cell viability of the biofilm was carried out according to Pierce et al.<sup>54</sup> with modifications. After incubation, the wells were gently washed with PBS three times to remove non-attached cells. Subsequently, 50 µL of menadione solution and 2,3-bis (2-methoxy-4-nitro-5-sulfophenyl)-2Htetrazolium-5-carboxanilide—MTT (Sigma-Aldrich—St. Louis, MO, USA) at a concentration of 0.5 mg/mL were added to the wells. After formazan formation, 100 µL of DMSO was pipetted into each well and incubated at room temperature for 10 min. Subsequently, 80 µL from each well was transferred to a new plate to be read at 490 nm. With this, it was possible to determine the lowest concentration capable of inhibiting cell viability by 50% or more (IC<sub>50</sub>)<sup>57</sup>. The antifungal Amphotericin B was evaluated against the yeasts tested, at a concentration of 0.031 to 16 µg/mL, being considered as test quality control. GraphPad Prism 8.0 was used to evaluate the quantitative data.

### Analysis of biofilm inhibition in scanning electron microscopy (SEM)

To evaluate the morphological changes caused by the samples in the cellular and biofilm structure, the scanning electron microscopy (SEM) analysis was performed, according to Melo et al.<sup>58</sup> with modifications. For so, the sub-inhibitory concentration (½MIC) of Rottlerin was used. The assay was carried out in 24-well plates containing sterilized Polyvinyl chloride (PVC) discs measuring 9 mm in diameter, following the same steps described in the 2.5 sub-item, with some modifications. After 24 h of incubation at 37 °C, the discs were fixed in a solution of glutaraldehyde (2.5%) and paraformaldehyde (2%) in 0.15 M sodium cacodylate buffer (pH 7.0) for two hours. Then, the discs were post-fixed in 1% osmium tetroxide solution (Sigma-Aldrich—St. Louis, MO, USA) for 2 h and dehydrated in ethanol at the following concentrations: 30%, 50%, 70%, 90% and 100% at intervals of 20 min each. Subsequently, the samples were subjected to critical point drying (SPC) using liquid carbon dioxide, coated with gold (20-nm thickness) and analyzed using a Tescan scanning electron microscope, model VEGA 3 LMU at magnifications of  $\times 50$ ,  $\times 800$ ,  $\times 10,000$  and  $\times 40,000$ , selecting the best image as representative for each well. The experiment was carried out in triplicate independently.

### C. elegans assay: in vivo assessment of toxicity and infection

The in vivo toxicity and infection assessment tests were carried out using the mutant strain of *Caenorhabditis elegans* AU37, according to Breger et al.<sup>59</sup>, with some modifications, as described below. The Rottlerin sample was evaluated at concentrations of 3.90 to 1000 µg/mL. DMSO was used as solvent (final concentration ≤ 1%). The mutant strain of *C. elegans* AU37 was grown on Nematode Growth Medium (NGM) plates seeded with *Escherichia coli* OP50 and incubated at 16 °C for 3 days. After incubation, the supernatant was washed with the bleaching solution (sodium hypochlorite + NaOH) to synchronize the larvae at the L4 stage. Plates containing larvae synchronized in the L4 phase were washed with M9 buffer and the supernatant was placed in 15-mL conical tubes. Subsequently, 20 µL of the larval suspension was added to each well of a 96-well flat-bottom microplate, along with 80 µL of Brain Heart Infusion (BHI) medium + antibiotics (200 mg/mL Streptomycin, 200 mg/mL ampicillin and 90 µg/mL kanamycin) and 100 µL of Rottlerin, and incubated for 24 h at 25 °C. Counting of live and dead larvae was performed on an EVOS M5000 Imaging System Microscope (Thermo Fisher Scientific, Massachusetts, USA) and the percentage of mortality was calculated.

In vivo infection tests were performed with the same yeasts selected for antibiofilm activity assays (*C. albicans*—ATCC 90028, *C. dubliniensis*—ATCC MYA-646 and *C. auris*—clinical isolate). For so, after the larvae synchronization procedure, 100 µL of L4 stage larvae was pipetted into NGM plates containing an inoculum of the evaluated yeasts and incubated for three hours at 25 °C. Subsequently, the already infected larvae were washed with M9 buffer and transferred to 15-mL falcon tubes, being centrifuged three times to remove excess yeast that may be adhered to the worm cup. Larvae were then added into wells of 96-well plates containing 60% M9 buffer, 40% BHI broth, 10 µg/mL cholesterol in ethanol, 90 µg/mL kanamycin and 200 mg/mL ampicillin. The larvae were divided into three groups: uninfected and untreated larvae, infected and untreated larvae and infected larvae treated with Rottlerin or Amphotericin B (used as control at concentrations of 1 to 16 µg/mL). The plates were incubated for 2 days at 25 °C and the mortality rate was calculated daily. On the first day of infection, worms were stained with SYTOX Green (Invitrogen, CA, USA) at a concentration of 1 µM and were incubated for 15 min at room temperature. Images were captured by EVOS M5000 Imaging System Microscope (Thermo Fisher Scientific, Massachusetts, USA).

Descriptive statistical analyses of numerical variables consisted of sample size, missing observations, arithmetic mean, median, standard deviation, 95% confidence interval of the mean and minimum and maximum values. To compare the survival percentage averages between treatments, concentrations and yeasts, the analysis of variance technique was used with the effect estimated by the partial eta squared statistics. To compare performance over the days, analysis of variance with repeated measures was used with the effect calculated by the partial eta squared statistics. Post-hoc comparisons for significant effects were performed using Tukey's test with the effect estimated using Cohen's D statistics. The significance level adopted was 0.05. The computational package used for statistical analyses was JASP version 0.17.3 for MacOS.

### Data availability

All data generated or analysed during this study are included in this published article (and its Supplementary Information files).

Received: 5 January 2024; Accepted: 2 May 2024

Published online: 15 May 2024

### References

- Pristov, K. E. & Ghannoum, M. A. Resistance of *Candida* to azoles and echinocandins worldwide. *Clin. Microbiol. Infect.* **25**, 792–798. <https://doi.org/10.1016/j.cmi.2019.03.028> (2019).
- da Costa, V. G., Quesada, R. M., Abe, A. T., Furlaneto-Maia, L. & Furlaneto, M. C. Nosocomial bloodstream *Candida* infections in a tertiary-care hospital in South Brazil: A 4-year survey. *Mycopathologia* **178**, 243–250. <https://doi.org/10.1007/s11046-014-9791-z> (2014).
- Daneshnia, F. et al. Worldwide emergence of fluconazole-resistant *Candida parapsilosis*: Current framework and future research roadmap. *Lancet Microbe* **4**, e470–e480. [https://doi.org/10.1016/S2666-5247\(23\)00067-8](https://doi.org/10.1016/S2666-5247(23)00067-8) (2023).
- Larkin, E. et al. The emerging pathogen *Candida auris*: Growth phenotype, virulence factors, activity of antifungals, and effect of SCY-078, a novel glucan synthesis inhibitor, on growth morphology and biofilm formation. *Antimicrob. Agents Chemother.* **61**, e02396–e02416. <https://doi.org/10.1128/AAC.02396-16> (2017).
- Lee, Y., Puumala, E., Robbins, N. & Cowen, L. E. Antifungal drug resistance: Molecular mechanisms in *Candida albicans* and beyond. *Chem. Rev.* **121**, 3390–3411. <https://doi.org/10.1021/acs.chemrev.0c00199> (2021).
- Mba, I. E. & Nweze, E. I. Mechanism of *Candida* pathogenesis: Revisiting the vital drivers. *Eur. J. Clin. Microbiol. Infect. Dis.* **39**, 1797–1819. <https://doi.org/10.1007/s10096-020-03912-w> (2020).
- El-Baz, A. M. et al. Back to nature: Combating *Candida albicans* biofilm, phospholipase and hemolysin using plant essential oils. *Antibiotics* **10**, 81. <https://doi.org/10.3390/antibiotics10010081> (2021).
- Lim, S. J. et al. Opportunistic yeast pathogen *Candida* spp.: Secreted and membrane-bound virulence factors. *Med. Mycol.* **59**, 1127–1144. <https://doi.org/10.1093/mmy/myab053> (2021).
- Abreu-Pereira, C. A. et al. DNase enhances photodynamic therapy against fluconazole-resistant *Candida albicans* biofilms. *Oral Dis.* <https://doi.org/10.1111/odi.14149> (2022).
- Pianalto, K. M. & Alspaugh, J. A. New horizons in antifungal therapy. *J. Fungi* **2**, 26. <https://doi.org/10.3390/jof2040026> (2016).
- Maioli, E. et al. Rottlerin inhibits ROS formation and prevents NFκB activation in MCF-7 and HT-29 cells. *J. Biomed. Biotechnol.* **2009**, 742936. <https://doi.org/10.1155/2009/742936> (2009).
- Kumar, D., Shankar, S. & Srivastava, R. K. Rottlerin induces autophagy and apoptosis in prostate cancer stem cells via PI3K/Akt/mTOR signaling pathway. *Cancer Lett.* **343**, 179–189. <https://doi.org/10.1016/j.canlet.2013.10.003> (2014).
- Ishii, N., Yamamoto, M., Yoshihara, F., Arisawa, M. & Aoki, Y. Biochemical and genetic characterization of Rbf1p, a putative transcription factor of *Candida albicans*. *Microbiology (Reading)* **143**, 429–435. <https://doi.org/10.1099/00221287-143-2-429> (1997).
- Zaidi, S. F. et al. Potent bactericidal constituents from *Mallotus philippinensis* against clarithromycin and metronidazole resistant strains of Japanese and Pakistani *Helicobacter pylori*. *Biol. Pharm. Bull.* **32**, 631–636. <https://doi.org/10.1248/bpb.32.631> (2009).

15. Teixeira, S. C. *et al.* Rottlerin impairs early and late steps of *Toxoplasma gondii* infection in human trophoblast cells and villous explants. *Chem. Biol. Interact.* **384**, 110716. <https://doi.org/10.1016/j.cbi.2023.110716> (2023).
16. Ietta, F. *et al.* Rottlerin-mediated inhibition of *Toxoplasma gondii* growth in BeWo trophoblast-like cells. *Sci. Rep.* **7**, 1279. <https://doi.org/10.1038/s41598-017-01525-6> (2017).
17. Kean, R. & Ramage, G. Combined antifungal resistance and biofilm tolerance: The global threat of *Candida auris*. *mSphere* **4**, 10–1128. <https://doi.org/10.1128/mSphere.00458-19> (2019).
18. Motia Fernandes, C. *et al.* The future of antifungal drug therapy: Novel compounds and targets. *Antimicrob. Agents Chemother.* **65**, 10–1128. <https://doi.org/10.1128/AAC.01719-20> (2021).
19. Genilloud, O. Natural products discovery and potential for new antibiotics. *Curr. Opin. Microbiol.* **51**, 81–87. <https://doi.org/10.1016/j.mib.2019.10.012> (2019).
20. Gschwendt, M. *et al.* Rottlerin, a novel protein kinase inhibitor. *Biochem. Biophys. Res. Commun.* **199**, 93–98 (1994).
21. Torricelli, C. *et al.* Alternative pathways of cancer cell death by rottlerin: Apoptosis versus autophagy. *Evid. Based Complement Altern. Med.* **2012**, 980658. <https://doi.org/10.1155/2012/980658> (2012).
22. Torricelli, C. *et al.* Phosphorylation-independent mTORC1 inhibition by the autophagy inducer Rottlerin. *Cancer Lett.* **360**, 17–27. <https://doi.org/10.1016/j.canlet.2015.01.04017-27> (2015).
23. Wang, L. *et al.* Rottlerin inhibits cell growth and invasion via down-regulation of Cdc20 in glioma cells. *Oncotarget* **7**, 69770. <https://doi.org/10.18632/oncotarget.11974> (2016).
24. Song, J., Zhou, Y., Gong, Y., Liu, H. & Tang, L. J. M. Rottlerin promotes autophagy and apoptosis in gastric cancer cell lines. *Mol. Med. Rep.* **18**, 2905–2913. <https://doi.org/10.3892/mmr.2018.9293> (2018).
25. Bharadwaj, R. *et al.* Rottlerin derivatives and other compounds from *Mallotus philippinensis* fruits and their potential antimicrobial activity. *Planta Med. Lett.* **2**, e28–e30. <https://doi.org/10.1055/s-0035-1557793> (2015).
26. Gangwar, M. *et al.* Qualitative phytochemical characterization and antibacterial evaluation of glandular hairs covering of *Mallotus philippinensis* fruit extract. *J. Pharm. Res.* **4**, 4214–4216 (2011).
27. Silva, P. T. D. *et al.* Cytotoxic and antifungal activity of chalcones synthesized from natural acetophenone isolated from *Croton anisodontus*. *Rev. Quim.* **12**, 712–723 (2020).
28. Mellado, M. *et al.* Design, synthesis, antifungal activity, and structure–activity relationship studies of chalcones and hybrid dihydrochromane–chalcones. *Mol. Divers.* **24**, 603–615. <https://doi.org/10.1007/s11030-019-09967-y> (2020).
29. Kulkarni, R. R. *et al.* Antifungal dimeric chalcone derivative kamalachalcone E from *Mallotus philippinensis*. *Nat. Prod. Res.* **28**, 245–250. <https://doi.org/10.1080/14786419.2013.843178> (2014).
30. de Barros, P. P. *et al.* *Candida* biofilms: An update on developmental mechanisms and therapeutic challenges. *Mycopathologia* **185**, 415–424. <https://doi.org/10.1007/s11046-020-00445-w> (2020).
31. Ghannoum, M. A. Potential role of phospholipases in virulence and fungal pathogenesis. *Clin. Microbiol. Rev.* **13**, 122–143. <https://doi.org/10.1128/CMR.13.1.122> (2000).
32. Menezes, R. P. *et al.* Antimicrobial, antivirulence, and antiparasitic potential of *Capsicum chinense* Jacq. extracts and their isolated compound capsaicin. *Antibiotics* **11**, 1154. <https://doi.org/10.3390/antibiotics11091154> (2022).
33. Riceto, E. B., Menezes Rde, P., Penatti, M. P. & Pedrosa Rdos, S. Enzymatic and hemolytic activity in different *Candida* species. *Rev. Iberoam. Micol.* **32**, 79–82. <https://doi.org/10.1016/j.riam.2013.11.003> (2015).
34. Hacıoglu, M., Oyardi, O. & Kirinti, A. Oregano essential oil inhibits *Candida* spp. biofilms. *Z. Nat. C J. Biosci.* **76**, 443–450. <https://doi.org/10.1515/znc-2021-0002> (2021).
35. Uppuluri, P. *Candida auris* biofilm colonization on skin niche conditions. *MSphere* **5**, 10–1128. <https://doi.org/10.1128/mSphere.00972-19> (2020).
36. Tsang, P. W., Wong, A. P., Yang, H. P. & Li, N. F. Purpurin triggers caspase-independent apoptosis in *Candida dubliniensis* biofilms. *PLoS ONE* **8**, e86032. <https://doi.org/10.1371/journal.pone.0086032> (2013).
37. Sullivan, D. & Coleman, D. *Candida dubliniensis*: Characteristics and identification. *J. Clin. Microbiol.* **36**, 329–334. <https://doi.org/10.1128/JCM.36.2.329-334.1998> (1998).
38. Jabri, B. *et al.* *Candida albicans* and *Candida dubliniensis* in periodontitis in adolescents and young adults. *Int. J. Microbiol.* **2022**, 4625368. <https://doi.org/10.1155/2022/4625368> (2022).
39. Camargo, G. A., Abreu, M. G., Cordeiro Rdos, S., Wenderosky Lde, F. & Duque, C. Prevalence of periodontopathogens and *Candida* spp. in smokers after nonsurgical periodontal therapy—A pilot study. *Braz. Oral Res.* **30**, e92. <https://doi.org/10.1590/1807-3107BOR-2016.vol30.0092> (2016).
40. Ribeiro, F. C. *et al.* Action mechanisms of probiotics on *Candida* spp. and candidiasis prevention: an update. *J. Appl. Microbiol.* **129**, 175–185. <https://doi.org/10.1111/jam.14511> (2020).
41. El-Houssaini, H. H., Elnabawy, O. M., Nasser, H. A. & Elkhatib, W. F. Influence of subinhibitory antifungal concentrations on extracellular hydrolases and biofilm production by *Candida albicans* recovered from Egyptian patients. *BMC Infect. Dis.* **19**, 54. <https://doi.org/10.1186/s12879-019-3685-0> (2019).
42. Vazquez-Munoz, R., Lopez, F. D. & Lopez-Ribot, J. L. Bismuth nanoantibiotics display anticandidal activity and disrupt the biofilm and cell morphology of the emergent pathogenic yeast *Candida auris*. *Antibiotics* **9**, 461. <https://doi.org/10.3390/antibiotics9080461> (2020).
43. Hao, W. *et al.* Activity of chlorhexidine acetate in combination with fluconazole against suspensions and biofilms of *Candida auris*. *J. Infect. Chemother.* **28**, 29–34. <https://doi.org/10.1016/j.jiac.2021.09.018> (2022).
44. Nett, J. E. & Andes, D. R. Contributions of the biofilm matrix to *Candida* pathogenesis. *J. Fungi* **6**, 11. <https://doi.org/10.3390/jof6010021> (2020).
45. Crisford, A. *et al.* Selective toxicity of the anthelmintic emodepside revealed by heterologous expression of human KCNMA1 in *Caenorhabditis elegans*. *Mol. Pharmacol.* **79**, 1031–1043. <https://doi.org/10.1124/mol.111.071043> (2011).
46. Singulani, J. L. *et al.* Activity of gallic acid and its ester derivatives in *Caenorhabditis elegans* and zebrafish (*Danio rerio*) models. *Future Med. Chem.* **9**, 1863–1872. <https://doi.org/10.4155/fmc-2017-0096> (2017).
47. Clinical and Laboratory Standards Institute. Reference method for broth dilution antifungal susceptibility testing of yeasts. Approved standard—fourth edition. CLSI document M27- A4 (2017).
48. Sarker, S. D., Nahar, L. & Kumarasamy, Y. Microtitre plate-based antibacterial assay incorporating resazurin as an indicator of cell growth, and its application in the in vitro antibacterial screening of phytochemicals. *Methods* **42**, 321–324. <https://doi.org/10.1016/j.ymeth.2007.01.006> (2007).
49. Siddiqui, Z. N., Farooq, F., Musthafa, T. N. M., Ahmad, A. & Khan, A. U. Synthesis, characterization and antimicrobial evaluation of novel halopyrazole derivatives. *J. Saudi Chem. Soc.* **17**, 237–243. <https://doi.org/10.1016/j.jscs.2011.03.016> (2013).
50. Luo, G., Samaranyake, L. P. & Yau, J. Y. *Candida* species exhibit differential in vitro hemolytic activities. *J. Clin. Microbiol.* **39**, 2971–2974. <https://doi.org/10.1128/JCM.39.8.2971-2974.2001> (2001).
51. Ruchel, R., Tegeler, R. & Trost, M. A comparison of secretory proteinases from different strains of *Candida albicans*. *Sabouraudia* **20**, 233–244. <https://doi.org/10.1080/00362178285380341> (1982).
52. Price, M. F., Wilkinson, I. D. & Gentry, L. O. Plate method for detection of phospholipase activity in *Candida albicans*. *Sabouraudia* **20**, 7–14. <https://doi.org/10.1080/00362178285380031> (1982).
53. Sanchez, M. & Colom, F. Extracellular DNase activity of *Cryptococcus neoformans* and *Cryptococcus gattii*. *Rev. Iberoam. Micol.* **27**, 10–13. <https://doi.org/10.1016/j.riam.2009.11.004> (2010).

54. Pierce, C. G. *et al.* A simple and reproducible 96-well plate-based method for the formation of fungal biofilms and its application to antifungal susceptibility testing. *Nat. Protoc.* **3**, 1494–1500. <https://doi.org/10.1038/nprot.2008.141> (2008).
55. O’Toole, G. A. Microtiter dish biofilm formation assay. *J. Vis. Exp.* **1**, e2437. <https://doi.org/10.3791/2437> (2011).
56. Wei, G. X., Campagna, A. N. & Bobek, L. A. Effect of MUC7 peptides on the growth of bacteria and on *Streptococcus mutans* biofilm. *J. Antimicrob. Chemother.* **57**, 1100–1109. <https://doi.org/10.1093/jac/dkl120> (2006).
57. Sebaugh, J. L. Guidelines for accurate EC<sub>50</sub>/IC<sub>50</sub> estimation. *Pharm. Stat.* **10**, 128–134. <https://doi.org/10.1002/pst.426> (2011).
58. Melo, R. T. *et al.* Intrinsic and extrinsic aspects on *Campylobacter jejuni* biofilms. *Front. Microbiol.* **8**, 1332. <https://doi.org/10.3389/fmicb.2017.01332> (2017).
59. Breger, J. *et al.* Antifungal chemical compounds identified using a *C. elegans* pathogenicity assay. *PLoS Pathog.* **3**, e18. <https://doi.org/10.1371/journal.ppat.0030018> (2007).

## Acknowledgements

The authors would like to thank Prof. Dr. Alberto da Silva Moraes from the Institute of Biomedical Sciences at the Federal University of Uberlândia for providing the reagents for SEM assays and the PhD student at Universidade Estadual Paulista “Júlio de Mesquita Filho”, Victória Riquena Grosche, for editing the design and layout of images of *C. elegans* included in this study. We also thank teacher Abilio Borghi for the assistance with the English language.

## Author contributions

N.B.S.S: Designed the experiments, functions/Writing—original draft; writing—proofreading and editing. R.P.M: Designed the experiments and carried out the experiments. D.S.G: Designed the experiments and carried out the experiments. M.B.S: Designed the experiments and carried out the experiments. N.C.C: Designed the experiments and carried out the experiments. S.L.S: Designed the experiments and carried out the experiments. A.L.O: Designed the experiments and carried out the experiments. R.S.S: Analysed the results and Writing—proofreading and editing. S.B.R: Analysed the results and validation. E.A.V.F: Analysed the results and Writing—proofreading and editing. C.H.G.M: Conceptualization, formal analysis, methodology, supervision, validation; visualization, functions/Writing—original draft; writing—proofreading and editing. All authors gave the final approval for publication.

## Funding

This work was supported by Fundação de Amparo a Pesquisa do Estado de Minas Gerais (FAPEMIG—Scholarship Grant Number 12138 and APQ Grant Number 02067-22).

## Competing interests

The authors declare no competing interests.

## Additional information

**Supplementary Information** The online version contains supplementary material available at <https://doi.org/10.1038/s41598-024-61179-z>.

**Correspondence** and requests for materials should be addressed to C.H.G.M.

**Reprints and permissions information** is available at [www.nature.com/reprints](http://www.nature.com/reprints).

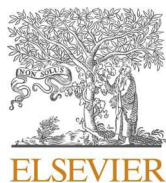
**Publisher’s note** Springer Nature remains neutral with regard to jurisdictional claims in published maps and institutional affiliations.



**Open Access** This article is licensed under a Creative Commons Attribution 4.0 International License, which permits use, sharing, adaptation, distribution and reproduction in any medium or format, as long as you give appropriate credit to the original author(s) and the source, provide a link to the Creative Commons licence, and indicate if changes were made. The images or other third party material in this article are included in the article’s Creative Commons licence, unless indicated otherwise in a credit line to the material. If material is not included in the article’s Creative Commons licence and your intended use is not permitted by statutory regulation or exceeds the permitted use, you will need to obtain permission directly from the copyright holder. To view a copy of this licence, visit <http://creativecommons.org/licenses/by/4.0/>.

© The Author(s) 2024





## Exploring the composition and properties of *Centella asiatica* metabolites and investigating their impact on BSA glycation, LDL oxidation and $\alpha$ -amylase inhibition

Ana Luiza Silva Borges<sup>a,1</sup>, Vinícius Prado Bittar<sup>a,1</sup>, Allisson Benatti Justino<sup>a</sup>, Maria Sol Peña Carrillo<sup>a</sup>, Renner Francisco Mateus Duarte<sup>a</sup>, Nagela Bernadelli Sousa Silva<sup>b</sup>, Daniela Silva Gonçalves<sup>b</sup>, Diego Godina Prado<sup>c</sup>, Iasmin Aparecida Cunha Araújo<sup>d</sup>, Mário Machado Martins<sup>e</sup>, Larissa Campos Motta<sup>f</sup>, Carlos Henrique Gomes Martins<sup>b</sup>, Françoise Vasconcelos Botelho<sup>a</sup>, Neide Maria Silva<sup>d</sup>, Alberto de Oliveira<sup>c</sup>, Wanderson Romão<sup>f,g</sup>, Foued Salmen Espíndola<sup>a,\*</sup>,<sup>2</sup>

<sup>a</sup> Laboratory of Biochemistry and Molecular Biology in Institute of Biotechnology, Federal University of Uberlândia, Uberlândia, MG 38400-902, Brazil

<sup>b</sup> Laboratory of Antimicrobial Testing, Institute of Biomedical Sciences, University of Uberlândia, Campus Umuarama, Uberlândia, MG 38405-320, Brazil

<sup>c</sup> Nucleus of Research in Natural Products (NuPpEn), Federal University of Uberlândia, Uberlândia, MG 38400-902, Brazil

<sup>d</sup> Laboratory of Immunoparasitology, Institute for Biomedical Sciences, Federal University of Uberlândia, Uberlândia, MG 38400-902, Brazil

<sup>e</sup> Laboratory of Nanobiotechnology "Dr. Luiz Ricardo Goulart Filho", in Institute of Biotechnology, Federal University of Uberlândia, Uberlândia, MG 38400-902, Brazil

<sup>f</sup> Laboratory of Petroleum and Forensics, of the Center of Competence in Petroleum Chemistry – NCQP, Federal University of Espírito Santo (UFES), Vitória, ES 29075-910, Brazil

<sup>g</sup> Federal Institute of Education, Science, and Technology of Espírito Santo, Vila Velha, 29106-010, Brazil

### ARTICLE INFO

#### Keywords:

*Centella asiatica*  
glycation  
LDL  
antioxidant

### ABSTRACT

*Centella asiatica* (L.) Urb. is a small herbaceous plant belonging to the Apiaceae family that is rich in triterpenes, such as asiaticoside and madecassoside. *Centella asiatica* finds broad application in promoting wound healing, addressing skin disorders, and boosting both memory and cognitive function. Given its extensive therapeutic potential, this study aimed not only to investigate the *Centella asiatica* ethanolic extract but also to analyze the biological properties of its organic fractions, such as antioxidant antiglycation capacity, which are little explored. We also identified the main bioactive compounds through spectrometry analysis. The ethanolic extract (EE) was obtained through a static maceration for seven days, while organic fractions (HF: hexane fraction; DF: dichloromethane fraction; EAF: ethyl acetate fraction; BF: n-butanol fraction and HMF: hydromethanolic fraction) were obtained via liquid-liquid fractionation. The concentration of phenolic compounds, flavonoids, and tannins in each sample was quantified. Additionally, the antiglycation (BSA/FRU, BSA/MGO, and ARG/MGO models) and antioxidant (FRAP, ORAC, and DPPH) properties, as well as the ability to inhibit LDL oxidation and hepatic tissue peroxidation were evaluated. The inhibition of enzyme activity was also analyzed ( $\alpha$ -amylase,  $\alpha$ -glucosidase, acetylcholinesterase, and butyrylcholinesterase). We also evaluated the antimicrobial and cytotoxicity against RAW 264.7 macrophages. The main compounds present in the most bioactive fractions were elucidated through ESI FT-ICR MS and HPLC-ESI-MS/MS analysis. In the assessment of antioxidant capacity (FRAP, ORAC, and DPPH), the EAF and BF fractions exhibited notable results, and as they are the phenolic compounds richest fractions, they also inhibited LDL oxidation, protected the hepatic tissue from peroxidation

**Abbreviations:** HPLC-ESI, High-performance liquid chromatography-electrospray ionization source; FRAP, Ferric reducing antioxidant power; DPPH, 2,2-diphenyl-1-picrylhydrazyl; ORAC, Oxygen radical absorbance capacity; AGEs, Advanced glycation end products; MGO, Methylglyoxal; FRU, Fructose; BSA, Bovine serum albumin; LDL, Low-density lipoprotein; ARG, Arginine; PBS, Phosphate buffer saline; OHT, Oxidized hepatic tissue; HT, Hepatic tissue; MIC, Minimum Inhibitory Concentration; AChE, Acetylcholinesterase; BChE, Butyrylcholinesterase; ROS, Reactive oxygen species; IC50, Inhibition concentration; CC50, cytotoxicity concentration; TBARS, thiobarbituric acid reactive substance; MDA, malondialdehyde; MTT, 3-(4,5-dimethylthiazol-2-yl)-2,5-diphenyltetrazolium bromide.

\* Correspondence to: Universidade Federal de Uberlândia, Instituto de Biotecnologia, Rua Acre s/n, Bloco 2E, Uberlândia, MG 38400-319, Brazil.

E-mail address: [foued@ufu.br](mailto:foued@ufu.br) (F.S. Espíndola).

<sup>1</sup> Equal contributions authors: & ALSB and VPB

<sup>2</sup> <https://orcid.org/0000-0002-6937-1411>

<https://doi.org/10.1016/j.jpba.2024.116143>

Received 21 December 2023; Received in revised form 26 March 2024; Accepted 31 March 2024

Available online 12 April 2024

0731-7085/© 2024 Published by Elsevier B.V.

and inhibited  $\alpha$ -amylase activity. Regarding glycation models, the EE, EAF, BF, and HMF fractions demonstrated substantial activity in the BSA/FRU model. However, BF was the only fraction that presented non-cytotoxic activity in RAW 264.7 macrophages at all tested concentrations. In conclusion, this study provides valuable insights into the antioxidant, antiglycation, and enzymatic inhibition capacities of the ethanolic extract and organic fractions of *Centella asiatica*. The findings suggest that further *in vivo* studies, particularly focusing on the butanol fraction (BF), may be promising routes for future research and potential therapeutic applications.

## 1. Introduction

*Centella asiatica* (L.) Urban is an herbaceous medicinal plant, also known as pegaga, pennywort or gotu kola. It belongs to the *Apiaceae* family and is native to Asia and especially found in India, China, and Malaysia [1,2]. Currently, the extract of *C. asiatica* has gained popularity among skincare products [3,4] and is also used in nutraceutical preparations, such as salads, teas, and juices [5]. However, Ayurveda and traditional Chinese medicine have employed and supported the use of this plant for centuries, and owing to its numerous health benefits, *C. asiatica* has attracted substantial attention from the scientific community [2,6].

Multiple studies have demonstrated the pharmacological effects of *C. asiatica* and its wide range of applications. The improvement of wound healing and its efficacy in treating various skin disorders have already been reported by many authors [7–9]. This plant also provides cognitive function, memory and learning improvement [10–12] and controls hyperglycemia in *in-vivo* models [13,14] among other properties. Available evidences also indicate that *C. asiatica* holds anti-inflammatory and antioxidant activity, which can support oxidative stress control [15–17].

*C. asiatica* leaves are a rich source of bioactive compounds, especially triterpenes, such as asiaticoside and madecassoside as well as their respective aglycones asiatic acid and madecasic acid, which are the main responsible for its pharmacological activity [2,6,18]. In addition to triterpenes, flavonoids, and phenolic compounds are also found in this plant, contributing to *C. asiatica*'s therapeutic effects.

The properties of ethanolic, methanolic, and aqueous extract of *C. asiatica* have already been studied. However, few researches have analyzed their liquid-liquid partitioning using organic solvents and their properties. This method aims to concentrate molecules according to their polarity increasing their therapeutical effects. The antioxidant and antiglycation capacities of organic fractions from *C. asiatica* have been little explored, in terms of the potential to inhibit LDL oxidation and hepatic tissue oxidation *in-vitro*.

This study aims to investigate the antioxidant, antiglycation, antimicrobial, and cytotoxic properties of the ethanolic extract of *C. asiatica* and its organic fractions using both *in-vitro* and *ex-vivo* methodologies. Furthermore, we employed mass spectrometry analysis to elucidate the bioactive compounds present in the samples.

## 2. Methodology

### 2.1. Reagents

Ethanol, methanol, and organic solvents hexane, dichloromethane, ethyl acetate, and n-butanol were purchased from Vetec Química Fina Ltda (Duque de Caxias, Rio de Janeiro, Brazil). Folin-Ciocalteu, gallic acid, vanillin, catechin, quercetin, 2,2-diphenyl-1-picrylhydrazyl, 2,4,6-Tris(2-pyridyl)-s-triazine, 6-hydroxy-2,5,7,8-tetramethylchroman-2-carboxylic acid (Trolox), 2,2'-azobis (2-amidino-propane)

dihydrochloride (AAPH), fluorescein, L-arginine, D-(-)-fructose, 2-Thiobarbituric

acid, aprotinin from bovine lung, acarbose, 2-chloro-4-nitrophenyl-4- $\beta$ -D-galactopyranosylmaltoside (GalG2CNP), acetylcholinesterase, butyrylcholinesterase, chlorhexidine, resazurin, were purchased from Sigma Aldrich (St. Louis, MO, USA). Dimethyl sulfoxide (DMSO) was

purchased from Merck (Darmstadt, HE, Germany). Brain Heart Infusion broth (BH1b) and Brain Heart Infusion agar (BH1a) Schaedler broth were purchased from BD Difco (Sparks, MD, EUA). Rivastigmine (drug) was purchased from ACHÉ Laboratórios Farmacêuticos, Brazil, and galantamine (drug) was purchased from Libbs Farmacêutica Ltda, Brazil.

### 2.2. Plant material

*C. asiatica* dried leaves were obtained from the Santos Flora Comércio de Ervas Ltda (Mariporã, São Paulo, Brasil) with a certificate of origin, attesting its purity and microbiology control. This company is registered under ANVISA (Authorization Number: 6.0.671–1) and the Regional Pharmacy Council - CRF (Registration Number: 0505). Spectrometry analysis was also employed to evaluate the presence of *C. asiatica* biomarkers, and the results were compared to those of the relevant literature.

### 2.3. Extraction and fractionation

To obtain the ethanolic extract of *C. asiatica* (EE), 500 g of dried and crushed leaves of *C. asiatica* were submitted to a static maceration procedure using two liters of 98 % pure ethanol (1:4 m/v) for seven days at room temperature in the absence of light. The solution was filtered with a common paper filter, and the remaining solvent was removed by rotary evaporation (Buchi Rotavapor R-210, Flawil, Switzerland) at 40°C under controlled and reduced pressure. Subsequently, the EE was submitted to lyophilization process to remove the remaining solvent and diluted in a 90 % (9:1 v/v 250 mL) hydro-methanolic (MeOH:H<sub>2</sub>O) solution to initiate the process of liquid-liquid partitioning. The organic solvents were added in an increasing polarity order: hexane (HF), dichloromethane (DF), ethyl acetate (EAF) and n-butanol (BF). The residue of the partitioning process represents the hydromethanolic fraction (HMF). The EE and the organic fractions were frozen at –20 °C and lyophilized.

### 2.4. ESI FT-ICR MS analysis

The EE and its organic fractions of *C. asiatica* were solubilized in 1 mL of methanol and submitted to Fourier transform ion cyclotron resonance mass spectrometry (FT-ICR MS) analysis using a 9.4 T Solarix, Bruker Daltonics (Bremen, Germany) equipped with an electrospray ionization source (ESI) at the negative mode, which was set to operate over a mass range of  $m/z$  150–15,000. To each sample, a flow rate of 5  $\mu$ L/min was chosen, and the ESI source conditions were as follows: a capillary voltage of 3.5 – 4.1 kV, a nebulizer gas pressure of 1 bar, and a transfer capillary temperature of 250 °C. The ion accumulation time and the time-of-flight in the hexapole were 0.02 and 0.9 ms, respectively. Each spectrum was acquired by accumulating 16 scans of time-domain transient signals in four mega-point time-domain data sets. All mass spectra were externally calibrated using an arginine solution ( $m/z$  from 150 to 1500). The resolution power was approximately 500,000 in  $m/z$  400. FT-ICR mass spectra were acquired and processed using the Software Data Analysis (Bruker Daltonics, Bremen, Germany), and the determination of the proposed structures for each molecular formula were assigned using the PubChem database.

## 2.5. HPLC-MS/ESI

The EAF, BF, and DF fractions were submitted to high-performance liquid chromatography coupled to an electrospray ionization mass spectrometer (HPLC-ESI/MS) in order to identify the compounds responsible for their high antioxidant and antiglycation activity. It was used a liquid chromatograph (Agilent - Infinity 1260) coupled to a high-resolution mass spectrometer (Agilent® model 6520 B) with ESI source. The mobile phase consisted of 0.1 % formic acid (v/v) (A) and methanol (B). The gradient system parameter applied was 10 % of B (0 min), 98 % of B (0–10 min), and 98 % (11–17 min). We set the ionization parameters as follows: a nebulizer pressure of 20 psi, a drying gas flow rate of 8 L/min, and a temperature of 220 °C. Additionally, an energy of 4.5 kV was applied to the capillary. To obtain information about the chemical connectivity of molecules, collision-induced dissociation (CID) experiments were performed using different collision energies ranging from 5 to 30 eV. The MS data was analyzed by Agilent MassHunter® software to obtain exact mass values, and all spectra obtained were compared to other already published studies, online libraries, such as Metlin, and databases (PubChem, ChemSpider, and MassBank).

## 2.6. In-vitro antioxidant activity

To evaluate the antioxidant properties of EE and its organic fractions, three assays were performed according to the study of [19]: ferric reducing antioxidant power (FRAP), oxygen radical absorbance capacity (ORAC), and 2,2-diphenyl-1-picrylhydrazyl (DPPH). For FRAP and DPPH assay, samples were prepared at a concentration of 1 mg/mL. For ORAC assay, samples were prepared at a concentration of 0.100 mg/mL.

### 2.6.1. FRAP

EE and its organic fractions were mixed with FRAP reagent (300 mM sodium acetate buffer pH 3.6, 10 mM 2,4,6-tris-(2-pyridyl)-s-triazine (TPTZ) and 20 mM ferric chloride at a 10:1:1 proportion) and were incubated at 37 °C for six min at a 96-well microplate. The absorbance was measured at 593 nm (Molecular Devices, Menlo Park, CA, USA). Quercetin was used as positive control, and sodium acetate buffer was used as negative control. The antioxidant capacity was calculated according to an analytical curve using 6-hydroxy-2,5,7,8-tetramethylchroman-2-carboxylic acid (Trolox) as standard, and the results were expressed as  $\mu\text{mol}$  of Trolox equivalents ( $\mu\text{mol TE/g}$ ).

### 2.6.2. ORAC

EE and its organic fractions at the concentration of 100  $\mu\text{g/mL}$  were incubated with 0.085 mM fluorescein and 153 mM 2,2'-azobis (2-amidinopropane) dihydrochloride (AAPH), and the fluorescence was measured at 485 nm<sub>ex</sub>/528 nm<sub>em</sub> (PerkinElmer LS 55, Massachusetts, USA) for 90 min at 37 °C in a 96-well microplate. All reagents were diluted in 75 mM phosphate buffer, pH 7.4. Quercetin was used as positive control, and phosphate buffer was used as negative control. The antioxidant capacity was calculated according to an analytical curve using 6-hydroxy-2,5,7,8-tetramethylchroman-2-carboxylic acid (Trolox) as standard and the results were expressed as  $\mu\text{mol}$  of Trolox equivalents ( $\mu\text{mol TE/g}$ ).

### 2.6.3. DPPH

EE and its organic fractions at the concentration of 250  $\mu\text{g/mL}$  were serially 10-point diluted in order to assess the  $\text{EC}_{50}$  values and were incubated with 0.06 M DPPH for 30 min in the absence of light, and the absorbance was measured at 517 nm (Molecular Devices, Menlo Park, CA, USA) in a 96-well microplate. Quercetin was used as positive control, and methanol was used as negative control. The DPPH scavenging capacity of the samples were determined using the following formula:  $\text{DPPH (\%)} = [(\text{Abs DPPH} - \text{Abs sample}) / (\text{Abs DPPH} - \text{A blank})] \times 100$ , where Abs DPPH refers to the absorbance of DPPH solution, Abs sample refers to the absorbance of the sample/positive control mixed with

DPPH solution and Abs blank refers to the absorbance of the sample mixed with only methanol.

## 2.7. Phytochemical analysis

To access the phytochemical analysis of *C. asiatica* EE and its organic fractions, phenolic, flavonoids, and condensed tannins content were performed according to the methodologies as already described [20,21]. All samples were used at a concentration of 5 mg/mL, and ethanol was used as blank.

### 2.7.1. Total Flavonoid content

The EE and its organic fractions were incubated with a solution of 5 % sodium nitrite and ultrapure water for six minutes at 25 °C in the dark. Subsequently, the mixture was incubated with 10 % aluminum chloride for more six minutes at 25 °C in the dark, and the absorbance was measured at 425 nm (Versamax, Molecular Devices, EUA). Quercetin was used as a standard to construct an analytical curve to determine the flavonoid content (mg QE/g).

### 2.7.2. Total phenolic content

The EE and its organic fractions were incubated with a solution of 10 % Folin-Ciocalteu for six minutes at 25 °C. After that, the mixture was incubated with 7 % of sodium carbonate for 2 h at 25 °C in the dark, and the absorbance was measured at 760 nm (Versamax, Molecular Devices, EUA). Gallic acid was used as a standard to construct an analytical curve to determine the total phenolic content (mg GAE/g).

### 2.7.3. Condensed tannin content

The EE and its organic fractions were incubated with 4 % of vanillin and HCl for 15 min at 25 °C. The absorbance was measured at a 500 nm (Versamax, Molecular Devices, EUA). Catechin was used as standard to construct an analytical curve to determine the total condensed tannin content (mg CE/g).

## 2.8. AGEs formation analysis

The inhibition of advanced glycation end products (AGEs) formation by EE and its organic fractions was verified as described by Franco et al., [22] with minor modifications. Bovine serum albumin (BSA) and arginine were used as glycation targets, and fructose (FRU) and methylglyoxal (MGO) were used as glycation inducers. The EE, its organic fractions, and positive control quercetin were serially diluted from a concentration of 10 mg/mL for  $\text{IC}_{50}$  determination. Phosphate buffer was used as a negative control. The glycation inhibition percentage (I%) was performed according to the following equation:  $\text{I (\%)} = [(\text{F control} - \text{F sample}) / \text{F control}] \times 100$ , in which F control represents the fluorescence value obtained in the negative control, F sample represents the fluorescence value obtained in the presence of EE, organic fractions and quercetin.

### 2.8.1. BSA/FRU model

In the BSA/FRU model, which was based on the methodology described by Wang et al., (2011), EE and its organic fractions were incubated with BSA at 9.37 mg/mL and 234 mM fructose (both diluted in 200 mM phosphate buffer, pH 7.4, with 0.02 % azide) in microtubes for 72 h at 37 °C in the dark. Following this period, 20 % trichloroacetic acid was added, and the mixture was submitted to centrifugation at  $10.000 \times g$  for 10 min. Phosphate buffer was used for pellet resuspension, and the fluorescence intensity was measured at 350 nm<sub>ex</sub>/420 nm<sub>em</sub> (Perkin-Elmer LS 55, Massachusetts, USA). Quercetin was used as a positive control, and phosphate buffer was used as a negative control.

### 2.8.2. BSA/MGO model

In the BSA/MGO model, which was based on the methodology

described by [23], EE and its organic fractions were incubated with BSA at 9.37 mg/mL and 10 mM methylglyoxal (MGO) (both diluted in 200 mM phosphate buffer, pH 7.4, with 0.02 % azide) in microtubes for 72 h at 37 °C in the dark. Following this period, 20 % trichloroacetic acid was added, and the mixture was submitted to centrifugation at 10,000×g for 10 min. Phosphate buffer was used for pellet resuspension, and the fluorescence intensity was measured at 340 nm<sub>ex</sub>/380 nm<sub>em</sub> (Perkin-Elmer LS 55, Massachusetts, USA). Quercetin was used as a positive control, and phosphate buffer was used as a negative control.

### 2.8.3. ARG/MGO model

In the ARG/MGO assay model, which was described as [23], EE and its organic fractions were incubated with 20 mM arginine and 10 mM methylglyoxal (MGO) (both diluted in 200 mM phosphate buffer pH 7.4, with 0.02 % azide) in microtubes for 72 h at 37 °C in the dark. After incubation, the fluorescence intensity was measured at 340 nm<sub>ex</sub>/380 nm<sub>em</sub> (Perkin-Elmer LS 55, Massachusetts, USA). Quercetin was used as a positive control, and phosphate buffer was used as a negative control.

## 2.9. Ex-vivo analysis in hepatic tissue

### 2.9.1. Liver tissue processing

Healthy male Wistar rats at 6–8 weeks of age were anesthetized and euthanized by cervical dislocation at the Federal University of Uberlândia (UFU) Center for Bioterism and Experimentation with official approval from the Animal Ethics Committee (Craft No.7/2022/CEUA/PROPP/REITO-UFU of July 14, 2022). The liver tissues were immediately removed, immersed in liquid nitrogen, and stored at a –70 °C ultrafreezer. The liver tissues were homogenized in phosphate buffer (1:10 w/v, pH 7.4) and centrifuged at 800×g for 15 min at 4 °C. Subsequently, the supernatant was used to perform the ex-vivo oxidation induction assay as already described by Justino et al., [24] with minor modifications. The supernatant was incubated for one hour at 37 °C in the absence of light with 0,01 mM FeSO<sub>4</sub> and 0,01 mM ascorbic acid (oxidized hepatic tissue – OHT) and with the EE and its organic fractions at a concentration of 50 µg/mL. Quercetin was used as a positive control at the same concentration as the samples tested.

### 2.9.2. Lipid peroxidation assay

Lipid peroxidation was determined according to thiobarbituric acid reactive species (TBARS) assay [25]. The samples were incubated with 10 % trichloroacetic acid (TCA) and 0.67 % thiobarbituric acid (TBA) for 2 h at 100 °C. Then, butanol was added to the samples, and they were centrifugated at 5000×g for 3 min. The fluorescence intensity was measured at 515 nm<sub>ex</sub>/553 nm<sub>em</sub> (Perkin-Elmer LS 55, Massachusetts, USA), and the results were expressed as nmol of malondialdehyde per milligram of protein.

## 2.10. Isolation, oxidation, and peroxidation of low-density lipoprotein (LDL)

Blood samples were collected from healthy, non-smoking volunteers in heparinized vacutainer tubes, adhering to the ethical principles outlined in the Declaration of Helsinki. The study received approval from the local Ethics Committee (Approval No. 61082522.4.0000.5704, report 5.671.038). Plasma was obtained by centrifuging blood at 3000 rpm for 10 min at 4 °C. LDL isolation followed the method by Byung H. Chung et al., [26]. Initially, the plasma density was adjusted to 1.22 g/mL through the addition of 0.326 g of KBr per mL of plasma. After the gentle dissolution of KBr, we added to the plasma aprotinin (5 µL per mL of plasma), 2 mM benzamidine (5 µL per mL of plasma), 0.5 mM phenylmethylsulfonyl fluoride (PMSF) (0.5 µL per mL of plasma), 0.25 % chloramphenicol (0.5 µL per mL of plasma), and a solution containing 5 % sodium azide, 8 % EDTA, and 0.1 % chloramphenicol (10 µL per mL of plasma). Three milliliters of this mixture were

placed in a centrifuge tube, and 7 mL of a KBr solution (density 1.006 g/mL) was overlaid on the top of the mixture. The mixture underwent single-step discontinuous gradient ultracentrifugation at 40,000 rpm for two hours and thirty minutes at 4 °C. The LDL band was collected and dialyzed using phosphate-buffered saline (PBS 20 mM, pH 7.4), and the protein concentration was determined using Bradford's methodology [27]. The LDL oxidation (ox-LDL) was induced by 5 µM CuSO<sub>4</sub>, and the process was monitored for two hours at 37 °C at 234 nm (Perkin-Elmer LS 55, Massachusetts, USA). To evaluate the potential inhibition of LDL oxidation, 2 µg/mL of EE and its organic fractions were tested. Quercetin was used as a positive control, and PBS was used as a negative control. After two hours, samples were submitted to TBARS assay.

## 2.11. Enzymatic activity inhibition

Inhibiting target enzymes represents a strategy for modulating cellular processes involved in disease pathogenesis, and therefore, the search for natural compounds with enzyme inhibitor behavior is becoming increasingly important. The enzymatic activity inhibition of EE and its organic fractions were evaluated in four different enzymes: α-amylase, α-glucosidase, acetyl-cholinesterase, and butyryl-cholinesterase. The inhibition calculation was performed using the following formula: I (%) = [(Auc control – Auc sample) / (Auc control)] x100, where Auc control refers to the area under the curve obtained in the absence of the samples and positive control and the Auc sample refers to the area under the curve obtained in the presence of the samples.

### 2.11.1. Inhibition of α-amylase

Saliva was collected from volunteers, and a human salivary α-amylase enriched fraction (HSA-f) was obtained by ion-exchange chromatography on Q-sepharose resin [28]. The HSA-f and the substrate 2-chloro-4-nitrophenyl-4-β-D-galactopyranosylmaltoside (GalG2CNP) were diluted in 50 mM 2-(N-morpholino)-ethane sulfonic acid (MES) buffer (5 mM calcium chloride, 140 mM potassium thiocyanate and 300 mM sodium chloride, pH 6.0) for the assay. To evaluate the α-amylase activity inhibition capacity of EE and its organic fractions, the samples were incubated with HSA-f (1:10) for 30 min at 37 °C. Subsequently, 12 mM of GalG2CNP was added, and the absorbance was immediately measured at 405 nm (Perkin-Elmer LS 55, Massachusetts, USA) every minute for five minutes. Acarbose and ethanol were used as positive and negative controls, respectively.

### 2.11.2. Inhibition of α-glucosidase

The α-glucosidase activity was accessed according to a modified method adapted by Justino et al., (2016) using 4-nitrophenyl α-D-glucopyranoside (p-NPG) as substrate and an α-glucosidase rich fraction from intestinal acetone powders from rats. EE and its organic fractions were incubated with α-glucosidase and 1.5 mM of reduced glutathione, both diluted in 50 mM phosphate buffer pH 6.8, for 20 min at 37 °C. Right away, 4 mM 4-nitrophenyl α-D-glucopyranoside in phosphate buffer was added and the absorbance was measured at 405 nm (Perkin-Elmer LS 55, Massachusetts, USA) every three minutes for 20 min at 37 °C. Acarbose and ethanol were used as positive and negative controls, respectively.

### 2.11.3. Inhibition of acetyl-cholinesterase (AChE) and butyryl-cholinesterase (BChE)

The evaluation of AChE and BChE inhibitory activity was performed as the following methods described by [29], with modifications. In this assay, three buffers were used: A) 50 mM Tris-HCl, pH 8; B) 50 mM Tris-HCl buffer with 1 % bovine serum albumin; C) 50 mM Tris-HCl with NaCl 0.6 % w/v and MgCl<sub>2</sub> 0.4 % w/v. The EE, its organic fractions, and positive controls (galantamine and rivastigmine) were prepared in buffer A to reach a concentration of 5.5 mg/mL and posteriorly

incubated with 3 mM acetylthiocholine iodide or 3 mM butyrylthiocholine iodide, 50 mM Tris-HCl buffer with 1 % bovine serum albumin, 3.06 mM 5,5'-dithiobis (2-nitrobenzoic acid) (DTNB) prepared in buffer C. To start the reaction, 0.2 U/mL AChE or BChE was added, and the absorbance was immediately measured at 405 nm (Molecular Devices, Menlo Park, CA, USA) for 30 min.

### 2.12. MTT (fibroblasts and macrophages)

The cytotoxicity concentration (CC<sub>50</sub>) of EE and its organic fractions was determined using the 3-(4,5-dimethylthiazol-2-yl)-2,5 diphenyltetrazolium bromide (MTT) assay [30]. RAW 264.7 macrophages (ATCC TIB-71), obtained from the American Type Culture Collection (ATCC), were seeded in 96-well flat-bottom plates (5 × 10<sup>4</sup> cells/well) and incubated at 37 °C and 5 % CO<sub>2</sub> until their full adhesion. Cells were treated with 10, 100, and 500 µg/mL of the samples completely diluted in RPMI and incubated for 24 h at 37 °C and 5 % CO<sub>2</sub>. Subsequently, an MTT solution (50 µg/well) was added, and the plates were incubated for four hours at the same previous conditions. Afterward the solution was removed, and DMSO was added to solubilize the formazan crystals, and the absorbance was measured at 570 nm (Spectramax M2). Cell viability was calculated by considering the untreated group as 100 % viability.

### 2.13. MIC assay

The antibacterial activity of EE and its organic fractions was evaluated using the broth microdilution method, and the minimum inhibitory concentration (MIC) was determined as recommended by the Clinical and Laboratory Standards Institute (CLSI, [31]) with modifications. The assay was conducted in triplicate on a 96-well microplate. Samples were solubilized in 5 % dimethyl sulfoxide (DMSO) and diluted in Brain Heart Infusion broth (BHI). The EE and its organic fractions were tested at concentrations of 0.98–2000 µg/mL. The cariogenic bacterial strains used in this study were *Enterococcus faecalis* (ATCC 4082), *Streptococcus salivarius* (ATCC 29975), *Streptococcus mitis* (ATCC 49456), *Streptococcus sanguinis* (ATCC 10556), *Streptococcus mutans* (ATCC 25175), *Lactobacillus paracasei* (ATCC 11578), obtained from the American Type Culture Collection (ATCC) and were incubated in Brain Heart Infusion agar (BHIa), added with defibrinated horse blood (5 %) in a microaerophilic incubator for 24 h at 37 °C with 10 % CO<sub>2</sub>, except for *E. faecalis* and *S. salivarius* which were incubated aerobically. The inoculum concentration was adjusted for each microorganism to 5 × 10<sup>5</sup> CFU/mL. 5 % DMSO was used as a negative control. The positive control used was chlorhexidine at concentrations ranging from 0.115 to 59 µg/mL. The plates containing the samples and bacteria were incubated under the conditions described previously. Subsequently, 30 µL of 0.02 % aqueous resazurin was added to each well in order to analyze bacterial growth. Resazurin serves as an oxidation-reduction indicator, where the blue hue indicates the absence of microbial viability, while the red color signifies the presence of microbial viability.

### 2.14. Statistical analysis

Results were expressed by mean ± standard deviation, except for the EC<sub>50</sub> calculation, which was expressed as mean ± standard error. One-way ANOVA and Tukey post-test were applied to analyze multiple comparisons. Values of p < 0.05 were considered significant. The statistical analyses and graphs were created using GraphPad Prism 8.0 software.

## 3. Results

### 3.1. Phytochemical prospection

The content of phenolic compounds, flavonoids, and condensed tannins in the EE and its organic fractions was quantified, and the results

are presented in Table 1. The EAF exhibited the highest phenolic compound content (237.4 ± 26.7 mg GAE/g), followed by the BF (111.6 ± 5.95 mg GAE/g). With the exception of HMF, all samples showed a flavonoid content sum above 100 mg QE/g, with the EE and DF fractions having the highest values at 299.2 ± 18.08 and 261.5 ± 2.72 mg QE/g, respectively. In terms of condensed tannin content, EE and BF exhibited the highest values at above 80 mg CE/g.

### 3.2. Antioxidant activity

The antioxidant capacity of EE and its organic fractions was analyzed according to FRAP, ORAC, and DPPH assays, and the results can be observed in Fig. 1. In the FRAP assay (Fig. 1a), EAF and BF (978.4 ± 26.05 µM and 753.2 ± 66.15 µM Trolox eq/g, respectively) exhibited the highest antioxidant capacity, however, only EAF didn't show significant difference when compared to the positive control quercetin (987.8 ± 10.15 µM Trolox eq/g). In the ORAC assay, all samples, with the exception of HF and EE (DF: 2408 ± 31.04; EAF: 2288 ± 30.51; BF: 2371 ± 54.63 and HMF: 2349 ± 75.28 Trolox eq/g), were statistically similar to the positive control quercetin (2279 ± 18.45 Trolox eq/g). In the DPPH assay, EAF (1.6 ± 0.48 µg/mL) exhibited the lowest IC<sub>50</sub> value among EE and its fractions and was not significantly different when compared to positive control quercetin (0.366 ± 0.1392 µg/mL). Although the IC<sub>50</sub> values of EE, DF, and BF were slightly higher, there was no statistically significant difference between these values and the positive control.

### 3.3. Antiglycation Properties

The antiglycation properties of EE and its organic fractions were analyzed using three different models (BSA/FRU, BSA/MGO, and ARG/MGO), and the results are presented in Fig. 2. In the BSA/FRU model (Fig. 2a), both EAF and the positive control quercetin were able to inhibit glycation over 80 % from the concentration of 19 µg/mL. Among the fractions, EAF and BF revealed the lowest IC<sub>50</sub> values (4.14 ± 2.52 and 6.46 ± 1.1 µg/mL, respectively) and were not significantly different from the positive control quercetin (1.672 ± 0.60 µg/mL). Additionally, EE and HMF also showed similar inhibitory effects to quercetin. Furthermore, EE, DF, and EAF inhibited glycation in BSA/MGO model (Fig. 2b) by over 55 % at 625 µg/mL. In the ARG/MGO method (Fig. 2c), there was no significant difference between the IC<sub>50</sub> values of the EAF, DF, and the positive control (194.6 ± 21.60; 252.8 ± 22.79 and 37.16 ± 3.34 µg/mL). At the highest concentration used in the assay, the positive control inhibited 96 % of the glycation, while EAF and DF inhibited 82 % and 69 %, respectively.

### 3.4. Lipid peroxidation inhibition in hepatic tissue

The inhibition of lipid peroxidation in liver tissue was also evaluated (Fig. 3). The organic fractions that presented the highest antioxidant

**Table 1**

Total phenols, flavonoids, and condensed tannins content of the ethanolic extract of *C. asiatica* and its organic fractions. Values are expressed as mean ± standard deviation, and different letters indicate statistical significance (p < 0.05). Note: EE: ethanolic extract, HF: hexane fraction, DF: dichloromethane fraction, EAF: ethyl acetate fraction, BF: n-butanol fraction, HMF: hydro-methanolic fraction.

	Total phenols (mg GAE/g)	Flavonoids (mg QE/g)	Condensed tannins (mg CE/g)
EE	73.3 ± 0.99 <sup>ab</sup>	299.2 ± 18.08 <sup>a</sup>	96.47 ± 7.93 <sup>a</sup>
HF	8.36 ± 1.19 <sup>c</sup>	123.8 ± 11.5 <sup>bc</sup>	10.94 ± 1.98 <sup>bd</sup>
DF	46.65 ± 3.76 <sup>ac</sup>	261.5 ± 2.72 <sup>a</sup>	26.36 ± 3.96 <sup>bc</sup>
EAF	237.4 ± 26.7 <sup>d</sup>	161.7 ± 8.13 <sup>b</sup>	31.97 ± 3.96 <sup>c</sup>
BF	111.6 ± 5.95 <sup>b</sup>	103.3 ± 0.72 <sup>c</sup>	82.45 ± 3.96 <sup>a</sup>
HMF	12.01 ± 3.96 <sup>c</sup>	48.5 ± 4.33 <sup>d</sup>	0 ± 0 <sup>d</sup>

**Table 2**MIC values of the *C. asiatica* EE and its organic fractions over cariogenic bacteria. Values are expressed as  $\mu\text{g/mL}$ .

	<i>E. faecalis</i> ATCC 4082	<i>S. salivarius</i> ATCC 29975	<i>S. sobrinus</i> ATCC 33448	<i>S. mitis</i> ATCC 49456	<i>S. sanguinis</i> ATCC 10556	<i>S. mutans</i> ATCC 25175	<i>L. paracasei</i> ATCC 11578
EE	>2000	250	125	62,5	62,5	125	1000
HF	1000	125	15,6	15,6	31,25	15,6	62,5
DF	2000	250	125	31,25	31,25	125	250
EAF	>2000	250	250	250	500	250	250
BF	>2000	250	250	250	250	250	250
HMF	1000	250	500	500	500	250	1000
Chlorhexidine	3688	0922	0922	3688	1844	0922	1844

Note: EE: ethanolic extract, HF: hexane fraction, DF: dichloromethane fraction, EAF: ethyl acetate fraction, BF: n-butanol fraction, HMF: hydromethanolic fraction.

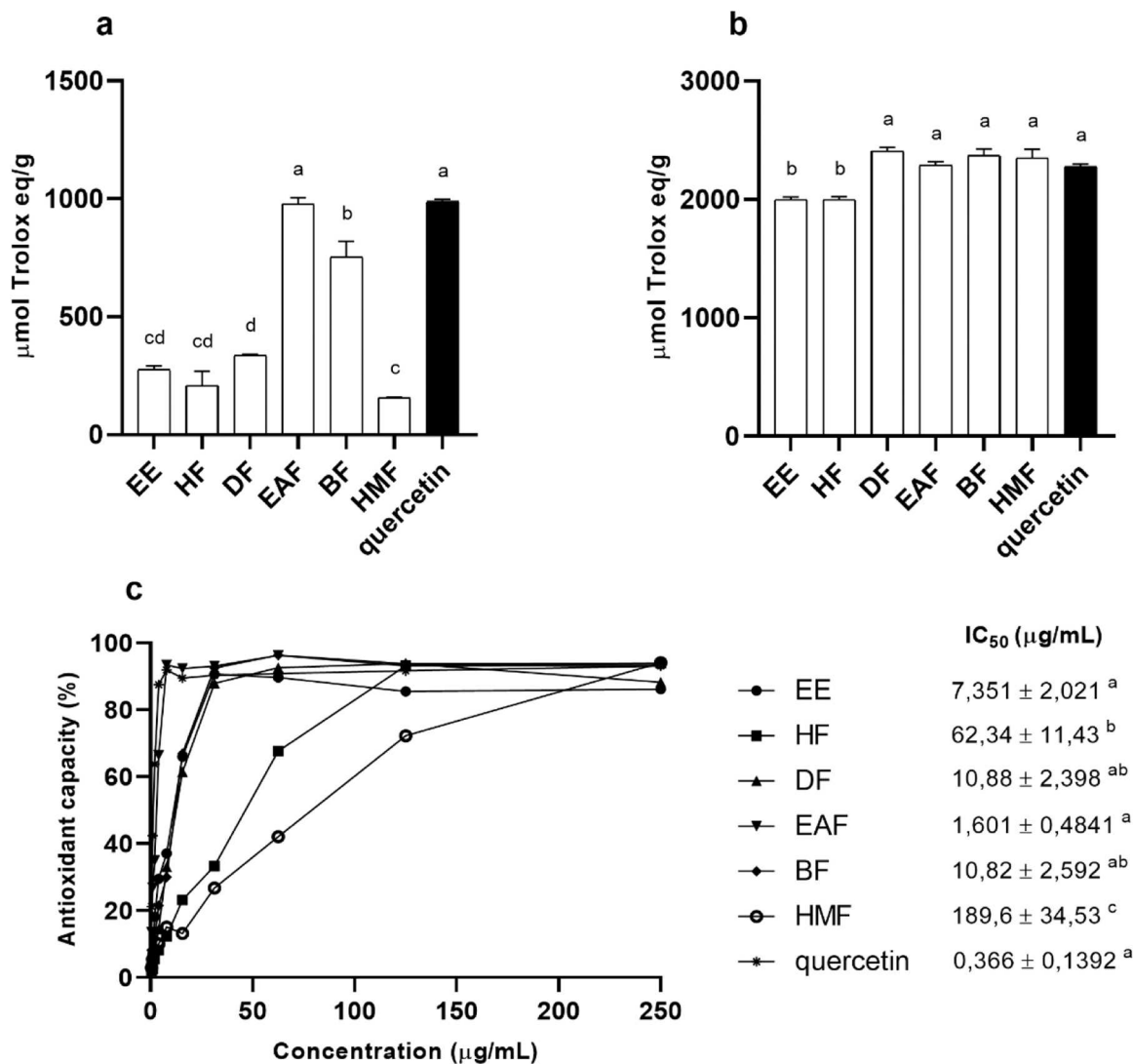


**Fig. 1.** Antioxidant capacity analysis of the ethanolic extract and organic fractions of *C. asiatica* by the methods FRAP (a), ORAC (b), and DPPH (c). Values (mean  $\pm$  standard deviation) are expressed as  $\mu\text{mol}$  Trolox equivalents (a and b) and percentage of antioxidant and  $\text{IC}_{50}$  values (c). Different letters indicate statistical significance ( $p < 0.05$ ). Note: EE: ethanolic extract, HF: hexane fraction, DF: dichloromethane fraction, EAF: ethyl acetate fraction, BF: n-butanol fraction, HMF: hydromethanolic fraction.

potential in the previous assays, EAF and BF, were also the most effective at protecting liver tissue from lipid peroxidation induced by  $\text{Fe}^{2+}$ -ascorbate, presenting significant difference when compared to the oxidized hepatic tissue (THO) control ( $p < 0.0001$ ) and no statistical difference versus positive control quercetin. It is also observed that malondialdehyde (MDA) levels are also reduced in the presence of EE and DF when compared to THO ( $p < 0.05$ ).

### 3.5. LDL oxidation and peroxidation inhibition

The inhibition of LDL oxidation and peroxidation by  $\text{Cu}^{2+}$  ions by EE and its organic fractions were evaluated (Fig. 4). It was observed that EE and its fractions DF, EAF, and BF were effective in inhibiting LDL oxidation (Fig. 4a), showing no significant difference when compared to control native LDL (without  $\text{Cu}^{2+}$  presence). Regarding the lipid peroxidation of LDL (Fig. 4b), the same fractions mentioned above, with the

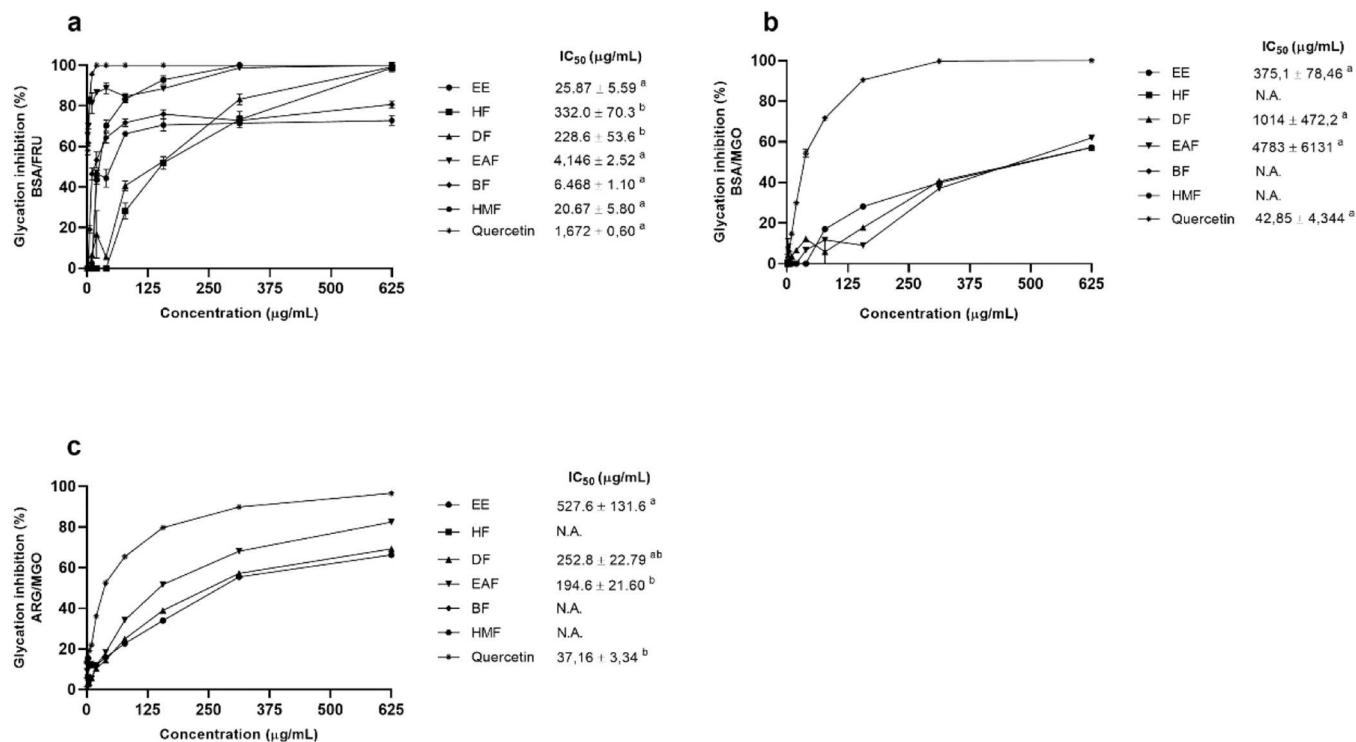


**Fig. 2.** Glycation inhibition of the ethanolic extract of *C. asiatica* and its organic fractions was evaluated by BSA-fructose (a), BSA-methylglyoxal (b) and arginine-methylglyoxal (c) models. Values (mean ± standard error) are expressed as glycation inhibition percentage and IC<sub>50</sub> values (µg/mL). Different letters indicate statistical significance ( $p < 0.05$ ). Note: EE: ethanolic extract, HF: hexane fraction, DF: dichloromethane fraction, EAF: ethyl acetate fraction, BF: n-butanol fraction, HMF: hydromethanolic fraction. N.A.: means no activity.

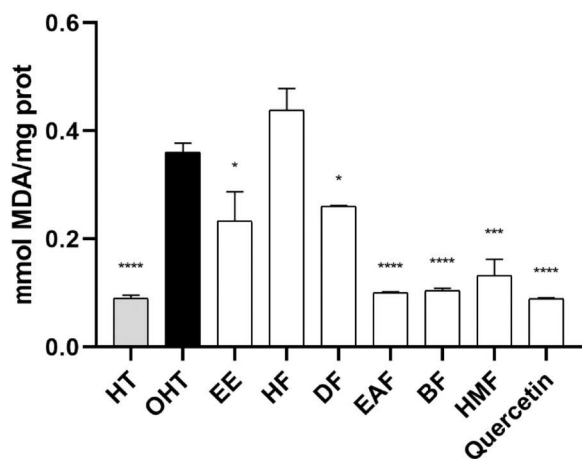


**Fig. 3.** Evaluation of the inhibition of lipid peroxidation in hepatic tissue by *C. asiatica* ethanolic extract and its organic fractions. Values are expressed as mean ± standard deviation. \*  $p < 0,05$ , \*\*  $p < 0,01$ , \*\*\*  $p < 0001$  e \*\*\*\*  $p < 0,0001$  when compared to OHT. Note: HT: hepatic tissue, OHT: oxidized hepatic tissue, EE: ethanolic extract, HF: hexane fraction, DF: dichloromethane fraction, EAF: ethyl acetate fraction, BF: n-butanol fraction, HMF: hydromethanolic fraction.

exception of EE, were able to reduce MDA levels.

### 3.6. $\alpha$ -amylase and $\alpha$ -glucosidase activity inhibition

Assays were conducted to verify the ability of *C. asiatica* EE and its organic fractions to inhibit  $\alpha$ -amylase and  $\alpha$ -glucosidase enzyme activity (Fig. 5). In the  $\alpha$ -amylase inhibition assay (Fig. 5a), our results revealed that the IC<sub>50</sub> values of EAF and BF ( $7.29 \pm 1.97$  and  $5.64 \pm 1.37$  µg/mL)

did not present significant difference when compared to the positive control, acarbose ( $0.15 \pm 0.03$  µg/mL). The EE had a higher IC<sub>50</sub> value when compared to the aforementioned fractions, indicating a lower inhibitory potential on the enzyme. However, at a concentration of 12 µg/mL, it still exhibited a significant inhibitory effect of  $72.67 \% \pm 1.01$ . In the  $\alpha$ -glucosidase inhibition analysis (Fig. 5b), acarbose showed an inhibition value of  $63.28 \pm 0.60 \%$  at a concentration of 231.4 µg/mL. However, at the same concentration, the EE and its fractions did not demonstrate significant inhibition of this enzyme, with all values below 50 % of inhibition, therefore it was not possible to obtain IC<sub>50</sub> values.

### 3.7. AchE and BchE inhibition assay

The inhibition of cholinesterases activity (AChE and BChE) by *C. asiatica* EE and its organic fractions were also evaluated, and the results are presented in Fig. 6. At a concentration of 100 µg/mL, the positive control galantamine, a drug already used to treat Alzheimer disease symptoms, demonstrated the ability to inhibit  $98.28 \pm 0,88 \%$  of AChE activity while EAF, at a concentration of 550 µg/mL, inhibited  $95.96 \pm 5.71 \%$ . DF inhibited  $66.09 \pm 10.65 \%$  of AChE activity at 550 µg/mL. However, it was statistically different when compared to galantamine and EAF. Regarding BChE inhibition, rivastigmine was used as control at a concentration of 100 µg/mL and inhibited  $92.07 \pm 0.44 \%$ . EAF and DF, at a concentration of 550 µg/mL, did not exhibit statistical difference when compared to rivastigmine.

### 3.8. Cytotoxicity in macrophages RAW 264.7 (MTT)

To evaluate cell viability, RAW 264.7 macrophages were treated with 10, 100 and 500 µg/mL of *C. asiatica* EE and its organic fractions (Fig. 7). At the lowest concentration, all samples, except for HF, did not reduce the cell viability. Notably, BF demonstrated exceptional non-cytotoxicity across all tested concentrations. At higher concentrations,

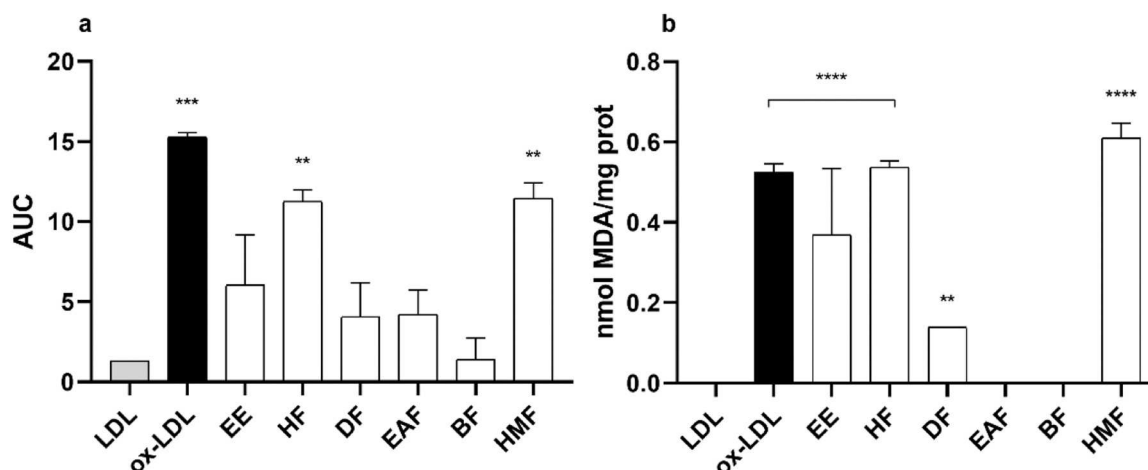


**Fig. 4.** Evaluation of the inhibition of oxidation (a) and peroxidation (b) of isolated LDL by the ethanolic extract of *C. asiatica* and its organic fractions. Values are expressed as mean  $\pm$  standard deviation. \*  $p < 0,05$ , \*\*  $p < 0,01$ , \*\*\*  $p < 0,001$  e \*\*\*\*  $p < 0,0001$  when compared to native LDL. Note: LDL: native LDL, ox-LDL: oxidized LDL, EE: ethanolic extract, HF: hexane fraction, DF: dichloromethane fraction, EAF: ethyl acetate fraction, BF: n-butanol fraction, HMF: hydromethanolic fraction.

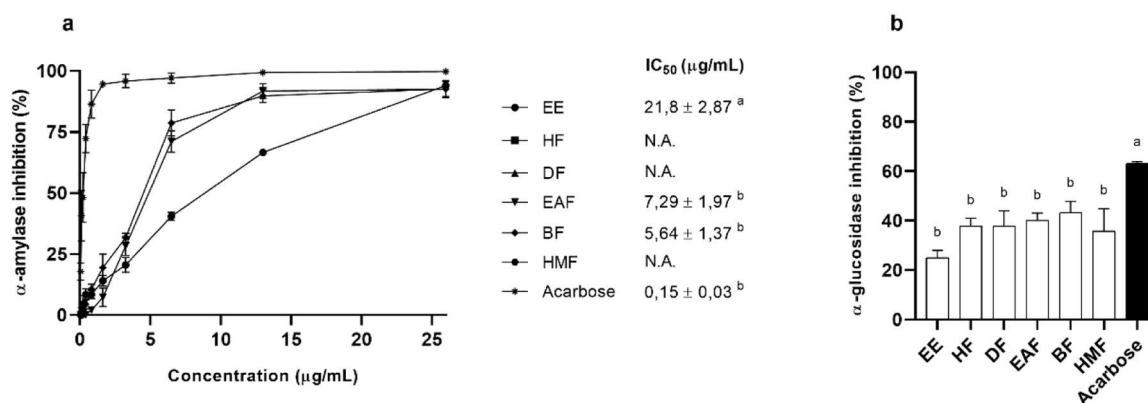


**Fig. 5.** Evaluation of the inhibitory potential of the activity of the enzymes  $\alpha$ -amylase (a) and  $\alpha$ -glucosidase (b) by the ethanolic extract of *C. asiatica* and its organic fractions. Values are expressed as IC<sub>50</sub> values (mean  $\pm$  standard error) (a) and as inhibition percentage (mean  $\pm$  standard deviation) (b). Different letters indicate statistical significance ( $p < 0.05$ ). Note: EE: ethanolic extract, HF: hexane fraction, DF: dichloromethane fraction, EAF: ethyl acetate fraction, BF: n-butanol fraction, HMF: hydromethanolic fraction. N.A.: means no activity.

apolar fractions, like HF and DF, were more cytotoxic than the polar ones, like EAF, BF, and HMF.

### 3.9. Antimicrobial activity

The antimicrobial activity of EE and its organic fractions was evaluated against bacteria associated to the development of caries and it is presented in Table 2. Both EE and its organic fractions demonstrated antibacterial activity against most cariogenic bacteria, demonstrating MIC values that varied from 15.6 to 2000  $\mu\text{g/mL}$ . The HF and DF fractions demonstrated the lowest values, where HF demonstrated MIC values of 15.6  $\mu\text{g/mL}$  against *Streptococcus sobrinus*, *Streptococcus mitis*, and *Streptococcus mutans* and 31.25  $\mu\text{g/mL}$  against *Streptococcus sanguinis*. The DF fraction presented a MIC value of 31.25  $\mu\text{g/mL}$  for *Streptococcus mitis* and *Streptococcus sanguinis*.

### 3.10. ESI FT-ICR mass spectra analysis

The ethanolic extract and its organic fractions were submitted for ESI FT-ICR MS analysis to identify the main compounds. Table 3 shows the detection of 23 compounds, of which 18 were identified, being mostly formed by phenolic acids and fatty acids compounds with values DBEs ranging from 1 to 28. This result indicates that their chemical structure

starts from typical linear fatty acids (palmitic acid,  $m/z$  255, for example) to compounds containing two aromatic rings, e.g., phenolic acids (digallic acid,  $m/z$  965). Information about the theoretical and obtained  $m/z$  values, mass error (in ppm) and DBE (double-bound equivalent) are supplied in Table 3.

### 3.11. HPLC-MS/ESI

As was observed in previous assays, DF, EAF, and BF demonstrated remarkable antioxidant activity, preventing LDL and hepatic tissue oxidation and a potential to inhibit the formation of AGEs. Therefore, these fractions were submitted to HPLC-MS/ESI analysis to identify the main compounds that contribute to the excellent performance of the samples mentioned above. Based on the retention times, error values, profile of fragmentation patterns, sequential mass spectra, and literature information, it was suggested the occurrence of some compounds listed in Table 4.

## 4. Discussion

Several studies have evaluated the therapeutic potential of *C. asiatica* leaf extract and its isolated triterpenes, however, researches about liquid-liquid fractionation using organic solvents are still little explored.



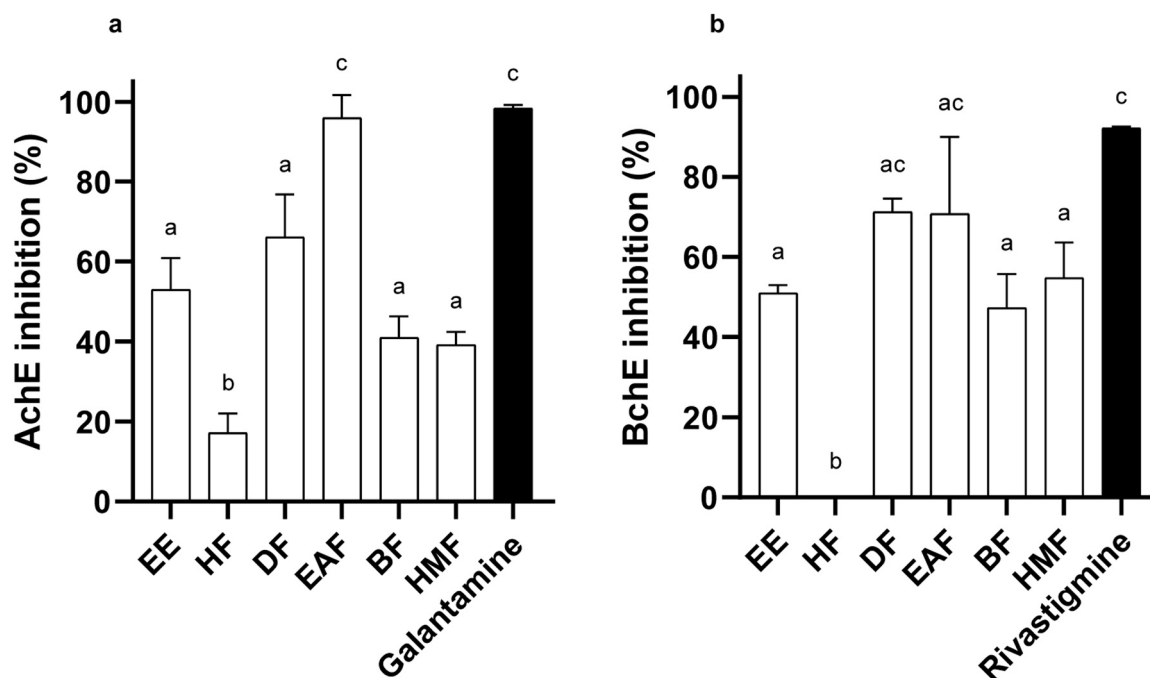


**Fig. 6.** Evaluation of AchE (a) and BchE (b) activity inhibition by *C. asiatica* EE and its organic fractions. Values are expressed as inhibition percentage (mean  $\pm$  standard deviation). Different letters indicate statistical significance ( $p < 0.05$ ). Note: EE: ethanolic extract, HF: hexane fraction, DF: dichloromethane fraction, EAF: ethyl acetate fraction, BF: n-butanol fraction, HMF: hydromethanolic fraction.

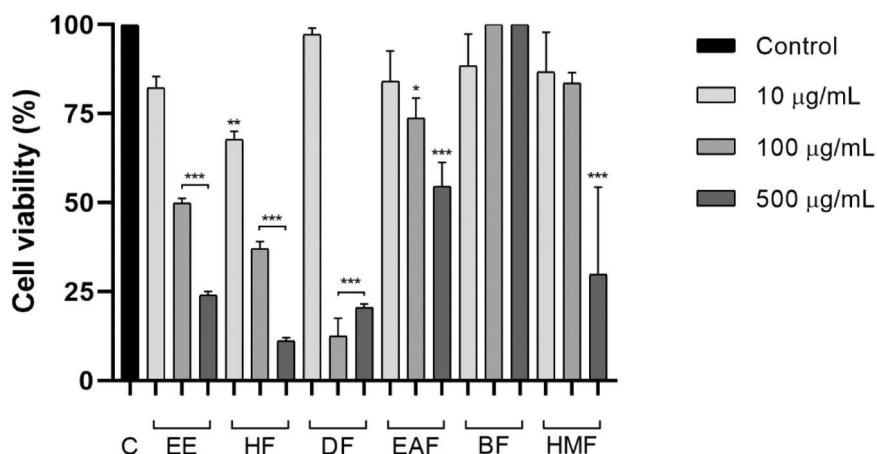


**Fig. 7.** Cell viability of RAW 264.7 macrophages treated with different concentrations of *C. asiatica* EE and its organic fractions. Values are expressed as the percentage of viable cells (mean  $\pm$  standard deviation) compared to the vehicle group. \*  $p < 0.01$ , \*\*  $p < 0.001$ , \*\*\*  $p < 0.001$  when compared to vehicle group. Note: EE: ethanolic extract, HF: hexane fraction, DF: dichloromethane fraction, EAF: ethyl acetate fraction, BF: n-butanol fraction, HMF: hydromethanolic fraction.

Therefore, this study provided a phytochemical prospection, ESI FT-ICR MS analysis, as well as the compounds elucidation of the most active fractions by HPLC-ESI-MS/MS. Furthermore, the antioxidant and anti-glycation potential, the inhibition of isolated LDL oxidation, the prevention of hepatic tissue peroxidation, and the enzymatic activity inhibition were evaluated. This study also determines the cytotoxicity and antimicrobial activity of EE and its organic fractions.

Based on phytochemical analysis, both EAF and BF demonstrated a high content of flavonoids and phenolic compounds (Table 1), which explains the superior antioxidant capacity of these fractions in the FRAP, ORAC, and DPPH assays (Fig. 1). In addition, these molecules possess the ability to chelate transition metal ions, which can inhibit ROS production [51]. Studies have reported the ability to reduce  $Fe^{3+}$  by the aqueous and ethanolic extract of *C. asiatica* [52,53], however, EAF and BF demonstrated higher reducing power than the EE due to the

concentration of polyphenols in these fractions.

Phenolic compounds and flavonoids are also capable of stabilizing radicals, such as DPPH and peroxy. According to Marques et al., [54], ethyl acetate and n-butanol fractions derived from *C. asiatica* aqueous extract exhibited  $IC_{50}$  values for DPPH assay of  $38.86 \pm 0.26$  and  $175.4 \pm 3.72 \mu\text{g/mL}$ , respectively. Meanwhile, our results presented  $1.60 \pm 0.48$  and  $10.82 \pm 2.59 \mu\text{g/mL}$   $IC_{50}$  values for EAF and BF, respectively.

The organic solvent used in the maceration process can significantly impact the yield and composition of extracted molecules in each fraction. According to both HPLC-ESI-MS/MS and ESI FT-ICR MS analysis, as shown in Tables 3 and 4, high antioxidants compounds were identified, such phenolic compounds (ellagic acid, gallic acid and its derivatives, protocatechuic acid, corilagin, chebulaninnale), tannins (geraniin, chebulic acid) and flavonoids (rutin, quercetin 3-rhamnoside-7-glucoside). In addition to ellagic acid and gallic acid, asiatic acid was

**Table 3**Compounds identified in *C. asiatica* leaves ethanolic extract and its organic fractions by ESI (-) FT-ICR MS.

ESI (-) FT-ICR MS: Ethanolic extract of <i>C. asiatica</i> and its organic fractions											
Compound	EE	HF	DF	EAF	BF	HMF	Molecular formula	<i>m/z</i> theoretical	<i>m/z</i> obtained	Error (ppm)	DBE
Palmitic acid	-	X	-	-	-	-	[C <sub>16</sub> H <sub>32</sub> O <sub>2</sub> - H] <sup>-</sup>	255.23295	255.23303	- 0.29	1
Alpha-linolenic acid	X	X	-	-	-	-	[C <sub>18</sub> H <sub>30</sub> O <sub>2</sub> - H] <sup>-</sup>	277.21735	277.21730	- 0.18	4
Linolenic acid	X	X	X	-	-	-	[C <sub>18</sub> H <sub>32</sub> O <sub>2</sub> - H] <sup>-</sup>	279.23295	279.23314	- 0.66	3
Oleic acid	X	X	-	-	-	-	[C <sub>18</sub> H <sub>34</sub> O <sub>2</sub> - H] <sup>-</sup>	281.24860	281.24868	- 0.28	2
Stearic acid	X	X	X	-	-	-	[C <sub>18</sub> H <sub>36</sub> O <sub>2</sub> - H] <sup>-</sup>	283.26425	283.26447	- 0.75	1
17-hydroxylinolenic acid	-	X	-	-	-	-	[C <sub>18</sub> H <sub>30</sub> O <sub>3</sub> - H] <sup>-</sup>	293.21222	293.21230	- 0.28	4
Elagic acid	X	-	X	X	X	-	[C <sub>14</sub> H <sub>6</sub> O <sub>8</sub> - H] <sup>-</sup>	300.99899	300.99921	- 0.73	12
13-hydroperoxy-11,9-octadecadienoic acid	X	X	X	-	-	-	[C <sub>18</sub> H <sub>32</sub> O <sub>4</sub> - H] <sup>-</sup>	311.22278	311.22296	- 0.57	3
Malynic acid	-	-	X	-	-	-	[C <sub>18</sub> H <sub>32</sub> O <sub>5</sub> - H] <sup>-</sup>	327.21770	327.21787	- 0.53	3
Chlorogenic acid	-	-	-	-	X	-	[C <sub>16</sub> H <sub>18</sub> O <sub>9</sub> - H] <sup>-</sup>	353.08781	353.08781	- 0.31	8
Tuberonic acid glucoside	X	-	X	X	X	X	[C <sub>18</sub> H <sub>28</sub> O <sub>9</sub> - H] <sup>-</sup>	387.16606	387.16635	- 0.76	5
Linolenic acid dimer	X	X	-	-	-	-	2 [C <sub>18</sub> H <sub>32</sub> O <sub>2</sub> - H] <sup>-</sup>	559.47318	559.47410	- 1.63	4
Oleic acid dimer	X	X	-	-	-	-	2 [C <sub>18</sub> H <sub>34</sub> O <sub>2</sub> - H] <sup>-</sup>	561.48883	561.48972	- 1.57	4
Non identified	X	X	X	-	-	-	[C <sub>33</sub> H <sub>42</sub> O <sub>8</sub> - H] <sup>-</sup>	565.28069	565.28181	- 1.98	13
Non identified	X	X	X	-	-	-	[C <sub>33</sub> H <sub>44</sub> O <sub>9</sub> - H] <sup>-</sup>	583.29126	583.29236	- 1.89	12
Non identified	X	-	X	X	X	X	[C <sub>26</sub> H <sub>22</sub> O <sub>17</sub> - H] <sup>-</sup>	605.07842	605.07959	- 1.93	16
Quercetin 3-rhamnoside-7-glucoside	X	-	-	X	X	-	[C <sub>27</sub> H <sub>30</sub> O <sub>16</sub> - H] <sup>-</sup>	609.14611	609.14672	- 1.01	13
Corilagin	X	X	-	X	X	X	[C <sub>27</sub> H <sub>22</sub> O <sub>18</sub> - H] <sup>-</sup>	633.07334	633.07452	- 1.87	18
Chebulanin	-	-	X	X	X	X	[C <sub>27</sub> H <sub>24</sub> O <sub>19</sub> - H] <sup>-</sup>	651.08390	651.08517	- 1.95	16
Non identified	X	X	X	-	-	-	[C <sub>37</sub> H <sub>78</sub> O <sub>17</sub> - H] <sup>-</sup>	793.51662	793.51564	1.24	0
Non identified	X	X	X	X	X	X	[C <sub>31</sub> H <sub>28</sub> O <sub>26</sub> - H] <sup>-</sup>	815.07960	815.07954	0.08	18
Geraniin	X	X	X	X	X	X	[C <sub>41</sub> H <sub>28</sub> O <sub>27</sub> - H] <sup>-</sup>	951.07452	951.07601	- 1.57	28
Digallic acid	X	X	X	X	X	X	3 [C <sub>14</sub> H <sub>10</sub> O <sub>9</sub> - H] <sup>-</sup>	965.09017	965.09066	- 0.51	28

Note: EE: ethanolic extract, HF: hexane fraction, DF: dichloromethane fraction, EAF: ethyl acetate fraction, BF: n-butanol fraction, HMF: hydromethanolic fraction

found in DF. The triterpenes found in *C. asiatica* also hold antioxidant activity and might be associated to DPPH and peroxy radical stabilization [2,55]. Beyond *in-vitro* antioxidant activity, asiatic acid increased the *in-vivo* antioxidant enzyme levels, like superoxide dismutase (SOD), catalase (CAT), and glutathione peroxidase (GPx) [56].

Usually, antioxidant compounds can also inhibit the formation of advanced glycation end products (AGEs) by inhibiting the formation of Schiff bases and Amadori products, neutralizing ROS production, and decreasing AGEs cell damage by blocking AGE-RAGE interaction. Glycation is a non-enzymatic reaction between a reducing sugar and the amino group of a protein, resulting in the formation of AGEs, which are associated with promoting oxidative stress and induce proinflammatory and inflammatory mediators' production [57] and are abundant in diabetic individuals. BSA and arginine were incubated with fructose and methylglyoxal, a dicarbonyl intermediate formed in the glycolysis pathway, to verify if EE and its organic fractions were capable of preventing AGEs formation, since glycation is one of the main causes of spontaneous damage to protein [58].

In the BSA/FRU model (Fig. 2a), the EE, EAF, BF, and HMF were able to inhibit AGEs formation and didn't demonstrate significant difference when compared to positive control, quercetin. In contrast, when using MGO as a glycation-inducing agent, the antiglycation activity of EE and its fractions were moderate, with high IC<sub>50</sub> values, since MGO is one of the strongest glycation agents and can be up to 50,000 times more potent than glucose [59].

An enriched *C. asiatica* extract with phenolic compounds inhibited 38 % of the AGEs formation in BSA glycated by glucose model at a concentration of 500 mM [60], in the meantime this study demonstrated that EE, DF and EAF inhibited 36–41 % of the glycation in BSA/MGO model in a concentration of 312.5 µg/mL. Another study also reported that the methanolic extract of *C. asiatica* at 1 mg/mL inhibited the formation of AGEs by 20 % in a BSA/MGO model [61].

Besides AGEs formation, oxidative stress stimulates LDL oxidation and promotes the development of atherosclerosis [62]. Therefore the search for antioxidant compounds that can control oxidative stress is relevant in order to avoid arterial occlusion by atherosclerotic plaques. Studies conducted by Meyer et al., [63] revealed that phenolic compounds interact physically with LDL lipid nucleus, in addition, these molecules have transition metals chelating activity, such as Cu<sup>2+</sup> ions.

Due to their high antioxidant capacity and significant phenolic compounds content, EE, EAF, and BF were capable of inhibiting oxidation and peroxidation of LDL (Fig. 4). Although DF did not present an antioxidant capacity similar to the aforementioned fractions, it also protected LDL from oxidation and peroxidation. Asiatic acid, a triterpene found in DF, has shown a potential to prevent atherosclerosis progression by inhibiting endothelial hyperpermeability and increasing the expression of adhesion molecules in ox-LDL exposed HUVEC cells [64].

The EAF, BF, and HMF were also able to inhibit lipid peroxidation in hepatic tissue oxidized by the Fe<sup>2+</sup>-ascorbate model (Fig. 5). Despite demonstrating little activity in previous assays and low content of phenolic compounds and flavonoids when compared to the other fractions, HMF surprised by demonstrating liver protection against oxidation, demonstrating low MDA levels. ESI FT-ICR MS analysis demonstrated the presence of tuberonic acid glucoside, corilagin, chebulanin, geraniin and digallic acid, which might explain this result, Table 3.

As observed by Lu et al., (2021), the n-butanol extract of *C. asiatica* increased the viability of L02 hepatocytes when exposed to oxidative stress induced by H<sub>2</sub>O<sub>2</sub> [65]. These results align with the outcomes presented in the current investigation, signifying not only the non-cytotoxic nature of the n-butanol fraction but also its capacity to provide hepatoprotective effects. Another study reported that the aqueous extract of *C. asiatica* inhibited lipid peroxidation induced by Fe<sup>2+</sup>-ascorbate in liver tissue homogenate [66].

Flavonoids and phenolic compounds found in EAF and BF, have already shown inhibition of lipid peroxidation and reduction of ROS in previous studies [67–69]. The results corroborate with the fact that the polar fractions own the most antioxidant activity in all the models studied.

The triterpenes present in *C. asiatica*, such as asiatic acid also protect the lipids from peroxidation, reducing MDA levels in the brain of rats pre-treated with d-Galactose [70], in the liver of hyperlipidemic rats [71] and in tissue repair model [9].

The EE and some of its organic fractions have also demonstrated potential inhibitory effects on glycoside hydrolases, which represents a potential strategy for the management of Diabetes mellitus and its associated complications. The inhibition of α-amylase by the ethanolic

Table 4

Compounds identified in DF, EAF, and BF of *C. asiatica* leaves ethanolic extract by HPLC-ESI-MS/MS in negative ionization mode.

$t_R$ (min)	$m/z$ obtained	$m/z$ theoretical	Error (ppm)	Fragment ions ( $m/z$ ) MS/MS	Molecular formula	Tentative identify	Sample	Reference
0.90	133.0133	133.0142	- 6.76	5 eV: 115, 87, 89, 71	C <sub>4</sub> H <sub>6</sub> O <sub>5</sub>	malic acid	BF, EAF	[32,33] MoNA <sup>a</sup>
1.15	355.0310	355.0307	0.84	15 eV: 337, 293, 249, 205	C <sub>14</sub> H <sub>12</sub> O <sub>11</sub>	chebulic acid	BF, DF, EAF	[34]
1.17	331.0673	331.0671	0.60	20 eV: 271, 241, 211, 169, 150, 125	C <sub>13</sub> H <sub>16</sub> O <sub>10</sub>	glucogalin (galloyl- hexoside)	BF, EAF	[35]
	169.0139	169.0142	- 1.77	20 eV: 125, 107, 79, 69	C <sub>7</sub> H <sub>6</sub> O <sub>5</sub>	galic acid	BF, DF, EAF	[33,36]
2.27	153.0189	153.0193	- 2.61	20 eV: 109, 108	C <sub>7</sub> H <sub>6</sub> O <sub>4</sub>	protocatechuic acid	DF, EAF	[33,36] MoNA <sup>a</sup>
2.43	325.0563	325.0565	- 0.61	30 eV: 169, 125, 111	C <sub>14</sub> H <sub>14</sub> O <sub>9</sub>	galloylshikimic acid	BF, EAF	[35,37]
2.45	483.0780	483.0787	1.45	30 eV: 331, 313, 271, 211, 169, 125	C <sub>20</sub> H <sub>20</sub> O <sub>14</sub>	digalloylglucose	EAF	[35,38]
2.87	633.0742	633.0733	- 1.42	30 eV: 301	C <sub>27</sub> H <sub>22</sub> O <sub>18</sub>	HHDP galloyl- glucose isomer I	BF, DF, EAF	[35,38]
3.02	183.0298	183.0299	- 0.54	15 eV: 168, 124	C <sub>8</sub> H <sub>8</sub> O <sub>5</sub>	methyl gallate	BF, DF, EAF	[33,35]
3.30	137.0244	137.0244	0	5 eV: 123, 98, 65	C <sub>7</sub> H <sub>6</sub> O <sub>3</sub>	hydroxybenzoic acid	DF	[39,40]
3.95	951.0738	951.0745	- 0.74	30 eV: 933, 907, 301, 169	C <sub>41</sub> H <sub>28</sub> O <sub>27</sub>	geraniin or isomer	BF, DF, EAF	[41]
4.25	633.0747	633.0733	2.21	30 eV: 463, 419, 301, 275	C <sub>27</sub> H <sub>22</sub> O <sub>18</sub>	HHDP galloyl- glucose isomer II	BF, DF, EAF	[35,38]
	291.0146	291.0153	2.41	25 eV: 247, 219, 191, 175, 145	C <sub>13</sub> H <sub>8</sub> O <sub>8</sub>	brevifolin carboxylic acid	BF, DF, EAF	[32,42]
4.42	387.1659	387.1661	- 0.51	20 eV: 207, 163, 119, 89, 71, 59	C <sub>18</sub> H <sub>28</sub> O <sub>9</sub>	tuberonic acid hexoside	DF	[43–45]
4.70	225.1127	225.1132	- 2.21	15 eV: 207, 163, 147, 97, 59	C <sub>12</sub> H <sub>18</sub> O <sub>4</sub>	tuberonic acid	DF	[43,46]
5.15	193.0503	193.0506	- 1.55	20 eV: 178, 134, 133, 106	C <sub>10</sub> H <sub>10</sub> O <sub>4</sub>	ferulic acid	DF	MoNA <sup>b</sup>
5.51	951.0759	951.0745	1.47	30 eV: 933, 907, 301, 300, 273	C <sub>41</sub> H <sub>28</sub> O <sub>27</sub>	geraniin or isomer	DF	[41]
5.57	319.0461	319.0459	0.62	20 eV: 273, 245, 229, 217, 201	C <sub>15</sub> H <sub>12</sub> O <sub>8</sub>	ethyl brevifolin carboxylate	DF, EAF	[42]
5.83	491.0850	491.0831	3.95	25 eV: 476, 328, 313, 297	C <sub>22</sub> H <sub>20</sub> O <sub>13</sub>	dimethylellagic acid glucoside	BF, DF, EAF	MoNA <sup>c</sup> PubChem <sup>d</sup>
5.95	609.1467	609.1461	0.98	30 eV: 463, 300, 301, 271, 179, 151	C <sub>27</sub> H <sub>30</sub> O <sub>16</sub>	rutin	BF, EAF	[47,48]
6.18	300.9986	300.9990	- 1.33	30 eV: 284, 257, 229, 201, 185, 173, 145	C <sub>14</sub> H <sub>6</sub> O <sub>8</sub>	elagic acid	BF, DF, EAF	[32,38]
8.48	327.2185	327.2177	2.44	25 eV: 291, 251, 229, 211, 183, 171, 137, 97, 85	C <sub>18</sub> H <sub>32</sub> O <sub>5</sub>	trihydroxy-octadecadienoic acid	DF, EAF	[49]
8.83	329.2338	329.2333	1.52	25 eV: 311, 293, 229, 211, 171, 139	C <sub>18</sub> H <sub>34</sub> O <sub>5</sub>	trihydroxy-octadecenoic acid	DF	[37,49]
9.05	307.1922	307.1915	2.28	20 eV: 235, 211, 185, 125, 123, 97, 71, 65	C <sub>18</sub> H <sub>28</sub> O <sub>4</sub>	dihydrocapsiate	DF	[37]
10.21	487.3442	487.3429	2.67	-	C <sub>30</sub> H <sub>48</sub> O <sub>5</sub>	asiatic acid	DF	[50]
10.58	293.2132	293.2122	3.41	20 eV: 275, 235, 223, 195, 121	C <sub>18</sub> H <sub>30</sub> O <sub>3</sub>	hydroxy-octadecatrienoic acid	DF	[45]

Note: BF: *n*-butanol fraction, DF: dichloromethane fraction and EAF: ethyl acetate fraction<sup>a</sup> <https://mona.fiehnlab.ucdavis.edu/spectra/display/MetaboBASE0107><sup>b</sup> <https://mona.fiehnlab.ucdavis.edu/spectra/display/MetaboBASE0970><sup>c</sup> <https://mona.fiehnlab.ucdavis.edu/spectra/display/CCMSLIB00000845290><sup>d</sup> [https://pubchem.ncbi.nlm.nih.gov/compound/3\\_3\\_-Di-O-Methylellagic-Acid-4\\_-Glucoside](https://pubchem.ncbi.nlm.nih.gov/compound/3_3_-Di-O-Methylellagic-Acid-4_-Glucoside)

extract of *C. asiatica* has already been reported and, according to Supkamonseni et al., [14], it was obtained an IC<sub>50</sub> value of 536.51 ± 8.80 µg/mL, while the present study reported an IC<sub>50</sub> value for EE of 21, 8 ± 2,87 µg/mL. It is important to emphasize that phenolic compounds rich fractions, EAF, and BF, demonstrated high α-amylase inhibition, representing a natural strategy to control hyperglycemia by the reduction of glucose absorption, a very common manifestation in patients diagnosed with type 2 diabetes mellitus. Phenolic compounds have exhibited α-amylase inhibition properties due to their chemical structure, position, and amount of free hydroxyl groups [22,72–74], this explains the higher inhibition activity of this enzyme by the fractions, which presented expressive content of total phenols. Compounds such as gallic acid, ellagic acid and rutin have several free hydroxyl groups, contributing to the inhibition of α-amylase. Thus, *in vivo* studies have demonstrated beneficial effects of *C. asiatica* use to aid in the treatment of Diabetes mellitus, since these compounds were identified by mass spectrometry [14,75,76]. Unlike α-amylase, α-glucosidase was just partially inhibited by the samples, with values which vary from 20 % to 50 % at the higher concentration. Some key factors are important to inhibit α-glucosidase according to Justino et al., (2022), such as a galloyl group esterified to the 3-position of the flavonoid C-ring, the number and localization of hydroxyl groups, specific hydroxylations at the A, B

and C flavonoids rings and some phenolic compounds such as myricetin, quercetin and kaempferol glucosides [77] [78]. Although some galloyl group-containing compounds being identified, such as glucocalin, galloylshikimic acid and digalloylglucose, their concentration might not be enough to inhibit α-glucosidase.

Cholinesterases, AChE and BChE, are serine hydrolases that hydrolyze the neurotransmitters acetyl and butyrylcholine into acetate and butyryl and choline in the cholinergic cleft. Its inhibition allows acetylcholine or butyrylcholine to remain longer in the cleft, potentiating cholinergic transmission, a desired effect in the treatment of diseases such as Alzheimer's [11,79]. Although many studies have stated that *C. asiatica* extract displays high AChE and BChE inhibitory effects, our observations revealed that the organic fractions, DF and EAF, have even higher inhibitory activity. According to studies conducted by Hafiz et al., [11], *C. asiatica* extract inhibited, in a concentration-dependent manner, AChE in human neuroblastoma cell line SH-SY5Y. Orhan et al., [80] reported inhibition of about 50 % of the enzymatic activity by the ethanolic extract of *C. asiatica*, containing 11% of triterpenes (asiaticoside and madecassoside), at 200 µg/mL. According to Rather et al., [79] asiatic acid inhibited AChE activity in the cortex and hippocampus in a rat model for Alzheimer. As stated by Nasir et al., [81], this triterpene competes with acetylcholine for the esterase active site of

the enzyme in an *in vitro* model. Moreover, investigations conducted by Firdaus et al., [12] revealed that the extract of *C. asiatica* effectively suppressed AchE activity. Additionally, this extract demonstrated significant potential in ameliorating cognitive deficits induced by AlCl<sub>3</sub>, mitigating oxidative stress, alleviating cholinergic dysfunction, and attenuating neurodegenerative processes in the rat brain.

Since *C. asiatica* is widely consumed and used in skincare products, the cytotoxicity of the EE and its organic fractions was evaluated (Fig. 7). It is also important to lay emphasis on how BF was not cytotoxic for macrophages at any tested concentrations. Hafiz et al., [11] demonstrated that *C. asiatica* ethanolic extract was not cytotoxic at the SH-SY5Y and RAW 264.7 cell lines. *C. asiatica* callus extract was not cytotoxic to human foreskin fibroblasts either [17]. Also, a recent study showed that madecassoside protected INS-1E cells from cell death [82].

ESI (-) FT-ICR MS technic also identified some fatty acids in HF and DF fractions besides some phenolic acids, such as linolenic acid and stearic acid. Free fatty acids are known to have antimicrobial effects, and although their mechanism remains unclear, the cell membrane appears to be their main target [83]. Both the HF and DF fractions exhibited low minimum inhibitory concentration (MIC) against bacteria that are commonly associated with the development of caries, suggesting that they may have potential for the prevention or treatment of dental caries. The polarity of extracts and fractions is a critical factor in determining their antimicrobial activity. Apolar solvents, such as hexane and dichloromethane, are effective in extracting lipophilic compounds, which have been shown to disrupt cell membranes and promote bacterial cell death [84]. The dichloro-methane/methanolic extract of *C. asiatica* inhibited the growth of *S. aureus*, *E. coli*, *S. typhi*, *B. subtilis*, and *Shigella sonnei*, indicating higher activity in gram-negative bacteria [85]. However, it was observed that the cariogenic bacteria most susceptible to HF are gram-positive. A recent study showed that *C. asiatica* ethanolic extract inhibited *S. aureus* growth, a gram-positive bacteria [86]. Another study evaluated the antibacterial activity of a *C. asiatica* pentacyclic triterpene rich extract and determined low MICs against *Streptococcus* spp [87].

## 5. Conclusion

In summary, our findings have established the antioxidant and antiglycation properties of *C. asiatica* ethanolic extract and its organic fractions. Notably, EAF and BF, polyphenol compounds richest fractions, exhibited remarkable antioxidant and antiglycation efficacy, particularly within the BSA/FRU model. Additionally, these fractions demonstrated the ability to effectively reduce LDL oxidation *in vitro* and attenuated peroxidation in the hepatic tissues, as well as inhibit  $\alpha$ -amylase activity. Notably, non-cytotoxic across all tested concentrations, BF emerges as a promising candidate for further exploration *in vivo* models, emphasizing its potential as a safe and effective therapeutic agent.

## Institutional review board statement

The study was conducted in accordance with the Declaration of Helsinki, and approved by the local Ethics Committee (CAAE 61082522.4.0000.5704) report 5.671.038.

## Funding

This work was supported by the Foundation for Research Support of the Minas Gerais State-FAPEMIG (grants # APQ-01856-14, APQ-01981-16 and APQ-01612-18) and the National Institute of Science and Technology in Theranostics and Nanobiotechnology—INCT—TeraNano (CNPq grant # 465669/2014-0, <http://www.teranano.ufu.br/>). VPB and ALSB received fellowships from the Coordination for the Improvement of Higher Education Personnel (CAPES). FSE received scholarship grants from FAPEMIG (PPM 00503-18) and CNPq (PQ—Research

productivity, process no. 312812/2021-3).

## CRediT authorship contribution statement

**Vinicius Prado Bittar:** Conceptualization, Data curation, Formal analysis, Methodology, Software, Validation, Visualization. **Larissa Campos Motta:** Data curation, Formal analysis, Investigation, Methodology, Validation. **Carlos Henrique Gomes Martins:** Data curation, Formal analysis, Investigation, Methodology, Validation. **Ana Luiza Silva Borges:** Investigation, Formal analysis, Data curation, Conceptualization, Methodology, Project administration, Software, Supervision, Validation, Visualization, Writing – original draft, Writing – review & editing. **Iasmin Aparecida Cunha Araújo:** Data curation, Investigation, Methodology, Validation. **Mário Machado Martins:** Data curation, Formal analysis, Investigation, Methodology, Validation. **Daniela Silva Gonçalves:** Data curation, Formal analysis, Investigation, Methodology, Validation. **Diego Godina Prado:** Data curation, Formal analysis, Investigation, Methodology, Validation. **Renner Francisco Mateus Duarte:** Data curation, Investigation, Methodology, Validation. **Wanderson Romão:** Data curation, Formal analysis, Investigation, Methodology, Validation. **Foued Espindola:** Visualization, Validation, Supervision, Resources, Methodology, Conceptualization, Data curation, Funding acquisition, Investigation. **Nagela Bernadelli Sousa:** Data curation, Formal analysis, Investigation, Methodology, Validation. **Allisson Benatti Justino:** Data curation, Investigation, Methodology, Validation. **Neide Maria Silva:** Data curation, Investigation, Methodology, Validation. **Maria Sol Peña Carrillo:** Data curation, Investigation, Methodology, Validation. **Alberto de Oliveira:** Data curation, Formal analysis, Investigation, Methodology, Validation. **Françoise Vasconcelos Botelho:** Data curation, Investigation, Methodology, Validation.

## Declaration of Competing Interest

The authors declare that they have no known competing financial interests or personal relationships that could have appeared to influence the work reported in this paper.

## Acknowledgements

The authors would like to thank the Institute of Biotechnology of the Federal University of Uberlandia and Rede de Biotérios (REBIR) for all the structure and support provided to make this study possible.

## References

- [1] R. Azerad, Chemical structures, production and enzymatic transformations of saponinins and saponins from *Centella asiatica* (L.) Urban, *Fitoterapia* 114 (2016) 168–187, <https://doi.org/10.1016/j.fitote.2016.07.011>.
- [2] B. Sun, L. Wu, Y. Wu, C. Zhang, L. Qin, M. Hayashi, M. Kudo, M. Gao, T. Liu, Therapeutic Potential of *Centella asiatica* and Its Triterpenes: A Review, *Front Pharm.* 11 (2020), <https://doi.org/10.3389/fphar.2020.568032>.
- [3] K.S. Park, Pharmacological Effects of *Centella asiatica* on Skin Diseases: Evidence and Possible Mechanisms, *Evid.-Based Complement. Altern. Med.* 2021 (2021), <https://doi.org/10.1155/2021/5462633>.
- [4] W. Poomanee, N. Yaowiwat, T. Pattarachaidaecharuch, P. Leelapornpisid, Optimized multiherbal combination and *in vivo* anti-skin aging potential: a randomized double blind placebo controlled study, *Sci. Rep.* 13 (2023), <https://doi.org/10.1038/s41598-023-32738-7>.
- [5] P. Hashim, H. Sidek, M.H.M. Helan, A. Sabery, U.D. Palanisamy, M. Ilham, Triterpene composition and bioactivities of *Centella asiatica*, *Molecules* 16 (2011) 1310–1322, <https://doi.org/10.3390/molecules16021310>.
- [6] L.R.L. Diniz, L.L. Calado, A.B.S. Duarte, D.P. de Sousa, *Centella asiatica* and Its Metabolite Asiatic Acid: Wound Healing Effects and Therapeutic Potential, *Metabolites* 13 (2023), <https://doi.org/10.3390/metabo13020276>.
- [7] L.R.L. Diniz, L.L. Calado, A.B.S. Duarte, D.P. de Sousa, *Centella asiatica* and Its Metabolite Asiatic Acid: Wound Healing Effects and Therapeutic Potential, *Metabolites* 13 (2023), <https://doi.org/10.3390/metabo13020276>.
- [8] E. Arribas-López, N. Zand, O. Ojo, M.J. Snowden, T. Kochhar, A Systematic Review of the Effect of *Centella asiatica* on Wound Healing, *Int J. Environ. Res Public Health* 19 (2022), <https://doi.org/10.3390/ijerph19063266>.

- [9] A. Shukla, A.M. Rasik, B.N. Dhawan, Asiaticoside-induced Elevation of Antioxidant Levels in Healing Wounds, 1999.
- [10] N.E. Gray, C.J. Harris, J.F. Quinn, A. Soumyanath, Centella asiatica modulates antioxidant and mitochondrial pathways and improves cognitive function in mice, *J. Ethnopharmacol.* 180 (2016) 78–86, <https://doi.org/10.1016/j.jep.2016.01.013>.
- [11] Z.Z. Hafiz, M.A. Mohd Amin, R.M. Johari James, L.K. Teh, M.Z. Salleh, M.I. Adenan, Inhibitory Effects of Raw-Extract Centella asiatica (RECA) on Acetylcholinesterase, Inflammations, and Oxidative Stress Activities via in Vitro and in Vivo, *Molecules* 25 (2020), <https://doi.org/10.3390/molecules25040892>.
- [12] Z. Firdaus, D. Kumar, S.K. Singh, T.D. Singh, Centella asiatica Alleviates AlCl<sub>3</sub>-induced Cognitive Impairment, Oxidative Stress, and Neurodegeneration by Modulating Cholinergic Activity and Oxidative Burden in Rat Brain, *Biol. Trace Elem. Res* 200 (2022) 5115–5126, <https://doi.org/10.1007/s12011-021-03083-5>.
- [13] A.B. Oyenih, S.O.P. Langa, S. Mukaratirwa, B. Masola, Effects of Centella asiatica on skeletal muscle structure and key enzymes of glucose and glycogen metabolism in type 2 diabetic rats, *Biomed. Pharmacother.* 112 (2019), <https://doi.org/10.1016/j.biopha.2019.108715>.
- [14] N. Supkamonsoni, A. Thinkratok, D. Meksuriyen, R. Srisawat, Hypolipidemic and hypoglycemic effects of Centella asiatica (L.) extract in vitro and in vivo, 2014.
- [15] N. Giribabu, K. Karim, E.K. Kilari, S.R. Nelli, N. Salleh, Oral administration of Centella asiatica (L.) Urb leave aqueous extract ameliorates cerebral oxidative stress, inflammation, and apoptosis in male rats with type-2 diabetes, *Inflammopharmacology* 28 (2020) 1599–1622, <https://doi.org/10.1007/s10787-020-00733-3>.
- [16] B. Masola, O.O. Oguntibeju, A.B. Oyenih, Centella asiatica ameliorates diabetes-induced stress in rat tissues via influences on antioxidants and inflammatory cytokines, *Biomed. Pharmacother.* 101 (2018) 447–457, <https://doi.org/10.1016/j.biopha.2018.02.115>.
- [17] V. Buranasudja, D. Rani, A. Malla, K. Kobtrakul, S. Vimolmangank, Insights into antioxidant activities and anti-skin-aging potential of callus extract from Centella asiatica (L.), *Sci. Rep.* 11 (2021), <https://doi.org/10.1038/s41598-021-92958-7>.
- [18] S. Bandopadhyay, S. Mandal, M. Ghorai, N.K. Jha, M. Kumar, Radha, A. Ghosh, J. Procków, J.M. Pérez de la Lastra, A. Dey, Therapeutic properties and pharmacological activities of asiaticoside and madecassoside: A review, *J. Cell Mol. Med* 27 (2023) 593–608, <https://doi.org/10.1111/jcmm.17635>.
- [19] R.R. Franco, A.B. Justino, M.M. Martins, C.G. Silva, P.R.V. Campana, J.C.D. Lopes, V.L. De Almeida, F.S. Espindola, Phytoscreening of Vochysiaceae species: Molecular identification by HPLC-ESI-MS/MS and evaluating of their antioxidant activity and inhibitory potential against human  $\alpha$ -amylase and protein glycation, *Bioorg. Chem.* 91 (2019), <https://doi.org/10.1016/j.bioorg.2019.103122>.
- [20] A.B. Justino, N.M. Pereira, D.D. Vilela, L.G. Peixoto, M.M. Martins, R.R. Teixeira, N.C. Miranda, M.N. da Silva, R.M.F. de Sousa, A. de Oliveira, F.S. Espindola, Peel of araticum fruit (*Annona crassiflora* Mart.) as a source of antioxidant compounds with  $\alpha$ -amylase,  $\alpha$ -glucosidase and glycation inhibitory activities, *Bioorg. Chem.* 69 (2016) 167–182, <https://doi.org/10.1016/j.bioorg.2016.11.001>.
- [21] Y. Zou, S.K.C. Chang, Y. Gu, S.Y. Qian, Antioxidant activity and phenolic compositions of lentil (*Lens culinaris* var. Morton) extract and its fractions, *J. Agric. Food Chem.* 59 (2011) 2268–2276, <https://doi.org/10.1021/jf104640k>.
- [22] R.R. Franco, V.H. Mota Alves, L.F. Ribeiro Zabisky, A.B. Justino, M.M. Martins, A. L. Saraiva, L.R. Goulart, F.S. Espindola, Antidiabetic potential of Bauhinia forficata Link leaves: a non-cytotoxic source of lipase and glycoside hydrolases inhibitors and molecules with antioxidant and antilycation properties, *Biomed. Pharmacother.* 123 (2020), <https://doi.org/10.1016/j.biopha.2019.109798>.
- [23] W. Wang, Y. Yagiz, T.J. Buran, C. do N. Nunes, L. Gu, Phytochemicals from berries and grapes inhibited the formation of advanced glycation end-products by scavenging reactive carbonyls, *Food Res. Int.* 44 (2011) 2666–2673, <https://doi.org/10.1016/j.foodres.2011.05.022>.
- [24] A.B. Justino, R.R. Franco, H.C.G. Silva, A.L. Saraiva, R.M.F. Sousa, F.S. Espindola, B. procyanidins of *Annona crassiflora* fruit peel inhibited glycation, lipid peroxidation and protein-bound carbonyls, with protective effects on glycated catalase, *Sci. Rep.* 9 (2019), <https://doi.org/10.1038/s41598-019-55779-3>.
- [25] K. Yagi, Simple Procedure for Specific Assay of Lipid Hydroperoxides in Serum or Plasma, 1998.
- [26] Byung H. Chung, Jere P. Segrest, Marjorie J. Ray, John D. Brunxell, John E. Hokanson, Ronald M. Krauss, Ken Beaudrie, John T. Cone, Preparation of Plasma Lipoproteins, 1986.
- [27] M.M. Bradford, A Rapid and Sensitive Method for the Quantitation of Microgram Quantities of Protein Utilizing the Principle of Protein-Dye Binding, 1976.
- [28] T.V. Da Silva Santos, R.R. Teixeira, D.L. Franco, J.M. Madurro, A.G. Brito-Madurro, F.S. Espindola, Bioelectrode for detection of human salivary amylase, *Mater. Sci. Eng. C.* 32 (2012) 530–535, <https://doi.org/10.1016/j.msec.2011.12.005>.
- [29] I.K. Rhee, M. Van De Meent, K. Ingkaninan, R. Verpoorte, Screening for Acetylcholinesterase Inhibitors from Amaryllidaceae Using Silica Gel Thin-layer Chromatography in Combination with Bioactivity Staining, 2001. [www.elsevier.com/locate/chroma](http://www.elsevier.com/locate/chroma).
- [30] T. Mosmann, Rapid Colorimetric Assay for Cellular Growth and Survival: Application to Proliferation and Cytotoxicity Assays, 1983.
- [31] Clinical and Laboratory Standards Institute, M.P. Weinstein, Methods for Dilution Antimicrobial Susceptibility Tests for Bacteria That Grow Aerobically, 2018.
- [32] D. Fraternali, D. Ricci, G. Verardo, A. Gorassini, V. Stocchi, P. Sestili, Activity of Vitis vinifera Tendrils Extract Against Phytopathogenic Fungi, 2015.
- [33] J.G. de, S. Corrêa, M. Bianchin, A.P. Lopes, E. Silva, F.Q. Ames, A.M. Pomini, S. T. Carpes, J. de Carvalho Rinaldi, R. Cabral Melo, E.S. Kioshima, C.A. Bersani-Amado, E.J. Pilau, J.E. de Carvalho, A.L.T.G. Ruiz, J.V. Visentainer, S.M. de, O. Santin, Chemical profile, antioxidant and anti-inflammatory properties of *Miconia albicans* (Sw.) Triana (Melastomataceae) fruits extract, *J. Ethnopharmacol.* 273 (2021), <https://doi.org/10.1016/j.jep.2021.113979>.
- [34] Y. Li, Y. Li, J. Chen, Screening and identification of acetylcholinesterase inhibitors from Terminalia chebula fruits based on ultrafiltration and ultra-performance liquid chromatography-quadrupole time-of-flight mass spectrometry, *Microchem. J.* 168 (2021), <https://doi.org/10.1016/j.microc.2021.106438>.
- [35] A. Singh, V. Bajpai, S. Kumar, R. Sharma, B. Kumar, Profiling of Gallic and Ellagic Acid Derivatives in Different Plant Parts of Terminalia arjuna by HPLC-ESI-QTOF-MS/MS, 2016.
- [36] M. Gómez-Romero, A. Segura-Carretero, A. Fernández-Gutiérrez, Metabolite profiling and quantification of phenolic compounds in methanol extracts of tomato fruit, *Phytochemistry* 71 (2010) 1848–1864, <https://doi.org/10.1016/j.phytochem.2010.08.002>.
- [37] I.M. Abu-Reidah, M.S. Ali-Shtayeh, R.M. Jamous, D. Arráez-Román, A. Segura-Carretero, HPLC-DAD-ESI-MS/MS screening of bioactive components from *Rhus coriaria* L. (Sumac) fruits, *Food Chem.* 166 (2015) 179–191, <https://doi.org/10.1016/j.foodchem.2014.06.011>.
- [38] P. Mena, L. Calani, C. Dall'Asta, G. Galaverna, C. García-Viguera, R. Bruni, A. Crozier, D. Del Rio, Rapid and comprehensive evaluation of (Poly)phenolic compounds in pomegranate (*Punica granatum* L.) Juice by UHPLC-MSn, *Molecules* 17 (2012) 14821–14840, <https://doi.org/10.3390/molecules171214821>.
- [39] K. Kramberger, D. Barlič-Maganja, D. Bandelj, A. Baruca Arbeiter, K. Peeters, A. Miklavčič Višnjevec, Z.J. Pražnikar, HPLC-DAD-ESI-QTOF-MS determination of bioactive compounds and antioxidant activity comparison of the hydroalcoholic and water extracts from two helichrysum italicum species, *Metabolites* 10 (2020) 1–25, <https://doi.org/10.3390/metabo10100403>.
- [40] D.D.C. Lima, T.E.A. Pitorro, M.B. Santiago, R.R. Franco, T. da C. Silva, D.G. Prado, L.C.S. Cunha, F.S. Espindola, D.C. Tavares, H.D. Nicoletta, C.H.G. Martins, V. R. Novais, In vitro evaluation of the antibacterial and cytotoxic activities of the *Euclea natalensis* crude extract and fractions against oral infection agents, *Arch. Oral. Biol.* 143 (2022), <https://doi.org/10.1016/j.archoralbio.2022.105546>.
- [41] A.D. Sousa, I.V. Maia, P.R.V. Ribeiro, K.M. Canuto, G.J. Zocolo, E. Sousa de Brito, UPLC-QTOF-MSE-based chemometric approach driving the choice of the best extraction process for *Phyllanthus niruri*, *Sep. Sci. Technol. (Phila.)* 52 (2017) 1696–1706, <https://doi.org/10.1080/01496395.2017.1298612>.
- [42] S. Luo, L. Guo, C. Sheng, Y. Zhao, L. Chen, C. Li, Z. Jiang, H. Tian, Rapid identification and isolation of neuraminidase inhibitors from mockstrawberry (*Duchesnea indica* Andr.) based on ligand fishing combined with HR-ESI-QTOF-MS, *Acta Pharm. Sin.* B 10 (2020) 1846–1855, <https://doi.org/10.1016/j.apsb.2020.04.001>.
- [43] M. Wang, Y. Liu, B. Guo, L. Wei, H. Teng, X. Chen, M. Ma, A dilute-and-shoot multispectral integration approach towards nontargeted component profiling of traditional herbal Yin-zhi-huang using liquid chromatography-photodiode array-trap/time-of-flight characterization, *J. Chromatogr. B Anal. Technol. Biomed. Life Sci.* 1087–1088 (2018) 118–132, <https://doi.org/10.1016/j.jchromb.2018.04.035>.
- [44] S. Kumar, P. Chandra, V. Bajpai, A. Singh, M. Srivastava, D.K. Mishra, B. Kumar, Rapid qualitative and quantitative analysis of bioactive compounds from *Phyllanthus amarus* using LC/MS/MS techniques, *Ind. Crops Prod.* 69 (2015) 143–152, <https://doi.org/10.1016/j.indcrop.2015.02.012>.
- [45] T. Danise, M. Innangi, E. Curcio, S. Piccolella, A. Fioretto, S. Pacifico, White poplar (*Populus alba* L.) leaf waste recovery and intercropping outcome on its polyphenols, *Ind. Crops Prod.* 171 (2021), <https://doi.org/10.1016/j.indcrop.2021.113866>.
- [46] S.K. Gidda, O. Miersch, A. Levitin, J. Schmidt, C. Wasternack, L. Varin, Biochemical and molecular characterization of a hydroxyjasmonate sulfotransferase from *Arabidopsis thaliana*, *J. Biol. Chem.* 278 (2003) 17895–17900, <https://doi.org/10.1074/jbc.M211943200>.
- [47] N. de A. Neves, P.C. Stringheta, S. Gómez-Alonso, I. Hermosín-Gutiérrez, Flavonols and ellagic acid derivatives in peels of different species of jaboticaba (*Plinia* spp.) identified by HPLC-DAD-ESI/MSn, *Food Chem.* 252 (2018) 61–71, <https://doi.org/10.1016/j.foodchem.2018.01.078>.
- [48] L.J. Quintans-Júnior, S.R. Gandhi, F.R.S. Passos, L. Heimfarth, E.W.M. Pereira, B. S. Monteiro, K.S. dos Santos, M.C. Duarte, L.S. Abreu, Y.M. Nascimento, J. F. Tavares, M.S. Silva, I.R.A. Menezes, H.D.M. Coutinho, Á.A.N. Lima, G. Zengin, J. S.S. Quintans, Dereplication and quantification of the ethanol extract of *Miconia albicans* (Melastomataceae) by HPLC-DAD-ESI-MS/MS, and assessment of its anti-hyperalgesic and anti-inflammatory profiles in a mice arthritis-like model: Evidence for involvement of TNF- $\alpha$ , IL-1 $\beta$  and IL-6, *J. Ethnopharmacol.* 258 (2020), <https://doi.org/10.1016/j.jep.2020.112938>.
- [49] S.T. Sakna, A. Mocan, H.N. Sultani, N.M. El-fiky, L.A. Wessjohann, M.A. Farag, Metabolites profiling of Ziziphus leaf taxa via UHPLC/PDA/ESI-MS in relation to their biological activities, *Food Chem.* 293 (2019) 233–246, <https://doi.org/10.1016/j.foodchem.2019.04.097>.
- [50] F. Masi, G. Chianese, F. Peterlongo, A. Riva, O. Tagliatalata-Scafati, Phytochemical profile of Centevita®, a Centella asiatica leaves extract, and isolation of a new oleanane-type saponin, *Fitoterapia* 158 (2022), <https://doi.org/10.1016/j.fitote.2022.105163>.
- [51] J. Dai, R.J. Mumper, Plant phenolics: Extraction, analysis and their antioxidant and anticancer properties, *Molecules* 15 (2010) 7313–7352, <https://doi.org/10.3390/molecules15107313>.
- [52] O. Kulkarni, S. Mukherjee, R. Bhandare, S. Jagtap, S. Dugad, N. Pawar, P. Pawar, Evaluation of comparative free-radical quenching potential of Brahmi (*Bacopa monnieri*) and Mandookparni (*Centella asiatica*), *AYU (Int. Q. J. Res. Ayurveda)* 32 (2011) 258, <https://doi.org/10.4103/0974-8520.92549>.

- [53] S. Rattanakom, P. Yasurin, Chemical profiling of *Centella asiatica* under different extraction solvents and its antibacterial activity, antioxidant activity, *Orient. J. Chem.* 31 (2015) 2453–2459, <https://doi.org/10.13005/ojc/310480>.
- [54] N.F. Marques, S.T. Stefanello, A.L.F. Froeder, A. Busanello, A.A. Boligon, M. L. Athayde, F.A.A. Soares, R. Fachineto, *Centella asiatica* and Its Fractions Reduces Lipid Peroxidation Induced by Quinolinic Acid and Sodium Nitroprusside in Rat Brain Regions, *Neurochem Res* 40 (2015) 1197–1210, <https://doi.org/10.1007/s11064-015-1582-5>.
- [55] N.N.M. Razali, C.T. Ng, L.Y. Fong, Cardiovascular Protective Effects of *Centella asiatica* and Its Triterpenes: A Review, *Planta Med* 85 (2019) 1203–1215, <https://doi.org/10.1055/a-1008-6138>.
- [56] P. Rameshreddy, V.V.S. Uddand Rao, P. Brahmanaidu, S. Vadivukkarasi, R. Ravindarnaik, P. Suresh, K. Swapna, A. Kalaivani, P. Parvathi, P. Tamilmani, G. Saravanan, Obesity-alleviating potential of asiatic acid and its effects on ACC1, UCP2, and CPT1 mRNA expression in high fat diet-induced obese Sprague–Dawley rats, *Mol. Cell Biochem* 442 (2018) 143–154, <https://doi.org/10.1007/s11010-017-3199-2>.
- [57] A. Perrone, A. Giovino, J. Benny, F. Martinelli, Advanced Glycation End Products (AGEs): Biochemistry, Signaling, Analytical Methods, and Epigenetic Effects, *Oxid. Med Cell Longev.* 2020 (2020), <https://doi.org/10.1155/2020/3818196>.
- [58] B.C.T. van Bussel, M.C.G. van de Poll, C.G. Schalkwijk, D.C.J.J. Bergmans, Increased dicarbonyl stress as a novel mechanism of multi-organ failure in critical illness, *Int J. Mol. Sci.* 18 (2017), <https://doi.org/10.3390/ijms18020346>.
- [59] P.J. Thornalley, Dicarbonyl intermediates in the Maillard reaction, in: *Ann N Y Acad Sci*, New York Academy of Sciences, 2005, pp. 111–117, <https://doi.org/10.1196/annals.1333.014>.
- [60] F.N. Eze, A.J. Tola, Protein glycation and oxidation inhibitory activity of *Centella asiatica* phenolics (CAP) in glucose-mediated bovine serum albumin glycoxidation, *Food Chem.* 332 (2020), <https://doi.org/10.1016/j.foodchem.2020.127302>.
- [61] A.S. Alqahtani, K.M. Li, V. Razmovski-Naumovski, A. Kam, P. Alam, G.Q. Li, Attenuation of methylglyoxal-induced glycation and cellular dysfunction in wound healing by *Centella cordifolia*, *Saudi J. Biol. Sci.* 28 (2021) 813–824, <https://doi.org/10.1016/j.sjbs.2020.11.016>.
- [62] P. Kong, Z.Y. Cui, X.F. Huang, D.D. Zhang, R.J. Guo, M. Han, Inflammation and atherosclerosis: signaling pathways and therapeutic intervention, *Signal Transduct. Target Ther.* 7 (2022), <https://doi.org/10.1038/s41392-022-00955-7>.
- [63] A.S. Meyer, M. Heinonen, E.N. Frankel, Antioxidant interactions of catechin, cyanidin, caffeic acid, quercetin, and ellagic acid on human LDL oxidation, 1997.
- [64] L. Jing, W. Haitao, W. Qiong, Z. Fu, Z. Nan, Z. Xuezheng, Anti-inflammatory effect of asiaticoside on human umbilical vein endothelial cells induced by ox-LDL, *Cytotechnology* 70 (2018) 855–864, <https://doi.org/10.1007/s10616-018-0198-4>.
- [65] J. Lu, C. Chen, R. Gai, H. Qiu, Y. Wu, Q. He, X. Yang, Protective effects and possible mechanisms of *Centella asiatica* (L.) urban extract against acute and chronic liver injury: Evidence from in vivo and in vitro studies, *Phytother. Res.* 35 (2021) 2785–2796, <https://doi.org/10.1002/ptr.7024>.
- [66] S. Kumari, M. Deori, R. Elancheran, J. Kotoky, R. Devi, In vitro and in vivo antioxidant, anti-hyperlipidemic properties and chemical characterization of *Centella asiatica* (L.) extract, *Front Pharm.* 7 (2016), <https://doi.org/10.3389/fphar.2016.00400>.
- [67] V. Aishwarya, S. Solaipriya, V. Sivaramakrishnan, Role of ellagic acid for the prevention and treatment of liver diseases, *Phytother. Res.* 35 (2021) 2925–2944, <https://doi.org/10.1002/ptr.7001>.
- [68] A. Gupta, A.K. Pandey, Basic Study Aceclofenac-induced hepatotoxicity: An ameliorative effect of Terminalia bellirica fruit and ellagic acid, *World J. Hepatol.* 12 (2020) 949–964, <https://doi.org/10.4254/wjh.v12.i11.949>.
- [69] C.H. Chen, T.Z. Liu, C.H. Chen, C.H. Wong, C.H. Chen, F.J. Lu, S.C. Chen, The efficacy of protective effects of tannic acid, gallic acid, ellagic acid, and propyl gallate against hydrogen peroxide-induced oxidative stress and DNA damages in IMR-90 cells, *Mol. Nutr. Food Res* 51 (2007) 962–968, <https://doi.org/10.1002/mnfr.200600230>.
- [70] X. Lin, S. Zhang, R. Huang, L. Wei, S. Tan, C. Liang, S. Lv, Y. Chen, S. Liang, Y. Tian, Z. Lu, Q. Huang, Protective effect of madecassoside against cognitive impairment induced by d-galactose in mice, *Pharm. Biochem Behav.* 124 (2014) 434–442, <https://doi.org/10.1016/j.pbb.2014.07.014>.
- [71] Y. Zhao, P. Shu, Y. Zhang, L. Lin, H. Zhou, Z. Xu, D. Suo, A. Xie, X. Jin, Effect of *Centella asiatica* on oxidative stress and lipid metabolism in hyperlipidemic animal models, *Oxid. Med Cell Longev.* 2014 (2014), <https://doi.org/10.1155/2014/154295>.
- [72] H. Rasouli, S.M.B. Hosseini-Ghazvini, H. Adibi, R. Khodarahmi, Differential  $\alpha$ -amylase/ $\alpha$ -glucosidase inhibitory activities of plant-derived phenolic compounds: A virtual screening perspective for the treatment of obesity and diabetes, *Food Funct.* 8 (2017) 1942–1954, <https://doi.org/10.1039/c7fo00220c>.
- [73] S. Gonçalves, E. Moreira, C. Grosso, P.B. Andrade, P. Valentão, A. Romano, Phenolic profile, antioxidant activity and enzyme inhibitory activities of extracts from aromatic plants used in Mediterranean diet, *J. Food Sci. Technol.* 54 (2017) 219–227, <https://doi.org/10.1007/s13197-016-2453-z>.
- [74] J.P. de Lima Júnior, R.R. Franco, A.L. Saraiva, I.B. Moraes, F.S. Espindola, *Anacardium humile* St. Hil as a novel source of antioxidant, antiglycation and  $\alpha$ -amylase inhibitors molecules with potential for management of oxidative stress and diabetes, *J. Ethnopharmacol.* 268 (2021), <https://doi.org/10.1016/j.jep.2020.113667>.
- [75] S. Jamil, Q. Nizami, M. Salam, Natural Product Radiance *Centella asiatica* (Linn.) Urban óA Review, 2007.
- [76] A.U. Kabir, M. bin Samad, N. Malrina D'costa, F. Akhter, A. Ahmed, J. Hannan, Anti-hyperglycemic activity of *Centella asiatica* is partly mediated by carbohydrase inhibition and glucose-fiber binding, 2014. <http://www.biomedcentral.com/1472-6882/14/31>.
- [77] A.B. Justino, H.C. Guerra Silva, R.R. Franco, I. de Oliveira Cavalcante Pimentel, N. F. Silva, A.L. Saraiva, F.S. Espindola, Flavonoids and proanthocyanidins-rich fractions from *Eugenia dysenterica* fruits and leaves inhibit the formation of advanced glycation end-products and the activities of  $\alpha$ -amylase and  $\alpha$ -glucosidase, *J. Ethnopharmacol.* 285 (2022), <https://doi.org/10.1016/j.jep.2021.114902>.
- [78] A.B. Justino, F.R.B. de Moura, R.R. Franco, F.S. Espindola,  $\alpha$ -Glucosidase and non-enzymatic glycation inhibitory potential of *Eugenia dysenterica* fruit pulp extracts, *Food Biosci.* 35 (2020), <https://doi.org/10.1016/j.fbio.2020.100573>.
- [79] M.A. Rather, A.J. Thenmozhi, T. Manivasagam, M. Dhivya Bharathi, M.M. Essa, G. J. Guillemin, Neuroprotective role of Asiatic acid in aluminium chloride induced rat model of Alzheimer's disease, 2018.
- [80] I.E. Orhan, E. Atasu, F.S. Senol, N. Ozturk, B. Demirci, K. Das, N. Sekeroglu, Comparative studies on Turkish and Indian *Centella asiatica* (L.) Urban (gotu kola) samples for their enzyme inhibitory and antioxidant effects and phytochemical characterization, *Ind. Crops Prod.* 47 (2013) 316–322, <https://doi.org/10.1016/j.indcrop.2013.03.022>.
- [81] M.N. Nasir, J. Abdullah, M. Habsah, R.I. Ghani, G. Rammes, Inhibitory effect of asiatic acid on acetylcholinesterase, excitatory post synaptic potential and locomotor activity, *Phytomedicine* 19 (2012) 311–316, <https://doi.org/10.1016/j.phymed.2011.10.004>.
- [82] S.C. Tan, R. Rajendran, S.K. Bhattamisra, P. Krishnappa, F. Davamani, E. Chitra, S. Ambu, B. Furman, M. Candamy, Protective effects of madecassoside, a triterpenoid from *Centella asiatica*, against oxidative stress in INS-1E cells, *Nat. Prod. Res.* (2024), <https://doi.org/10.1080/14786419.2024.2315499>.
- [83] S.W. Jung, S. Thamphiwatana, L. Zhang, M. Obonyo, Mechanism of antibacterial activity of liposomal linolenic acid against helicobacter pylori, *PLoS One* 10 (2015), <https://doi.org/10.1371/journal.pone.0116519>.
- [84] M.M. Cowan, Plant Products as Antimicrobial Agents, 1999.
- [85] B.M. Sieber, G.I. Omwenga, R.K. Wambua, J.C. Samoei, M.P. Ngugi, Screening of the Dichloromethane: Methanolic Extract of *Centella asiatica* for Antibacterial Activities against *Salmonella typhi*, *Escherichia coli*, *Shigella sonnei*, *Bacillus subtilis*, and *Staphylococcus aureus*, *Sci. World J.* 2020 (2020), <https://doi.org/10.1155/2020/6378712>.
- [86] M. Taghizadeh, S. Jalili, Phytochemical content, antioxidant properties, and antibacterial activities of *Centella asiatica* L., *Nat. Prod. Res.* (2023), <https://doi.org/10.1080/14786419.2023.2258439>.
- [87] P. Puttarak, P. Panichayupakaranant, A new method for preparing pentacyclic triterpene rich *Centella asiatica* extracts, *Nat. Prod. Res.* 27 (2013) 684–686, <https://doi.org/10.1080/14786419.2012.686912>.



## Bioactive compounds from the leaves of *Maytenus ilicifolia* Mart. ex Reissek: Inhibition of LDL oxidation, glycation, lipid peroxidation, target enzymes, and microbial growth

Vinicius Prado Bittar<sup>a,1</sup>, Ana Luiza Silva Borges<sup>a,1</sup>, Allisson Benatti Justino<sup>a</sup>, Maria Sol Peña Carrillo<sup>a</sup>, Renner Francisco Mateus Duarte<sup>a</sup>, Nagela Bernadelli Sousa Silva<sup>e</sup>, Daniela Silva Gonçalves<sup>e</sup>, Diego Godina Prado<sup>b</sup>, Iasmin Aparecida Cunha Araújo<sup>d</sup>, Mário Machado Martins<sup>c</sup>, Carlos Henrique Gomes Martins<sup>e</sup>, Françoise Vasconcelos Botelho<sup>a</sup>, Neide Maria Silva<sup>d</sup>, Alberto de Oliveira<sup>b</sup>, Foued Salmen Espíndola<sup>a,\*</sup>

<sup>a</sup> Laboratory of Biochemistry and Molecular Biology in Institute of Biotechnology, Federal University of Uberlândia, Uberlândia, MG, 38400-902, Brazil

<sup>b</sup> Nucleus of Research in Natural Products (NuPpE), Federal University of Uberlândia, Uberlândia, MG, 38400-902, Brazil

<sup>c</sup> Laboratory of Nanobiotechnology "Dr. Luiz Ricardo Goulart Filho", Institute of Biotechnology, Federal University of Uberlândia, Uberlândia, MG, 38400-902, Brazil

<sup>d</sup> Laboratory of Immunopathology, Institute of Biomedical Sciences, Federal University of Uberlândia, Uberlândia, MG, 38400-902, Brazil

<sup>e</sup> Laboratory of Antimicrobial Testing, Institute of Biomedical Sciences, University of Uberlândia, Campus Umuarama, Uberlândia, MG, 38405-320, Brazil

### ARTICLE INFO

#### Keywords:

Antioxidant  
Phytochemical analysis  
Lipid peroxidation  
Antiglycant

### ABSTRACT

**Ethnopharmacological relevance:** *Maytenus ilicifolia* Mart. ex Reissek, a medicinal plant used for treating gastritis, ulcers, and gastric disorders, possesses therapeutic properties attributed to diverse leaf compounds—terpenoids, alkaloids, flavonoids, phenols, and tannins, reflecting the ethnopharmacological knowledge of traditional users. **Aims of the study:** We aimed to assess the antioxidant and antiglycant capacities of *Maytenus ilicifolia*'s ethanolic extract and organic fractions, identify bioactive compounds through HPLC-MS/MS analysis, and conduct phytochemical assessments. We also assessed their potential to inhibit digestive and cholinesterase enzymes, mitigate oxidation of human LDL and rat hepatic tissue, and examine their antimicrobial and cytotoxic properties.

**Materials and methods:** Organic fractions (hexane - HF-Mi, dichloromethane - DMF-Mi, ethyl acetate - EAF-Mi, n-butanol - BF-Mi, and hydromethanolic - HMF-Mi) were obtained via liquid-liquid partitioning. Antioxidant (DPPH, FRAP, ORAC) and antiglycant (BSA/FRU, BSA/MGO, ARG/MGO/LDL/MGO models) capacities were tested. Phytochemical analysis employed HPLC-MS/MS. We also studied the inhibitory effects on  $\alpha$ -amylase, acetylcholinesterase, butyrylcholinesterase, human LDL and rat hepatic tissue oxidation, antimicrobial activity, and cytotoxicity against RAW 264.7 macrophages.

**Results:** HPLC-ESI-MS/MS identified antioxidant compounds such as catechin, quercetin, and kaempferol derivatives. Ethanolic extract (EE-Mi) and organic fractions demonstrated robust antioxidant and antiglycant activity. EAF-Mi and BF-Mi inhibited  $\alpha$ -amylase (2.42  $\mu$ g/mL and 7.95  $\mu$ g/mL) compared to acarbose (0.144  $\mu$ g/mL). Most organic fractions exhibited ~50% inhibition of acetylcholinesterase and butyrylcholinesterase, rivaling galantamine and rivastigmine. EAF-Mi, BF-Mi, and EE-Mi excelled in inhibiting lipid peroxidation. All fractions, except HMF-Mi, effectively countered LDL oxidation, evidenced by the area under the curve. These fractions protected LDL against lipid peroxidation.

**Conclusion:** This study unveils *Maytenus ilicifolia*'s ethanolic extract and organic fractions properties. Through rigorous analysis, we identify bioactive compounds and highlight their antioxidant, antiglycant, enzyme inhibition, and protective properties against oxidative damage. These findings underline its significance in modern pharmacology and its potential applications in healthcare.

\* Corresponding author. Universidade Federal de Uberlândia, Instituto de Biotecnologia, Rua Acre s/n, Bloco 2E, 38400-319, Uberlândia, MG, Brazil.

E-mail address: [foued@ufu.br](mailto:foued@ufu.br) (F.S. Espíndola).

<sup>1</sup> Equal contributions authors: VPB and ALSB.

## 1. Introduction

In traditional medicine, natural products have been used for several years (Atanasov et al., 2015). The advancement of metabolomics has allowed the identification of diverse molecules present in medicinal plants, enabling the investigation of their biological potential through *in*

MO, USA). Dimethyl sulfoxide was purchased from Merck (Darmstadt, HE, Germany). Brain Heart Infusion broth (BHI) and Schaedler broth were purchased from BD Difco (Sparks, MD, EUA). Rivastigmine (drug) was purchased from ACHÉ Laboratórios Farmacêuticos, Brazil, and galantamine (drug) was purchased from Libbs Farmacêutica Ltda, Brazil.

### Abbreviations

<b>EE-Mi</b>	Ethanol extract of <i>Maytenus ilicifolia</i>	<b>BSA</b>	Bovine serum albumin
<b>HF-Mi</b>	Hexane fraction of <i>Maytenus ilicifolia</i>	<b>LDL</b>	Low-density lipoprotein
<b>DMF-Mi</b>	Dichloromethane fraction of <i>Maytenus ilicifolia</i>	<b>ARG</b>	Arginine
<b>EAF-Mi</b>	Ethyl acetate fraction of <i>Maytenus ilicifolia</i>	<b>PBS</b>	Phosphate buffer saline
<b>BF-Mi</b>	<i>n</i> -butanol fraction of <i>Maytenus ilicifolia</i>	<b>OHT</b>	Oxidized hepatic tissue
<b>HMF-Mi</b>	Hydromethanolic fraction of <i>Maytenus ilicifolia</i>	<b>HT</b>	Hepatic tissue
<b>HPLC-ESI</b>	High-performance liquid chromatography-electrospray ionization source	<b>MIC</b>	Minimum Inhibitory Concentration
<b>FRAP</b>	Ferric reducing antioxidant power	<b>AChE</b>	Acetylcholinesterase
<b>DPPH</b>	2,2-diphenyl-1-picrylhydrazyl	<b>BChE</b>	Butyrylcholinesterase
<b>ORAC</b>	Oxygen radical absorbance capacity	<b>ROS</b>	Reactive oxygen species
<b>AGEs</b>	Advanced glycation end products	<b>EC<sub>50</sub></b>	Effective concentration
<b>MGO</b>	Methylglyoxal	<b>CC<sub>50</sub></b>	cytotoxicity concentration
<b>FRU</b>	Fructose	<b>TBARs</b>	thiobarbituric acid reactive substance
		<b>MDA</b>	malondialdehyde
		<b>MTT</b>	3-(4,5-dimethylthiazol-2-yl)-2,5 diphenyltetrazolium bromide

*in vitro* analysis (Harvey et al., 2015). *Maytenus*, a genus from the Celastraceae family, is found in various biomes of South America (Grosso et al., 2014). *Maytenus ilicifolia* Mart. ex Reissek, also known as “espinaheira-santa,” is a species found in southern Brazil, and its leaves are commonly used in traditional medicine due to their antacid and anti-ulcerogenic effects (Baggio et al., 2007).

Other reported benefits of *M. ilicifolia* include analgesic, antiseptic, and wound-healing activities (de Moura et al., 2021; Paula et al., 2021; Veloso et al., 2017). These properties are associated with the presence of flavonoids, terpenes, alkaloids, and polyphenols such as catechin, epicatechin, afzelechin, epiafzelechin, quercetin, rutin, kaempferol, malic acid found in the leaves of *M. ilicifolia* (de Souza et al., 2008; Olivaro et al., 2022).

Until now, few studies have investigated the *in vitro* activity of the ethanolic extract of *M. ilicifolia* and its organic fractions partitioned by liquid-liquid separation. This study aims to investigate the antioxidant and antiglycating capacity of the ethanolic extract of *M. ilicifolia* leaves and its organic fractions, as well as to identify the compounds present in the most bioactive fractions through phytochemical analysis using HPLC-MS/MS analysis. Additionally, we aim to analyze the inhibitory capacity of  $\alpha$ -amylase, acetylcholinesterase, and butyrylcholinesterase enzymes, the prevention of human LDL and rat hepatic tissue oxidation, antimicrobial activity, and cytotoxicity against murine RAW 264.7 macrophages.

## 2. Materials and methods

### 2.1. Reagents

Ethanol, hexane, dichloromethane, ethyl acetate, *n*-butanol, and methanol were purchased from Vetec Química Fina Ltda (Duque de Caxias, Rio de Janeiro, Brazil). Folin-Ciocalteu, gallic acid, vanillin, catechin, quercetin, 2,2-diphenyl-1-picrylhydrazyl, 2,4,6-Tris(2-pyridyl)-s-triazine, 6-hydroxy-2,5,7,8-tetramethylchroman-2-carboxylic acid (Trolox), 2,2'-azobis (2-amidino-propane) dihydrochloride (AAPH), fluorescein, L-arginine, D-(−)-fructose, 2-Thiobarbituric acid, aprotinin from bovine lung, acarbose, 2-chloro-4-nitrophenyl-4- $\beta$ -D-galactopyranosylmaltoside (GalG2CNP), acetylcholinesterase, and butyrylcholinesterase were purchased from Sigma Aldrich (St. Louis,

### 2.2. Plant material

The dried leaves of *M. ilicifolia* were purchased from Santos Flora Comércio de Ervas Ltda (Mariporã, São Paulo, Brazil), an officially registered enterprise under ANVISA (Authorization Number: 6.0.671-1) and the Regional Pharmacy Council - CRF (Registration Number: 0505). The plant material possessed a certificate of origin, attesting to its purity and lack of contaminants. Its authenticity was established through its sensory and macroscopic characteristics, supplemented by an analysis of phytochemical markers. These markers were identified using HPLC-MS/MS and cross-referenced with the relevant literature. This analysis revealed a series of catechin derivatives commonly reported in this species, providing robust confirmation of the quality and purity of the dried material supplied by the company.

### 2.3. Extraction and fractionation

To obtain the ethanolic extract of *M. ilicifolia*, we used 800 g of dried leaves that were subjected to static maceration in 4 L of ethanol (1:5 m/v) at room temperature and protected from light for seven days (Lima Júnior et al., 2021). After seven days, the solution was filtered through a common paper filter, and the remaining solvent was removed using a rotary evaporator (Buchi Rotavapor R-210, Flawil, Switzerland) in a water bath at 40 °C under controlled and reduced pressure. Finally, the ethanolic extract was subjected to lyophilization to completely remove any remaining water in the sample.

To obtain the organic fractions, 4 g of the ethanolic extract of *M. ilicifolia* (EE-Mi) were diluted in a 90% (9:1 v/v 250 mL) hydromethanolic (MeOH:H<sub>2</sub>O) solution. After dilution, the mixture underwent a liquid-liquid partitioning process (Justino et al., 2020). The solvents were added at a fixed volume of 200 mL in the increasing order of polarity: hexane (HF-Mi), dichloromethane (DMF-Mi), ethyl acetate (EAF-Mi), and *n*-butanol (BF-Mi). The hydromethanolic fraction (HMF-Mi) represented the final residue of the partitioning process. The solvents remaining at each step of the partitioning process were removed by lyophilization and drying. The dried samples of EE-Mi, HF-Mi, DMF-Mi, EAF-Mi, BF-Mi, and HMF-Mi were stored at −20 °C until use in the experiments.



## 2.4. HPLC-ESI-MS/MS analysis

The ethyl acetate (EAF-Mi) and n-butanol (BF-Mi) fractions of *M. ilicifolia* were evaluated by high-performance liquid chromatography hyphenated to mass spectrometry with an electrospray ionization source (HPLC-MS/ESI). These fractions were chosen based on their performance in biological assays. The analysis was conducted using a liquid chromatograph (Agilent - Infinity 1260) coupled to a high-resolution mass spectrometer (Agilent® model 6520 B) with an ESI source located at Nanobiotechnology Laboratory Prof. Dr. Luiz Ricardo Goulart Filho (IBTEC/UFU). The eluents used were water acidified with 0.1% v/v formic acid (A) and methanol (B). The analytical parameters were set as follows: 10% of B (0 min), 98% of B (0–10 min), and 98% (11–17 min). The ionization parameters were a nebulizer pressure of 20 psi, drying gas at 8 L min<sup>-1</sup> at a temperature of 220 °C, and an energy of 4.5 KV applied to the capillary. Sequential mass spectra (MS/MS) were obtained by applying energy values between 5 and 30 eV to obtain spectra with the best fragmentation pattern for each compound present. For analysis, all spectra obtained ([Supplementary Material](#)) were evaluated in the Agilent Mass Hunter® B.07.00 software and compared with online libraries such as MassBank and other literature studies.

## 2.5. Phytochemical analysis

The phytochemical screening of the ethanolic extract of *M. ilicifolia* and its organic fractions HF-Mi, DMF-Mi, EAF-Mi, BF-Mi, and HMF-Mi, was performed to determine the concentrations of total phenols, total flavonoids, and condensed tannins ([Zou et al., 2011](#)). Spectrophotometric measurements were performed at a concentration of 1 mg/mL for each sample. Ethanol was used as a blank sample for the measurements.

### 2.5.1. Total phenolic content

The ethanolic extract of *M. ilicifolia* (EE-Mi) and its organic fractions were analyzed for total phenolic content using the Folin-Ciocalteu assay. Briefly, 1 mg/mL of each sample was mixed with 10% Folin-Ciocalteu and incubated at 25 °C for 6 min. Then, 7% sodium carbonate (Na<sub>2</sub>CO<sub>3</sub>) was added, and samples were further incubated for 2 h at 25 °C in the dark. After incubation, absorbance was measured at 760 nm using a microplate reader (Versamax, Molecular Devices, USA). The total phenolic content was expressed as mg gallic acid equivalents per gram of sample (mg GAE/g), using a standard analytical curve of gallic acid.

### 2.5.2. Total flavonoid content

To determine the total flavonoids content in EE-Mi and its organic fractions, we incubated them in the dark with a solution of 5% sodium nitrite and ultrapure water for 6 min at 25 °C. After incubation, we added 10% aluminum chloride to the tested samples and incubated them for another 6 min at 25 °C. The absorbance was measured at 425 nm using a microplate reader (Versamax, Molecular Devices, USA). A standard analytical curve of quercetin was used to determine the total flavonoid content (mg QE/g).

### 2.5.3. Condensed tannin content

To determine the condensed tannin content (mg CE/g) in EE-Mi and its organic fractions, we incubated them with 4% vanillin (diluted in methanol) and HCl for 15 min at 25 °C. After incubation, we measured the absorbance at 500 nm using a microplate reader (Versamax, Molecular Devices, USA). A standard analytical curve constructed with catechin was used to determine the condensed tannin content.

## 2.6. Antioxidant activity

To determine the antioxidant capacity of the samples, we performed three different assays: ferric reducing antioxidant power (FRAP), 2,2-diphenyl-1-picrylhydrazyl (DPPH) antioxidant activity, and oxygen

radical absorbance capacity (ORAC). We diluted different sample concentrations in ethanol for each assay. The FRAP method evaluates the sample's capacity to reduce iron molecules, while the ORAC method measures its ability to sequester the peroxy radical. In the DPPH method, the sample is challenged to reduce the DPPH radical to hydrazine.

### 2.6.1. FRAP assay

EE-Mi and its organic fractions were mixed with the FRAP reagent (composed of 300 mM sodium acetate buffer pH 3.6, 2,4,6-tri-(2-pyridyl)-s-triazide (TPTZ), and 20 mM ferric chloride in a 10:1:1 ratio, respectively) and incubated for 6 min at 37 °C. After incubation, absorbance was measured at 593 nm using a microplate reader (Versamax, Molecular Devices, USA). A standard curve for 6-hydroxy-2,5,7,8-tetramethylchroman-2-carboxylic acid (Trolox) was constructed. Quercetin was used as a positive control and sodium acetate buffer was used as a negative control. The results were expressed as μmol of trolox (eq. g<sup>-1</sup>) ([Benzie and Devaki, 2017](#)).

### 2.6.2. ORAC assay

EE-Mi and its organic fractions were incubated with 0.085 mM fluorescein and 153 mM of 2,2'-azobis(2-amidinopropane) dihydrochloride (AAPH), both reagents were diluted in 75 mM phosphate buffer (pH 7.4). Fluorescence was measured at 485 nm excitation and 528 nm emission for 90 min at 37 °C in a microplate reader (EnSpire, PerkinElmer, USA). An analytical standard curve of trolox was constructed to measure the antioxidant capacity of the samples in the assay. Phosphate buffer was used as a negative control, and quercetin was used as a positive control. The results were expressed as μmol of trolox (eq. g<sup>-1</sup>) ([Prior et al., 2003](#)).

### 2.6.3. DPPH assay

The DPPH assay was conducted following the method described before ([Brand-Williams et al., 1995](#)), with modifications ([Lima Júnior et al., 2021](#)). EE-Mi and its organic fractions were tested at an initial concentration of 250 μg/mL, and a serial 10-point dilution was performed to a final concentration of 0.48 μg/mL to estimate the EC<sub>50</sub> value. The samples were incubated with 60 mM DPPH radical (diluted in methanol) for 30 min at 37 °C in the absence of light. Subsequently, absorbance was measured at 517 nm in a microplate reader (Versamax, Molecular Devices, USA). The antioxidant activity of the samples was calculated using the following equation:  $DPPH (\%) = [(X \text{ control} - X \text{ sample}) / (X \text{ control} - X \text{ blank})] \times 100$ , where "X control" refers to the absorbance of DPPH diluted in methanol, "X sample" refers to the absorbance of the DPPH + sample set, and "X blank" refers to the samples diluted in methanol without the presence of DPPH (methanol + samples). Methanol was used as a negative control and quercetin was used as a positive control.

## 2.7. AGEs formation analysis

The methods for evaluating the ability to inhibit the formation of advanced glycation end products (AGEs) were based on methodologies described previously ([Alqahtani et al., 2021](#); [Wang et al., 2011](#)), with some modifications. Initially, EE-Mi and its organic fractions were serially diluted in ethanol at a concentration of 625 μg/mL to determine the EC<sub>50</sub> values. The percentage of glycation inhibition was calculated using the following equation:  $I (\%) = (X \text{ control} - X \text{ sample}) / X \text{ control} \times 100$ , where "X control" represents the fluorescence value obtained in the absence of the samples/positive control, "X sample" represents the fluorescence value obtained in the presence of the samples/positive control, and "X blank" is the fluorescence value obtained in the absence of the agent that will promote glycation (fructose or methylglyoxal) and of the samples/positive control. In all models, phosphate buffer (200 mM, pH 7.4) was used to replace the glycation-causing agents, while ethanol was used to dilute the samples and served as a negative control.

Quercetin was used as a positive control.

### 2.7.1. BSA and methylglyoxal (MGO) model

EE-Mi and its organic fractions were incubated with bovine serum albumin (BSA) at a concentration of 50 mg/mL and methylglyoxal (MGO) at a concentration of 53.3 mM. The reaction was performed in 200 mM phosphate buffer (pH 7.4) containing 0.02% sodium azide for 72 h at 37 °C in the absence of light. After the incubation period, a 20% trichloroacetic acid (TCA) solution was added to the reaction mixture, which was then centrifuged at 10,000×g for 10 min. The supernatant was discarded, and the pellet was resuspended in a phosphate buffer. The fluorescence intensity of the samples was measured using a microplate reader (EnSpire, PerkinElmer, USA) at an excitation wavelength of 340 nm and an emission wavelength of 380 nm. Ethanol was used as the negative control, and quercetin was used as a positive control. In the blank sample, MGO was replaced with phosphate buffer.

### 2.7.2. BSA and fructose (FRU) model

EE-Mi and its organic fractions were incubated with bovine serum albumin (BSA) at a concentration of 50 mg/mL and fructose at a concentration of 1.25 M in 200 mM phosphate buffer (pH 7.4) containing 0.02% sodium azide for 72 h at 37 °C in the absence of light. After the incubation, a 20% trichloroacetic acid (TCA) solution was added to the reaction mixture, which was then centrifuged at 10,000×g for 10 min. The supernatant was discarded, and the pellet was resuspended in a phosphate buffer. The fluorescence intensity of the samples was measured using a microplate reader (EnSpire, PerkinElmer, USA) at an excitation wavelength of 350 nm and an emission wavelength of 420 nm. Ethanol was used as the negative control, and quercetin was used as a positive control. In the blank sample, fructose was replaced with phosphate buffer.

### 2.7.3. Arginine (ARG) and methylglyoxal model

EE-Mi and its organic fractions were incubated with arginine at a concentration of 106.6 mM and methylglyoxal (MGO) at a concentration of 53.3 mM in 200 mM phosphate buffer (pH 7.4) containing 0.02% sodium azide. The reaction was carried out for 72 h at 37 °C in the absence of light. After the incubation period, the fluorescence intensity of the samples was measured using a microplate reader (EnSpire, PerkinElmer, USA) at an excitation wavelength of 340 nm and an emission wavelength of 380 nm. Ethanol was used as a negative control, and quercetin was used as a positive control. In the blank sample, MGO was replaced with phosphate buffer.

### 2.7.4. Low-density lipoprotein (LDL) and methylglyoxal model

Human LDL was isolated according to a previously described method (Chung et al., 1986). The isolated LDL was incubated with EE-Mi and its organic fractions at a concentration of 190 µg/mL, along with one mM methylglyoxal (MGO) and phosphate buffer (100 mM, pH 7.4, and 0.02% azide) for 72 h at 37 °C in the absence of light. Fluorescence intensity was measured at 340 nm excitation and 380 nm emission using a microplate reader (EnSpire, PerkinElmer, USA). Ethanol was used as a negative control, and quercetin was used as the positive control.

## 2.8. Ex vivo analysis of hepatic tissue

### 2.8.1. Liver tissue processing

Liver tissue analysis was conducted using the induction and tissue oxidation methodology with Fe<sup>2+</sup>-ascorbate (Justino et al., 2019). The liver tissue samples were obtained from Wistar rats (6–8 weeks old) at the Center for Bioterism and Experimentation of the Federal University of Uberlandia (UFU) with official approval from the animal ethics committee (Craft No. 7/2022/CEUA/PROPP/REITO-UFU of July 14, 2022). The animals were anesthetized and euthanized by cervical dislocation, and the liver was removed and stored in liquid nitrogen before being transported to an ultra-freezer at –70 °C until the time of

the analysis. The liver samples were homogenized in phosphate-buffered saline (PBS) at a ratio of 1:10 and centrifuged at 3,000×g for 10 min at 4 °C. The supernatant obtained after centrifugation was incubated for 60 min at 37 °C with 0.1 mM iron sulfate and 0.1 mM ascorbic acid to form Fe<sup>2+</sup>-ascorbate, resulting in oxidized hepatic tissue (OHT). EE-Mi and its organic fractions, along with the positive control quercetin, were simultaneously added at a concentration of 160 µg/mL, diluted in ethanol. A sample containing only PBS was used as a negative control.

### 2.8.2. Lipid peroxidation

Samples were incubated with 10% trichloroacetic acid (TCA) and 0.67% thiobarbituric acid (TBA) for 2 h in a water bath at 100 °C. After incubation, 400 µL of butanol was added to extract malondialdehyde (MDA), a product of lipid peroxidation. The mixture was then centrifuged at 3,000×g for 10 min, and the fluorescence was measured at 532 nm using an EnSpire spectrophotometer (PerkinElmer, USA). The results were expressed as nmol of malondialdehyde per milligram of protein (Yagi, 1998).

## 2.9. Isolation, oxidation, and peroxidation of low-density lipoprotein (LDL)

### 2.9.1. Isolation of LDL

The LDL isolation was performed following the method already described (Chung et al., 1986). Blood samples were obtained from healthy, non-smoking human volunteers in accordance with the approval of the Human Research Ethics Committee of the UNA University Center, located in Uberlandia - Minas Gerais, Brazil (protocol: 5.671.038; National Health Council Resolution CNS 466/12). The samples were collected in vacutainer tubes containing 10% EDTA and subsequently centrifuged at 800×g for 10 min at 4 °C to isolate the plasma. Plasma density was elevated to 1.21 g/mL by adding potassium bromide. Aprotinin (5 µL per 1 mL of plasma), benzamidine two mM (5 µL per 1 mL of plasma), phenylmethylsulfonyl fluoride (PMSF) 0.5 mM (0.5 µL per 1 mL of plasma), chloramphenicol 0.25% (0.5 µL per 1 mL of plasma), and a solution containing sodium azide 5%, EDTA 8%, and chloramphenicol 0.1% (10 µL per 1 mL of plasma) were also added to the plasma. LDL was isolated using sequential ultracentrifugation (Sorvall WX 90+ ultracentrifuge - ThermoFisher Scientific) at 53,000×g for 2 h and 30 min at 4 °C. The orange layer corresponding to LDL was collected using a syringe and dialyzed in phosphate buffer solution (PBS 1x) at 4 °C and pH 7.4 for 24 h with exchanges every 6 h. After this procedure, LDL was stored at 4 °C in the absence of light until the analysis. Protein quantification was performed using the Bradford method (Bradford, 1976) with modifications.

### 2.9.2. Induction of LDL oxidation and peroxidation

LDL oxidation was induced using 5 µM copper (II) sulfate, and the process was monitored for 2 h with readings taken every 2 min. The goal was to determine the intercept of the tangents between the slow and fast absorption of conjugated dienes (Gieseg and Esterbauer, 1994) at a temperature of 37 °C in a microplate at 234 nm using an EnSpire spectrophotometer from PerkinElmer, USA. EE-Mi and its organic fractions were evaluated at a concentration of 1 µM, and PBS was used as a negative control. After the monitoring period, the samples were taken directly from the plate, and the quantification of lipid peroxidation was performed using the malondialdehyde method previously described in this study.

## 2.10. Analysis of enzyme inhibitory capacity

The α-amylase enzyme inhibition assay utilizes a fraction enriched in α-amylase (HAS-f) and 2-chloro-4-nitrophenyl-4-β-D-galactopyranosylmaltoside (GAL-G2-CNP) as a substrate (Da Silva Santos et al., 2012) with modifications. The inhibitory activity of the enzymes butyrylcholinesterase (BChE) and acetylcholinesterase (AChE) was

determined using methods already described (Ellman et al., 1961; Marston et al., 2002; Rhee et al., 2001). To calculate the inhibition percentages, the following formula was used:  $I (\%) = (X_{\text{control}} - X_{\text{sample}}/X_{\text{control}}) \times 100$ . Here, “X control” represents the area under the curve calculated using the absorbance measurement obtained in the absence of the compounds, whereas “X sample” represents the area under the curve calculated using the absorbance measurement obtained in the presence of the ethanolic extract, organic fractions, and positive controls.

### 2.10.1. Inhibition of $\alpha$ -amylase

Saliva was collected from healthy human volunteers. The collected samples were then dialyzed and fractionated using Q-Sepharose ion exchange chromatography to obtain an  $\alpha$ -amylase enriched fraction (Navazesh, 1993). This fraction was then diluted in 50 mM MES (2-tanesulfonic acid) buffer at pH 6.4, which was prepared using 300 mM sodium chloride (NaCl), five mM calcium chloride (CaCl<sub>2</sub>), and 140 mM potassium thiocyanate (KSCN) in ultrapure water. The  $\alpha$ -amylase enriched fraction was incubated with the samples diluted in ethanol for 30 min at 37 °C. After that, 2-chloro-4-nitrophenyl-4- $\beta$ -D-galactopyranosylmaltoide (GalG2CNP) was added, and the absorbance of the samples was measured at 405 nm for 3 min at 1-min intervals using a Versamax spectrophotometer (Molecular Devices, USA). Ethanol was used as the negative control, and acarbose was used as the positive control.

### 2.10.2. Inhibition of butyrylcholinesterase and acetylcholinesterase

Three different buffers were prepared: buffer A (50 mM Tris-HCl at pH 8), buffer B (50 mM Tris-HCl containing 0.1% bovine serum albumin), and buffer C (50 mM Tris-HCl containing 0.1 M NaCl and 0.02 M MgCl<sub>2</sub>·6H<sub>2</sub>O). The substrates butyrylcholine and acetylthiocholine (3 mM) were diluted in water, and 5,5'-dithio-bis-[2-nitrobenzoic acid] (DTNB) (3 mM) was diluted in buffer C. The samples to be tested were diluted in buffer A. To perform the assay, the following reagents were added: substrate, buffer B, DTNB, EE-Mi, and its organic fractions diluted in buffer A. The enzymes acetylcholinesterase or butyrylcholinesterase at 0.2 U/mL were then added to initiate the reaction, and the absorbance was measured at 405 nm every 30 s for 20 min at 30 °C using a microplate reader (Versamax, Molecular Devices, USA). The percentage inhibition was calculated using the following equation:  $I (\%) = (X_{\text{blank}} - X_{\text{sample}}/X_{\text{blank}}) \times 100$ , where “X blank” represents the reading obtained without the sample or positive control (10% ethanol, the same solvent used for diluting the samples, in buffer A), and “X sample” represents the reading obtained in the presence of the sample or positive control. The positive controls were galantamine and rivastigmine.

### 2.11. In vitro cytotoxicity of extracts toward RAW 264.7 macrophages

RAW 264.7 macrophages (ATCC TIB-71) were obtained from the American Type Culture Collection (ATCC). To determine the cytotoxicity concentration (CC<sub>50</sub>) of the substances against RAW 264.7 macrophages, it was employed the 3-(4,5-dimethylthiazol-2-yl)-2,5 diphenyltetrazolium bromide (MTT) assay (Mosmann, 1983). For the assay, RAW 264.7 cells were seeded in 96-well flat-bottom plates (3 × 10<sup>4</sup> cells/well and 5 × 10<sup>4</sup> cells/well, respectively) and incubated at 37 °C and 5% CO<sub>2</sub> until they fully adhered. After incubation, the wells were emptied, and EE-Mi and organic fractions diluted in complete RPMI were added at concentrations of 1000, 500, 100, and 10  $\mu$ g/mL. The cells were then exposed to the extracts for 24 h at 37 °C and 5% CO<sub>2</sub>. Next, the wells were emptied again, and an MTT solution (50  $\mu$ g/well) was added. The plates were incubated for an additional 4 h at 37 °C and 5% CO<sub>2</sub>. Subsequently, DMSO was added to solubilize the formazan crystals produced, and the plates were read on a spectrophotometer (570 nm emission, on Spectramax M2). Each experiment was repeated three times, and the optical density (OD) was obtained by subtracting

the average OD value of the wells containing only cells incubated with complete medium (considered 100% viability) from the mean value of the sample readings performed in triplicate.

### 2.12. Analysis of antimicrobial activity

The minimum inhibitory concentration (MIC) was determined in triplicate using the methodology recommended by the Clinical and Laboratory Standards Institute (CLSI) in 2007 and 2012. EE-Mi and organic fractions were prepared by solubilizing them in 5% dimethyl sulfoxide (DMSO) and diluting them in Brain Heart Infusion broth (BHI) for aerobic bacteria and in Schaedler broth supplemented with hemin (5 mg/mL) and menadione (1 mg/mL) for anaerobic bacteria. Twelve concentrations (0.195–400  $\mu$ g/mL) of the samples were tested. The pathogenic bacterial strains “*Staphylococcus aureus* ATCC 29213”, “*Staphylococcus epidermidis* ATCC 12228”, “*Pseudomonas aeruginosa* ATCC 27853”, and “*Burkholderia cepacia* ATCC 25416” were obtained from the American Type Culture Collection (ATCC) and standardized at a concentration of 5 × 10<sup>5</sup> colonies per unit (CFU/mL) for aerobic bacteria and 1 × 10<sup>6</sup> for anaerobic bacteria. These bacteria were part of the Antimicrobial Laboratory Testing collection at the University of Uberlandia and were cryopreserved at –20 °C until use. To check the toxicity of the medium, 5% DMSO and the tested microorganisms were incubated separately, and bacterial growth was observed at this concentration. After this step, the plates containing anaerobic microorganisms were incubated at 37 °C for 72 h in an anaerobic oven with a gas mixture of 5–10% H<sub>2</sub>, 10% CO<sub>2</sub>, and 80–85% N<sub>2</sub> (Don Whitley Scientific, Bradford, UK), while the aerobic bacteria were incubated at 37 °C for 24 h under standard aerobic conditions. Following incubation, 30  $\mu$ L of 0.02% aqueous solution of resazurin was added to each well. Resazurin is an oxy-reducing compound that allows bacterial growth to be immediately analyzed. Non-proliferating bacteria are indicated by the blue color, while the pink color represented bacterial growth (Sarker et al., 2007). Each experiment was performed in triplicate, and the MIC was the lowest concentration of the sample that inhibited bacterial growth.

### 2.13. Statistical analysis

The results are expressed as the mean  $\pm$  standard deviation, except for the EC<sub>50</sub> calculation, where the mean  $\pm$  standard error was used. Analysis of variance between groups was performed using one-way ANOVA with Tukey's post-test for multiple comparisons. A p-value less than 0.05 (p < 0.05) was considered significant. Statistical analysis and graph plotting were performed using GraphPad Prism 8.0 software.

## 3. Results

### 3.1. Fractionation yield

A total of 800 g of shredded leaves were used to obtain 32 g of ethanolic extract of *M. ilicifolia* (yield: 4%). To obtain the organic fractions, 4 g of EE-Mi were used, and the yields of each fraction were: HF-Mi (3.17%), DMF-Mi (19.12%), EAF-Mi (37.12%), BF-Mi (26.75%), and HMF-Mi (11.92%). Additional information on the fractions can be found in the Supplementary Material.

### 3.2. HPLC-ESI-MS/MS analysis of the organic fraction ethyl acetate and n-butanol of *M. ilicifolia* leaves

To identify the compounds present in the organic fraction ethyl acetate (EAF-Mi) and n-butanol (BF-Mi) of *M. ilicifolia*, HPLC-ESI-MS/MS analyses were conducted. MS/MS spectra were analyzed, considering the retention times, error values, fragmentation patterns, sequential mass spectra, and literature information. Based on this analysis, we propose the compounds listed in Table 1.

Table 1

Compounds identified in EAF-Mi and BF-Mi fractions of *M. ilicifolia* leaves extract by HPLC-ESI-MS/MS in negative ionization mode.

$t_R$ (min)	[M - H] <sup>-</sup>	Exact Mass	Error (ppm)	Fragment ions (m/z) MS/MS	Molecular formula	Suggested compound	Sample	Reference
0.76	181.0721	181.718	1.66	15 eV: 163, 101, 89, 71, <b>59</b> , 55	C <sub>6</sub> H <sub>14</sub> O <sub>6</sub>	Sorbitol	BF-Mi	Lima et al. (2022)
0.83	133.0143	133.0142	0.75	10 eV: <b>115</b> , 71	C <sub>4</sub> H <sub>6</sub> O <sub>5</sub>	malic acid	BF-Mi, EAF-Mi	(Gómez-Romero et al., 2010; Fraternali et al., 2015)
1.43	849.2045	849.2036	1.06	25 eV: 831, 723, 697, 679, <b>577</b> , 559, 425, 407, 397, 289, 287, 125	C <sub>45</sub> H <sub>38</sub> O <sub>17</sub>	(epi)afz-(epi)cat-(epi)cat I	BF-Mi, EAF-Mi	(Gu et al., 2003; Ge et al., 2016; Olivaro et al., 2022)
1.98	315.0727	315.0722	1.59	25 eV: 153, <b>152</b> , 109, 108	C <sub>13</sub> H <sub>16</sub> O <sub>9</sub>	protocatechuic acid hexoside	BF-Mi	Abu-Reidah et al. (2015a)
2.02	305.0669	305.0667	0.66	20 eV: 261, 219, 167, 165, <b>137</b> , <b>125</b>	C <sub>15</sub> H <sub>14</sub> O <sub>7</sub>	(epi)galocatechin	BF-Mi, EAF-Mi	(de Moura Martins et al., 2020; de Moura et al., 2021; Olivaro et al., 2022)
2.03	833.2085	833.2087	-0.24	30 eV: 561, 543, 407, <b>289</b> , 273, 125	C <sub>45</sub> H <sub>38</sub> O <sub>16</sub>	(epi)afz-(epi)afz-(epi)cat I	BF-Mi, EAF-Mi	(Gu et al., 2003; de Souza et al., 2008; Olivaro et al., 2022)
2.60	593.1309	593.1301	1.35	20 eV: 575, 467, 441, <b>423</b> , 407, 305, 289, 273, 177, 125	C <sub>30</sub> H <sub>26</sub> O <sub>13</sub>	(epi)cat-(epi)gal	BF-Mi, EAF-Mi	(Ge et al., 2016; Olivaro et al., 2022)
2.95	577.1355	577.1351	0.69	25 eV: 559, 451, 425, 407, <b>289</b> , 245, 161, 125	C <sub>30</sub> H <sub>26</sub> O <sub>12</sub>	(epi)cat-(epi)cat	BF-Mi, EAF-Mi	(de Souza et al., 2008; Sobeh et al., 2018; Olivaro et al., 2022)
3.15	849.2044	849.2036	0.94	25 eV: 723, 697, 679, 577, 561, <b>559</b> , 543, 407, 289, 271, 125	C <sub>45</sub> H <sub>38</sub> O <sub>17</sub>	(epi)afz-(epi)cat-(epi)cat II	EAF-Mi	(Gu et al., 2003; Ge et al., 2016; Olivaro et al., 2022)
	865.1985	865.1985	0.0	25 eV: 847, 739, 713, 695, 577, 575, 451, 425, 305, 287, 245, 125	C <sub>45</sub> H <sub>38</sub> O <sub>18</sub>	(epi)cat-(epi)cat-(epi)cat ou (epi)afz-(epi)cat-(epi)gal	EAF-Mi	Olivaro et al. (2022)
3.31	305.0670	305.0667	0.98	20 eV: 287, 261, 219, 179, 167, 165, 137, 135, <b>125</b>	C <sub>15</sub> H <sub>14</sub> O <sub>7</sub>	(epi)galocatechin	BF-Mi, EAF-Mi	(de Moura Martins et al., 2020; de Moura et al., 2021; Olivaro et al., 2022)
	289.0719	289.0718	0.35	20 eV: 271, 245, 203, 151, 137, 125, 123, <b>109</b>	C <sub>15</sub> H <sub>14</sub> O <sub>6</sub>	(epi)catechin	BF-Mi, EAF-Mi	(do Nascimento et al., 2020; de Moura et al., 2021; Olivaro et al., 2022)
3.51	561.1410	561.1402	1.43	20 eV: 435, 407, <b>289</b> , 271, 245, 125	C <sub>30</sub> H <sub>26</sub> O <sub>11</sub>	(epi)afz-(epi)cat I	BF-Mi, EAF-Mi	(de Souza et al., 2008; Ge et al., 2016; Olivaro et al., 2022)
3.56	833.2099	833.2087	1.44	25 eV: 707, 561, <b>543</b> , 289, 271, 125	C <sub>45</sub> H <sub>37</sub> O <sub>16</sub>	(epi)afz-(epi)afz-(epi)cat II	EAF-Mi	(de Souza et al., 2008; Ge et al., 2016; Olivaro et al., 2022)
3.70	577.1351	577.1351	2.08	20 eV: 451, 425, <b>407</b> , 289, 245, 161, 125	C <sub>30</sub> H <sub>26</sub> O <sub>12</sub>	(epi)cat-(epi)cat	BF-Mi, EAF-Mi	(Sobeh et al., 2018; Olivaro et al., 2022)
4.30	289.0723	289.0718	1.73	20 eV: 271, 245, 203, 151, 137, 125, 123, <b>109</b>	C <sub>15</sub> H <sub>14</sub> O <sub>6</sub>	(epi)catechin	BF-Mi, EAF-Mi	(do Nascimento et al., 2020; de Moura et al., 2021; Olivaro et al., 2022)
4.48	849.2044	849.2036	0.94	25 eV: 723, 697, 679, <b>559</b> , 433, 425, 407, 289, 271, 125	C <sub>45</sub> H <sub>37</sub> O <sub>17</sub>	(epi)afz-(epi)cat-(epi)cat III	BF-Mi, EAF-Mi	(Gu et al., 2003; Ge et al., 2016; Olivaro et al., 2022)
4.50	545.1477	545.1453	4.40	20 eV: 419, <b>273</b> , 164, 125	C <sub>30</sub> H <sub>26</sub> O <sub>10</sub>	(epi)afz-(epi)afz	EAF-Mi	(Ge et al., 2016; Costa Silva et al., 2019)
4.66	833.2081	833.2087	-0.72	25 eV: 707, 561, <b>543</b> , 435, 289, 271, 125	C <sub>45</sub> H <sub>37</sub> O <sub>16</sub>	(epi)afz-(epi)afz-(epi)cat III	BF-Mi, EAF-Mi	(de Souza et al., 2008; Ge et al., 2016; Olivaro et al., 2022)
4.85	273.0772	273.0768	1.46	15 eV: 255, 229, 205, 187, 169, 151, <b>137</b> , 125, 109, 87	C <sub>15</sub> H <sub>13</sub> O <sub>5</sub>	afzelechin	EAF-Mi	Costa Silva et al. (2019)
5.25	755.2034	755.2040	-0.79	30 eV: 301, <b>300</b>	C <sub>33</sub> H <sub>40</sub> O <sub>20</sub>	quercetin rhamnosyl-rutinoside	BF-Mi, EAF-Mi	(de Moura et al., 2021; Olivaro et al., 2022)
5.30	609.1474	609.1461	2.13	30 eV: 343, <b>300</b> , 271, 178	C <sub>27</sub> H <sub>30</sub> O <sub>16</sub>	quercetin robinoside I	BF-Mi, EAF-Mi	(de Souza et al., 2008; Sakna et al., 2019; Olivaro et al., 2022)
5.61	561.1409	561.1402	2.85	20 eV: 435, 407, <b>289</b> , 271, 245, 125	C <sub>30</sub> H <sub>26</sub> O <sub>11</sub>	(epi)afz-(epi)cat II	EAF-Mi	(de Souza et al., 2008; Ge et al., 2016; Olivaro et al., 2022)
5.66	739.2094	739.2091	0.41	20 eV: 593, 575, 285, <b>284</b> , 257, 255	C <sub>33</sub> H <sub>39</sub> O <sub>19</sub>	kaempferol dirhamnosyl-hexoside	BF-Mi, EAF-Mi	(Sakna et al. (2019)
5.73	593.1527	593.1512	2.53	30 eV: 327, 285, <b>284</b> , 255, 178	C <sub>27</sub> H <sub>30</sub> O <sub>15</sub>	kaempferol robinoside	BF-Mi, EAF-Mi	(de Souza et al., 2008; Sakna et al., 2019)
6.02	609.1477	609.1461	2.63	30 eV: 301, <b>300</b> , 271, 178	C <sub>27</sub> H <sub>30</sub> O <sub>16</sub>	quercetin robinoside II	BF-Mi	(de Souza et al., 2008; Sakna et al., 2019; Olivaro et al., 2022)
6.04	463.0890	463.0882	1.72	30 eV: <b>301</b> , 271, 255, 179, 151, 121	C <sub>21</sub> H <sub>20</sub> O <sub>12</sub>	quercetin hexoside	BF-Mi, EAF-Mi	(de Souza et al., 2008; Sakna et al., 2019; Olivaro et al., 2022)
	833.2083	833.2087	-0.48	25 eV: 707, <b>561</b> , 543, 435, 289, 271, 125	C <sub>45</sub> H <sub>38</sub> O <sub>16</sub>	(epi)afz-(epi)afz-(epi)cat IV	EAF-Mi	(de Souza et al., 2008; Ge et al., 2016; Olivaro et al., 2022)
6.34	447.0949	447.0933	3.58	30 eV: 327, 284, <b>285</b> , 255, 227, 151	C <sub>21</sub> H <sub>20</sub> O <sub>11</sub>	kaempferol hexoside or luteolin hexoside	EAF-Mi	(Abu-Reidah et al., 2015b; de Moura et al., 2021)
6.43	563.1414	563.1406	1.42	30 eV: 285, <b>284</b> , 255, 227, 179	C <sub>26</sub> H <sub>27</sub> O <sub>14</sub>	kaempferol rhamnosyl-hexoside	BF-Mi, EAF-Mi	Hamed et al. (2016)

The numbers in bold indicate the base peak. Note: BF-Mi: n-butanol fraction; EAF-Mi: ethyl acetate fraction; cat: catechin, afz: afzelechin, gal: galocatechin. <sup>a</sup><https://mona.fiehnlab.ucdavis.edu/spectra/display/CCMSLIB00000845599>.

### 3.3. Phytochemical prospections - total phenols, flavonoids, and condensed tannins

The fractions with the lowest reference values (mg of GAE/g) in total phenols content were HMF-Mi ( $50.71 \pm 38.87$ ) and DMF-Mi ( $72.87 \pm 13.09$ ), while the other fractions showed values above 100 mg GAE/g. EAF-Mi ( $656.52 \pm 32.19$ ) and BF-Mi ( $439.38 \pm 34.72$ ) were the fractions with the highest reference values (mg QE/g) in flavonoid content, and the fraction with the lowest value was HMF-Mi ( $60.61 \pm 6.14$ ). In the condensed tannin analysis, the fractions with the highest reference values (mg CE/g) were again EAF-Mi ( $2676.38 \pm 182.42$ ) and BF-Mi ( $1014.86 \pm 61.47$ ), while the fractions with the lowest values were HMF-Mi ( $67.02 \pm 1.98$ ) and DMF-Mi ( $152.55 \pm 3.96$ ). Additional details can be found in the Supplementary Material.

### 3.4. Antioxidant property of *M. ilicifolia* leaves extract and its fractions

The antioxidant results are presented in Fig. 1. In the evaluation of total antioxidant capacity using the FRAP method (Fig. 1A), EAF-Mi exhibited the highest values, reaching levels similar to the reference molecule quercetin ( $954 \pm 51.43$  and  $987.8 \pm 10.15$   $\mu\text{mol Trolox eq. eg}^{-1}$ , respectively). When comparing the extract and other fractions of *M. ilicifolia*, they showed decreasing antioxidant capacity in the following order: BF-Mi (752), EE-Mi (671), HF-Mi (524.6), DMF-Mi (512), and HMF-Mi (174), with values ranging from 752 to 174  $\mu\text{mol Trolox eq. eg}^{-1}$ . In addition, all fractions showed values higher than quercetin ( $2279 \pm 18.45$   $\mu\text{mol Trolox eq. eg}^{-1}$ ) in the ORAC method

(Fig. 1B) against the oxidation of the peroxy radical but without statistical significance. EAF-Mi had the highest gross value ( $2510 \pm 67.98$ ). In the DPPH assay (Fig. 1C), quercetin and the samples EAF-Mi and EE-Mi exhibited the lowest  $\text{EC}_{50}$  values ( $0.36 \pm 0.13$ ;  $2.42 \pm 0.57$ ;  $5.66 \pm 1.2$ , respectively). The other fractions exhibited higher  $\text{EC}_{50}$  values and were statistically different from quercetin.

### 3.5. *M. ilicifolia* leaves extract and its fractions decrease protein glycation and AGEs productions

The measurement of antiglycation activity assesses the ability of both reference molecules, such as quercetin, and molecules present in the ethanolic extract of *M. ilicifolia* leaves and its organic fractions to inhibit the glycation of proteins (albumin and LDL) and the amino acid arginine by methylglyoxal (MGO) or fructose models. The inhibition results were presented in Fig. 2 as percent values of antiglycation activity and  $\text{EC}_{50}$  values. In the BSA/FRU model (Fig. 2A), the samples that demonstrated better antiglycation activity against fructose were BF-Mi ( $18.26 \pm 2.04$   $\mu\text{g/mL}$ ) and HMF-Mi ( $43.82 \pm 13.72$   $\mu\text{g/mL}$ ). In contrast, quercetin showed a much lower value ( $1.62 \pm 0.60$   $\mu\text{g/mL}$ ), and DMF-Mi and EAF-Mi fractions did not show sufficient antiglycation activity. In the BSA/MGO model (Fig. 2B), all samples showed lower antiglycation activities compared to the positive control, quercetin. The  $\text{EC}_{50}$  values for quercetin ( $43.3 \pm 4.8$ ) were at least four times lower than those of the fractions. Among the fractions, the best  $\text{EC}_{50}$  values were EAF-Mi ( $166.1 \pm 25.95$   $\mu\text{g/mL}$ ) and HF-Mi ( $355.2 \pm 57.28$   $\mu\text{g/mL}$ ), while the hydromethanolic residual fraction did not show activity.

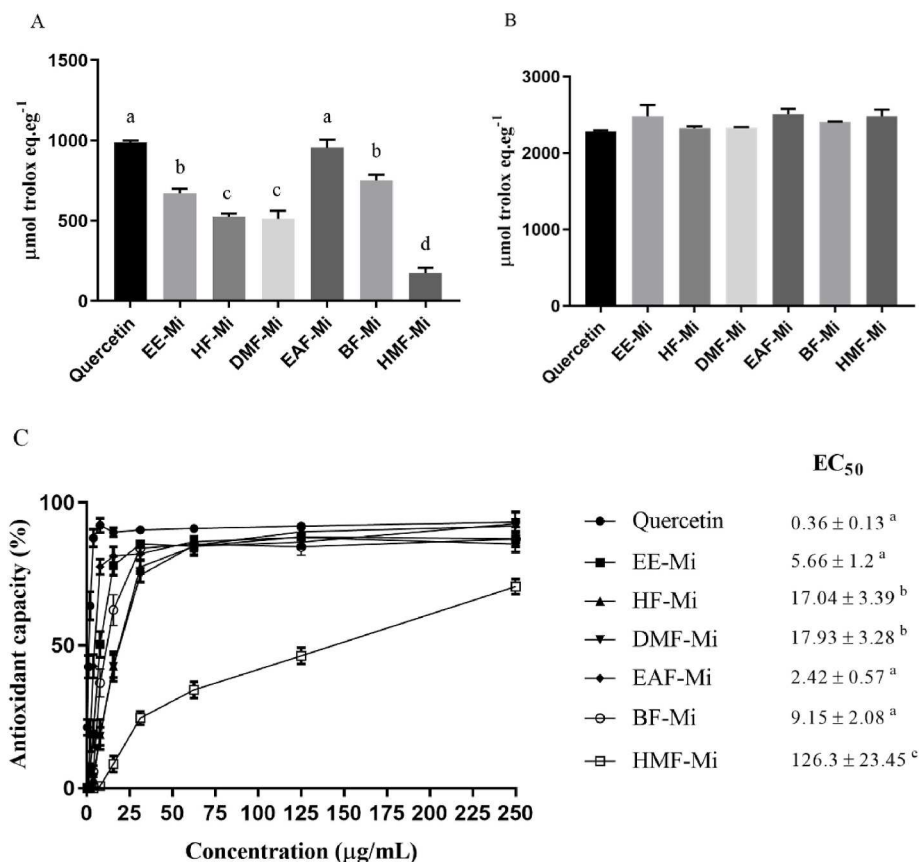
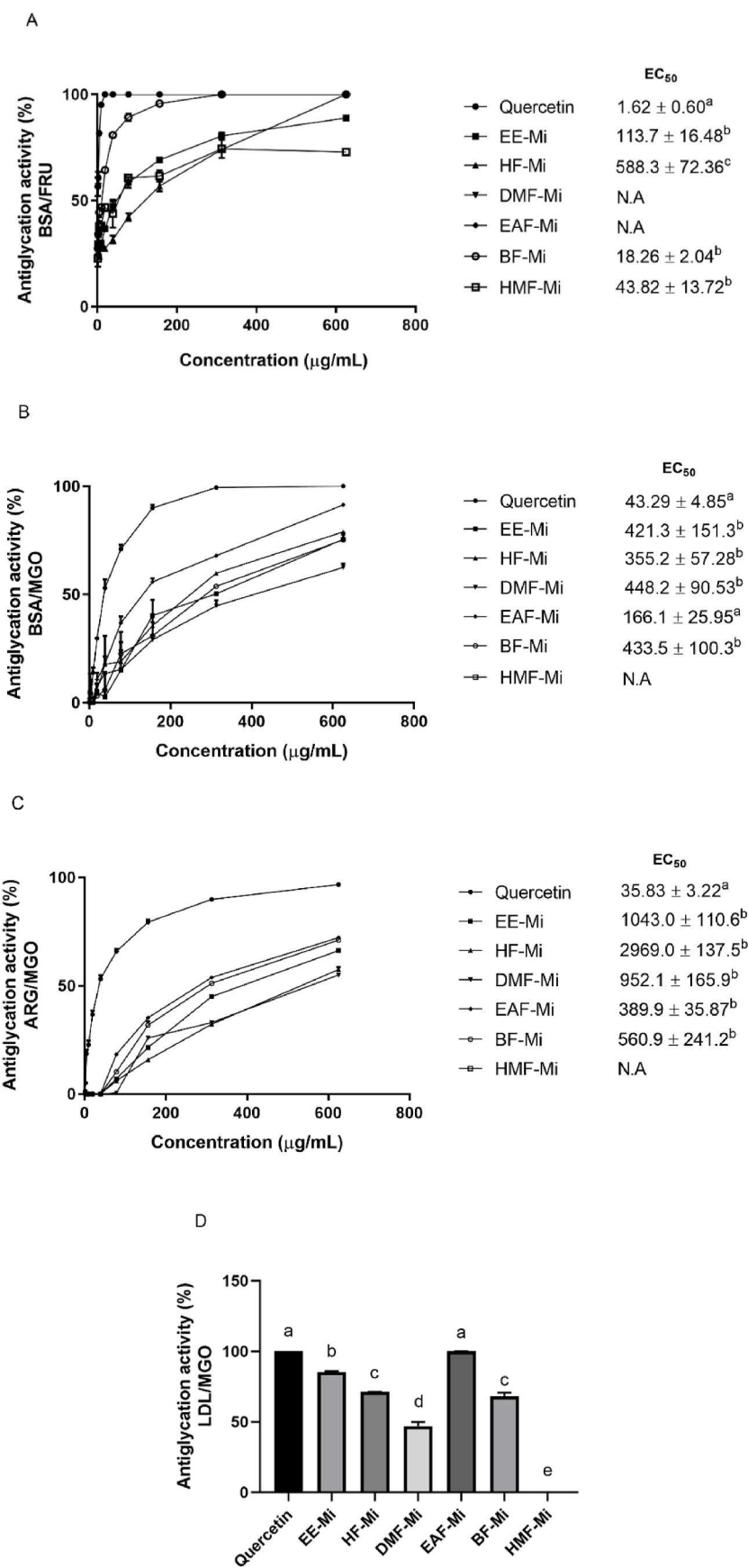


Fig. 1. Analysis of antioxidant capacity of *M. ilicifolia* ethanolic extract and organic fractions using FRAP (A), ORAC (B), and DPPH (C) methods. The data is presented as mean values with standard deviation ( $\pm$ ) expressed as  $\mu\text{mol}$  of trolox equivalents per gram ( $\text{eq. g}^{-1}$ ) for FRAP and ORAC assays and as a percentage of antioxidant capacity for DPPH assay. The  $\text{EC}_{50}$  values are presented as the mean and standard error of the mean ( $\pm$ ). The concentration of 285  $\mu\text{g/mL}$  and 100  $\mu\text{g/mL}$  were used for FRAP and ORAC assays, respectively, while for the DPPH assay, a serial dilution starting at 250  $\mu\text{g/mL}$  was made. Note: EE-Mi: ethanolic extract, HF-Mi: hexane fraction, DMF-Mi: dichloromethane fraction, EAF-Mi: ethyl acetate fraction, BF-Mi: *n*-butanol fraction, HMF-Mi: aqueous fraction. Quercetin was used as a positive control. Different letters indicate statistical significance ( $p < 0.05$ ).



(caption on next page)

**Fig. 2.** Analysis of the glycation inhibition capacity of fructose (FRU) or methylglyoxal (MGO) in the target models of bovine serum albumin (BSA), low-density lipoprotein (LDL), and the amino acid arginine (ARG) by quercetin and the ethanolic extract of *M. ilicifolia* and its organic fractions. The EC<sub>50</sub> values of BSA/Fructose (A), BSA/MGO (B), BSA/ARG (C), and LDL/MGO (D) models are expressed as mean and standard error ( $\pm$ ). A serial dilution starting at 600  $\mu\text{g/mL}$  was made for BSA/Fructose, BSA/MGO, and BSA/ARG models, while the LDL/MGO model was tested with a concentration of 100  $\mu\text{g/mL}$ . Quercetin was used as a positive control in all models. N.A.: No activity. Note: EE-Mi: ethanolic extract, HF-Mi: hexane fraction, DMF-Mi: dichloromethane fraction, EAF-Mi: ethyl acetate fraction, BF-Mi: *n*-butanol fraction, HMF-Mi: aqueous fraction. Different letters indicate statistical significance ( $p < 0.05$ ).

In the ARG/MGO model (Fig. 2C), EAF-Mi ( $218.6 \pm 35.87 \mu\text{g/mL}$ ) and DMF-Mi ( $416.8 \pm 165.9 \mu\text{g/mL}$ ) obtained the lower EC<sub>50</sub>. The other fractions obtained similar values, and HMF-Mi did not show significant results. Quercetin in this ARG/MGO model presented significantly lower values ( $35.83 \pm 3.22 \mu\text{g/mL}$ ).

To investigate the potential of *M. ilicifolia* samples on human LDL, the antiglycation activity was extended to the LDL/MGO model. The results are presented as the percentage of glycation inhibition activity (Fig. 2D). The EAF-Mi sample ( $99.91 \pm 0.12\%$ ) showed the best response and was statistically similar to quercetin. The other fractions also exhibited inhibitory activity, with inhibition capacity ranging between 85.71% and 68% for EE-Mi, HF-Mi, and BF-Mi, respectively. The DMF-Mi fraction had an inhibition capacity of less than 50%. The residual HMF-Mi fraction did not show any inhibitory activity on LDL glycation.

### 3.6. *M. ilicifolia* leaves extract and its fractions prevent lipid peroxidation and production of ROS in hepatic tissue

The hepatic tissue underwent oxidation and lipid peroxidation (OHT) induced by *in vitro* incubation with Fe<sup>2+</sup>-ascorbate, as indicated by the dosage of malondialdehyde expressed as nmol of MDA/mg of proteins by the thiobarbituric acid reactive substance (TBARS) method (Fig. 3). The value obtained ( $0.36 \pm 0.011$ ) was significantly higher than that obtained when the supernatant was incubated with PBS alone ( $0.09 \pm 0.03$ ). However, when the liver supernatant exposed to the oxidation inducer was simultaneously incubated with quercetin or *M. ilicifolia* samples, the ascending order of protection was as follows: quercetin ( $0.09 \pm 0.03$ ), BF-Mi ( $0.09 \pm 0.008$ ), EAF-Mi (0.10), EE-Mi ( $0.11 \pm 0.005$ ), and HMF-Mi ( $0.17 \pm 0.002$ ). The DMF-Mi fraction ( $0.26 \pm$

$0.008$ ) was not very effective in this protection. HF-Mi ( $0.39 \pm 0.024$ ) induced an oxidative state equivalent to Fe<sup>2+</sup>-ascorbate.

### 3.7. *M. ilicifolia* leaves extract and its fractions inhibit oxidation and lipid peroxidation of LDL

To investigate *in vitro* LDL oxidation, copper ion incubation was used, and the LDL oxidation status was inhibited with quercetin, and *M. ilicifolia* samples (Fig. 4A). The level of lipid peroxidation of LDL induced by the oxidative state in the presence of copper ions was also determined (Fig. 4B). The crude ethanolic extract EE-Mi showed the greatest inhibition potential (expressed as area under the curve, AUC) ( $0.76 \pm 0.38$ ), followed by the organic fractions HF-Mi ( $1.50 \pm 0.34$ ) and BF-Mi ( $2.35 \pm 0.58$ ), which were all statistically similar to non-oxidized LDL ( $1.30 \pm 0.002$ ) (Fig. 4A). The inhibitory effect was more pronounced in the quantification of MDA resulting from LDL oxidation (Fig. 4B), where quercetin and all *M. ilicifolia* samples were able to inhibit 100% of lipid peroxidation. The oxidized LDL obtained a value of  $0.52 \pm 0.02 \mu\text{mol MDA/mg protein}$ .

### 3.8. *M. ilicifolia* leaves extract and its organic fractions inhibit $\alpha$ -amylase, butyrylcholinesterase, and acetylcholinesterase

The  $\alpha$ -amylase inhibitory activity of *M. ilicifolia* samples was evaluated, and acarbose was used as a positive control in the inhibition assay. The samples underwent a 10-point serial dilution, starting at 250  $\mu\text{g/mL}$ . The results of  $\alpha$ -amylase inhibition by *M. ilicifolia* are presented in Fig. 5A. The EC<sub>50</sub> values ( $\mu\text{g/mL}$ ) were statistically similar for acarbose ( $0.144 \pm 0.03$ ), EAF-Mi ( $2.42 \pm 0.57$ ), and BF-Mi ( $7.95 \pm 2.52$ ). However, the EC<sub>50</sub> for EE-Mi was higher and significantly different from the others ( $23.83 \pm 6.94$ ). HF-Mi, DMF-Mi, and HMF-Mi did not show any inhibitory activity on  $\alpha$ -amylase.

Acetylcholinesterase (AChE) and butyrylcholinesterase (BuChE) enzymes were incubated with drugs that inhibit their activity and *M. ilicifolia* samples (550  $\mu\text{g/mL}$ ). The percentage inhibition results are shown in Fig. 5B and C. The DMF-Mi (56.84%) and EAF-Mi (52.18%) fractions showed inhibitory activity on BuChE with values significantly similar to galanthamine and rivastigmine controls, which inhibited BuChE above 80%. The other fractions showed results below 50% inhibition. In contrast, AChE inhibition was below 50% in all samples. The organic fractions that inhibited AChE close to 50% were EAF-Mi (49.49%) and BF-Mi (44.77%). As expected, galantamine was very efficient in inhibiting AChE, whereas rivastigmine exhibited lower inhibitory activity than all samples.

### 3.9. Analysis of the cellular viability of *M. ilicifolia* ethanolic extract and its organic fractions

The effects of EE-Mi and its organic fractions on cellular viability were tested *in vitro* using murine RAW 264.7 macrophages. All samples of *M. ilicifolia* at a dose of 10  $\mu\text{g/mL}$  induced low cytotoxicity in murine RAW 264.7 macrophages, presenting the following values: EE-Mi (88.36%), HF-Mi (73.57.07%), DMF-Mi (96.60%), EAF-Mi (100%), BF-Mi (100%), and HMF-Mi (100%). At 100  $\mu\text{g/mL}$ , DMF-Mi caused high toxicity (15.40%) in macrophages, while the other samples (EE-Mi, HF-Mi, EAF-Mi, BF-Mi, and HMF-Mi) were able to maintain cell viability. However, at concentrations of 500 and 1000  $\mu\text{g/mL}$ , murine RAW 264.7 macrophages showed high toxicity, and cell viability did not

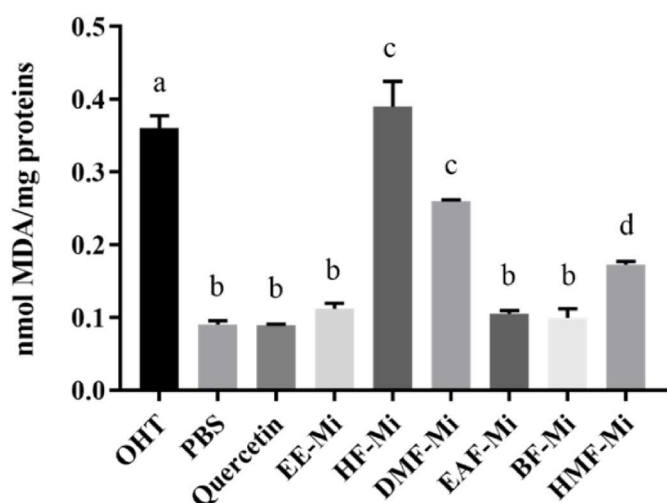


**Fig. 3.** Analysis of lipid peroxidation (MDA content) in healthy rat liver supernatant challenged *in vitro* with Fe<sup>2+</sup>-ascorbate (oxidized hepatic tissue - OHT) and co-treated with the ethanolic extract and organic fractions of *M. ilicifolia* (50  $\mu\text{g/mL}$ ). The mean and standard deviation ( $\pm$ ) values are expressed as nmol MDA/mg protein. Note: EE-Mi: ethanolic extract, HF-Mi: hexane fraction, DMF-Mi: dichloromethane fraction, EAF-Mi: ethyl acetate fraction, BF-Mi: *n*-butanol fraction, HMF-Mi: aqueous fraction. Quercetin (50  $\mu\text{g/mL}$ ) was used as a positive control. Different letters indicate statistical significance ( $p < 0.05$ ).

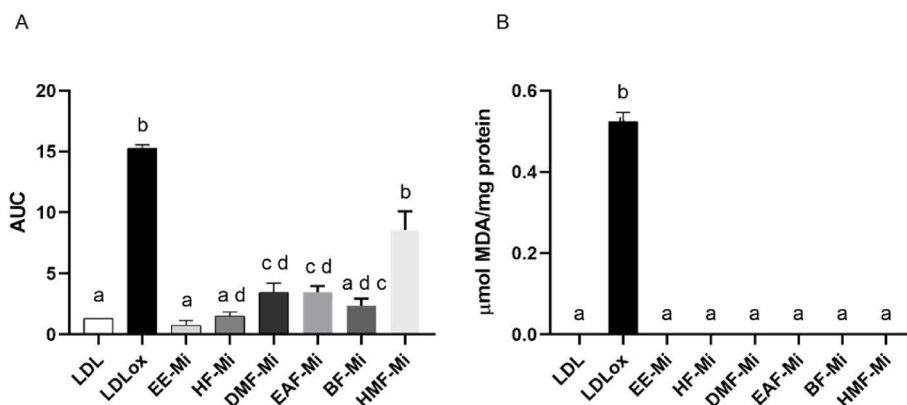


**Fig. 4.** In vitro analysis of human low-density lipoprotein (LDL) exposed to  $\text{Cu}^{2+}$  oxidation and co-treated with quercetin, the ethanolic extract, and the organic fractions of *M. ilicifolia*. LDL oxidation was measured as AUC (area under the curve) (A), and lipid peroxidation was measured as MDA content (B). Mean and standard deviation ( $\pm$ ) values are expressed as AUC and  $\mu\text{mol}$  MDA/mg protein, respectively. All samples were tested at a concentration of  $1 \mu\text{g}/\text{mL}$ . Note: EE-Mi: ethanolic extract, HF-Mi: hexane fraction, DMF-Mi: dichloromethane fraction, EAF-Mi: ethyl acetate fraction, BF-Mi: *n*-butanol fraction, HMF-Mi: aqueous fraction. LDLox: oxidized low-density lipoprotein. Quercetin was used as a positive control. Different letters indicate statistical significance ( $p < 0.05$ ).

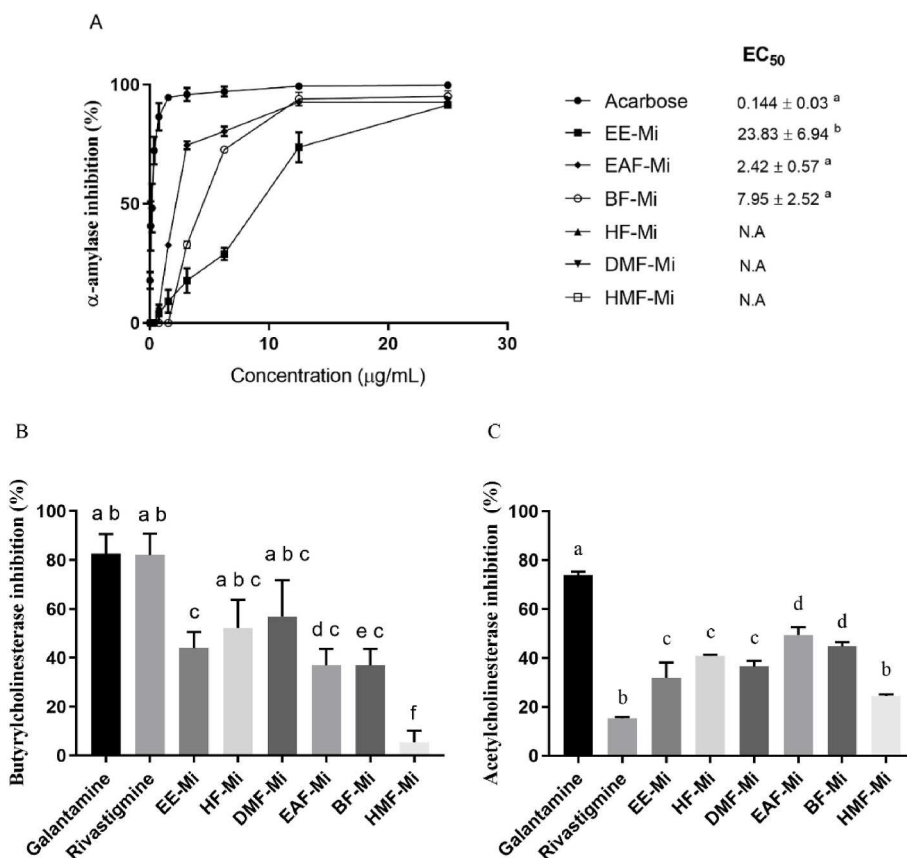


**Fig. 5.** Inhibition activities of  $\alpha$ -amylase (A), butyrylcholinesterase (B), and acetylcholinesterase (C) by the ethanolic extract and organic fractions of *M. ilicifolia*. The EC<sub>50</sub> values are expressed as the mean and standard error of the mean ( $\pm$ ). For all samples, the butyrylcholinesterase and acetylcholinesterase assays used a concentration of  $550 \mu\text{g}/\text{mL}$ , while a serial dilution starting at  $25 \mu\text{g}/\text{mL}$  was used for  $\alpha$ -amylase. Note: EE-Mi: ethanolic extract, HF-Mi: hexane fraction, DMF-Mi: dichloromethane fraction, EAF-Mi: ethyl acetate fraction, BF-Mi: *n*-butanol fraction, HMF-Mi: aqueous fraction. Acarbose, galantamine, and rivastigmine were used as positive controls. N.A: No activity. Different letters indicate statistical significance ( $p < 0.05$ ).

exceed 30%. The calculated cytotoxic concentrations (CC<sub>50</sub>) for EE-Mi (242.66), DMF-Mi (407.93), BF-Mi (366), EAF-Mi (371.85), HF-Mi (241.75), and HMF-Mi (365.84). Details can be found in the Supplementary Material.

### 3.10. Analysis of the antimicrobial activity of *M. ilicifolia* ethanolic extract and its organic fractions

Although all tested samples did not show significant results against aerobic skin bacteria, including *Staphylococcus aureus* ATCC 29213, *Staphylococcus epidermidis* ATCC 1228, *Pseudomonas aeruginosa* ATCC 27853, and *Burkholderia cepacia* ATCC 25416, EAF-Mi showed the



highest inhibition value (62.5 µg/mL) against *Burkholderia cepacia* ATCC 25416 (details can be found in the [Supplementary Material](#)).

#### 4. Discussion

Bioactive molecules extracted from natural compounds with therapeutic potential have become an increasingly popular alternative for the treatment of various pathologies in recent years (Harvey et al., 2015). *Maytenus ilicifolia* leaves have been used in traditional medicine to treat gastritis, ulcers, and other gastric disorders (de Carvalho Meirelles et al., 2022). In this study, Our aim was to characterize the ethanolic extract of *Maytenus ilicifolia* leaves, as well as its organic fractions obtained by liquid-liquid partitioning, in terms of their *in vitro* antioxidant and anti-glycation activities, their capacity to inhibit lipid peroxidation in rat hepatic tissue and human LDL, their potential to inhibit enzyme activity, antimicrobial activity, and cell viability. Additionally, the molecules extracted from the organic solvents ethyl acetate and *n*-butanol were elucidated through HPLC-ESI-MS/MS analysis. The total phenols, polyphenols, and tannins in the ethanolic extract of *M. ilicifolia* and its organic fractions support their antioxidant potential and their capacity to inhibit human LDL oxidation and lipid peroxidation, as well as inhibit lipid peroxidation in rat hepatic tissue. Kaempferol, quercetin, and derivatives of catechin are molecules with high antioxidant capacity (Xu et al., 2019; Ahmadi et al., 2020; Lima Júnior et al., 2021; Simunkova et al., 2021) that were found in the EAF-Mi and BF-Mi organic fractions. This may explain the protective effect of these fractions against the glycation of human LDL.

In this study, three methods were used to assess the total antioxidant activity of the samples. Each method elucidated a different antioxidation pathway. The FRAP assay was used to determine the sample's ability to chelate metal ions through electron donation, while the DPPH assay was used to evaluate the sample's radical scavenging ability. The ORAC assay was used to assess the sample's ability to reduce hydrogen molecules (Fig. 1A/B/C). The results showed that all the samples, except for HMF-Mi in the FRAP assay, had antioxidant capacity. This capacity was attributed to the active compounds found in the samples that can scavenge free radicals, reduce hydrogen molecules, and act as electron donors (Grzesik et al., 2018; Xu et al., 2019). Previous studies have already shown that the antioxidant capacity of *M. ilicifolia* is proportional to its total polyphenol content (Pessuto et al., 2009). Moreover, the highest amount of total phenols was observed in EAF-Mi and BF-Mi, as identified through phytochemical prospection. This finding may explain the higher antioxidant capacity of these fractions compared to the others.

The oxidation of LDL can be initiated by oxidative stress, which may cause complications in the body and even lead to the onset of atherosclerosis in the long term (Niki, 2018). The present study highlights the significant potential of *M. ilicifolia* in protecting LDL from oxidation. It has been shown that polyphenols, such as quercetin and catechin, can interact with the surface of LDL through sites containing fatty acids or sugar residues, thereby shielding these structures from free radical attack. Additionally, these molecules can protect LDL from oxidation by scavenging free radicals and chelating transition metal ions (Grzesik et al., 2018; Xu et al., 2019).

The ethanolic extract and fractions of *M. ilicifolia*, at a concentration as low as 1 µg/mL, inhibit 100% of lipid peroxidation induced by LDL oxidation. *M. ilicifolia* contains molecules that can inhibit the lipid peroxidation process by interacting with the metal ion Cu<sup>2+</sup>, which is used in the experiment to induce LDL oxidation (Kaurinovic and Vastag, 2019). Additionally, these molecules can interact directly with the hydrophobic portion of membrane lipids, thereby protecting them from oxidation and maintaining membrane integrity, or they can donate an electron to stabilize a free radical present in the medium (Ciumârnean et al., 2020). In the malondialdehyde quantification test in liver tissue, EE-Mi, EAF-Mi, and BF-Mi showed a high capacity to reduce lipid peroxidation. The presence of antioxidant compounds can decrease the

process of lipid peroxidation by controlling the production of reactive oxygen species (Gaschler and Stockwell, 2017). A previous study showed that the ethanolic extract and organic fractions of *Annona muricata* were able to inhibit lipid peroxidation due to the high concentration of glycosylated derivatives of quercetin, kaempferol, and catechin, which are the same molecules found in the most active fractions in this study, EAF-Mi and BF-Mi (Justino et al., 2018). Furthermore, LDL oxidation is associated with LDL glycation, which can lead to an increase in vascular dysfunction (Younis et al., 2008; Chen et al., 2010).

Advanced glycation end products (AGEs) result from a non-enzymatic reaction between reducing sugars and amino acids, and various factors such as high blood glucose levels, diet, and smoking habits can increase their production. The accumulation of AGEs can modify various biological structures, such as long-lived proteins, including bovine serum albumin (Singh et al., 2001; Muraoka et al., 2022). *In vitro* methods have been developed to evaluate the anti-glycation ability of a given compound. In the present study, it was observed that EAF-Mi exhibited the strongest inhibitory activity against BSA and arginine glycation induced by methylglyoxal, with the lowest EC<sub>50</sub> value among the other fractions. Additionally, BF-Mi demonstrated satisfactory glycation inhibition activity, particularly in the BSA/FRU model.

A previous study has shown that AGEs formation can be prevented by compounds with antioxidant and metal ion chelating properties (Xie and Chen, 2013). Molecules possessing these properties were found in both EAF-Mi and BF-Mi, suggesting that these fractions act against the glycation process. Catechins and proanthocyanidins have the ability to inhibit the binding of amino groups, reactive carbonyl compounds, and the auto-oxidation of sugars, thus blocking the formation of Schiff bases (Perez Gutierrez and Velazquez, 2020). Preventing the formation of AGEs helps to maintain the integrity of biological structures and reduces the binding of AGE-RAGE, thereby contributing to a decrease in oxidative stress (Singh et al., 2001).

Plants with therapeutic potential have become a complementary treatment for various diseases, including type 2 diabetes. Inhibition of glycosidic hydrolases may reduce postprandial blood hyperglycemia levels and consequently decrease ROS and AGEs formation in diabetic patients (Tan et al., 2017). In the present study, EAF-Mi and BF-Mi inhibited α-amylase enzyme activity. These samples contain catechin and its analogs, which are known to be strong inhibitors of α-amylase due to their non-hydrolyzable oligomeric structures that can occupy the substrate binding site on the enzyme (Yilmazer-Musa et al., 2012). Other studies have also demonstrated the high inhibitory ability of organic compounds with catechin groups and kaempferol derivatives against α-amylase enzyme activity (Franco et al., 2020; Justino et al., 2022).

In addition to α-amylase, the inhibitory potential of *M. ilicifolia* against AChE and BChE enzymes was investigated, as these enzymes play a crucial role in the development of Alzheimer's disease. The inhibitory potential of AChE and BChE of the ethanolic extract and the organic fractions of *M. ilicifolia* had not been previously elucidated. Our results demonstrate that the DMF-Mi, EAF-Mi, and BF-Mi fractions showed the highest inhibition values. Previous research has shown that both enzymes have 50% structural similarity (Rosenberry et al., 2017; Silman and Sussman, 2017) and are susceptible to the action of organic compounds (Novales and Schwans, 2022). Therefore, further studies should be conducted to investigate the inhibitory activity of the compounds found in *M. ilicifolia* leaves against these enzymes.

Compounds derived from botanical sources have attracted considerable attention from researchers due to their proven efficacy in combating bacteria, as well as their potential to possess other beneficial properties, including anti-inflammatory, antioxidant, and wound-healing effects (Pineau et al., 2019). The fractions EE-Mi, HF-Mi, EAF-Mi, and BF-Mi have demonstrated significant growth inhibition activity against *Staphylococcus epidermidis* and *Burkholderia cepacia*. MIC values below 100 µg/mL for hydroalcoholic crude extracts or below 10 µg/mL for isolated compounds are considered promising when

evaluating the antibacterial activity of plant extracts, essential oils, and compounds isolated from natural sources (Ríos and Recio, 2005; Sarker et al., 2007). Based on the findings of these authors, the EE-Mi, HF-Mi, EAF-Mi, and BF-Mi samples exhibited promising antibacterial activity in this study.

Until now, the use of organic fractions of *M. ilicifolia* in the treatment of *Staphylococcus epidermidis* and *Burkholderia cepacian* had not been investigated. The antimicrobial activity of *M. ilicifolia* was documented in a previous study; however, in that study, the plant was used to combat *Helicobacter pylori*, a bacterium responsible for gastritis and ulcers that lodged in the stomach mucosa (Paula et al., 2021). The results of the study showed that the adhesion of the bacterium to the stomach mucosal cell was reduced in the presence of the plant.

At concentrations of 10 and 100 µg/mL, *M. ilicifolia* and its organic fractions did not exhibit cytotoxicity toward murine RAW 264.7 macrophages. Based on these promising *in vitro* results, this study encourages further *in vivo* studies on the ethanolic extract of *M. ilicifolia* and its organic fractions to better understand their mechanisms of action.

The present study provides valuable insights into the therapeutic potential of *Maytenus ilicifolia* leaves as a source of bioactive molecules with various beneficial properties. The characterization of the ethanolic extract and its organic fractions, along with the identification of key molecules such as kaempferol, quercetin, and derivatives of catechin, highlights their biological activities. These findings contribute to our understanding of *Maytenus ilicifolia* and pave the way for further research. Future *in vivo* studies are warranted to validate and explore the therapeutic efficacy of *Maytenus ilicifolia* and its organic fractions.

## 5. Conclusion

Overall, this study highlights the therapeutic potential of bioactive molecules extracted from *M. ilicifolia* leaves. The ethanolic extract and its organic fractions exhibited significant antioxidant activity, inhibitory effects on lipid peroxidation and glycation, inhibition of enzymes related to diabetes and Alzheimer's disease, and antimicrobial properties. These findings contribute to the growing body of evidence supporting the use of *Maytenus ilicifolia* as a natural alternative for the treatment of various pathologies. Further research should focus on exploring the *in vivo* effects and mechanisms of action of these bioactive compounds, which could potentially lead to the development of novel therapeutic strategies.

## Funding

This work was supported by the Foundation for Research Support of the Minas Gerais State-FAPEMIG (grants # APQ-01856-14, APQ-01981-16 and APQ-01612-18) and the National Institute of Science and Technology in Theranostics and Nanobiotechnology—INCT—TeraNano (CNPq grant # 465669/2014-0, <http://www.teranano.ufu.br/>). VPB and ALSB received fellowships from the Coordination for the Improvement of Higher Education Personnel (CAPES). FSE received scholarship grants from FAPEMIG (PPM-00503-18) and CNPq (PQ—Research productivity, process no. 312812/2021-3).

## Institutional review board statement

The study was conducted in accordance with the Declaration of Helsinki, and approved by the local Ethics Committee (CAAE 61082522.4.0000.5704) report 5.671.038.

## CRedit authorship contribution statement

**Vinicius Prado Bittar:** Conceptualization, Methodology, Software, Validation, Formal analysis, Investigation, Resources, Data curation, Writing – original draft, Writing – review & editing, Visualization, Supervision, Project administration, Methodology, Validation,

Investigation, Data curation. **Ana Luiza Silva Borges:** Conceptualization, Methodology, Software, Validation, Formal analysis, Investigation, Resources, Data curation, Writing – original draft, Writing – review & editing, Visualization, Supervision, Project administration, Methodology, Validation, Investigation, Data curation. **Allisson Benatti Justino:** Methodology, Validation, Investigation, Data curation. **Maria Sol Peña Carrillo:** Methodology, Validation, Investigation, Data curation. **Renner Francisco Mateus Duarte:** Methodology, Validation, Investigation, Data curation. **Nagela Bernadelli Sousa Silva:** Methodology, Validation, Investigation, Data curation, Formal analysis. **Daniela Silva Gonçalves:** Methodology, Validation, Investigation, Data curation, Formal analysis. **Diego Godina Prado:** Methodology, Validation, Investigation, Data curation, Formal analysis. **Iasmin Aparecida Cunha Araújo:** Methodology, Validation, Investigation, Data curation. **Mário Machado Martins:** Methodology, Validation, Investigation, Data curation, Formal analysis. **Carlos Henrique Gomes Martins:** Methodology, Validation, Investigation, Data curation, Formal analysis. **Françoise Vasconcelos Botelho:** Methodology, Validation, Investigation, Data curation. **Neide Maria Silva:** Methodology, Validation, Investigation, Data curation. **Alberto de Oliveira:** Methodology, Validation, Investigation, Data curation, Formal analysis. **Foued Salmen Espíndola:** Conceptualization, Methodology, Software, Validation, Formal analysis, Investigation, Resources, Data curation, Writing – original draft, Writing – review & editing, Visualization, Supervision, Project administration, Funding acquisition.

## Declaration of competing interest

The authors declare that they have no known competing financial interests or personal relationships that could have appeared to influence the work reported in this paper.

## Data availability

No data was used for the research described in the article.

## Acknowledgements

The authors would like to thank the Institute of Biotechnology of the Federal University of Uberlandia and Rede de Biotérios (REBIR) for all the structure and support provided to make this study possible.

## Appendix A. Supplementary data

Supplementary data to this article can be found online at <https://doi.org/10.1016/j.jep.2023.117315>.

## References

- Abu-Reidah, I.M., Ali-Shtayeh, M.S., Jamous, R.M., Arráez-Román, D., Segura-Carretero, A., 2015a. HPLC-DAD-ESI-MS/MS screening of bioactive components from *Rhus coriaria* L. (Sumac) fruits. *Food Chem.* 166, 179–191. <https://doi.org/10.1016/j.foodchem.2014.06.011>.
- Abu-Reidah, I.M., Ali-Shtayeh, M.S., Jamous, R.M., Arráez-Román, D., Segura-Carretero, A., 2015b. Comprehensive metabolite profiling of *Arum palaestinum* (Araceae) leaves by using liquid chromatography-tandem mass spectrometry. *Food Res. Int.* 70, 74–86. <https://doi.org/10.1016/j.foodres.2015.01.023>.
- Ahmadi, S.M., Farhoosh, R., Sharif, A., Rezaie, M., 2020. Structure-antioxidant activity relationships of luteolin and catechin. *J. Food Sci.* 85, 298–305. <https://doi.org/10.1111/1750-3841.14994>.
- Alqahtani, A.S., Li, K.M., Razmovski-Naumovski, V., Kam, A., Alam, P., Li, G.Q., 2021. Attenuation of methylglyoxal-induced glycation and cellular dysfunction in wound healing by *Centella cordifolia*. *Saudi J. Biol. Sci.* 28, 813–824. <https://doi.org/10.1016/j.sjbs.2020.11.016>.
- Atanasov, A.G., Waltenberger, B., Pferschy-Wenzig, E.M., Linder, T., Wawrosch, C., Uhrin, P., Temml, V., Wang, L., Schwaiger, S., Heiss, E.H., Rollinger, J.M., Schuster, D., Breuss, J.M., Bochkov, V., Mihovilovic, M.D., Kopp, B., Bauer, R., Dirsch, V.M., Stuppner, H., 2015. Discovery and resupply of pharmacologically active plant-derived natural products: a review. *Biotechnol. Adv.* 33, 1582–1614. <https://doi.org/10.1016/j.biotechadv.2015.08.001>.

- Baggio, C.H., Freitas, C.S., Otofujii, G. de M., Cipriani, T.R., Souza, L.M. de, Sasaki, G.L., Iacomini, M., Marques, M.C.A., Mesia-Vela, S., 2007. Flavonoid-rich fraction of *Maytenus ilicifolia* Mart. ex. Reiss protects the gastric mucosa of rodents through inhibition of both H<sup>+</sup>K<sup>+</sup>-ATPase activity and formation of nitric oxide. *J. Ethnopharmacol.* 113, 433–440. <https://doi.org/10.1016/j.jep.2007.06.015>.
- Benzie, I.F.F., Devaki, M., 2017. The ferric reducing/antioxidant power (FRAP) assay for non-enzymatic antioxidant capacity: concepts, procedures, limitations and applications. In: *Measurement of Antioxidant Activity & Capacity*. JWS, Ltd, Chichester, UK, pp. 77–106. <https://doi.org/10.1002/9781119153388.ch5>.
- Bradford, M., 1976. A rapid and sensitive method for the quantitation of microgram quantities of protein utilizing the principle of protein-dye binding. *Anal. Biochem.* 72, 248–254. <https://doi.org/10.1006/abio.1976.9999>.
- Brand-Williams, W., Cuvelier, M.E., Berset, C., 1995. Use of a free radical method to evaluate antioxidant activity. *LWT-Food Sci. Technol.* 28, 25–30. [https://doi.org/10.1016/S0023-6438\(95\)80008-5](https://doi.org/10.1016/S0023-6438(95)80008-5).
- Chen, K.C., Chuang, C.M., Lin, L.Y., Chiu, W.T., Wang, H.E., Hsieh, C.L., Tsai, T., Peng, R. Y., 2010. The polyphenolics in the aqueous extract of *Psidium guajava* kinetically reveal an inhibition model on LDL glycation. *Pharm. Biol.* 48, 23–31. <https://doi.org/10.3109/13880200903029365>.
- Chung, B.H., Segrest, J.P., Ray, M.J., Brunzell, J.D., Hokanson, J.E., Krauss, R.M., Beaudrie, K., Cone, J.T., 1986. [8] Single vertical spin density gradient ultracentrifugation. *Methods Enzymol.* 181–209. [https://doi.org/10.1016/0076-6879\(86\)28068-4](https://doi.org/10.1016/0076-6879(86)28068-4).
- Ciumărnean, L., Milaciu, M.V., Runcan, O., Vesa, Ștefan C., Răchișan, A.L., Negrean, V., Perné, M.-G., Donca, V.I., Alexescu, T.-G., Para, I., Dogaru, G., 2020. The effects of flavonoids in cardiovascular diseases. *Molecules* 25, 4320. <https://doi.org/10.3390/molecules25184320>.
- Costa Silva, T. da, Justino, A.B., Prado, D.G., Koch, G.A., Martins, M.M., Santos, P. de S., Morais, S.A.L. de, Goulart, L.R., Cunha, L.C.S., Sousa, R.M.F. de, Espindola, F.S., de Oliveira, A., 2019. Chemical composition, antioxidant activity and inhibitory capacity of  $\alpha$ -amylase,  $\alpha$ -glucosidase, lipase and non-enzymatic glycation, in vitro, of the leaves of *Cassia bakeriana* Craib. *Ind. Crops Prod.* 140, 111641. <https://doi.org/10.1016/j.indcrop.2019.111641>.
- Da Silva Santos, T.V., Teixeira, R.R., Franco, D.L., Madurro, J.M., Brito-Madurro, A.G., Espindola, F.S., 2012. Bioelectrode for detection of human salivary amylase. *Mater. Sci. Eng. C* 32, 530–535. <https://doi.org/10.1016/j.msec.2011.12.005>.
- de Carvalho Meirelles, G., Bianchi, S.E., Siqueira, I.R., Bassani, V.L., 2022. Phytochemistry and pharmaceutical Technology studies on *monteverdia ilicifolia* (Maytenus ilicifolia): a traditionally used medicinal plant. *Rev Bras Farmacog* 32, 859–870. <https://doi.org/10.1007/s43450-022-00311-4>.
- de Moura, F.B.R., Ferreira, B.A., Deconte, S.R., Landim, B.C., Justino, A.B., Aro, A.A. de, Espindola, F.S., Rodrigues, R.A.F., Ribeiro, D.L., Araújo, F. de A., Tomiosso, T.C., 2021. Wound healing activity of the hydroethanolic extract of the leaves of *Maytenus ilicifolia* Mart. *Ex Reiss. J. Tradit. Complement Med.* 11, 446–456. <https://doi.org/10.1016/j.jtcm.2021.03.003>.
- de Moura Martins, C., Morais, S.A.L. de, Martins, M.M., Cunha, L.C.S., v. da Silva, C., Teixeira, T.L., B. Santiago, M., de Aquino, F.J.T., Nascimento, E.A., Chang, R., Martins, C.H.G., de Oliveira, A., 2020. Antifungal and cytotoxicity activities and new proanthocyanidins isolated from the barks of *Inga laurina* (Sw.) Willd. *Phytochem. Lett.* 40, 109–120. <https://doi.org/10.1016/j.phytol.2020.10.001>.
- de Souza, L.M., Cipriani, T.R., Iacomini, M., Gorin, P.A.J., Sasaki, G.L., 2008. HPLC/ESI-MS and NMR analysis of flavonoids and tannins in bioactive extract from leaves of *Maytenus ilicifolia*. *J. Pharm. Biomed. Anal.* 47, 59–67. <https://doi.org/10.1016/j.jpba.2007.12.008>.
- do Nascimento, M.N.G., Machado Martins, M., Scalon Cunha, L.C., de Souza Santos, P., Goulart, L.R., de Souza Silva, T., Gomes Martins, C.H., de Morais, S.A.L., Pivatto, M., 2020. Antimicrobial and cytotoxic activities of *Senna* and *Cassia* species (Fabaceae) extracts. *Ind. Crops Prod.* 148, 112081. <https://doi.org/10.1016/j.indcrop.2019.112081>.
- Ellman, G.L., Courtney, K.D., Andres, V., Featherstone, R.M., 1961. A new and rapid colorimetric determination of acetylcholinesterase activity. *Biochem. Pharmacol.* 7, 88–95. [https://doi.org/10.1016/0006-2952\(61\)90145-9](https://doi.org/10.1016/0006-2952(61)90145-9).
- Franco, R.R., Hugo, V., Alves, M., Fernando, L., Zabisky, R., Justino, A.B., Martins, M.M., Saraiva, A.L., Goulart, L.R., Espindola, F.S., 2020. Biomedicine & Pharmacotherapy Antidiabetic potential of *Bauhinia forficata* Link leaves: a non-cytotoxic source of lipase and glycoside hydrolases inhibitors and molecules with antioxidant and antiglycation properties. *Biomed. Pharmacother.* 123, 109798. <https://doi.org/10.1016/j.biopha.2019.109798>.
- Fraternal, D., Ricci, D., Verardo, G., Gorassini, A., Stocchi, V., Sestili, P., 2015. Activity of *vitis vinifera* tendrils extract against phytopathogenic fungi. *Nat. Prod. Commun.* 10, 1037–1042. <https://doi.org/10.1177/19345578x1501000661>.
- Gaschler, M.M., Stockwell, B.R., 2017. Lipid peroxidation in cell death. *Biochem. Biophys. Res. Commun.* 482, 419–425. <https://doi.org/10.1016/j.bbrc.2016.10.086>.
- Ge, Y.W., Zhu, S., Kazuma, K., Wei, S.L., Yoshimatsu, K., Komatsu, K., 2016. Molecular ion index assisted comprehensive profiling of B-type oligomeric proanthocyanidins in rhubarb by high performance liquid chromatography-tandem mass spectrometry. *Anal. Bioanal. Chem.* 408, 3555–3570. <https://doi.org/10.1007/s00216-016-9433-z>.
- Gieseg, S.P., Esterbauer, H., 1994. Low density lipoprotein is saturable by pro-oxidant copper. *FEBS Lett.* 343, 188–194. [https://doi.org/10.1016/0014-5793\(94\)80553-9](https://doi.org/10.1016/0014-5793(94)80553-9).
- Gómez-Romero, M., Segura-Carretero, A., Fernández-Gutiérrez, A., 2010. Metabolite profiling and quantification of phenolic compounds in methanol extracts of tomato fruit. *Phytochemistry (Elsevier)* 71, 1848–1864. <https://doi.org/10.1016/j.phytochem.2010.08.002>.
- Groppo, M., Simmons, M.P., Cappa, J.J., Biral, L., Lombardi, J.A., 2014. A new species of *maytenus* (Celastraceae) with fleshy fruits from eastern Brazil, with notes on the delimitation of *maytenus*. *Syst. Bot.* 39, 478–484. <https://doi.org/10.1600/036364414X680726>.
- Grzesik, M., Napparlo, K., Bartosz, G., Sadowska-Bartos, I., 2018. Antioxidant properties of catechins: comparison with other antioxidants. *Food Chem.* 241, 480–492. <https://doi.org/10.1016/j.foodchem.2017.08.117>.
- Gu, L., Kelm, M.A., Hammerstone, J.F., Zhang, Z., Beecher, G., Holden, J., Haytowitz, D., Prior, R.L., 2003. Liquid chromatographic/electrospray ionization mass spectrometric studies of proanthocyanidins in foods. *J. Mass Spectrom.* 38, 1272–1280. <https://doi.org/10.1002/jms.541>.
- Hamed, A.I., Said, R. ben, Kontek, B., Al-Ayed, A.S., Kowalczyk, M., Moldoch, J., Stochmal, A., Olas, B., 2016. LC-ESI-MS/MS profile of phenolic and glucosinolate compounds in samh flour (*Mesembryanthemum forsskalei* Hochst. ex Boiss) and the inhibition of oxidative stress by these compounds in human plasma. *Food Res. Int.* 85, 282–290. <https://doi.org/10.1016/j.foodres.2016.04.009>.
- Harvey, A.L., Edrada-Ebel, R., Quinn, R.J., 2015. The re-emergence of natural products for drug discovery in the genomics era. *Nat. Rev. Drug Discov.* 14, 111–129. <https://doi.org/10.1038/nrd4510>.
- Justino, A.B., Barbosa, M.F., Neves, T.V., Silva, H.C.G., Brum, E. da S., Fialho, M.F.P., Couto, A.C., Saraiva, A.L., Avila, V. de M.R., Oliveira, S.M., Pivatto, M., Espindola, F. S., Silva, C.R., 2020. Stephalagine, an aporphine alkaloid from *Annona crassiflora* fruit peel, induces antinociceptive effects by TRPA1 and TRPV1 channels modulation in mice. *Bioorg. Chem.* 96. <https://doi.org/10.1016/j.bioorg.2019.103562>.
- Justino, A.B., Franco, R.R., Silva, H.C.G., Saraiva, A.L., Sousa, R.M.F., Espindola, F.S., 2019. B procyanidins of *Annona crassiflora* fruit peel inhibited glycation, lipid peroxidation and protein-bound carbonyls, with protective effects on glycated catalase. *Sci. Rep.* 9, 1–15. <https://doi.org/10.1038/s41598-019-55779-3>.
- Justino, A.B., Guerra Silva, H.C., Franco, R.R., de Oliveira Cavalcante Pimentel, I., Silva, N.F., Saraiva, A.L., Espindola, F.S., 2022. Flavonoids and proanthocyanidin-rich fractions from *Eugenia dysenterica* fruits and leaves inhibit the formation of advanced glycation end-products and the activities of  $\alpha$ -amylase and  $\alpha$ -glucosidase. *J. Ethnopharmacol.* 285. <https://doi.org/10.1016/j.jep.2021.114902>.
- Justino, A.B., Miranda, N.C., Franco, R.R., Martins, M.M., Silva, N.M. da, Espindola, F.S., 2018. *Annona muricata* Linn. leaf as a source of antioxidant compounds with in vitro antidiabetic and inhibitory potential against  $\alpha$ -amylase,  $\alpha$ -glucosidase, lipase, non-enzymatic glycation and lipid peroxidation. *Biomed. Pharmacother.* 100, 83–92. <https://doi.org/10.1016/j.biopha.2018.01.172>.
- Kaurinovic, B., Vastag, D., 2019. Flavonoids and phenolic acids as potential natural antioxidants. In: *Antioxidants*. Intech. <https://doi.org/10.5772/intechopen.83731>.
- Lima, D.D.C., Pitorro, T.E.A., Santiago, M.B., Franco, R.R., Silva, T. da C., Prado, D.G., Cunha, L.C.S., Espindola, F.S., Tavares, D.C., Nicoletta, H.D., Martins, C.H.G., Novais, V.R., 2022. In vitro evaluation of the antibacterial and cytotoxic activities of the *Euclea natalensis* crude extract and fractions against oral infection agents. *Arch. Oral Biol.* 143. <https://doi.org/10.1016/j.archoralbio.2022.105546>.
- Lima Júnior, J.P. de, Franco, R.R., Saraiva, A.L., Moraes, I.B., Espindola, F.S., 2021. *Anacardium humile* St. Hil as a novel source of antioxidant, antiglycation and  $\alpha$ -amylase inhibitors molecules with potential for management of oxidative stress and diabetes. *J. Ethnopharmacol.* 268. <https://doi.org/10.1016/j.jep.2020.113667>.
- Marston, A., Kissling, J., Hostettmann, K., 2002. A rapid TLC bioautographic method for the detection of acetylcholinesterase and butyrylcholinesterase inhibitors in plants. *Phytochem. Anal.* 13, 51–54. <https://doi.org/10.1002/pca.623>.
- Mosmann, T., 1983. Rapid colorimetric assay for cellular growth and survival: application to proliferation and cytotoxicity assays. *J. Immunol. Methods* 65, 55–63. [https://doi.org/10.1016/0022-1759\(83\)90303-4](https://doi.org/10.1016/0022-1759(83)90303-4).
- Muraoka, M.Y., Justino, A.B., Caixeta, D.C., Queiroz, J.S., Sabino-Silva, R., Espindola, F. S., 2022. Fructose and methylglyoxal-induced glycation alters structural and functional properties of salivary proteins, albumin and lysozyme. *PLoS One* 17. <https://doi.org/10.1371/journal.pone.0262369>.
- Navazesh, M., 1993. Methods for collecting saliva. *Ann. N. Y. Acad. Sci.* 694, 72–77. <https://doi.org/10.1111/j.1749-6632.1993.tb18343.x>.
- Niki, E., 2018. Free Radical Biology and Medicine Oxidant-specific biomarkers of oxidative stress. Association with atherosclerosis and implication for antioxidant effects. *Free Radic. Biol. Med.* 120, 425–440. <https://doi.org/10.1016/j.freeradbiomed.2018.04.001>.
- Novales, N.A., Schwans, J.P., 2022. Comparing the effects of organic cosolvents on acetylcholinesterase and butyrylcholinesterase activity. *Anal. Biochem.* 654, 114796. <https://doi.org/10.1016/j.ab.2022.114796>.
- Olivaro, C., Escobal, M., de Souza, G., Mederos, A., 2022. Chemical characterisation and in vitro anthelmintic activity of phenolic-rich extracts from the leaves and branches of *Maytenus ilicifolia*, a native plant from South America. *Nat. Prod. Res.* 36, 3168–3172. <https://doi.org/10.1080/14786419.2021.1948844>.
- Paula, M.N. De, Kelm, M., Symma, N., Garcia, R., Pilatti, F., Sendker, J., Hensel, A., Carlos, J., Mello, P. De, 2021. Anti-adhesive Activity of *Maytenus ilicifolia* against *Helicobacter pylori*. *Rev. Bras. Farmacogn.* 726–731. <https://doi.org/10.1007/s43450-021-00214-w>.
- Perez Gutierrez, R.M., Velazquez, E.G., 2020. Glucopyranoside flavonoids isolated from leaves of *Spinacia oleracea* (spinach) inhibit the formation of advanced glycation end products (AGEs) and aldose reductase activity (RLAR). *Biomed. Pharmacother.* 128, 110299. <https://doi.org/10.1016/j.biopha.2020.110299>.
- Pessuto, M.B., Costa, I.C. da, Souza, A.B. de, Nicoli, F.M., Mello, J.C.P. de, Petereit, F., Luftmann, H., 2009. Atividade antioxidante de extratos e taninos condensados das folhas de *Maytenus ilicifolia* Mart. ex Reiss. *Quim Nova* 32, 412–416. <https://doi.org/10.1590/S0100-40422009000200027>.
- Pineau, R.M., Hanson, S.E., Lyles, J.T., Quave, C.L., 2019. Growth inhibitory activity of *callicarpa americana* leaf extracts against cutibacterium acnes. *Front. Pharmacol.* 10, 1–12. <https://doi.org/10.3389/fphar.2019.01206>.

- Prior, R.L., Hoang, H., Gu, L., Wu, X., Bacchiocca, M., Howard, L., Hampsch-Woodill, M., Huang, D., Ou, B., Jacob, R., 2003. Assays for hydrophilic and lipophilic antioxidant capacity (oxygen radical absorbance capacity (ORACFL)) of plasma and other biological and food samples. *J. Agric. Food Chem.* 51, 3273–3279. <https://doi.org/10.1021/jf0262256>.
- Rhee, I.K., van de Meent, M., Ingkaninan, K., Verpoorte, R., 2001. Screening for acetylcholinesterase inhibitors from Amaryllidaceae using silica gel thin-layer chromatography in combination with bioactivity staining. *J. Chromatogr. A* 915, 217–223. [https://doi.org/10.1016/S0021-9673\(01\)00624-0](https://doi.org/10.1016/S0021-9673(01)00624-0).
- Ríos, J.L., Recio, M.C., 2005. Medicinal plants and antimicrobial activity. *J. Ethnopharmacol.* <https://doi.org/10.1016/j.jep.2005.04.025>.
- Rosenberry, T.L., Brazzolotto, X., MacDonald, I.R., Wandhammer, M., Trovaslet-Leroy, M., Darvesh, S., Nachon, F., 2017. Comparison of the binding of reversible inhibitors to human butyrylcholinesterase and acetylcholinesterase: a crystallographic, kinetic and calorimetric study. *Molecules* 22, 1–21. <https://doi.org/10.3390/molecules22122098>.
- Sakna, S.T., Mocan, A., Sultani, H.N., El-fiky, N.M., Wessjohann, L.A., Farag, M.A., 2019. Metabolites profiling of Ziziphus leaf taxa via UHPLC/PDA/ESI-MS in relation to their biological activities. *Food Chem.* 293, 233–246. <https://doi.org/10.1016/j.foodchem.2019.04.097>.
- Sarker, S.D., Nahar, L., Kumarasamy, Y., 2007. Microtitre plate-based antibacterial assay incorporating resazurin as an indicator of cell growth, and its application in the in vitro antibacterial screening of phytochemicals. *Methods* 42, 321–324. <https://doi.org/10.1016/j.jymeth.2007.01.006>.
- Silman, I., Sussman, J.L., 2017. Recent developments in structural studies on acetylcholinesterase. *J. Neurochem.* 142, 19–25. <https://doi.org/10.1111/jnc.13992>.
- Simunkova, M., Barbierikova, Z., Jomova, K., Hudcova, L., Lauro, P., Alwasel, S.H., Alhazza, I., Rhodes, C.J., Valko, M., 2021. Antioxidant vs. Prooxidant properties of the flavonoid, kaempferol, in the presence of cu(ii) ions: a ros-scavenging activity, fenton reaction and dna damage study. *Int. J. Mol. Sci.* 22, 1–17. <https://doi.org/10.3390/ijms22041619>.
- Singh, R., Barden, A., Mori, T., Beilin, L., 2001. Advanced glycation end-products: a review. *Diabetologia* 44, 129–146. <https://doi.org/10.1007/s001250051591>.
- Sobeh, M., Mahmoud, M.F., Abdelfattah, M.A.O., Cheng, H., El-Shazly, A.M., Wink, M., 2018. A proanthocyanidin-rich extract from *Cassia abbreviata* exhibits antioxidant and hepatoprotective activities in vivo. *J. Ethnopharmacol.* 213, 38–47. <https://doi.org/10.1016/j.jep.2017.11.007>.
- Tan, Y., Chang, S.K.C., Zhang, Y., 2017. Comparison of  $\alpha$ -amylase,  $\alpha$ -glucosidase and lipase inhibitory activity of the phenolic substances in two black legumes of different genera. *Food Chem.* 214, 259–268. <https://doi.org/10.1016/j.foodchem.2016.06.100>.
- Veloso, C.C., Soares, G.L., Perez, A.C., Rodrigues, V.G., Silva, F.C., 2017. Pharmacological potential of maytenus species and isolated constituents, especially tingenone, for treatment of painful inflammatory diseases. *Rev Bras Farmacogn.* <https://doi.org/10.1016/j.bjp.2017.02.006>.
- Wang, J., Zhou, Y., Hu, Y., 2011. Facile synthesis of nanocrystalline TiO<sub>2</sub> mesoporous microspheres for lithium-ion batteries. *J. Phys. Chem.* 2529–2536.
- Xie, Y., Chen, X., 2013. Structures required of polyphenols for inhibiting advanced glycation end products formation. *Curr. Drug Metabol.* 14, 414–431. <https://doi.org/10.2174/1389200211314040005>.
- Xu, D., Hu, M.J., Wang, Y.Q., Cui, Y.L., 2019. Antioxidant activities of quercetin and its complexes for medicinal application. *Molecules* 24. <https://doi.org/10.3390/molecules24061123>.
- Yagi, K., 1998. Simple procedure for specific assay of lipid hydroperoxides in serum or plasma. In: *Free Radic Antioxid Protocols*. Humana Press, New Jersey, pp. 107–110. <https://doi.org/10.1385/0-89603-472-0:107>.
- Yilmazer-Musa, M., Griffith, A.M., Michels, A.J., Schneider, E., Frei, B., 2012. Grape seed and tea extracts and catechin 3-gallates are potent inhibitors of  $\alpha$ -amylase and  $\alpha$ -glucosidase activity. *J. Agric. Food Chem.* 60, 8924–8929. <https://doi.org/10.1021/jf301147n>.
- Younis, N., Sharma, R., Soran, H., Charlton-Menys, V., Elseweidy, M., Durrington, P.N., 2008. Glycation as an atherogenic modification of LDL. *Curr. Opin. Lipidol.* 19, 378–384. <https://doi.org/10.1097/MOL.0b013e328306a057>.
- Zou, Y., Chang, S.K.C., Gu, Y., Qian, S.Y., 2011. Antioxidant activity and phenolic compositions of lentil (*Lens culinaris* var. Morton) extract and its fractions. *J. Agric. Food Chem.* 59, 2268–2276. <https://doi.org/10.1021/jf104640k>.

## REVIEW ARTICLE

# Diagnosis of biofilm infections: current methods used, challenges and perspectives for the future

N.B.S. Silva<sup>1</sup> , L.A. Marques<sup>2</sup> and D.D.B. Röder<sup>3</sup>

1 Applied Immunology and Parasitology, Institute of Biomedical Sciences, Federal University of Uberlândia, Uberlândia, Minas Gerais, Brazil

2 Health Sciences, Medical School, Federal University of Uberlândia, Uberlândia, Minas Gerais, Brazil

3 Institute of Biomedical Sciences, Federal University of Uberlândia, Uberlândia, Minas Gerais, Brazil

## Keywords

clinical practice, diagnosis of biofilm, *in vitro* methods, *in vivo* methods, MALDI-TOF MS, omics analysis.

## Correspondence

Nagela B.S. Silva, Applied Immunology and Parasitology, Institute of Biomedical Sciences, Federal University of Uberlândia, Av. Amazonas, S/N - Umuarama, Uberlândia, Minas Gerais, Brazil.

E-mail: nagela\_bernadelli.mg@hotmail.com

2021/1947: received 6 June 2020, revised 1 February 2021 and accepted 23 February 2021

doi:10.1111/jam.15049

## Introduction

Biofilms are microbial communities adhered to biotic or abiotic surfaces and protected by an extracellular polymeric matrix; they have been extensively investigated in recent decades (Costa-Orlandi *et al.* 2017). It is estimated that approximately 65% of microbial infections are caused by biofilm-forming microorganisms, representing a serious public health problem due to the evasion of the host immune system and the resistance of most antimicrobials used for treatment, increasing the persistence of the infection (Mooney *et al.* 2018). Additionally, biofilms contribute to the increase in morbidity and mortality rates and hospital costs, making it difficult to treat and eradicate infections, especially those formed in and on invasive devices such as catheters and implants (Jamal *et al.* 2018).

The diagnosis of biofilm-related infections continues to be a challenge since in most infections, the signs and

## Summary

The diagnosis of biofilms continues to be a challenge, and there is no standardized protocol for such a diagnosis in clinical practice. In addition, some proposed methodologies are expensive to require significant amounts of time and a high number of trained staff, making them impracticable for clinical practice. In recent years, mass spectrophotometry/matrix-assisted laser desorption ionization time of flight (MALDI-TOF) has been applied in biofilm studies. However, due to several problems and limitations of the technique, MALDI-TOF is far from being the gold standard for identifying biofilm formation. The omics analysis may prove to be a promising strategy for the diagnosis of biofilms in clinical laboratories since it allows the identification of pathogens in less time than needed for conventional techniques and in a more specific manner. However, omic tools are expensive and require qualified technical expertise, and an analysis of the data obtained needs to be careful not to neglect subpopulations in the biofilm. More studies must therefore be developed for creating a protocol that guarantees rapid biofilm identification, ensuring greater chances of success in infection control. This review discusses the current methods of microbial biofilm detection and future perspectives for its diagnosis in clinical practice.

symptoms that the patient presents are nonspecific (Jamal *et al.* 2018). Although there are several methods for diagnosing biofilms in research laboratories, there is no standardized protocol for such a diagnosis in clinical practice. Additionally, susceptibility tests to antimicrobials continue to be performed on planktonic bacteria, not representing the clinical reality in the case of an infection associated with biofilms (Ferrer *et al.* 2016).

This review discusses the current methods of microbial biofilm detection and future perspectives for its diagnosis in clinical practice.

## Clinical and laboratory diagnosis of microbial biofilms

In 2014, the European Society for Clinical Microbiology and Infectious Disease published a guideline to assist healthcare professionals in the diagnosis of infections associated with biofilms, with emphasis on clinical and

laboratory procedures to facilitate diagnosis as well as to make patient treatment faster and more effective (Høiby *et al.* 2015). According to this guideline, the most frequent clinical signs of an infection associated with biofilms consist of inflammatory reactions, redness, pain, loss of function and fever. The patient must have a history of predisposition to infection, such as the use of a medical device or self-limiting diseases, as well as presenting a persistent infection over more than 7 days and failure of antibiotic therapy. Regarding biofilm laboratory diagnosis, the guideline suggests some detection methods, such as electron microscopy and polymerase chain reaction (PCR), where it is possible to identify microbial aggregates around inflammatory cells and the presence of mucoid or small cells in positive cultures, indicating antibiotic recalcitrance (Kamaruzzaman *et al.* 2018).

In the literature, the methods for diagnosis of infections caused by free-living bacteria, such as those related to catheter and chronic wounds, are well established (Frickmann *et al.* 2017; Stoica *et al.* 2017; Rajapaksha *et al.* 2019). However, when it comes to the diagnosis of biofilms, there are few consistent reports and data available, especially regarding biofilms formed in and on medical devices (Høiby *et al.* 2015). It is estimated that 2% of knee and breast implants, 4% of mechanical heart valves, pacemakers and defibrillators, 10% of ventricular devices and 40% of ventricular assist devices are affected by biofilms (Del Pozo 2018). The pathogens are generally derived from the hands of healthcare workers, contaminated water or fluids and the hospital environment (Yadav *et al.* 2020). Biofilms formed in medical devices are responsible for the worsening of the patient's clinical condition. Currently, although many methods allow identification of biofilms in catheters and other devices, such as electronic microscopy, biofilms on these materials are not routinely investigated in clinical practice (Stoica *et al.* 2017).

Also, the conventional methods used in clinical laboratories for the identification of pathogens, which are based on the use of a specific agar, the incubation of the sample, the isolation of the microorganisms and the enumeration of viable cells, can only detect free-living bacteria and cannot identify biofilm-forming microorganisms, generating results that may not represent the clinical reality of the patient (Mooney *et al.* 2018). Besides that, even with the use of automated growth detection systems, microbial identification takes approximately 5–7 days. In the wait for the result, mainly with the presence of the biofilm, these pathogens have already multiplied, worsening the patient's clinical condition and forcing doctors to start empirical therapy even without identifying the pathogen, which can lead to errors in antibiotic therapy and, in some cases, to the death of the patient

(Rajapaksha *et al.* 2019). To overcome this problem, new and more sophisticated methodologies for the identification of microorganisms in medical devices and clinical samples must be implemented in clinical practice to make the identification of microorganisms faster and to facilitate the routine investigation of biofilm formation in clinical practice (Gaudreau *et al.* 2018; Ordonez *et al.* 2019).

The literature describes several methods of biofilm detection, and the choice depends on the place of its formation and the sample to be analysed; these methods have greater specificity and sensitivity and are much less time-consuming than other conventional techniques. Biopsy is considered the most reliable way to detect biofilms (Ordonez *et al.* 2019; Rajapaksha *et al.* 2019). Biopsy samples are stained for the visualization of microbial aggregates, the extracellular matrix of the biofilm and cells of the immune system, and the larger the size of the tissue and the number of biopsies collected, the more sensitive and specific the result will be (Kamaruzzaman *et al.* 2018). The viability method of LIVE/DEAD uses green and red fluorescing markers and can be used as a qualitative and quantitative technique because it can differentiate healthy cells (stained green) from damaged cells (stained red) in the biopsy (Chevalier *et al.* 2017).

However, in many clinical situations, biopsies cannot be collected or are not indicated, and other samples could be sent to the laboratory, such as sputum, blood, fluids and secretions (Percival 2017). In the laboratory, analysis of these samples is difficult since the microorganisms in the biofilm are adhered to each other and a surface, forming a microbial aggregate. Therefore, sonication is generally performed, using energy to agitate particles in a solution, removing the aggregated and adhered bacteria from biomaterial surfaces (Galli *et al.* 2018). After sonication, the aggregated microorganisms detach themselves from the surface of the material and can be analysed by several methods, as described below.

### Polymerase chain reaction

This technique is used for the detection of biofilm-forming pathogens directly in clinical samples. It is based on the amplification of specific regions, providing high specificity and sensitivity in the identification of genes involved in biofilm formation, after the sonication process (Rajapaksha *et al.* 2019). Some examples of developed PCR methods are real-time PCR, multiplex PCR and reverse transcriptase PCR. These techniques can be used to identify clinical samples that produce biofilms, as in the study of Shahmoradi *et al.* (2019), who identified biofilm-forming isolates of *Staphylococcus aureus* in urine,

blood, sputum, cerebrospinal fluid, pleural fluid and wound samples of hospitalized patients.

Moreover, PCR can be used to identify genes involved in biofilm formation, as in the study of Klančnik *et al.* (2015), who used the PCR-based method for the identification of genes involved in the adhesion of different strains of *Listeria monocytogenes*.

### Fluorescence in situ hybridization

This method consists of the binding of short fluorescence-labelled oligonucleotides, which can bind to the specific ribosomal RNA of the target organisms. It has the advantage of allowing the analysis of the sample without prior treatment, easily identifying microbial aggregates; the samples are analysed via microscopy (Frickmann *et al.* 2017). Bernardi *et al.*, (2019) used the fluorescence in situ hybridization (FISH) method and confocal laser scanning microscopy (CLSM) in their study with halitosis to visualize and quantify the biofilm formed in the dorsum of the tongue, in which they identified *Fusobacterium nucleatum* and *Streptococcus* sp. biofilm-forming strains. This method also has been tested in bacterial vaginosis, identifying biofilm-forming bacteria in vaginal samples, with greater specificity than for other common methods (Machado *et al.* 2015).

### Electronic microscopy

This approach allows the visualization of microbial aggregates after sonication or FISH. Scanning electron microscopy (SEM), transmission electron microscopy (TEM) and CLSM are the most used tools in biofilm visualization (Costa-Orlandi *et al.* 2017). The high resolution of this microscopy allows analysis of all biofilm structures, facilitating direct detection and visualization of the biofilm where it was formed, such as in a catheter (Sugimoto *et al.* 2016; Schlafer and Meyer 2017).

Via SEM, samples can be fixed, dehydrated and stained, but in all these processes, mainly in dehydration, the morphology and structure of the biofilm can be altered, which is a disadvantage of this technique (Costa-Orlandi *et al.* 2017). The TEM is widely used for biofilm architecture visualization and has an advantage over SEM since the microbial aggregate is treated with resin, which ensures greater stability of the extracellular polymeric matrix of the biofilm. However, it has the disadvantage of not allowing visualization of the biofilm topography (Mohammed *et al.* 2017).

The CLSM guarantees the 3D visualization of the complete biofilm architecture, besides allowing the identification of macromolecules such as polysaccharides, proteins, nucleic acids and lipids through the use of fluorescent

dyes, which mark the different components of the biofilm as well as the extracellular matrix and spatial relationships of the biofilm (Costa-orlandi *et al.* 2017).

The analysis of biofilms in vitro contributed to the advancement of biofilm research; however, in most existing methodologies, biofilm is treated and analysed in a different place from where it was formed, which can damage its structure due to the lack of exact reproducibility of the appropriate temperature, pH and availability of nutrients from the site of origin (Sugimoto *et al.* 2016). To overcome this problem, a sophisticated microscopic technique can be used in the detection of the biofilm in situ, such as multiphoton laser scanning microscopy, making it possible to analyse the biofilm at the site where it was formed, such as catheters and implants, preserving its structure and architecture. This methodology is indicated for the acquisition of images of autofluorescence materials, where the researcher can obtain high-resolution images of the biofilm structure without losing any important components of the biofilm and without previous treatment of the sample (Neu and Lawrence 2015).

Other types of microscopy are also used in biofilm research, such as scanning transmission X-ray microscopy, which is associated with X-ray absorption spectroscopy, Hoffman modulation contrast microscopy and atomic force microscopy; however, they are associated with high costs (Costa-Orlandi *et al.* 2017).

Even with the publication of the guidelines proposed by the European Society for Clinical Microbiology and Infectious Disease in 2014 and the current discussion, until the present moment, the data about biofilm diagnosis and treatment are largely inconsistent, with little information to support definitive conclusions for containment and prevention strategies. In addition, some proposed methodologies are expensive or require significant amounts of time and a large number of trained staff, making them impracticable for clinical practice (Mooney *et al.* 2018).

However, of all the methodologies mentioned above, PCR and electron microscopy stand out due to their high cost-benefit, short experimental time and high sensitivity and specificity in the identification of microorganisms (Rajapaksha *et al.* 2019). These techniques, associated with the evaluation of signs and symptoms and clinical samples of the patient, can modernize and improve the way of diagnosing infections in the hospital, generating faster results and using less laboratory inputs than conventional techniques (Ordonez *et al.* 2019). In addition, with the use of these methods, the doctor would be able to distinguish infections caused by free-living or sessile microorganisms, which will reflect in a better prognosis for the patient, since the antimicrobial used would be

more specific and efficient for the infection, decreasing the patient's length of stay as well as the morbidity and mortality rates in the unit (Høiby *et al.* 2015).

### Antimicrobial susceptibility testing against biofilms

Recently, there was a discussion in the literature, on the implementation of a specific breakpoint value to assess the bacterial susceptibility of biofilm-forming microorganisms in laboratory diagnosis, but there was low applicability; further studies and other pharmacological and microbiological tests are needed for this value to be used safely and effectively (Ruiz *et al.* 2019). Furthermore, it is still early to determine a successful antibacterial regimen against biofilms, as currently available indirect screening tests may generate false negatives in the presence of antimicrobial treatment, with the risk of relapse after treatment discontinuation (Mooney *et al.* 2018).

Some studies recommend the use of combined antimicrobial therapy for the treatment of infections associated with biofilms by Gram-negative bacteria through the use of macrolides (erythromycin, clarithromycin and azithromycin); however, determining a specific antibiotic therapy for these infections is difficult due to the variety of microorganisms that live in biofilms (Cepas *et al.* 2019). This makes it difficult to determine a minimum inhibitory concentration (MIC) of eradication for these sessile microorganisms since to inhibit a biofilm, a drug at a high concentration is required, and considering the side effects and toxicity that antimicrobials have on human cells, this type of treatment becomes impracticable (Mooney *et al.* 2018).

Bacteria and fungi in biofilms are more resistant to antimicrobials than free-living microorganisms, with minimum eradication concentrations of 10–1000 times higher compared to planktonic bacteria (Mooney *et al.* 2018). In biofilms, gene expression is altered, with negative regulation of genes associated with glycolysis, carbon metabolism and ribosomal proteins. In addition, the transcription of genes encoding peptideoglycan, cell wall synthesis and efflux pump activity are greater in sessile cells than in planktonic cells (Castro *et al.* 2017; Nielsen *et al.* 2019).

Vuotto *et al.* (2017), in their study with *Klebsiella pneumoniae* urinary strains, demonstrated a correlation between biofilm production and resistance profile, showing that the samples that showed extensive resistance to antimicrobials showed a greater ability to form biofilms compared with sensitive samples. Neopane *et al.* (2018) also observed that the *S. aureus* biofilm-forming samples collected from wounds of hospitalized patients showed higher levels of microbial resistance when compared to

nonforming ones. Furthermore, Mohammadi *et al.* (2020) described a significant correlation between phospholipase activity and biofilm production in *Candida albicans* isolated from nails, discussing the importance of biofilm formation to the reduction of azole drug penetration into the biofilm matrix and the increased expression of gene resistance associated with antifungal resistance.

The relationship between biofilm production and antibiotic resistance is not clear; however, a possible explanation is that the plasmids that harbour antimicrobial resistance genes also harbour genes involved in the production of biofilms (Vuotto *et al.* 2017), which would explain why multiresistant microorganisms are also biofilm producers. In addition, within biofilms, bacteria have a cellular communication system called *quorum-sensing*, which facilitates the exchange of genes within the community, including antimicrobial resistance genes (Osman *et al.* 2019).

Therefore, several bacterial mechanisms may be involved in microbial resistance within biofilms, such as low antimicrobial penetration due to matrix presence, antimicrobial and antifungal release strategies, altered microbial multiplication rate and bacterial physiological changes (Singh *et al.* 2017).

In 1999, the first strategy of the minimum biofilm inhibitory concentration (MBIC) and the minimum biofilm eradication concentration (MBEC) was created using the Calgary biofilm device method. In this technique, biofilm formation is tested with stakes that fit into the wells of the microtiter plate, containing growth medium and bacteria. Thus, microbes do not sediment and only develop in the sessile form (Azeredo *et al.* 2017). Since then, other procedures have been proposed, such as models based on bioreactors, flow cell systems and MBIC definitions evaluating biomass, but the application and standardization of these procedures in the clinic are still pending (Di Luca *et al.* 2017).

The MBIC of biofilm and the MBEC are used to determine the efficacy of antimicrobials against biofilms (Azeredo *et al.* 2017). These values are generally considerably higher than the MIC of planktonic bacteria. Some studies have been successful in developing drugs for the treatment of catheter-related infections, taking into account the MBIC and MBEC values of the biofilm, while other clinical trials have failed to replicate these results with other microorganisms from different sites. In addition, most microbial resistance studies of biofilms are based on *in vitro* assays, questioning whether these tests can be reproduced *in vivo* (Coenye *et al.* 2018).

Although several microbial susceptibility tests on biofilms have already been described, so far, none has been approved as a reference method in clinical microbiology, generating an increasing interest in the development of



new specific sensitivity tests for sessile bacteria (Singh *et al.* 2017).

### Advances in scientific research: *In vitro* and *in vivo* biofilm detection methods

Many *in vitro* and *in vivo* methods have been used for a better understanding of the biology of biofilms and their detection. Colorimetric assays are the most widely used ones and commonly applied in studies related to the development and susceptibility of biofilms to drugs and the quantification of specific biofilm structures (Shukla and Rao 2017). These methods, although requiring significant amounts of time and a high number of trained staff, are important allies in identifying biofilm formation and for a better understanding, mainly of the susceptibility of biofilms to anti-biofilms and antimicrobial compounds, which can assist in the development of new methods of diagnosis and treatment that can be useful in clinical practice (Qu *et al.* 2017). The main *in vitro* and *in vivo* tests used by the academic community are listed in Table 1 and described below.

#### *In vitro* biofilm detection models

##### *Congo red agar test*

This agar allows the differentiation of the colonies in two colours, with black indicating strong biofilm production

and red indicating no biofilm production (Lee *et al.* 2015). This is a quantitative test because it is based on a subjective chromatic evaluation (Melo *et al.* 2013). Solati *et al.* (2015) have used it to assess *Staphylococcus epidermidis* produced by biofilm collected from the urine and blood of patients with urinary tract infections and septicemia, respectively, in which they identified 55% of the isolates with the greatest potential for biofilm formation; most were collected from urine.

##### *Tube biofilm formation test*

This test consists of the use of plastic tubes containing sample inoculum stained with 0.1% violet crystal. After several washing processes with phosphate buffer saline and fixation with sodium acetate, the tubes are inverted in an adsorbent paper, and those with the presence of the stained film on the bottom and walls of the tube, indicating the presence of biofilm, are being considered positive (Halim *et al.* 2018).

Some studies have used this method to detect clinical isolates producing biofilms; for example, Neopane *et al.* (2018) have identified 30 *S. aureus* biofilm-forming isolates collected from wounds of hospital-admitted patients, while Hassan and Khider (2019) have evaluated the correlation of the formation of biofilms in clinical samples of *Acinetobacter baumannii* using the tube biofilm formation test and molecular tests. Despite being a low-cost test, it is a qualitative and subjective test.

**Table 1** Main *in vitro* and *in vivo* biofilm detection methods

Method	Advantages	Disadvantages	References
<i>In vitro</i> biofilm detection			
Congo red agar test	High accuracy in the detection of <i>Staphylococcus</i> sp. biofilm producers	Low reproducibility	Melo <i>et al.</i> (2013)
Tube biofilm formation test	Low cost	Subjective reading	Halim <i>et al.</i> (2018)
Microplate test	Low cost Several tests can be done simultaneously	Lack of standardization in the interpretation of results	Qu <i>et al.</i> (2017)
Crystal violet	Low cost Simple technique High replicability	Low specificity	Xu <i>et al.</i> (2016)
Safranin	Non-toxic dye	Low replicability and sensitivity	Stepanović <i>et al.</i> (2007); Ommen <i>et al.</i> (2017)
XTT	Simple technique High replicability	High cost Low sensitivity salt Retention by the pathogens that can interfere with the result	Costa-Orlandi <i>et al.</i> (2017)
<i>In vivo</i> biofilm detection			
<i>D. melanogaster</i>	High homologies between the <i>Drosophila</i> and human genomes Easy to handle Inexpensive to maintain	Preference for yeasts and <i>Escherichia coli</i> for having small genomes Does not have haemoglobin	Yamaguchi and Yoshida (2018)
<i>C. elegans</i>	Powerful methods for studying physiological processes	Nematode culture standardization factors may interfere with its survival	Park <i>et al.</i> (2017)

### Microplate test

This test uses microplates with flat bottom or U-shaped wells, where all stages of biofilm formation occur within these wells (Di Luca *et al.* 2017). It is a cheap technique that requires few reagents, and several tests can be done simultaneously. For the detection of biofilm production, the wells with the samples are stained with specific dyes that quantify the main structures of the biofilm. This part of the experiment is the so-called 'colorimetric test' (Qu *et al.* 2017). According to the absorbance result of each isolate in these colorimetric tests, it is possible to classify them into nonproducers, weak, moderate or strong producers of biofilms. However, this classification is highly subjective and can vary according to the species and the cut-off value that the researcher uses as a reference (Shukla and Rao 2017).

*Crystal violet.* In addition to the use of this dye in tube tests, it can also be applied in microplate tests for an assessment of the total biomass of the biofilm. It is a cost-efficient substance, and the test is easy to interpret and has high replicability (Shukla and Rao 2017). However, this dye has the disadvantage of staining the entire structure of the biofilm, without specificity. Moreover, after being deposited in the plate, the wells need to be washed, culminating in the loss of important biofilm components and structures (Xu *et al.* 2016). It is the most used colorimetric test in the microplate test, making it possible to quantify the entire biomass and matrix of biofilms (Di Luca *et al.* 2017).

In the literature, there are several studies that use crystal violet in the identification and quantification of biofilm production in bacteria and fungi (Xu *et al.* 2016; Vuotto *et al.* 2017; Mohammadi *et al.* 2020).

*Safranin.* Safranin is a nontoxic dye, and its use is similar to that of crystal violet. However, it is less frequently used in the quantification of biomass and results in lower optical densities than crystal violet staining (Ommen *et al.* 2017). Some authors, such as Babapour *et al.* (2016) and Karami *et al.* (2020), have used safranin as a dye in the microplate test for the identification of clinical isolates of biofilm producers.

Some researchers believe that this dye specifically stains the mucopolysaccharides of the extracellular matrix because of their high affinity with these compounds. Mucopolysaccharides are molecules produced by cells within the biofilm that will compose the extracellular matrix of the biofilm (Stepanović *et al.* 2007). However, not all biofilms have polysaccharides as a matrix

component, which is replaced by DNA and other compounds. In addition, each microorganism has a type of extracellular matrix which varies in its cellular localisation, chemical composition, nature and functions; many are polyanionic, but others are neutral or polycationic (Limoli *et al.* 2015).

*The use of 2,3-bis (2-methoxy-4-nitro-5-sulfophenyl)-5-[(phenylamino) carbonyl 2H-tetrazolium hydroxide (XTT).* The tetrazolic salt XTT is used to evaluate the number of viable cells and the metabolic activity of biofilms. When microorganisms in the biofilm produce metabolites, XTT changes their chemical conformation and is transformed into formazan, which is seen in the microtiter plate by a colour change from neutral to orange (Costa-Orlandi *et al.* 2017). This compound is most frequently used in detecting and evaluating the metabolic activity of biofilms produced by fungi, as in the study by Di Domenico *et al.* (2018), who detected 38 clinical isolates of *Candida* sp. biofilm producers, but it can also be used for bacterial evaluation, as in the study by Xu *et al.* (2016), who reported that 77% of *S. aureus* isolates were biofilm-forming.

Some researchers use (3-[4,5-dimethylthiazol-2-yl]-2,5-phenyltetrazolium bromide) MTT, which is a salt that behaves in a similar way to XTT, albeit with a colour change from neutral to purple. Comparing the two salts, XTT has more advantages because after its reduction in formazan, the wells can be read immediately, while MTT requires other steps prior to reading, such as cell lysis (Costa-Orlandi *et al.* 2017). Another disadvantage of the MTT salt is the insolubility of formazan in water, making it necessary to dissolve the precipitate before measuring absorbance. In addition, reduced MTT can react with some compounds, forming large intracellular deposits, capable of damaging microbial cells during the test, producing false positive or negative results (Grela *et al.* 2015).

However, XTT has some disadvantages, such as the lack of a linear relationship between the number of microorganisms present in the biofilm and the colorimetric signal, salt retention by these pathogens in planktonic and sessile form and a high cost (Alonso *et al.* 2017). Additionally, XTT can react with some nanoparticles and also be reduced by O<sub>2</sub>. Toxicity testing of engineered nanomaterials including nano-TiO<sub>2</sub> has generated a many number of publications in the last several years (Wang *et al.* 2011). Furthermore, problems regarding intraspecies and interspecies variability have been reported, making the use of these methods unfeasible in some susceptibility tests for both planktonic cells and biofilms (Peeters *et al.* 2008).

### Detection of biofilms in vivo

Some researchers have used animal models to advance the research and detection of biofilms in vivo. Due to some difficulties encountered by the researchers in mammalian studies, including the approval of the Ethics Committee for such studies, other nonmammalian models are being used, such as *Drosophila melanogaster* (McLaughlin and Bratu 2015) and *Caenorhabditis elegans* (Park *et al.* 2017).

For example, Kamareddine *et al.* (2018) have used *D. melanogaster* in their study of infection by *Vibrio cholerae*, where they discovered that quorum-sensing, besides being a cellular communication mechanism in biofilms, also exercises control over the host's metabolic pathways. Another important study model for biofilms is *C. elegans*, which is used for the evaluation of the progression of intestinal infection caused by *Salmonella* sp., where it was possible to identify a toxin that is secreted by these bacteria in biofilm formation (Desai *et al.* 2019).

The advantages of such an approach are the ease of handling and the lower costs. Moreover, the small size of the models makes it easy to keep them in microtiter plates, thus facilitating the high-performance screening of biofilm formation and making them important tools in understanding the pathogen-host relationship (Costa-Orlandi *et al.* 2017).

### Matrix-assisted laser desorption ionization time-of-flight mass spectrometry (MALDI-TOF MS): Is it the diagnostic method of the future?

In recent years, mass spectrophotometry has been used by some clinical laboratories for the identification of bacteria and fungi. It is a method that compares the microbial protein profile, obtained from a database of reference mass spectra, for the identification of genera, species and subspecies. Microbial identification is performed in 60 s and has been used in the diagnosis of several infectious diseases around the world (Singhal *et al.* 2015). Currently, this methodology is the target of researchers and applied biofilm studies, since MALDI-TOF allows the differentiation of planktonic cells and biofilms due to profiles of different mass spectra (Caputo *et al.* 2018). The method was tested on different species of Gram-positive and negative bacteria and fungi (Kubesova *et al.* 2012; Pereira *et al.* 2015; Caputo *et al.* 2018), showing that it is possible, through MALDI-TOF, to differentiate microorganisms that form weak or strong biofilms, based on their molecular mass size.

However, due to several problems and limitations of this technique, MALDI-TOF is far from being the gold standard for identifying biofilm formation. A common

problem encountered by researchers is that the same microorganisms may present different mass spectra when analysed repeatedly (Singhal *et al.* 2015). Another limitation of the technique is the difficulty in differentiating microbial samples with a high degree of similarity due to the several similar compounds included in their cells. In addition, other intracellular compounds that vary within each microorganism may not be detected by the equipment; especially if they belong to low- or high-mass proteins, which are generally not ionized by the apparatus (Mlynáriková *et al.* 2016). However, according to Gaudreau *et al.* (2018), sample preparation for analysis is crucial for the success of the test, and when the sample is transferred directly to the analysis, together with the presence of formic acid and the matrix, the chances of interference are lower compared to other types of preparation with acetonitrile, water and ethanol.

New studies are necessary to prove the efficacy of this methodology in the detection of biofilms, since it presents limitations and low reproducibility. While MALDI-TOF is not yet fully effective in the detection of biofilms, conventional in vitro and in vivo techniques are still most frequently used in research labs (Singhal *et al.* 2015).

### Omics analysis: The role of proteomic, transcriptomic and metabolomic analyses in the diagnosis of biofilms

The traditional methods of microbiological diagnosis in clinical laboratories include the growth and isolation of the microorganism, the detection of antibodies or antigens in serological tests and, in some laboratories, genetic identification (DNA or RNA) through the PCR technique (Ordonez *et al.* 2019). While most molecular tests target only a limited number of pathogens using specific primers, omics analysis allows to analyse the entire microbiome of the pathogen and to identify specific proteins and metabolites produced by pathogens (Otto *et al.* 2012). These technologies are also being developed to detect differences in the transcription, translation and metabolism of microorganisms in biofilms, describing important information of these communities, such as the influence of environmental factors on biofilm adhesion and formation as well as physiological and mutational factors (Chiu and Miller 2019). Table 2 shows the main methods used in the omics analysis as well as the samples that can be evaluated and the infections that can be diagnosed.

The study of proteomics in biofilms allows the identification of specific proteins that are produced in this community, as well as the distribution, posttranslational modifications, structure, function and quantity of these proteins (Washio and Takahashi 2016). The success of

**Table 2** Omics analysis in the clinical diagnosis of biofilms

Detection methods	Clinical samples	Clinical indication	Reference
Transcriptomic			
The express sequence tag (EST)	Blood	Sepsis	Hrdlickova <i>et al.</i> (2017)
Serial Gene Expression Analysis (SAGE)	Peripheral blood mononuclear cel	Urinary Tract Infection	
DNA microarrays	Several body fluids and tissues	Multiplexed pathogen detection	
RNA-Seq (4sU-Seq, RIP-Seq, (Riboseq))	Cerebrospinal fluid	Meningitis	
Proteomic			
2D gels (DIGE)	Blood	Sepsis	Otto <i>et al.</i> (2012)
Gel free (iTRAQ, TMT)			
Spiked-in peptides	Secretions	Urinary Tract Infection	
Label-free quantitation	Cell-free body fluids	Respiratory infections	
Metabolomic			
Capillary electrophoresis (CE)	Blood Fluids	Sepsis	Chiu and Miller (2019) Washio and Takahashi (2016)
Time-of-flight mass spectrometer (TOF-MS)	Stool sample	Infections by <i>Clostridium difficile</i>	
CE-TOFMS	Cerebrospinal fluid	Meningitis	

proteomics studies is due to the invention of the 2DE gel, which is applied in orthogonal separation to classify species according to their molecular weight, where samples are stained and identified using software (Otto *et al.* 2012). Despite being a technique similar to MALDI-TOF, it is more sensitive and can differentiate nonstressed from stressed cells, cellular mutations and different time points from the same organism. The combination of proteomics analysis with the use of 2D gel and MALDI-TOF can generate more sensitive and specific data, revealing cases of multiple proteins found in the same place and those with low mass, reducing false values and improving the disadvantages of MALDI-TOF (Otto *et al.* 2012; Singhal *et al.* 2015).

Erdmann *et al.* (2019) used proteomics analysis and identified 1021 different proteins in the biofilms produced by 27 samples of *Pseudomonas aeruginosa* and a protein for mRNA that was common among species, even under different conditions, suggesting a posttranscriptional pattern. If researchers were able to identify proteins common in most biofilms produced, it would be possible, through the methods mentioned above, to reduce the time needed for the identification of microorganisms, facilitating our understanding of the main regulatory pathways and adaptation strategies for bacterial biofilms, which can be useful in the development of new treatment strategies for these biofilms (Chiu and Miller 2019).

Transcriptomics analysis allows identifying an RNA molecule in a live cell. In the 1990s, several methodologies were created that allowed sequencing specific RNA

molecules on a large scale, such as the express sequence tag (EST) method, serial gene expression analysis (SAGE) and DNA microarrays; however, they have numerous disadvantages, such as high costs, and demand for information on the sample genome and transcriptome, impeding discoveries (Hrdlickova *et al.* 2017). The method of choice for studying gene expression and identifying new species of RNA is RNA-Seq, as it offers less background noise and greater detection than previous methodologies (Hrdlickova *et al.* 2017). The transcriptomic approach is of great interest in biofilm research, as it allows the detection of specific genes in the formation of biofilms and new mechanisms of survival and antimicrobial resistance (Chiu and Miller 2019). For example, Kean *et al.* (2018) used this approach to investigate the mechanisms of biofilm formation and resistance in *Candida auris*, a recently discovered yeast.

The metabolic analysis is based on the identification and quantification of metabolite features in living cells, including gene transcription, mRNA translation, protein analysis and enzymatic reactions (Zhang and Powers 2012). In the 2000s, several devices with a metabolic approach were used, such as capillary electrophoresis and time-of-flight mass spectrometer (TOF MS), which identify metabolites according to their ionic charge and mass spectrometry, respectively. By connecting these two devices, these techniques can separate small ionic molecules and accurately measure their masses; they have been widely used since then. The metabolic approach provides data that allow the diagnosis of a disease as well as its progress (Washio and Takahashi 2016).

This allows, for example, the identification of chemical signalling molecules, so-called ‘autoinducers’, responsible for cellular communication within biofilms. Autoinducers are targets of promising drugs for biofilms since these molecules are not present in the human organism and can therefore be used as biofilm markers (Mooney *et al.* 2018). The molecular structure of a biofilm can positively impact the biology of systems and, consequently, the development of new diagnostic and/or therapeutic tools (Zhang and Powers 2012).

### Advantages and disadvantages of omic analysis

The new omic approaches allow an evaluation of several biological units of biofilms, such as gene expression, proteins and metabolites. This generates highly relevant data for a better understanding of biofilms, allowing the discovery of new biomarkers for various diseases and the development of new methods of diagnostics and therapies (Chiu and Miller 2019). The application of these omic methods in the health area can generate opportunities for clinical interventions, as in the study by Nascimento *et al.* (2017), who through omic analyses identified new oral *Streptococcus* and their phenotypic characterization revealed promising candidates for probiotic therapy. To investigate complex multispecies biofilms, the use of omic tools is the promise of a breakthrough regarding the understanding of bacterial interaction and physiology within biofilms.

However, although the transcriptomic, proteomic and metabolomic analysis are complementary methods to investigate the cellular physiology of biofilms, these omic methods were not designed to be evaluated together; that is, it is not possible to validate or compare one data with the other (Azeredo *et al.* 2017). Also, biofilm is by definition heterogeneous, varying according to its location, stage of development and physiology of microbial cells. In the omic analysis, the data result from a cell that will represent the entire population, consequently, a subpopulation can be neglected or be different from the cell collected for analysis.

Therefore, the results of the omic analysis should be analysed with caution, considering that the results obtained are averages with margins of error (Jamal *et al.* 2018). However, flow cell cameras can work around this problem, as microbial cells grow statically. Another solution is the laser capture microdissection microscopy as it allows the comparison and identification of the physiology of cells and their special distribution within the biofilm, for example, the differences between cells that reside on the periphery of biofilms with those that live in the superficial regions. The main challenge that remains unsolved is how much biomass

is needed to perform molecular analyses (Azeredo *et al.* 2017).

Another question that remains under investigation concerns the reference to compare the omic data obtained. Often a planktonic cell is used as a control, but it may not be the most appropriate, since the biofilm has several stages of development and any attempt at correlation would be incorrect. The best choice for the investigation of biofilm physiology remains to compare a wild-type strain with an isogenic mutant (Zhang and Powers 2012). The biofilm matrix can also be a problem for proteomic analysis since it can make access to different intracellular membrane and parietal subproteomes difficult (Washio and Takahashi 2016). Also, the analysis of exoproteoma, that is, proteins that are secreted into the extracellular environment, is also a challenge (Desvaux *et al.* 2009). In addition, omic analysis requires qualified technical expertise and is expensive.

Despite the challenges that these techniques still confront, the development of omic technologies is essential for a better understanding of the development and evolution of biofilms, allowing the creation of new methods of diagnosis and treatments in the health area (Chiu and Miller 2019).

### Conclusions

Despite all advances in research, biofilm-producing microorganisms remain a serious public health problem, often neglected in various health areas. Biofilm contributes to increased microbial resistance, making treatment more difficult and worsening the clinical conditions of patients, contributing to the increase in morbidity and mortality rates. The diagnosis of biofilms is challenging, since the current screening methodologies performed in the clinic, such as susceptibility tests, detect only planktonic colonies, not representing the clinical reality of the patient.

Also, even with several biofilm detection methods described in the literature, there is currently no routine test or protocol established for this purpose in the clinic. Omics analysis is a promising form of diagnosis in clinical laboratories since it allows the identification of pathogens in less time than needed for conventional techniques, and it is possible to analyse the entire pathogen microbiome, including an identification of production of proteins and metabolites, which allows a better understanding of its pathogenesis and a more specific identification.

More studies must therefore be developed to facilitate the development of efficient and reliable protocols for rapid biofilm identification, ensuring greater chances of success in infection control in clinical practice.

## Conflicts of Interest

No conflicts of interest are declared.

## References

- Alonso, B., Cruces, R., Pérez, A., Sánchez-Carrillo, C. and Guembe, M. (2017) Comparison of the XTT and resazurin assays for quantification of the metabolic activity of *Staphylococcus aureus* biofilm. *J Microbiol Methods* **139**, 135–137. <https://doi.org/10.1016/j.mimet.2017.06.004>.
- Azeredo, J., Azevedo, N.F., Briandet, R., Cerca, N., Coenye, T., Costa, A.R., Desvaux, M., Bonaventura, G.D. et al. (2017) Critical review on biofilm methods. *Crit Rev Microbiol* **43**, 313–351. <https://doi.org/10.1080/1040841X.2016.1208146>.
- Babapour, E., Haddadi, A., Mirnejad, R., Angaji, S.A. and Amirmozafari, N. (2016) Biofilm formation in clinical isolates of nosocomial *Acinetobacter baumannii* and its relationship with multidrug resistance. *Asian Pac J Trop Biomed* **6**, 528–533. <https://doi.org/10.1016/j.apjtb.2016.04.006>.
- Bernardi, S., Continenza, M.A., Al-Ahmad, A., Karygianni, L., Follo, M., Filippi, A. and Macchiarelli, G. (2019) *Streptococcus* spp. and *Fusobacterium nucleatum* in tongue dorsum biofilm from halitosis patients: a fluorescence in situ hybridization (FISH) and confocal laser scanning microscopy (CLSM) study. *New Microbiol* **42**, 108–113.
- Caputo, P., Di Martino, M.C., Perfetto, B., Iovino, F. and Donnarumma, G. (2018) Use of MALDI-TOF MS to discriminate between biofilm-producer and non-producer strains of *Staphylococcus epidermidis*. *Int J Environ Res Public Health* **15**, 1695. <https://doi.org/10.3390/ijerph15081695>.
- Castro, J., França, A., Bradwell, K.R., Serrano, M.G., Jefferson, K.K. and Cerca, N. (2017) Comparative transcriptomic analysis of *Gardnerella vaginalis* biofilms vs. planktonic cultures using RNA-seq. *NPJ Biofilms Microbiomes* **3**, 1–7.
- Cepas, V., López, Y., Muñoz, E., Rolo, D., Ardanuy, C., Martí, S., Xercavins, M., Horcajada, J.P. et al. (2019) Relationship between biofilm formation and antimicrobial resistance in Gram-negative bacteria. *Microbial Drug Resist* **25**, 72–79. <https://doi.org/10.1089/mdr.2018.0027>.
- Chevalier, M., Ranque, S. and Prêcheur, I. (2017) Oral fungal-bacterial biofilm models *in vitro*: a review. *Med Mycol* **56**, 653–667. <https://doi.org/10.1093/mmy/myx111>.
- Chiu, C.Y. and Miller, S.A. (2019) Clinical metagenomics. *Nat Rev Genet* **20**, 341. <https://doi.org/10.1038/s41576-019-0113-7>.
- Coenye, T., Goeres, D., Bамbeke, F.V. and Bjarnsholt, T. (2018) Should standardized susceptibility testing for microbial biofilms be introduced in clinical practice? *Clin Microbiol Infect* **24**, 570–572. <https://doi.org/10.1016/j.cmi.2018.01.003>.
- Costa-Orlandi, C.B., Sardi, J.C.O., Pitangui, N.S., Oliveira, H.C., Scorzoni, L., Galeane, M.C., Medina-Alarcón, K.P., Melo, W.C.M.A. et al. (2017) Fungal biofilms and polymicrobial diseases. *J Fungi* **3**, 22. <https://doi.org/10.3390/jof3020022>.
- Del Pozo, J.L. (2018) Biofilm-related disease. *Expert Rev Anti Infect Ther* **16**, 51–65. <https://doi.org/10.1080/14787210.2018.1417036>.
- Desai, S.K., Padmanabhan, A., Harshe, S., Zaidel-Bar, R. and Kenney, L.J. (2019) *Salmonella* biofilms program innate immunity for persistence in *Caenorhabditis elegans*. *Proc Natl Acad Sci* **116**, 12462–12467. <https://doi.org/10.1073/pnas.1822018116>.
- Desvaux, M., Hebraud, M., Talon, R. and Henderson, I.R. (2009) Secretion and subcellular localizations of bacterial proteins: a semantic awareness issue. *Trends Microbiol* **17**, 139–145. <https://doi.org/10.1016/j.tim.2009.01.004>.
- Di Domenico, E.G., Cavallo, I., Guembe, M., Prignano, G., Gallo, M.T., Bordignon, V., D'Agosto, B., Sperduti, I. et al. (2018) The clinical Biofilm Ring Test: a promising tool for the clinical assessment of biofilm-producing *Candida* species. *FEMS Yeast Res* **18**. <https://doi.org/10.1093/femsyr/foy025>.
- Di Luca, M., Navari, E., Esin, S., Menichini, M., Barnini, S., Trampuz, A., Casani, A. & Batoni, G. (2017) Detection of biofilms in biopsies from chronic rhinosinusitis patients: in vitro biofilm forming ability and antimicrobial susceptibility testing in biofilm mode of growth of isolated bacteria. In Donelli, G., ed. *Advances in Microbiology, Infectious Diseases and Public Health*, Vol. **1057**, pp. 127. Advances in Experimental Medicine and Biology. Cham: Springer. [https://doi.org/10.1007/5584\\_2017\\_34](https://doi.org/10.1007/5584_2017_34)
- Erdmann, J., Thöming, J.G., Pohl, S., Pich, A., Lenz, C. and Häussler, S. (2019) The core proteome of biofilm-grown clinical *Pseudomonas aeruginosa* isolates. *Cells* **8**, 1129. <https://doi.org/10.3390/cells8101129>.
- Ferrer, M.D., Rodriguez, J.C., Álvarez, L., Artacho, A., Royo, G. and Mira, A. (2016) Effect of antibiotics on biofilm inhibition and induction measured by real-time cell analysis. *J Appl Microbiol* **122**, 640–650. <https://doi.org/10.1111/jam.13368>.
- Frickmann, H., Zautner, A.E., Moter, A., Kikhney, J., Hagen, R.M., Stender, H. and Poppert, S. (2017) Fluorescence in situ hybridization (FISH) in the microbiological diagnostic routine laboratory: a review. *Crit Rev Microbiol* **43**, 263–293. <https://doi.org/10.3109/1040841X.2016.1169990>.
- Galli, J., Calo, L., Meucci, D., Giuliani, M., Lucidi, D., Paludetti, G., Torelli, M.S., Sanguinetti, M. et al. (2018) Biofilm in voice prosthesis: a prospective cohort study and laboratory tests using sonication and SEM analysis. *Clin Otolaryngol* **43**, 1260–1265. <https://doi.org/10.1111/coa.13141>.
- Gaudreau, A.M., Labrie, J., Goetz, C., Dufour, S. and Jacques, M. (2018) Evaluation of MALDI-TOF mass spectrometry for the identification of bacteria growing as biofilms. *J Microbiol Methods* **145**, 9–81. <https://doi.org/10.1016/j.mimet.2018.01.003>.

- Grela, E., Ząbek, A. and Grabowiecka, A. (2015) Interferences in the optimization of the MTT assay for viability estimation of *Proteus mirabilis*. *Avicenna J Med Biotechnol* **7**, 159.
- Halim, R.M.A., Kassem, N.N. and Mahmoud, B.S. (2018) Detection of biofilm producing staphylococci among different clinical isolates and its relation to methicillin susceptibility. *Open Access Maced J Med Sci* **6**, 1335. <https://doi.org/10.3889/oamjms.2018.246>.
- Hassan, P.A. and Khider, A.K. (2019) Correlation of biofilm formation and antibiotic resistance among clinical and soil isolates of *Acinetobacter baumannii* in Iraq. *Acta Microbiol et Immunol Hungarica* 1–10. <https://doi.org/10.1556/030.66.2019.026>.
- Høiby, N., Bjarnsholt, T., Moser, C., Bassi, G.L., Coenye, T., Donelli, G., Hall-Stoodley, L., Imbert, C. *et al.* (2015) ESCMID guideline for the diagnosis and treatment of biofilm infections 2014. *Clin Microbiol Infect* **21**, S1–S25. <https://doi.org/10.1016/j.cmi.2014.10.024>.
- Hrdlickova, R., Toloue, M. and Tian, B. (2017) RNA-Seq methods for transcriptome analysis. *Adv Rev* **8**, e1364. <https://doi.org/10.1002/wrna.1364>.
- Jamal, M., Ahmad, W., Andleeb, S., Jalil, F., Imran, M., Nawaz, M.S., Hussain, T., Ali, M. *et al.* (2018) Bacterial biofilm and associated infections. *J Chin Med Assoc* **81**, 1–5. <https://doi.org/10.1016/j.jcma.2017.07.012>.
- Kamareddine, L., Wong, A.C.N., Vanhove, A.S., Hang, S., Purdy, A.E., Kierek-Pearson, K., Asara, J.M., Ali, A. Jr *et al.* (2018) Activation of *Vibrio cholerae* quorum sensing promotes survival of an arthropod host. *Nat Microbiol* **3**, 243–252.
- Kamaruzzaman, N.F., Tan, L.P., Yazid, K.A.M., Saeed, S.I., Hamdan, R.H., Choong, S.S., Wong, W.K., Chivu, A. *et al.* (2018) Targeting the bacterial protective armour; challenges and novel strategies in the treatment of microbial biofilm. *Materials* **11**, 1705. <https://doi.org/10.3390/ma11091705>.
- Karami, P., Khaledi, A., Mashoof, R.Y., Yaghoobi, M.H., Karami, M., Dastan, D. and Alikhani, M.Y. (2020) The correlation between biofilm formation capability and antibiotic resistance pattern in *Pseudomonas aeruginosa*. *Gene Reports* **18**, <https://doi.org/10.1016/j.genrep.2019.100561>.
- Kean, R., Delaney, C., Sherry, L., Borman, A., Johnson, E.M., Richardson, M.D., Rautema-Richardson, R., Williams, C. *et al.* (2018) Transcriptome assembly and profiling of *Candida auris* reveals novel insights into biofilm-mediated resistance. *MSphere* **3**, <https://doi.org/10.1128/mSphere.00334-18>.
- Klančnik, A., Toplak, N., Kovač, M., Marquis, H. and Jeršek, B. (2015) Quantification of *Listeria monocytogenes* cells with digital PCR and their biofilm cells with real-time PCR. *J Microbiol Methods* **118**, 37–41. <https://doi.org/10.1016/j.mimet.2015.08.012>.
- Kubesova, A., Salplachta, J., Horka, M., Ruzicka, F. and Slais, K. (2012) *Candida* ‘‘Psilosis’’ - electromigration techniques and MALDI-TOF mass spectrometry for phenotypical discrimination. *Analyst* **137**, 1937–1943.
- Lee, J.S., Bae, Y.M., Lee, S.Y. and Lee, S.Y. (2015) Biofilm formation of *Staphylococcus aureus* on various surfaces and their resistance to chlorine sanitizer. *J Food Sci* **80**, M2279. <https://doi.org/10.1111/1750-3841.13017>.
- Limoli, D.H., Jones, C.J. and Wozniak, D.J. (2015) Bacterial extracellular polysaccharides in biofilm formation and function. *Microbial Biofilms* 223–247, <https://doi.org/10.1128/9781555817466.ch11>.
- Machado, A., Castro, J., Cereija, T., Almeida, C. and Cerca, N. (2015) Diagnosis of bacterial vaginosis by a new multiplex peptide nucleic acid fluorescence in situ hybridization method. *PeerJ* **3**, e780. <https://doi.org/10.7717/peerj.780>.
- McLaughlin, J.M. and Bratu, D.P. (2015) *Drosophila melanogaster* oogenesis: an overview. In Bratu, D. and McNeil, G., eds. *Drosophila Oogenesis*, pp 1–20. New York, NY: Humana Press.
- Melo, P.C., Ferreira, L.M., Filho, A.N., Zafalon, L.F., Vicente, H.I.G. and Souza, V. (2013) Comparison of methods for the detection of biofilm formation by *Staphylococcus aureus* isolated from bovine subclinical mastitis. *Braz J Microbiol* **44**, 119–124.
- Mlynáriková, K., Šedo, O., Růžička, F., Zdráhal, Z., Holá, V. and Mahelová, M. (2016) Evaluation of capacity to detect ability to form biofilm in *Candida parapsilosis* sensu stricto strains by MALDI-TOF MS. *Folia Microbiol* **61**, 465–471. <https://doi.org/10.1007/s12223-016-0458-7>.
- Mohammadi, F., Ghasemi, Z., Familsatarian, B., Salehi, E., Sharifynia, S., Barikani, A., Mirzadeh, M. and Hosseini, M.A. (2020) Relationship between antifungal susceptibility profile and virulence factors in *Candida albicans* isolated from nail specimens. *Rev Soc Bras de Med Trop* **53**, <https://doi.org/10.1590/0037-8682-0214-2019>.
- Mohammed, S.A., Vianna, M.E., Penny, M.R., Hilton, S.T., Mordan, N. and Knowles, J.C. (2017) Confocal laser scanning, scanning electron, and transmission electron microscopy investigation of *Enterococcus faecalis* biofilm degradation using passive and active sodium hypochlorite irrigation within a simulated root canal model. *Microbiology Open* **6**, e00455. <https://doi.org/10.1002/mb.03.455>.
- Mooney, J.A., Pridgen, E.M., Manasherob, R., Suh, G., Blackwell, H.E., Barron, A.E., Bollyky, P.L., Goodman, S.G. *et al.* (2018) Periprosthetic bacterial biofilm and quorum sensing. *J Orthop Res* **36**, 2331–2339. <https://doi.org/10.1002/jor.24019>.
- Nascimento, M.M., Zaura, E., Mira, A., Takahashi, N. and Ten Cate, J.M. (2017) Second era of OMICS in caries research: moving past the phase of disillusionment. *J Dent Res* **96**, 733–740. <https://doi.org/10.1177/0022034517701902>.
- Neopane, P., Nepal, H.P., Shrestha, R., Uehara, O. and Abiko, Y. (2018) *In vitro* biofilm formation by *Staphylococcus aureus* isolated from wounds of hospital-admitted patients and their association with antimicrobial

- resistance. *Int J Gen Med* **11**, 25–32. <https://doi.org/10.2147/IJGM.S153268>.
- Neu, T.R. and Lawrence, J.R. (2015) Innovative techniques, sensors, and approaches for imaging biofilms at different scales. *Trends Microbiol* **23**, 233–242. <https://doi.org/10.1016/j.tim.2014.12.010>.
- Nielsen, S.M., Penstoft, L.N. and Nørskov-Lauritsen, N. (2019) Motility, biofilm formation and antimicrobial efflux of sessile and planktonic cells of *Achromobacter xylosoxidans*. *Pathogens* **8**, 14. 10.3390.
- Ommen, P., Zobek, N. and Meyer, R.L. (2017) Quantification of biofilm biomass by staining: non-toxic safranin can replace the popular crystal violet. *J Microbiol Methods* **141**, 87–89. <https://doi.org/10.1016/j.mimet.2017.08.003>.
- Ordonez, A.A., Sellmyer, M.A., Gowrishankar, G., Ruiz-Bedoya, C.A., Tucker, E.W., Palestro, C.J., Hammoud, D.A. and Jain, S.K. (2019) Molecular imaging of bacterial infections: overcoming the barriers to clinical translation. *Sci Transl Med* **11**, 508. <https://doi.org/10.1126/scitranslmed.aax8251>.
- Osman, K., Orabi, A., Elbehiry, A., Hanafy, M.H. and Ali, A.M. (2019) *Pseudomonas* species isolated from camel meat: quorum sensing-dependent virulence, biofilm formation and antibiotic resistance. *Future Microbiol* **14**, 609–622. <https://doi.org/10.2217/fmb-2018-0293>.
- Otto, A., Bernhardt, J., Hecker, M. and Becher, D. (2012) Global relative and absolute quantitation in microbial proteomics. *Curr Opin Microbiol* **15**, 364–372. <https://doi.org/10.1016/j.mib.2012.02.005>.
- Park, H.E.H., Jung, Y. and Lee, S.J.V. (2017) Survival assays using *Caenorhabditis elegans*. *Moll Cells* **40**, 90. <https://doi.org/10.14348/molcells.2017.0017>.
- Peeters, E., Nelis, H.J. and Coenye, T. (2008) Comparison of multiple methods for quantification of microbial biofilms grown in microtiter plates. *J Microbiol Methods* **72**, 157–165. <https://doi.org/10.1016/j.mimet.2007.11.010>.
- Percival, S.L. (2017) Importance of biofilm formation in surgical infection. *Br J Surg* **104**, e85–e94. <https://doi.org/10.1002/bjs.10433>.
- Pereira, F.D., Bonatto, C.C., Lopes, C.A., Pereira, A.L. and Silva, L.P. (2015) Use of MALDI-TOF mass spectrometry to analyse the molecular profile of *Pseudomonas aeruginosa* biofilms grown on glass and plastic surfaces. *Microb Pathog* **86**, 32–37. <https://doi.org/10.1016/j.micpath.2015.07.005>.
- Qu, Y., Thissen, H., McGiffin, D.C. and Peleg, A.Y. (2017) Optimizing microplate biofilm assays to screen anti-infective surfaces. *Trends Biotechnol* **35**, 3–5. <https://doi.org/10.1016/j.tibtech.2016.09.001>.
- Rajapaksha, P., Elbourne, A., Gangadoo, S., Brown, R., Cozzolino, D. and Chapman, J. (2019) A review of methods for the detection of pathogenic microorganisms. *Analyst* **144**, 396–411.
- Ruiz, J., Sanjuan, E., Amaro, C., Gordon, M., Villarreal, E., Castellanos-Ortega, Á. and Ramirez, P. (2019) *In vitro* study of antimicrobial activity on *Klebsiella Pneumoniae* biofilms in endotracheal tubes. *J Chemother* **31**, 202–208. <https://doi.org/10.1080/1120009X.2019.1601801>.
- Schlafer, S. and Meyer, R.L. (2017) Confocal microscopy imaging of the biofilm matrix. *J Microbiol Methods* **138**, 50–59. <https://doi.org/10.1016/j.mimet.2016.03.002>.
- Shahmoradi, M., Faridifar, P., Shapouri, R., Mousavi, S.F., Ezzedin, M. and Mirzaei, B. (2019) Determining the biofilm forming gene profile of *Staphylococcus aureus* clinical isolates via multiplex colony PCR method. *Rep Biochem Mol Biol* **7**, 181.
- Shukla, S.K. and Rao, T.S. (2017) An improved crystal violet assay for biofilm quantification in 96-well microtitre plate. *Biorxiv* 100214, <https://doi.org/10.1101/100214>.
- Singh, S., Singh, S.K., Chowdhury, I. and Singh, R. (2017) Understanding the mechanism of bacterial biofilms resistance to antimicrobial agents. *Open Microbiol J* **11**, 53–62. <https://doi.org/10.2174/1874285801711010053>.
- Singhal, N., Kumar, M., Kanaujia, P.K. and Virdi, J.S. (2015) MALDI-TOF mass spectrometry: an emerging technology for microbial identification and diagnosis. *Front Microbiol* **6**, <https://doi.org/10.3389/fmicb.2015.00791>.
- Solati, S.M., Tajbakhsh, E., Khamesipour, F. and Guhnani, H.C. (2015) Prevalence of virulence genes of biofilm producing strains of *Staphylococcus epidermidis* isolated from clinical samples in Iran. *AMB Express* **5**, 47. <https://doi.org/10.1186/s13568-015-0134-3>.
- Stepanović, S., Vuković, D., Hola, V., Bonaventura, G.D., Djukić, S., Ćirković, I. and Ruzicka, F. (2007) Quantification of biofilm in microtiter plates: overview of testing conditions and practical recommendations for assessment of biofilm production by staphylococci. *Apmis* **115**, 891–899. [https://doi.org/10.1111/j.1600-0463.2007.apm\\_630.x](https://doi.org/10.1111/j.1600-0463.2007.apm_630.x).
- Stoica, P., Chifiriuc, M.C., Rapa, M. and Lazăr, V. (2017). Overview of biofilm-related problems in medical devices. In Deng, Y. and Lv, W., eds. *Biofilms and Implantable Medical Devices*, pp. 3–23. Oxford, UK: Woodhead Publishing.
- Sugimoto, S., Okuda, K.I., Miyakawa, R., Sato, M., Arita-Morioka, K.I., Chiba, A., Yamanaka, K., Ogura, T. et al. (2016) Imaging of bacterial multicellular behaviour in biofilms in liquid by atmospheric scanning electron microscopy. *Sci Rep* **6**, 1–13. <https://doi.org/10.1038/srep25889>.
- Vuotto, C., Longo, F., Pascolini, C., Donelli, G., Balice, M.P., Libori, M.F., Tiracchia, V., Salvia, A. et al. (2017) Biofilm formation and antibiotic resistance in *Klebsiella pneumoniae* urinary strains. *J Appl Microbiol* **123**, 1003–1018. <https://doi.org/10.1111/jam.13533>.
- Wang, S., Yu, H. and Wickliffe, J.K. (2011) Limitation of the MTT and XTT assays for measuring cell viability due to superoxide formation induced by nano-scale TiO<sub>2</sub>. *Toxicol in Vitro* **25**, 2147–2151. <https://doi.org/10.1016/j.tiv.2011.07.007>.



- Washio, J. and Takahashi, N. (2016) Metabolomic studies of oral biofilm, oral cancer, and beyond. *Int J Mol Sci* **17**, 870.
- Xu, Z., Liang, Y., Lin, S., Chen, D., Li, B., Li, L. and Deng, Y. (2016) Crystal violet and XTT assays on *Staphylococcus aureus* biofilm quantification. *Curr Microbiol* **73**, 474–482. <https://doi.org/10.1007/s00284-016-1081-1>.
- Yadav, M.K., Vidal, J.E. and Song, J.J. (2020) Microbial biofilms on medical indwelling devices. In *New and Future Developments in Microbial Biotechnology and Bioengineering: Microbial Biofilms*, pp. 15–28. <https://doi.org/10.1016/B978-0-444-64279-0.00002-5>.
- Yamaguchi, M. and Yoshida, H. (2018) *Drosophila* as a model organism. In Yamaguchi, M., ed. *Drosophila Models for Human Diseases*, pp 1–10. Singapore: Springer.
- Zhang, B. and Powers, R. (2012) Analysis of bacterial biofilms using NMR-based metabolomics. *Future Med Med* **4**, 1273–1306. <https://doi.org/10.4155/fmc.12.59>.



OPEN

## Potential in vitro anti-periodontopathogenic, anti-*Chikungunya* activities and in vivo toxicity of Brazilian red propolis

Nagela Bernadelli Sousa Silva<sup>1</sup>, Jonathan Henrique de Souza<sup>1</sup>, Mariana Brentini Santiago<sup>1</sup>, Jhennyfer Rodrigues da Silva Aguiar<sup>1</sup>, Daniel Oliveira Silva Martins<sup>1,2</sup>, Rafael Alves da Silva<sup>3</sup>, Igor de Andrade Santos<sup>1</sup>, Jennyfer A. Aldana-Mejía<sup>4</sup>, Ana Carolina Gomes Jardim<sup>1,2</sup>, Reginaldo dos Santos Pedroso<sup>5</sup>, Sergio Ricardo Ambrósio<sup>6</sup>, Rodrigo Cássio Sola Veneziani<sup>6</sup>, Jairo Kenupp Bastos<sup>4</sup>, Regina Helena Pires<sup>7</sup> & Carlos Henrique Gomes Martins<sup>1</sup>✉

Bacterial and viral infections are serious public health issue. Therefore, this study aimed to evaluate the antibacterial, antibiofilm and antiviral potential of the Brazilian Red Propolis (BRP) crude hydroalcoholic extract, fractions, and isolated compounds, as well as their in vivo toxicity. The antibacterial activity was evaluated by determining the Minimum Inhibitory Concentration and the antibiofilm activity by determining the Minimum Inhibitory Concentration of Biofilm (MICB<sub>50</sub>). The viable bacteria count (Log<sub>10</sub> UFC/mL) was also obtained. The antiviral assays were performed by infecting BHK-21 cells with *Chikungunya* (CHIKV) *nanoluc*. The toxicity of the BRP was evaluated in the *Caenorhabditis elegans* animal model. The MIC values for the crude hydroalcoholic extract sample ranged from 3.12 to 100 µg/mL, while fractions and isolated compounds the MIC values ranged from 1.56 to 400 µg/mL. The BRP crude hydroalcoholic extract, oblongifolin B, and gutiferone E presented MICB<sub>50</sub> values ranging from 1.56 to 100 µg/mL against monospecies and multispecies biofilms. Neovestitol and vestitol inhibited CHIKV infection by 93.5 and 96.7%, respectively. The tests to evaluate toxicity in *C. elegans* demonstrated that the BRP was not toxic below the concentrations 750 µg/mL. The results constitute an alternative approach for treating various infectious diseases.

Despite important advances in the health area, infectious diseases have constituted a serious public health issue over time<sup>1</sup>. One example is periodontitis, an inflammatory disease that affects tooth-supporting apparatus and which is caused by microorganisms present in dysbiosis plaque biofilms<sup>2</sup>. According to Mehrotra and Singh<sup>3</sup>, about 2.6% of African Americans, 5% of Africans, 0.2% of Asians, 1% of North Americans, and 0.3% of South Americans have been diagnosed with periodontitis in its most severe form. Periodontal treatment is essential not only for dental parameters, but also to avoid other pathological conditions such as adverse reactions in pregnancy, cardiovascular and respiratory diseases, cancer, lupus, rheumatoid arthritis, diabetes mellitus, and chronic kidney disease<sup>4</sup>. Even if the illness can be treated with antibiotics, the infection can be aggravated in patients lacking treatment or in the presence of resistant periodontopathogenic bacteria<sup>5</sup>.

Viral diseases also burden the global health system due to lack of vaccines and approved antivirals to combat important human viruses, including the *Chikungunya* Fever, caused by the *Chikungunya* virus (CHIKV)<sup>6</sup>. CHIKV was identified in 2014 and has become hyperendemic in Brazil<sup>7</sup>. This virus causes dengue-like symptoms such

<sup>1</sup>Institute of Biomedical Sciences (ICBIM), Federal University of Uberlândia, Uberlândia, Brazil. <sup>2</sup>Institute of Biosciences, Letters and Exact Sciences (IBILCE), Sao Paulo State University, São José Do Rio Preto, Brazil. <sup>3</sup>Faculty of Medicine (FAMED), Federal University of Uberlândia, Uberlândia, Brazil. <sup>4</sup>Faculty of Pharmaceutical Sciences of Ribeirão Preto, University of São Paulo (USP), Ribeirão Preto, Brazil. <sup>5</sup>Technical School of Health (ESTES), Federal University of Uberlândia, Uberlândia, Brazil. <sup>6</sup>Exact and Technological Sciences Nucleus, University of Franca (UNIFRAN), Franca, Brazil. <sup>7</sup>Postgraduate Program in Health Promotion, University of Franca (UNIFRAN), Franca, Brazil. ✉email: carlos.martins2@ufu.br

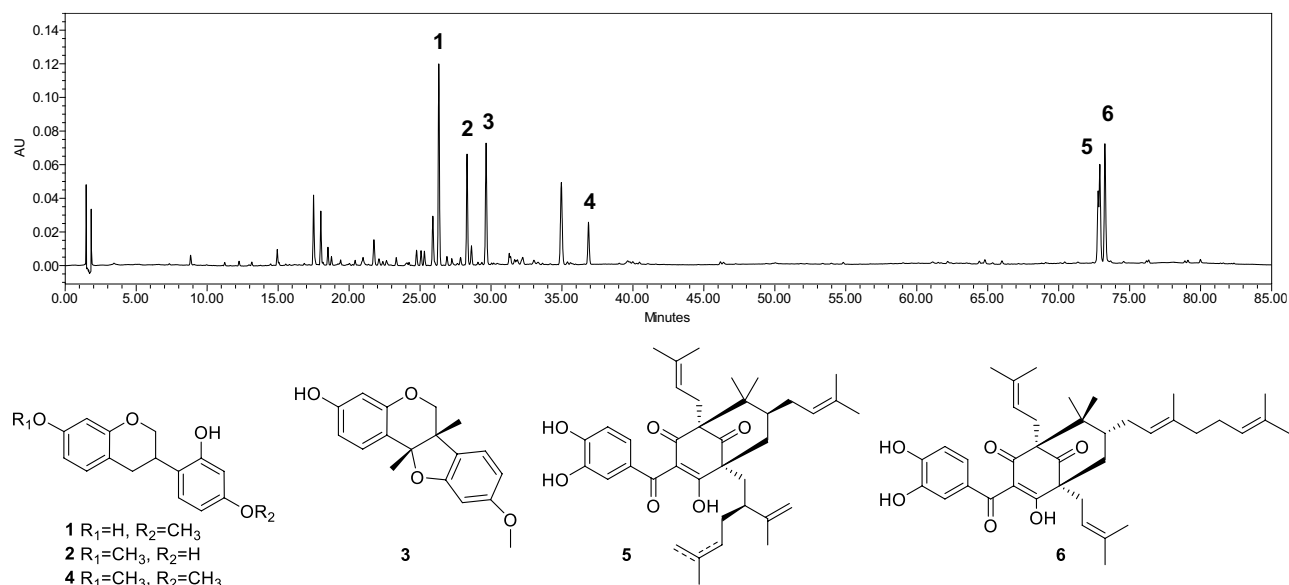


**Figure 1.** Chromatographic profile of Brazilian red propolis extract and chemical structures of their main compounds. Numbers correspond to: vestitol (1); neovestitol (2); medicarpin (3); 7-*O*-methylvestitol (4); guttiferone E/xanthochymol<sup>59</sup>; and oblongifolin B (6).

as fever, fatigue, arthralgia, and polyarthralgia<sup>8</sup>. By April 2022, 28,291 suspected cases of *Chikungunya Fever* had been registered and five deaths had been confirmed in Brazil; another eight deaths are under investigation<sup>9</sup>.

According to the World Health Organization, a considerable part of the worldwide population still depends on traditional medicine and employs natural products to treat several diseases<sup>10</sup>. Developing countries mainly use such products. In this scenario, Brazil is a valuable source of natural products given that it possesses diverse fauna and flora<sup>11</sup>. Brazilian Red Propolis (BRP), a resinous material produced by *Apis mellifera* bees through the collection of the exudates of two plant species: *Dalbergia ecastaphyllum*<sup>12,13</sup> and *Symphonia globulifera*<sup>14</sup> has excellent potential for developing new medicines. BRP is currently one of the most produced and commercialized types of Brazilian propolis. It is mainly found in the Brazilian mangroves of the Northeast, especially in Alagoas and Bahia states<sup>15</sup>.

BRP is composed of 50% resin, 30% wax, 10% essential oils, 5% pollen, and 5% other compounds, including secondary metabolites like flavonoids, isoflavonoids, cinnamic acid derivatives, esters, polyprenylated benzophenones, and some terpenes, which are considered the main biologically active constituents of this type of propolis<sup>16</sup>. The molecules isolated from BRP do not occur in any other type of propolis, which makes them rare and unique natural products<sup>17</sup>. Variations of this composition have been observed between locations. Some studies revealed that compounds such as formononetin and isoliquiritigenin are the most abundant in samples of Alagoas<sup>18</sup>. Instead, in “Canaveiras” sample, vestitol, neovestitol, medicarpin, and polyprenylated benzophenones have been identified as the main compounds and<sup>17</sup>. In this sense, BRP has been reported to possess antibacterial<sup>15,18–20</sup> antiparasitic<sup>21–27</sup>, and antiviral activities<sup>28</sup>.

Considering the lack of treatment options for periodontitis and CHIKV infection, we have hypothesized that BRP and its isolated compounds are a promising candidate for treating these diseases. To the best of our knowledge, there are no data on the BRP antiviral action against CHIKV, and few studies have reported on its antibacterial action against periodontopathogenic bacteria<sup>13,18,28–30</sup>. The use of BRP as a therapeutic option could reduce the use of antibiotics in periodontitis cases and become a novel antiviral strategy against CHIKV<sup>28</sup>.

This study aimed to evaluate the *in vitro* antibacterial, antibiofilm, and antiviral potential of the BRP crude hydroalcoholic extract, fractions, and isolated compounds, as well as their toxicity in an *in vivo* model.

## Results

**BRP crude extract characterization.** The chromatographic analysis revealed the presence of isoflavanes (vestitol, neovestitol, 7-*O*-methylvestitol), pterocarpans (medicarpin), and polyprenylated acylphloroglucinols (a mixture of guttiferone E/xanthochymol, and oblongifolin B) (Fig. 1), as main compounds of the BRP. The chromatographic profile of the fractions revealed the prominent presence of polyprenylated acylphloroglucinols on the hexane fraction, whereas the dichloromethane, ethyl acetate, and *n*-butanol fractions were composed mainly of isoflavanes (see Supplementary Figure S1).

**Minimum inhibitory concentration of the BRP crude hydroalcoholic extract, fractions, and isolated compounds.** Tables 1 and 2 show the MIC results for the crude hydroalcoholic extract, fractions and isolated compounds against periodontal bacteria included in the study. The MIC values for the crude hydroalcoholic extract sample ranged from 3.12 to 100  $\mu\text{g/mL}$ , for the dichloromethane fraction from 1.56 to 200  $\mu\text{g/mL}$ , ethyl acetate from 12.5 to 400  $\mu\text{g/mL}$ , hexane from 3.12 to 400  $\mu\text{g/mL}$ , and *n*-Butanol from 100 to 400  $\mu\text{g/mL}$  (Table 1).

Minimum Inhibitory Concentration ( $\mu\text{g/mL}$ )					
Crude extract		Fractions			
Bacteria		Dichloromethane	Ethyl acetate	Hexane	<i>n</i> -Butanol
<i>Porphyromonas gingivalis</i> (ATCC 49417)	3.12	1.56	12.5	3.12	100
<i>Porphyromonas gingivalis</i> (clinical isolate)	12.5	25	400	100	–
<i>Fusobacterium nucleatum</i> (ATCC 10953)	100	200	400	–	–
<i>Fusobacterium nucleatum</i> (clinical isolate)	12.5	12.5	–	400	–
<i>Prevotella intermedia</i> (ATCC 15033)	6.25	6.25	200	200	200
<i>Prevotella intermedia</i> (clinical isolate)	50	100	–	400	–
<i>Actinomyces naeslundii</i> (ATCC 19039)	25	25	–	400	–
<i>Actinomyces naeslundii</i> (clinical isolate)	100	100	400	400	400

**Table 1.** Minimum inhibitory concentration of the Brazilian Red Propolis crude hydroalcoholic extract, and fractions against periodontopathogenic bacteria. <sup>a</sup>Technique control strains: *Bacteroides fragilis* (ATCC 25285) and *Bacterioides thetaiotaomicron* (ATCC 29741)—Metronidazole: 1.47 and 2.95  $\mu\text{g/mL}$ , respectively.—> 400  $\mu\text{g/mL}$  was considered inactive.

Minimum Inhibitory Concentration ( $\mu\text{g/mL}$ )						
Isolated compounds						
Bacteria	Metilvestitol	Medicarpin	Vestitol	Neovestitol	Oblongifolin B	Guttiferone E
<i>Porphyromonas gingivalis</i> (ATCC 49,417)	25	50	12.5	12.5	50	1.56
<i>Porphyromonas gingivalis</i> (clinical isolate)	100	200	100	100	6.25	6.25
<i>Fusobacterium nucleatum</i> (ATCC 10,953)	50	50	25	12.5	50	200
<i>Fusobacterium nucleatum</i> (clinical isolate)	–	50	100	50	3.12	3.12
<i>Prevotella intermedia</i> (ATCC 15,033)	–	100	100	50	6.25	12.5
<i>Prevotella intermedia</i> (clinical isolate)	–	–	200	100	50	50
<i>Actinomyces naeslundii</i> (ATCC 19,039)	400	100	200	50	6.25	6.25
<i>Actinomyces naeslundii</i> (clinical isolate)	–	–	200	100	25	50

**Table 2.** Minimum inhibitory concentration of the BRP isolated compounds against periodontopathogenic bacteria. <sup>a</sup>Technique control strains: *Bacteroides fragilis* (ATCC 25285)—Metronidazole: 1.47  $\mu\text{g/mL}$  and *Bacterioides thetaiotaomicron* (ATCC 29741)—Metronidazole: 2.95  $\mu\text{g/mL}$ . – > 400  $\mu\text{g/mL}$  was considered inactive.

For the methylvestitol, the MIC values ranged from 25 to 400  $\mu\text{g/mL}$ , medicarpin from 50 to 400  $\mu\text{g/mL}$ , vestitol from 12.5 to 200  $\mu\text{g/mL}$ , neovestitol from 12.5 to 100  $\mu\text{g/mL}$ , oblongifolin B from 3.12 to 50  $\mu\text{g/mL}$ , and guttiferone E from 1.56 to 200  $\mu\text{g/mL}$  (Table 2).

**Antibiofilm activity of the BRP crude hydroalcoholic extract and isolated compounds.** The BRP crude hydroalcoholic extract reduced the monospecies biofilm formation of the standard strains (ATCC) and their clinical isolates (Fig. 2). Additionally, the number of viable cells in the monospecies biofilm expressed as  $\text{Log}_{10}$  CFU/mL decreased (Fig. 2). The lowest MIC<sub>50</sub> value obtained for the BRP crude hydroalcoholic extract against the monospecies biofilms was 3.12  $\mu\text{g/mL}$  against *A. naeslundii* (ATCC 19039) and *F. nucleatum* (clinical isolate) (Fig. 2e and f). Against the other evaluated monospecies biofilms, the BRP crude hydroalcoholic extract presented MIC<sub>50</sub> of 6.25  $\mu\text{g/mL}$ , except for *P. intermedia* (clinical isolate), against which MIC<sub>50</sub> was 12.5  $\mu\text{g/mL}$ . However, even at concentrations above MIC<sub>50</sub>, we detected viable biofilm cells (Fig. 2a–f).

As for the tested isolated compounds, they also reduced monospecies biofilm formation. In the presence of oblongifolin B (Fig. 3), the lowest MIC<sub>50</sub> was 0.78  $\mu\text{g/mL}$  against *A. naeslundii* (ATCC 19039) (Fig. 3c). Against the other evaluated monospecies biofilms, the MIC<sub>50</sub> values ranged from 1.56 to 6.25  $\mu\text{g/mL}$ . Oblongifolin B at 6.25  $\mu\text{g/mL}$  eliminated *P. gingivalis* (clinical isolate) viable cells and, at 12.5  $\mu\text{g/mL}$ , it eliminated *P. intermedia* (ATCC 15033) and *F. nucleatum* (clinical isolate) viable cells (Fig. 3a,b and d).

Guttiferone E presented low MIC<sub>50</sub> (0.78  $\mu\text{g/mL}$ ) against *A. naeslundii* (ATCC 19,039) (Fig. 4d). Against the other evaluated monospecies biofilms, MIC<sub>50</sub> ranged from 1.56 to 25  $\mu\text{g/mL}$  (Fig. 4a,b,c and e). Guttiferone E eliminated all the biofilm cells from a concentration of 3.12  $\mu\text{g/mL}$  against *P. gingivalis* (clinical isolate), 6.25  $\mu\text{g/mL}$  against *P. intermedia* (ATCC 15033), 25  $\mu\text{g/mL}$  against *F. nucleatum* (clinical isolate), and 1.56  $\mu\text{g/mL}$  against *A. naeslundii* (ATCC 19039). As for *P. gingivalis* (ATCC 49417), we verified the presence of viable biofilm cells even at concentrations above MIC<sub>50</sub> (Fig. 4a).

We also assessed the activity of the BRP crude hydroalcoholic extract and isolated compounds against multispecies biofilm formed by standard strains (group 1) and clinical isolates (group 2) (Fig. 5). The BRP crude

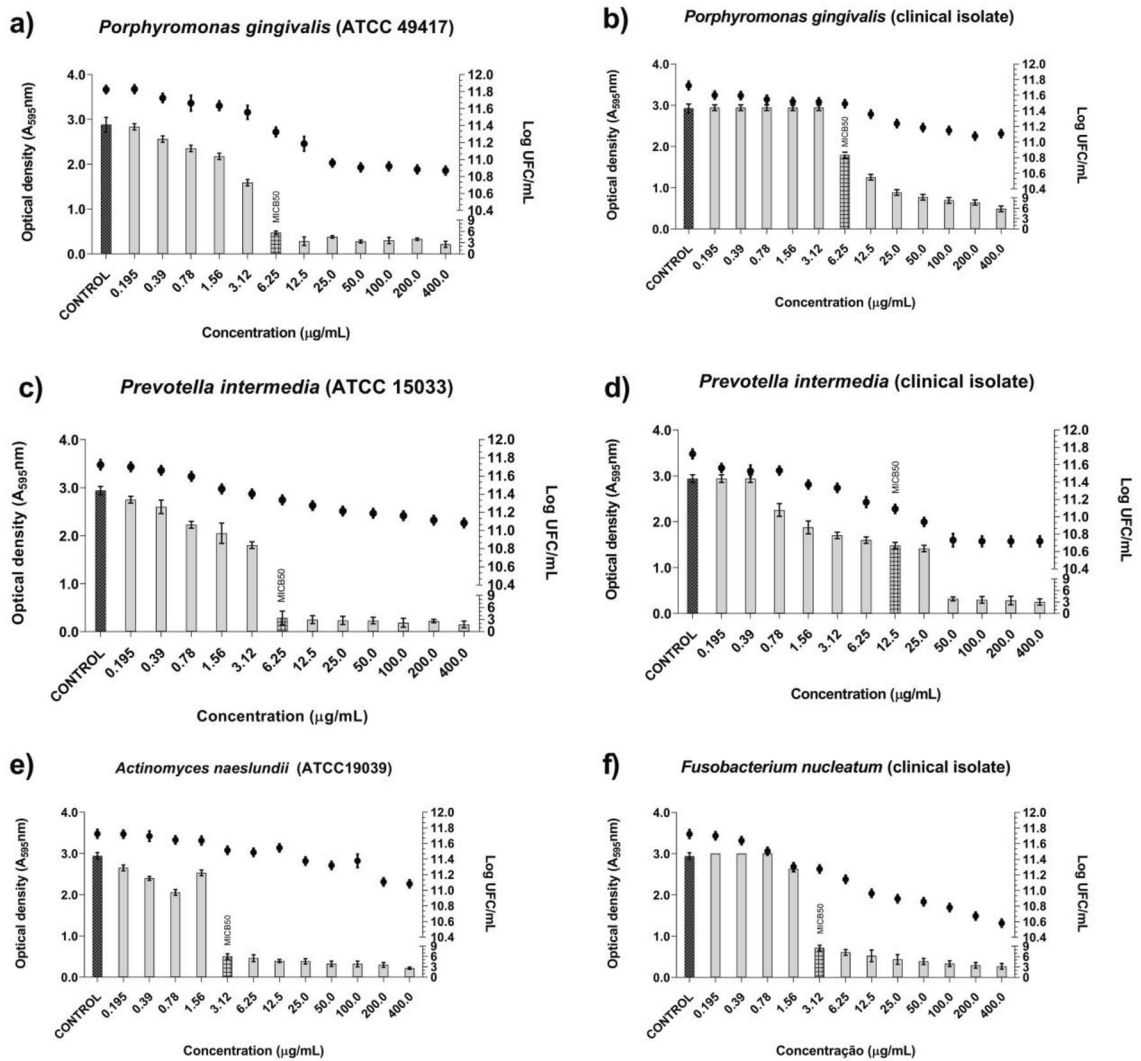


**Figure 2.** Antibiofilm activity of Brazilian Red Propolis crude hydroalcoholic extract samples and number of viable cells in monospecies biofilms formed by ATCC strains and clinical isolates included in the study. (a) *P. gingivalis* (ATCC 49417). (b) *P. gingivalis* (clinical isolate). (c) *P. intermedia* (ATCC 15033). (d) *P. intermedia* (clinical isolate). (e) *A. naeslundii* (ATCC 19039). (f) *F. nucleatum* (clinical isolate).

hydroalcoholic extract had MICB<sub>50</sub> of 6.25 µg/mL against the group 1 multispecies biofilm. However, even at higher concentrations, viable cells were still found in the biofilm. Similar results were found against the group 2 multispecies biofilm: MICB<sub>50</sub> was 6.25 µg/mL, and there also were viable biofilm cells above the MICB<sub>50</sub> concentration (Fig. 5A).

Concerning oblongifolin B, it had the lowest MICB<sub>50</sub> against the group 1 multispecies biofilm (1.56 µg/mL); however, at concentrations above MICB<sub>50</sub>, cells remained viable in the biofilm. Against the group 2 multispecies biofilm, oblongifolin B presented MICB<sub>50</sub> of 50 µg/mL and eliminated all the biofilm cells from the biofilm at this same concentration (Fig. 5B). On the other hand, guttiferone E showed MICB<sub>50</sub> of 3.12 µg/mL against the group 1 multispecies biofilm, and 6.25 µg/mL guttiferone E eliminated all the cells from the biofilm. Against the group 2 multispecies biofilm, guttiferone E had higher MICB<sub>50</sub> (100 µg/mL), but 50 µg/mL guttiferone E also eliminated all the viable cells from the biofilm (Figs. 5C).

Regarding the control (metronidazole), the MICB<sub>50</sub> of monospecies biofilms ranged from 2.95 to 5.9 µg/mL. As for the mixed biofilms, the MICB<sub>50</sub> was 2.95 µg/mL for both the biofilm formed by group 1 and the biofilm formed by group 2 (see supplementary material Figures S2 and S3).

**Effects of the BRP crude hydroalcoholic extract and isolated compounds on CHIKV replication.** To further evaluate the effects of BRP extract and its isolated compounds, BHK 21 cells were treated with each extract at 50, 10 and 2 µg/mL and cell viability was measured 16 h later. The results demonstrated that cells tolerated *n*-Butanol at 50 µg/mL (98.4%), ethyl acetate at 10 µg/mL (95.9%), while the crude extract, dichloromethane, and hexane at 2 µg/mL (99.3, 99.8, and 100%, respectively), (Table 3). Through the employment of BHK-21 cells infected with CHIKV-*nanoluc*, the anti-CHIKV activities of each sample were evaluated,

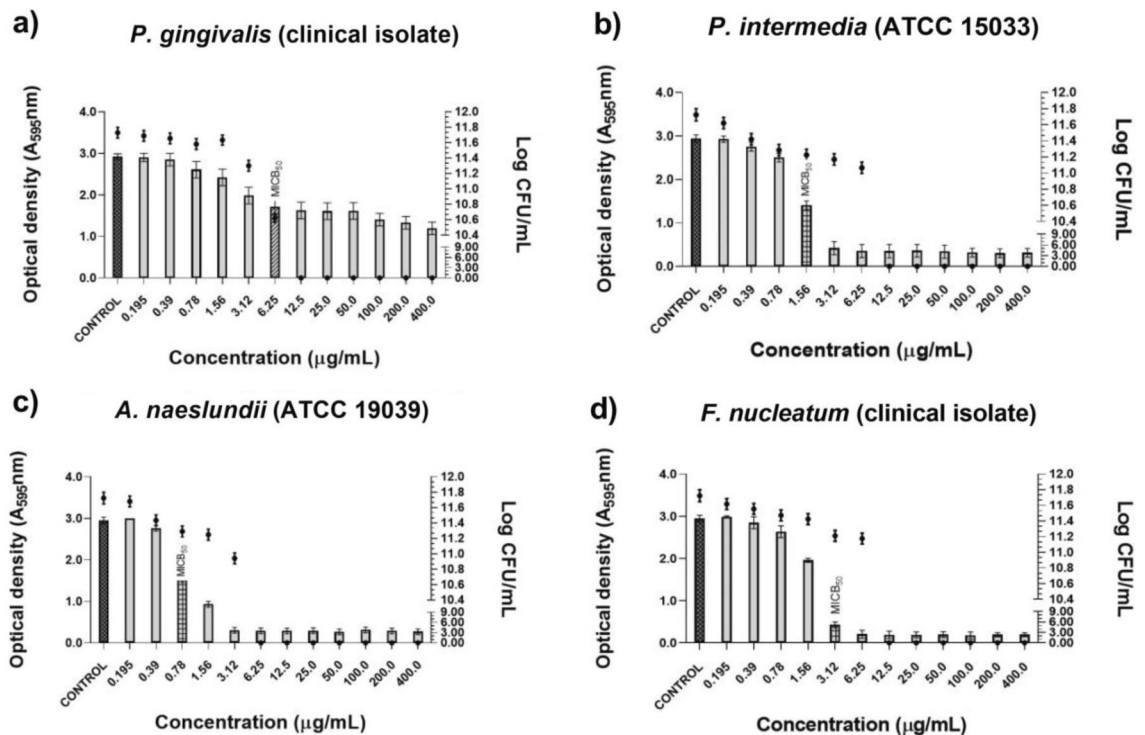


**Figure 3.** Antibiofilm activity of oblongifolin B and number of viable cells in monospecies biofilms formed by ATCC strains and clinical isolates included in the study. (a) *P. intermedia* (clinical isolate) (b) *P. intermedia* (ATCC 15033). (c) *A. naeslundii* (ATCC 19039). (d) *F. nucleatum* (clinical isolate).

at the maximum non-cytotoxic concentrations selected through the viability assay. The results demonstrated that *n*-Butanol significantly inhibited 69% of CHIKV replication (Fig. 6). The other samples presented no effect on CHIKV infection (Fig. 6).

For the isolated substances (medicarpin, neovestitol, vestitol, oblongifolin B, methylvestitol and, guttiferone E), BHK-21 cells were treated with concentrations of each compound ranging from 32 to 0.5 µg/mL. As an outcome, the treatment with compounds in concentrations over 3 µg/mL presented cell viability rates higher than 80% (Table 4), and the highest non-cytotoxic concentration of each compound was selected for the antiviral assay. Since medicarpin, neovestitol and vestitol at 14 µg/mL presented cytotoxicity (Table 4), and at 3 µg/mL showed no antiviral activity (Supplementary Figure S4), the alternative concentration of 11 µg/mL was selected to the further assays. Therefore, the antiviral activity of medicarpin, neovestitol and vestitol was tested at 11 µg/mL, guttiferone E and oblongifolin B at 6 µg/mL, and methylvestitol at 14 µg/mL. The compounds medicarpin, neovestitol and vestitol inhibited CHIKV replication in vitro in 86%, 94%, and 97% respectively (Fig. 7).

**Toxicity assessment in *Caenorhabditis elegans*.** To assess the toxicity of the BRP crude hydroalcoholic extract and isolated compounds in an in vivo system, the technique for determining the lowest concentration capable of killing 50% (LC<sub>50</sub>) of the larvae in relation to the incubation time was employed. Figure 8 shows the toxicity evaluation of the BRP crude hydroalcoholic extract, oblongifolin B, and guttiferone E as a function of time and concentration. The LC<sub>50</sub> of the BRP crude hydroalcoholic extract and oblongifolin B was 1500 µg/mL, determined on the second day of incubation (Fig. 8A and B). On the other hand, guttiferone E had LC<sub>50</sub> of 750 µg/mL, determined on the last day of incubation (Fig. 8C).

## Discussion

For years, propolis has been used to treat infections in folk medicine, and its antimicrobial potential has been demonstrated by the scientific community<sup>15</sup>. This biological potential can be related to its differentiated chemical composition.

Sesquiterpenes, pterocarpan, and isoflavans characterize Brazilian red propolis. Red propolis chemical composition is much different from other propolis types, such as brown propolis, which is characterized by hydrocarbons, aldehydes, and monoterpenes; and green propolis, which is characterized by polycyclic aromatic hydrocarbons, sesquiterpenes, and naphthalene derivatives<sup>31</sup>.

Vestitol, neovestitol, and medicarpin have been reported as major compounds in red propolis from Canavieiras, Bahia State, Brazil. On the other hand, formononetin, calycosin, biochanin A, and isoliquiritigenin were detected at lower concentrations<sup>17</sup>. Guttiferone E and oblongifolin B were described as chemical markers of red propolis<sup>14</sup>, but they appear to be at lower concentrations in the studied sample compared to the isoflavans. The triterpenes β-amyrin and glutinol have also been described in BRP from this location<sup>14</sup>.

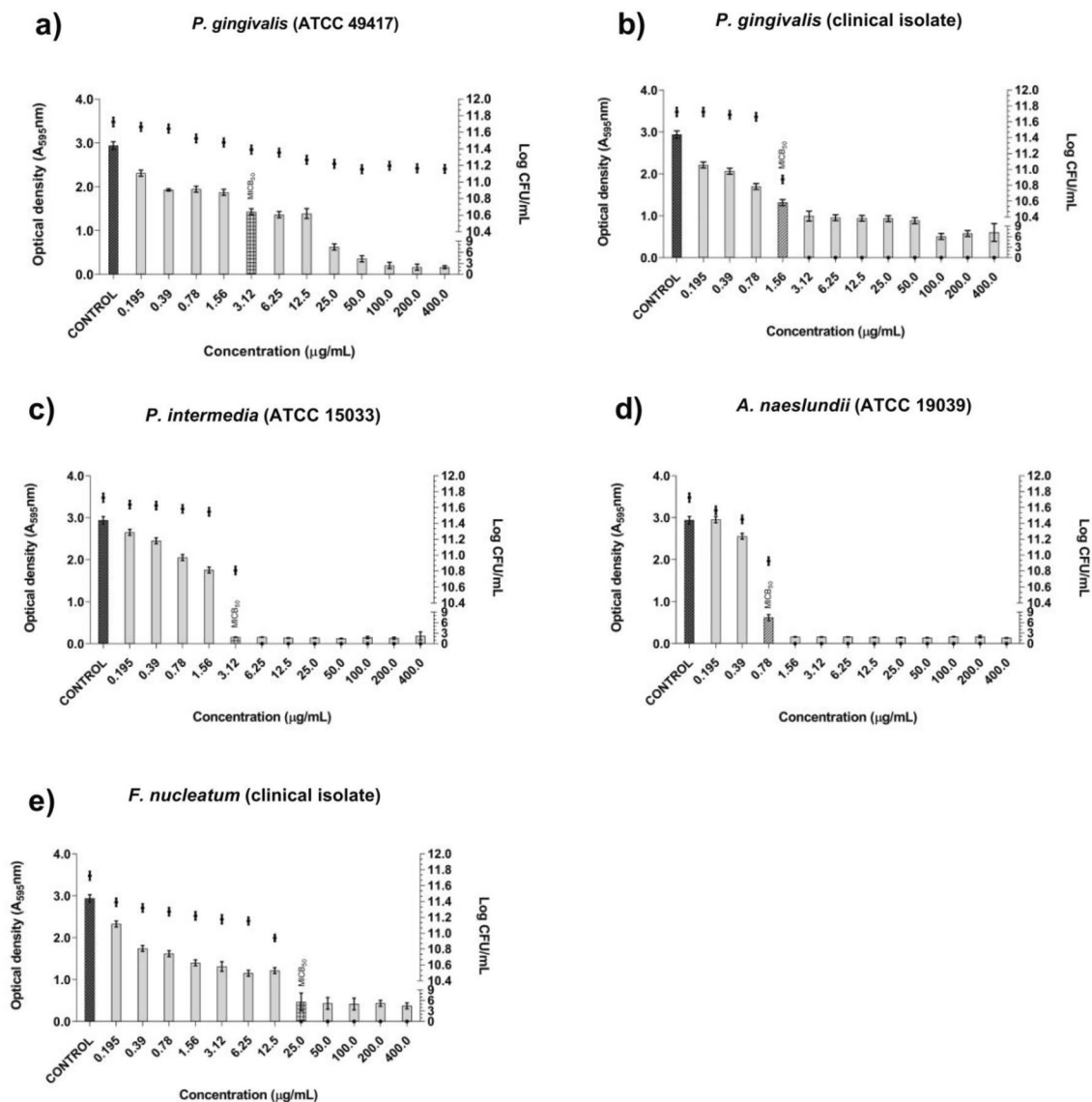


**Figure 4.** Antibiofilm activity of guttiferone E and number of viable cells in monospecies biofilms formed by ATCC strains and clinical isolates included in the study. (a) *P. gingivalis* (ATCC 49417). (b) *P. gingivalis* (clinical isolate). (c) *P. intermedia* (ATCC 15033). (d) *A. naeslundii* (ATCC 19039). (e) *F. nucleatum* (clinical isolate).

According to Rios and Recio<sup>32</sup> and Gibbons<sup>33</sup>, MIC values below 100 µg/mL for crude hydroalcoholic extract or below 10 µg/mL for isolated compounds are considered promising when evaluating the antibacterial activity of plant extracts, essential oils, and compounds isolated from natural sources. On the basis of these criteria and considering the MIC values presented here for all the evaluated BRP samples, the BRP crude hydroalcoholic extract and the isolated compounds guttiferone E and oblongifolin B displayed the best inhibition activity against most of the evaluated bacteria.

The red propolis dichloromethane fraction was not tested since the selection was based on the effect of the individual constituents of each fraction. The main compounds of hexane fraction, oblongifolin B and guttiferone E, displayed good activity at the individual testing, compared with the dichloromethane fraction individual compounds.

These samples showed antibacterial activity mainly against *P. gingivalis* (ATCC 49417), considered the most clinically important species in the development of periodontal disease<sup>34</sup> and *F. nucleatum* (clinical isolate) bacteria, also considered a relevant pathogen since it worsens gingival inflammation and tooth loss<sup>35</sup>. These results demonstrated the relevance of these natural products in periodontal disease control and treatment. In this paper, the BRP crude hydroalcoholic extract, fractions (*n*-hexane, dichloromethane, ethyl acetate, and *n*-butanol), and isolated compounds (methylvestitol, medicarpin, vestitol, neovestitol, oblongifolin B, and guttiferone E) were analyzed for their antibacterial activity against clinical isolates and the ATCC strains. The ATCC strains are more stable from a genetic viewpoint and would thus represent the bacterium species, thereby enabling comparison with other investigations. The in vitro assay furnishes a reliable indication of how the microorganism responds to the target agent, and extrapolation of the results for that species or even genus should be accepted. Clinical

### Crude extract

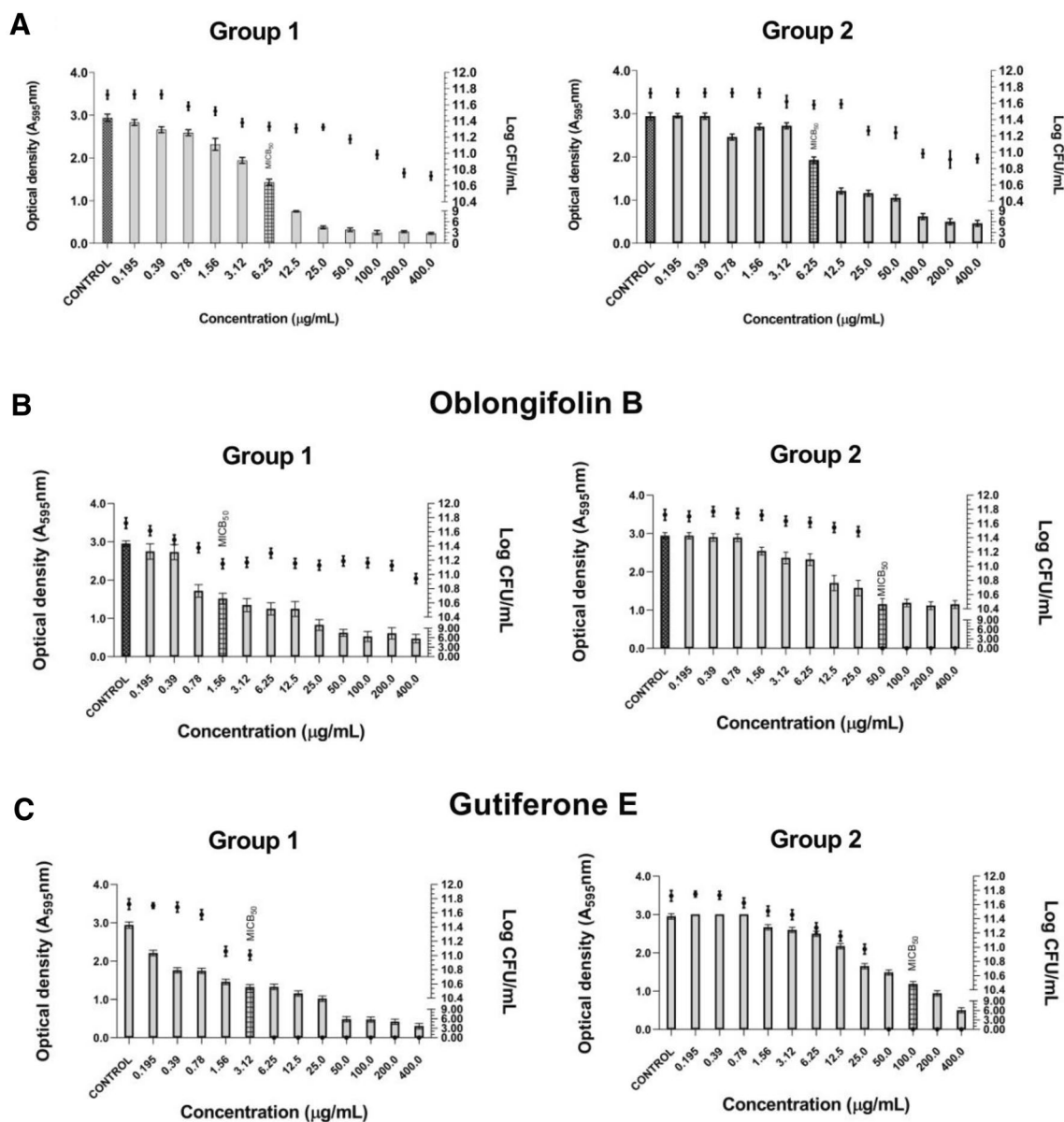


**Figure 5.** Antibiofilm activity of samples of Brazilian Red Propolis crude hydroalcoholic extract, oblongifolin B and guttiferone E and number of viable cells in multispecies biofilms formed by bacteria from groups 1 (standard strains) and 2 (clinical isolates). (A) Crude extract. (B) Oblongifolin B. (C) Guttiferone E.

Sample/concentration	50 µg/mL	10 µg/mL	2 µg/mL
Crude extract	57.3	83.2	99.3
<i>n</i> - Butanol	98.4	100.3	100.6
Dichloromethane	48.3	85.1	99.8
Hexane	45.7	83.3	100.0
Ethyl acetate	66.4	95.9	96.4

**Table 3.** Cell viability percentage in the presence of the BRP crude hydroalcoholic extract or fractions at 50, 10, and 2 µg/mL.



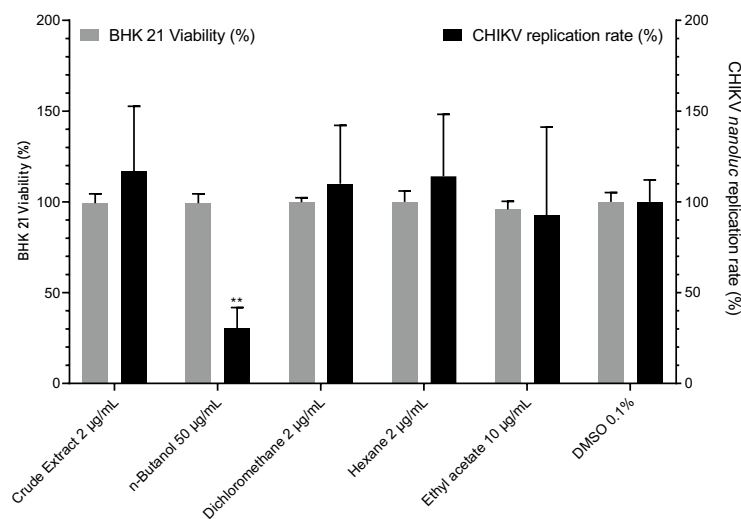


**Figure 6.** Cell viability and CHIKV replication rates in the presence of Brazilian Red Propolis crude hydroalcoholic extract and fractions.

Sample	Concentration (µg/mL)	Cell viability (%)
Medicarpin	14	84
	3	122
	0.5	113
Neovestitol	14	66
	3	110
	0.5	120
Vestitol	14	74
	3	117
	0.5	125
Oblongifolin B	32	72
	6	98
	1	99
Methylvestitol	14	108
	3	103
	0.5	103
Guttiferone E	32	15
	6	88
	1	90

**Table 4.** BHK-21 cell viability in the presence of the BRP isolated substances at concentrations ranging from 32 to 0.5 µg/mL.

isolates (also known as wild strains) are bacteria that can have their metabolism altered by environmental conditions and their genetics modified by circulation in the population, which would justify the relevance of evaluating these two types of strains.

The MIC values (1.56–400 µg/mL) for the other evaluated bacteria were significantly lower as compared to literature data. Bueno-Silva et al.<sup>29</sup> evaluated the antibacterial activity of the crude extract and isolated compounds neovestitol and vestitol obtained from BRP from the same botanical origin against *A. naeslundii* (ATCC 12104), and they reported MIC values of 25, 25, and 50 µg/mL, respectively. Here, neovestitol and vestitol were not promising against several of the evaluated periodontal bacteria. Another point to emphasize is that the MIC value for the crude extract reported by Bueno-Silva et al.<sup>29</sup> against *A. naeslundii* (ATCC 12104) resembled the value we obtained against *A. naeslundii* (ATCC 19039), suggesting a species susceptibility relation for the crude extract.

Santos et al.<sup>36</sup> evaluated the antibacterial activity of the aqueous hydroalcoholic extract and fractions (hexane, dichloromethane, and ethyl acetate) obtained from a different type of propolis, from the region of “Cachoeira da Prata”, Minas Gerais—Brazil, which is also collected from *Apis mellifera* bees. The tested bacteria were periodontal *F. nucleatum* (ATCC 10953), *P. gingivalis* (ATCC 33277), and *P. intermedia* (ATCC 25611). The extract gave MIC values of 1024, 256, and 256 µg/mL against *F. nucleatum* (ATCC 10953), *P. gingivalis* (ATCC 33277), and *P.*

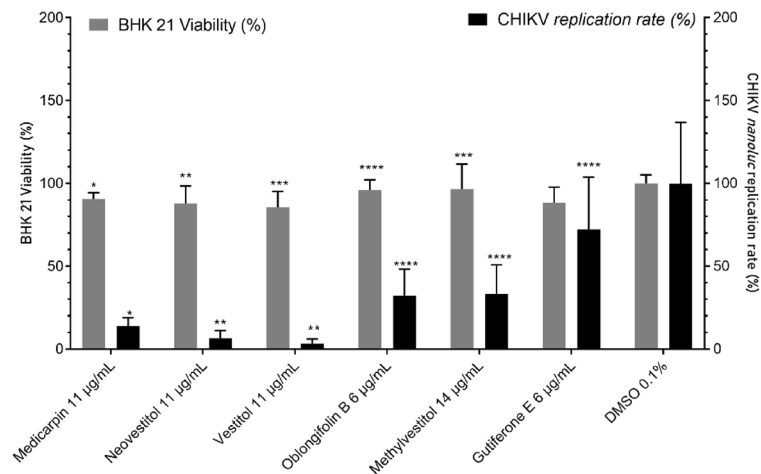


**Figure 7.** Effects of isolated compounds at on CHIKV infection and cell viability.

*intermedia* (ATCC 25611), respectively. As for the fractions, the MIC values ranged from 512 to > 1024 µg/mL. The MIC results against these bacteria were higher than those presented here for the BRP crude hydroalcoholic extract and fractions against the same bacterial species but from different strains: we found MIC values of 100, 3.12, and 6.25 µg/mL for the crude extract against *F. nucleatum* (ATCC 10953), *P. gingivalis* (ATCC 49417), and *P. intermedia* (ATCC 15033), respectively. As for the fractions, we found MIC values ranging from 12 to 400 µg/mL against the same bacteria. Therefore, compared to the results described by these authors, the BRP crude hydroalcoholic extract and fractions employed here were more effective against periodontal bacteria.

Additionally, these authors compared the MIC results they obtained with the crude extract and fractions by ANOVA analysis. They did not find any differences in the antibacterial activity of the fractions or extract against the evaluated bacteria. This corroborates our results: the BRP crude hydroalcoholic extract was more promising than the fractions and gave better values against all the evaluated bacteria, while the fractions presented antibacterial activity against only two bacteria (*P. gingivalis* ATCC 49417 and clinical isolate).

Shabbir et al.<sup>37</sup> evaluated the activity of the crude propolis extract collected in Skardu (Pakistan) originating from *Robinia pseudoacacia*, *Elegnus agustifolia* (Russian olive), and *Acacia modesta*, collected from *Apis mellifera* bees. The natural products afforded MIC values ranging from 64 to 512 µg/mL against *P. gingivalis* and *P. intermedia* clinical isolates. Our results suggested that BRP is more effective than the propolis used by Shabbir et al.<sup>37</sup> since the MIC values we obtained for the BRP crude hydroalcoholic extract against *P. gingivalis* and *P. intermedia* clinical isolates were lower (12.5 and 6.25 µg/mL, respectively). Therefore, BRP proved to have more promising activity than propolis from other countries given that it is composed of unique compounds that do not normally occur in other types of propolis<sup>15</sup>.

Inhibiting biofilm formation by these bacteria can contribute to reducing periodontitis. Indeed, Al-Ahmad et al.<sup>38</sup> described that *A. naeslundii* and *F. nucleatum* play the roles of initial colonizing bacterium and late colonizer, respectively. The latter bacterium was shown to be present at rates greater than 50% after 62 h of biofilm formation, contributing to increased inflammation and tooth loss<sup>38</sup>.

Other studies have evaluated the BRP monospecies antibiofilm activity against other types of bacteria. de Souza Silva et al.<sup>39</sup> evaluated the antibiofilm activity of the BRP crude hydroalcoholic extract (BRP collected in the same region as the BRP used in our study) coated on polymeric nanoparticles against *Staphylococcus aureus* (ATCC 25923), *Staphylococcus aureus* (ATCC 33591), *Staphylococcus aureus* (ATCC 43300), and *Pseudomonas aeruginosa* (ATCC 27853). The free BRP crude hydroalcoholic extract and the extract coated on nanoparticles inhibited the biofilm formed by the Gram-positive strains more effectively as compared to the biofilm formed by the Gram-negative strains, with biofilm inhibitory concentration values ranging from 15.6 to 125 µg/mL against the *S. aureus* strains and from 100 to 1560 µg/mL against the *P. aeruginosa* strain. These results corroborated our findings given that we verified the lowest MIC<sub>50</sub> values against the Gram-positive bacterium *A. naeslundii* (ATCC 19039) 3.12 µg/mL for the crude extract and 0.78 µg/mL for the isolated compounds oblongifolin B and guttiferone E.

Miranda et al.<sup>13</sup> evaluated the antibiofilm activity of the crude hydroalcoholic extract of BRP from the same botanical origin as the BRP used here. These authors divided the evaluated bacteria into complexes (*Actinomyces*, purple, yellow, green, orange, red, and others). At extract concentrations of 800 and 1,600 µg/mL, the authors showed a 40 and 45% decrease in the metabolic activity of the multispecies biofilms formed by these complexes, respectively. de Figueiredo et al.<sup>30</sup> also evaluated the antibiofilm activity of the BRP crude extract at 1600, 800, and 400 µg/mL and obtained 56, 56, and 57% reduction in the biofilm metabolic activity, respectively. Our study did not assess eradication, but it evaluated the ability of the BRP samples to inhibit biofilm formation. According to Wei et al.<sup>40</sup> inhibiting biofilm formation is much more important than eradicating it because biofilm formation inhibition prevents bacterial growth and, hence, bacterial maturation. The results presented here demonstrated that the BRP samples inhibited multispecies biofilm formation by periodontal bacteria by at least 50%. Oblongifolin B gave the lowest MIC<sub>50</sub> value (1.56 µg/mL) against the multispecies biofilm formed by the ATCC strains.

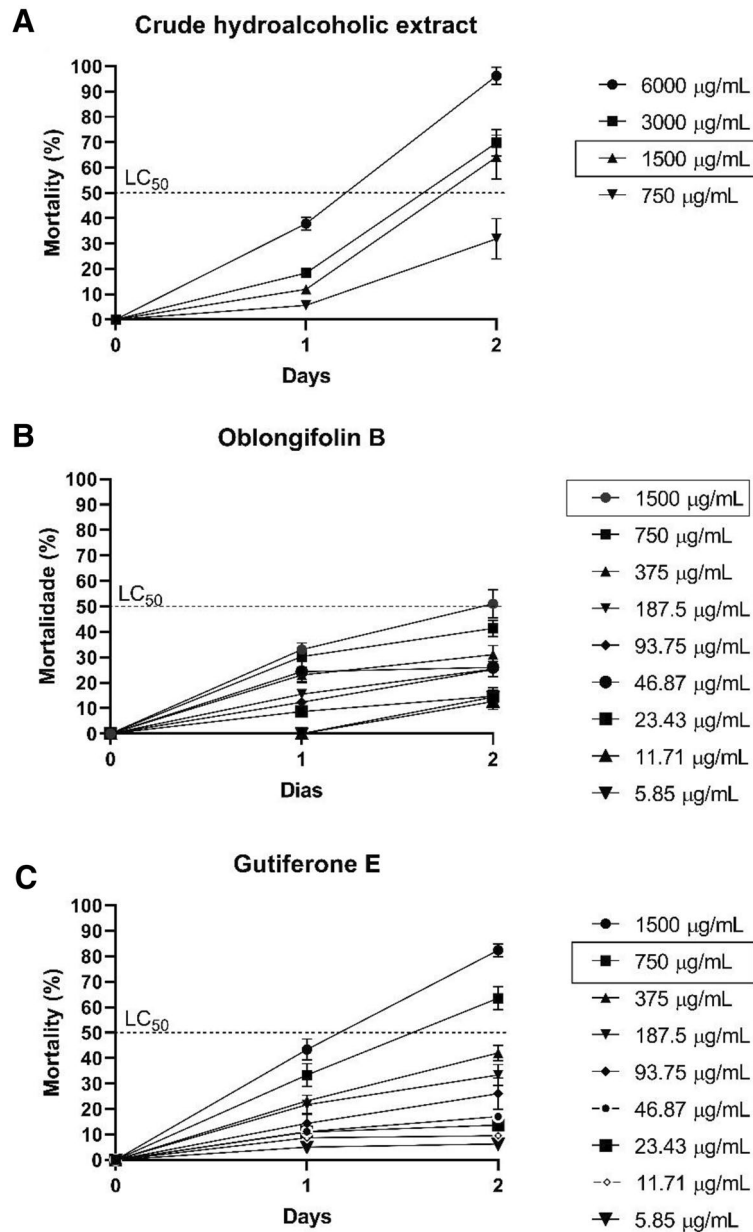


**Figure 8.** Evaluation of the toxicity of the Brazilian Red Propolis crude hydroalcoholic extract and isolated compounds guttiferone E and oblongifolin B in the *C. elegans* in vivo model. (A) Crude hydroalcoholic extract. (B) Oblongifolin B. (C) Guttiferone E.

As for the multispecies biofilm formed by the clinical isolates, the lowest MIC<sub>50</sub> value was 6.25  $\mu\text{g/mL}$ . These results suggested that the isolated compounds oblongifolin B and guttiferone E inhibited all the viable cells of most monospecies and multispecies biofilms formed by the bacteria included in this study. This pointed out that the BRP samples can inhibit biofilm formation and reach the cells within this bacterial community, eliminating them and leaving only the glycoprotein conjugate without live cells<sup>13</sup>.

It is worth mentioning that the MIC<sub>50</sub> values found in this paper are relatively low, especially for clinical isolates that are generally more resistant and demand higher concentrations. However, at the lowest concentration capable of inhibiting biofilm formation by at least 50%, the so-called MIC<sub>50</sub>, we demonstrated an inhibition of at least 50% of the biofilm. In other words, this did not correspond to total inhibition of the biofilm, which would probably require a higher concentration.

Propolis bioactive components such as flavonoids, esters, alcohols, essential oils, and other organic compounds have already been demonstrated to display antiviral activity against viruses such as herpes viruses (HSV-1 and HSV-2), sindbis virus, parainfluenza virus, cytomegalovirus, HIV, and *Varicella zoster* (HSV-1 and HSV-2), sindbis virus, parainfluenza virus, cytomegalovirus, HIV, and *Varicella zoster*<sup>41,42</sup>. In addition to the BRP antibacterial and antibiofilm activities demonstrated in this study, we evaluated the anti-CHIKV activity of the

BRP crude hydroalcoholic extract, fractions, and pure substances. We assessed the BHK-21 cell viability in the presence of the BRP samples by the MTT assay. In drug discovery, samples are considered non-toxic when the cell viability rate is above 50%, moderately cytotoxic when the cell viability rate varies between 25 and 50%, and highly cytotoxic when the cell viability rate is less than 25%<sup>43</sup>. In this study, all samples evaluated showed cell viability equal to or higher than 80% at a concentration of 50 µg/mL for the crude extract and fractions and 3 µg/mL for isolated compounds (Tables 3 and 4). All the BRP samples evaluated in this study provided BHK-21 cell viability equal to or higher than 80% (Tables 3 and 4), which was higher than the cell viability found by Rufatto et al.<sup>20</sup>, (between 14.5 and 46%).

Regarding the infection assays, the isolated compounds neovestitol and vestitol furnished the most promising results, with virus infection inhibition rates of 94 and 97%, respectively (Fig. 7). Even though several natural compounds with antiviral activity, including anti-CHIKV activity, have been described, neovestitol and vestitol have not had their antiviral potential screened. Our results showed higher inhibition rates than those reported in other studies with natural molecules, such as the study of Pohjala et al.<sup>44</sup>, who obtained an infection inhibition limit of at most 75% when they screened 356 compounds, being 123 of them natural compounds. To the best of our knowledge, there are no reports on the anti-CHIKV activity of BRP or isolated compounds. This shows the importance of capitalizing the BRP potential as candidate for antiviral treatment. Our study has pioneered evaluation of the BRP anti-CHIKV activity and has achieved expressive inhibition rates, paving the way for the development of antivirals against CHIKV as well as other viruses.

For BRP to be safely applicable, its toxicity must be evaluated in different experimental models. The murine model is the most used in vivo model to assess the toxicity of treatments, but it has disadvantages such as high cost, difficult maintenance, and delay in obtaining results, among others<sup>45</sup>. Therefore, here we evaluated toxicity by using another in vivo model, the nematode *C. elegans*, a complete animal with digestive, reproductive, endocrine, and neuromuscular systems. Apart from being small, having a short life cycle, and being easy to maintain, *C. elegans* possesses 60–80% genetic homology with humans<sup>46</sup>. In this context, we evaluated the most promising BRP samples for their toxicity against *C. elegans*. The lowest concentration capable of killing at least 50% of the larvae (LC<sub>50</sub>) was 1500 µg/mL for the BRP crude hydroalcoholic extract and oblongifolin B and 750 µg/mL for guttiferone E. These values were significantly higher than all the MIC and MIC<sub>50</sub> concentrations reported in this study.

Moreover, below this concentration, even after the larvae had been exposed to BRP samples for two days, LC<sub>50</sub> was not reached, demonstrating the non-toxic profile of these natural products. Interestingly, the LC<sub>50</sub> values of the BRP samples against *C. elegans* obtained in this study were higher than the LC<sub>50</sub> values of other types of Brazilian propolis evaluated against *C. elegans*. For example, Campos and collaborators (2015)<sup>47</sup> reported that propolis samples possessed LC<sub>50</sub> of 461.8 µg/mL. Here, the BRP concentrations determined as toxic were high, above the highest MIC value (400 µg/mL). Therefore, propolis is not toxic at the concentrations used in this study and can be safely employed at concentrations below 1500 and 750 µg/mL. The results obtained here are extremely relevant, because through different methodologies the antibacterial activity of Brazilian red propolis was demonstrated against a panel of periodontopathogenic bacteria. Another point to highlight is the anti-CHIKV activity of the BRP isolated compounds. *Chikungunya* infection has a high incidence and severity, therefore, the search for new treatment options is highly desirable. Our results constitute an initial step for further studies of BRP as an alternative approach for treating various infectious diseases.

## Conclusion

The Brazilian red propolis used in this study has antibacterial activity against a panel of periodontopathogenic bacteria. Furthermore, its crude extract and isolated compounds oblongifolin B and guttiferone E at concentrations similar to or slightly above the MIC concentrations inhibits monospecies and multispecies biofilms by over 50%. Medicarpin, neovestitol, and vestitol strongly inhibit CHIKV infection in vitro. Besides, toxicity tests on *C. elegans* demonstrated that the crude extract, oblongifolin B, and guttiferone E are non-toxic, proving to be safe and promising so that in the future, these samples of propolis can be used as medicine.

## Methods

**Crude hydroalcoholic extract, fractions, and isolated compounds.** BRP was collected in Canavieiras Bahia State, Brazil, in March 2019 at the Canavieiras Beekeepers Association (COAPER). BRP was frozen and extracted with 70% hydroalcoholic ethanol solution, as described by Santiago et al.<sup>48</sup>. The BRP crude hydroalcoholic extract was partitioned with organic solvents (hexane, dichloromethane, ethyl acetate, and *n*-butanol). Authentic standards from BRP (7-*O*-methylvestitol, medicarpin, vestitol, neovestitol, oblongifolin B, and guttiferone E) previously isolated by our research group were used to characterize the samples<sup>17</sup>.

Chromatographic analysis of BRP extract and its fractions were performed on a Waters 2695 HPLC instrument, coupled to a 2998 photodiode array detector (PDA), with Empower 3 software as a controller. Chromatographic profiles were carried out on a Supelco Ascentis Express C-18 (150 × 4.6 mm, 2.7 µm) column. Mobile phase with water (A) (0.1% formic acid) and acetonitrile (B) was used as follows: 10 → 100% of B until 80 min; 100% of B in 89 min; 100 → 10% in 90 min, maintaining the condition until 95 min. The injections were performed on a flow rate of 1 mL/min, a 40 °C, and an injection volume of 10 µL. Chromatograms were recorded at 275 nm.

For the antibacterial, antiviral, and toxicity assays were used the crude hydroalcoholic extract of BRP, fractions in dichloromethane, hexane, ethyl acetate, *n*-butanol, as well as the isolated compounds guttiferone E, oblongifolin B, methylvestitol, medicarpin, vestitol, and neovestitol.

**Bacterial strains, *Chikungunya* virus and animal model employed in the study.** The periodontopathogenic bacterial strains employed in the antibacterial and antibiofilm activity assays were obtained from the *American Type Culture Collection* (ATCC); their respective clinical isolates were obtained from human periodontal infections. The strains included *Porphyromonas gingivalis* (ATCC 49417 and clinical isolate), *Fusobacterium nucleatum* (ATCC 10953 and clinical isolate), *Prevotella intermedia* (ATCC 15033 and clinical isolate), and *Actinomyces naeslundii* (ATCC 19039 and clinical isolate). These bacteria are part of the collection of the Antimicrobial Assays Laboratory (LEA, abbreviation in Portuguese) of the Federal University of Uberlândia (UFU) and were cryopreserved at  $-20\text{ }^{\circ}\text{C}$ . For the in vivo toxicity assays, the mutant strain *Caenorhabditis elegans* AU37, obtained from the Genetics Center (CGC, University of Minnesota), was used.

For the antiviral assays, a CHIKV expressing the *Nanoluciferase* reporter (CHIKV-*nanoluc*) based on the CHIKV LR2006PYY1 strain (East/Central/South African genotype) was rescued<sup>49</sup>. The protocols were carried out as described previously<sup>50</sup>.

**Determination of the minimum inhibitory concentration<sup>51</sup>.** The antibacterial activity of the BRP crude hydroalcoholic extract, fractions, and isolated compounds were evaluated by the broth microdilution method, in triplicate. The assays were conducted in 96-well microplates; the methodology recommended by the Clinical and Laboratory Standards Institute<sup>52</sup>, with modifications, was followed. The inoculum was standardized to the McFarland 0.5 scale and diluted to a bacterial concentration of  $1.5 \times 10^6$  CFU/mL in the wells. To prepare the samples, the BRP crude hydroalcoholic extract, fractions, or isolated compounds were solubilized in 5% dimethyl sulfoxide (DMSO) and diluted in Brucella broth supplemented with hemin (5.0 mg/mL) and menadione (1.0 mg/mL); a twofold serial dilution with concentrations ranging from 0.195 to 400  $\mu\text{g/mL}$  was used. Control of 5% DMSO was performed, and the solvent did not interfere with bacterial growth at this concentration. It was also performed the following controls: inoculum (all the bacteria used in the test + the culture medium), to observe the viability of the bacteria; broth, to guarantee that the culture medium is sterile; and BRP sample, to guarantee that this solution is sterile. The microplates were incubated in an anaerobic chamber (Don Whitley Scientific, Bradford, U.K.) under anaerobic conditions (80%  $\text{N}_2$ , 10%  $\text{CO}_2$ , and 10%  $\text{H}_2$ ) at  $37\text{ }^{\circ}\text{C}$  for 72 h. Resazurin was used to reveal bacterial growth—the blue color indicated absence of bacterial growth, and the pink color indicated presence of bacteria<sup>53</sup>. As a control technique, metronidazole from 0.0115 to 5.9  $\mu\text{g/mL}$  was used against the control bacteria *Bacteroides fragilis* (ATCC 25285) and *Bacteroides thetaiotaomicron* (ATCC 29741)<sup>52</sup>.

**Evaluation of antibiofilm activity monospecies and multispecies by Minimum Inhibitory Concentration of Biofilm (MICB<sub>50</sub>).** To assess the antibiofilm activity, the BRP samples that presented the most promising MIC results against four or more bacteria were submitted to the Minimum Inhibitory Concentration of Biofilm (MICB<sub>50</sub>) assay. MICB<sub>50</sub> is defined as the lowest concentration of the microbial agent that can inhibit biofilm formation by at least 50%<sup>40</sup> and is calculated using the following equation:

$$1 - \frac{(\text{Absorbance (595nm) of the well containing the treated sample})}{\text{Absorbance (595nm) of the untreated control well}} \times 100$$

Here, MICB<sub>50</sub> was determined as described in the CLSI guidelines (2007)<sup>52</sup>, with modifications. First, the capacity of the analyzed strains to grow in the sessile mode was verified. All the strains at  $1.5 \times 10^6$  CFU/mL formed monospecies and multispecies biofilms after incubation at  $37\text{ }^{\circ}\text{C}$  for 72 h (data not shown).

For the monospecies biofilms, 100  $\mu\text{L}$  of each bacterium inoculum at  $1.5 \times 10^6$  CFU/mL was added to the well with the propolis samples to be evaluated at concentrations from 0.195 to 400  $\mu\text{g/mL}$  (crude hydroalcoholic extract, oblongifolin B and guttiferone E). The microplates were incubated in an anaerobic chamber at  $37\text{ }^{\circ}\text{C}$  for 72 h. For the multispecies biofilms, the main periodontopathogenic bacteria found in the oral biofilm were selected and divided into two groups: group 1 consisted only of the standard bacteria (*P. gingivalis* ATCC 49417, *P. intermedia* ATCC 15033, and *A. naeslundii* ATCC 19039), while group 2 was composed only by the *P. gingivalis*, *P. intermedia*, and *F. nucleatum* clinical isolates. The antibiofilm activity of the most promising BRP samples was evaluated against the multispecies biofilm formed by group 1 bacteria and against the multispecies biofilm composed by group 2 bacteria. For this purpose, 33.33  $\mu\text{L}$  of each evaluated bacterium, totaling 100  $\mu\text{L}$  of bacterial inoculum, at  $1.5 \times 10^6$  CFU/mL was added to the wells with the propolis samples to be evaluated at concentrations from 0.195 to 400  $\mu\text{g/mL}$  (crude hydroalcoholic extract, oblongifolin B and guttiferone E). The microplates were incubated under the same conditions as the monospecies biofilm microplates. The standard antibiotic metronidazole was used as a control at concentrations from 0.0115 to 5.9  $\mu\text{g/mL}$  with MIC<sub>50</sub> (see supplementary material, Figures S2 and S3). Control of 5% DMSO was performed, and the solvent did not interfere with bacterial growth at this concentration. It was also performed the following controls: inoculum (all the bacteria used in the test + the culture medium), to observe the viability of the bacteria; broth, to guarantee that the culture medium is sterile; and BRP sample, to guarantee that this solution is sterile. After incubation, the supernatant culture was withdrawn, and the planktonic cells were removed by washing the wells with ultrapure distilled water. Monospecies and multispecies biofilms were fixed with methanol and stained with 2% crystal violet<sup>54</sup>. The reading was performed in a microplate reader (GloMax<sup>®</sup>) at 595 nm. Reading was performed in a microplate reader (GloMax<sup>®</sup>) at 595 nm. The experiments were carried out in triplicate and independent events.

**Evaluation of the inhibition of biofilm formation by counting microorganism.** This assay was performed for monospecies and multispecies biofilms according to de Souza Silva et al.<sup>39</sup>, as described below. Two microplates were incubated, one for MICB<sub>50</sub> determination, and the other for microorganism count. After the microorganism count microplate was incubated, the supernatant was withdrawn, and the planktonic cells

were removed by washing the wells with ultrapure distilled water. Subsequently, supplemented Brucella broth was added to all the microplate wells, and the biofilm was detached from the well after an ultrasound bath. Then, tenfold serial dilutions were performed in each well of a 96-well microplate, and 50  $\mu$ L of each well, corresponding to each dilution available was placed on two plates of Brucella agar supplemented with horse blood (5%), hemin (5.0 mg/mL), and menadione (1.0 mg/mL). Each of the plates were fractionated into eight parts, as described by Harrison et al.<sup>55</sup> and incubated in an anaerobic chamber for 37 °C. After 72 h, the Colony Forming Units (CFU) count was performed in each plate. The results were expressed as Log<sub>10</sub> (CFU/mL), and the assays were independently performed in triplicate.

**Mammalian cells for antiviral assays.** The BHK-21 cells (fibroblasts derived from Syrian golden hamster kidney; ATCC CCL-10) were maintained in Dulbecco's modified Eagle's medium (DMEM, Sigma-Aldrich) supplemented with 100 U/mL penicillin (Hyclone Laboratories), 100 mg/mL streptomycin (Hyclone Laboratories), 1% dilution of stock of non-essential amino acids (Hyclone Laboratories), and 1% fetal bovine serum (FBS, Hyclone Laboratories) in a humidified 5% CO<sub>2</sub> incubator at 37 °C.

**Cell viability through MTT for antiviral assays.** BHK-21 cell viability in the presence of the tested BRP samples was measured by the MTT [3-(4,5-dimethylthiazol-2-yl)-2,5-diphenyl tetrazolium bromide] (Sigma-Aldrich) assay. BHK-21 cells were cultured in 48-well microplates and treated with different concentrations of the tested BRP sample at 37 °C for 16 h. Then, media containing the tested BRP sample was removed from the 48-well microplate. Next, 1 mg/mL MTT solution was added to each well, incubated for 30 min, and replaced with 300  $\mu$ L of DMSO to solubilize the formazan crystals. Absorbance was measured at 490 nm on a Glomax microplate reader (Promega). Cell viability was calculated according to the equation  $(T/C) \times 100\%$ , where T and C represent the optical density of the treated well and control groups, respectively. DMSO was used as untreated control<sup>50</sup>.

**Antiviral activity against CHIKV infection in vitro.** For initial screening of the anti-CHIKV activity of the BRP crude hydroalcoholic extract and isolated compounds, HK-21 cells were seeded at a density of  $5 \times 10^4$  cells per well in 48-well microplates 24 h before the infection. CHIKV-*nanoluc* at a multiplicity of infection<sup>56</sup> of 0.1 and the tested isolated compound or extract were simultaneously added to the cells. The cells were harvested in Renilla luciferase lysis buffer (Promega) 16 h post-infection (h.p.i.), and virus replication was quantified by measuring nanoluciferase activity with the Renilla luciferase Assay System (Promega). The CHIKV replication rates were calculated according to the equation  $(T/C) \times 100\%$ , where T and C represent the optical density of the treated well and control groups, respectively. DMSO 0.1% was used as untreated control.

**Toxicity assessment in *Caenorhabditis elegans*.** Toxicity evaluation was performed for the most promising BRP samples in the CIM, using the in vivo model of *C. elegans*, according to Andrade et al.<sup>57</sup> and Singulani et al.<sup>58</sup>. The *C. elegans* AU37 mutant strain was cultivated in Nematode Growth Medium (NGM) plates seeded with *Escherichia coli* OP50 and incubated at 16 °C for 72 h. After incubation, the NGM plates containing larvae and eggs were washed with M9 buffer, and the supernatant was placed in 15-mL conical tubes. A bleaching solution (hypochlorite + NaOH) was further added, to kill the adult larvae. The eggs were placed in NGM plates and incubated again at 15 °C for 24 h. Later, the NGM plates containing the larvae at the L1/L2 stages were washed with M9 buffer, and the supernatant was transferred to NGM plates seeded with *E. coli* OP50 and incubated at 16 °C for 24 h. After synchronization, 20  $\mu$ L of the NGM plate contents containing from 10 to 20 L4 stage larvae was added to each well of a 96-well flat-bottomed microplate and incubated at 16 °C for 72 h. The BRP crude hydroalcoholic extract was evaluated from 750 to 6000  $\mu$ g/mL, and the isolated compounds oblongifolin B and guttiferone E were evaluated from 5.85 to 1500  $\mu$ g/mL. DMSO was used as solvent (final concentration  $\leq 1\%$ ).

Larvae were counted every 24 h for three consecutive days under an inverted microscope. Larvae with movement were considered alive and static even after touching they were considered dead. For each sample, the lowest concentration that was able to kill 50% of the larvae, called Lethal Concentration (LC<sub>50</sub>), was determined according to time.

**Statistical analysis.** Individual experiments were performed in triplicate, and all the assays were performed a minimum of three times to confirm the reproducibility of the results. Differences between the means of the readings were compared by analysis of variance (one-way or two-way ANOVA) or Student's t-test conducted with the software Graph Pad Prism 8.0 (Graph Pad Software). The *p* values  $\leq$  than 0.05 were considered statistically significant.

## Data availability

All data generated or analysed during this study are included in this published article (and its Supplementary Information files).

Received: 22 August 2022; Accepted: 21 November 2022

Published online: 07 December 2022

## References

1. Ellwanger, J. H. et al. Beyond diversity loss and climate change: Impacts of Amazon deforestation on infectious diseases and public health. *An. Acad. Bras. Cienc.* **92**, e20191375. <https://doi.org/10.1590/0001-3765202020191375> (2020).

2. Papapanou, P. N. *et al.* Periodontitis: Consensus report of workgroup 2 of the 2017 World Workshop on the Classification of Periodontal and Peri-Implant Diseases and Conditions. *J. Clin. Periodontol.* **45**(Suppl 20), S162–S170. <https://doi.org/10.1111/jcpe.12946> (2018).
3. Mehrotra, N. & Singh, S. *Periodontitis* (StatPearls Publishing, 2020).
4. Slots, J. Periodontitis: Facts, fallacies and the future. *Periodontol.* **2000** **75**, 7–23. <https://doi.org/10.1111/prd.12221> (2017).
5. Cooley, L. & Teng, J. Anaerobic resistance: Should we be worried?. *Curr. Opin. Infect. Dis.* **32**, 523–530. <https://doi.org/10.1097/QCO.0000000000000595> (2019).
6. Silva, L. A. & Dermody, T. S. Chikungunya virus: Epidemiology, replication, disease mechanisms, and prospective intervention strategies. *J. Clin. Invest.* **127**, 737–749. <https://doi.org/10.1172/JCI84417> (2017).
7. Reilly, J. M. *et al.* Postmortem chikungunya diagnosis: A case report and literature review. *Am. J. Forensic Med. Pathol.* **41**, 48–51. <https://doi.org/10.1097/PAF.0000000000000519> (2020).
8. Vairo, F. *et al.* Chikungunya: Epidemiology, pathogenesis, clinical features, management, and prevention. *Infect. Dis. Clin. North Am.* **33**, 1003–1025. <https://doi.org/10.1016/j.idc.2019.08.006> (2019).
9. Department, H. S. Vol. 53 (ed Ministry of Health) (2022).
10. WHO. (World Health Organization, 2018).
11. Valli, M. *et al.* Development of a natural products database from the biodiversity of Brazil. *J. Nat. Prod.* **76**, 439–444. <https://doi.org/10.1021/np3006875> (2013).
12. Batista, L. L. *et al.* Comparative study of topical green and red propolis in the repair of wounds induced in rats. *Rev. Col. Bras. Cir.* **39**, 515–520. <https://doi.org/10.1590/s0100-69912012000600012> (2012).
13. Miranda, S. L. F. *et al.* Brazilian red propolis reduces orange-complex periodontopathogens growing in multispecies biofilms. *Biofouling* **35**, 308–319. <https://doi.org/10.1080/08927014.2019.1598976> (2019).
14. Ccana-Capatinta, G. V. *et al.* *Dalbergia ecastaphyllum* (L.) Taub. and *Symphonia globulifera* L.f.: The botanical sources of Isoflavonoids and Benzophenones in Brazilian Red Propolis. *Molecules* <https://doi.org/10.3390/molecules25092060> (2020).
15. Reis, J. H. O. *et al.* Evaluation of the antioxidant profile and cytotoxic activity of red propolis extracts from different regions of northeastern Brazil obtained by conventional and ultrasound-assisted extraction. *PLoS ONE* **14**, e0219063. <https://doi.org/10.1371/journal.pone.0219063> (2019).
16. Boeing, T. *et al.* The gastroprotective effect of red propolis extract from Northeastern Brazil and the role of its isolated compounds. *J. Ethnopharmacol.* **267**, 113623. <https://doi.org/10.1016/j.jep.2020.113623> (2021).
17. Aldana-Mejia, J. A. *et al.* A validated HPLC-UV method for the analysis of phenolic compounds in Brazilian red propolis and *Dalbergia ecastaphyllum*. *J. Pharm. Biomed. Anal.* **198**, 114029. <https://doi.org/10.1016/j.jpba.2021.114029> (2021).
18. Bueno-Silva, B., Marsola, A., Ikegaki, M., Alencar, S. M. & Rosalen, P. L. The effect of seasons on Brazilian red propolis and its botanical source: Chemical composition and antibacterial activity. *Nat. Prod. Res.* **31**, 1318–1324. <https://doi.org/10.1080/14786419.2016.1239088> (2017).
19. Freires, I. A., de Alencar, S. M. & Rosalen, P. L. A pharmacological perspective on the use of Brazilian Red Propolis and its isolated compounds against human diseases. *Eur. J. Med. Chem.* **110**, 267–279. <https://doi.org/10.1016/j.ejmech.2016.01.033> (2016).
20. Rufatto, L. C. *et al.* Brazilian red propolis: Chemical composition and antibacterial activity determined using bioguided fractionation. *Microbiol. Res.* **214**, 74–82. <https://doi.org/10.1016/j.micres.2018.05.003> (2018).
21. Ayres, D. C., Marcucci, M. C. & Giorgio, S. Effects of Brazilian propolis on *Leishmania amazonensis*. *Mem. Inst. Oswaldo Cruz* **102**, 215–220. <https://doi.org/10.1590/s0074-02762007005000020> (2007).
22. Dantas Silva, R. P. *et al.* Antioxidant, antimicrobial, antiparasitic, and cytotoxic properties of various Brazilian propolis extracts. *PLoS ONE* **12**, e0172585. <https://doi.org/10.1371/journal.pone.0172585> (2017).
23. do Nascimento, T. G. *et al.* Comprehensive multivariate correlations between climatic effect, metabolite-profile, antioxidant capacity and antibacterial activity of Brazilian red propolis metabolites during seasonal study. *Sci. Rep.* **9**, 18293. <https://doi.org/10.1038/s41598-019-54591-3> (2019).
24. Morsy, A. S. *et al.* Effect of Brazilian red propolis administration on hematological, biochemical variables and parasitic response of Santa Ines ewes during and after flushing period. *Trop. Anim. Health Prod.* **45**, 1609–1618. <https://doi.org/10.1007/s11250-013-0406-3> (2013).
25. Regueira-Neto, M. D. S. *et al.* Antitrypanosomal, antileishmanial and cytotoxic activities of Brazilian red propolis and plant resin of *Dalbergia ecastaphyllum* (L.) Taub. *Food Chem. Toxicol.* **119**, 215–221. <https://doi.org/10.1016/j.fct.2018.04.029> (2018).
26. Sena-Lopes, A. *et al.* Chemical composition, immunostimulatory, cytotoxic and antiparasitic activities of the essential oil from Brazilian red propolis. *PLoS ONE* **13**, e0191797. <https://doi.org/10.1371/journal.pone.0191797> (2018).
27. Sinott, F. A. *et al.* Essential oil from Brazilian Red Propolis exhibits anthelmintic activity against larvae of *Toxocara cati*. *Exp. Parasitol.* **200**, 37–41. <https://doi.org/10.1016/j.exppara.2019.03.014> (2019).
28. Silva-Beltran, N. P., Balderrama-Carmona, A. P., Umsza-Guez, M. A. & Souza Machado, B. A. Antiviral effects of Brazilian green and red propolis extracts on Enterovirus surrogates. *Environ. Sci. Pollut. Res. Int.* **27**, 28510–28517. <https://doi.org/10.1007/s11356-019-07458-z> (2020).
29. Bueno-Silva, B. *et al.* Anti-inflammatory and antimicrobial evaluation of neovestitol and vestitol isolated from Brazilian red propolis. *J. Agric. Food Chem.* **61**, 4546–4550. <https://doi.org/10.1021/jf305468f> (2013).
30. de Figueiredo, K. A. *et al.* Brazilian Red propolis is as effective as amoxicillin in controlling red-complex of multispecies subgingival mature biofilm in vitro. *Antibiotics (Basel)* <https://doi.org/10.3390/antibiotics9080432> (2020).
31. Ribeiro, V. P. *et al.* Chemical characterization of Brazilian propolis using automated direct thermal desorption-gas chromatography-mass spectrometry. *J. Sci. Food Agric.* **102**, 4345–4354. <https://doi.org/10.1002/jsfa.11788> (2022).
32. Rios, J. L. & Recio, M. C. Medicinal plants and antimicrobial activity. *J. Ethnopharmacol.* **100**, 80–84. <https://doi.org/10.1016/j.jep.2005.04.025> (2005).
33. Gibbons, S. Phytochemicals for bacterial resistance—strengths, weaknesses and opportunities. *Planta Med.* **74**, 594–602. <https://doi.org/10.1055/s-2008-1074518> (2008).
34. Yoshimasu, Y. *et al.* Rapid bactericidal action of propolis against porphyromonas gingivalis. *J. Dent. Res.* **97**, 928–936. <https://doi.org/10.1177/0022034518758034> (2018).
35. Han, Y. W. *Fusobacterium nucleatum*: A commensal-turned pathogen. *Curr. Opin. Microbiol.* **23**, 141–147. <https://doi.org/10.1016/j.mib.2014.11.013> (2015).
36. Santos, F. A. *et al.* Antibacterial activity of Brazilian propolis and fractions against oral anaerobic bacteria. *J. Ethnopharmacol.* **80**, 1–7. [https://doi.org/10.1016/s0378-8741\(02\)00003-x](https://doi.org/10.1016/s0378-8741(02)00003-x) (2002).
37. Shabbir, A., Rashid, M. & Tipu, H. N. Propolis, a hope for the future in treating resistant periodontal pathogens. *Cureus* **8**, e682. <https://doi.org/10.7759/cureus.682> (2016).
38. Al-Ahmad, A. *et al.* The in vivo dynamics of *Streptococcus* spp., *Actinomyces naeslundii*, *Fusobacterium nucleatum* and *Veillonella* spp. in dental plaque biofilm as analysed by five-colour multiplex fluorescence in situ hybridization. *J. Med. Microbiol.* **56**, 681–687. <https://doi.org/10.1099/jmm.0.47094-0> (2007).
39. de Souza Silva, T. *et al.* Green and Red Brazilian propolis: Antimicrobial potential and anti-virulence against ATCC and clinically isolated multidrug-resistant bacteria. *Chem Biodivers* **18**, e2100307. <https://doi.org/10.1002/cbdv.202100307> (2021).
40. Wei, G. X., Campagna, A. N. & Bobek, L. A. Effect of MUC7 peptides on the growth of bacteria and on Streptococcus mutans biofilm. *J. Antimicrob. Chemother.* **57**, 1100–1109. <https://doi.org/10.1093/jac/dkl120> (2006).

41. Gonzalez-Burquez, M. J. *et al.* Comparison between in vitro antiviral effect of Mexican propolis and three commercial flavonoids against canine distemper virus. *Evid. Based Complement Alternat. Med.* **2018**, 7092416. <https://doi.org/10.1155/2018/7092416> (2018).
42. Labska, K., Plodkova, H., Pumannova, M. & Sensch, K. H. Antiviral activity of propolis special extract GH 2002 against *Varicella zoster virus in vitro*. *Pharmazie* **73**, 733–736. <https://doi.org/10.1691/ph.2018.8672> (2018).
43. de Carvalho, F. M. A. *et al.* Brazilian red propolis: Extracts production, physicochemical characterization, and cytotoxicity profile for antitumor activity. *Biomolecules* <https://doi.org/10.3390/biom10050726> (2020).
44. Pohjala, L. *et al.* Inhibitors of alphavirus entry and replication identified with a stable *Chikungunya* replicon cell line and virus-based assays. *PLoS ONE* **6**, e28923. <https://doi.org/10.1371/journal.pone.0028923> (2011).
45. Hunt, P. R. & The, C. The *C. elegans* model in toxicity testing. *J Appl Toxicol* **37**, 50–59. <https://doi.org/10.1002/jat.3357> (2017).
46. Ruszkiewicz, J. A. *et al.* *C. elegans* as a model in developmental neurotoxicology. *Toxicol. Appl. Pharmacol.* **354**, 126–135. <https://doi.org/10.1016/j.taap.2018.03.016> (2018).
47. Campos, J. F. *et al.* Antimicrobial, antioxidant, anti-inflammatory, and cytotoxic activities of propolis from the stingless bee *Tetragonisca fiebrigi* (Jatai). *Evid. Based Complement Alternat. Med.* **2015**, 296186. <https://doi.org/10.1155/2015/296186> (2015).
48. Santiago, M. B. *et al.* Brazilian red propolis presents promising anti-*H. pylori* activity in in vitro and in vivo assays with the ability to modulate the immune response. *Molecules* <https://doi.org/10.3390/molecules27217310> (2022).
49. Matkovic, R. *et al.* The host DHX9 DExH-box helicase is recruited to *Chikungunya* virus replication complexes for optimal genomic RNA translation. *J. Virol.* <https://doi.org/10.1128/JVI.01764-18> (2019).
50. de Oliveira, D. M. *et al.* Organometallic complex strongly impairs *Chikungunya* virus entry to the host cells. *Front. Microbiol.* **11**, 608924. <https://doi.org/10.3389/fmicb.2020.608924> (2020).
51. Shaughnessy, M. K. *et al.* Evaluation of hospital room assignment and acquisition of *Clostridium difficile* infection. *Infect. Control Hosp. Epidemiol.* **32**, 201–206. <https://doi.org/10.1086/658669> (2011).
52. CLSI. Vol. Approved Standard M11-A7, CLSI (Clinical and Laboratory Standards Institute Wayne, PA, 2007).
53. Sarker, S. D., Nahar, L. & Kumarasamy, Y. Microtitre plate-based antibacterial assay incorporating resazurin as an indicator of cell growth, and its application in the in vitro antibacterial screening of phytochemicals. *Methods* **42**, 321–324. <https://doi.org/10.1016/j.ymeth.2007.01.006> (2007).
54. Stepanovic, S. *et al.* Quantification of biofilm in microtiter plates: overview of testing conditions and practical recommendations for assessment of biofilm production by staphylococci. *APMIS* **115**, 891–899. [https://doi.org/10.1111/j.1600-0463.2007.apm\\_630.x](https://doi.org/10.1111/j.1600-0463.2007.apm_630.x) (2007).
55. Harrison, J. J., Turner, R. J. & Ceri, H. High-throughput metal susceptibility testing of microbial biofilms. *BMC Microbiol.* **5**, 53. <https://doi.org/10.1186/1471-2180-5-53> (2005).
56. Moise, A. R. & Bobis, O. *Baccharis dracunculifolia* and *Dalbergia ecastophyllum*, main plant sources for bioactive properties in green and red Brazilian propolis. *Plants (Basel)* <https://doi.org/10.3390/plants9111619> (2020).
57. Andrade, G. *et al.* Brazilian Copaifeira species: Antifungal activity against clinically relevant *Candida* species, cellular target, and in vivo toxicity. *J Fungi (Basel)* <https://doi.org/10.3390/jof6030153> (2020).
58. Singulani, J. L. *et al.* Activity of gallic acid and its ester derivatives in *Caenorhabditis elegans* and zebrafish (*Danio rerio*) models. *Future Med. Chem.* **9**, 1863–1872. <https://doi.org/10.4155/fmc-2017-0096> (2017).

## Author contributions

N.B.S.S. designed the experiments, functions/Writing—original draft; writing—proofreading and editing. J.H.S. designed the experiments and carried out the experiments. M.B.S. designed the experiments and carried out the experiments. J.R.S.A. designed the experiments and carried out the experiments. D.O.S.M. designed the experiments and analysed the results. R.A.S. designed the experiments and carried out the experiments. I.A.S. analysed the results and Writing—proofreading and editing. J.A.A. designed the experiments and carried out the experiments and analysed the results and Writing—proofreading and editing. A.C.J. analysed the results and Writing—proofreading and editing. R.P.S. Writing—proofreading and editing, methodology, supervision. S.R.A. Acquisition of financing, writing—proofreading and editing. R.C.S.V. Writing—proofreading and editing, acquisition of financing. J.K.B. Writing—proofreading and editing, acquisition of financing. R.H.P. Methodology. C.H.G.M. Conceptualization, formal analysis, methodology, supervision, validation; visualization, functions/Writing—original draft; writing—proofreading and editing. All authors gave the final approval for publication.

## Funding

This work was funded by Fundação de Amparo à Pesquisa do Estado de São Paulo (FAPESP Grant # 2017/04138–8), Fundação de Amparo à Pesquisa do Estado de Minas Gerais (FAPEMIG # 12138—Scholarship granted; APQ-03385–18 and APQ-01487–22), Coordenação de Aperfeiçoamento de Pessoal de Nível Superior (CAPES Finance Code 001—Scholarship granted and Prevention and Combat of Outbreaks, Endemics, Epidemics and Pandemics—Finance Code #88881.506794/2020–01) and Conselho Nacional de Desenvolvimento Científico e Tecnológico (CNPq Grant # 307974/2019–7).

## Competing interests

The authors declare no competing interests.

## Additional information

**Supplementary Information** The online version contains supplementary material available at <https://doi.org/10.1038/s41598-022-24776-4>.

**Correspondence** and requests for materials should be addressed to C.H.G.M.

**Reprints and permissions information** is available at [www.nature.com/reprints](http://www.nature.com/reprints).

**Publisher's note** Springer Nature remains neutral with regard to jurisdictional claims in published maps and institutional affiliations.





**Open Access** This article is licensed under a Creative Commons Attribution 4.0 International License, which permits use, sharing, adaptation, distribution and reproduction in any medium or format, as long as you give appropriate credit to the original author(s) and the source, provide a link to the Creative Commons licence, and indicate if changes were made. The images or other third party material in this article are included in the article's Creative Commons licence, unless indicated otherwise in a credit line to the material. If material is not included in the article's Creative Commons licence and your intended use is not permitted by statutory regulation or exceeds the permitted use, you will need to obtain permission directly from the copyright holder. To view a copy of this licence, visit <http://creativecommons.org/licenses/by/4.0/>.

© The Author(s) 2022

# Rapid detection of biofilm-producing *Candida* species via MALDI-TOF mass spectrometry

Get access >

P.A.D.F. Aguiar ✉, R.P. Menezes, M.P.A. Penatti, T.A. Moreira, J.P. Pimenta, N.B.S. Silva, D.V.D.B. Röder


*Journal of Applied Microbiology*, Volume 131, Issue 4, 1 October 2021,  
Pages 2049–2060, <https://doi.org/10.1111/jam.15066>

**Published:** 01 October 2021



**Article history** ▼

Rapid Communication

# **Volatile compounds of hexane extract from *Pterodon pubescens* Benth seeds and its significant *in vitro* potential against different bacterial strains**

Jaciel G. dos Santos, Cassia C. Fernandes, Nagela B. S. Silva, Gabriel G. Calefi, Carlos H. G. Martins ,  
Guilherme A. Volpini, ...show all

Received 16 Aug 2023, Accepted 11 Dec 2023, Published online: 24 Dec 2023

 Cite this article  <https://doi.org/10.1080/14786419.2023.2297405>

